Cathrin Zeppek, BSc MSc

Amine Base Induced Polymerization of Aryltin Hydrides: Mechanistic Insights & Nanomaterial Characterization

DOCTORAL THESIS

to achieve the university degree of

Doktorin der technischen Wissenschaften

submitted to

Graz University of Technology

supervisor
Univ.-Prof. Dipl.-Chem. Dr.rer.nat. Frank Dieter Uhlig

Institute of Inorganic Chemistry
Faculty of Technical Chemistry, Process Engineering and Biotechnology

Graz, November 2015

Eidesstattliche Erklärung

Ich erkläre an Eides statt, dass ich die vorliegende Arbeit selbstständig verfasst, andere als die angegebenen Quellen/Hilfsmittel nicht benutzt, und die den benutzten Quellen wörtlich und inhaltlich entnommenen Stellen als solche kenntlich gemacht habe. Das in TUGRAZonline hochgeladene Textdokument ist mit der vorliegenden Dissertation identisch.

Affidavit

I declare that I have authored this thesis independently, that I have not used other than the declared sources/resources, and that I have explicitly indicated all material which has been quoted either literally or by content from the sources used. The text document uploaded to TUGRAZonline is identical to the present doctoral thesis.

Datum/ Date

Unterschrift/ Signature

Abstract

The lack of knowledge on the synthesis, structural and spectroscopical characterization of aryltin halogenides and especially hydrides provided motivation to successfully generate a variety of novel compounds. These exhibit aryl moieties in a steric range from *o*-tolyl, 2,4-xylyl, 2,6-xylyl, mesityl, 1-naphthyl, 2-naphthyl, *p*-^{n}butylphenyl, *p*-biphenyl to 9-anthracenyl. Detailed ^{1}H, ^{13}C and ^{119}Sn NMR studies, based on experimental data, as well as DFT calculations for these compound classes is provided, which represent a comprehensive work of reference particularly for ^{119}Sn NMR shifts of Sn(IV) halogenides and hydrides. These findings are complemented by investigations on the stabilizing, non-covalent interactions in the solid state structure of aryltin halogenides and hydrides, which have simply been unmentioned or overlooked in literature.

Since the use of aryltin trihydrides as potential monomeric building blocks in the generation of novel material has been neglected thus far, this work deals with the dehydrogenative coupling reaction of the latter applying the cheap and easy to handle amine base TMEDA as polymerization catalyst. Within this work we propose a reductive dehydropolymerization reaction mechanism, based on DFT calculations and *in situ* synchrotron EXAFS measurements of aryltin trihydrides. The mechanism proceeds *via* a short term Sn(II) intermediate which allows for Sn–Sn bond formation and hydrogen evolution upon insertion. Finally, this conversion forms hitherto unknown aryl decorated nanoparticles (aryl@Sn) containing Sn in oxidation zero.

The shape and size of these nanostructures formed can be controlled by the nature of the solvent which is elucidated by *in situ* synchrotron SAXS measurements. Ethereal, donating solvents such as diethyl ether and dimethoxyethane lead to spherical nano-substructures in the size range of 1-2 nm, whereas the use of cyclohexane or toluene results in nanorods. Furthermore, size and shape can be altered by the aryl substituent bonded to the tintrihydride.

The tailoring of the nanomorphology generated upon dehydrogenative coupling reaction of aryltin trihydrides with amine bases is a valuable tool, which can be seen as a “chemical file”. This allows for the efficient fine tuning of the materials on a nanometer scale and makes aryl decorated nanoparticles (aryl@Sn) potential high energy anode materials for lithium ion batteries.

Kurzfassung

Die Synthese, sowie die strukturelle und spektroskopische Charakterisierung von Arylzinnchloriden und vor allem Arylzinnhydriden erweist sich in der Literatur als vielerseits lückenhaft, was die erfolgreiche Herstellung einer Vielzahl an neuartigen Verbindungen dieser Substanzklassen in unser Interesse rückte. Der sterische Anspruch des Arylrestes variiert dabei von *o*-tolyl, 2,4-xylyl, 2,6-xylyl, mesityl, 1-naphthyl, 2-naphthyl, *p*-^{n}butyl, *p*-biphenyl bis 9-anthracenyl. Detaillierte ^{1}H, ^{13}C und ^{119}Sn NMR Studien, sowohl experimentell, als auch basierend auf DFT Berechnungen, ergeben ein umfassendes Nachschlagewerk für ^{119}Sn NMR Verschiebungen von Sn(IV)Halogeniden und -hydriden. Desweiteren werden stabilisierende, nicht kovalente Wechselwirkungen in der Festkörperstruktur von Arylzinnhalogeniden und -hydriden näher diskutiert, welche bis *dato* in der Literatur unerwähnt, oder schlicht weg übersehen wurden.

Die Rolle von Arylzinntrihydriden als potentielle, monomere Bausteine in der Bildung von neuartigen Materialen findet in dieser Arbeit zum ersten Mal Erwähnung. Diese beschäftigt sich mit der dehydrogenierenden Kupplung von Arylzinntrihydriden unter der Zugabe der Aminbase TMEDA, einem billigen und einfach zu hantierbaren Polymerisationskatalysator. Im Zuge dieser Arbeit wird, unterstützt von sowohl DFT Berechnung, als auch *in situ* Synchrotron EXAFS Messungen, ein reduktiver, dehydrogenierender Reaktionsmechanismus postuliert. Dieser verläuft über die Bildung eines kurzlebigen und reaktiven Sn(II) Zwischenproduktes, welcher unter Insertion die Entstehung von Sn–Sn Bindung und das Abspalten von H_2 ermöglicht. Diese Reaktion führt zur schlussendlichen Erzeugung von Nanopartikeln, die Zinn in Oxidationsstufe null enthalten, welches von Arylresten umgeben ist (Aryl@Sn).

Durch *in situ* Synchrotron SAXS Messungen konnte demonstriert werden, dass die Größe, sowie auch die Form dieser Nanostrukturen durch die Art des verwendeten Lösungsmittels gesteuert werden kann. In diesem Sinne führen etherische, donierende Lösungsmittel wie Diethylether und Dimethoxyethan zu sphärischen Nanosubstrukturen in der Größenordnung von 1-2 nm, wohingegen Toluol oder Cyclohexan in der Bildung von Nanostäbchen resultieren. Desweiteren kann die Größe und Form durch den Arylrest, welcher an das Zinntrihydrid gebunden ist, beeinflusst werden.

Dieses Wissen erlaubt die Bildung maßgeschneiderter Nanomorphologien, als hätte man eine „chemische Feile“ als Werkzeug. Die effiziente Feinanpassung von Aryl@Sn im Nanometerbereich macht diese Substanzen zu potentiellen Anodenmaterialien.

Danksagung

Hiermit will ich die Chance ergreifen, all jenen Menschen Danke zu sagen, die für das erfolgreiche Zustandekommen dieser Arbeit einen essentiellen Beitrag lieferten und deren Unterstützung maßgeblich zum Gelingen beigetragen hat.

Mein primärer Dank geht an meinen Doktorvater Frank Uhlig, der mir die Möglichkeit gab diese Dissertation in seiner Arbeitsgruppe verfassen zu können. Besonders möchte ich mich bei dir für deine Empathie und Menschlichkeit bedanken, die du mir in privat und beruflich schwierigen Situationen entgegenbracht hast, sowie für dein fortwährendes Vertrauen in mich und meine Arbeit. Deine wertschätzende Haltung mir gegenüber, dein offenes Ohr, sowie professionelle und fachlichen Ratschläge, aber auch optimistischer und motivierenden Zuspruch deinerseits will ich hier dankend hervorheben.

Natürlich geht mein Dank auch an alle Mitglieder der AG Uhlig und AG Stüger, die durch das angenehme Arbeitsklima, ihre Hilfsbereitschaft und den Wissensaustausch viel zum erfolgreichen Heranwachsen dieser Arbeit beigetragen haben. So seien auch diverse Reiberein und Kommunikationsschwierigkeiten nicht unerwähnt, deren gemeinsame, erfolgreiche Lösung ein großer Teil dieser persönlichen Lernerfahrungen waren. Herzlich bedanken möchte ich mich bei den „drei Engeln für Frank“- Astrid, Babsi und Monika- weil ihr hier unermüdlich im Hintergrund den Laden schmeißt. Ein großes Danke auch an Johann, Hansipansi, Pichler für unzählige Hilfestellungen was Fachliches betrifft, sowie auch den schlussendlich (manchmal muss man sich zusammenraufen) unterhaltsamen und kurzweiligen Büro- und Laboralltag. Vielen Dank für SAXSing und WAXSing an Manfred Kriechbaum. Grazie mille auch an dich, Heinz Enzo Amenitsch, den verrückten Professor für die „synchrotron world tour“ bei der du es geschafft hast Humor, aber zur selben Zeit Wissenschaftlichkeit miteinander zu verbinden. Danke auch dir, Resi für deine sonnige Art und deine lieben und aufbauenden Worte.

Just some words are not enough to express how grateful I am to have you, Ana. Not only have you been a talented teacher and crystallographer extraordinaire supporting me immensely in the course of this thesis with your professionalism and knowledge, but you have also become one of my best friends. I cannot think of anyone better to travel around Europe to lose sleep over synchrotron measurements and trust so much in being a great scientist and wonderful, reliable person at the same

time. De mi corazón, quiero darte las gracias por tu amistad, apoyo y honestidad. Te conozco bacalao, aunque vengas disfrazao! Gracias por hacer mi vida más completa.

Jedoch gilt mein größter Dank meinen Eltern Carmen und Edmund Zeppek, die mir die Möglichkeit gaben dieses Studium zu beginnen und mich fortwährend nicht nur finanziell, sondern auch emotional unterstützten. Durch eure kompromisslose und aufopfernde Liebe und Hingabe, weiß ich welche Werte im Leben wirklich wichtig sind und dass ich an mich glauben kann.

Ebenso möchte ich mich bei zwei sehr besonderen Menschen in meinem Leben bedanken. Einerseits bei Bartholomäus Pieber, meiner besseren Hälfte, dem Fels in der Brandung- du erlaubst mir zu jedem Zeitpunkt ich zu sein und den Blick auf die wesentlichen Dinge im Leben nie zu verlieren. Danke, für deine kompromisslose, immerwährende Unterstützung in all der Zeit. Danke, dass ich mich immer auf dich verlassen kann und deine liebevolle Art mir jeden Tag mit dir zum Geschenk macht.

Andererseits bei Eva Fischereder, für unsere innige Freundschaft, die mein Leben bereichert und es einfach so viel schöner macht. Mit dir an meiner Seite ist es mir ein Leichtes das Leben mit Humor zu nehmen. Ich sage danke, für unseren schwesterlichen Zusammenhalt, deine Ehrlichkeit und Loyalität in jeder Situation. Ich bin der Baum und du der Pilz- oder umgekehrt?!

Komplett ist das Dreamteam, das „trio infernale“, erst mit dir, Cornelia Hojnik. Danke dafür, dass du eine Quelle der Heiterkeit und des positiven Denkens für mich bist. Danke an euch, an die vielen lieben, unverwechselbare Studienkollegen, die ihr mir alle meine Studienzeit zu einem wunderbaren Lebensabschnitt gemacht habt.

Last but not least, danke ich den „Golden Girls“ Simone Bohne und Marlene für unsere langjährige Freundschaft, die jegliche Tiefschläge und Hochs überdauert, in der ich mich immer angekommen und daheim fühle auch wenn uns oft viele Kilometer voneinander trennen. Auch danke ich dir, Angelika für deine unbeschreiblich empathische, liebevolle und verständnisvolle Art. Kein anderer vermag es mir neue Blickwinkel auf Situationen zu geben, um Dinge reflektieren zu können, wie du.

Danke

Meinen Eltern, Carmen & Edmund, in Dankbarkeit gewidmet

Sich verwirrt zu fühlen, ist der Anfang des Wissens.

Khalil Gibran

Table of Contents

Introduction

1 Introduction 3

1.1 Objectives 4

1.2 Tin in a General Approach: Sources, Industrial Production, Application 4

1.3 Toxicity of Organotin Compounds 6

1.4 The History of Organotin Compounds 7

1.4.1 Tetraorgano Stannanes *8*

1.5 Organotin Halides 12

1.5.1 Triorganotin Halides R_3SnX *12*

1.5.2 Diorganotin Dihalides R_2SnX_2 *15*

1.5.3 Monoorganotin Trihalides $RSnX_3$ *19*

1.6 Organotin Hydrides 22

1.6.1 Properties of Organotin Hydrides *25*

1.7 Linear Polystannanes 26

1.7.1 Synthesis of Polystannanes *26*

1.7.2 Characteristics of Polystannanes *31*

Part A- Synthesis and Characterization of Aryltin Hydrides: Building Blocks towards Polyarylstannanes

2 Aryltin Chlorides and Hydrides: Preparation, Detailed NMR Studies and DFT Calculations 37

2.1 Introduction 38

2.2 Results and Discussion 40

2.2.1 Synthesis *40*

2.2.2 NMR- Spectroscopy and Theoretical Calculations *43*

2.3 Conclusions 54

3 Anthracenyltin Compounds 57

3.1 Introduction 58

3.2 Results and Discussion 59

3.2.1 Synthesis of ASnCl$_3$ via the Lithiation Route (a) 59

3.2.2 Synthesis of ASnCl$_3$ via the Grignard Route (b) 79

3.2.3 Synthesis of ASnCl$_3$ via a Sn(II) Species (c) 81

3.2.4 Synthesis of ASnCl$_3$ via Oxidative Addition (d) 82

3.3 Conclusions 83

4 Stabilizing, Non-covalent Interactions in the Solid State Structure of Novel Aryltin Hydrides and Halogenides 85

4.1 Introduction 86

4.2 Results and Discussion 88

4.2.1 Crystallographic Studies 88

4.3 Conclusions 109

Part B- Dehydrogenative Coupling of Aryltin Hydrides: Mechanistic Insights and Characterization of Aryl@Sn

5 Crystal Structure and Polymerization Studies of Diphenyltin Dihydride 112

5.1 Introduction 113

5.2 Results and Discussion 115

5.2.1 VT-NMR Studies 115

5.2.2 Synthesis 117

5.2.3 X-Ray Crystallography 118

5.2.4 Conformational Analysis and Theoretical Calculations 123

5.3 Conclusions 127

6 Towards Aryl Decorated Tin Nanoparticles (Aryl@Sn)- Insights in an Unknown Reaction Pathway 129

6.1 Introduction 130

6.2 Results and Discussion 132

6.2.1 Synthesis 132

6.2.2 Material Characterization 134

6.2.3 Particle Formation – In situ Synchrotron SAXS Measurements 137

6.2.4 TEM Imaging 142

6.2.5 In situ DLS Measurements 144

6.2.6 Insights into the Reaction Mechanism 147

6.2.7 Proposed Reaction Mechanism 148

6.2.8 Thermally Induced Dehydrocoupling 155

6.2.9 In situ Synchrotron Stopped Flow EXAFS and XANES Studies 159

6.3 Conclusions 167

7 “Basic” Changes in the Dehydrogenative Coupling Reaction of Aryltin Trihydrides 169

7.1 Introduction 170

7.2 Results and Discussion 171

7.3 SWAXS Measurements and Elemental Composition 172

7.4 SEM Imaging 175

7.5 Conclusions 177

8 Control the Morphology of Aryl Decorated Tin Nanoparticles 179

8.1 Introduction 180

8.2 Results and Discussion 181

8.2.1 Synthesis 182

8.2.2 SAXS Measurements 182

8.2.3 SEM Imaging 184

8.2.4 In situ Synchrotron Stopped Flow SAXS Measurements 185

8.2.5 In situ Synchrotron Stopped Flow EXAFS Measurements 193

8.3 Conclusions 196

9 Hydrogenation of *C,N*- Chelated Organotin Halides- Autocatalytic Reductive Dehydropolymerization 197
9.1 Introduction 198
9.2 Results and Discussion 199
9.2.1 VT-NMR Studies and DFT Calculations 204
9.2.2 X-Ray Crystallography 210
9.3 Conclusions 213

Part C

10 Summary & Outlook 216
11 Experimental Part 222
11.1 Materials and Methods 222
11.2 NMR Spectroscopy 222
11.3 GC-MS Measurements 222
11.4 Impedance Spectroscopy 223
11.5 Theoretical Calculations 223
11.6 Crystal Structure Determination 223
11.7 Powder Diffraction Studies 224
11.8 EPR Measurements 225
11.9 SAXS Mesurements 225
11.10 SEM and FESEM Measurements 226
11.11 TEM Measurements 226
11.12 *In situ* UV-VIS Measurements 227
11.13 *In situ* DLS Measurements. 227
11.14 *In situ* Synchrotron Measurements 228
11.14.1 SAXS 228
11.14.2 EXAFS/XANES 230
11.14.3 General Procedure for Stopped Flow Experiments 231

11.15 Synthesis 233
11.15.1 List of Compounds 233
11.15.2 Published Compounds 234
11.15.3 Chapter 2 & 4 236
11.15.4 Chapter 3 248
11.15.5 Chapter 5 256
11.15.6 Chapter 6 257
11.15.7 Chapter 7 & 8 257
11.15.8 Chapter 9 258

12 References 261

13 Appendix I
13.1 Crystal Structure Analysis Data I
13.2 DFT Calculations V
13.2.1 Chapter 2 V
13.2.2 Chapter 5 VIII
13.2.3 Chapter 6 XXVI
13.2.4 Chapter 9 XXXIII

Introduction

1 Introduction

Since the Bronze Age (3500 BC), representing one of the milestones in the evolution of mankind, tin has been a highly appreciated metal and raw material for further processing. But when Frankland[1,2] first described the successful synthesis of an organotin compound shortly after Cadet[3] and Zeise[4] had been established as the pioneers in organometallic chemistry, much attention had been drawn to the organic derivatives of tin, especially to tetra coordinated species. More advanced analytical techniques including Sn NMR, X-ray diffraction or appropriate computational methods were implemented helping organotin chemistry to be a growing field of interest. Besides being used as fungicides, insecticides or stabilizers in PVC, organostannanes are currently widely used in chemical synthesis. They exhibit dominance in many homolytic mechanisms, where in particular, organotin hydrides are the main used agents for performing ring-closing cyclizations.[5] Nevertheless, due to the acute toxicity of organo substituted tin compounds their use in synthetic chemistry has been conotated quite negatively.

Apart from the afore mentioned use of organotin hydrides as mediator in radical additions, rearrangement and elimination reactions, especially diorganotin dihydrides have been investigated as precursors in the formation of polymeric materials exhibiting a linear backbone of covalently bonded tin atoms. Organotin hydrides can undergo a catalytic dehydropolymerization using metal complexes based on palladium, zirconium, rhodium, lanthanides, or platinum as well as “non-traditional” iron and molybdenum alkyls as catalysts.[6-9] Moreover, a solvent and catalyst free dehydrogenation reaction was described as a successful route towards polystannanes.[10] In 2011, amine bases such as TMEDA (*N*,*N*,*N’*,*N’*-tetramethylethylenediamine) have been reported to efficiently catalyze the polymerization reaction of organotin dihydrides leading to poly(diarylstannane)s.[11] These linear polystannanes harbor a covalently linked metal (tin) backbone, which can be seen as a molecular metal wire embedded in an organic jacket, feature an increased degree of electron delocalization by catenation leading to promising materials in charge-transfer devices.[12,13]

1.1 Objectives

In comparison to the use of organotin monohydrides (R_3SnH) as a versatile synthetic tool and the synthesis and characterization of dihydrides (R_2SnH_2)[12-15] as well as their use as polymerization monomers, less is known on the synthesis, properties, as well as applications of organotin trihydrides ($RSnH_3$). Mainly alkyl substituted species have been reported, but have not been fully characterized.[15] This lack of synthetic information provided motivation for this work to synthesize and fully characterize a range of aryltin trihydrides (arylSnH_3). Furthermore, this novel compound class gives rise to a trifunctionalized educt family in a dehydrogenative coupling reaction with TMEDA forming hitherto unknown aryl decorated tin nanoparticles (aryl@Sn). They are promising materials for the use as high energy density anode materials in lithium ion batteries as they are suggested to offer an increased number of electrochemically active sites as well as a high ability to buffer the stress which is induced upon lithiation and delithiation.

1.2 Tin in a General Approach: Sources, Industrial Production, Application

Tin and its ubiquitous uses have been known and appreciated since its discovery in about 3500 BC. The major source of tin is found in the earth's crust with an abundance of 2 ppm, which is scarce in comparison to other metals such as Zn, Pb or Cu. The extraction technique of choice to gain Sn in its metallic form involves the reduction of cassiterite (SnO_2) using carbon monoxide or carbon at elevated temperatures as shown below (Scheme 1).[16,17]

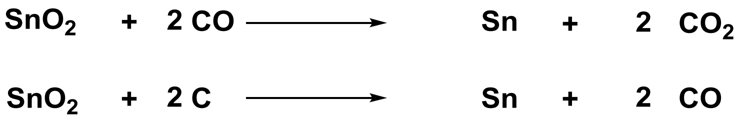
$SnO_2 + 2\,CO \longrightarrow Sn + 2\,CO_2$
$SnO_2 + 2\,C \longrightarrow Sn + 2\,CO$

Scheme 1: *Preparation of metallic tin from cassiterite using carbon monoxide or carbon.*

Apart from being obtained from natural sources, tin is also recycled from used food and drink cans. The major tin producing countries are China and Indonesia. Table 1 depicts the tin production and reserves in the year 2013 and 2014 in tons worldwide.[18]

Table 1: *Worldwide production of tin in 2013 and 2014.*

	mine production (t)	
	2013	**2014**
United States	-	-
Australia	6,470	6,100
Bolivia	19,300	18,000
Brazil	12,000	12,000
Burma	11,000	11,000
China	110,000	125,000
Congo	3,000	3,000
Indonesia	95,200	84,000
Laos	800	800
Malaysia	3,700	3,500
Nigeria	570	500
Peru	23,700	23,700
Russia	420	350,00
Rwanda	1,900	200
Thailand	200	5,400
Vietnam	5400	NA
other countries	100	100

Due to the high demand in the production of the growing field of telecommunication devices, approximately 50 % of the produced tin is used as soldering material. Approximately 20 % of the production refers to the generation of tin plate used intensively in the fabrication of cans. Only about 14 % of the tin occurrence belongs to the elaboration of basic chemicals subjected to further chemical conversion. In addition, application of tin in glass, brass and bronze makes up 2 and 6 %, respectively. Table 2 lists the use of organotin compounds in industrial applications.[19]

Interestingly, tin in its metallic form and its organometallic derivatives exhibit a wide range of different and important applications including as stabilizers, industrial catalysts, industrial and agricultural biocides, fungicides, wood-preserving and antifouling agents, surface disinfectants, slimicides, laundry sanitizers or hospital and veterinary disinfectants.[22,23]

Table 2: *Industrial applications of organotin compounds (OTC) and their function.*

industrial application	function	OTC
PVC stabilizer	stabilization against decomposition by heat and light	R_2SnX_2 and $RSnX_3$
antifouling paints	biocide	R=Me, Bu, Oct
		R_3SnX
agrochemicals	fungicide, insecticide, miticide, antifeedant	R=Bu, Ph
		R_3SnX, , $RSnX_3$ R=Me,Bu
wood preservation, glass treatment	precursors for tin (IV) oxide films on glass	Me_2SnX_2
materials protection (stone leather, paper)	fungicide, algaecide, bactericide	Bu_3SnX
impregnation of textile	insecticide, antifeedant	Ph_3SnX
poultry farming	dewormer	Bu_2SnX_2

1.3 Toxicity of Organotin Compounds

Due to the increased production of tin organometallic derivatives for commercial uses during the last 60 years, concerns regarding their toxicity have become prevalent specifically regarding the penetration of worldwide ecosystems and their persistence in the latter. Currently, a wide span of different organotin compounds is known and aside from methyltins, which are generated upon biomethylation, these do not stem from anthropogenic origin.[20] While tin in its metallic form is not considered to exhibit harmful effects on the environment, the toxicological aspect of their organic derivatives is quite complex.[19] Since the biocidal properties of the latter were described in detail by van der Kerk and Luijten[21,22] in the late 1950s it is known that derivatives of R_3SnX, the trialkyl, triaryl tin hydroxides and tin salts harbour the highest fungitoxicity. The toxicity only depends on R (hydrocarbon radical residue) and not on X, as long as X itself is not a toxic compound.

Hence, the biological effects strongly depend on both, the nature and the size of the organic moiety, resulting in a more or less cationic tin species, which is indeed highly toxic. Therefore, the maximum toxicity level is reached regarding trisubstituted compounds R_nSnX_{4-n}.[19] Thus, the toxicity towards organisms decreases as followed: $R_3SnX > R_2SnX_2 > RSnX_3$.[23] However, according to Smith, triethyltin acetate can be seen as the most toxic organostannane for mammals, with an LD_{50} value of 4mg/kg in rats.[24]

Much attention has been drawn to the extended toxicity of TBT (tributyltin hydride) as a water pollutant, as well as contaminating sediments, due to its harmful effect on the aquatic life and terrestrial ecosystems.[25] Bioaccumulation and persistence in the environment is one major criterion regarding the toxicity of organostannane due to their lipophility.[26] Apart from bioaccumulation, the persistence of organotin compounds, especially regarding butyltins is an environmental issue.[27]

1.4 The History of Organotin Compounds

Organotin compounds or organostannanes are chemical compounds containing at least one Sn−C bond. The first organotin compound described in literature was published by Frankland more than 160 years ago synthesized *via* a direct method by heating up ethyl iodide in the presence of metallic tin leading to a yellow oily fluid (Scheme 2). [1,2]

$$2\ \mathrm{EtI} + \mathrm{Sn} \xrightarrow{h\nu \text{ or } 160\ ^\circ\mathrm{C}} \mathrm{Et_2SnI_2}$$

Scheme 2: *Synthesis of the first organo stannane via a direct method.*

Subsequently, Buckton generated tetraethyltin *via* the so-called indirect route, by treating tin(IV) chloride with diethyl zinc (Scheme 3).[28]

$$2\ Et_2Zn + SnCl_4 \longrightarrow Et_4Sn + 2\ ZnCl_2$$

Scheme 3: *First indirect route synthesizing tetraalkyl stannanes using diethyl zinc and* $SnCl_4$.

Replacement of tin(IV) chloride by tin(II) chloride improved the indirect route due to easier handling of the starting material and reaction processing in a more controllable fashion (Scheme 4).

$$2\ Et_2Zn + SnCl_2 \longrightarrow Et_4Sn + ZnCl_2 + Zn$$

Scheme 4: *Improvement of the indirect route by Frankland diethyl zinc and* $SnCl_2$.

With the discovery of organomagnesium halides in ether solution, by Grignard in 1900 the synthetic scope for organostannanes was widely broadened. Pope and Peachey showed an improved application for Grignard reagents realizing the formation of several simple and mixed tetraalkyl tin derivatives.[29] Pfeiffer *et al.* generated arylstannanes.[30,31]

Sander *et al.* published a comprehensive review on the synthetic aspects of tetraorganotins and organotin (IV) halides.[32]

1.4.1 Tetraorgano Stannanes

The best known and used protocol for generating tetra organostannanes is the reaction of the appropriate Grignard reagent (RMgX) or the organolithium compound (RLi) with a tin halide, in most cases tin(IV) chloride (Scheme 5) in ethereal solvents such as diethyl ether, dibutyl ether or tetrahydrofuran.[33-41]

$$4\ RMgX + SnX_4 \longrightarrow R_4Sn + 4\ MX$$

Scheme 5: *Conversion of a Grignard reagent with* SnX_4 *generating tetraorgano stannanes.*

By using an excess of Grignard reagent the reaction is driven to full conversion but might contain R_3SnX as a side product. Hence, using the Grignard route, tetravinyl,[42] tetrallyl,[43-45] tetraalkyl[36-41] and tetraaryl stannanes[30,46-48] are easily prepared up to 90 % yield and higher. An interesting procedure was described by Kipping and Smith generating tetra organostannanes without preparation of the Grignard reagent, adding the organic halide to magnesium powder and tin(IV) chloride in ether.[49] This reaction procedure was further discussed in the literature, whereby diethyl ether frequently was replaced by hydrocarbon solvents.[50,51] For tetraalkyl organostannanes with alkyl moieties longer than C_4, the Grignard route might not be the reaction pathway of choice due to low yields. In that case, a Wurtz-type coupling reaction of $SnCl_4$ with a sodium-tin alloy in a hydrocarbon solvent is more successful as shown by van der Kerk and Luijten. They generated the butyl derivative in relatively high yields, but with difficult to control reaction conditions and distannanes as side products (Scheme 6).[13,52]

$$\mathrm{SnX_4} + 4\ \mathrm{BuX} + 8\ \mathrm{Na} \longrightarrow \mathrm{R_4Sn} + 8\ \mathrm{NaX}$$

Scheme 6: *Wurtz-type coupling reaction generating tetraalkyl organostannanes.*

Lithiation of the organohalide and treatment with SnX_4 turned out to be a suitable route for tetraaryl stannanes and Me_4Sn.[35,55] However, product yields for this approach can be declared as rather low due to distannane formation as a side reaction. Concerning the preparation of tetraaryltins, diarylzinc reagents have proven to be more successful, since in this transarylation reaction no formation of distannanes can be detected and therefore diphenylzinc results in Ph_4Sn in higher than 90 % yield (Scheme 7).[53]

$$2\ \mathrm{R_2Zn} + \mathrm{SnX_4} \longrightarrow \mathrm{R_4Sn} + 2\ \mathrm{ZnX_2}$$

Scheme 7: *Preparation of tetraorgano stannanes using diorgano zinc reagents.*

Also, by employing triorganoaluminum reagents, distannane formation can be avoided (Scheme 8).[54,55] Nowadays, this route is employed in the industrial preparation of tetraalkyltins.

$$4\ \mathbf{R_3Al} + 3\ \mathbf{SnX_4} \longrightarrow 3\ \mathbf{R_4Sn} + 2\ \mathbf{AlX_3}$$

Scheme 8: *Preparation of tetraorgano stannanes using triorgano aluminum reagents.*

The tetraaryl species is only obtained with about 10 % yield when carrying out the reaction using stoichiometric amounts of $SnCl_4$ and R_3Al. The remaining product can be assigned as the stable complexes $R_2SnCl_2(AlCl_3)$ and $R_3SnCl(AlCl_3)$. Hence, an excess of R_3Al is necessary to perform complete alkylation. To overcome this disadvantage, Sundermeyer and Verbeek introduced a modified method preparing the alkylating agent $Na[AlMeCl_3]$ in one step, which then reacts quantitatively with $SnCl_4$ to afford $SnMe_4$ with 95 % yield.[56] All so far mentioned techniques can be performed with the use of $SnCl_4$, whereas organotin halides can be applied as described by Sisido and Kozima (Scheme 9).[57]

$$n\text{-}Bu_2SnCl_2 \xrightarrow{Zn,\ Et_3N} n\text{-}Bu_4Sn + n\text{-}Bu_3SnCl$$

Scheme 9: *Generating tetraorgano stannanes by reduction of the corresponding dichloride with zinc.*

Alternatively, a trialkyl or triaryltin hydride can be transformed into a nucleophile by deprotonation with a strong base, *e.g.* LDA (lithium diisopropylamide) generating an anionic tin species which further displaces halides to afford tetraalkyl tins (Scheme 10).[58-60]

$$R^1{}_3SnH \xrightarrow{LDA} R^1{}_3SnLi \xrightarrow{R^2X} R^1{}_3SnR^2$$

Scheme 10: *Nucleophilic attack of a deprotonated tin species generating tetraorgano stannanes.*

Competition between an S_N2 mechanism and radical processes are considered to be responsible for complete inversion of the configuration using Ph_3SnM as an educt as illustrated in Scheme 11. Not limited to halides, also the well established leaving group tosylate is displaced under full inversion (Scheme 12). However, leaving groups other than Ts (tosylate) and halides have found limited use.

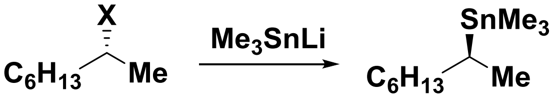

Scheme 11: *Displacement of a halide with Me_3SnLi under full inversion.*

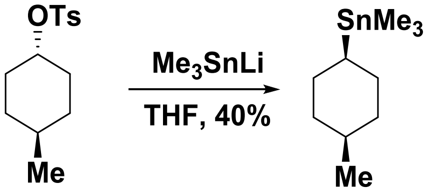

Scheme 12: *Displacement of a tosylate with Me_3SnLi under full inversion.*

In 2006 Shaikh *et al.* discovered that the Ulmann coupling reaction conditions can be modified by using an activated copper bronze (9:1 mixture of copper and tin) in order to obtain tetraaryl stannanes along with the production of substituted biaryls (Scheme 13).[61]

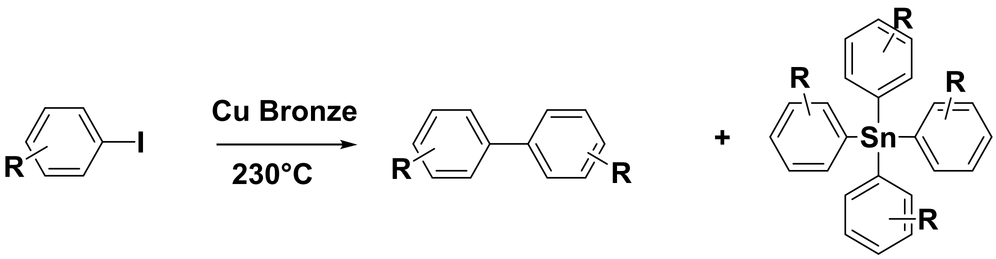

Scheme 13: *Ulmann coupling using copper bronze generating tetraaryl stannanes.*

Regarding this work, tetraorgano stannanes are important precursor for the synthesis of $RSnX_3$ (organotin trihalides) compounds (Part A, Chapter 2).

1.5 Organotin Halides

1.5.1 Triorganotin Halides R_3SnX

The most common route for the synthesis of triorganotin halides (R_3SnX) is the Kozeshkov redistribution reaction where three equivalents of a tetraorgano stannane are treated with one equivalent of $SnCl_4$ (Scheme 14).[33,62,63]

$$3\ R_4Sn + SnX_4 \xrightarrow{\text{neat}} 2\ R_3SnX$$

Scheme 14: *Kozeshkov redistribution reaction of tetraorgano stannanes producing triorganotin halides.*

Utilizing this synthetic method triallyl,[43,44] triphenyl[13,64,65] and trialkyltin halides[35,39,66,22,67,68] can be generated in good yields. Usually, the reaction proceeds at elevated temperature (100-200 °C) without the use of solvent. Instead of employing $SnCl_4$, tin(II) chloride can be used as well, reacting with the starting material R_4Sn generating metallic tin, R_3SnX and a C–C coupled product (Scheme 15).[69]

$$2\ R_4Sn + SnX_2 \longrightarrow 2\ R_3SnX + Sn + R\text{-}R$$

Scheme 15: *Synthesis of R_3SnX using tin(II) chloride.*

Another selective method for the synthesis of triorganotin halides is the cleavage of a Sn–C bond with dihalogens, such as Cl_2, Br_2 or I_2. Selective cleavage of one Sn–C bond can be achieved performing the reaction in an equimolar scale at a temperature of -50 °C (Scheme 16).[70-72]

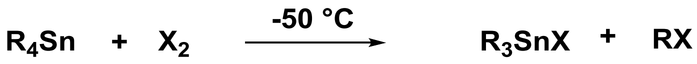
$R_4Sn + X_2 \xrightarrow{-50\ °C} R_3SnX + RX$

Scheme 16: *Generating R_3SnX by selective Sn–C cleavage using X_2.*

In most cases Br_2 is used, due to a faster reaction progress. Subsequent hydrolysis of the triorganotin bromide results in the formation of the trialkyltin oxide in high yields. The latter then serve as a convenient starting materials for the conversion with HX to afford halide exchange (Scheme 17).

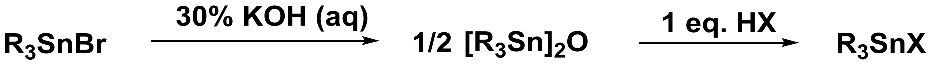
$R_3SnBr \xrightarrow{30\%\ KOH\ (aq)} 1/2\ [R_3Sn]_2O \xrightarrow{1\ eq.\ HX} R_3SnX$

Scheme 17: *Conversion of trialkyltin oxide with HX resulting in R_3SnX.*

Furthermore, trialkyltin chlorides are generated as side products in the conversion of tetraorgano stannanes with Co(TPP)Cl (TPP = dianion of tetraphenylporphyrin), where the organostannane is utilized as a soft alkylation agent (Scheme 18).[73]

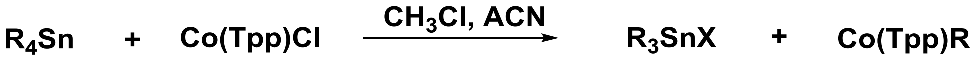
$R_4Sn + Co(Tpp)Cl \xrightarrow{CH_3Cl,\ ACN} R_3SnX + Co(Tpp)R$

Scheme 18: *Synthesis of R_3SnX using Co(Tpp)Cl.*

Apart from selective Sn−C bond cleavage, also selective formation of a Sn−C bond is possible by adding one equivalent of alkylating aluminum reagent (R_3Al, $R_3Al_2Cl_3$) to one equivalent of $SnCl_4$. The reaction proceeds in the presence of the base Et_3N using diethyl ether as solvent leading to higher than 90 % yield (Scheme 19).[74,75] However, this method is limited to the synthesis of Et_3SnCl, because no further examination on the possible scope have been carried out.

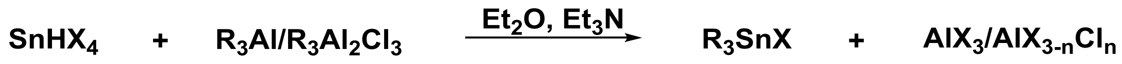

Scheme 19: *Selective formation of a Sn–C bond using alkylating aluminum reagents.*

Moreover, the preparation of triphenyl trichloride can be accomplished in high yields (92 %) by selective trisubstitution of $SnCl_4$ with phenylcopper, which itself is generated by the reaction of PhLi with cuprous bromide (Scheme 20).[76]

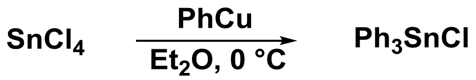

Scheme 20: *Generation of Ph_3SnCl by selective trisubstitution of $SnCl_4$ with PhCu.*

Besides of utilizing tin tetrahalides and tetraalkyltins, also diorganotin dihalides can be applied in the generation of triorganotin halides. As an example *n*-Bu_2SnCl_2 can be transformed into the corresponding triorganotin compound by reduction with metallic tin powder carried out in water at 160 °C (Scheme 21).[57] Modification of the water-based protocol applying butyl chloride and pyridine even leads to full conversion to the desired product.

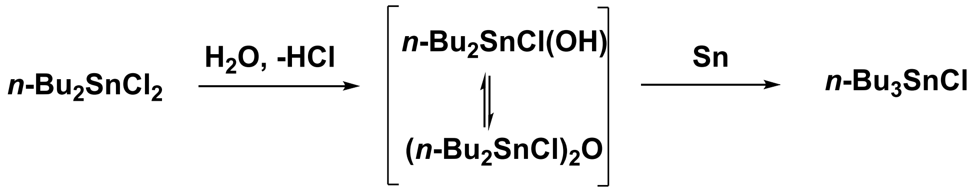

Scheme 21: *Production of n-Bu_3SnCl carried out in water in the presence of metallic tin.*

As a last synthetic route towards triorganotin halides, the direct conversion of metallic tin and benzyl chloride in water selectively affording tribenzyl tinchloride should be mentioned. Applying the reaction on *ortho*, *meta* or *para* substituted benzyl chlorides showed the formation of the desired product, but in significantly lower yields (Scheme 22).[71,68]

$$3\ \mathrm{BzCl} + 2\ \mathrm{Sn} \xrightarrow{\mathrm{H_2O}} \mathrm{Bz_3SnCl}$$

Scheme 22: *Direct conversion of benzyl chloride and metallic tin yielding in* Bz_3SnCl

Recently, Coffer *et al.* showed the formation of Ar_3SnCl by selective lithiation of CF_3 substituted aryl groups with *n*-BuLi and subsequent conversion with $SnCl_4$. However, the corresponding $(2,5\text{-}(CF_3)_2C_6H_3)_3SnCl$ is generated in the presence of Ar_4Sn as well as the higher chlorinated Ar_2SnCl_2. This product distribution can be overcome by using $SnBr_4$ as tin source, exclusively forming $(2,5\text{-}(\text{-}(CF_3)_2C_6H_3)_3SnCl$ (Scheme 23).[77]

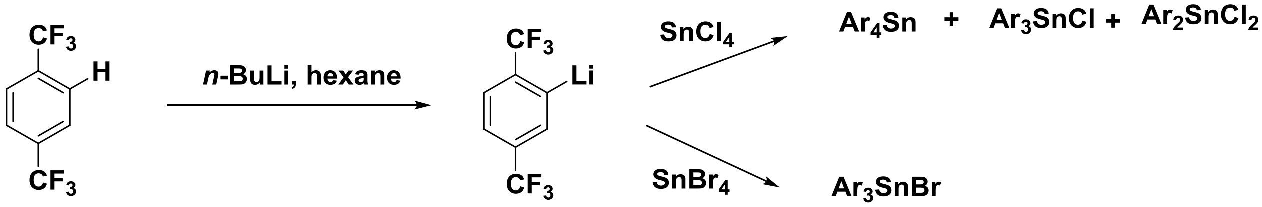

Scheme 23: *Selective formation of* Ar_3SnBr *harboring a* $2,5\text{-}(CF_3)_2C_6H_3$ *moiety.*

1.5.2 Diorganotin Dihalides R_2SnX_2

In accordance to triorganotin halides, also diorganotin dihalides are preferably generated *via* a Kozeshkov redistribution reaction using stoichiometric amounts of SnX_4 and the corresponding tetraorgano stannane in the absence of solvents at elevated temperature (150-200 °C) (Scheme 24).

$$\mathrm{R_4Sn} + \mathrm{SnX_4} \xrightarrow{\text{neat}} 2\ \mathrm{R_2SnX_2}$$

Scheme 24: *Kozeshkov redistribution for the formation of diorganotin dihalides.*

The synthesis of diallyltin-,[43,44] diarylltin-,[63,78-82] divinyltin-[83] and dialkyltin dihalides[13,52,66,84] (up to propyl) can be realized in 80-90 % yield and goes to completion within few hours.

Buschhoff suggested the use of SnF_2 as a catalyst in the redistribution reaction of organotin halides with SnX_4, however no clear proof for its catalytic activity has been published so far.[85] Apart from SnX_4 acting as a Lewis acid in the redistribution reaction, also other halogenides such as $SbCl_5$ and BCl_3 can be applied to successfully convert *e.g.* Me_4Sn to the corresponding dichloride. In this case, BCl_3 can be used in excess as the resulting product Me_2SnCl_2 does not undergo further redistribution with BCl_3. However, comparably weaker Sn–C bonds as found in Ph_2SnCl_2 and other aryltin dichlorides cannot be prepared using other Lewis acids than SnX_4 due to phenyl group migration from tin to antimony or bismuth forming $SnCl_4$, and Ph_2SbCl_3 or a mixture of $PhBCl_2$and Ph_2BCl, respectively.[86]

Another approach for selective dialkylation of $SnCl_4$ is the use of alkylaluminum reagents such as R_3Al, R_2AlCl[75] in the presence of R_3N, R_2O or KCl,[74] as well as $R_3Al_2Cl_3$. Using the latter reagent, no addition of R_3N, R_2O or KCl is required as well as it is reported to be very effective in the synthesis of diethyltin dihalides.[87] For this purpose, ethylaluminum sesquihalides are easily prepared by reacting metallic aluminum with ethyl halide leading to an alkylation reagent that can be used under mild conditions in a temperature range from 50-70 °C as compared to elevated temperatures (120-140 °C) in the case of R_3Al.[88]

In addition organonocopper and -lithium compounds can be applied to synthesize diorganotin dihalides from $SnCl_4$. However, the scope of substituents is limited to *e.g.* mesitylene. When $[CuMes]_5$(toluene) is converted with $SnCl_4$ the corresponding $Mesityl_2SnCl_2$ can be obtained in 87 % yield and 97 % purity, whereas reaction of MesitylLi with $SnCl_4$ yields the dichloride only in 21 %.[89,90]

A selective cleavage of two Sn–C bonds can be realized by converting tetraorgano stannanes with HCl or $SOCl_2$, respectively forming diorganotin dichlorides (Scheme 25).[91-93] The reactivity of tetraorgano stannanes (R_4Sn) towards $SOCl_2$ decreases as followed: R = n-C_4H_9> n-C_3H_7> C_2H_5 >CH_3> $C_6H_5CH_2$≫ $C_6H_4CH_3$.[93]

$$R_4Sn \quad + \quad 2\ HCl/\ SOCl_2 \longrightarrow 4 \quad R_2SnX_2 \ + \ 2\ RH/\ RSOCl$$

Scheme 25: *Formation of diorganotin dihalides by Sn–C bond cleavage.*

As already mentioned in Chapter 1.4, the first organotin compound reported in literature is Et_2SnCl_2 which was synthesized *via* a direct route reacting Sn foil with EtI (Scheme 2).[1,2] In a general approach using RX in the formation of R_2SnX_2, the following reactivity has been observed: R= Me> Et> Pr and X= I> Br> Cl (Scheme 26).[94,95] Thus, the reaction only takes place at relatively low temperatures when RI is used. Benzylchloride has to be mentioned as an exception concerning the reactivity row of halogenides because it easily reacts with metallic tin.[68]

$$2\ RX \quad + \quad Sn \xrightarrow{160\text{-}180\ °C} R_2SnX_2$$

Scheme 26: *Direct synthesis of diorganotin dihalides.*

The reactivity of organic chlorides and bromides in a direct alkylation with elemental tin is increased in the presence of catalysts such as magnesium,[96] $HgCl_2$,[97] hexamethyl phosphoric triamide (HMPT) ,[98] copper powder[99] and crown ethers[100]. Smith and Rochow successfully reported the generation of Me_2SnCl_2 in five mechanistic steps by continuously flowing methyl chloride gas through a reactor charged with metallic tin and the copper powder catalyst (Scheme 27). The reaction proceeds until Sn reaches oxidation IV by rearrangement of the methyl and chlorine forming almost exclusively Me_2SnCl_2.[99]

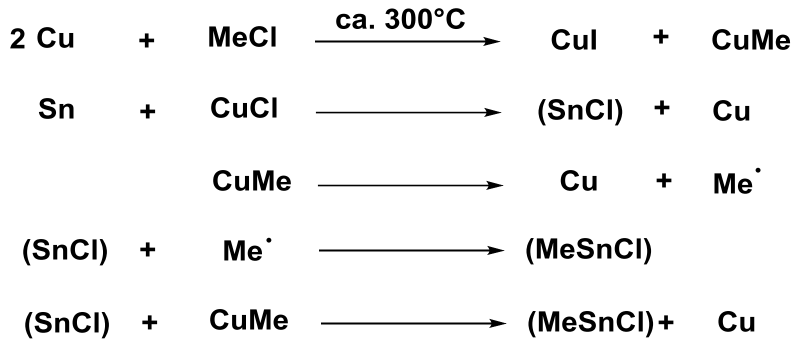

Scheme 27: *Suggested mechanism for the generation of diorganotin dihalides by copper catalysis.*

For the synthesis of R_2SnCl_2 exhibiting longer chained alkyl groups such as *n*-butyl or *n*-octyl, crown ethers as *e.g.* dicyclohexyl-18-crown-6 and dibenzo-18-crown-6 have to be applied as catalysts. The selectivity of the reaction can be driven up to 95-99 % if it is carried out in DMF using butyl iodide as a co-catalyst at temperatures from 100-160 °C. According to Scheme 28, it is suggested that the crown ether as well as the butyl iodide assist in the nucleophilic substitution by halogen interchange forming RI which readily reacts with metallic tin under the formation of R_2SnI_2. The following nucleophilic substitution with X^- yields in R_2SnX_2.[100]

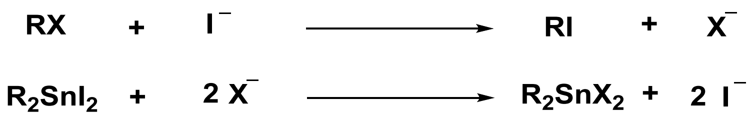

Scheme 28: *Assisted nucleophilic substitution by butyl iodide in the formation of R_2SnX_2 (X= Cl, Br).*

Kocheshkov's protocol that reacts tin(II) halides with $(p\text{-}XC_6H_4)_2Hg$ to give the aromatic $(p\text{-}XC_6H_4)_2SnX_2$ and metallic mercury has been quite neglected due to the use of toxic mercury compounds although yields are reported up to 99 % depending on the used halide (Scheme 29).[101]

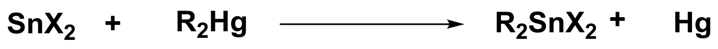

$$SnX_2 + R_2Hg \longrightarrow R_2SnX_2 + Hg$$

Scheme 29: *Formation of organotin dihalides from organomercury compounds.*

1.5.3 Monoorganotin Trihalides $RSnX_3$

Among the compound class of organotin halides, organotin trihalides ($RSnX_3$) tend to undergo a second substitution forming R_2SnX_2. Hence, methods using $SnCl_4$ with an organometallic reagent such as RMgX or RLi do not show high selectivities.

However, Kozeshkov described one of the first methods for successful preparation of $RSnX_3$ in the 1930s starting from the corresponding tetraorgano stannane subjecting it to a redistribution reaction with a tin tetrahalide at elevated temperatures without the use of solvents.[81,84,102,103] Scheme 30, shows the overall reaction, which in fact consists of three consecutive redistribution reactions including R_2SnX_2 as an intermediate (Scheme 31).

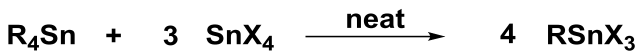

$$R_4Sn + 3\ SnX_4 \xrightarrow{\text{neat}} 4\ RSnX_3$$

Scheme 30: *Overall reaction sequence for the Kozeshkov redistribution reaction generating $RSnX_3$.*

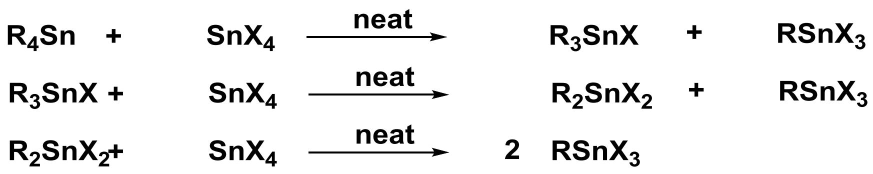

$$R_4Sn + SnX_4 \xrightarrow{\text{neat}} R_3SnX + RSnX_3$$
$$R_3SnX + SnX_4 \xrightarrow{\text{neat}} R_2SnX_2 + RSnX_3$$
$$R_2SnX_2 + SnX_4 \xrightarrow{\text{neat}} 2\ RSnX_3$$

Scheme 31: *Kozeshkov redistribution reaction proceeding in three steps.*

However, this reaction sequence is limited to the R-moieties such as vinyl,[83,42] aryl,[63,80,82,104] allyl[43-45] and acryl esters[105], since the third redistribution reaction fails using alkyl substituents. For that reason monoalkyltin halides are generated using a modified procedure, affording R_2SnX_2 and the desired product $RSnX_3$ in an one to two ratio (Scheme 32).

$$R_4Sn \;+\; 2\; SnX_4 \xrightarrow{\text{neat}} R_2SnX_2 \;+\; 2\; RSnX_3$$

Scheme 32: *Preparation of monoalkyl tinhalides via Kozeshkov redistribution reaction.*

As already mentioned in the synthesis of R_2SnX_2, other Lewis acids than SnX_4 can be applied in the redistribution reaction in order to form $RSnX_3$. In this manner Me_2SnCl_2 is treated with $SbCl_5$ to generate $MeSnCl_3$. However, phenyl groups are more likely to be transferred from the tin to the antimony resulting in Ph_2SbCl_3. This disadvantage can be avoided by using a less strong Lewis acid such as BCl_3 (Scheme 33).[86]

$$R_2SnCl_2 \;+\; SbCl_5 \longrightarrow RSnCl_3 \;+\; RSbCl_4$$

Scheme 33: *Preparation of $MeSnCl_3$ using $SbCl_5$.*

As already reported in Chapter 1.4.1, the synthesis of R_4Sn compounds can be achieved by using aluminum trialkyls to substitute the $SnCl_4$. Müller and Buschhoff described that R_3Al also displays a convenient agent for the monoalkylation of $SnCl_4$.[106] In order to minimize the alkylating effect of the aluminum reagent, an ether or tertiary amine complex is formed which subsequently reacts with $SnCl_4$ yielding in $RSnCl_3$ (R=*n*-butyl or octyl) up to 90 % yield (Scheme 34).

$$3\; SnX_4 \;+\; R_3Al(OR'_2)/R_3Al(NR'_3) \longrightarrow 3\; RSnCl_3 \;+\; AlCl_3(OR_2)/AlCl_3(NR'_3)$$

Scheme 34: *Monoalkylation of tin(IV) chloride using R_3Al complexes.*

In comparison to the less selective organolithium and Grignard reagents, mesitylcopper $[CuMes]_5$(toluene), described by Jäkle and Manners, easily and selectively reacts with $SnCl_4$ resulting in $MesSnCl_3$ with 92 % yield.[90]

Furthermore, an oxidative addition of a tin(II) halide provides a convenient and selective one-step method preparing monoorganotin trihalides (Scheme 35). Janiak and Schwichtenberger described the selective addition using pentaphenylcyclopentadienyl as an organic substituent.[107] However, in some other cases the reaction does not proceed selectively. Therefore, catalysts like primary amines, organic disulfides, quaternary ammonium halides and trialkylantimony have to be applied to obtain reasonable yields of $RSnCl_3$.[108]

$$SnX_2 \quad + \quad RX \quad \xrightarrow{\hspace{3em}} \quad RSnX_3$$

Scheme 35: *Preparation of $RSnX_3$ via oxidative addition.*

The Grignard route is applied by Elhamzaoui in order to prepare an arylmagnesium bromide which is then treated with trimethyl tinchloride to obtain a mixed tetraorgano stannane. Since alkyl groups are more likely to be exchanged, further conversion with $SnCl_4$ leads to the corresponding aryltrichloro stannane (Scheme 36).[109]

$$ArBr \xrightarrow{Mg} ArMgBr \xrightarrow{Me_3SnCl} ArSnMe_3 \xrightarrow{SnCl_4} ArSnCl_3$$

Scheme 36: *Synthesis of $ArSnCl_3$ on the Grignard route via $ArSnMe_3$ as an intermediate.*

Moreover, Matsuda and coworkers published a protocol generating Me_3SnCl by reacting MeCl and $SnCl_2$ in the presence of a small amount of I_2 and magnesium in 95 % yield (Scheme 37).[110]

$$SnCl_2 \quad + \quad MeCl \quad \xrightarrow{I_2,\ Mg} \quad MeSnCl_3$$

Scheme 37: *Oxidative addition of tin(II) chloride in the presence of iodide and magnesium.*

Lazarev reported the selective cleavage of a Si–C induced by $SnCl_4$ affording the corresponding $ArSnCl_3$ species (Scheme 38).[111]

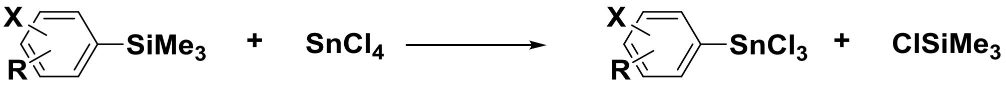

Scheme 38: *Selective cleavage of a Si–C bond with* $SnCl_4$*.*

An additional interesting route for the preparation of aryltrichloro stannanes is the *in situ* generation of a chlorostannylene by treating the lithiated aryl compound with tin(II) chloride and subsequent reduction with CCl_4 as illustrated in Scheme 39. Saito described the reaction for R= terphenyl with a yield of 45 %.[112]

$$SnCl_2 \xrightarrow[THF]{ArLi,\ -LiCl} Ar(Cl)Sn: \xrightarrow{CCl_4} ArSnCl_3$$

Scheme 39: *Generating* $ArSnCl_3$ *via a tin(II) intermediate.*

1.6 Organotin Hydrides

The sensitivity towards oxygen or temperature of Group 14 metal hydrides increases as descending the group. This is in accordance with the dissociation energy of the M−H bond.[113] Stannane (SnH_4) itself is highly labile and undergoes rapid decomposition at room temperature under the formation of elementary tin and hydrogen.[12] This sensitivity towards elevated temperatures can be lowered by the substitution of a hydrogen atom with an alkyl or aryl moiety. Furthermore, the reactivity towards atmospheric oxygen increases with the number of hydride functionalities leading to poorly soluble precipitates.[114]

Although Paneth was first in describing stannane (SnH_4), as well as taking into account the investigation on elements of group 14 generating hydrides in 1920, the preparation of organic derivatives received little attention.[115] Subsequently, Kraus and Greer published the first synthesis of trimethyl stannane and described its properties in 1922.[116] The preparation method involved treating organotin sodium with ammonium chloride or bromide in liquid ammonia (Scheme 40).

$$R_3SnNa + NH_4X \xrightarrow{NH_3} R_3SnH + NaX + NH_3$$

$$R_2SnNa_2 + 2\ NH_4X \xrightarrow{NH_3} R_2SnH_2 + 2\ NaX + 2\ NH_3$$

Scheme 40: *First synthesis of organotin hydrides by Kraus and Greer.*

In this manner the afore mentioned trimethyltin hydride as well as triphenyltin hydride[53,117] and dimetyhlethyltin hydride[118] were generated. Further investigations concerning the preparation, characteristics and reaction behaviour of organotin hydrides were quite neglected due to their instability. This lasted until 1947, when Finholt and coworkers developed a novel and more convenient route, generating hydrides of Group 14 elements and their organic derivatives using $LiAlH_4$ (lithium aluminum hydride) starting with the corresponding chloride in solvents such as dioxane, diethyl ether or THF.[12] The reaction proceeds smoothly forming organotin hydrides in high purity and good yields (Scheme 41). They were able to generate stannane, methyltin trihydride, dimethyltin dihydride, and trimethyltin hydride. The reaction sequence has been established as standard synthetic route towards organotin mono-, di-, and trihydrides.[63,80]

$$4\ SnR_yX_{4-y} + 4\text{-}y\ LiAlH_4 \xrightarrow{Et_2O} 4\ SnR_yH_{4-y} + 4\text{-}y\ LiX + 4\text{-}y\ AlX_3$$

Scheme 41: *General route synthesizing organotin hydrides with* $LiAlH_4$.

Subsequently, Gilman and Eisch employed this procedure to synthesize triphenyltin hydride.[119] Various other novel tinhydrides were first mentioned by van der Kerk, Noltes and Luijten by slight modifications to the isolation procedure.[83] Until 1963, triphenyltin hydride was the only known tin hydride harbouring an aryl group. Afterwards also following aryltin hydrides were generated using $LiAlH_4$: tris(*p*-tolyl), tris(*p*-fluorophenyl), trismesityl tin hydrides[120] and tris(*m*-tolyl), tris(*o*-tolyl) and tris(*o*-biphenylyl)tin hydrides.[121] Lithium aluminum hydride also reduces bis(tri-*n*-butyl)oxide to yield in tri-*n*-butyltin hydride in 88 % yield.[122]

Afterwards, Ziegler and Gellert reported the formation of organotin hydrides using DIBAL (diisobutylaluminum hydride) as hydrogenation agent in the absence of solvent. Organotin hydrides are synthesized at -20 to 0 °C in good yields (Scheme 42).[123]

$$R_{4-n}SnX_n + n\ R'_2AlH \longrightarrow R_{4-n}SnH_n + n\ R'_2AlCl$$

Scheme 42: *Preparation of organotin hydrides using dialkylaluminum hydrides.*

Furthermore, di-*n*-butylaluminum hydride transforms diethylamino stannanes into the corresponding hydrides as shown in Scheme 43.[124]

$$R_{4-n}Sn[N(C_2H_5)_2]_n + n\ (n\text{-}C_4H_9)_2AlH \longrightarrow R_{4-n}SnH_n + n\ (n\text{-}C_4H_9)_2AlN(C_2H_5)_2$$

Scheme 43: *Synthesis of organotin hydrides via reduction of diethylamino stannanes.*

Van der Kerk, Noltes and Luijten also reported that organotin halides can be reduced in good yields with amalgamated aluminum and water, but yields were not satisfying.[125]

As another route the hydrolysis of for instance (triphenyltin)magnesium in a THF solution, itself generated by reaction of triphenyltin chloride with magnesium using ethyl bromide as initiator, with aqueous ammonium chloride yielding in 82 % triphenyltin hydride can be mentioned (Scheme 44).[126]

$$2\ (C_6H_5)_3SnCl + Mg \xrightarrow{\text{THF, EtBr}} (C_6H_5)_3Sn\text{-}Sn(C_6H_5)_3 + MgCl_2$$

$$(C_6H_5)_3Sn\text{-}Sn(C_6H_5)_3 + Mg \xrightarrow{\text{THF, EtBr}} [(C_6H_5)_3Sn]_2Mg \xrightarrow{2\ H_2O} 2\ (C_6H_5)_3SnH + MgOH_2$$

Scheme 44: *Hydrolysis of triphenylmagnesium resulting in Ph_3SnH.*

In comparison to the latter method, the hydrolysis of triphenyltinlithium with 1 M hydrochloric acid affords 69 % of the corresponding hydride[127] and hydrolysis of tri-*n*-butyl lithium using water results in 54 % yield of the hydride.[128]

Finally, organotin hydrides can be obtained in excellent yields by the reaction of organotin methoxides with diborane (Scheme 45).[129]

$$4/n\ R_{4-n}SnOCH_n + B_2H_6 \longrightarrow 4/n\ R_{4-n}SnH_n + 2\ HB(OCH_3)_2$$

Scheme 45: *Generating organotin hydrides by reduction of organotin methoxides with diborane.*

1.6.1 Properties of Organotin Hydrides

Most organotin hydrides are colourless, distillable liquids, which in function of the number of organic substituents, decompose very easily at room temperature under disproportion and formation of metallic tin as shown in the Scheme 46.[33] For alkyl compounds stability increases with the size of the substituent.[130]

$$\begin{aligned}4\ R_3SnH &\longrightarrow 3\ R_4Sn + Sn + 2\ H_2\\ 2\ R_2SnH_2 &\longrightarrow R_4Sn + Sn + 2\ H_2\\ 4\ RSnH_3 &\longrightarrow R_4Sn + 3\ Sn + 6\ H_2\end{aligned}$$

Scheme 46: *Decomposition of organotin hydrides.*

Organotin monohydrides harbouring an aryl group are colorless solids, as well as dihydrides exhibiting exhibiting bigger organic moieties than phenyl such as 1- and 2-naphthyl are yellowish solids.[63,80,131] In the case of organotin trihydrides, MesitylSnH_3 is the first one found to be solid.

Especially when exposed to atmospheric oxygen, organotin hydrides decompose resulting in a white to yellow or grey precipitate (tin oxides).[114,119,132,133] For example, triphenyltin hydride gives hexaphenyl distannane in the presence of oxygen,[53] while ethyldimethyltin hydride and triethyltin hydride lead to the corresponding hydroxide shown in Scheme 47.[12,114]

$$\begin{aligned}4\ Ph_3SnH + O_2 &\longrightarrow 2\ Ph_3Sn\text{-}SnPh_3 + 2\ H_2O\\ 2\ Ph_3SnH + O_2 &\longrightarrow 2\ R_3SnOH\end{aligned}$$

Scheme 47: *Reaction of organotin hydrides with oxygen.*

1.7 Linear Polystannanes

Linear polystannanes are compounds with the general formula $(R_2Sn)_n$, harboring a covalently linked metal (tin) backbone, which can be seen as a molecular metal wire embedded in an organic jacket.[134] At the same time, being the formally structural analogues of saturated polymeric hydrocarbons, the polymers of group 14 elements have the capacity to catenate.[135] Induced by a very low band gap as well as σ-conjugation between the Sn sp^3 orbitals in the metallic backbone, these polymers exhibit an increased degree of electron delocalization with catenation.[136,137] These compounds bear strong σ→σ* transitions at about 390-340 nm. Even lower band gaps should be achieved if π-electrons in terms of covalently bond aromatic groups, can be found on the "tin-wire" additionally leading to σ→π delocalization.[138] The mentioned outstanding property of a potentially highly conductive metallic material could be promising for applications in charge-transport, photoresists in microlithography, non-linear optical materials, semiconductors in doping and electronic devices.[139-141] Furthermore, those electronic properties make them thinkable as one dimensional quantum wires in printed electronic applications.[142] Those features are highly dependent on the already mentioned σ-delocalization which is not only a function of the substituents attached to the main chain, but also depends on the changes in solid state structures, backbone conformation and chain length.

1.7.1 Synthesis of Polystannanes

Over the years, different polymerization methods have been established in order to synthesize polystannanes, however, these are often accompanied by the formation of side products.

1.7.1.1 Wurtz-Type Coupling

The first described oligo- or polystannanes were published by Löwig in 1852. Shortly after, the first organotin compound was synthesized by Frankland[1,2] generated *via* the reaction of Sn/K or Sn/Na alloys with iodoethane in the presence of quartz sand in order to improve the reaction control. However, it was found out that Sn/Na is more convenient for that preparation. The elemental composition of the afforded compounds were very similar to oligo(diethylstannane) or poly(diethylstannane).[143] Subsequently, Cahours isolated a compound with elemental composition corresponding to the formula $(SnEt_2)_n$ generated by heating iodoethane in the presence of metallic tin and sodium. With those findings, Cahours was the pioneer in applying a Wurtz-type reaction for the preparation of polystannanes. He also tried to afford poly(dimethylstannane) by a Wurtz reaction, but was not able to prove his results[144,145] until Price *et al.* confirmed that poly(dibutylstannane) synthesized *via* Wurtz coupling leads to a bimodal molar mass distribution.[146]

Wurtz-type coupling reactions with sodium in organic solvents such as toluene are widely used to gain poly(dialkylstannane)s of high molar mass. However, the reaction conditions lead to oligomeric stannanes or cyclic oligomers in poor yields.[31,143,147-151] Scheme 48 displays the Wurtz-type coupling for the preparation of polystannanes.

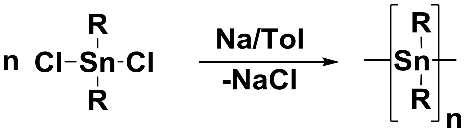

Scheme 48: *Wurtz-type coupling for the preparation of polystannanes.*

Mechanistic suggestions consider that polymerization (chain growth) occurs at the surface of metallic sodium followed by a second slower step of chain prolongation by condensation reactions.[152,153]

In 2011, Caseri *et al.* proposed a modification of the traditional Wurtz-type polymerization method converting R_2SnCl_2 compounds with sodium in liquid ammonia, whereby polymers are generated either in an one-step polymerization using two equivalents of sodium or *via* a two-step proceeding with four equivalents. The reaction is very likely to proceed *via* stannide ions including a radical mechanism.[154]

Jousseaume reported on the use of Mg activated with 1,2-dibromoethane in a milder reduction of Bu_2SnCl_2 in THF at 60 °C. This reaction provides an almost equimolar mixture of five and six-membered perbutylated Sn rings. However, no high molecular weight fractions could be obtained.[155] The same reaction behavior was reported by Beckmann *et al.* in 2008 when trying to generate chiral polystannanes by converting optically active bis(myrtanyl)tin compounds (*cis*-Myr_2SnX_2) with Mg. This reduction exclusively forms pentastannane rings.[156]

1.7.1.2 Polycondensation

Based on Neumanns results on the condensation of stannylamines with organotin hydrides mainly forming cyclostannanes,[157] Foucher *et al.* have very recently reported on a synthetic protocol for the generation of alternating polystannanes which involves the stoichiometric reaction of organotin dihydrides and organotin diamides in diethyl ether or toluene under mild reaction conditions (Scheme 49). This procedure afforded three novel moderate molecular weight alternating polystannanes in yields up to 86 %: –[Ph_2Sn-*alt*-Sn(*n*-Bu)$_2$]$_n$-, -[Ph_2Sn-*alt*-SnMe_2]$_n$-) and (–[Me_2Sn-*alt*-Sn(*n*-Bu)$_2$]$_n$-.

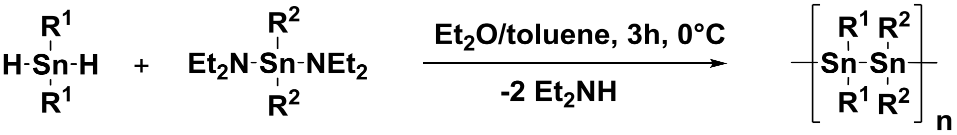

Scheme 49: *Preparation of alternating polystannanes by condensation.*

By introducing both, diaryl and dialkyl substituents alternatively into the tin backbone, solubility as well as light stability of the product can be ensured in contrast to homopolymers such as (Ph_2Sn)$_n$.[158,159]

1.7.1.3 Electrochemical Synthesis

The electrochemical pathway for the reduction of diorganotin dihalides can be seen as a promising route for the synthesis of moderate molecular weight polymers in good as well as reproducible yields (Scheme 50).[160,161]

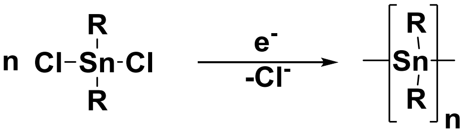

Scheme 50: *Electrochemical synthesis of polystannanes.*

Electrochemical conversions are performed in an one-compartment cell furnished with a platinum cathode and a silver anode using 1,2-dimethoxyethane as solvent and tetrabutylammonium chloride as supporting electrolyte. The reaction is carried out for Bu_2SnCl_2 as well as for Oct_2SnCl_2 yielding up to 56 % of the corresponding polymer.[161] Using R_3SnCl compounds as starting material, crosslinked polystannanes with a network-σ-conjugated system are generated. However, the product still exhibits Sn–Cl groups after reaction completion, in addition the conversion proceeds under the formation of unknown fractions of cyclic oligomers.[162]

1.7.1.4 Solvent- and Catalyst Free Dehydrogenation

In 2010 Foucher *et al*. reported the successful preparation of oligo- and polystannanes *via* thermal hydrocoupling under inert conditions. *n*-Bu_2SnH_2 is heated for 6 h yielding in a hydride terminated distannane, cyclic species and a polymer. Generated polystannanes show modest molecular weight and broad polydispersity.[10]

1.7.1.5 Catalytic Dehydropolymerization

So far, the most common and widely applied method of generating organo polystannanes is the catalytic dehydrocoupling of tin hydrides with early transition metal complexes based on palladium, zirconium, rhodium, platinum or lanthanides (Scheme 51).[6-8,139,150,163-167]

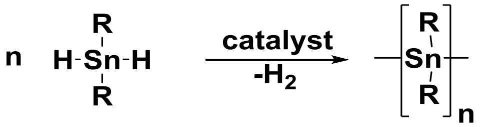

Scheme 51: *Catalytic dehydropolymerization generating polystannanes.*

Initial polymerization attempts on this field in most cases led to a significant number of side products including cyclic oligomers or other impurities. More recently, investigations on the use of a Wilkison's catalyst $[RhCl(PPh_3)_3]$ turned out to be very successful affording polyalkylstannanes in high yields (65-90 %) without significant byproducts.[135,163,168] This method allows the systematic investigation on material properties without the disturbing influence of the side products. However, use of the Wilkinson catalyst is not suitable for two aromatic substituents on the tin educt. A synthetic route applying lanthanide diamide based catalysts for the generation of polystannanes and distannanes has been reported by Choffat *et al.*[168] On the quest for chiral polystannanes, Beckmann *et al.* were able to synthesize a mixture of poly(*cis*-Myrtanyl$_2$Sn)$_n$ and poly(*trans*-Myrtanyl$_2$Sn)$_n$ subjecting the enatiomerically pure *cis*- and *trans*-Myrtanyl$_2$SnCl$_2$ to a dehydropolymerization a Wilkons catalyst.[156] Very recently, Foucher *et al.* reported on the synthesis of C,O-chelated organotin dihydrides which were converted to asymmetrical hyperconjugated polystannanes *via* a dehydrogenative coupling reaction with a Wilkinson catalyst. These novel protected polystannanes exhibit improved light stability.[169]

The same working group could show the use of Pd(PPh$_3$)$_4$ in the insertion of acetylene and phenylacetylene into the backbone of poly[di-(*n*-butyl)]stannane in order to form novel, modest molecular weight, partially inserted alkene tin polymers.[170] Furthermore, Foucher and coworkers were able to prepare polybis(dimethylstannyl)ferrocene with a modest moderate molecular weight using a Karstedt's catalyst in DMF in 50 % yield.[171]

1.7.1.6 Dehydrogenative Coupling Using an Amine Base

Adding a nitrogen base such as pyridine to a tin hydride solution in order to afford the formation of a Sn–Sn bond was first described by Neumann[55] and successfully further applied by Davies and Mathiasch (Scheme 52).[172,173]

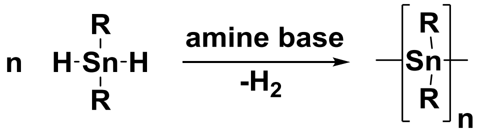

Scheme 52: *Dehydrogenative coupling using an amine base.*

Although further investigations on the reaction mechanisms have been neglected thus far, the reaction progress is considered to occur *via* either a polar process or a radical chain mechanism. It is possible that the polar mechanism proceeds *via* the formation of a four-membered transition state as involving a R_3SnX species as shown in Scheme 53.[174,175]

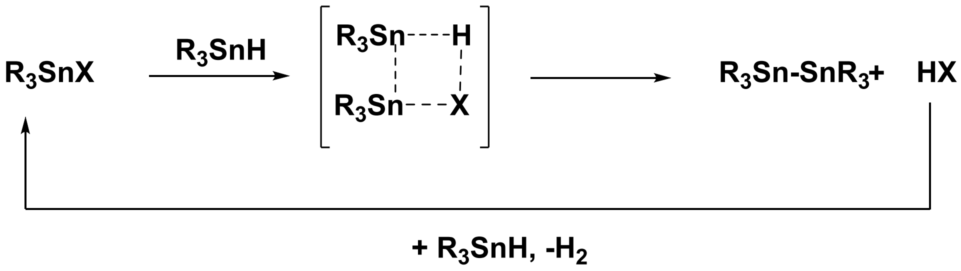

Scheme 53: *Polar transitions state in dehydrogenative coupling.*

Regarding the radical formation pathway a $R_3Sn\cdot$ radical would displace a hydrogen atom from another tin hydride resulting in a $H\cdot$ species which subsequently leads to the production of H_2 through abstracting a hydrogen from another tin center.[173]

In 2011, Uhlig *et al*. described the application of TMEDA (*N,N,N',N'*-tetramethylethylenediamine) as a convenient amine base generating poly(dialkylstannane)s as well as poly(diarylstannane)s. Also for this synthetic route a radical mechanism is considered but not published yet.[11]

1.7.2 Characteristics of Polystannanes

Much attention concerning the properties of polystannanes had been drawn to the visible spectroscopic properties, whereas the stability investigations had been quite neglected until Caseri *et al.* dedicated themselves to the topic.[176]

1.7.2.1 Visible Properties of Polystannanes: Color and Absorption Maxima

Polystannanes are reported to exhibit a characteristic yellow or orange-yellow color leading to absorption maxima in UV-VIS spectra at around 375-410 nm which are attributed to $\sigma \rightarrow \sigma^*$ band-gap transitions.[135,150,163,177] Long-chain polystannanes strongly absorb light in the

UV, indicated by their high ε-values ranging from 4200 to 63000. Furthermore, those energies are independent of the polymer being neat or in solution.

1.7.2.2 Thermal Stability

Under common TGA conditions, *i.e.* heating rate of 10 °Cmin^{-1}, thermal decomposition of poly(dialkylstannane)s, as well as for polystannanes with phenyl terminated alkyl groups does not proceed below 200 °C under inert conditions as well being exposed to the ambient.[55,163] However, the maximum decomposition rate regarding poly(alkylstannane)s could be detected in the range of 250-300 °C under nitrogen and 240-300 °C under oxygen containing atmosphere, respectively. There is no general, systematic trend detectable referring to the dependency of decomposition and chain length. Regardless, it is established that poly(diphenylstannane)s exhibit more stability than poly(dialkylstannane)s. Concerning copolymers of butyl and phenyl moieties, the aromatic substituent did not improve thermal stability as shown on the example of poly(dibutylstannane-*ran*-diphenylstannane).[160]

1.7.2.3 Light Stability

Caseri *et al*. investigated the stability of polystannanes towards light under controlled exposure and compared results of the polymer in solution where a consistent illumination is more accessible than to the neat polymer. The degradation process was monitored *via* NMR spectroscopy and GPC. A correlation between the length of the alkyl side groups and the stability of the polymer has not been found, but indeed the used solvent exhibits a strong influence on the degradation rate. Hereby, chlorinated solvents as well as styrenes repress the decomposition, whereas degradation proceeds rapidly in aromatic and aliphatic hydrocarbons.[177] In 2011, it was found that poly(diarylstannane)s exhibit a higher stability towards light than poly(dialkylstannane)s in THF as well as in dichloromethane.[178]

Foucher *et al.* very recently showed that alternating polystannanes consisting of alkyl and aryl groups such as, –[Ph_2Sn-*alt*-Sn(*n*-Bu)$_2$]$_n$-, -[Ph_2Sn-*alt*-$SnMe_2$]$_n$-) and (–[Me_2Sn-*alt*-Sn(*n*-

$Bu)_2]_n$- show increased light stability.[158] Furthermore, he reported the successful synthesis of protected polystannanes which display dramatically improved light stability due to a suggested dative interaction between an electron donor, in this case oxygen of aryloxy side chain, to the tin.[169]

1.7.2.4 Processing and Orientation

Poly(dialkylstannane)s (alkyl= butyl, octyl, dodecyl) are blended with ultrahigh molar mass polyethylene to afford mixtures containing typically about 10 % or 25 % w/w polystannane. The resulting blends were homogenous, but however opaque. Poly(alkylstannane)s exhibit liquid-crystalline behavior at room temperature or even below. Hence, their orientation is achieved by shearing on a glass slide at ambient temperature or even at 60 °C. Furthermore, they can be grown out of solution onto a glass slide coated with a PTFE layer. Depending on the procedure the polystannane backbone is either oriented parallel or perpendicular, evidenced by UV-VIS spectra using polarized light.[179]

Part A

Synthesis and Characterization of Aryltin Hydrides:

Building Blocks towards Polyarylstannanes

2 Aryltin Chlorides and Hydrides: Preparation, Detailed NMR Studies and DFT Calculations

Graphical Abstract

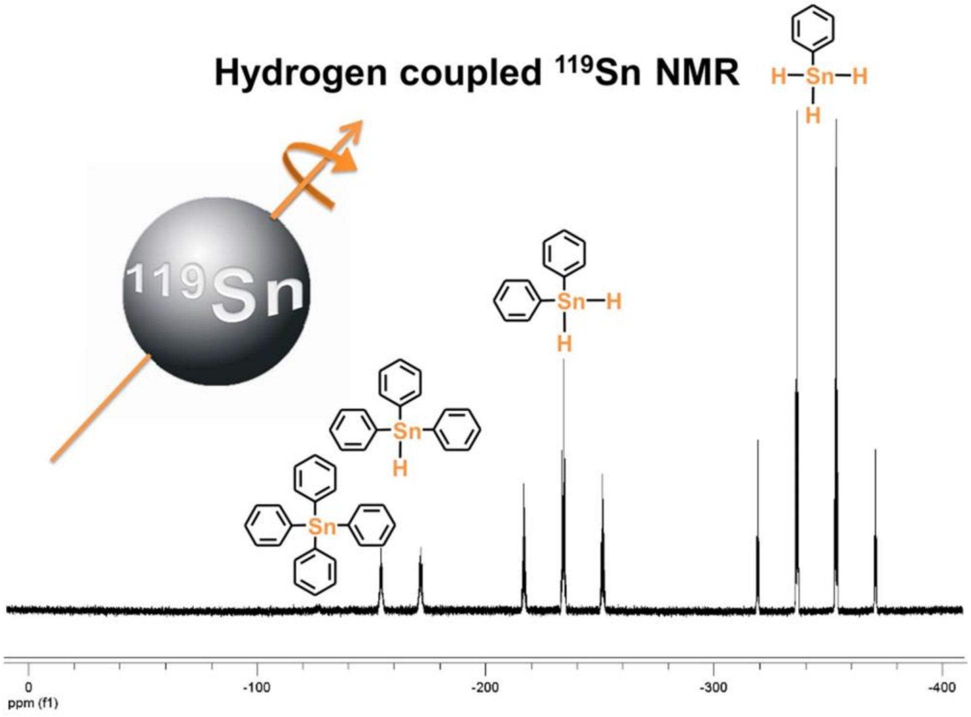

Abstract

A series of novel tin chlorides R_nSnCl_{4-n} *and respective hydrides* R_nSnH_{4-n} *were synthesized displaying a range of substituted phenyl residues, as well as naphthyl moieties (R= Ph, o-tolyl, 2,4-xylyl, 2,6-xylyl, p-*^{n}*butylphenyl, p-biphenyl, mesityl, 1-naphthyl, 2-naphthyl). These compounds were characterized using* ^{1}*H,* ^{13}*C and* ^{119}*Sn NMR spectroscopy. DFT calculations were carried out to compare experimental NMR data with calculated* ^{13}*C and* ^{119}*Sn shifts, as well as* ^{13}*C-*^{119}*Sn coupling constants.*

2.1 Introduction

The sensitivity towards oxygen or temperature of Group 14 metal hydrides increases descending the group. This is in accordance with the dissociation energy of the M−H bond.[180] Stannane (SnH_4) itself is highly labile and undergoes rapid decomposition at room temperature under the formation of elementary tin and hydrogen.[12] This sensitivity towards elevated temperatures can be lowered by the substitution of a hydrogen atom with an alkyl or aryl moiety. Furthermore, the reactivity towards atmospheric oxygen increases with the number of hydride functionalities leading to poorly soluble precipitates.[114]

Initial preparation methods of organotin hydrides involved treating organotin sodium with ammonium chloride or bromide in liquid ammonia.[116] In this manner, Kraus and Greer were the first to successfully synthesize trimethyltin hydride and triphenyltin hydride. Further investigations concerning the preparation, characteristics and reaction behaviour of organotin hydrides were quite neglected due to their instability. This lasted until 1947, when Finholt and coworkers developed a novel and more convenient route, generating hydrides of Group 14 elements and their organic derivatives using $LiAlH_4$ (lithium aluminum hydride) starting with the corresponding chloride.[12] They were able to generate stannane, methyltin trihydride, dimethyltin dihydride, and trimethyltin hydride. Afterwards, Ziegler and Gellert reported the formation of organotin hydrides using DIBAL (diisobutylaluminum hydride) as hydrogenation agent.[123] However, using $LiAlH_4$ as a straight forward synthetic procedure has been applied as general approach for the successful formation of mono-, di- and trihydride organotin compounds (R_3SnH, R_2SnH_2, and $RSnH_3$) in high yields and purity (Scheme 54).[12]

$$R_nSnCl_{4-n} \xrightarrow{LiAlH_4,\ Et_2O} R_nSnH_{4-n}$$

Scheme 54: *Formation of organotin mono-, di- and trihydrides via hydrogenation of the corresponding chloride using $LiAlH_4$.*

Synthetic applications for triorganotin hydrides (R_3SnH) are a well investigated field in organometallic and organic synthesis, especially in mediating radical additions, rearrangement and elimination reactions. Specifically, Bu_3SnH (TBTH, tributyltin hydride) is widely used to bring about hydrostannolysis or hydrostannation by radical chain mechanisms.[5] Furthermore, in the last decade, organotin dihydrides have been studied as precursors in the formation of polymeric materials exhibiting a linear backbone of covalently bonded tin atoms. Organotin hydrides can also undergo a catalytic dehydropolymerization using metal complexes based on palladium, zirconium, rhodium, lanthanides, or platinum as well as "non-traditional" iron and molybdenum alkyls as catalysts.[6-9] Moreover, a solvent and catalyst free dehydrogenation reaction was described as a successful route towards polystannanes.[10] More recently, amine bases such as TMEDA (*N*,*N*,*N'*,*N'*-tetramethylethylenediamine) have been reported to efficiently catalyze the polymerization reaction of organotin dihydrides leading to poly(diarylstannane)s.[11] Linear polystannanes harboring a covalently linked metal (tin) backbone, which can be seen as a molecular metal wire embedded in an organic jacket, feature an increased degree of electron delocalization by catenation leading to promising materials in charge-transfer devices.[134,137]In comparison to the use of organotin monohydrides (R_3SnH) as a versatile synthetic tool, less is known about the synthesis, properties, as well as applications of dihydrides (R_2SnH_2).[12-14] In case of trihydrides ($RSnH_3$), mainly alkyl substituted species have been reported, but have not been fully characterized.[15] In most cases, ^{119}Sn and ^{13}C NMR spectroscopy was not performed and only ^{1}H NMR shifts or elemental analysis were reported. In addition, all reported trihydrides are liquids leading to a lack of structural information. Even less is known on tin trihydride derivatives containing aromatic substituents. Apart from the published compounds $PhSnH_3$, $tripSnH_3$ (trip= 2,4,6-triisopropylphenyl) and Ar^*SnH_3 (Ar*= 2,6-bis-2',4',6'-triisopropylphenyl)phenyl) all other known trihydrides exhibit alkyl moieties.[112,181,182] $TerphenylSnH_3$ has only been mentioned as a calculated intermediate in the activation of hydrogen by distannanes leading to a tin (II) hydride product.[183]

The limited number of investigations on the synthesis and spectral data of dihydrides and especially trihydrides and their potential use as polymerization educts provided motivation for the synthesis and full characterization of a series of novel aryltin di- and trihydrides and to provide extensive ^{1}H, ^{13}C and ^{119}Sn NMR studies. Furthermore, theoretical DFT calculations were carried out to supplement the experimental NMR data.

2.2 Results and Discussion

2.2.1 Synthesis

The tin containing starting compound for all further conversions discussed herein is the corresponding tetraaryl stannane (**2-6**). In the case of already published and spectroscopically well described tetraaryl stannanes, no further information is provided. All aryltin di- and trichlorides (**12-16**,**20-27**) as well as di- and trihydrides (**31-41**) were synthesized according to Scheme 55. 2,6-Xylyl$_3$SnBr (**9**) was synthesized as main product in the Grignard reaction of 2,6-xylylBr and could subsequently be hydrogenated according to Scheme 55. Phenyl$_3$SnCl (**7**) was synthesized according to literature.[81] A wide range of substituted phenyl residues was chosen in order to provide information on the influence of steric pressure as well as electronic factors on structural and spectroscopic parameters. All synthesized compounds and their corresponding numbers can be found in Table 24 in Chapter 11.15.1.

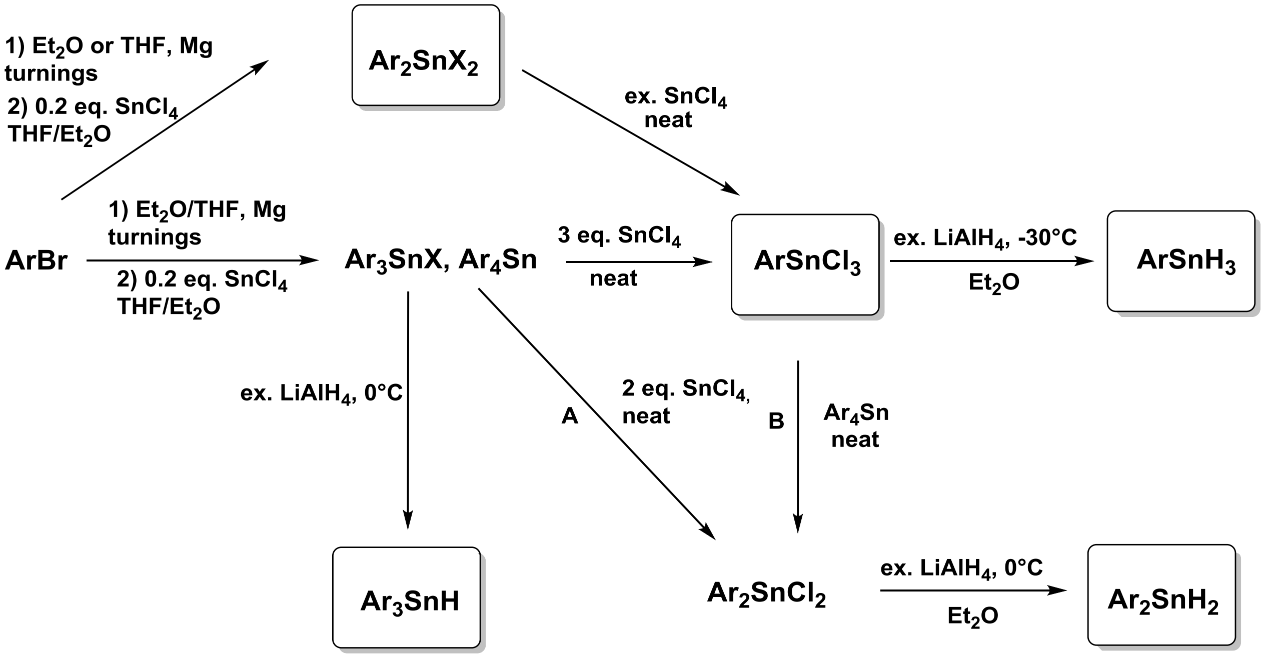
1) Et$_2$O or THF, Mg turnings
2) 0.2 eq. SnCl$_4$ THF/Et$_2$O
Ar$_2$SnX$_2$
ex. SnCl$_4$ neat
ArBr
1) Et$_2$O/THF, Mg turnings
2) 0.2 eq. SnCl$_4$ THF/Et$_2$O
Ar$_3$SnX, Ar$_4$Sn
3 eq. SnCl$_4$ neat
ArSnCl$_3$
ex. LiAlH$_4$, -30°C Et$_2$O
ArSnH$_3$
ex. LiAlH$_4$, 0°C
A
2 eq. SnCl$_4$, neat
B
Ar$_4$Sn neat
Ar$_3$SnH
Ar$_2$SnCl$_2$
ex. LiAlH$_4$, 0°C Et$_2$O
Ar$_2$SnH$_2$

Ar= phenyl (**2**,**7**,**12**,**20**,**29**,**31**,**35**), *p*-^{n}butylphenyl (**3**, **13**, **25**, **37**), *p*-biphenyl (**4**, **14**, **34**) *o*-tolyl (**21**,**36**), 2,4-xylyl (**22**,**38**), 2,6-xylyl (**23**,**39**), mesityl (**10**, **18**, **24**, **40**), 1-naphthyl (**5**,**15**,**26**,**32**,**41**), 2-naphthyl (**6**,**16**,**33**)

Scheme 55: *General synthetic scheme towards aryltin dihydrides (Ar$_2$SnH$_2$) and trihydrides (ArSnH$_3$).*

In each case, the commercially available arylbromide was converted into the Grignard reagent in THF or Et_2O, respectively and subsequently treated with $SnCl_4$ in order to generate the corresponding tetraaryl stannane (Ar_4Sn).[184,185] In the case of the sterically demanding 2,6-xylyl and mesityl aryl residue, the formation of 2,6-xylyl$_4$Sn or mesityl$_4$Sn was not observed and 2,6-xylyl$_3$SnBr (**9**) and mesityl$_3$SnBr (**10**) were isolated as main products. This halogen interchange has already been described for the preparation of sterically encumbered species of mesityl tin compounds.[89] In accordance to the steric demand of the *ortho* substituent, the ratio of the desired Ar_4Sn product was observed to decrease, giving rise to a higher amount of the Ar_3SnX species. The formation of mixtures was tried to be avoided in the synthesis of mesitylSnCl$_3$ (**24**) by converting mesitylMgBr with $SnCl_4$ in a 2:1 ratio. This stoichiometry should generate mesityl$_2$SnCl$_2$ as a single product (Scheme 55). However, a mixture of 73 % mesityl$_2$SnBr$_2$ (**18**), 11 % mesityl$_3$SnBr (**10**) and 16 % mesityl$_2$SnClBr could be observed according to ^{119}Sn NMR measurements. Isolation of the different aryltin species as well as optimization of the reaction conditions was not necessary because the mixtures were treated with excess $SnCl_4$ to generate the desired aryltin trichloride according to the Kozeshkov equilibrium (Scheme 31).[84,102] This type of redistribution reaction was first mentioned by Buckton.[186] MesitylSnCl$_2$Br was detected as a side product from synthesizing mesitylSnCl$_3$ (**24**) by a redistribution reaction from the above described halogen mixture.

Nevertheless, product distribution could probably be influenced by the stoichiometry of the Grignard reagent, solvent and reaction time. Moreover, it was reported that for the generation of organosilicon halides, Grignard reagents permit a better control of product composition but are sensitive towards sterically demanding organic groups which limit their reactivity.[187] Therefore, organolithium compounds could alter the ratio of the formed products. In addition, the use of more reactive tin educts could be considered, such as replacing $SnCl_4$ by $SnBr_4$ or SnI_4, which would also lead to a facilitated salt formation.

In contrast to the formation of aryltin trichlorides, the stoichiometric ratio of $SnCl_4$ reacted with tetraaryl stannane in the preparation of the dichlorides has to be regulated 2:1 to avoid product mixtures. This pathway is illustrated in Scheme 55 as **A**. Route **B** (Scheme 55) employing the Kocheskov equilibrium depicted in Scheme 31, is a more convenient method towards diaryltin dichlorides. Herein, the aryltin trichloride is formed as an intermediate and subsequently treated with 0.5 eq. of the respective tetraorgano stannane (R_4Sn). Tetraorgano stannanes have the advantage of being solid and more stable at atmospheric conditions than

$SnCl_4$ and therefore the stoichiometry can be adjusted easily. The reaction progress for aryltin trichlorides and diaryltin dichlorides was monitored *via* ^{119}Sn NMR in $CDCl_3$ comparing the shifts to known literature data.[89,185,188]

Diaryltin dichlorides were isolated in high purity employing a standard work-up procedure. In this manner residual aryltin trichlorides present were also removed. Di-1-naphthyltin dichlorides (**15**) as well as di-2-naphthyltin dichloride (**16**) were recrystallized from ethyl acetate at room temperature. Di-*p*-biphenyltin dichloride (**14**) was recrystallized from toluene at room temperature. Aryltin trichlorides with less sterically demanding substituents on the aromatic ring (**20**,**21**,**22**) could be purified by distillation, whereas twofold *ortho* substitution in 2,6-position of the aromatic ring (**23**) leads to a change from the liquid to the solid state at room temperature. Therefore, 2,6-xylyltin trichloride (**23**), mesityltin trichloride (**24**), 1-naphthyltin trichloride (**26**) as well as naphthyltin trichloride (**27**) were successfully recrystallized and analyzed by X-ray crystallography which is discussed at length in Chapter 4.

In order to obtain the aryltin hydride species (Ar_3SnH **29**, **30**, Ar_2SnH_2 **31-34**, $ArSnH_3$ **35-41**), the respective aryltin monobromides, di- and trichlorides were subjected to a hydrogenation reaction in Et_2O with an excess of $LiAlH_4$ (lithium aluminum hydride) as described in literature.[12]

Syntheses of aryltin monohydrides and diaryltin dihydrides were carried out at 0 °C, whereas aryltin trihydrides were generated at -30 °C. For the trihydrides, the ether was removed gently at approximately 200 mbar to avoid loss of product. In the case of di-*p*-biphenyltin dihydride (**34**) the reaction was performed in a mixture of Et_2O and THF, due to the poor solubility of the educt (**14**) and therefore the work-up procedures differ. With the exception of phenyl$_2$SnH$_2$ (**31**) the presented dihydrides (**32-34**) are solid at room temperature, whereas the aryltin trihydrides are liquids with the exception of mesityltin trihydride (**40**). Thermal stability of organotin hydrides was reported to decrease with replacement of each organic group by a hydrogen atom as evidenced by trihydrides being the least stable.[114] However, liquid aryltin trihydrides were able to be purified by distillation as well as mesityltin trihydride (**40**) could be recrystallized from diethyl ether and therefore displays the first solid state structure of an aryltin trihydride reported (Figure 1). The distillation was carried out at the lowest temperature possible according to their boiling point. All dihydrides and trihydrides were stored at -80 °C under inert conditions due to their reported instability towards oxygen and their disposition to radical reaction even at room temperature.[33]

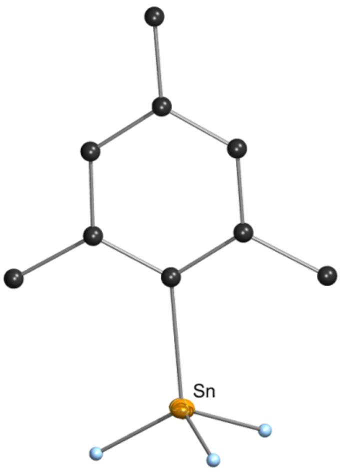

Figure 1: *Crystal structure of mesityltin trichloride (***40***). All non-carbon atoms shown as 30 % shaded ellipsoids. Hydrogen atoms removed for clarity.*

2.2.2 NMR- Spectroscopy and Theoretical Calculations

Herein, an extensive spectroscopic study on the synthesized, tetraaryl stannanes (Ar_4Sn), triaryltin bromide (Ar_3SnBr), mono-, di- and trichlorides (Ar_3SnCl, Ar_2SnCl_2, $ArSnCl_3$) as well as mono-, di- and trihydrides (Ar_2SnH_2, $ArSnH_3$) is presented. For the mentioned stannanes, theoretical DFT calculations were carried out to supplement the experimental ^{119}Sn and ^{13}C NMR data. For comparison purposes, phenyl substituted monochlorides and hydrides are also included in the study.

Spectral parameters such as coupling constants and shifts are dependent on the solvent used.[189] Therefore, C_6D_6 was chosen as a non-coordinating, non-reacting and comparable solvent system. Although the synthesis of tetraorgano stannanes, organotin mono- , di and organotin trichlorides exhibiting a phenyl residue (**2**,**7**,**12**,**20**,**29**,**31**,**35**) is already well described in literature [81,84,102,184,185] either no detailed NMR data is available or compounds were measured in solvents other than C_6D_6.[14,89,184,185,188,190,191-194] The experimental data is supplemented by DFT calculations for the phenyl compound series (Ph_nSnY_{4-n}, Y= Cl, H), for methyl substituted aryltin trichlorides (*o*-tolyl$SnCl_3$, 2,4-xylyl$SnCl_3$, 2,6-xylyl$SnCl_3$, *p*-tolyl$SnCl_3$), as well as for 1-naphthyl$SnCl_3$ (Table 3). ^{119}Sn and ^{13}C NMR shifts, $^{1}J(^{13}C\text{-}^{119}Sn)$ coupling constants, partial charges (q) at the tin and the *ipso* carbon as well as Sn–C_{ipso} bond lengths were calculated. Molecules were regarded in the gas phase and not in solution or solid state. This accounts for the expected bond lengths deviations of up to 0.02 Å between calculated structures and those measured for the molecules in the solid state. As depicted in Figure 2 with a correlation coefficient of R^2= 0.9972, coupling constants are correctly reproduced and results permit a qualitative interpretation. A certain deviation between measured and calculated values could be observed, especially for compounds containing chlorines. The neglect of relativistic effects of the heavy atoms (Cl and Sn) account for part of the deviations.[195] However, Casella *et al.* could show that calculated ^{119}Sn-^{13}C coupling constants basing on non-relativistic levels of theory reproduce trends well and give reliable results. This can most likely be explained by error compensation.[196]

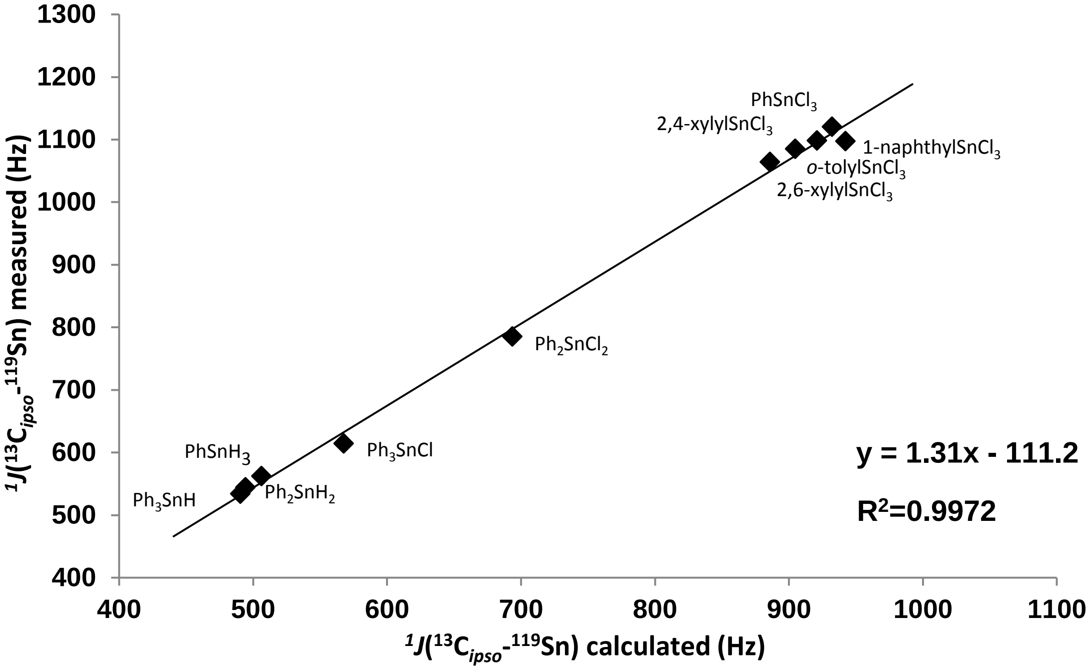

Figure 2: *Correlation between measured and calculated* $^1J(^{13}C-^{119}Sn)$ *coupling constants (Hz).*

Table 3: *Sn–C_{ipso} bond lengths (Å), partial charges of Sn and C_{ipso} and $^{1}J(^{13}C\text{-}^{119}Sn)$ (Hz) for Ph_nSnY_{4-n}, methyl substituted aryltin trichlorides and 1-naphthylSnCl_3 obtained by DFT calculations. Measured values are shown in parenthesis.*

	Ph_3SnH (29)	**Ph_2SnH_2 (31)**	**$PhSnH_3$ (35)**	**Ph_3SnCl (7)**	**Ph_2SnCl_2 (12)**	**$PhSnCl_3$ (20)**	***o*-tolylSnCl_3 (21)**	**2,4-xylylSnCl_3 (22)**	**2,6-xylylSnCl_3 (23)**	***p*-tolylSnCl_3**	**1-naphthylSnCl_3 (26)**
Sn–C_{ipso}	2.15	2.15	2.15	2.14	2.12	2.12	2.12	2.12	2.14	2.11	2.12
q(Sn)	1.55	1.30	1.04	1.81	1.77	1.67	1.66	1.67	1.65	1.67	1.67
q(C_{ipso})	-0.45	-0.44	-0.43	-0.49	-0.51	-0.51	-0.49	-0.52	-0.49	-0.52	-0.51
$^{1}J(^{119}Sn\text{-}^{13}C)$	-490.6	-494.5	-506.5	-567.8	-693.6	-932.4	-904.9	-921.1	-886.1	-950.5	-942.3
	(534)	(544)	(562)	(614)	(785)	(1120)	(1085)	(1098)	(1064)		(1098)

The experimental ^{13}C NMR data as well as a detailed summary of ^{13}C-^{119}Sn coupling constants are listed in Table 4. For comparison, coupling constants of *p*-biphenyl$_4$Sn in $CDCl_3$ were taken from literature due to its poor solubility in C_6D_6.[197] Figure 3 displays the numbering scheme used in Table 4. In order to assign ^{13}C and ^{1}H peaks, 2D-NMR experiments were carried out as well (H,H-COSY and H,C-HETCOR). For the substituted phenyl derivatives, the size of long range coupling constants provides sufficient information on the position in the aromatic ring system according to the following sequence $J_{ipso}>J_{meta}>J_{ortho}>J_{para}$. It should be noted that the ^{3}J coupling constant is bigger than the ^{2}J (Table 4). This trend was also observed for ^{13}C-X-couplings for the heavier homologues of the fourth group, such as X= Sn or Pb. In the case of sterically encumbered compounds, a dihedral angle relationship according to the Karplus type exists.[198] However, for X= Si long range coupling constants are rarely detected, because of their small size.[199] This coupling constants sequence can be explained by negative hyperconjugation effects. Natural bonding analyses showed that the $\sigma_{Sn\text{-}C\mathit{ipso}}$ orbital donates additional electron density into the $\sigma^*_{C2\text{-}C3}$ and $\sigma^*_{C5\text{-}C6}$, while there is no comparable interaction between $\sigma_{Sn\text{-}C\mathit{ipso}}$ and any other antibonding σ^* orbital in the phenyl ring. A higher electron density leads to higher coupling constants.[200]

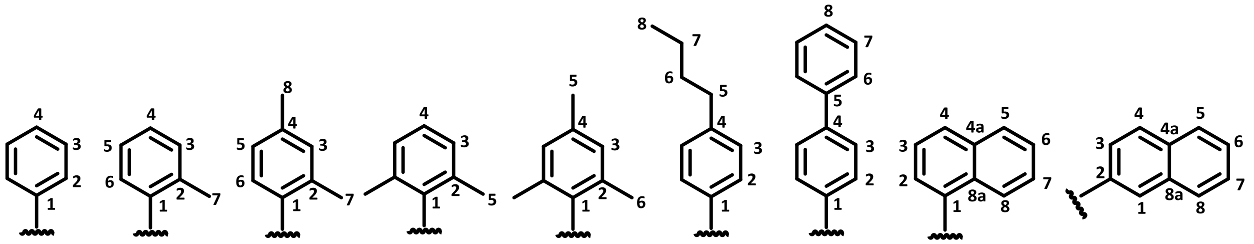

Figure 3: *Numbering scheme for aryl moieties listed in Table 4.*

Table 5 summarizes ^{119}Sn NMR shifts for all included compounds as well as for comparable arylstannanes reported in literature. The signals lie in a range of -9.0 to -421 ppm. Figure 4 illustrates the relationship between the number of chlorine atoms and the ^{119}Sn NMR shift in ppm. For the aryltin chloride species (aryl$_n$SnCl$_{4-n}$), an increase in number of chlorines results in a lower shielding of the ^{119}Sn nucleus, thus in a highfield shift in ^{119}Sn NMR, which can be graphically depicted as a U-shaped curve (Figure 4). For comparison, $SnCl_4$, Ph_3SnCl and Ph_4Sn were included in the graph. Wrackmeyer reported the modified shielding of the Sn as a dependency of the number (n) of groups X bonded in $Me_{4-n}SnX_n$. If X= Cl, an almost linear relationship is observed. The graph becomes more U-shaped if X is a heavier halogen like Br and I.[15] Thus, the aromatic residue reveals great influence on the shape of the ^{119}Sn shift dependency graph. Major changes in the shielding and therefore the shift are reported if tetrahedral symmetry is lowered to *e.g.* C_{3v} or C_{2v}, as can be observed for $aryl_2SnCl_2$.[15]

Table 4: *^{13}C-NMR data and J(^{13}C-^{119}Sn) coupling constants for compounds* ***2-7, 12-16, 20-29, 31-41***.

	C(1)		C(2)		C(3)		C(4)		C(4a)		C(5)		C(6)		C(7)		C(8)		C(8a)	
compound	δ	*J*(^{13}C-^{119}Sn)	δ	*J*(^{13}C-^{119}Sn)	δ	*J*(^{13}C-^{119}Sn)	δ	*J*(^{13}C-^{119}Sn)	δ	*J*(^{13}C-^{119}Sn)	δ	*J*(^{13}C-^{119}Sn)	δ	*J*(^{13}C-^{119}Sn)	δ	*J*(^{13}C-^{119}Sn)	δ	*J*(^{13}C-^{119}Sn)	δ	*J*(^{13}C-^{119}Sn)
phenyl$_4$Sn **2**	138.3	530	137.7	37.0	129.0	50.7	129.4	11.1			36.0		33.9		22.6		14.1			
p-^{n}butylphenyl$_4$Sn **3**	135.4	535	137.8	39.2	129.3	53.0	143.9	11.5												
p-biphenyl$_4$Sn **4**	142.1		137.6	38.3	127.4	53.0	141.0				136.6		127.2		128.8		127.5			
1-naphthyl$_4$Sn **5**	140.7	520	137.6	38.1	126.8	43.8	130.6	32.2	134.5	37.7	129.3	6.7	126.1	n.r.	126.4	n.r.	130.3	11.7	139.4	34.7
2-naphthyl$_4$Sn **6**	138.7	36.9	135.9	529	133.7	40.3	128.6	50.6	134.5	10.0	128.3	4.6	126.8	n.r.	126.4	4.3	128.2	under C_6D_6		57.8
phenyl$_3$SnCl **7**	137.6	614	136.5	50.7	129.4	64.5	130.6	13.0												
phenyl$_2$SnCl$_2$ **12**	137.1	785	135.2	64.7	129.8	86.3	131.7	17.5												
p-^{n}butylphenyl$_2$SnCl$_2$ **13**	134.0	793	135.3	65.8	130.1	86.4	147.1	17.0			35.9		33.6		22.6					
p-biphenyl$_2$SnCl$_2$ **14**	135.7	795	135.7	67.1	128.5	88.8	144.9	17.9			140.4	7.7	127.5	n.r.	129.2	n.r.	128.3	n.r.		
1-naphthyl$_2$SnCl$_2$ **15**	138.1	771	135.8	54.4	126.2	95.6	132.4	13.21	134.8	66.2	129.5	13.8	126.9	n.r.	128.0	24.4	128.4	52.4	136.8	67.1
2-naphthyl$_2$SnCl$_2$ **16**	137.0	64.1	134.5	788	130.0	67.5	129.6	84.3	135.0	16.2	128.7	3.1	128.0	3.69	127.0	7.4	128.2	6.8	133.8	96.8
phenylSnCl$_3$ **20**	135.8	1120	133.9	78.8	130.3	126.3	132.9	121												
o-tolylSnCl$_3$ **21**	136.7	1085	142.9	75.2	131.6	119	133.3	24.0			127.2	128	134.4	77.8	24.3	55.3				
2,4-xylylSnCl$_3$ **22**	133.4	1098	142.8	79.5	132.5	124	144.0	24.3			128.0	132	134.2	82.2	24.2	54.8	21.4	14.3		
2,6-xylylSnCl$_3$ **23**	138.5	1064	143.6	75.5	129.3	121	132.9	23.4			24.9	57.5								
mesitylSnCl$_3$ **24**	135.2	1076	143.5	79.8	130.1	127	143.3	n.r.			20.9	15.1	24.7	56.3						
p-^{n}butylphenylSnCl$_3$ **25**	132.8	1137	133.9	82.2	130.5	130	148.6	28.8			35.7	12.4	33.4	5.8	22.5		14.0			
1-naphthylSnCl$_3$ **26**	136.1	1098	134.8	63.4	125.8	141	133.3	27.5	134.8	103	129.4	20.8	127.3	n.r.	128.7	6.9	127.5	58.3	135.1	85.5
2-naphthylSnCl$_3$ **27**	136.0	74.6	135.2	1130	85.4	81.8	130.1	124.7	135.1	23.1	128.8	5.5	128.1	n.r.	128.7	5.8	127.4	11.3	133.4	141.4
phenyl$_3$SnH **29**	137.3	534	137.7	41.4	129.0	53.0	129.3	11.4												
phenyl$_2$SnH$_2$ **31**	135.5	544	137.8	41.3	128.9	54.4	129.2	11.9												
1-naphthyl$_2$SnH$_2$ **32**	136.7	544	134.3	36.3	126.1	62.7	130.1	12.4	137.4	39.2	129.3	7.3	126.7	n.r.	126.1	5.8	130.6	41.2	139.2	36.3
2-naphthyl$_2$SnH$_2$ **33**	138.7	40.0	133.0	542	133.8	44.3	128.2	52.5	134.2	9.8	128.2	5.2	126.6	n.r.	126.3	4.40	128.1	under C_6D_6	134.1	63.9
p-biphenyl$_2$SnH$_2$ **34**	134.2	546	138.3	42.8	127.7	55.7	142.4	11.8			141.4	5.5	127.5	n.r.	129.1	n.r.	127.7	n.r.		
phenylSnH$_3$ **35**	132.7	562	138.1	44.0	128.8	57	129.1	14.0												
o-tolylSnH$_3$ **36**	134.4	569	144.8	32.4	129.3	43.0	129.8	11.4			126.0	57.8	139.0	44.4	25.8	40.3				
p-^{n}butylphenylSnH$_3$ **37**	129.0	571	131.8	45.2	129.1	62.6	143.8	11.9			35.9		33.9		22.6		14.8			
2,4-xylylSnH$_3$ **38**	130.4	579	144.6	34.4	130.4	44.5	139.3	11.6			126.8	59.5	139.0	n.r.	25.7	40.8	21.5	n.r.		
2,6-xylylSnH$_3$ **39**	135.4	582	144.9	30.4	127.0	43.5	129.4	8.8			26.7	47.3								
mesitylSnH$_3$ **40**	131.3	592	144.9	32.2	128.0	under C_6D_6	138.8	9.7			26.4	48.3	21.1	5.2						
1-naphthylSnH$_3$ **41**	134.4	534	138.2	39.2	125.9	64.5	123.0	12.6	134.1	37.6	129.2	7.2	126.6	n.r.	126.0	10.9	130.7	42.5	139.1	35.8

n.r.= not resolved

***Table 5**: ^{119}Sn NMR shifts (C_6D_6) of included compounds and similar compounds in literature.*

compound	^{119}Sn NMR shift (ppm)	compound	^{119}Sn NMR shift (ppm)
SnCl$_4$ (**1**)	-148.6		
aryl$_4$Sn			
phenyl$_4$Sn (**2**)	-126.5		
o-tolyl$_4$Sn[184]	-122.6[a]		
m-tolyl$_4$Sn[188]	-128.0[a]		
p-tolyl$_4$Sn[185]	-124.6[a]		
2,4-xylyl$_4$Sn[185]	-119.3[a]		
3,5-xylyl$_4$Sn[188]	-127.5[a]		
p-^{n}butylphenyl$_4$Sn (**3**)	-121.5		
p-biphenyl$_4$Sn (**4**)	-124.5[a]		
1-naphthyl$_4$Sn (**5**)	-118.8		
2-naphthyl$_4$Sn (**6**)	-117.6		
p-hexylphenyl$_4$Sn[138]	-127.1[a]		
o-ethylphenyl$_4$Sn[138]	-116.1		
aryl$_3$SnX		**aryl$_3$SnH**	
phenyl$_3$SnCl (**7**)	-44.4	phenyl$_3$SnH (**29**)	-162.8
o-tolyl$_3$SnCl[188]	-32.3[a]	2,6-xylyl$_3$SnH (**30**)	-286.6
m-tolyl$_3$SnCl[188]	-42.3[a]		
3,5-xylyl$_3$SnCl[188]	-39.7[a]		
mesityl$_3$SnCl[188]	-84.4[a]		
1-naphthyl$_3$SnCl	-37.2[a]		
phenyl$_3$SnBr[201]	-59.8[a]		
o-tolyl$_3$SnBr [185]	-54.0[a]		
m-tolyl$_3$SnBr [185]	-56.9[a]		
p-tolyl$_3$SnBr[197]	-52.2[a]		
3,5-xylyl$_3$SnBr[188]	-53.6[a]		
2,6-xylyl$_3$SnBr (**9**)	-131.6		
mesityl$_3$SnBr[185,188] (**10**)	-121.0[a]		
aryl$_2$SnX$_2$		**aryl$_2$SnH$_2$**	
phenyl$_2$SnCl$_2$ (**12**)	-26.4	phenyl$_2$SnH$_2$ (**31**)	-233.7
o-tolyl$_2$SnCl$_2$**	-18.1	*o*-tolyl$_2$SnH$_2$**	-253.5
p-^{n}butylphenyl$_2$SnCl$_2$ (**13**)	-19.9	1-naphthyl$_2$SnH$_2$ (**32**)	-249.7
p-biphenyl$_2$SnCl$_2$ (**14**)	-22.0	2-naphthyl$_2$SnH$_2$ (**33**)	-230.0
1-naphthyl$_2$SnCl$_2$ (**15**)	-9.0	*p*-biphenyl$_2$SnH$_2$ (**34**)	-233.2
2-naphthyl$_2$SnCl$_2$ (**16**)	-23.9	*p*-^{n}butylphenyl$_2$SnH$_2$[11]	-234.3[c]
mesityl$_2$SnCl$_2$[89]	-51.6[a]	mesityl$_2$SnH$_2$[8]	-256.3
p-^{t}butylphenyl$_2$SnCl$_2$[202]	-18.2	*p*-^{t}butylphenyl$_2$SnH$_2$[202]	-234.1
o-ethylphenyl$_2$SnCl$_2$[138]	-15.8	*p*-hexylphenyl$_2$SnH$_2$[138]	-232.1
phenyl$_2$SnClBr[203]	-52[b]	*o*-ethylphenyl$_2$SnH$_2$[138]	-249.3
p-hexylphenyl$_2$SnCl$_2$[138]	-18.6		
mesityl$_2$SnClBr[89]	-97.8		
mesityl$_2$SnBr$_2$[89]	-148.1		

compound	^{119}Sn NMR shift (ppm)	compound	^{119}Sn NMR shift (ppm)
arylSnX$_3$		**arylSnH$_3$**	
phenylSnCl$_3$ (**20**)	-61.0	phenylSnH$_3$ (**35**)	-344.9
o-tolylSnCl$_3$ (**21**)	-60.7	*o*-tolylSnH$_3$ (**36**)	-358.4
2,4-xylylSnCl$_3$ (**22**)	-56.5	*p*-^{n}butylphenylSnH$_3$ (**37**)	-344.6
2,6-xylylSnCl$_3$ (**23**)	-90.5	2,4-xylylSnH$_3$ (**38**)	-352.5
mesitylSnCl$_3$ (**24**)	-84.9	2,6-xylylSnH$_3$ (**39**)	-417.5
p-^{n}butylphenylSnCl$_3$ (**25**)	-58.2	mesitylSnH$_3$ (**40**)	-420.7
1-naphthylSnCl$_3$ (**27**)	-62.3	1-naphthylSnH$_3$ (**41**)	-353.9
2-naphthylSnCl$_3$ (**26**)	-63.5	Ar*SnH$_3$[112]	-384.7[a]
phenylSnBr$_3$[191]	-225[b]		
mesitylSnBr$_3$[89]	-294.2[a]		
phenylSnCl$_2$Br[191]	-114[b]		
mesitylSnCl$_2$Br[89]	-150.1[a]		

a = measured in CDCl$_3$ b= measured in CD$_2$Cl$_2$ c= measured in D$_2$O **= found as side product

Ar*= 2,6-bis-2',4',6'-triisopropylphenyl)phenyl

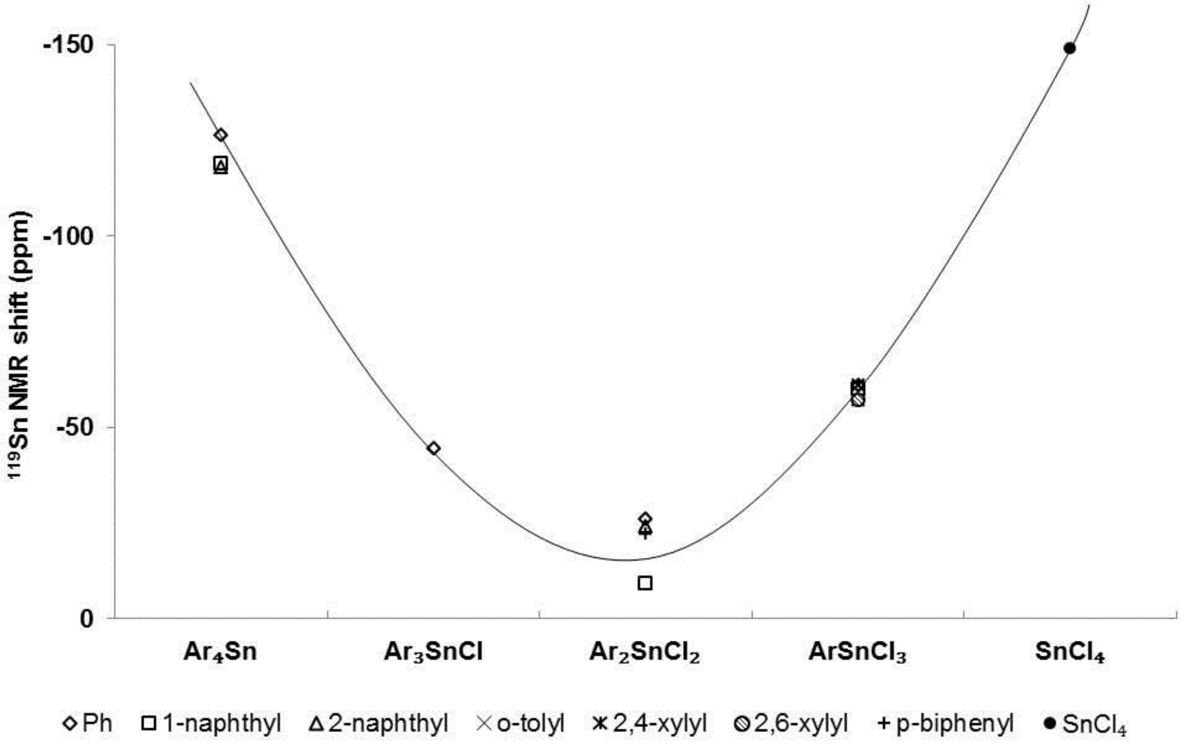

Figure 4: *Correlation between number of chlorine atoms and ^{119}Sn NMR shift (ppm).*

A change of the shielding of the tin nucleus and therefore the ^{119}Sn NMR signal is also observed for Ar_nSnH_{4-n}, leading to a significant high field shift of the central tin atom as the number of bonded hydrogens increases. The effect is similar to the one observed for chlorinated organotin compounds, showing a nonlinear relationship, however it is less pronounced. This has also been described for silicon hydrides and is supported by theoretical calculations.[204]

Both, 2,6-xylyltin trichloride (**23**) and trihydride (**39**) follow the ^{119}Sn shift trend, but show a deviation in comparison to the other trichlorides and hydrides (Figure 4). DFT calculations support that methyl substitution in both *ortho* positions alters the electronic environment on the tin leading to a high field shift of ^{119}Sn NMR shifts (Table 5). Table 6 depicts calculated and measured ^{13}C and ^{119}Sn NMR shifts. The NMR chemical shifts are calculated by referencing to the magnetic shieldings of $SiMe_4$ (σ_C= 186.5 ppm) and $SnMe_4$ (σ_{Sn}= 2552.5 ppm).

The neighboring methyl groups make the *ipso* carbon less negative causing a slightly higher electron density on the tin (Table 3). All measured $^{13}C_{ipso}$ signals lie in a small range of 7 ppm (135.8-140.7 ppm). A decrease of C_{ipso} shifts progressing from Ar_4Sn to $ArSnCl_3$ or $ArSnH_3$, respectively. This trend was also observed for Ph_nSnCl_{4-n}.[192] However, these findings are in contrast to $^{13}C_{ipso}$ chemical shifts of the methyl series Me_nSnCl_{4-n} where an increase of ^{13}C shifts is reported.

Table 6: *δ ^{119}Sn (ppm) and δ $^{13}C_{ipso}$ (ppm) for Ph_nSnY_{4-n}, methyl substituted aryltin trichlorides and 1-naphthyl$SnCl_3$ obtained by DFT calculations. Measured values are shown in parenthesis.*

	Ph_3SnH (16)	**Ph_2SnH_2 (17)**	**$PhSnH_3$ (21)**	**Ph_3SnCl (6)**	**Ph_2SnCl_2 (7)**	**$PhSnCl_3$ (11)**	***o*-tolyl$SnCl_3$ (12)**	**2,4-xylyl$SnCl_3$ (13)**	**2,6-xylyl$SnCl_3$ (14)**	***p*-tolyl$SnCl_3$**	**1-naphthyl$SnCl_3$ (15)**
δ ^{119}Sn	-192.4	-251.0	-367.5	-46.7	-14.2	-30.0	-28.2	-25.9	-43.5	-27.1	-28.1
	(-163)	(-233)	(-345)	(-44.4)	(-26.4)	(-61.0)	(-60.7)	(-56.5)	(-90.5)		(-62.3)
δ $^{13}C_{ipso}$	143.5	142.9	141.0	142.4	140.2	140.6	141.5	137.7	143.3	136.9	137.0
	(137.3)	(135.5)	(132.7)	(137.6)	(137.1)	(135.8)	(136.7)	(133.4)	(138.5)		(136.1)

Table 4 summarizes ^{13}C-^{119}Sn coupling constants illustrating a significant increase of *ipso* coupling with rising number of chlorines attached to the tin. The *ipso* coupling constant of the previously reported *o*-tolyl$_4$Sn is included.[188] This effect was previously described for a series of compounds R_nSnCl_{4-n}, (R= Me, *n*-Bu, Ph).[192] Concerning the compound family Ar_nSnH_{4-n}, the changes in $^{1}J(^{13}C-^{119}Sn)$ constants by increasing the number of hydrogens are not significant. These trends are confirmed by DFT calculations (Figure 2).

Conversely, a replacement of an aryl group by a chlorine leads to a $\Delta((^{1}J(^{13}C-^{119}Sn))$ of about 80-90 Hz. Further chlorine substitution augments the *ipso* coupling by $\Delta\approx170$ Hz. The difference between Ar_2SnCl_2 and $ArSnCl_3$ is about 330 Hz. In addition, DFT calculations support that with every aryl replacement by a chlorine atom, the increment for the *ipso* coupling increases (Figure 5). This effect can be explained by the high electronegativity (EN(Cl)= 3.16) and therefore electron withdrawing properties of the chlorine leading to a shortening of the Sn–C$_{ipso}$ bond and thus an increase in $(^{1}J(^{13}C-^{119}Sn)$ coupling constants as already reported by Bent.[200] As the electronegativity of hydrogen is smaller (EN(H)= 2.2) changes in coupling constants are not significant.

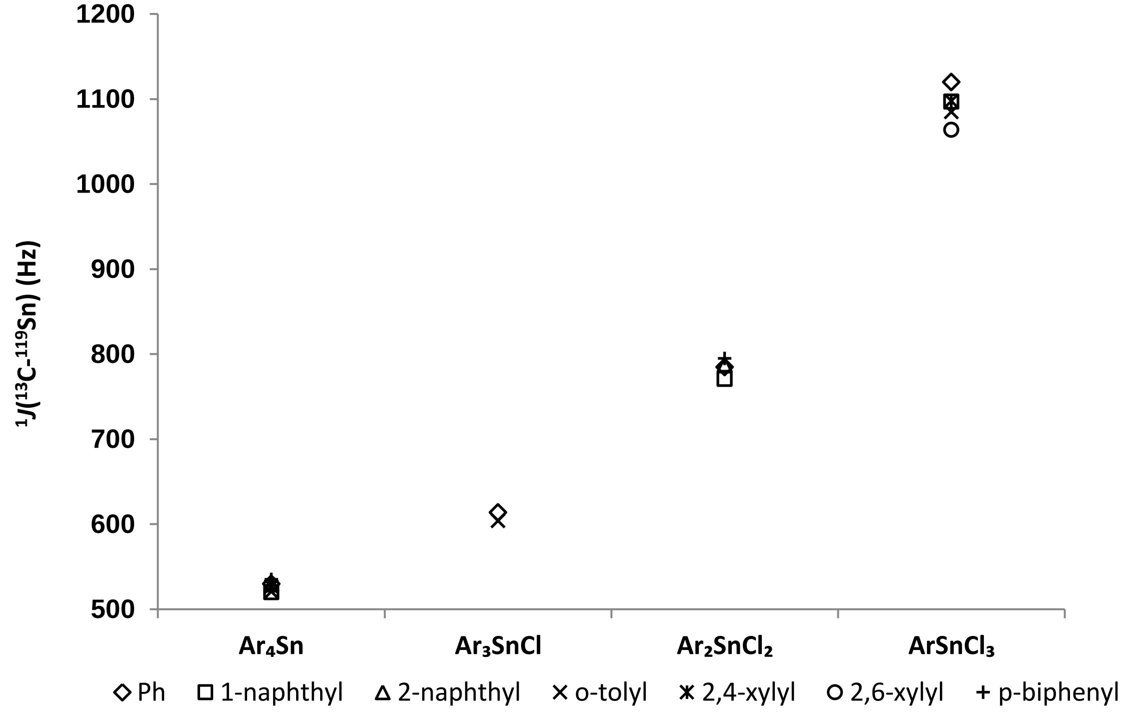

Figure 5: *Correlation between number of chlorine atoms and* $^{1}J(^{13}C-^{119}Sn)$ *(Hz).*

These observations are in accordance with calculated bond lengths, which decrease with the substitution of an organic residue by an electronegative chlorine, and remain similar regarding organotin hydrides. Bond lengths acquired by X-ray analysis are comparable to DFT calculated ones (1-naphthyl$SnCl_3$: measured: 2.114(10) Å, calculated: 2.12 Å; 2,6-xylyl$SnCl_3$: measured: 2.123(2) Å, calculated: 2.14 Å) and therefore calculated values allow a reliable comparison. Calculations show that a high number of chlorine substituents shortens the $Sn{-}C_{ipso}$ bond lengths, which can be explained by the back donation of electron density of the chlorine's free electron pairs in the $Sn{-}C_{ipso}$ antibonding orbital, which is also considered as the +M effect.

2.3 Conclusions

In summary, we were able to synthesize and fully characterize a series of novel aryltin dichlorides, dihydrides as well as aryltin trichlorides and trihydrides featuring at least one *ortho*-substituent on the phenyl ring, a naphthyl, *p*-^{n}butylphenyl or a *p*-biphenyl group as organic residue. Organotin chlorides were generated according to the Kozeshkov equilibrium and subsequently hydrogenated to the corresponding organotin hydride using $LiAlH_4$. Apart from solid dihydrides, structural information by X-ray crystallography was gained for all investigated solid compounds 1-naphthyl$_2SnCl_2$ (**15**), 2-naphthyl$_2SnCl_2$ (**16**), *p*-biphenyl$_2SnCl_2$ (**14**), 2,6-xylyl$SnCl_3$ (**23**) and 1-naphthyl$SnCl_3$ (**26**). In contrast to the herein reported aryltin dihydrides, 1-naphthyl$_2SnH_2$ (**32**), 2-naphthyl$_2SnH_2$ (**33**) and *p*-biphenyl$_2SnH_2$ (**34**), all published aryltin trihydrides as well as those presented in this work are liquids. While reported to easily decompose at room temperature, they could be purified by distillation. All reported organotin compounds were subjected to an extensive ^{119}Sn, ^{13}C and ^{1}H NMR study in the appropriate solvent C_6D_6. Shifts and coupling constants were compared to already published aryltin compounds. Experimental NMR data of ^{13}C and ^{119}Sn shifts as well as ^{13}C-^{119}Sn coupling constants is supplemented by DFT calculations and confirms that an increased number of chlorines attached to the tin leads to an U-shaped ^{119}Sn shift dependency, as well as augmentation of $^1J(^{13}C\text{-}^{119}Sn)$ coupling constants is observed. These effects are less pronounced regarding an increased number of bonded hydrogens to the tin, because of its smaller electronegativity in contrast to chlorine. A detailed long range coupling constants overview reveals, as reported in literature, that $J_{ipso}>J_{meta}>J_{ortho}>J_{para}$. This is supported by NBO analyses showing a negative hyperconjugation from the $\sigma_{\text{Sn-C}ipso}$ orbital into the C2-C3 and C5-C6 antibonding sigma orbital.

3 Anthracenyltin Compounds

Graphical Abstract

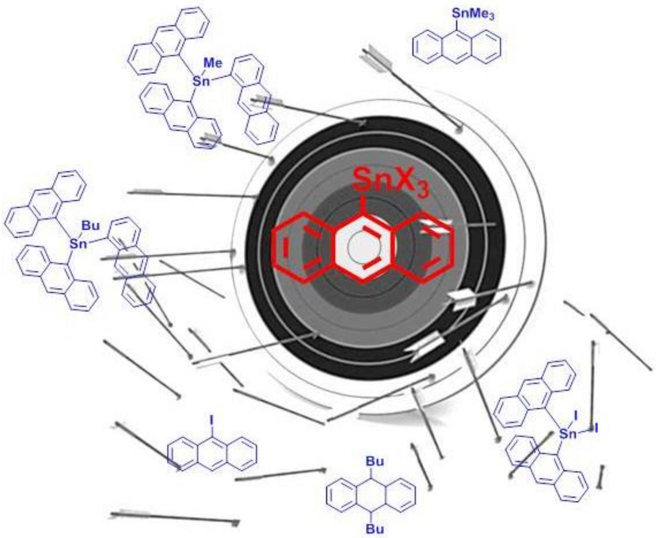

Abstract

This chapter summarizes various approaches towards the synthesis of 9-anthracenyltin halogenides (9-anthracenyl$_n$*SnX*$_{4-n}$*, X= Cl, I) via already established synthetic protocols for aryltin halogenides. The desired products 9-anthracenyl*$_n$*SnX*$_{4-n}$ *with X being either chloride or iodide should serve as educt in the subsequent generation for the corresponding anthracenyltin hydrides. It could be shown that the synthesis of these polyaromatic aryltin halogenides is not as straight forward as reported for less sterically demanding aromatic derivatives such as o-tolyl*$_n$*SnX*$_{4-n}$ *or 1-naphthylSn*$_n$*X*$_{4-n}$*. This can be explained by the elevated thermodynamic stability of anthracene, which is usually formed as a byproduct, as well as by the propensity to stabilize radical anions and therefore avoiding product formation. Thus, formed anthracenyltin compounds easily decompose by formation of anthracene and therefore exhibit temperature lability. However, it could be established that the lithiation of 9-bromo- or iodoantrhacene using n-BuLi is the synthetic route of choice, efficiently forming 9-lithioanthracene which could then be converted to a mixture of anthracenyltin halogenides in the presence of several aromatic byproducts. Additionally, it could be shown that the conversion of 9-lithioanthracene with SnI*$_4$ *instead of SnCl*$_4$ *is more successful since less anthracene is produced as byproduct. A detailed*

*^{119}Sn NMR study of 9-anthracenyl$_3$SnCl (**8**), 9-anthracenyl$_2$SnCl$_2$ (**17**), 9-anthracenylSnCl$_3$ (**28**), 9-anthracenyl$_3$SnI (**11**), 9-anthracenyl$_2$SnI$_2$ (**19**) and 9-anthracenylSnI$_3$ is presented as well as X-ray diffraction studies of **8**, **17**, **28**, **11** and **19** are depicted.*

3.1 Introduction

Polycyclic aromatic carbon compounds, including fullerenes and carbon nanotubes are a fascinating and potentially useful class of compounds. Therefore, substituted anthracenes are valuable building blocks and widely used in metal organic chemistry. Their synthesis and utilization has been well established in the field of semiconductors in OTFTs (organic thin-film transistors,[205] molecular ratchets[201,206] or functionalization of OLC (onion like carbon) nanoparticles.[203] Especially the three dimensional structure stabilized by $\pi-\pi$ interaction in the solid state also allowing for electron conjugation, has been reported to lead to interesting self-assemblies and highly promising materials in the field of nanoelectronics. Sufficient conjugative interaction is expected to create a single extended π-system with a drastically lowered HOMO-LUMO energy gap.[207] However, the synthesis of this class of compounds has been reported to be accompanied by formation of aromatic side products especially anthracene as thermodynamic sink.

In 1976, Bullpitt and coworkers reported on the synthesis of 9-anthracenyltin trimethyl (9-anthracenylSnMe$_3$) converting 9-bromoanthracene with *n*-BuLi to yield 9-lithioanthracene which subsequently is converted with Me$_3$SnX (X= halogenide). However, a substantial amount of anthracene could be observed even before the addition of Me$_3$SnX which leads to poor yields of the desired product. These findings are in stark contrast to the formation of phenyl, 1- and 2-naphthyl as well as *p*-biphenyl derivatives which can be afforded in reasonable to high yields.[208] Kitching reported on a modified synthesis of 9-anthracenylSnMe$_3$ converting 9-bromoanthracene with Me$_3$SnLi also forming anthracene as a side product and yielding the desired, thermally unstable product only in 19 % yield.[209] Better yields (62 %) could be realized by subjecting 9-bromoanthracene to a metathesis reaction with NaSnMe$_3$.[210] Senge could synthesize 9-anthracenylSnBu$_3$ in 75 % yield subjecting 9-bromoanthracene to a lithiation reaction with 2.5 eq. *t*-BuLi at -78 °C in THF.[211] Additionally, 9-anthracenylMgBr could be synthesized as a reaction intermediate which is for example further converted in an acid catalyzed cross coupling reaction to yield sterically crowded biaryls in high yields.[212-215] More recently, Gerbino *et al.* have successfully generated 9-anthracenyl$SnBu_3$ (60 % yield) *via* a Barbier like reaction applying a sonochemical protocol. In this manner, 9-bromoanthracene was converted with *n*-Bu_3SnCl in the presence of dibromoethane and magnesium while sonication.[216]

Nevertheless, the application of *n*-BuLi seems to be the protocol of choice according to literature.[217-222] Only vague description of the formation of side products and the product purification in the literature provided motivation to carefully optimize the formation of 9-anthracenylM (M= Li, MgBr) and the subsequent conversion with SnX_4 (X= Cl, I) in order to generate anthracenyltin halogenides. The latter should serve as educts in the synthesis of corresponding anthracenyltin hydrides representing valuable monomers in the formation of polyaromatic polystannanes.

3.2 Results and Discussion

The experimental procedure is reported in detail in chapter 11.15.4. For all following reaction sequences the abbreviations **ABr** (9-bromoanthracene), **AI** (9-iodoanthracene), **ALi** (9-lithioanthracene) and **A_nSnX_{4-n}** (anthracenyltin halide; X= Cl, I) will be mentioned.

3.2.1 Synthesis of $ASnCl_3$ *via* the Lithiation Route (*a*)

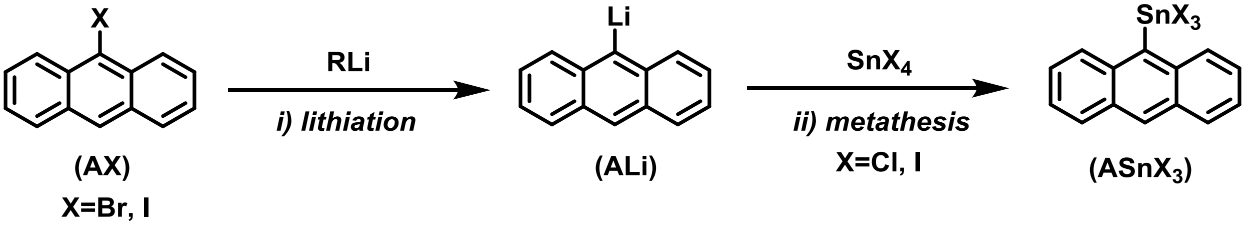

Scheme 56: *General reaction scheme for the lithiation route (**a**) towards anthracenyltin trihalides **$ASnX_3$**.*

Scheme 56 depicts the general synthetic route towards anthracenyltin trihalides (**$ASnX_3$**). In order to further functionalize the 9-anthracenyl moiety the conversion of 9-bromoanthracene, or 9-iodoanthracene (**ABr**, **AI**) with organolithium reagents such as *n*-BuLi, MeLi or *t*-BuLi is the synthetic protocol of choice reported in literature. Therefore, various attempts to successfully lithiate 9-bromoanthracene (**ABr**), or 9-iodoanthracene (**AI**), respectively to generate 9-lithioanthracene (**ALi**) in reaction (***i***) and further convert it with SnX_4 (X=Cl, Br) to generate anthracenyltin trihalides (**$ASnX_3$**) have been carried out (***ii***).

3.2.1.1 a1- i) 1 eq. n-BuLi (-78 °C) ii) 1 eq. **$SnCl_4$** ***(0 °C)***

$$\mathbf{ABr} \xrightarrow[\text{-78°C, THF}]{\text{1 eq. } n\text{-BuLi}} \mathbf{ALi} \xrightarrow[\text{0°C, THF}]{\text{1 eq. } SnCl_4} \mathbf{ASnCl_3}$$

Scheme 57: *Reaction sequence for* ***a1****.*

Converting **ABr** with 1 equivalent of *n*-BuLi in THF at -78 °C and further conversion to the lithiated species (**ALi**) with an equimolar amount of $SnCl_4$ (Scheme 57) led to the formation of an amber colored reaction mixture. Evaporating the solvents yielded an orange to brown solid, which was taken up in $CDCl_3$ to measure a ^1H and ^{119}Sn NMR. Formed precipitates were separated and measured in THF/D_2O. By integration of the ^1H NMR, it could be asserted that approximately 50 % of the resulting solid which was soluble in chloroform belongs to anthracene. However, no unreacted 9-bromoanthracene (**ABr**) could be found. The ^{119}Sn NMR showed two product peaks at -49.6, -84.8 ppm. In comparison to reported compounds, the two shifts could be assigned as **A_3SnCl** (**8**) and **$ASnCl_3$** (**28**), respectively. For a full work-up, the residual solid was taken up in toluene and the resulting precipitate filtered off to afford a red solution. The latter formed a precipitate when standing for a longer time. The supernatant liquid was removed and the toluene evaporated under reduced pressure. The resulting brownish solid was washed with pentane and the soluble parts (pentane solution) removed from pentane under *vacuo*. The resulting brown powder was very poorly soluble in $CDCl_3$, showing a product distribution of 50:50 product/anthracene. Attempts to recrystallize the product were not successful.

3.2.1.2 a2- i) 1 eq. n-BuLi (-78 °C) ii) 0.3 eq. $SnCl_4$ (-50 °C)

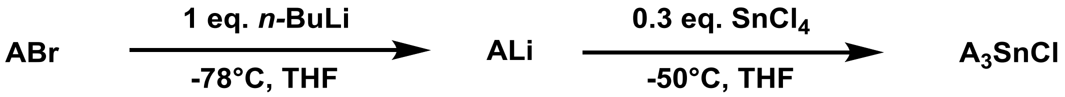

***Scheme 58:** Reaction sequence for **a2**.*

Converting **ABr** with one equivalent of *n*-BuLi in THF at -78 °C and further conversion to the lithiated species (**ALi**) with 0.3 equivalents of $SnCl_4$ (Scheme 58) led to the formation of a clear, dark red solution. After removing the solvent, the resulting solid was taken up in toluene to precipitate salts. These were filtered off to yield a dark yellow solution. After evaporating toluene the ^{1}H NMR ($CDCl_3$) showed that approximately 50 % of the reaction mixture could be assigned as anthracene, however no unreacted 9-bromoanthracene **ABr** could be observed. The ^{119}Sn NMR showed three different peaks when measured for 10 h (-45.0, -84.7 and -92.7 ppm). The main signal was the shift at -84.7 ppm which corresponds to the desired product **$ASnCl_3$** (**28**), as well as -45.0 ppm is in accordance to ***a1*** being assigned as **A_3SnCl** (**8**).

3.2.1.3 a3- i) 1 eq. n-BuLi (-78 °C) ii) 1 eq. $SnCl_4$ (-50 °C)

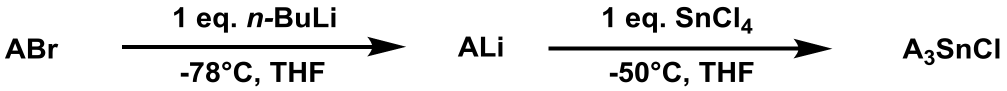

***Scheme 59:** Reaction sequence for **a3**.*

Converting **ABr** with one equivalent of *n*-BuLi in THF at -78 °C and further conversion to the lithiated species (**ALi**) with 1 equivalent of $SnCl_4$ (Scheme 59) led to the formation of a clear, dark red solution. After removing the solvent, the resulting solid was taken up in $CDCl_3$ to precipitate salts. The latter were filtered off and the solution subjected to a ^{1}H NMR. The observed ^{1}H NMR did not show unreacted 9-bromoanthracene (**ABr**) nor anthracene. A ^{119}Sn NMR measurement of 10 h depicted two defined peaks at -84.3 and -258.9 ppm. The first corresponds to **$ASnCl_3$** (**28**).

3.2.1.4 *a4- i) 1 eq. n-BuLi (-78 °C) ii) 1 eq. SnCl$_4$ (RT)*

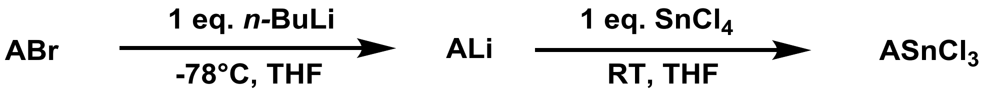

Scheme 60: *Reaction sequence for* ***a4****.*

Converting **ABr** with one equivalent of *n*-BuLi in THF at -78 °C and further conversion to the lithiated species (**ALi**) with 1 equivalent of SnCl$_4$ (Scheme 60) at room temperature led to the formation of a dark red solution with a brownish precipitate. After removing the solvent, the resulting brown red solid was taken up in toluene to precipitate salts. The latter were filtered off and the solvent removed in *vacuo* to afford a yellow solid which was subjected to a ^{1}H NMR in CDCl$_3$. The ^{1}H NMR showed unreacted 9-bromoanthracene **ABr**, anthracene, as well as another aromatic product mixture. This was also revealed by ^{119}Sn measurements showing two peaks at -45.1 and -84.5 ppm which is in accordance to **A1** and **A2**. The insoluble part precipitating from toluene and CDCl$_3$ was composed of salt as well as a single aromatic product with a ^{119}Sn NMR shift at -91.8 ppm (D$_2$O/THF).

3.2.1.5 *a5- i) 1 eq. n-BuLi (-78 °C) ii) 1 eq. SnCl$_4$ (-78 °C)*

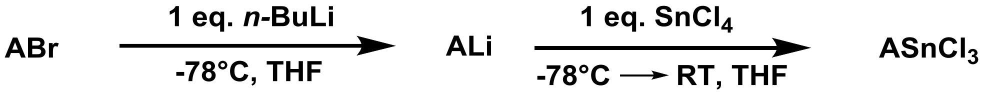

Scheme 61: *Reaction sequence for* ***a5****.*

The used amounts of reagents were in accordance with reaction ***a4***, however in this experiment the lithiation as well as the conversion with SnCl$_4$ was carried out at -78 °C (Scheme 61). The latter was stirred for 3h at -78 °C. Afterwards the red brown reaction mixture was allowed to warm up to room temperature resulting in a clear solution without formation of salt precipitation. For a micro work-up a small amount of solution was transferred to a separate flask and the solvent evaporated under reduced pressure. The resulting yellow oil was taken up in CDCl$_3$ and ^{1}H and ^{119}Sn NMR measurements were performed. The ^{1}H spectra did not show anthracene or unreacted educt **ABr**, as well as the ^{119}Sn spectra revealed two signals at -50.6 and

-84.0 ppm. The residual reaction solution was pumped down and toluene was added. The crystals formed in toluene could be verified as di-9-anthracenyltin dichloride (**17**) (Figure 6). **17** probably gives rise to the broader shift at -50.6 ppm in presence of **ASnCl$_3$** (**28**) at -84.0 ppm. **A$_2$SnCl$_2$** (**17**) crystallizes in the monoclinic space group P2$_1$/c. The compound displays intermolecular interactions in the solid state as seen in the extended structure (Chapter 4). In the presence of the product **17**, a THF complex of SnCl$_4$ saturated with a Li atom [SnCl$_5$(THF)][Li(THF)$_4$] could be identified (Figure 7) which leads to a ^{119}Sn shift at 142.5 ppm in CDCl$_3$. Therefore, it can be concluded that the lithiation reaction does not proceed quantitatively.

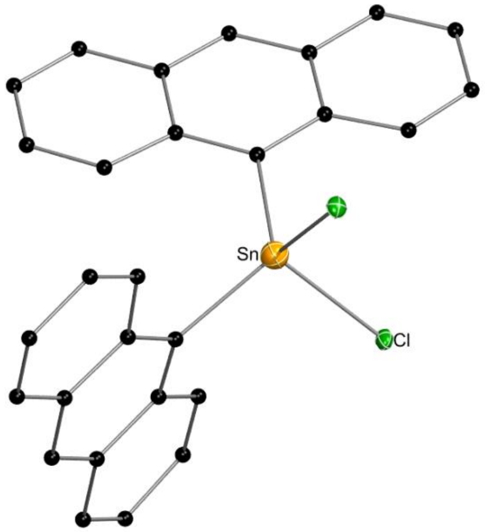

Figure 6: *Crystal structure of di-9-anthracenyltin dichloride **A$_2$SnCl$_2$** (**17**). All non-carbon atoms shown as 30 % shaded ellipsoid. Hydrogen atoms removed for clarity.*

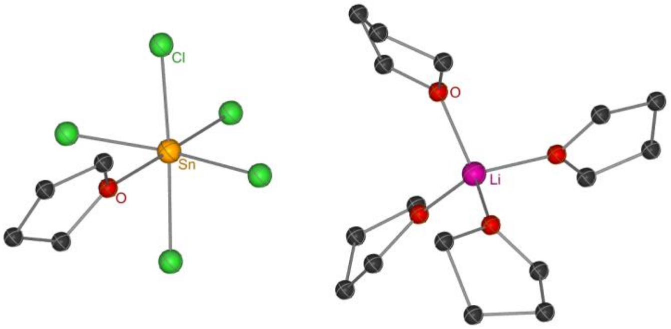

Figure 7: *Crystal structure of [SnCl$_5$(THF)][Li(THF)$_4$]. All non-carbon atoms shown as 30 % shaded ellipsoid. Hydrogen atoms removed for clarity.*

3.2.1.6 a6- i) 2 eq. n-BuLi (-78 °C) ii) 1 eq. $SnCl_4$ (0 °C)

$$\mathrm{ABr} \xrightarrow[\text{-78°C, THF}]{\text{2 eq. } n\text{-BuLi}} \mathrm{ALi} \xrightarrow[\text{0°C, THF}]{\text{1 eq. } \mathrm{SnCl_4}} \mathrm{ASnCl_3}$$

Scheme 62: *Reaction sequence for* ***a6****.*

As the side product $[SnCl_5(THF)][Li(THF)_4]$ generated in ***a5*** suggests that the lithiation reaction does not proceed in a quantitative manner, 2 eq. of *n*-BuLi were used in the case of ***a6*** (Scheme 62). The conversion of **ALi** with $SnCl_4$ was carried out at 0 °C. A micro work-up with $CDCl_3$ and subsequent ^{119}Sn and ^{1}H measurements did not show the existence of anthracene nor unreacted educt in the reaction mixture. However, no adequate ^{119}Sn signal could be found.

3.2.1.7 a7- i) 1.2 eq. n-BuLi (-78 °C) ii) 1 eq. $SnCl_4$ (0 °C)

$$\mathrm{ABr} \xrightarrow[\text{-78°C, THF}]{\text{1.2 eq. } n\text{-BuLi}} \mathrm{ALi} \xrightarrow[\text{0°C, THF}]{\text{1 eq. } \mathrm{SnCl_4}} \mathrm{ASnCl_3}$$

Scheme 63: *Reaction sequence for* ***a7****.*

In the case of ***a7***, **ABr** was converted with slight excess of *n*-BuLi (1.2 eq.) at -78 °C (Scheme 63). However, the lithiation reaction was allowed to warm up to room temperature and stirred overnight before being converted with $SnCl_4$ at 0 °C. Afterwards, the solvent was evaporated to result in a brown solid which was taken up in $CDCl_3$. The ^{1}H NMR revealed the formation of anthracene, however the ^{119}Sn signal did not show a tin signal although even when the sample was measured over 10 h. Therefore, it can be stated that the lithiation reaction needs to be carried out fast and at low temperature otherwise the formation of a radical anion giving rise to a dark green color of is favored. Subsequently, the reactive radical anion easily reacts under the formation of anthracene.

3.2.1.8 a8- i) 2.2 eq. n-BuLi (-78 °C) ii) 1 eq. $SnCl_4$ (0 °C)

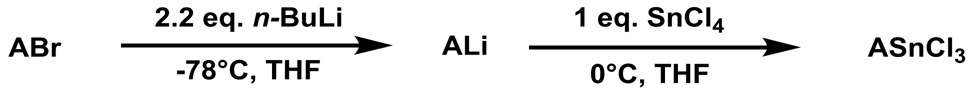

Scheme 64: *Reaction sequence for* ***a8****.*

For ***a8***, **ABr** was converted with 2.2 eq. of *n*-BuLi at -78 °C and stirred for 1h resulting in a dark orange reaction mixture. The conversion with $SnCl_4$ was carried out at 0 °C using 1 eq. $SnCl_4$ (Scheme 64). The reaction mixture turned turbid yellow and became clear after 10 min reaction time. For reaction monitoring, a small amount of the reaction solution was transferred into a separate flask and the solvent removed under *vacuo*. The resulting solid was taken up in $CDCl_3$ and ^1H, ^{119}Sn NMR were recorded. The ^{119}Sn spectrum showed two signals at -62.3 and -100.1 ppm. These two shifts did not correspond with any spectrum measured before. Also, the ^1H NMR showed as a main compound anthracene. For the work-up, THF was completely removed under reduced pressure and the resulting residue taken up in dichloromethane. The supernatant orange, slightly turbid solution was separated and dichloromethane removed in *vacuo*. This yielded an orange to brown oil. The ^1H NMR mainly showed anthracene and the butylated byproduct **ABu** (9-butylanthracene). However, no reliable ^{119}Sn NMR shifts were found. Recrystallization from toluene yielded in anthracene as colorless blocks. When carrying out the reaction according to Scheme 64, but slightly changing the work-up procedure a different result was obtained. THF was removed under *vacuo* and the resulting brown suspension taken up in toluene. The precipitate was filtered off to afford an orange to yellow clear solution. Toluene was evaporated and the solid taken up in $CDCl_3$. The ^{119}Sn NMR showed several peaks: 1.5, -32.2, -45.0, -92.0, -92.4, -145.2, -153.7 and -165.4 ppm. From this sample di-9-anthracenyltin dichloride $\mathbf{A_2SnCl_2}$ (**17**) could be recrystallized which belongs to the shift at -92.0 or -92.4 ppm which was surprisingly not found in ***a5*** (Figure 6).

3.2.1.9 a9- i) 1.38 eq. n-BuLi (RT) ii) 1 eq. SnCl₄ (0 °C→ RT)

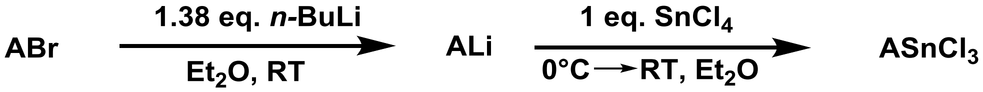

Scheme 65: *Reaction sequence for* ***a9****.*

In the case of ***a9***, **ABr** was converted with 1.38 eq. *n*-BuLi in Et_2O at room temperature. This procedure is in accordance to a published synthesis.[217] The lithiated species, **ALi**, was added to a solution of $SnCl_4$ in Et_2O at 0 °C which led to an immediate color change to brightly yellow and the formation of a precipitate which was filtered off and washed with cold Et_2O. Afterwards, the solvent was removed under reduced pressure to afford a yellow powder. The filtrate mainly consisted of anthracene, 9-butylanthracene (**ABu**) and unreacted **ABr** according to ^1H NMR. The yellow powder was taken up in chloroform to precipitate the salt and the resulting solution was subjected to a ^{119}Sn NMR measurements revealing the following signals in $CDCl_3$: -44.5 and -84.7 ppm. The main signal at -44.5 ppm belonged to tri-9-anthracenyltin chloride **A_3SnCl** (**8**) which could be recrystallized from ethyl acetate as yellow crystals (Figure 8). **8** crystallizes in the cubic space group Pa-3 and exhibits intermolecular interactions in the solid state structure (Chapter 4). The high field shifted peak could be assigned as the desired product **$ASnCl_3$** (**28**), however both products were found in the presence of anthracene.

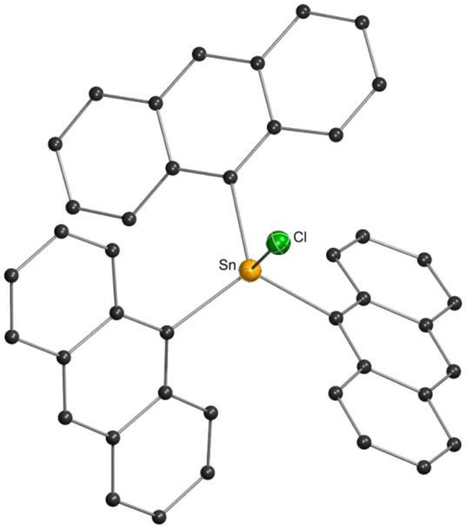

Figure 8: *Crystal structure of tri-9-anthracenyltin chloride **A$_3$SnCl** (**8**). All non-carbon atoms shown as 30 % shaded ellipsoid. Hydrogen atoms removed for clarity.*

3.2.1.9.1 a10- i) 2.5 eq. t-BuLi (-95 °C) ii) 1 eq. SnCl$_4$ (-50 °C)

$$\text{ABr} \xrightarrow[\text{-95°C, THF}]{\text{2.5 eq. } t\text{-BuLi}} \text{ALi} \xrightarrow[\text{0°C, THF}]{\text{1.5 eq. SnCl}_4} \text{ASnCl}_3$$

Scheme 66: *Reaction sequence for **a10**.*

In the case of ***a10***, 9-bromanthracene, **ABr** was dissolved in THF and converted with 2.5 eq. of *t*-BuLi at -95 °C resulting in a dark orange reaction mixture. Afterwards, the reaction mixture was allowed to warm up to -50 °C and 1.5 eq. of SnCl$_4$ were added and the formation of an orange turbid solution which became clear after stirring was observed (Scheme 66). After 30 min reaction time the mixture slowly warmed up to room temperature. The solvent was removed and the resulting solid taken up in toluene which led to the formation of a yellow precipitate and surprisingly a supernatant solution consisting of two different phases. The lower phase was dark orange, clear and the upper phase slightly orange and clear. For NMR analysis, the two phases as well as the precipitate were separated. Toluene was completely removed under reduced pressure and the resulting solids taken up in CDCl$_3$. The lower phase did not show a tin signal. However, the upper phase and the precipitate showed two signals at -45.3 and -92.3 ppm. Di-9-

anthracenyltin dichloride **A_2SnCl_2** (**17**) and tri-9-anthracenyltrin chloride **A_3SnCl** (**8**) could be recrystallized from toluene. The NMR shift of -92 ppm is in accordance with the one found in ***a8***.

3.2.1.9.2 a11- i) 1.1 eq. n-BuLi (0 °C) ii) 1 eq. $SnCl_4$ (0 °C)

$$\mathbf{ABr} \xrightarrow[\substack{0°\mathrm{C} \rightarrow \mathrm{RT,\ overnight} \\ \mathrm{Et_2O}}]{\mathrm{1.1\ eq.}\ n\text{-}\mathrm{BuLi}} \mathbf{ALi} \xrightarrow[\mathrm{0°C,\ toluene}]{\mathrm{1.2\ eq.\ SnCl_4}} \mathbf{ASnCl_3}$$

Scheme 67: *Reaction sequence for* ***a11***.

For ***a11***, **ABr** was converted with 1.1 eq. of *n*-BuLi at 0 °C in Et_2O and stirred overnight resulting in a yellow precipitate and a yellowish supernatant liquid (Scheme 67). The supernatant liquid was subjected to a NMR analysis showing the presence of anthracene as a side product. For that reason, the supernatant liquid was filtered off and the resulting yellow residue washed twice with diethyl ether and then taken up in toluene. The conversion with 1.2. eq. $SnCl_4$ was carried out at 0 °C. For reaction monitoring, a small amount of the reaction solution was transferred into a separate flask and the solvent removed under *vacuo*. The resulting solid was taken up in C_6D_6 and ^1H, ^{119}Sn NMR were recorded. The ^1H NMR mainly showed anthracene and unreacted 9-bromoanthracene (**ABr**). The ^{119}Sn spectrum showed a single signal at -85 ppm, however very low in intensity. Afterwards, the reaction mixture was refluxed for 1h which led to decomposition of the product. Thus, it can be suggested that the desired product is thermally unstable, as well as the lithiation reaction should be carried out quickly at low temperatures.

3.2.1.9.3 a12- i) 1.1 eq. n-BuLi (0 °C) ii) 1 eq. $SnCl_4$ (RT)

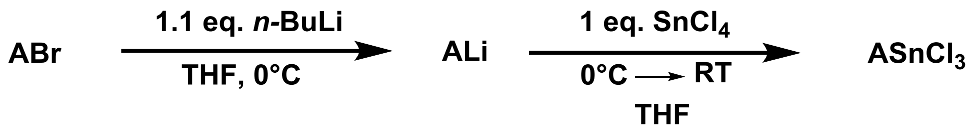

Scheme 68: *Reaction sequence for* ***a12****.*

For ***a12***, **ABr** was converted with 1.1 eq. of *n*-BuLi at 0 °C in THF and stirred for 25 min resulting in an orange, turbid reaction mixture. Subsequently, 1 eq. of $SnCl_4$ was added at 0 °C and the reaction allowed to warm up to room temperature. After stirring overnight, the THF was completely removed under *vacuo* to afford a brown oily solid, which mainly showed anthracene in the ^{1}H NMR. The ^{119}Sn NMR showed one peak at -201 ppm. A lithium coordinated anthraquinone derivative **47** could be recrystallized from toluene, however the desired product could not be detected (Figure 9).

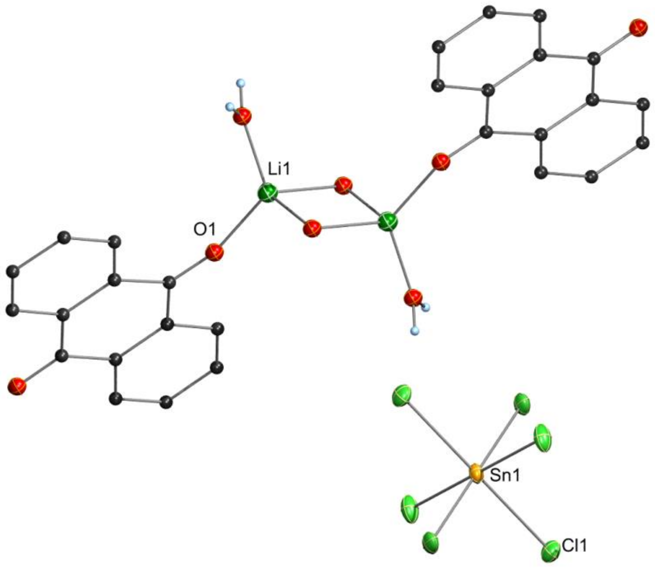

Figure 9: *Crystal structure of* ***47****. All non-carbon atoms shown as 30 % shaded ellipsoid. Hydrogen atoms removed for clarity.*

3.2.1.9.4 a13- i) 1.1 eq. n-BuLi, TMEDA (0 °C) ii) 1 eq. $SnCl_4$ (RT)

$$\mathrm{ABr} \xrightarrow[\text{pentane, 0°C}]{\text{1.1 eq. } n\text{-BuLi, 1 eq. TMEDA}} \mathrm{ALi_2{*}TMEDA_2} \xrightarrow[\substack{\text{0°C} \longrightarrow \text{RT} \\ \text{THF}}]{\text{1 eq. SnCl}_4} \mathrm{ASnCl_3}$$

Scheme 69: *Reaction sequence for* ***a13****.*

For ***a13***, **ABr** was suspended in pentane in addition with TMEDA and cooled to 0 °C. Subsequently, 1.1 eq. of *n*-BuLi was added at 0° to form a clear dark red solution which then turned yellow under the formation of an orange precipitate (Scheme 69). The orange solid easily reacted with air resulting in a black solid. The latter could be isolated by filtration and recrystallization from toluene (Figure 10). In the presence of the donor TMEDA, a stabilized, mixed lithium bromide complex [RLi(TMEDA)·LiX(TMEDA)] was formed (**46**). These findings are in accordance with results published by Stern *et al.*, who reported on the assessment of LiX salt effect in anthracenyl lithiums. Herein, it could be established that the presence of a donor (DME, THF) leads to dimer formation $[\mathrm{RLi(Donor)}]_2$ whereas the addition of LiBr and a donor forms structures such as 9-anthracenylLi(TMEDA)·LiBr(TMEDA) (**46**).[223] Comparable dimers $[\mathrm{RLi(Donor)}]_2$ lacking a coordinated LiX salt could be isolated when 1-bromonaphthaline was converted with *n*-BuLi and TMEDA (Figure 12), although Neugebauer and coworkers postulated a monomer according to ^{1}H NMR.[224]

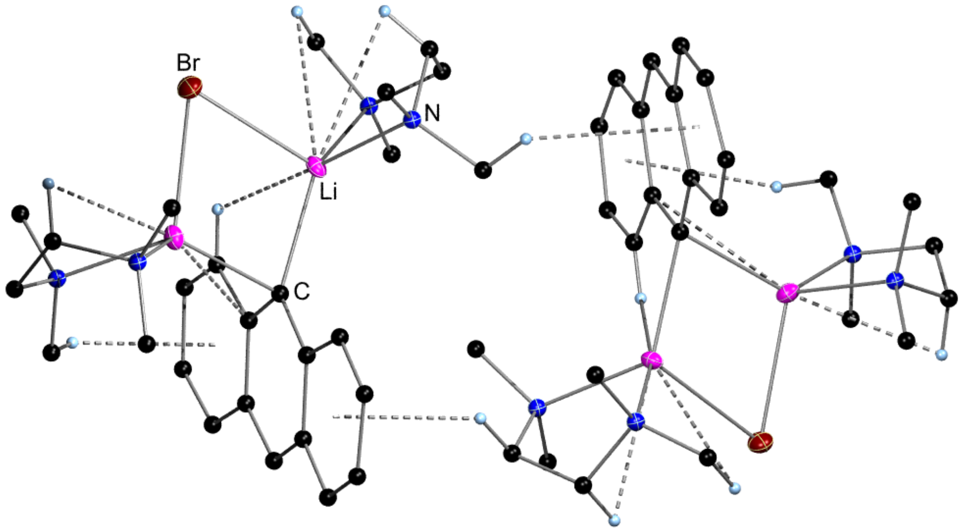

Figure 10: *Crystal packing diagram of 9-anthracenylLi(TMEDA)·LiBr(TMEDA) (**46**). C-H–π stacking and Cl–H interactions are highlighted by dashed bonds. All non-carbon atoms shown as 30 % shaded ellipsoid. Hydrogen atoms removed for clarity.*

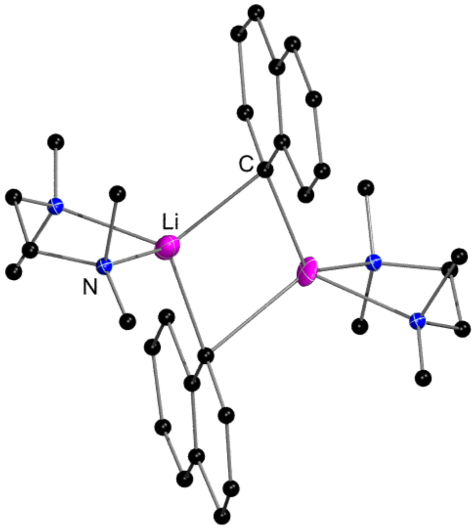

Figure 11: *Crystal structure of [1-naphthylLi(TMEDA)]$_2$. All non-carbon atoms shown as 30 % shaded ellipsoid. Hydrogen atoms removed for clarity.*

X-Ray analysis of the supernatant liquid gained during the lithiation reaction showed the existence of a μ,μ'-dihalo-bridged binuclear species [(TMEDA)LiBr$_2$Li(TMEDA)] (Figure 12). The doubled lithiated 9-anthracenyl species 9-anthracenylLi(TMEDA)·LiBr(TMEDA) (**46**) was dissolved in THF and converted with 1 eq. $SnCl_4$ at room temperature. The orange suspension was stirred for 5 h at room temperature and the reaction progress monitored by NMR giving rise to the following ^{119}Sn NMR (D_2O) signals: -88, -142, -200 ppm. Additionally, ^{119}Sn shifts for a THF-$SnCl_4$-TMEDA complex (-506 ppm) and $SnCl_4 \cdot 2THF$ (-610 ppm) could be found. Subsequently, the solvent was removed under reduced pressure and the resulting brownish residue taken up in toluene to precipitate salts. The salts were filtered off and the filtrate subjected to an NMR analysis giving rise to a ^{119}Sn shift of -45 ppm in $CDCl_3$ which did not match the previously mentioned shifts. Tri-9-anthracenyltin chloride **A_3SnCl** (**8**) could be isolated by recrystallization from toluene (Figure 8).

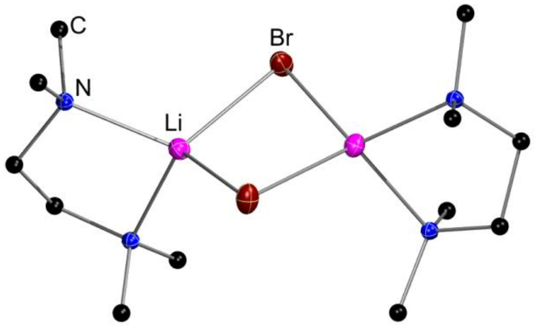

Figure 12: *Crystal structure of [(TMEDA)LiBr$_2$Li(TMEDA)].*

3.2.1.9.5 a14- i) 1.1 eq. n-BuLi, TMEDA (0 °C) ii) 1.4 eq. SnCl₄ (RT)

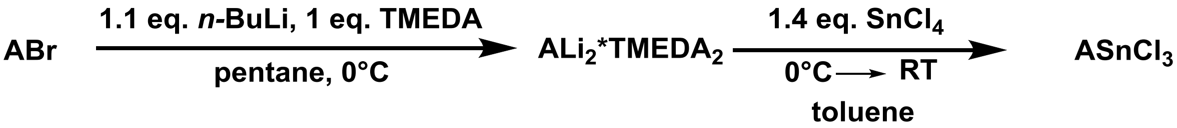

Scheme 70: *Reaction sequence for **a14**.*

For reaction ***a14***, the conditions were the same as described for ***a13***, however the solvent for conversion of ALi_2*$TMEDA_2$ (**46**) was changed to toluene, as well as an excess of $SnCl_4$ was used (Scheme 70). After stirring overnight at room temperature, the precipitated salts were filtered off and the filtrate subjected to ^{1}H and ^{119}Sn NMR measurements revealing 44 % of anthracene, 15 % of unreacted **ABr** and 41 % of a Sn containing anthracenyl compound with a shift of -80.5 ppm in the ^{119}Sn NMR. This is evidenced by $J(^{1}\text{H-}^{117/119}\text{Sn})$ coupling constants from one of the aromatic protons to the Sn nucleus of 20 Hz. After removing the solvent under reduced pressure a yellow powder could be obtained which was subjected to sublimation at 80 °C for 1.5 h. In this manner the desired product 9-anthracenyltin trichloride **ASnCl$_3$** (**28**) could be recrystallized from the described mixture using toluene (Figure 13). Anthracene could be successfully removed, as well as the content of the educt **ABr** could be decreased to 10 %. However, it was observed that the product is temperature labile and therefore decomposed when heated while sublimation. This led to the formation of anthracene and black insoluble powder.

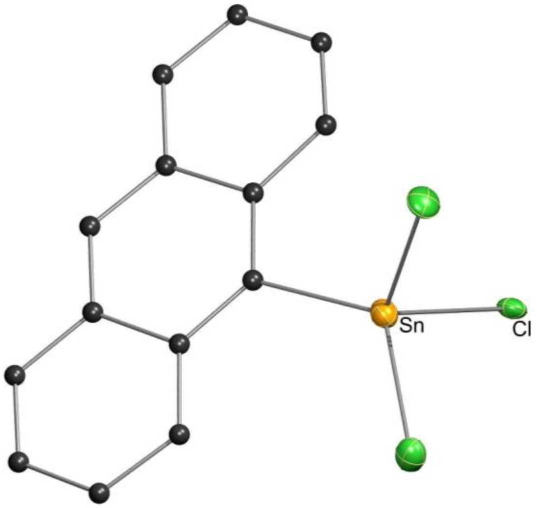

Figure 13: *Crystal structure of 9-anthracenyltin trichloride (**28**). All non-carbon atoms shown as 30 % shaded ellipsoids. Hydrogen atoms removed for clarity.*

3.2.1.9.6 a15- i) 2.2 eq. n-BuLi, TMEDA (0 °C) ii) 1.2 eq. $SnCl_4$ (RT)

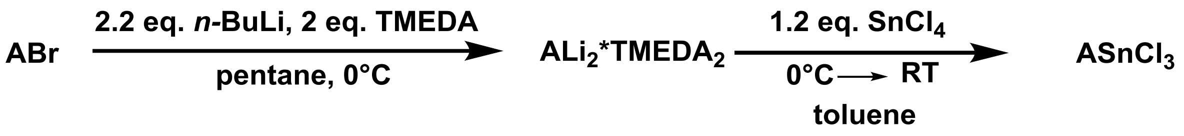

Scheme 71: *Reaction sequence for* ***a15****.*

The use of solvents was in accordance to ***a14***, however 2.2 eq. of *n*-BuLi as well as 2 eq. of TMEDA were used, in order to fulfill the stoichiometry for the doubly lithiated, TMEDA stabilized intermediate ALi_2TMEDA_2 (**47**) (Scheme 71). After stirring the mixture overnight, the precipitated salts were filtered off and the filtrate subjected to a ^{119}Sn, as well as an ^{1}H NMR. The ^{119}Sn spectrum showed two signals (C_6D_6) at -84 and -154 ppm. The lowfield shifted signal could be assigned as the desired product **$ASnCl_3$**. The ^{1}H NMR showed the formation of anthracene as a side product as well as unreacted **ABr**. These impurities could be removed by sublimation over 8 h to yield an orange to brown solid. Tri-9-anthracenyltinbutyl **A_3SnBu** (**48**) could be recrystallized from the mixture using toluene, however the crystal structure data was not satisfying (Figure 14). Thus, it can be suggested that **48** belongs to the ^{119}Sn NMR shift at -154 ppm. The formation of the butylated product can be explained by the excess of *n*-BuLi lithiating the partially formed **A_3SnCl** yielding in **A_3SnLi** and BuCl which subsequently forms **A_3SnBu** (**48**) and LiCl.

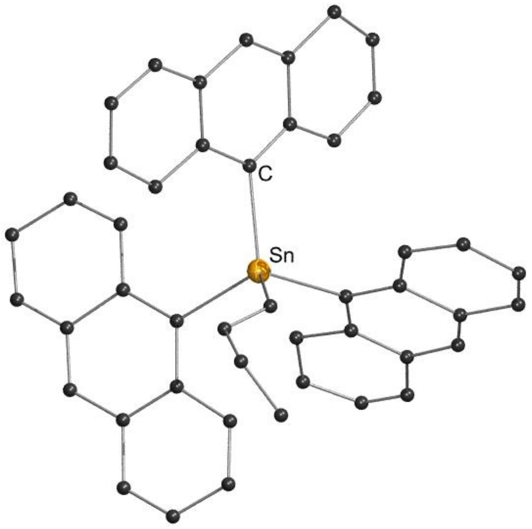

Figure 14: *Crystal structure of tri-9-anthracenyltin butyl* ***A_3SnBu (48)****. All non-carbon atoms shown as 30 % shaded ellipsoids. Hydrogen atoms removed for clarity.*

3.2.1.9.7 a16- i) 2.2 eq. MeLi, TMEDA (0 °C) ii) 1.2 eq. $SnCl_4$ (RT)

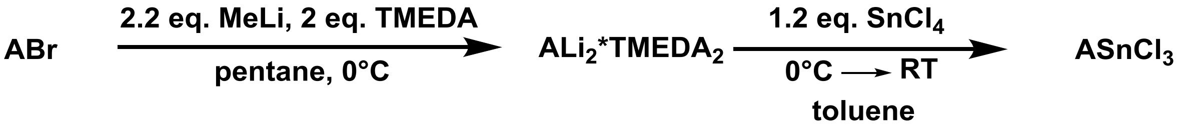

Scheme 72: *Reaction sequence for* ***a16****.*

For ***a16***, **ABr** was converted with an excess of MeLi in pentane at 0 °C in the presence of TMEDA to give a yellow suspension (Scheme 72). The yellow precipitate was filtered off and suspended in toluene to give an orange solution which was then converted with 1.2 eq. of $SnCl_4$ in toluene at 0 °C to yield a yellow, turbid reaction mixture. After filtration of the precipitate the following ^{119}Sn NMR shifts could be found in the filtrate (C_6D_6): -48.8, -84.0, -102.2, -165.3 and -172.9 ppm. By subjecting the orange powder to sublimation, unreacted **ABr** and anthracene could be removed. Tri-9-anthracenyltin methyl **A_3SnMe** (**45**) could be recrystallized from the mixture using benzene (Figure 15). According to the previous experiments and results described in this chapter it can be suggested that the -48.8 and -84.0 ppm belong to **A_3SnCl** (**8**) and **$ASnCl_3$** (**28**), respectively, as well as the signal at -102.2 ppm corresponds to **45**. This is in good comparison to phenyl$_3$SnMe which shifts to -93 ppm (CH_2Cl_2) in ^{119}Sn NMR.[15]

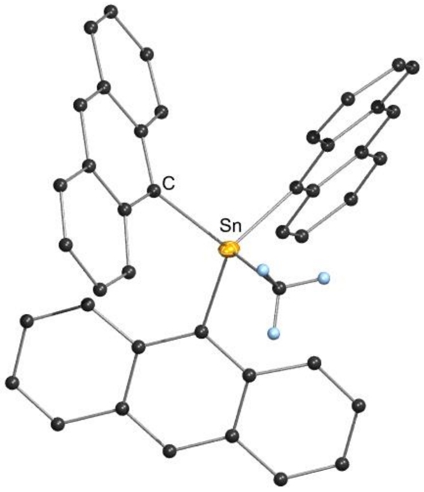

***Figure 15:** Crystal structure of tri-9-anthracenyltin methyl **A_3SnMe (45)**. All non-carbon atoms shown as 30 % shaded ellipsoids. Hydrogen atoms removed for clarity.*

3.2.1.9.8 a17- i) 1.1 eq. MeLi, TMEDA (0 °C) ii) 1.2 eq. $SnCl_4$ (RT)

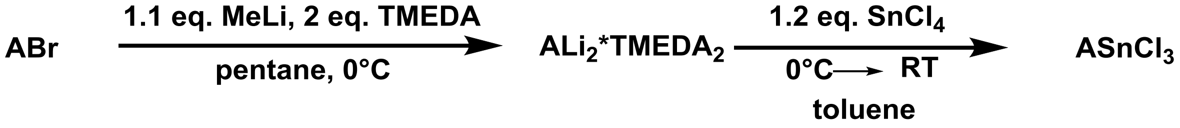

***Scheme 73:** Reaction sequence for **a17**.*

In order to avoid methylation of the anthracenyltin halogenide formed in the reaction, the amount of employed MeLi equivalents was reduced from 2.2 to 1.1 (Scheme 73). The procedure is according to the description for ***a14***, however reaction monitoring *via* ^{119}Sn NMR (C_6D_6) revealed the following signals: -43.7, -50.4, -87.0 ppm which might be assigned as **A_3SnCl** and **$ASnCl_3$**. However, peak integration in the ^{1}H NMR showed the presence of 50 % unreacted **ABr**, as well as 30 % anthracene as a side product. If the educt (**ABr**) is dissolved in a mixture of diethyl ether and pentane and subsequently converted with MeLi in the absence of TMEDA, no lithiation reaction was observed.

3.2.1.9.9 a18- i) 2 eq. t-BuLi (RT) ii) 1 eq. SnI_4 (RT)

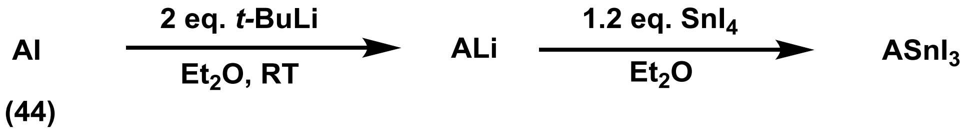

Scheme 74: *Reaction sequence for* ***a18****.*

9-Iodoanthracene (**44, AI**) was synthesized according to literature procedure converting 9-bromoanthracene (**ABr**) with 1.38 eq. of *n*-BuLi at room temperature in diethyl ether to realize the formation of 9-lithioanthracene (**ALi**), which was subsequently converted with excess of SnI_4 to result in the desired **$ASnI_3$** (Scheme 74).[217] Since **AI** was able to be synthesized in reasonable yields and high purity (63 % after recrystallization, 95 % purity), it is obvious that the lithiation reaction is feasible implementing the described procedure. Byproducts, including anthracene, 9-butylanthracene, 9,10-dibutyl-9,10-dihydroanthracene and unreacted 9-bromoanthracene (**ABr**) could be removed entirely by sublimation. By using 9-iodoanthracene **AI** (**44**) as educt and SnI_4 as electrophile instead of $SnCl_4$, the formation of halogen mixtures was avoided. When SnI_4 is added to **ALi** and stirred at room temperature a yellow precipitate was formed. The latter was filtered off and subjected to ^{119}Sn NMR showing the following signals ($CDCl_3$): -222, -437 ppm. These shifts are comparable to those reported for the phenyl derivatives: phenyl$_2$$SnI_2$ (-246 ppm) and phenylSnI_3 (-475 ppm). The ^{1}H NMR did not show anthracene or unreacted **44**. Di-9-anthracenyltin diiodide **A_2SnI_2** (**19**) could be recrystallized from chloroform (Figure 16). In contrast, the filtrate mainly showed **AI** (**44**) and anthracene.

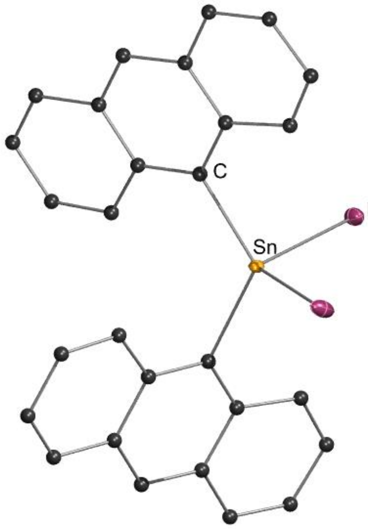

Figure 16: *Crystal structure of di-9-anthracenyltin diiodide* ***A_2SnI_2*** *(**19**). All non-carbon atoms shown as 30 % shaded ellipsoids. Hydrogen atoms removed for clarity.*

3.2.1.9.9.1 a19- i) 1.38 eq. n-BuLi (RT) ii) 1 eq. SnI_4 (RT)

$$\mathbf{AI} \xrightarrow[\text{Et}_2\text{O, RT}]{1.38\text{ eq. } n\text{-BuLi}} \mathbf{ALi} \xrightarrow[\text{Et}_2\text{O}]{1\text{ eq. SnI}_4} \mathbf{ASnI_3}$$

(44)

Scheme 75: *Reaction sequence for* ***a19****.*

AI (**44**) was converted with 1.38 eq. of *n*-BuLi to form **ALi** which was then added to a solution of SnI_4 in diethyl ether to form a dark red reaction mixture containing a yellow precipitate which was isolated by filtration (Scheme 75). The filtrate contained anthracene and unreacted **AI** (**44**) according to ^{1}H NMR. Thus, the synthesized anthracenyltin derivatives only exhibit poor to no solubility in diethyl ether. Therefore, the solid was taken up in chloroform to precipitate salts which were removed and the filtrate subjected to ^{119}Sn NMR measurements showing the following signals in $CDCl_3$: -221.5, -223.6 and -438.4 ppm which correspond to **A_2SnI_2** (**19**) at -222 and **$ASnI_3$** at -438 ppm. Di-9-anthracenyltin diiodide **A_2SnI_2** (**19**) (Figure 16), as well as tri-9-anthracenyltin iodide **Ar_3SnI** (**11**) (Figure 17) could be recrystallized from the mixture using chloroform at 4 °C giving rise to the shift at -224 ppm. However the main product **$ASnI_3$** remained in solution and could not be recrystallized.

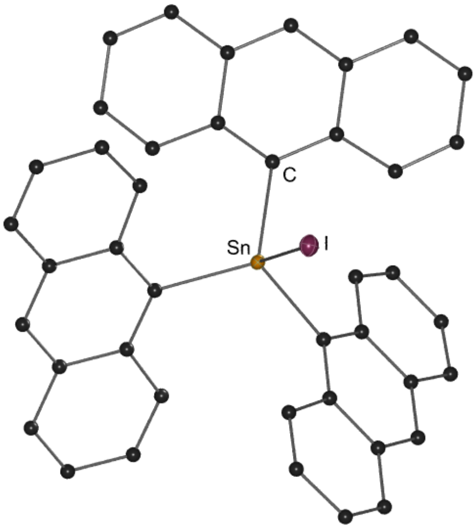

Figure 17: *Crystal structure of tri-9-anthracenyltin iodide* ***Ar_3SnI (11)****. All non-carbon atoms shown as 30 % shaded ellipsoids. Hydrogen atoms removed for clarity.*

3.2.2 Synthesis of $ASnCl_3$ *via* the Grignard Route (*b*)

A second common method to obtain aryltin trichlorides, which has been applied successfully for a range of compounds, is the formation of a Grignard species (ArylMgBr) which is further converted to the corresponding tetraaryl stannane ($Aryl_4Sn$). The latter serves as starting material in the formation of the desired aryltin trichloride ($ArylSnCl_3$).[80] This chapter sums up the attempts towards anthracenyltin halogenides *via* a Grignard reaction sequence (Scheme 76).

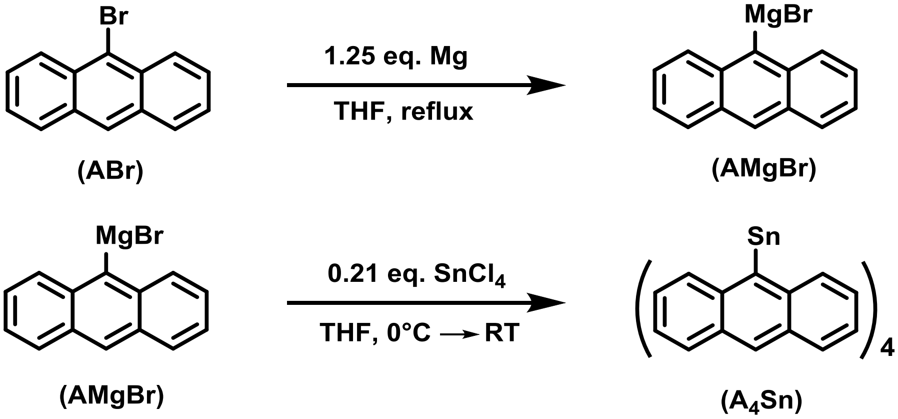

Scheme 76: *Formation of anthracenyltin compounds via a Grignard reaction* (***b1***).

The formation of **AMgBr** (9-anthracenylmagnesium bromide) could be achieved by adding dibromoethane to start the reaction. However, the reaction mixture did not turn as dark brown as seen for other arylMgBr such as *o*-tolylMgBr, 1-naphthylMgBr or 2,6-xylylMgBr. The yield of the **AMgBr** was estimated as 80 % to further calculate 0.23 eq. of $SnCl_4$ in the subsequent reaction step forming $\mathbf{A_4Sn}$ (Scheme 76). After removing THF under reduced pressure, a brown solid could be afforded. ^{119}Sn NMR in $CDCl_3$ revealed two ^{119}Sn NMR shifts at -124.0 and 145.9 ppm. The shifts could correspond to a mixture of different degrees of aryl substitution or to products of a halogen interchange. Recrystallization attempts from pentane, toluene, ethyl acetate and diethyl ether did not give any results.

In order to successfully elucidate the aryl substitution degree, the brown solid was subjected to a hydrogenation reaction using $LiAlH_4$ (***b1****) (Scheme 77). Therefore, the product mixture was converted with an excess of $LiAlH_4$ at -30 °C in diethyl ether (Scheme 77). The excess of $LiAlH_4$ was quenched with degassed water, phases were separated, the organic phase dried and the diethyl ether removed under *vacuo*. The resulting solid was subjected to ^{1}H as well as to a ^{119}Sn hydrogen coupled NMR measurement in C_6D_6 revealing that anthracene was the main product which has not been affected by addition of $LiAlH_4$. However, also two sets of $^{1}J(^{1}\text{H-}^{119}\text{Sn})$ and $^{1}J(^{1}\text{H-}^{117}\text{Sn})$ couplings could be detected with very low signal intensity. These findings are in accordance with the decoupled ^{119}Sn NMR spectrum, where the signals may be assigned to $\mathbf{A_2SnH_2}$ (-346 ppm) and $\mathbf{A_3SnH}$ (-273 ppm). The latter one could be supported by a coupled ^{119}Sn spectrum giving rise to a triplett and doublet, respectively. Recrystallization attempts from toluene were not successful.

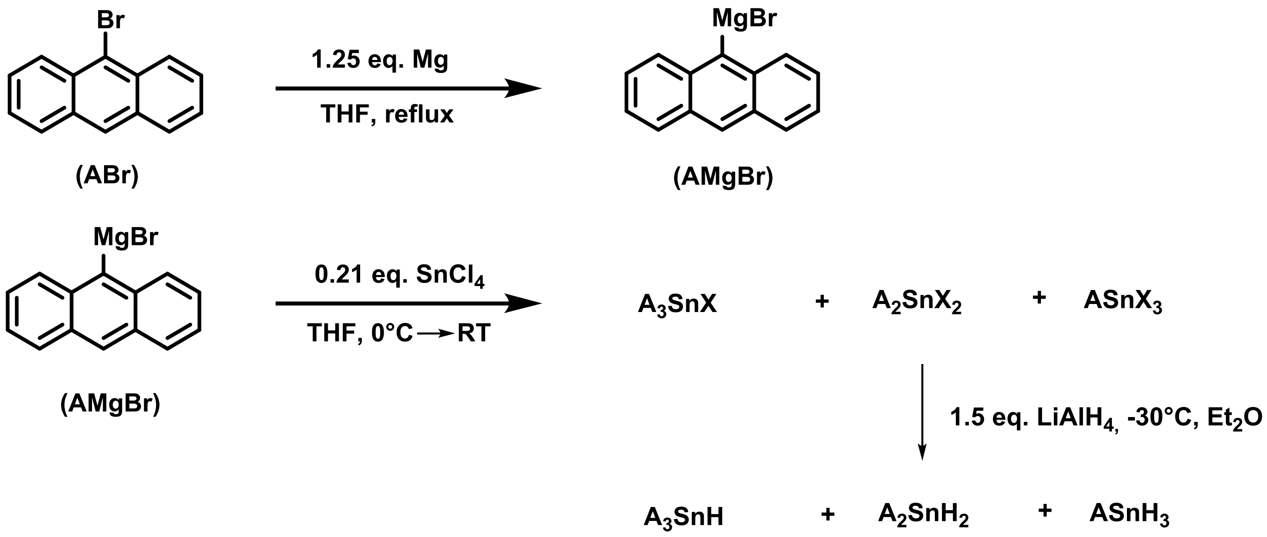
Br
1.25 eq. Mg
THF, reflux
MgBr
(ABr)
(AMgBr)
MgBr
0.21 eq. SnCl4
THF, 0°C → RT
A3SnX + A2SnX2 + ASnX3
(AMgBr)
1.5 eq. LiAlH4, -30°C, Et2O
A3SnH + A2SnH2 + ASnH3

Scheme 77: *Hydrogenation of an anthracenyltin compound mixture (**b1***).*

3.2.3 Synthesis of $ASnCl_3$ *via* a Sn(II) Species (*c*)

Following the procedure published by Saito and coworkers, who described the formation of aryltin trichlorides exhibiting sterically demanding aryl groups, **ABr** was lithiated with 1.1 eq. of *n*-BuLi in THF at -78 °C in order to form **ALi**.[112] The latter was then reacted with $SnCl_2$ to generate AClSn: which should then react with CCl_4 (Scheme 78).

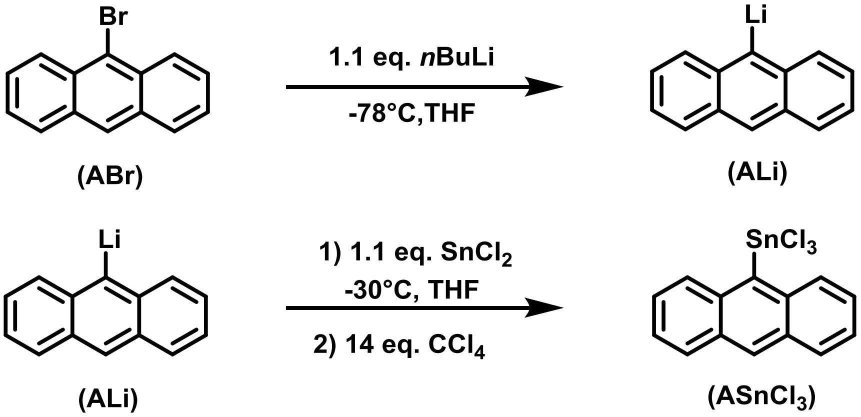
Br
1.1 eq. nBuLi
-78°C,THF
Li
(ABr)
(ALi)
Li
1) 1.1 eq. SnCl2
-30°C, THF
2) 14 eq. CCl4
SnCl3
(ALi)
(ASnCl3)

Scheme 78: *Synthesis of $ASnCl_3$ via AClSn: (Route **c**).*

After removing the solvent, the resulting brown solid was taken up in toluene leading to the formation of a precipitate. The ^{1}H NMR does not show unreacted **ABr**, however about 50 % anthracene could be found in the presence of 50 % product. The precipitate formed in toluene and taken up in $CDCl_3$ only showed marginal amounts of anthracene in the presence of product, which gave a ^{119}Sn NMR shift of -45.4 ppm. The latter may be assigned as $\mathbf{ASnCl_3}$ or $\mathbf{A_3SnCl}$ according to region in the spectrum. Apparently, the synthesized product showing a ^{119}Sn shift of -45.4 ppm has a low solubility in toluene, however is well soluble in $CDCl_3$. Therefore it was easily separated from anthracene which is well soluble in toluene. Anthracene was recrystallized from the product mixture using toluene.

3.2.4 Synthesis of $\mathbf{ASnCl_3}$ *via* Oxidative Addition (*d*)

It was attempted to subject 9-bromoanthracene (**ABr**) and 9-iodanthracene (**AI**) (**44**) to an oxidative addition using $SnCl_2$ in THF and SnI_2 in toluene, respectively (Scheme 79). After 2d of stirring at room temperature and 5d of reflux no reaction was observed.

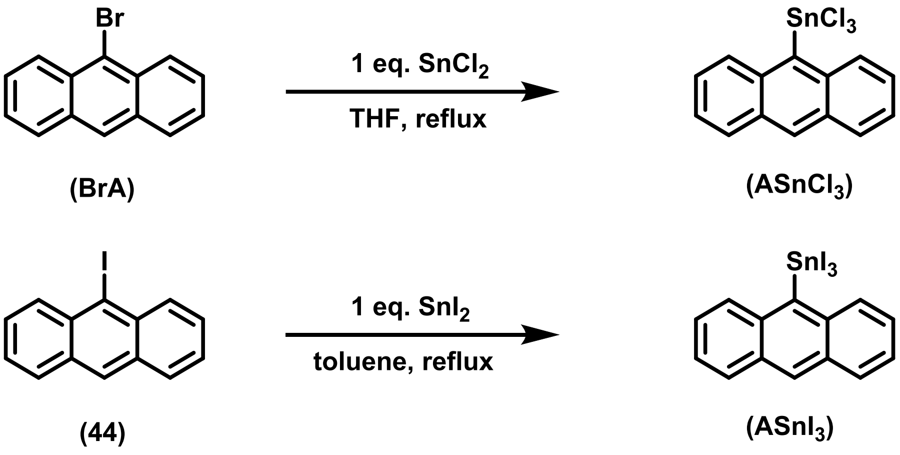

Scheme 79: *Oxidative addition of 9-bromoanthracene and 9-iodoanthracene (**44**) to $SnCl_2$ and SnI_2 (**d**).*

3.3 Conclusions

As previously reported in literature, obstacles were encountered in the synthesis of anthracenyltin compounds based on the thermodynamic stability of anthracene. This led to the formation of anthracene as a side product in the lithiation reaction of 9-bromoanthracene (**ABr**), as well as 9-iodoanthracene (**AI**). However, we could show that the lithiation needs to be carried out quickly at low temperatures to avoid anthracene or radical anion formation. A big excess of organolithium reagents should be avoided in order circumvent alkylation of the anthracenyl moiety as well as of the tin generating 9-butylanthracene (**ABu**) and tri-9-anthracenyltin butyl (**A_3SnBu**), respectively. Surprisingly, the Grignard route did not lead to useful results. Furthermore, it could be found out that the conversion of 9-lithioanthracene (**ALi**) with SnI_4 as an electrophile, instead of $SnCl_4$, reduces the generated amount of anthracene. Additionally, it could be observed that synthesized compounds exhibiting a Sn–anthracenyl bond are very likely to decompose upon heating. Thus, the applied work-up has to be chosen accordingly. Nevertheless, a series of novel 9-anthracenyltin compounds could be synthesized and characterized *via* X-ray diffraction studies and ^{119}Sn NMR. NMR assignments could be carried out comparing to already known data on similar compounds as well as after isolation by crystallization. The most highfield shifted signals were found for iodo compounds revealing signals at -438 ppm (**$ASnI_3$**) and -222 ppm (**A_2SnI_2 19**). Surprisingly, a signal at -224 ppm was found for **A_2SnI_2** (**11**), which was expected to be lowfield shifted. The signals found for the chlorinated derivatives are in accordance with the shift sequence reported for less encumbered aryltin species. Hence, **A_2SnCl_2** (**17**) is the most high filed shifted at -92 ppm, followed by **A_3SnCl** (**8**) at -85 ppm and **$ASnCl_3$** (**28**) at -45 ppm.

4 Stabilizing, Non-covalent Interactions in the Solid State Structure of Novel Aryltin Hydrides and Halogenides

Graphical Abstract

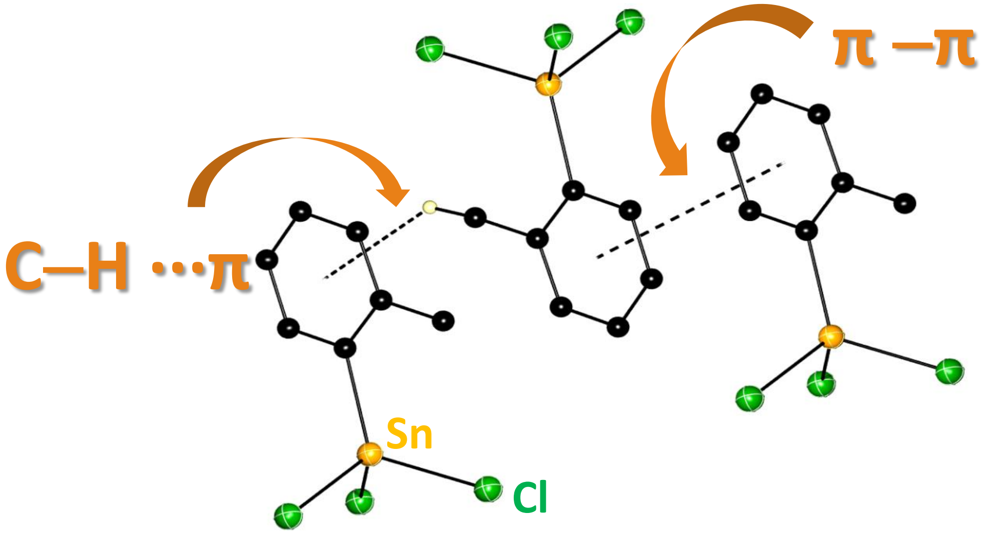

Abstract

A group of novel aryltin chlorides, bromides, and hydrides (Ar_nSnY_{4-n}*) (Ar= o-tolyl, 2,6-xylyl, mesityl, 1-naphthyl, 2-naphthyl, p-biphenyl p-*^{n}*butylphenyl, 9-anthracenyl, Y= Cl, Br, I, H) have been synthesized and structurally characterized via X-ray diffraction. These compounds display non-covalent intermolecular interactions in the form of edge to face, π–π stacking and C–H···π interactions resulting in discrete arrangements in the solid state. The strength of these interactions and their effect on resulting structural parameters, as well as the consequence of the aromatic substituent, on the type of interactions present, will be highlighted and discussed.*

4.1 Introduction

The synthesis and detailed characterization of various tetraaryl stannanes (Ar_4Sn) exhibiting aliphatic substituents on the aromatic ring *via* a Grignard reaction pathway has been well established and is reported in detail in Chapter 2.[80,185] In the case of 9-anthracenyltin compounds a conversion of either 9-bromoanthracene or 9-iodoanthracene using organo lithium reactants has been carried out as described in detail in Chapter 3. These compounds serve as starting materials for the generation of aryltin halogenides (Ar_nSnX_{4-n}) which themselves act as major precursors for the formation of highly oxygen and temperature labile aryltin hydrides. Hence, the majority of crystallographically studied aryl substituted tin species reported have been tetraaryl stannanes[61,225-230] and aryltin mono-[77,188,231-236] and dichlorides.[142,237-243] However, solid state examples of trichlorides are limited and the only aryltin hydride species to have been characterized crystallographically is mesityl$_2$SnH$_2$ (mesityl = 2,4,6-trimethylphenyl).[8] Chapter 2 reports on the synthesis, detailed characterization and DFT studies of novel aryltin chloride and hydride species.[80] Their potential use as starting materials for polyarylstannanes provided motivation to establish the generation of aryltin trihydrides displaying a hitherto more or less neglected compound class of organotins. On the way towards these crucial starting materials, we were able to generate a large variety of aromatic tin compounds as well as elucidating their solid state structure *via* single crystal X-ray crystallography. While not previously mentioned in literature, aryltin chlorides and hydrides exhibit non-covalent interactions in the solid state stemming from the aromatic substituents. The role of aromatic non-covalent interactions in the stabilization of compounds in solid state and their importance in chemical and biological processes have been well documented.[244-248] However, their presence and ultimately their effect on aryltin species have never been studied. In an effort to expand the existing library of compounds and study the underlying factors leading to solid state structures, we present a series of novel aryltin compounds with aryl substituents ranging in steric demand from *o*-tolyl to polyaromatic substituents such as naphthyl and 9-anthracenyl (**3,5,6,8,9,11,14,15,16,17,19,21,23,24,26,27,28**). In addition, a novel aryltin monohydride species 2,6-xylyl$_3$SnH (**30**) as well as the second solid state structure of an organotin trihydride (mesitylSnH$_3$ **40**) are reported (Table 7). The types of non-covalent interactions present in these systems will be highlighted and compared to previously reported compounds. In addition, the nature of the aromatic substituent and its direct effects on the type of electrostatic interaction that arises in these structures will be discussed.

Table 7: *Summary of presented compounds in Chapter 4.*

	Compound	no.
Ar_4Sn	$phenyl_4Sn$	**2**
	p-^{n}butylphenyl$_4$Sn[63]	**3**
	1-naphthyl$_4$Sn[63,80]	**5**
	2-naphthyl$_4$Sn[63,80]	**6**
Ar_3SnCl	phenyl$_3$SnCl	**7**
	9-anthracenyl$_3$SnCl	**8**
Ar_3SnBr	2,6-xylyl$_3$SnBr[63]	**9**
	mesityl$_3$SnBr	**10**
Ar_3SnBr	9-anthracenyl$_3$SnI	**11**
Ar_2SnCl_2	*p*-^{n}butylphenyl$_2$SnCl$_2$	**13**
	p-biphenyl$_2$SnCl$_2$[80]	**14**
	1-naphthyl$_2$SnCl$_2$[80]	**15**
	2-naphthyl$_2$SnCl$_2$ [80]	**16**
	9-anthracenyl$_2$SnCl$_2$	**17**
Ar_2SnBr_2	mesityl$_2$SnBr$_2$	**18**
Ar_2SnI_2	9-anthracenyl$_2$SnI$_2$	**19**
$ArSnCl_3$	*o*-tolylSnCl$_3$ [63,80]	**21**
	2,6-xylylSnCl$_3$ [80]	**23**
	mesitylSnCl$_3$	**24**
	1-naphthylSnCl$_3$[63,80]	**26**
	2-naphthylSnCl$_3$[63]	**27**
	anthracenylSnCl$_3$	**28**
Ar_3SnH	phenyl$_3$SnH[131]	**29**
	2,6-xylyl$_3$SnH[63]	**30**
Ar_2SnH_2	phenyl$_2$SnH$_2$	**31**
$ArSnH_3$	mesitylSnH$_3$	**40**

4.2 Results and Discussion

For the generation of aryltin halogenides and hydrides (**12-16,21-27,31-41**) the corresponding tetraaryl stannane (**1-6**) was synthesized first and then used for all further conversions (Scheme 55, Chapter 2). In each case, the commercially available arylbromide was converted into the Grignard reagent in THF or Et_2O, respectively and subsequently treated with $SnCl_4$ in order to generate the corresponding tetraaryl stannane (Ar_4Sn).[185] The synthesis of tetraaryl stannanes as well as their use as precursors in the generation of aryltin halogenides and hydrides have been well established and are discussed in detail in Chapter 2 (Scheme 55).[80,185] In the case of 9-anthracenyltin compounds a conversion of either 9-bromoanthracene or 9-iodoanthracene using organo lithium reactants has been carried out as described in detail in Chapter 3.

4.2.1 Crystallographic Studies

The presence of aromatic secondary interactions and their importance as stabilizing factors for these aryltin derivatives in the solid state has been rarely discussed or simply overlooked. Specifically, interactions attributed to the aromatic substituents including π–π stacking, edge to face or C–H···π interactions have been neglected. Figure 18 summarizes the types of aromatic non-covalent interactions and acceptable ranges found in biological and organic systems.[244-246] All novel aryltin compounds presented display non-covalent interactions in the solid state through the aromatic substituents. These stabilizing interactions are described and compared to those present in previously reported species. In addition, interactions for model aromatic systems (benzene, toluene, naphthalene) are included for comparison. The crystallographic data and details for all compounds presented can be found in Chapter 13.1.

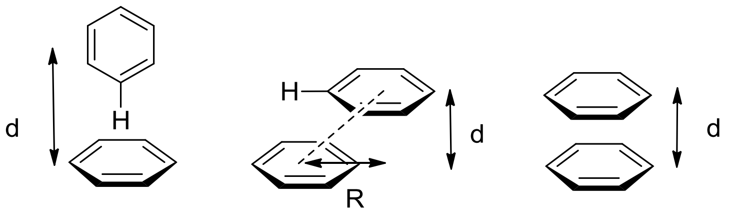

a) edge to face d = 2.4–3.1 Å

b) parallel displaced d = 3.4–3.6 Å R = 1.6–1.8

c) C–H···π d = 2.3–3.4 Å

Figure 18: *Types of π–π interactions.*

4.2.1.1 Tetraaryl Stannanes (2-6)

Compounds *p*-^{n}butylphenyl$_4$Sn (**3**), 1-naphthyl$_4$Sn (**5**), 2-naphthyl$_4$Sn (**6**) are comparable to previously reported tetraaryl stannanes (Table 8). Each Sn atom is in a near tetrahedral environment with C−Sn−C angles ranging from 107-114°. With respect to averaged Sn−C bonds, these fall within a narrow range of 2.13-2.15 Å and are not affected by the degree of bulkiness caused by the organic substituent on Sn. In most cases and as seen for phenyl$_4$Sn (**1**),[225] tetraaryl stannanes crystallize in high symmetry space groups, mainly tetragonal, and display highly ordered packing motifs. These consist of columns of symmetry related molecules. This packing motif is also seen in 2-naphthyl$_4$Sn (**6**) (Figure 19), which crystallizes in the I-4 space group. For this compound, each of these columns consists of interlocking neighboring molecules by edge to face interactions (2.50 Å) through the naphthyl substituents (Table 8). These values fall within range for edge to face interactions found in biological and organic systems (2.4-3.1 Å).[244,245] While not reported in literature, slightly longer interactions are observed for phenyl$_4$Sn (**1**) (2.95 Å). In the case of 1-naphthyl$_4$Sn (**5**) which crystallizes in the monoclinic space group P2$_1$/n, discrete column formation is not observed in agreement with the lower symmetry (Figure 20). This results in the molecules orienting themselves to maximize interactions between neighboring molecules and numerous edge to face interactions ranging from 2.53-2.95 Å are observed. 1-naphthyl$_4$Sn (**5**) and 2-naphthyl$_4$Sn (**6**) compare well with the herringbone packing structure of naphthalene which also exhibits edge to face interactions (2.81 Å).[249]

Table 8: *List of Sn–C bond lengths and non-covalent interactions for selected tetraaryl stannanes and model aromatic system.*

	space group	**Sn–C (Å) (avg.)**	**edge to face (Å)**	**C–H···π (Å)**
phenyl$_4$Sn [225] (**2**)	P42$_1$c	2.14(5)	2.86–3.14	—
o-tolyl$_4$Sn [226]	P42$_1$c	2.15(5)	—	3.36
m-tolyl$_4$Sn[227]	I4$_1$/a	2.15(3)	3.13	—
p-tolyl$_4$Sn[228]	I4	2.15(6)	2.78	3.22
3,5-xylyl$_4$Sn[229]	P42$_1$c	2.13(5)	—	3.39
2,4-xylyl$_4$Sn [61]	P1	2.14(2)	3.07	2.95–3.39
p-ethylphenyl$_4$Sn[230]	C2/c	2.13(4)	3.21	3.24
p-^{n}butylphenyl$_4$Sn (**3**)	P-1	2.14(2)	2.96	2.91
p-^{t}butylphenyl$_4$Sn[230]	P4$_2$/n	2.14(5)	2.98	—
1-naphthyl$_4$Sn (**5**)	P2$_1$/n	2.15(6)	2.53–2.95	—
2-naphthyl$_4$Sn (**6**)	I-4	2.14(3)	2.50–3.15	—
benzene[248]	Pbca	—	2.84	—
toluene[248]	P2$_1$/c	—	2.78	2.61
naphthalene[249]	P2$_1$/a	—	2.81	—

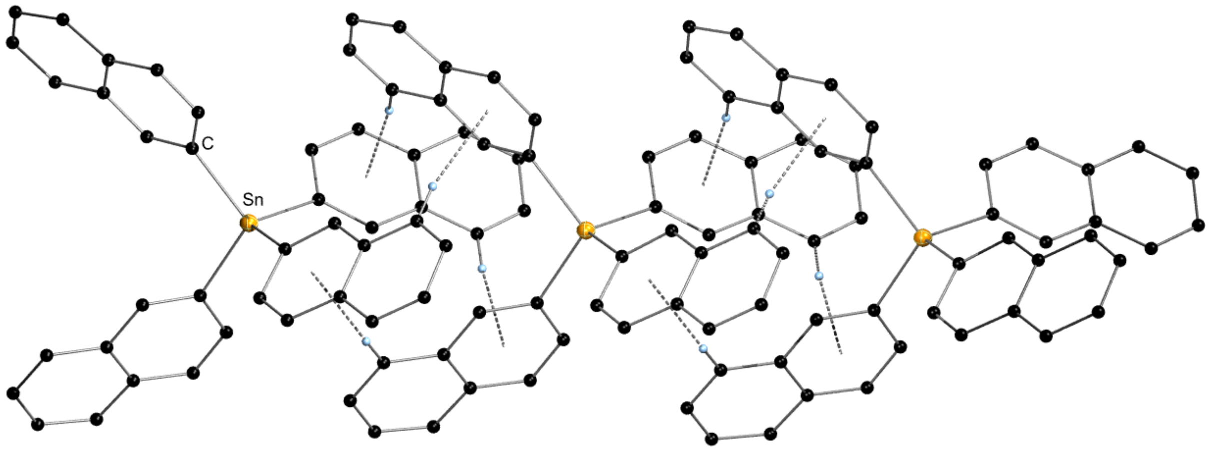

Figure 19: *Crystal packing diagram for 2-naphthyl$_4$Sn (**6**). Edge to face interactions are highlighted by dashed bonds. All non-carbon atoms shown as 30 % shaded ellipsoids. Hydrogen atoms not involved in intermolecular interactions removed for clarity.*

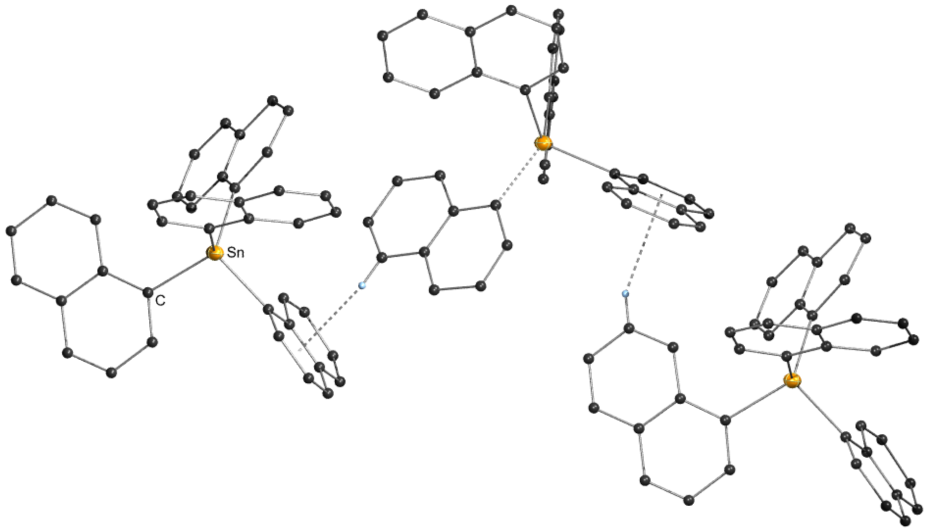

Figure 20: *Crystal packing diagram for 1-naphthyl$_4$Sn (**5**). Edge to face interactions are highlighted by dashed bonds. All non-carbon atoms shown as 30 % shaded ellipsoids. Hydrogen atoms not involved in intermolecular interactions removed for clarity.*

Introduction of ^{n}butyl groups in the *para* position of the phenyl substituent in *p*-^{n}butylphenyl$_4$Sn (**3**) results in crystallization in the low symmetry space group P-1 (Figure 21). This is due to the higher degree of rotation of the ^{n}butyl groups as compared to the ^{t}butyl groups of *p*-^{t}butylphenyl$_4$Sn[230] which is tetragonal (P4$_2$/n). In addition to the presence of edge to face interactions (2.96 Å) in compound **3**, C–H···π interactions are observed between the methylene hydrogens of the butyl substituents and the phenyl groups of neighboring molecules (2.91 Å) (Table 8). However, despite the potential for the ^{t}butyl group in *p*-^{t}butylphenyl$_4$Sn for C–H···π interactions, only an edge to face interaction (2.98 Å) is observed between the phenyl substituents of neighboring molecules.

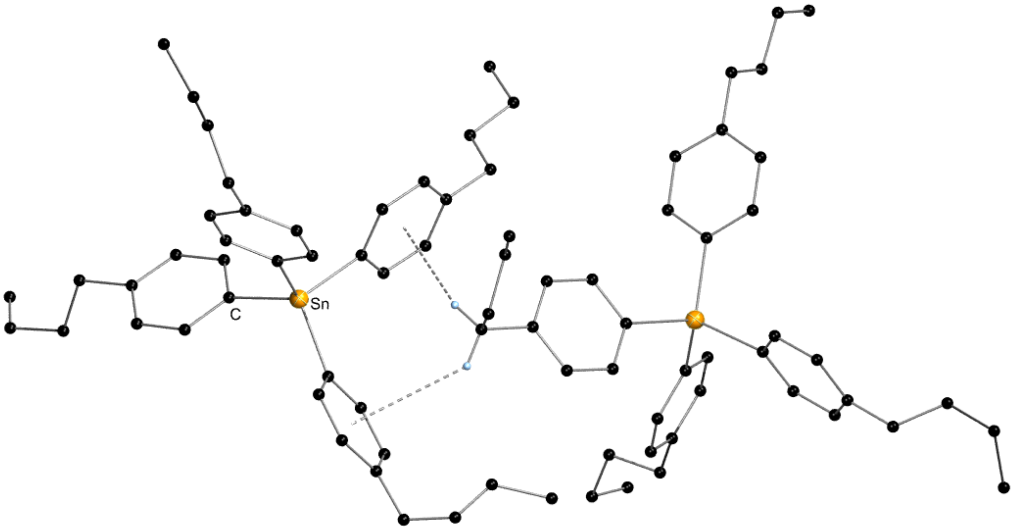

Figure 21: *Crystal packing diagram for p-^{n}butylphenyl$_4$Sn (**4**). C–H···π interactions are highlighted by dashed bonds. All non-carbon atoms shown as 30 % shaded ellipsoids. Hydrogen atoms not involved in intermolecular interactions removed for clarity.*

4.2.1.2 Aryltin Hydrides (30,40) Monohalogenides (8, 9, 11, 30)

While compounds **5** and **6** show a propensity towards edge to face interactions due to the nature of the naphthyl moiety, addition of methyl groups on the aryl substituent of Sn should lead to C–H···π interactions being preferred in packing motifs. This is indeed the case for 2,6-xylyl$_3$SnBr (**9**) (Figure 22), mesityl$_3$SnBr (**10**) (Figure 23), 2,6-xylyl$_3$SnH (**30**) (Figure 26) and mesitylSnH$_3$ (**40**) (Figure 27) where the molecules in the solid state arrange themselves in order to maximize these interactions (Table 9). It should be noted that Aryl$_3$SnCl species are better studied and therefore not included in these discussions with the exception of 9-anthracenyl$_3$SnCl (**8**) which is compared to 9-anthracenyl$_3$SnI (**11**).[188,231-233,250] As shown in Figure 22 and 23, molecules of compound xylyl$_3$SnBr (**9**) and mesityl$_3$SnBr (**10**) are arranged in a staggered formation creating chains propagated through C–H···π interactions from a methyl group and a neighboring 2,6-xylyl or mesityl substituent, respectively. Xylyl$_3$SnBr (**9**) exhibits shorter C–H···π interactions (2.778 Å) than the threefold methyl substituted derivatives **10** (3.01 Å) which is due to the interaction of the *para* located methyl group to the neighboring molecule lacking in the case of **9**. These interactions are well within range for reported C–H···π interactions (2.3-3.4 Å).[244] These latter are also visible in the solid state packing motif for toluene,[248] which in addition to edge to face interactions, (2.78 Å) exhibits closer C−H···π interactions from the methyl group (2.61 Å) (Table 9). While no Sn−Br interactions were seen between neighboring molecules, the closest distances being well over 8 Å, C−H···Br interactions were observed (3.03-3.01 Å) between chains. As compared to phenyl$_3$SnBr (2.11(8) Å), a slight increase in the average Sn−C bond lengths is seen for 2,6-xylyl$_3$SnBr (**9**) (2.16(8) Å) and mesityl$_3$SnBr (**10**) (2.17(5) Å) consistent with increased steric bulk around the Sn center due to the methyl groups at the 2 and 6-positions of the aryl substituent (Table 9). This increased steric bulk around the Sn center is also manifested by an increased Sn−Br bond in 2,6-xylyl$_3$SnBr (**9**) and mesityl$_3$SnBr (**10**) (2.547(1) Å) as compared to phenyl$_3$SnBr (2.495(2) Å). While 2,6-xylyl$_3$SnBr (**9**) does not exhibit any edge to face interactions within acceptable ranges, lack of methyl groups in Ph$_3$SnBr allows for very close contacts (2.63 Å).

Table 9: *Selected bond lengths and angles of aryltin hydrides and monohalogenides.*

	space group	**Sn–C (Å) (avg.)**	**Sn–X (Å) (avg.)**	**edge to face (Å)**	**π–π interaction (Å)**		**C–H···π (Å)**	**C–H···X (Å)**	**Sn–H···π (Å)**
					d	**R**			
phenyl$_3$SnH[131]	P2$_1$/c	2.141(4)	1.13(5)	2.78	—	—	—	—	3.09
2,6-xylyl$_3$SnH (**30**)	P-1	2.162(5)	—	2.87	—	—	2.70–2.81	—	—
mesityl$_2$SnH$_2$[8]	C2/c	2.154(3)	1.669(2)	—	—	—	2.70–2.75	—	—
phenyl$_2$SnH$_2$ (**31**)	P2$_1$/c	2.134(9)	1.65(6)	2.86	—	—	—	—	—
mesitylSnH$_3$ (**40**)	P-1	2.149(5)	1.658(8)	—	3.59	1.44	2.67-2.85	—	—
tripSnH$_3$	P2$_1$/c	2.155(1)	1.627(2)	—	—	—	2.77		3.05
phenyl$_3$SnCl[231,251-253]	P2$_1$/c	2.116(4)	2.356(4)	2.67–2.76	—	—	—	2.95	—
o-tolyl$_3$SnCl[254]	P2$_1$/n	2.132(3)	2.376(10)	3.01–3.32	—	—	2.91	—	—
m-tolyl$_3$SnCl[188]	R3	2.123(1)	2.379(2)	—	—	—	—	—	—
p-tolyl$_3$SnCl[231]	P-1	2.118(18)	2.373(6)	—	—	—	2.85–3.14	3.13	—
p-^{t}butylphenyl $_3$SnCl[233]	C2/c	2.349(2)	2.108(6)	2.99	—	—	3.19	3.08	—
3,5-xylyl$_3$SnCl[188]	R3c	2.124(2)	2.358(4)	—	—	—	—	—	—
mesityl$_3$SnCl[250]	P21/n	2.158(5)	2.390(13)	3.11	—	—	—	2.85	—
9-anthracenyl$_3$SnCl (**8**)	Pa-3	2.154(3)	2.426(13)	2.99	—	—	—	2.79-2.83	—
phenyl$_3$SnBr[255]	P2$_1$/c	2.114(8)	2.495(2)	2.63–3.14	—	—	—	3.03	—
2,6-xylyl$_3$SnBr (**9**)	P2$_1$/c	2.164(8)	2.547(3)	—	—	—	2.78	3.03	—
mesityl$_3$SnBr (**10**)[256]	P-1	2.169(5)	2.547(1)	3.17	—	—	3.005	2.96	—
phenyl$_3$SnI[257]	P-1	2.124(3)	2.705(2)	2.88–3.14	—	—	—	—	—
mesityl$_3$SnI[258]	P-1	2.165(2)	2.752(2)	—	—	—	3.38	2.99	—
9-anthracenyl$_3$SnI (**11**)	Pbca	2.185(3)	2.763(4)	2.98–2.76	3.40	1.69	—	—	—

X= H,Cl,Br,I Mesityl= (2,4,6-Me)Ph, trip= (2,4,6-iPr)Ph

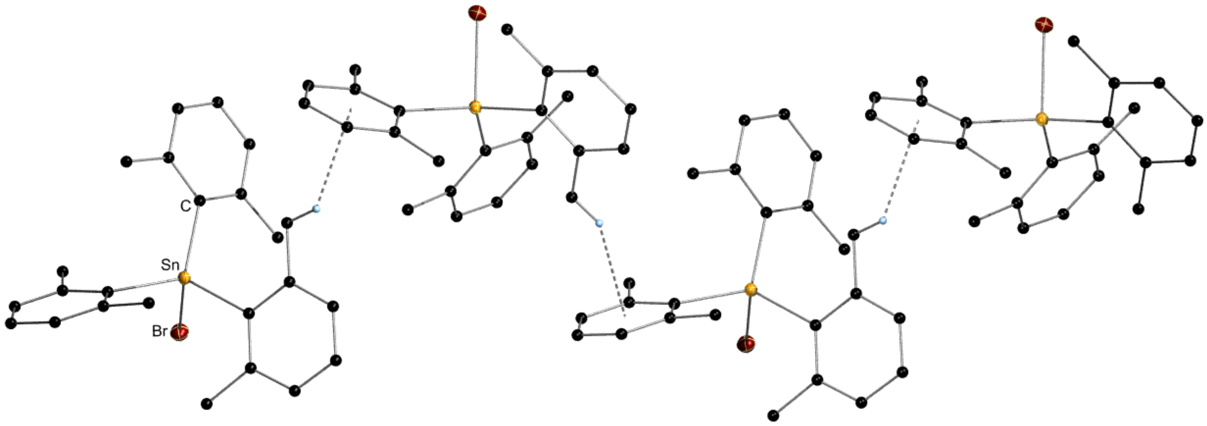

Figure 22: *Crystal packing diagram for 2,6-xylyl$_3$SnBr (**9**). C–H···π interactions are highlighted by dashed bonds. All non-carbon atoms shown as 30 % shaded ellipsoids. Hydrogen atoms not involved in intermolecular interactions removed for clarity.*

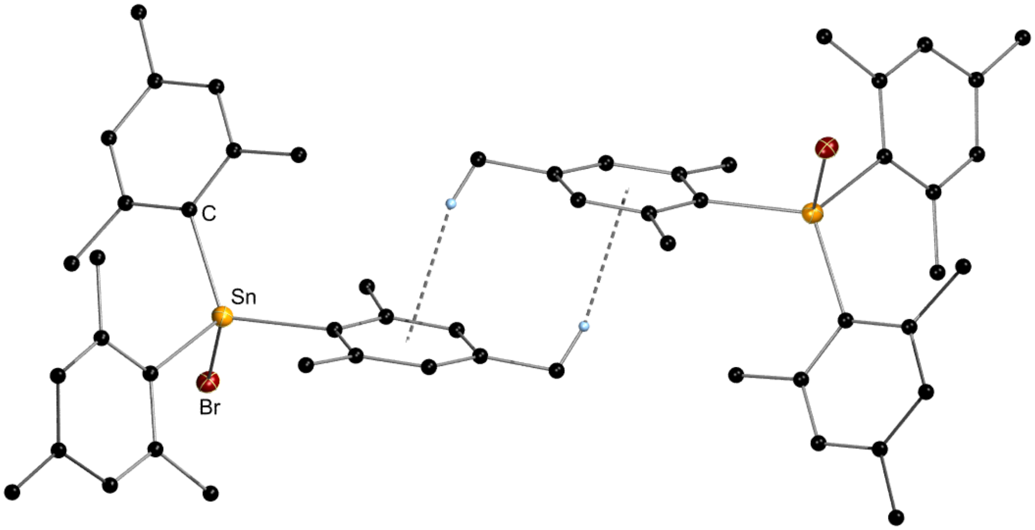

Figure 23: *Crystal packing diagram for mesityl$_3$SnBr (**10**). C–H···π interactions are highlighted by dashed bonds. All non-carbon atoms shown as 30 % shaded ellipsoids. Hydrogen atoms not involved in intermolecular interactions removed for clarity*

9-Anthracenyl$_3$SnCl (**8**) crystallizes in the highly symmetric space group Pa-3 exhibiting edge to face interactions (Figure 24). In accordance to the steric demand of the 9-anthracenyl substituent the average Sn–C bond increases from *o*-tolyl$_3$SnCl (2.132(3) Å) to **8** (2.154 (3) Å). Not surprisingly, the same trend for bond length increase in accordance with the steric demand of the polyaromatic residue is seen in the case of 9-anthracenyl$_3$SnI (**11**) compared to phenyl$_3$SnI and mesityl$_3$SnI extending from 2.124(3) Å for phenyl$_3$SnI to 2.185(3) Å (**11**) (Figure 25). This effect is also observed for the Sn–X (X= Cl, I) bond of 2.426(13) Å and 2.185(3) Å, respectively which are the longest one found in their compound family (Table 9). The found edge to face interactions of 2.99 Å for **8** and 2.98-2.76 for **11** fall in the range of distances found for comparable compounds, however the C–H···Cl is slightly shorter (2.79-2.83 Å) compared to all literature known compounds (Table 9). Apart from edge to face interactions, **11** also displays parallel displaced π–π stacking in the solid state structure with an interplanar distance of 3.40 Å and an off-set of 1.69 Å.

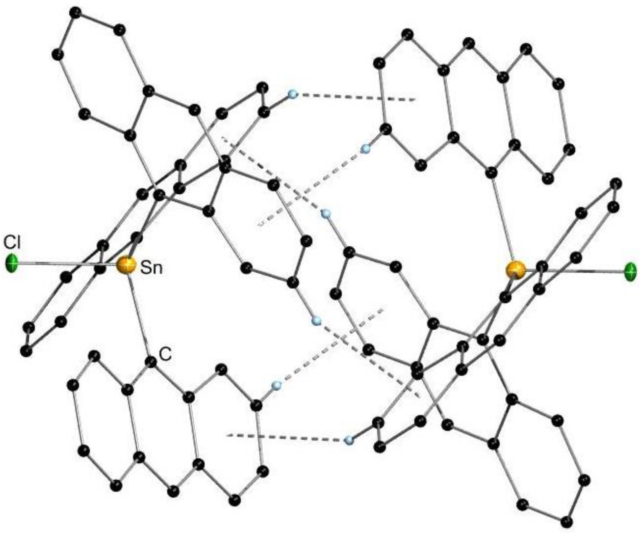

Figure 24: *Crystal packing diagram for 9-anthracenyl$_3$SnCl (**8**). C–H···π interactions are highlighted by dashed bonds. All non-carbon atoms shown as 30 % shaded ellipsoids. Hydrogen atoms not involved in intermolecular interactions removed for clarity.*

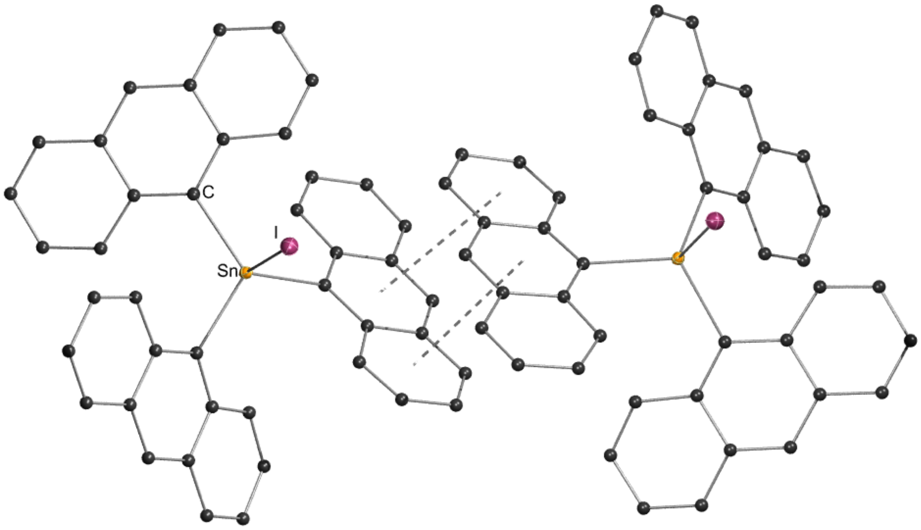

Figure 25: *Crystal packing diagram for 9-anthracenyl$_3$SnCl (**11**). $\pi-\pi$ interactions are highlighted by dashed bonds. All non-carbon atoms shown as 30 % shaded ellipsoids. Hydrogen atoms not involved in intermolecular interactions removed for clarity.*

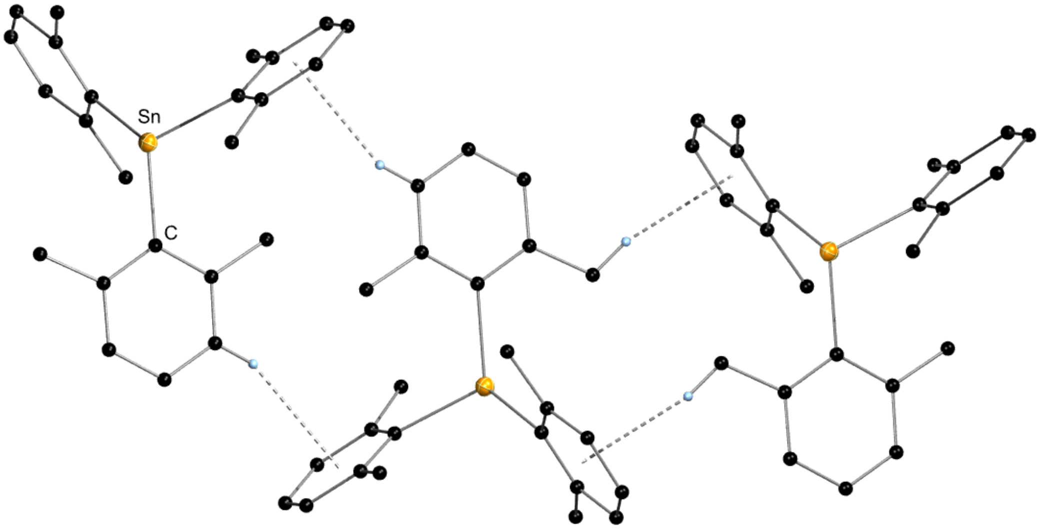

Figure 26: *Crystal packing diagram for 2,6-xylyl$_3$SnH (**30**). C–H···π and edge to face interactions are highlighted by dashed bonds. All non-carbon atoms shown as 30 % shaded ellipsoids. Hydrogen atoms not involved in intermolecular interactions removed for clarity*

Synthetic applications for triorgano tin hydrides (R_3SnH) are a well investigated field in organometallic and organic synthesis, especially in mediating radical additions, rearrangement and elimination reactions.[5] Furthermore, in the last decade, organotin dihydrides (R_2SnH_2) have been explored as precursors in the formation of polymeric materials exhibiting a linear backbone of covalently bonded tin atoms.[6-8] However, the solid state structures of organotin hydrides have not been well studied. While alkyl tin hydrides are liquid, the majority of solid state examples of aryltin hydrides known to date have been isolated by our working group and include phenyl$_2$SnH$_2$ (**31**), mesityl$_2$SnH$_{2,}$[8] phenyl$_3$SnH[131] 2,6-xylyl$_3$SnH (**30**) and mesitylSnH$_3$ (**40**) (Table 10). The only exception is tripSnH$_3$ (trip= (2,4,6-iPr)Ph) which has been reported only very recently.[259] MesitylSnH$_3$ (**40**), as the second example known for the solid state structure of aryltin trihydrides exhibits a C–H···π interaction (2.67-2.85 Å), which is comparable to the one found for tripSnH$_3$ (2.77 Å) (Figure 28). However, **40** does not show any Sn–H···π as reported for tripSnH$_3$. The solid state structure of the liquid **31** is discussed in detail in chapter 5.4.1. and thus will not be highlighted herein. As mentioned above, presence of methyl groups at the 2- and 6-position of the aryl substituent results in a slight increase of the average Sn–C bond length in 2,6-xylyl$_3$SnH (**30**) (2.162(5) Å) and mesityl$_2$SnH$_2$ (2.154(9) Å) as compared to phenyl$_3$SnH (2.141(4) Å). However, Sn–H bonds cannot be compared due to difficulties in reliably locating hydrogen atoms in difference maps as Sn is such a heavy atom. Nevertheless, packed structures of **30** (Figure 27) reveal staggered chains of alternating edge to face (2.87 Å) and C–H···π interactions (2.70-2.81 Å). The lack of these methyl substituents on phenyl$_3$SnH results exclusively in the presence of edge to face interactions, however an additional Sn–H···π interaction, 3.092(3) Å, is observed.[131] In mesityl$_2$SnH$_2$, only C–H···π interactions ranging from 2.701 and 2.75 Å are observed.

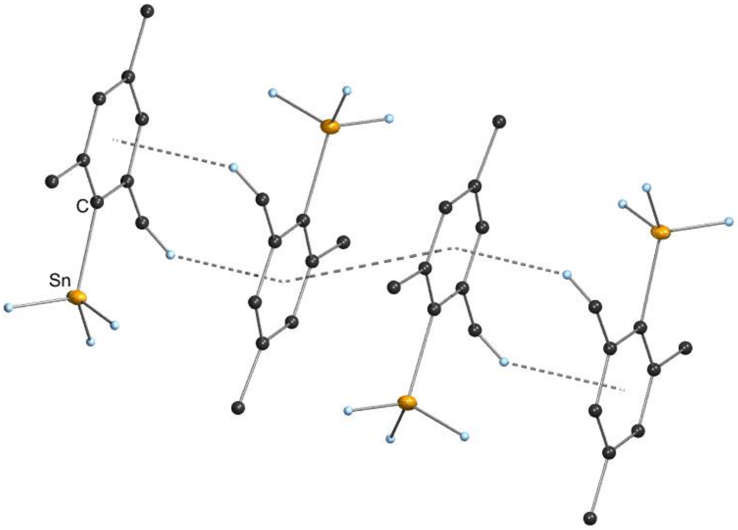

Figure 27: *Crystal packing diagram for mesitylSnH$_3$ (**40**). C–H···π interactions are highlighted by dashed bonds. All non-carbon atoms shown as 30 % shaded ellipsoids. Hydrogen atoms not involved in intermolecular interactions removed for clarity*

4.2.1.3 Aryltin Dihalogenides (14-17, 19)

Di-1-naphthyltin dichloride (**15**) (Figure 28), di-2-naphthyltin dichloride (**16**) (Figure 29) and di-*p*-biphenyltin dichloride (**14**) (Figure 30) crystallize at room temperature from ethyl acetate. Di-9-anthracenyl$_2$SnCl$_2$ (**17**) (Figure 31), as well as di-9-anthracenyl$_2$SnI$_2$ (**19**) (Figure 32) crystallize from chloroform. In each case, the tin is found in a distorted tetrahedral environment bound to two halogens and two aryl substituents. Table 10 summarizes average bond lengths and angles of **14**, **15**, **16**, **17**, **19** and of comparable aryltin dichlorides (Ar= Ph, biphenylyl, mesityl, supermesityl or Mes*, Trip). The average Sn–C bond for compound **15** (2.118(2) Å) compares nicely with Ph$_2$SnCl$_2$ (2.112(5) Å) and Mes$_2$SnCl$_2$ (2.117(2) Å), while for compound **16** (2.106(8) Å) and **14** (2.102(3) Å), the bond is slightly shorter. In the case of the 9-anthracenyl substituted compounds **19** the average Sn–C bond increases to 2.167(2) which is explained by the steric demand of the aryl residue. The average C–Sn–C angles for all three compounds do not show a significant deviation in comparison to published species. Only compound **15** shows deviations concerning the average Cl–Sn–Cl angle. The average Cl–Sn–Cl angle of **15** is 114.6(6)° which is wider than for the other species presented. The two phenyl rings of the substituents in compound (**14**) show a twisting of 38.05° with respect to each other.

Table 10: *Selected bond lengths diaryltin dichlorides.*

	space group	bond length avg. [Å]		angle avg. [°]			π–π interaction (Å)	
compound		*Sn–C*	*Sn–Cl*	*C–Sn–Cl*	*Cl–Sn–Cl*	*C–Sn–C*	d	R
phenyl$_2$SnCl$_2$ (**12**) [239]	P-1	2.112(5)	2.345(2)	107.3(2)	101.7(1)	123.9(2)	3.67	1.41
1-naphthyl$_2$SnCl$_2$ (**15**)	P2/n	2.118(2)	2.359(1)	105.2(5)	114.6(6)	116.6(11)	3.59	1.42
2-naphthyl$_2$SnCl$_2$ (**16**)	P2$_1$/n	2.106(8)	2.354(19)	108.7(2)	101.4(8)	119.1(3)	3.40	1.67
p-biphenyl$_2$SnCl$_2$ (**14**)	C2/c	2.102(3)	2.337(9)	108.0(9)	104.4(5)	119.3(17)	—	—
(biphenylyl)$_2$SnCl$_2$ [238]	P2$_1$/n	2.130(9)	2.386(3)	105.6(2)	99.71(9)	130.8(3)	—	—
mesityl$_2$SnCl$_2$ [241]	Pbcn	2.117(2)	2.414(2)	115.4(2) 102.4(2)	100.3(2)	119.7(2)	—	—
mesityl*$_2$SnCl$_2$ [243]	P2$_1$/c	2.198(4)	2.371(1)	118.2(1) 103.7(1)	95.5(1)	116.9(1)	—	—
trip$_2$SnCl$_2$ [237]	C2/c	2.147(4)	2.353(2)	100.1(1) 118.5(1)	98.0(1)	120.4(2)	—	—
9-anthracenyl$_2$SnCl$_2$ (**17**)	P21/c	2.134(6)	2.351(15)	109.6(18)	96.24(5)	119.7(2)	3.39 3.59	1.69 1.47
phenyl$_2$SnI$_2$	P21/c	2.135(2)	2.693(2)	108.5(3)	105.17(3)	116.7(4)	3.49	1.50
9-anthracenyl$_2$SnI$_2$ (**19**)	P21/c	2.167(2)	2.724(2)	106.98(5)	105.750 (7)	122.66 (7)	3.33 3.37 3.45	1.95 1.79 1.57

Mes= (2,4,6-Me)Ph, Mes*= Supermes or (2,4,6-^{t}Bu)Ph, Trip= (2,4,6-^{i}Pr)Ph

Apart from *p*-biphenyl$_2$SnCl$_2$ (**14**) not being polyaromatic, the herein presented compounds 1-naphthyl$_2$SnCl$_2$ (**15**), 2-naphthyl$_2$SnCl$_2$ (**16**), 9-anthracenyl$_2$SnCl$_2$ (**17**) and 9-anthracenyl$_2$SnI$_2$ (**19**) all exhibit parallel displaced π–π interactions as predominant stabilizing, non-covalent interaction in the solid state structure (Table 10) forming infinite linear chains between neighboring molecules.[80] These interactions fall into the range reported for benzene[244] (3.4-3.6 Å) or graphite (3.35Å).[260] 1-Naphthyl$_2$SnCl$_2$ (**15**) shows an interplanar distance (d) of 3.60 Å while 2-naphthyl$_2$SnCl$_2$ (**16**) is slightly tighter packed with a distance of 3.40 Å (Figure 28 and 29). The shortest interplanar distances are found for 9-anthracenyltin derivatives with approximately 3.4 Å for both mentioned compounds **17** and **19**. The off-sets for these polyaromatic species (X=Cl: 1.69 Å, X=I: 1.95 Å) are increased in comparison to phenyl$_2$SnX$_2$ (X=Cl: 1.41 Å, X=I: 1.50 Å) (Figure 31 and 32).

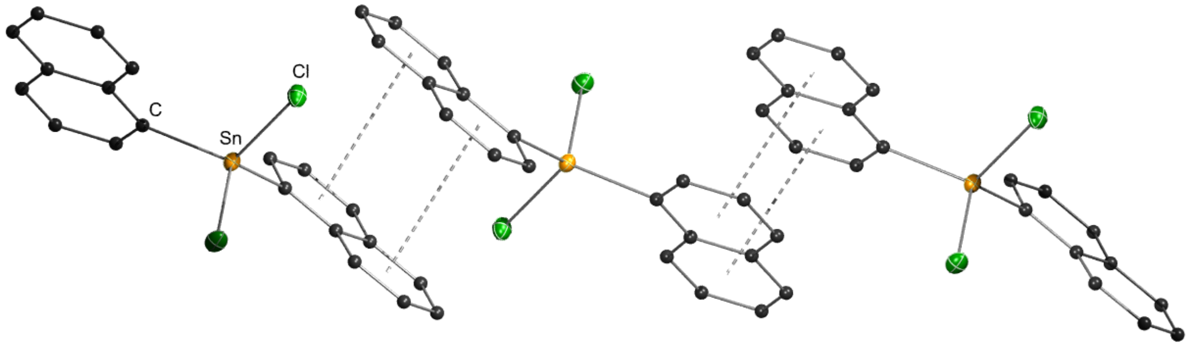

Figure 28: *Crystal packing diagram for 1-naphthyl$_2$SnCl$_2$ (**15**).[80] π–π stacking interactions are highlighted by dashed bonds. All non-carbon atoms shown as 30 % shaded ellipsoids. Hydrogen atoms not involved in intermolecular interactions removed for clarity.*

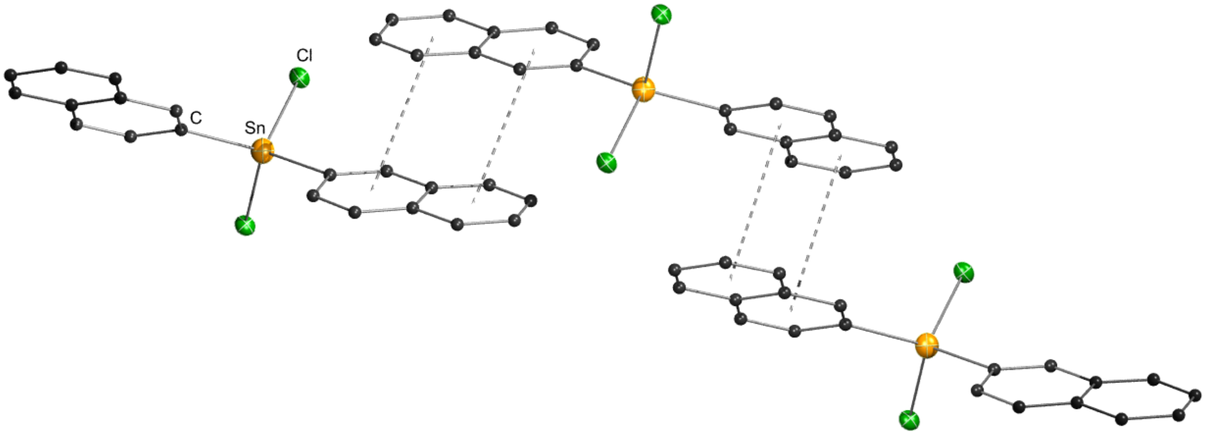

Figure 29: *Crystal packing diagram for 2-naphthyl$_2$SnCl$_2$ (**16**).*[80] *π–π stacking interactions are highlighted by dashed bonds. All non-carbon atoms shown as 30 % shaded ellipsoids. Hydrogen atoms not involved in intermolecular interactions removed for clarity.*

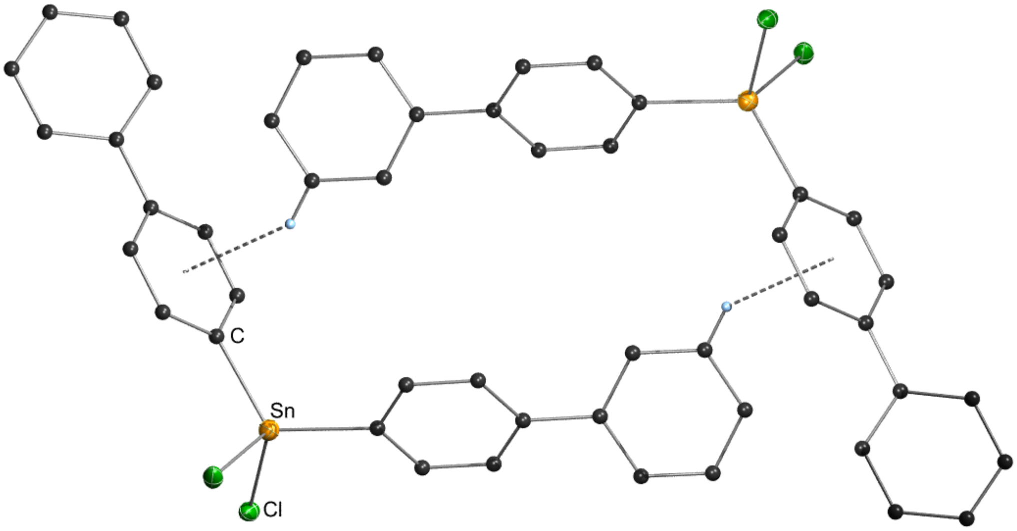

Figure 30: *Crystal packing diagram for p-biphenyl$_2$SnCl$_2$ (**14**). Edge to face interactions are highlighted by dashed bonds. All non-carbon atoms shown as 30 % shaded ellipsoids. Hydrogen atoms not involved in intermolecular interactions removed for clarity.*

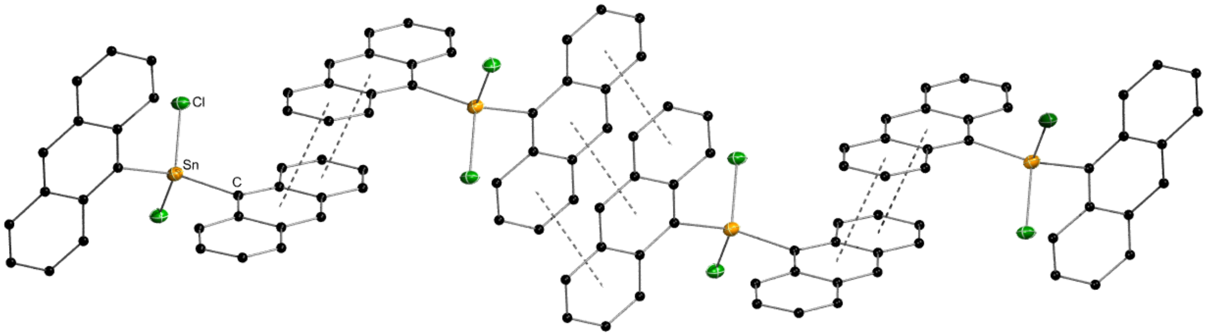

Figure 31: *Crystal packing diagram for 9-anthracenyl$_2$SnCl$_2$ (**17**). π–π stacking interactions are highlighted by dashed bonds. All non-carbon atoms shown as 30 % shaded ellipsoids. Hydrogen atoms not involved in intermolecular interactions removed for clarity.*

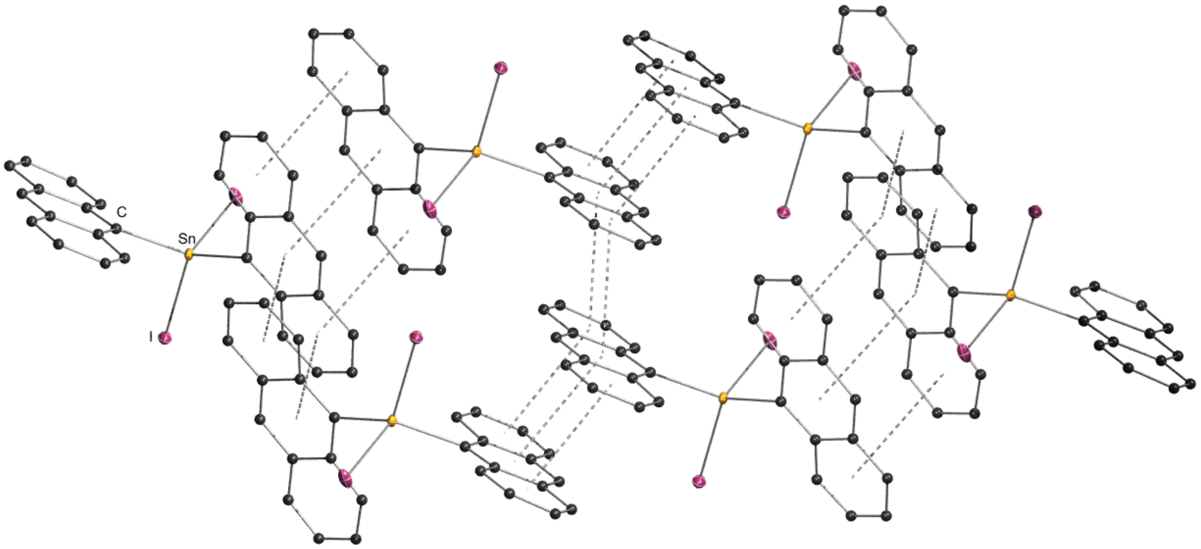

Figure 32: *Crystal packing diagram for 9-anthracenyl$_2$SnI$_2$ (**19**). π–π stacking and π···I interactions are highlighted by dashed bonds. All non-carbon atoms shown as 30 % shaded ellipsoids. Hydrogen atoms not involved in intermolecular interactions removed for clarity.*

4.2.1.4 Aryltin Trichlorides (21,23,24,26,27,28)

Until a recent contribution from this working group,[80] only two examples of structurally characterized aryl trichloro stannanes had been reported in literature (Table 11).[261,262] The compounds (2,6-Mes)PhSnCl$_3$ (Mes = (2,4,6-Me)Ph) and Ph*SnCl$_3$ (Ph*= (2,6-Trip)Ph, Trip= (2,4,6-*i*Pr)Ph) employ sterically hindered substituents containing methylated aryl moieties on the phenyl substituents only exhibit C–H···π interactions (Table 11). More recent examples include methyl substituted phenyl, naphthyl and 9-anthracenyl derivatives. In the case of 1-naphthylSnCl$_3$ (**26**)[80] and 2-naphthylSnCl$_3$ (**27**), large deviations from Sn–C or Sn–Cl bond lengths are not observed. However, the naphthyl derivatives display much different crystal packing motifs than for the aforementioned bulkier substituents. In both 1-naphthylSnCl$_3$ (**26**) (Figure 33) and 2-naphthylSnCl$_3$ (**27**) (Figure 34), the naphthyl substituents show a large propensity towards π–π stacking. The same packing motif is found for 9-anthracenylSnCl$_3$ (**28**). In each case, molecules arrange in order to maximize these interactions creating infinite layers of parallel stacked polyaromatic derivatives with a specific distance between the ring centers (d). They are also found to be parallel-displaced to each other with a certain off-set R. This is in stark contrast to the previously mentioned herringbone structure present for naphthalene, which is dominated by edge to face interactions and corresponds more to larger polycyclic aromatic molecules coronene, kekulene, or graphite.[244,260]1-NaphthylSnCl$_3$ (**26**) and 2-naphthylSnCl$_3$ (**27**) show similar interplanar distances of 3.56 Å and 3.54 Å, respectively. These findings are in accordance to a reported range of 3.4-3.6 Å for benzene[244] or 3.35 Å in graphite.[260] 2-NaphthylSnCl$_3$ (**27**) shows a slightly larger displacement I of 1.76 Å. Off-set distances for other benzyl systems are found in a range of 1.6-1.8 Å.[244] Likewise to 9-anthracenyl$_2$SnX$_2$ (**17**, **19**) (X= Cl, I), also 9-anthracenylSnCl$_3$ (**28**) as well displays the shortest intermolecular distance (3.36 Å) of all reported aryltin trichlorides and thus the most tightly packed among the latter (Figure 35). In addition to π–π stacking C–H···Cl, interactions are observed between layers for naphthyl and anthracenyl compounds (Table 11, Figures 34 and 35).

Table 11: *List of Sn–C bond lengths and non-covalent interactions for aryltin tri- and dichlorides.*

	space group	**Sn–C (Å) (avg.)**	**Sn–Cl (Å) (avg.)**	**π–π interaction (Å)**		**edge to face (Å)**	**C–H···π (Å)**	**C–H···Cl (Å)**
				d	**R**			
o-tolylSnCl$_3$ (**21**)	P-1	2.109(4)	2.132(2)	3.46	1.65	—	2.89	2.95
2,6-xylylSnCl$_3$ (**23**)[80]	Pbcn	2.123(2)	2.332(1)	—	—	—	2.74	2.91
(2,6-Mes)PhSnCl$_3$[261]	P2$_1$/c	2.128(6)	2.332(1)	—	—	3.04	2.90	2.79
phenyl*SnCl$_3$ [207]	P-1	2.155(5)	2.315(2)	—	—	—	3.15	—
mesitylSnCl$_3$ (**24**)	P-1	2.110 (6)	2.341(1)	—	—	—	2.67-2.99	—
1-naphthylSnCl$_3$ (**26**)[80]	P2$_1$/c	2.114(11)	2.324(3)	3.56	1.63	—	—	2.90
2-naphthylSnCl$_3$ (**27**)	Pnma	2.097(3)	2.306(7)	3.54	1.76	—	—	2.86
9-anthracenylSnCl$_3$ (**28**)	P-1	2.122 (6)	2.335(3)	3.36	1.41	—	—	2.79–2.84

Mesityl = (2,4,6-Me)phenyl; phenyl*= (2,6-Trip)phenyl, Trip= (2,4,6-iPr)phenyl

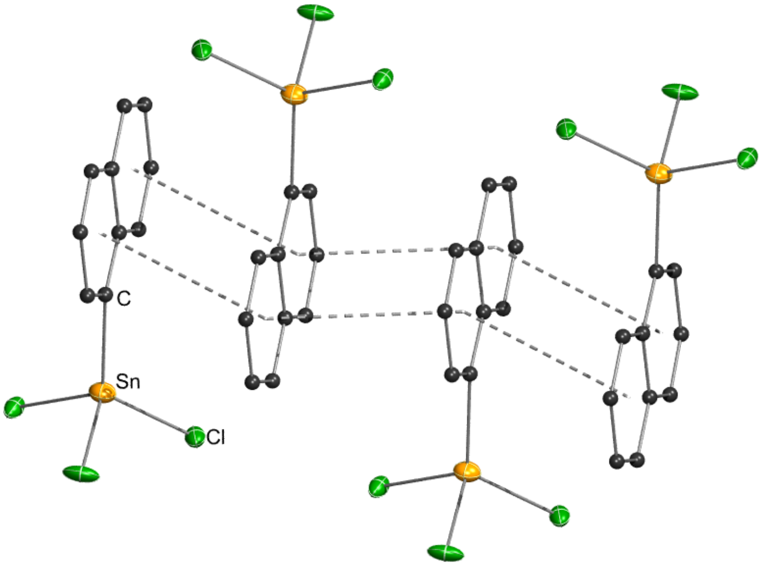

Figure 33: *Crystal packing diagram for 1-naphthylSnCl$_3$ (**26**).*[80] *π–π stacking interactions are highlighted by dashed bonds. All non-carbon atoms shown as 30 % shaded ellipsoids. Hydrogen atoms not involved in intermolecular interactions removed for clarity.*

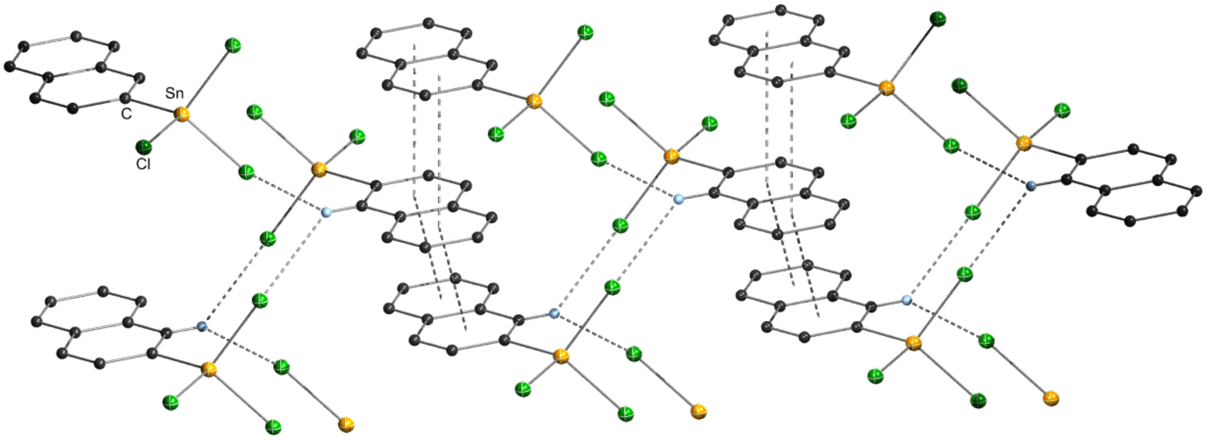

Figure 34: *Crystal packing diagram for 2-naphthyl$_2$SnCl$_2$ (**27**).*[80] *π–π stacking* and *C–H···Cl interactions are highlighted by dashed bonds. All non-carbon atoms shown as 30 % shaded ellipsoids. Hydrogen atoms not involved in intermolecular interactions removed for clarity.*

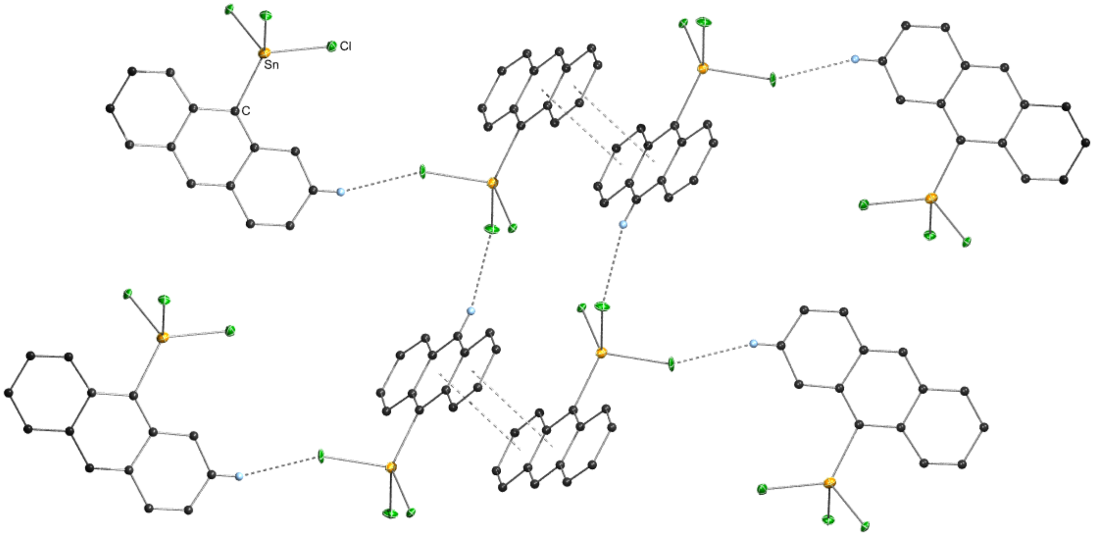

Figure 35: *Crystal packing diagram for 9-anthracenylSnCl$_3$* ***(28)****. π–π stacking and C–H···Cl interactions are highlighted by dashed bonds. All non-carbon atoms shown as 30 % shaded ellipsoids. Hydrogen atoms not involved in intermolecular interactions removed for clarity.*

Also exhibiting close π–π stacking interactions (d = 3.46, R = 1.65 Å) in the solid state is *o*-tolylSnCl$_3$ (**21**), which is a low melting solid (4 °C) and subsequently obtaining a suitable solid state structure proved challenging (Table 11). Crystal packing diagrams of *o*-tolylSnCl$_3$ (**21**) display neighboring molecules positioned to maximize C–H···π interactions from methyl groups (2.89 Å) while allowing π–π stacking interactions (Figure 36). If methyl substitution is increased as seen for 2,6-xylylSnCl$_3$ (**23**) and mesitylSnCl$_3$ (**24**), only C–H···π interactions are present (Figures 37 and 38). For **23** the latter show a distance of 2.74 Å, which is comparable to the range found for the more sterically encumbered species **24** (2.67-2.99 Å).[80] It should be noted that *o*-tolylSnCl$_3$ (**21**) displays the shortest Sn–Cl bond (2.132(2) Å) due to the lower steric hindrance afforded to the Sn atom by the *o*-tolyl substituent as compared to 2,6-xylylSnCl$_3$ (**23**) (2.123(2) Å).

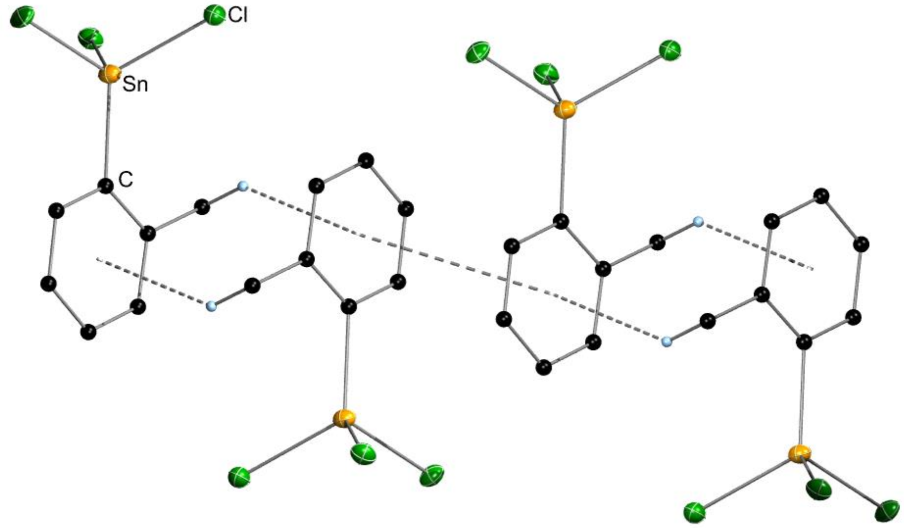

***Figure 36:** Crystal packing diagram for o-tolylSnCl$_3$ (**21**). C–H···π and π–π stacking interactions are highlighted by dashed bonds. All non-carbon atoms shown as 30 % shaded ellipsoids. Hydrogen atoms not involved in intermolecular interactions removed for clarity.*

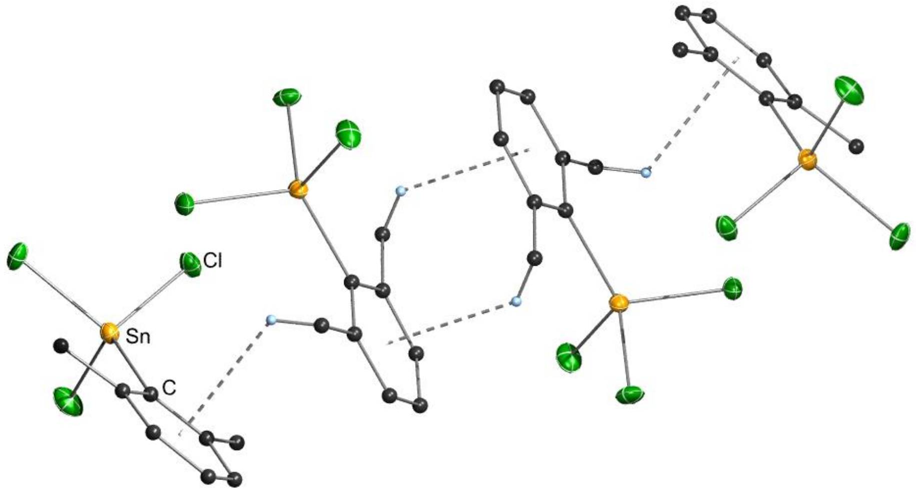

***Figure 37:** Crystal packing diagram for 2,6-xylylSnCl$_3$ (**23**).*[80] *C–H···π interactions are highlighted by dashed bonds. All non-carbon atoms shown as 30 % shaded ellipsoids. Hydrogen atoms not involved in intermolecular interactions removed for clarity.*

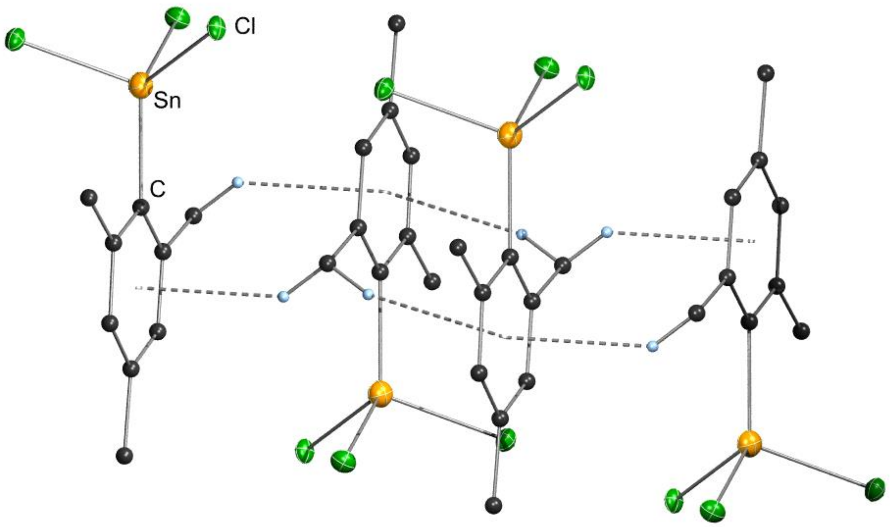

Figure 38: *Crystal packing diagram for mesitylSnCl$_3$ (**24**). C–H···π interactions are highlighted by dashed bonds. All non-carbon atoms shown as 30 % shaded ellipsoids. Hydrogen atoms not involved in intermolecular interactions removed for clarity.*

4.3 Conclusions

A series of novel organotin species containing methyl or ^{n}butyl substituted phenyl, naphthyl and anthracenyl residues have been synthesized and fully characterized by X-ray crystallography. In addition, the presence and nature of non-covalent interactions in the solid state of the presented compounds is studied and compared to those existing but never mentioned and simply overlooked in literature. Three different types of aromatic, non-covalent interactions could be detected including the most prominent edge to face interaction, a parallel displaced stacking as well as a C–H···π interaction of methyl groups to the neighboring ring system. The first one mentioned is found in the solid state structure of all presented organotins mostly in the presence of additional interactions bringing about typical packing motifs. However, the discussed tetraarylstannanes 1-naphthyl$_4$Sn (**5**) and 2-naphthyl$_4$Sn (**6**) exclusively display edge to face interaction as stabilizing element in the solid state. Substitution with aliphatic chains to the aromatic ring as seen for *p*-^{n}butylphenyl$_4$Sn (**3**) results in both, edge to face intermolecular and C–H···π interactions. Additionally, mesitylSnH$_3$ (**40**), as the second example known for the solid state structure of aryltin trihydrides exhibiting a C–H···π interaction is presented. 1- and 2-naphthylSnCl$_3$ (**26**, **27**) and similar naphthyltin mono- and dichlorides and hydrides arrange themselves in the solid state to accommodate π–π stacking interactions through the naphthyl substituents of neighboring molecules. The same packing motif is found for the sterically more encumbered 9-anthracenyl (**11**, **17**, **19**, **28**) species which form staggered structures *via* π–π interactions. The only exception not displaying the latter non-covalent interaction is 9-anthracenyl$_3$SnCl (**8**) which exclusively shows edge to face and C–H···Cl interactions. Onefold methyl substitution in the *ortho* positions of the phenyl ring, in the case of *o*-tolylSnCl$_3$ (**21**), gives rise to the coexistence of π–π stacking interactions through the aromatic rings as well as C–H···π interactions through the methyl groups and the aromatic rings of neighboring substituents as stabilizing factors. If methyl substitution is increased, as seen for 2,6-xylylSnCl$_3$ (**23**) and mesitylSnCl$_3$ (**24**), only C–H···π interactions are present.

Part B

Dehydrogenative Coupling of Aryltin Hydrides: Mechanistic Insights and Characterization of Aryl@Sn

5 Crystal Structure and Polymerization Studies of Diphenyltin Dihydride

Graphical Abstract

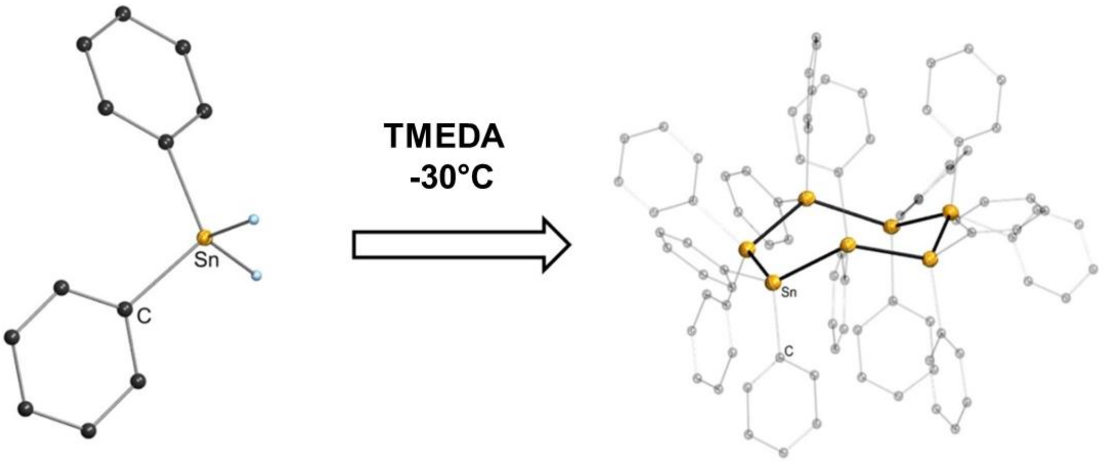

Abstract

*Diphenyltin dihydride phenyl$_2$SnH$_2$ (**31**), a colorless liquid at ambient conditions was managed to be recrystallized via an in situ recrystallization process in a glass capillary affording the first solid state structure of a liquid diorganotin dihydride. When diphenyltin dihydride (**31**) was subjected to a dehydrogenative coupling reaction using the cheap and easy to be handled amine base TMEDA (N,N,N',N'-tetramethylethylenediamine) as catalyst, not only the insoluble polystannane (phenyl$_2$Sn)$_n$ was generated. This work elucidates the soluble side products formed upon a dehydrogenative coupling reaction of phenyl$_2$SnH$_2$ **31**. In this manner, it could be proven by single crystal X-ray analysis as well as via variable temperature ^{119}Sn NMR study, that the hitherto unknown seven membered perphenylated tin ring (phenyl$_2$Sn)$_7$ **43** formed as a soluble side product in the presence of low amounts of (phenyl$_2$Sn)$_6$ **42**, when the dehydropolymerization towards (phenyl$_2$Sn)$_n$ was carried out at -30 °C. (Phenyl$_2$Sn)$_7$ (**43**) crystallized in a disordered mixture of a chair (**C**) and a twist chair conformation (**TC**), which is accordance to DFT calculations. However, these quantum mechanical calculations reveal a marginal relative energy difference between the ground state **C** and the twist chair conformation (**TC**) of 0.09 kcal/mol rationalizing the disorder found in the crystal.*

5.1 Introduction

Investigation on the synthesis and use of organotin hydrides was quite neglected until Finholt and coworkers published a convenient route to synthesize this class of compounds by treating the corresponding organotin chloride with lithium aluminumhydride ($LiAlH_4$).[12]

Thus, synthetic applications of organotin monohydrides (R_3SnH) are a well investigated field in organometallic and organic synthesis, especially in mediating radical additions, rearrangement and elimination reactions. Specifically, Bu_3SnH (TBTH, tributyltin hydride) is widely used to bring about hydrostannolysis or hydrostannation by radical chain mechanisms.[5] In the last decade, diorganotin dihydrides have been reported to efficiently serve as monomers in the preparation of polystannanes: polymeric materials exhibiting a linear backbone of covalently bonded tin atoms. Organotin hydrides perform catalytic dehydropolymerization using metal complexes based on palladium, zirconium, rhodium, lanthanides, or platinum as well as "non-traditional" iron and molybdenum alkyls as catalysts.[6-9] In most cases, the formation of polymeric products is accompanied by low molecular oligomers and cyclic products in low yields which were found to be five and six membered rings.[138,156,168] Moreover, a solvent and catalyst free dehydrogenation reaction was described as a successful route towards polystannanes, as well as five and six membered perbutylated tin rings starting with *n*-Bu_2SnH_2.[10] Furthermore, Neumann *et al.* suggested the formation of five, six or seven membered rings by means of fractional evaporation and mass chromatography of crude $(R_2Sn)_n$ mixture generated by the conversion of organotin dihydrides with *t*-Bu_2Hg. The observed ring size was found to be in accordance with the nature of R (alkyl or aryl).[263] Additionally, organotin hydrides can be used as dehydrogenative coupling educts evolving hydrogen and forming Sn–Sn bonds when reacted with amine bases as catalysts, which was also mentioned by Neumann in 1962. The dehydropolymerization was carried out exposing phenyl$_2$SnH$_2$ to dimethylformamide (DMF) as well as pyridine leading to soluble, cyclic, lower mass products in the presence of an insoluble precipitate. In the case of DMF, a five membered perphenylated ring structure was suggested, whereas conversion with the aromatic base pyridine supposedly led to the generation of (phenyl$_2$Sn)$_6$. In the same manner, using pyridine as a base, the author claimed to gain a seven membered cyclostannane, which has not been proven by any means yet. The product assignment was mainly based on degradation experiments using I_2.[264,265] These findings are in contrast to

Dräger *et al.* who published the first crystal structure of (phenyl$_2$Sn)$_6$, which was synthesized *via* a dehydropolymerization of phenyl$_2$SnH$_2$ using pyridine. The formation of (phenyl$_2$Sn)$_5$ was not observed.[266] The synthesis of aliphatic cyclostannanes was essentially achieved by subjecting the corresponding organotin dihydrides (R_2SnH_2) to catalytic dehydrogenation with dialkylstannylen diamines ($R_2[N(C_2H_5)_2]$). In this way, dimethyl, diethyl and dibutyltin dihydride led to the formation of the corresponding six membered rings, whereas conversion of the dicyclohexyl derivative gave the five membered cycle. Furthermore, *t*-buty$_2$SnH$_2$ formed a nine membered ring in presence of the dialkylstannylen diamine.[267,268] The resulting ring size apparently depends on the nature of R (alkyl moiety), as well as the reaction conditions. These findings have not been proven by crystal structure analysis yet. A thermal route towards cyclopolystannanes was reported by Sita heating Bu$_2$SnH(OEt) in heptane for 12 h in order to form five and six membered perbutylated tin rings.[269] More recently, amine bases such as TMEDA (*N,N,N',N'*-tetramethylethylenediamine) have been reported to efficiently catalyze the polymerization reaction of organotin dihydrides leading to poly(diarylstannane)s. The drawback of badly soluble polymers, such as (phenyl$_2$Sn)$_n$ can be overcome by using *p*-butylphenyl$_2$SnH$_2$ as monomer to result in well characterized materials.[11] The limited knowledge on the reaction process using amine bases, and in our case TMEDA, provided motivation to investigate the formation of soluble side products apart from (phenyl$_2$Sn)$_6$ in the dehydrogenative coupling reaction of phenyl$_2$SnH$_2$ (Scheme 80).

$$\textbf{phenyl}_2\textbf{SnH}_2 \xrightarrow[\textbf{Et}_2\textbf{O, VT}]{\textbf{1 eq. TMEDA}} (\textbf{phenyl}_2\textbf{Sn})_n \quad + \quad \textbf{soluble side products}$$

Scheme 80: *Dehydrogenative coupling of phenyl$_2$SnH$_2$ leading to an insoluble polystannane (phenyl$_2$Sn)$_n$ and soluble side products (VT= variable temperature).*

As the nature of the Sn–H bond is known to be very versatile according to its reaction behavior with nucleophiles, electrophiles and radicals, it is important to gain insight in the bonding situation by elucidating the crystal structure.[270] Structural information for diorganotin dihydrides (R_2SnH_2) is very limited as the sensitivity towards oxygen or temperature of Group 14 metal hydrides increases as descending Group 14, as well as with the number of hydrogens attached to the metal.[113] Additionally, the vast majority of known organotin dihydrides is found to be liquid. The only published solid state structure so far concerns the solid mesityl$_2$SnH$_2$ (mesityl=2,4.6-trimethylphenyl),[8] however we were able to elucidate the crystal structure of the liquid and air sensitive phenyl$_2$SnH$_2$ realized *via in situ* crystallization and displays, to the best of our knowledge, the first structure of a liquid diorganotin dihydride.

5.2 Results and Discussion

5.2.1 VT-NMR Studies

In order to investigate the formation of soluble side products during the dehydrogenative coupling reaction of phenyl$_2$SnH$_2$ (**31**), a variable temperature NMR (VT-NMR) study was carried out using screw cap NMR tubes with septa. The dihydride **31** was dissolved in dried and degassed diethyl ether in the NMR tube, cooled to -80 °C and TMEDA was added *via* the septum. Immediately, the sample was transferred in the precooled NMR probe (-50 °C).^{1}H, ^{119}Sn decoupled and coupled NMR measurements were carried out at seven different temperature steps (-50, -30, -20, -10, 0, 10, 25 °C). However, measuring ^{1}H NMR spectra at temperatures higher than -10 °C turned out to be not possible due to formation of the insoluble polymer leading to the loss of the lock signal. Therefore, the intensity of the ^{119}Sn NMR signals decreased and the acquisition of ^{1}H NMR spectra did not lead to any useful signals. As Waltz decoupling of the hydrogen signals in ^{119}Sn NMR led to significant decoupling side bands, the Sn–H was decoupled using continuous wave decoupling with a decoupler power of 63 dB. This effect is also known for ^{13}C NMR signals.[271] The ^{119}Sn NMR spectrum at -20 °C showed the formation of an unknown soluble side product **43** at -220 ppm. While warming up the reaction mixture to -10 °C, a second peak arose at -208 ppm, which was assigned to the literature known perphenylated six membered tin ring (phenyl$_2$Sn)$_6$ **42**,[266] in the presence of residual dihydride **31** (-233 ppm) and the peak at -220 ppm. After completion of the reaction at room temperature, the supernatant liquid in the NMR tube was separated from the polymer and the resulting filtrate measured once again to give the ^{119}Sn NMR spectrum shown in Figure 39. Figure 39 displays the two soluble side products obtained during the dehydropolymerization reaction. Thus, the generation of the perphenylated six membered ring **42** and the hitherto unknown second byproduct (**43**) is temperature dependent.

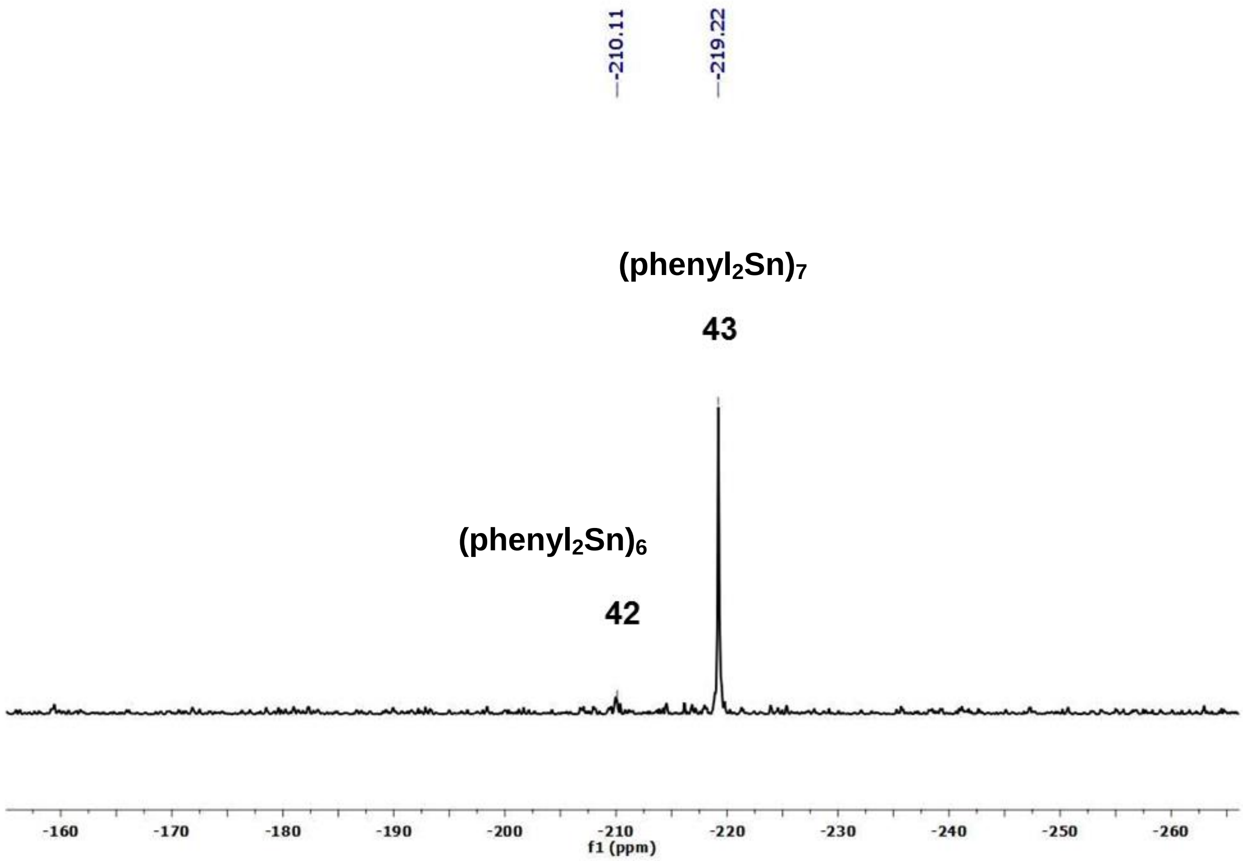

Figure 39: *VT-NMR study @ -30 °C → RT, ^{119}Sn NMR of the filtrate (Et$_2$O, D$_2$O).*

Therefore, a second small scale reaction was carried out, using the same amount of educts, however reacting them at room temperature. Afterwards, the supernatant liquid was subjected to a ^{119}Sn NMR measurement using a D$_2$O capillary leading to the ^{119}Sn spectrum displayed in Figure 40. Figure 40 shows that carrying out the polymerization reaction at room temperature mainly formed the perphenylated six membered ring **42**. In order to identify the unknown compound exhibiting a ^{119}Sn NMR shift at -210 ppm, the dehydrogenative coupling reaction was carried out in a bigger scale to afterwards isolate it for further analysis.

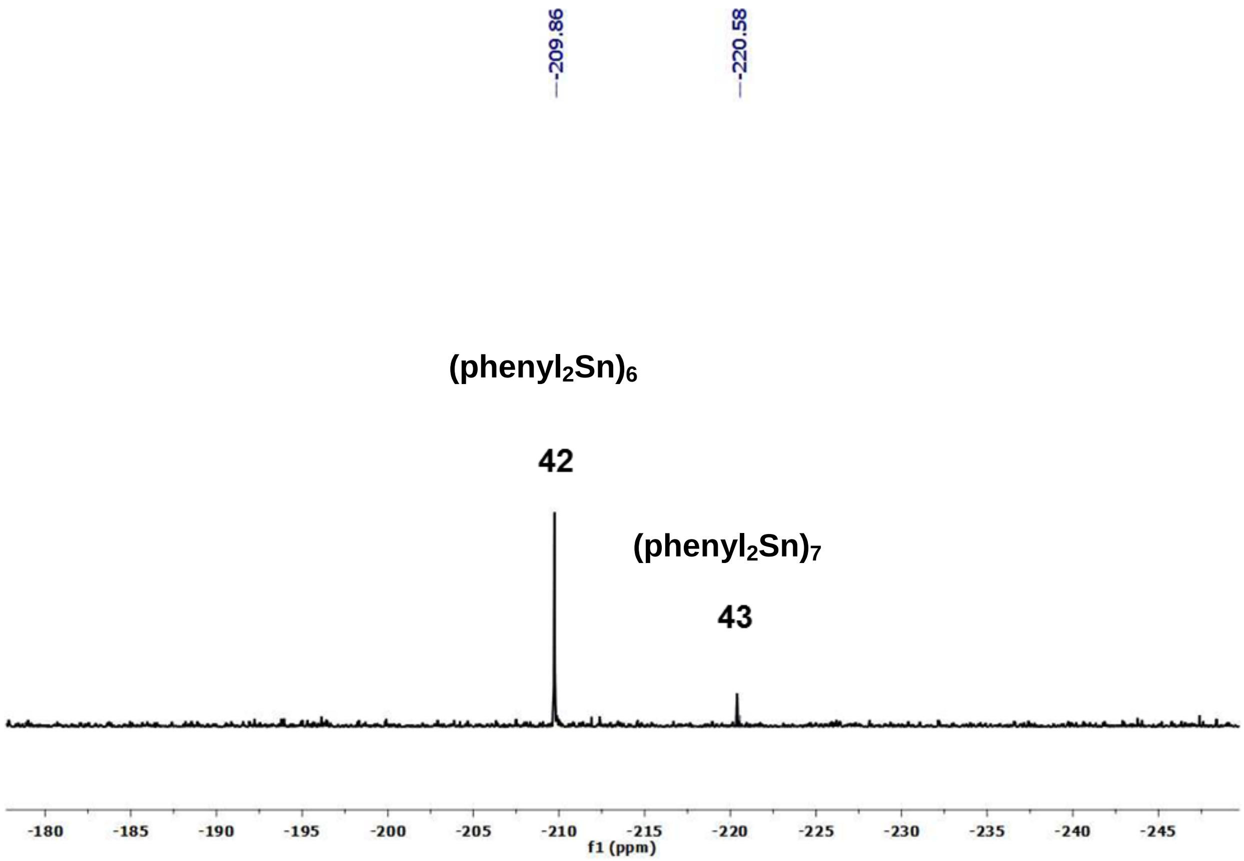

Figure 40: *Dehydropolymerization carried out at RT → ^{119}Sn NMR of the filtrate (Et_2O, D_2O).*

5.2.2 Synthesis

According to the findings of the variable temperature NMR studies, the formation of (phenyl$_2$Sn)$_6$ (**42**) and another soluble side product **43** in the presence of the insoluble polymer was carried out using standard Schlenk technique (Scheme 81) .

$$\underset{\textbf{31}}{\text{phenyl}_2\text{SnH}_2} \xrightarrow[\text{Et}_2\text{O, -30°C} \rightarrow \text{RT}]{\text{1.4 eq. TMEDA}} (\text{phenyl}_2\text{Sn})_n + \underset{\textbf{42}}{(\text{phenyl}_2\text{Sn})_6} + \underset{\textbf{43}}{(\text{phenyl}_2\text{Sn})_7}$$

Scheme 81: *Dehydrogenative coupling of phenyl$_2$SnH$_2$ **31** generating an insoluble polymer and soluble cyclic byproducts **42** and **43**.*

According to Scheme 81, phenyl$_2$SnH$_2$ (**31**) was dissolved in dried and degassed diethyl ether and cooled to -30 °C using an ethanol/liquid nitrogen bath. Subsequently, 1.4 eq. of TMEDA were added with a syringe *via* a septum. The reaction started immediately, forming a turbid solution and turns bright yellow after approximately 15 minutes. The reaction mixture was kept at -30 °C for 2 h and then allowed to warm up to room temperature overnight. The insoluble, strong yellow polystannane, (phenyl$_2$Sn)$_n$, precipitated. Afterwards, the supernatant liquid was filtered off using a filter cannula to result in a colorless liquid. ^{119}Sn NMR of the diethyl ether solution showed **43** as a main product in the presence of **42**. In order to isolate the unknown species **43**, the diethyl ether was removed under reduced pressure and the resulting white solid taken up in dried toluene. Two different crystals could be isolated showing on one hand the structure of the already literature known compound (phenyl$_2$Sn)$_6$ **42** and on the other hand X-ray analysis revealed that the second formed product is a hitherto unknown seven membered tin ring (phenyl$_2$Sn)$_7$ (**43**). Although Neumann *et al.* suggested the formation of a seven membered tin ring using pyridine as a catalyst for the dehydrogenative coupling reaction of phenyl$_2$SnH$_2$ **31**, the actual evidence by crystallography or NMR spectroscopy has never been mentioned in literature.[265] Further, a seven membered tin ring exhibiting any organic residues has not been synthesized *via* any other synthetic method thus far.

5.2.3 X-Ray Crystallography

This section summarizes the crystallographic data of compounds **31**, **42** and **43** and compares it to already published compounds. The crystallographic data and details for compounds **31**, **42** and **43** can be found in Chapter 13.1.

5.2.3.1 Diphenyltin Dihydride 31

Crystallographic data on the compound class of organotin hydrides is very limited due to their high reactivity towards atmospheric oxygen and their thermal lability in accordance to the number of hydrogens attached to tin. Further, the majority of known organotin hydrides are liquids and therefore not suitable for usual single crystal analysis. Recently, we have been able to elucidate the solid structure of two triorganotin hydrides (R_3SnH) (2,6-xylyl$_3$SnH **29**, phenyl$_3$SnH **30**) which were the first ones to be reported.[63,131] Fischer *et al.* could also show the first X-ray structure of a diorganotin dihydride mesityl$_2$SnH$_2$ (mesityl= 2,4,6-trimethylphenyl), which is solid at room temperature due to the sterically demanding residues on the bonded to the tin.[8] phenyl$_2$SnH$_2$ (**31**) crystallizes in the monoclinic space group $P2_1$ *via* an *in situ* technique in a capillary, which is described in detail in 11.6. Mesityl$_2$SnH$_2$ crystallizes in C2/c from diethyl ether at -30 °C. It has to be stressed that **31** is the first liquid diorganotin dihydride which has been crystallized so far (Figure 41). In the solid state structure of phenyl$_2$SnH$_2$ (**31**), as well as mesityl$_2$SnH$_2$ the tin is found in a distorted tetrahedral environment bound to two hydrogens and two aryl substituents. Table 12 summarizes average bond lengths and angles of **31** and mesityl$_2$SnH$_2$. The average Sn–C bond lengths of **31** (2.134 (19) Å) is slightly shorter than for mesityl$_2$SnH$_2$ (2.154 (1) Å) which can be explained by the higher steric demand of the methyl groups in both *ortho* position of the mesityl moiety. However, in the case of aryltin dihydrides bond angles are not affected by the steric pressure of the substituent as it was also shown for a series of diaryltin dichlorides.[80] Phenyl$_2$SnH$_2$ (**31**) shows an C–Sn–C angle of 114.4(7)°, Mesityl$_2$SnH$_2$ of 111.1(4)°. The average H–Sn–C angle is almost the same (**31**: 109.2 (15)°, Mesityl$_2$SnH$_2$: 109.2(15)°) however the average H–Sn–H angle of **31** is found to be a little bit wider (105.0(2)°) than the other one (103.1(1)°). In contrast to mesityl$_2$SnH$_2$, **31** exhibits an edge to face interaction in the solid state structure due to the lack of methyl groups attached to the aromatic ring. These interaction falls in the range reported in literature (2.86 Å) (Figure 41) and is also comparable to the one found for phenyl$_3$SnH (**29**) (2.78 Å).[131,244] Noteworthy, phenyl$_2$SnH$_2$ (**31**) does not show Sn–H interactions as reported for phenyl$_3$SnH (**29**).

***Table 12:** Average bond lengths, angles and non-covalent interactions of diphenyltin dihydride (**31**) and dimesityltin dihydride.*

	Space group	**Sn–C (Å) (avg.)**	**Sn–H(Å) (avg.)**	**C–Sn–C (°) (avg.)**	**H–Sn–H (°) (avg.)**	**C–Sn–H (°) (avg.)**	**π–π Stacking (Å)**		**Edge to Face (Å)**	**CH$_3$···π (Å)**
							d	**R**		
phenyl$_2$SnH$_2$ **(31)**	P2$_1$	2.134(19)	1.65(6)	114.4(7)	105.0(2)	109.2(15)	—	—	2.86	—
mesityl$_2$SnH$_2$^{8}	C2/c	2.154(3)	1.669(2)	111.07(2)	103.1(1)	110.35(2)	—	—	—	2.75–2.78

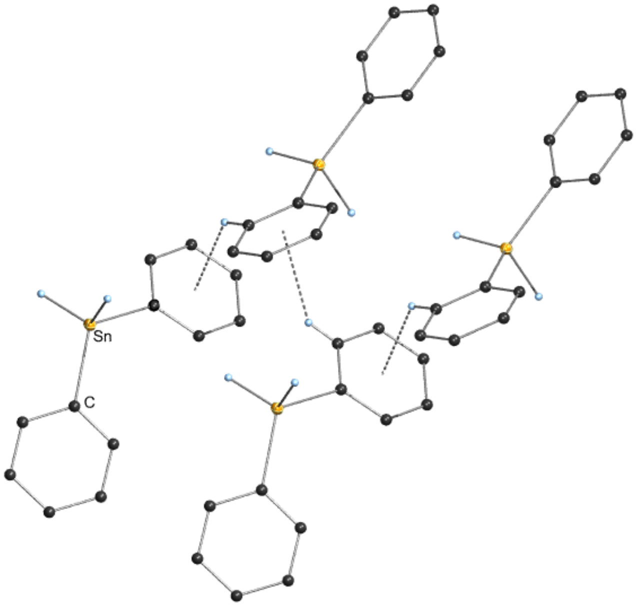

***Figure 41:** Crystal packing diagram for phenyl$_2$SnH$_2$ (**31**). Edge to face interactions are highlighted by dashed bonds (2.86 Å). All non-carbon atoms shown as 30 % shaded ellipsoids. Hydrogen atoms not involved in intermolecular interactions removed for clarity.*

5.2.3.2 Perphenylated Tin Rings 42, 43

The two different perphenylated tin rings **42** and **43** crystallize from toluene at room temperature as colorless crystals. (phenyl$_2$Sn)$_6$ (**42**) crystallizes very nicely forming well diffracting crystals, whereas (phenyl$_2$Sn)$_7$ (**43**) generates small, weakly diffracting crystals due to its bad solubility in warm toluene. Table 13 summarizes selected bond lengths and angles of **42** and **43**. Crystallographic data and details for compounds **42** and **43** are found in Chapter 13.1. Figure 42 displays the crystal structure of **42**.

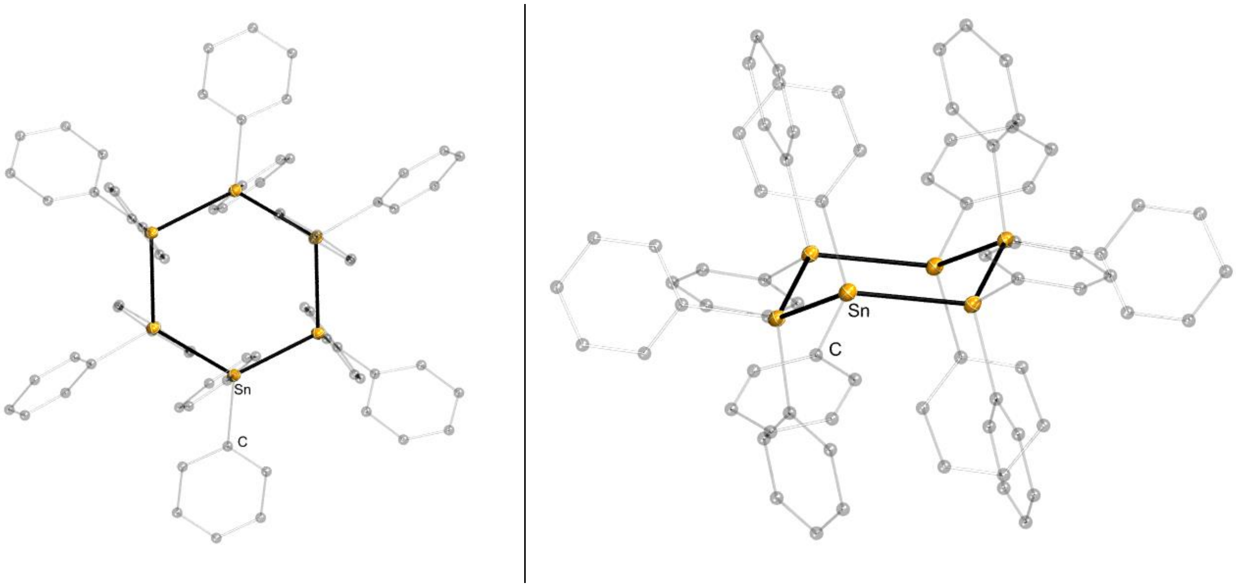

Figure 42: *Crystal structure of (phenyl$_2$Sn)$_6$ (**42**). All non-carbon atoms shown as 30 % shaded ellipsoids. Hydrogen atoms removed for clarity.*

(Phenyl$_2$Sn)$_6$ (**42**) crystallizes in the monoclinic space group P2$_1$/c from toluene at room temperature as colorless crystals and contains two cocrystallizing molecules of toluene. The tin is found in a distorted tetrahedral environment bonded to two other tin atoms of the ring and two phenyl rings. In accordance to already published structure, (phenyl$_2$Sn)$_6$ (**42**) is found in the chair conformation which is the most favored one.[266,272,273] Average bond lengths and angles fall in the expected range.

Figure 43 illustrates the solid state structure of (phenyl$_2$Sn)$_7$ (**43**) which was crystallized at room temperature from toluene.

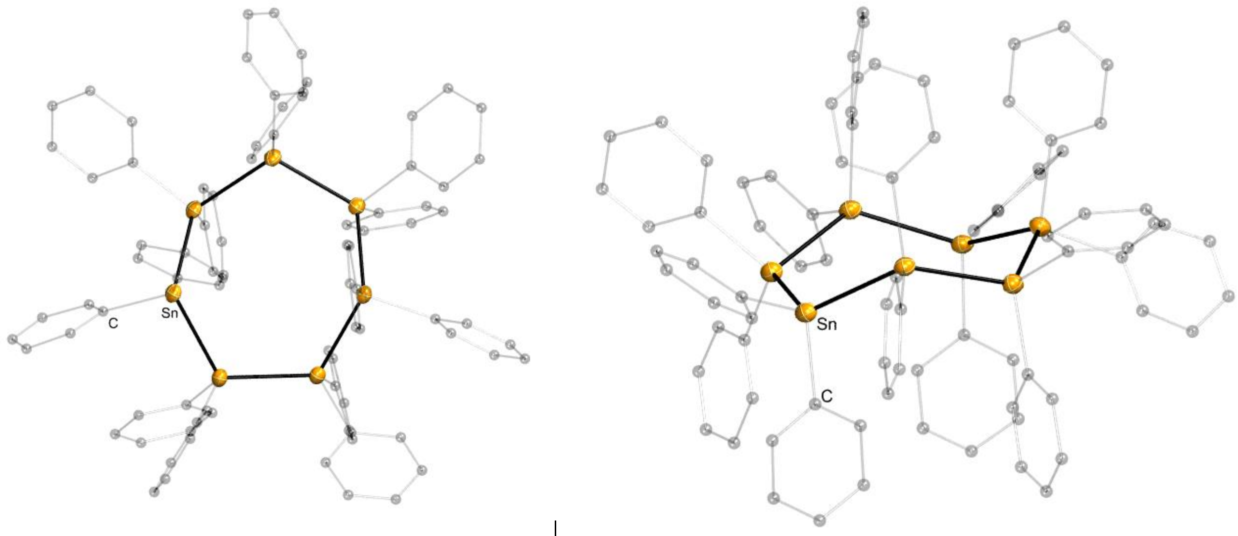

Figure 43: *Crystal structure of (phenyl$_2$Sn)$_7$ (**43**). All non-carbon atoms shown as 30 % shaded ellipsoids. Hydrogen atoms removed for clarity.*

(Phenyl$_2$Sn)$_7$ (**43**) crystallizes in the triclinic space group P-1 and is found as a disordered mixture of the chair (**C**) and twist chair (**TC**) conformation. According to DFT calculations, **C** is the global minimum separated by only 0.4 kJ/mol (0.09 kcal/mol) from the local minimum **TC**. This marginal energy differences rationalizes the coexistence of both conformers in the solid state structure of **43** which strongly affects a successful recrystallization process (Figure 43).

Table 13: *Selected bond lengths and angles of (phenyl$_2$Sn)$_6$ (**42**) and (phenyl$_2$Sn)$_7$ (**43**).*

	space group	**bond length avg. (Å)**		**angle avg. (°)**			
compound		*Sn–C*	*Sn–Sn*	*Sn–Sn–Sn*	*C–Sn–Sn*	*C–Sn–C*	*C–C–Sn*
(phenyl$_2$Sn)$_6$ (**42**)	P2$_1$/c	2.149 (7)	2.772 (7)	112.6 (2)	107.3 (8)	107.0 (3)	121.1 (6)
(phenyl$_2$Sn)$_7$ (**43**)	P-1	2.16 (3)	2.784 (2)	118.2 (7)	107.5 (7)	106.2 (9)	120.0 (20)

5.2.4 Conformation Analysis and Theoretical Calculations

VT-NMR studies, as well as the synthetic approach could show that the formation of soluble side products in the dehydrogenative coupling reaction of diphenyltin dihydride (**31**) is strongly temperature dependent. By lowering the temperature to -30 °C, the less thermodynamically stable seven membered, perphenylated tin ring (phenyl$_2$Sn)$_7$ (**43**) could be obtained as evidenced by single crystal analysis in presence of (phenyl$_2$Sn)$_6$ (**42**). However, crystal structure data including thermal parameters did not show satisfying quality, due to weak crystal formation. Furthermore, two different conformations of **43** were found in the crystal, as a disordered mixture explained by a high degree of freedom in the possible conformation of **43**. Therefore, DFT studies were carried out in order to support the understanding of the stability of the found ring conformations as a function of temperature.

The four basic conformations of seven membered rings have been identified and carefully studied for cycloheptane *via* molecular mechanics applying a modified force field method (MM2) by Bocian and Strauss[274] and by Ivanov and Osawa[210]: chair (**C**), boat (**B**), twist-chair (**TC**) and twist-boat (**TB**). The chair (**C**), as well as the boat (**B**), exhibit C_s symmetry, whereas the other ones (**TC** and **TB**) are of C_2 symmetry. The **TC** conformer exhibits the lowest energy, as the global minimum and undergoes pseudorotation *via* the **C** conformer as a transition state by overcoming the activation energy of only 0.96 kcal/mol. Therefore, **C** forms are saddle points on a pseudorotational route connecting all possible **TC** minima. Furthermore, the local minimum **TB** conformer participates in a free pseudorotation *via* the **B** conformer requiring only little activation energy. Examination on the MP2 level by Wiberg reported an activation energy of 1.5 kcal/mol from **TC** to **C** and 1 kcal/mol from **TB** to **B**. Finally, there is a transition state (**T3**) that connects the **TC** and **B** conformers (Figure 44).[274-277]

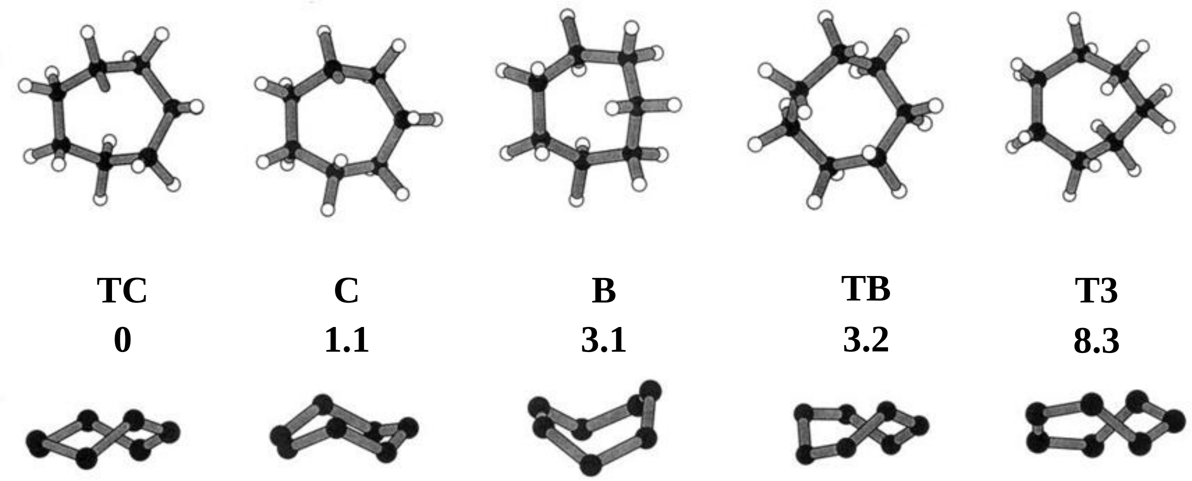

Figure 44: *Possible conformations of cycloheptane conformers, transition states and relative energies E (kcal/mol), MP2/6-311+G*).*[277]

West and coworkers intensively studied the temperature dependent redistribution equilibria between permethylated cyclopolysilanes. During a study of the reaction of dimethyl dichloro silane with Na/K alloy in THF, a temperature dependent formation between $(Me_2Si)_5$, $(Me_2Si)_6$ and $(Me_2Si)_7$ could be observed. The results showed that $(Me_2Si)_6$ is more stable than $(Me_2Si)_5$ and $(Me_2Si)_7$. This is in accordance with cyclopentane, cylcoheptane and cyclohexane, however stability differences are found to be less than for the corresponding hydrocarbons.[278] Watanabe *et al.* realized the Wurtz type coupling reaction of dialkyldichlorosilane using lithium in THF and could show that bulky substituents such as *i*-Pr, *i*-Bu and *t*-Bu afford smaller rings, mainly four membered ones, whereas less hindered silicones (R= Me,Pr) give rise to large cyclopolysilanes $(R_2Si)_n$ (n= 5,7).[279]

West *et al.* presented the solid state structure of $(Me_2Si)_7$, as well as carried out EFF (empirical force field) calculations elucidating that $(Me_2Si)_7$ adopts a similar twisted chair ground state structure as cycloheptane, however significant differences could be noted in the structure of other possible conformations. The relative energy difference of the most favored **TC** and the **C** transition state could be calculated with only 0.9 kcal/mol.[280] The decrease of relative energies difference between the **TC** and **C** conformer in comparison to cycloheptane can be highlighted. This effect can rationalized by larger Si−Si distances and weaker vicinal interactions compared to cycloalkanes.[281] Generally, not only barrier heights but also energy differences between conformers decrease descending the group from carbon to the heavier homologues (Si, Sn, Ge). This is accompanied by a considerable decrease in the conformers' lifetimes.[282]

With the help of quantum chemical DFT calculations applying SDD pseudopotentials on the Sn atoms (MPW1PW91/sdd), the geometries and energies of the conformers of (SnH$_2$)$_7$ and (phenyl$_2$Sn)$_7$ (**43**) were investigated. Studying the possible conformations of the hydrogen substituted seven membered tin ring (SnH$_2$)$_7$ showed the same results as reported for cycloalkanes, however energy differences between conformations decrease as already seen for the silicon derivative (Me$_2$Si)$_7$. In this manner, **TC** is the global minimum, whereas **C** (0.53 kJ/mol, 0.13 kcal/mol) was found to be a transition state. Furthermore, **TB** (1.49 kJ/mol, 0.36 kcal/mol) was calculated as a local minimum and **B** (1.52 kJ/mol, 0.36 kcal/mol) as a transition state.

Additionally, we could show that changing the hydrogen to the larger substituent phenyl (phenyl$_2$Sn)$_7$ (**43**) leads to a global minimum for the **C** conformation in contrast to cycloheptane, (Me$_2$Si)$_7$ and (SnH$_2$)$_7$ where **C** is a transition state. **TC1** forms a local minimum with a relative energy of only 0.4 kJ/mol (0.09 kcal/mol) in comparison to **C**. Two twist boat conformations **TB1** and **TB2** with relative of 10.3 kJ/mol and 26.0 kJ/mol, respectively could be found in addition with another **TC2** conformation (14.5 kJ/mol, 3.5 kcal/mol). No **B** conformations could be calculated (Figure 45).

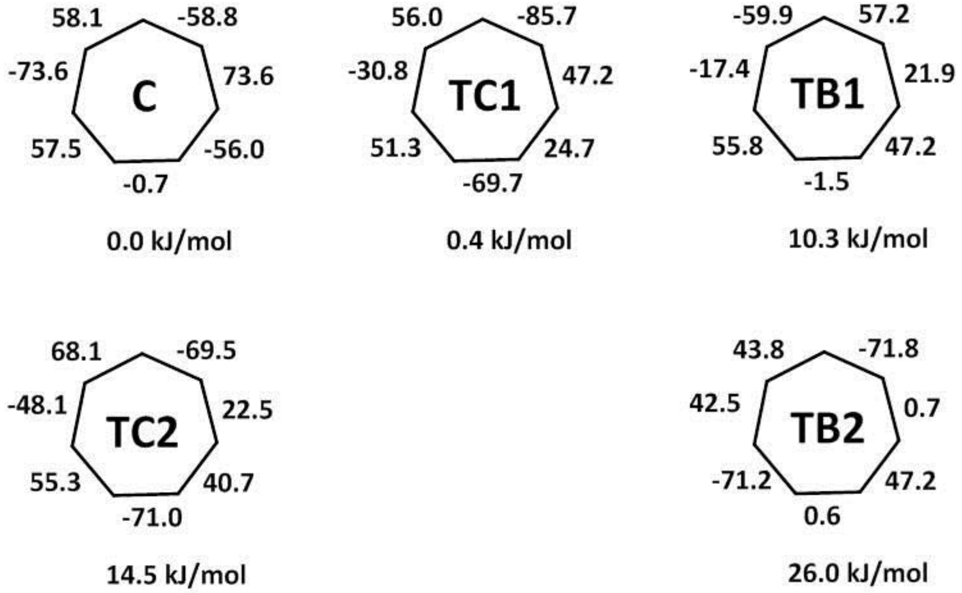
58.1
-58.8
-73.6
C
73.6
57.5
-56.0
-0.7
0.0 kJ/mol
56.0
-85.7
-30.8
TC1
47.2
51.3
24.7
-69.7
0.4 kJ/mol
-59.9
57.2
-17.4
TB1
21.9
55.8
47.2
-1.5
10.3 kJ/mol
68.1
-69.5
-48.1
TC2
22.5
55.3
40.7
-71.0
14.5 kJ/mol
43.8
-71.8
42.5
TB2
0.7
-71.2
47.2
0.6
26.0 kJ/mol

Figure 45: *Possible conformations of (phenyl$_2$Sn)$_7$ (**43**), energy differences (ΔE) in kJ/mol and Dieder angles.*

The theoretical results are nicely supported by the crystal data elucidating the presence of a **C** and a **TC** conformer in a disordered mixture in the unit cell. As the energy difference between these two conformers is only assigned with 0.4 kJ/mol, it is not surprising that (phenyl$_2$Sn)$_7$ (**43**) crystallizes in both conformers simultaneously resulting in unsatisfying thermal parameters of the diffraction data. Electron diffraction studies of cycloheptane in the gas phase also revealed a discorded mixture of **TC** and **C** as reported by Dillen and Geise.[205]

Figure 46 illustrates the Dieder angles found for the **C** and **TC** conformer in the unit cell of **43** which compare nicely to the theoretical ones.

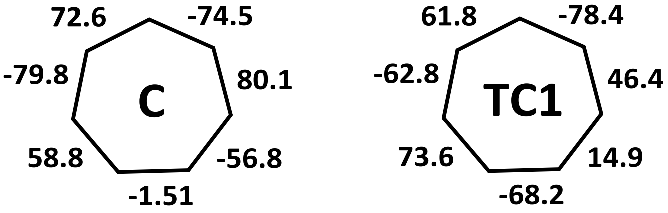

***Figure 46**: Dieder angles found in the solid state structure of (phenyl$_2$Sn)$_7$ (**43**).*

Table 14 summarizes the calculated ^{119}Sn NMR shifts for **C**, **TC1** and **TB1**. The average ^{119}Sn chemical shift for the chair conformation of (phenyl$_2$Sn)$_7$ (**43**) is -233 ppm. DFT calculations revealed that the shift for the **C** conformation of (phenyl$_2$Sn)$_6$ (**42**) is downfield shifted in comparison to **43** which is in accordance to the measured ^{119}Sn chemical shifts.

***Table 14:** δ ^{119}Sn (ppm) of (phenyl$_2$Sn)$_7$ (**43**) and (phenyl$_2$Sn)$_6$ (**42**) obtained by DFT calculations.*

conformer (phenyl$_2$Sn)$_7$	**calculated δ ^{119}Sn (ppm)**							**avg. (ppm)**	**measured δ ^{119}Sn (ppm)**
C	-221	-225	-228	-229	-233	-237	-257	**-233**	**-220**
TC1	-220	-223	-230	-239	-246	-249	-250	-237	
TB1	-228	-240	-244	-253	-266			-246	
conformer (phenyl$_2$Sn)$_6$									
C	-214	-221	-234					**-223**	**-210**

5.3 Conclusions

In summary, we were able to identify the soluble side products of the dehydrogenative coupling reaction of phenyl$_2$SnH$_2$ (**31**) using TMEDA as a catalyst. The formation of the insoluble, strong yellow colored (phenyl$_2$Sn)$_n$ is accompanied by the formation of lower molecular weight cyclic side products. Depending on the reaction temperature, the generation of a thermodynamically stable six membered, perphenylated tin ring (phenyl$_2$Sn)$_6$ (**42**), or the seven membered derivative (phenyl$_2$Sn)$_7$ (**43**) is favored. Carrying out the reaction at room temperature yields **42**, which can easily be recrystallized from toluene at room temperature. However, variable temperature NMR studies at -30 °C indicated the formation of an unknown tin species as soluble side product. When phenyl$_2$SnH$_2$ (**31**) is subjected to a dehydrogenative coupling reaction at -30 °C on a laboratory scale, the unknown species can be identified by means of single crystal analysis as a seven membered, perphenylated tin ring (phenyl$_2$Sn)$_7$ (**43**). The seven membered tin ring (**43**) crystallizes in a discorded mixture of a chair (**C**) and twist chair conformation (**TC1**). These findings are supported by DFT calculations revealing an energy difference of only 0.4 kJ/mol between **C** and **TC1**. This marginal energy barrier rationalizes the presence of both conformations in the solid state structure of **43** and strongly affects crystal growth. Additionally, another twist chair (**TC2**) with a relative energy of 14.5 kJ/mol, as well as two twist boat conformations exhibiting a relative energy of 10.3 kJ/mol and 26.0 kJ/mol can be found as local minima. No boat conformation could be detected. DFT calculations showed an upfield shift for **42** in comparison to **43**, which is in accordance with the experimental data.

6 Towards Aryl Decorated Tin Nanoparticles (Aryl@Sn)- Insights into an Unknown Reaction Pathway

Graphical Abstract

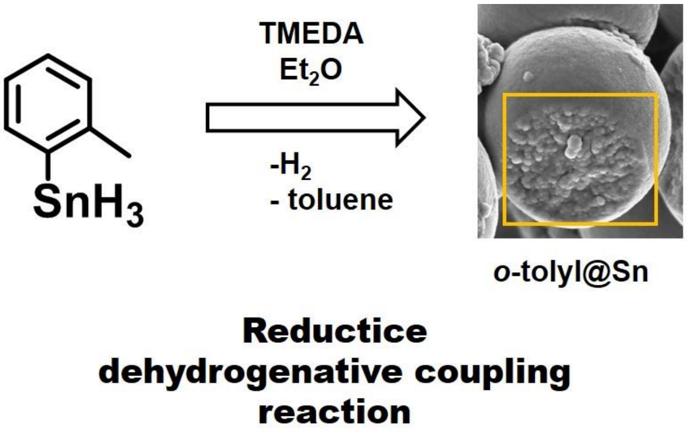

Abstract

o-tolylSnH_3 was subjected to a dehydrogenative coupling reaction with the amine base TMEDA (N,N,N',N'-tetramethylethylenediamine) forming hitherto unknown aryltin decorated nanoparticles (aryl@Sn). Detailed in situ synchrotron SAXS measurements revealed the evolution of spherical nanoparticles over reaction time. Furthermore, a reductive dehydropolymerization via a reactive Sn(II) mechanism is proposed based on DFT calculations, in situ synchrotron EXAFS studies and in situ UV-VIS measurements. Additionally, thermally induced dehydrocoupling of o-tolylSnH_3 allowed the isolation of a suggested intermediate upon Sn–Sn bond formation and H_2 abstraction.

6.1 Introduction

The use of organotin dihydrides (R_2SnH_2) exhibiting aryl moieties as building blocks in the synthesis of linear polystannanes has gained high attention in the last decade. The monomers easily undergo catalytic dehydropolymerization applying metal complexes based on palladium, zirconium, rhodium, lanthanides, or platinum as well as "non-traditional" iron and molybdenum alkyls as catalysts.[6-9] Moreover, a solvent and catalyst free thermal based dehydrogenation reaction was described as a successful route towards polystannanes exhibiting modest molecular weight and broad polydispersity.[10] More recently, amine bases such as TMEDA (*N*,*N*,*N'*,*N'*-tetramethylethylenediamine) have been reported to efficiently catalyze the polymerization reaction of organotin dihydrides leading to poly(diarylstannane)s.[11]

The gained polymeric materials with the general formula $(R_2Sn)_n$ harbor a covalently linked metal (tin) backbone, which can be seen as a molecular metal wire embedded in an organic jacket. The molecular wire features an increased degree of electron delocalization by catenation, leading to promising materials in charge-transfer devices.[134,137] In particular, substitution by aryl groups leading to polyarylstannanes are suggested to additionally exhibit $\sigma-\pi$ transitions as well as are reported to display increased light stability.[138,178] However, the latter have not been well characterized due to their insolubility in common organic solvents. Lechner and coworkers could increase the solubility of the polyarylstannanes by substituting the phenyl ring with a butyl group in the *para* position allowing for standard polymer characterization techniques, such as ^{119}Sn NMR and GPC. In this manner, *p*-^{n}butylphenyl$_2$SnH$_2$ was converted with TMEDA in Et_2O to result in poly[bis(*p*-^{n}butylphenyl)stannane] exhibiting a molar mass of 46 000 $gmol^{-1}$ which corresponds to approximately 120 (*p*-^{n}butylphenyl)$_2$Sn units.[11] Although the use of amine bases as catalysts in the dehydrogenative coupling reaction of organotin mono- and dihydrides has already been described by Neumann applying pyridine to allow for H_2 abstraction and Sn−Sn bond formation, further detailed investigations on the reaction mechanisms and the role of the amine base in the polystannane formation have been neglected thus far.[265,266]

However, the use of aryl moieties leads to poorly soluble polymeric materials and therefore a lack of analytical data on polyarylstannanes. Furthermore, the conversion of organotin trihydrides ($RSnH_3$) as trifunctionalized educts has been neglected thus far, but presents an auspicious starting point to the formation of nanostructured organometallic particles. Sindlinger and coworkers have very recently reported on the reductive dihydrogen elimination of the highly sterically encumbered aryltin trihydride Ar*SnH_3 (Ar*= 2,6-trip$_2$(C_6H_3), trip= 2,4,6-triisopropylphenyl) forming an aryltin (II) hydride species applying a variety of amine bases such as pyridine, DMAP (4-dimethylaminopyridine) and TMEDA. In case where catalytic amounts of base were used, the dehydrocoupling product diorganodistannane Ar*H_2Sn–SnH_2Ar* could be obtained quantitatively; whereas the use of excessive amounts (>4 eq.) led to almost exclusive formation of the monomeric base adduct Ar*SnH being thermally relatively robust. The formation of higher molecular Sn species by full hydrogen release has not been observed. The authors suggested two different reaction mechanisms for the amine promoted dehydrogenative reduction of Ar*SnH_3. Both rely on the polarizability of the Sn–H bond. Mechanism I assumes a nucleophilic attack of the amine base at the tin center forming a Lewis adduct (**LA**), whereas mechanism II proposes the heterolytic cleavage of a proton from Ar*SnH_3 via a Brønsted adduct (**TS-B1**) (Figure 47).[259]

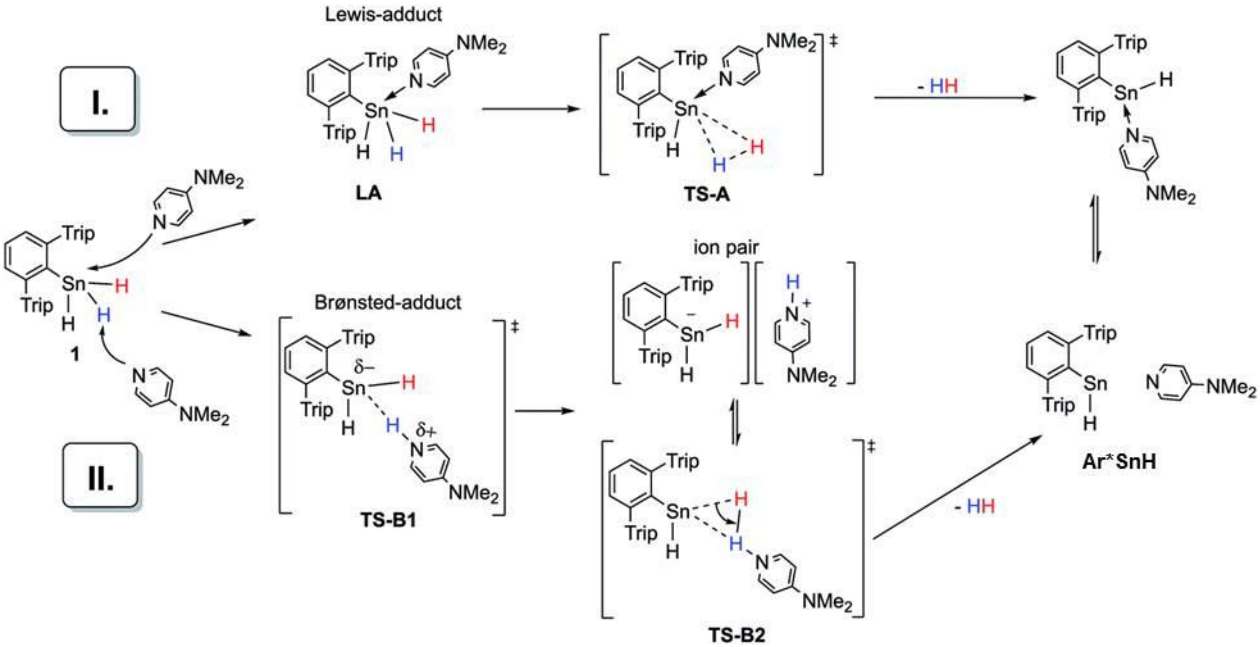

Figure 47: *Possible reductive dihydrogen elimination mechanisms of Ar*SnH_3 *using DMAP. Mechanism I proceeds via a Lewis-adduct formation. Mechanism II proposes a heterolytic cleavage of a hydrogen atom.*[259]

However, due to the large nature of the aryl residue of the converted aryltin trihydride Ar*SnH_3, Sindlinger has not observed the formation of higher molecular species, since the stability of the formed distannane as well as stannylene species does not allow for further hydrogen abstraction.

In an effort to provide trifunctionalized, sterically less hindered building blocks for the generation of higher molecular species exhibiting Sn–Sn bonds, polyarylstannanes, we have been able to present the synthesis and characterization of a series of novel aryltin trihydrides, arylSnH_3 (aryl= tolyl, xylyl, naphthyl), in a recent contribution from our working group (Chapter 2).[80] Specifically, *o*-tolylSnH_3 (**36**) has been subjected to a dehydrogentive coupling reaction using the amine base TMEDA in order to generate novel, insoluble Sn based materials.

This conversion forms hitherto unknown nanostructured polymers which can be described as aryl decorated nanoparticles (aryl@Sn). Detailed morphology studies were performed applying SAXS, SEM and TEM analyses. In addition, conventional analytic techniques (elemental analysis, UV-VIS, GC-MS, solid and solution state NMR, TGA-MS) and EXAFS/XANES studies were applied in order to gain insight into the mechanism. Supported by DFT calculations, we are able to propose a reductive dehydrogenative coupling mechanism for the formation of polymeric materials exhibiting a discrete nanostructure, which can exclusively be afforded by the conversion of small aryltin trihydrides.

6.2 Results and Discussion

6.2.1 Synthesis

The educt *o*-tolylSnH_3 (**36**) was synthesized *via* a literature known procedure subjecting *o*-tolylSnCl_3 (**21**) to a hydrogenation reaction using excess LiAlH_4 at -30 °C. The resulting thermally labile compound was stored at -80 °C.[80] In a typical dehydrogenative coupling reaction, an equimolar amount of TMEDA was added to a 0.4 M solution of dried and degassed diethyl ether and **36** at room temperature to obtain ***o*-tolyl@Sn** (Scheme 82).

$$o\text{-tolylSnH}_3 \xrightarrow[\text{-toluene, -H}_2]{\text{1 eq. TMEDA}} o\text{-tolyl@Sn}$$

Scheme 82: *Formation of o-tolyl decorated Sn nanoparticles (**o-tolyl@Sn**) by dehydrogenative coupling of o-tolylSnH$_3$ (**36**) with TMEDA.*

The addition of TMEDA immediately led to a strong color change from colorless to yellowish orange and the formation of hydrogen. After a few minutes a dark red mixture was obtained which turned darker over approximately 40 min to form a black, insoluble precipitate ***o*-tolyl@Sn** (Figure 48). A similar color change due to the generation of Sn–Sn bonds which allow for σ–σ* and σ–π transitions, as well as the generation of hydrogen, has already been reported for the dehydrogenative coupling reaction of diphenyltin dihydride (phenyl$_2$SnH$_2$) applying pyridine or TMEDA forming (phenyl$_2$Sn)$_n$.[135,150,163,177]

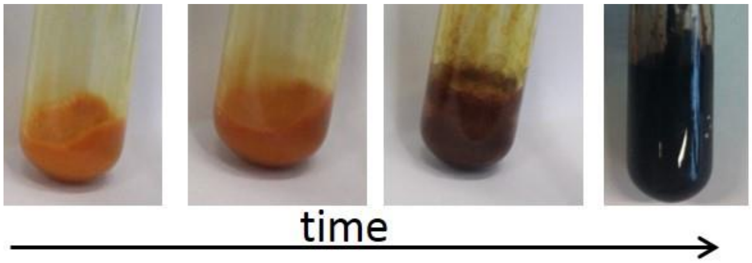

Figure 48: *Visible reaction progress in the dehydrogenative coupling reaction of o-tolylSnH$_3$ (**36**) forming **o-tolyl@Sn**.*

This black precipitate could be filtered off and washed with diethyl ether. The latter is not soluble in common organic solvents, as already reported for linear polyarylstannanes which consequently does not allow for standard polymer characterization techniques (*e.g.* liquid state ^{1}H, ^{13}C, ^{119}Sn NMR, GC-MS, GPC). The gained filtrate did not show unreacted educt according to ^{1}H and ^{119}Sn NMR. According to GC-MS measurements of the filtrate, toluene was detected as a side product due to Sn–C bond cleavage. It could be observed that the product easily undergoes oxidation when coming into contact with air, changing color from black to yellowish white (Figure 49). This oxidation process forming tin oxides is exothermic which suggests the presence of a high number of reaction sites due to an increased surface area.

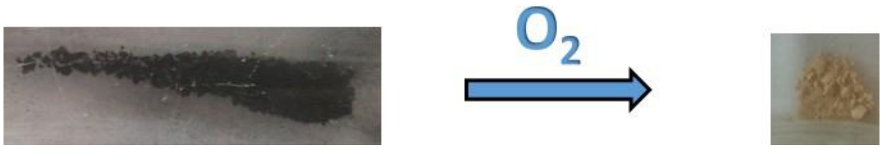

Figure 49: *Color change caused by oxidation of **o-tolyl@Sn**.*

Surprisingly, MAS-^{119}Sn NMR measurements did not show any Sn signals, as well as no reflections could be observed in powder diffraction studies. These findings strongly suggest that the formed material exhibits reduced particle sizes, as this leads to major difficulties in characterization by *e.g.* X-ray diffraction (XRD) arising from peak broadening. Furthermore, impedance measurements showed a dielectric behavior of the material.

6.2.2 Material Characterization

As stated above, the formation of reduced sized particles in the material has been suggested which provided motivation to characterize the insoluble product *via* FESEM imaging and SAXS measurements.

FESEM measurements of the black, insoluble powder showed a discrete spherical morphology suggesting a controlled and homogenous particle formation during the reaction. The particles seen in FESEM exhibit a diameter of approximately 1 µm (Figure 50). Increased magnification displays that these spheres (superstructures) are composed by smaller subunits, which seem to also be of spherical nature in a size range of 7-30 nm (Figure 51).

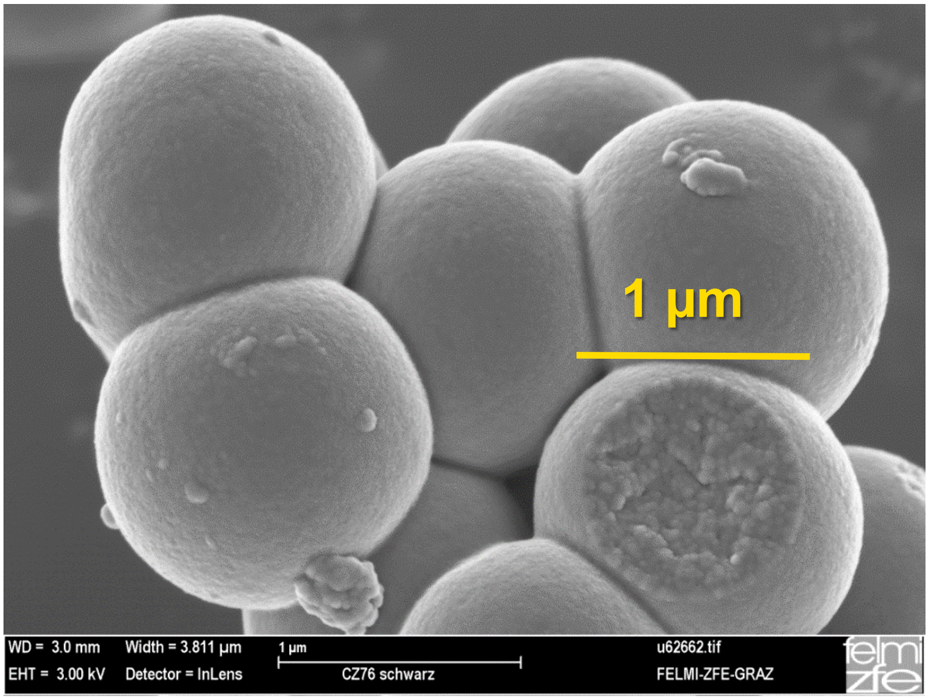
1 µm
WD = 3.0 mm
EHT = 3.00 kV
Width = 3.811 µm
Detector = InLens
1 µm
CZ76 schwarz
u62662.tif
FELMI-ZFE-GRAZ
felmi zfe

Figure 50: *FESEM showing spherical superstructures of* ***o-tolyl@Sn*** *(~ 1 µm).*

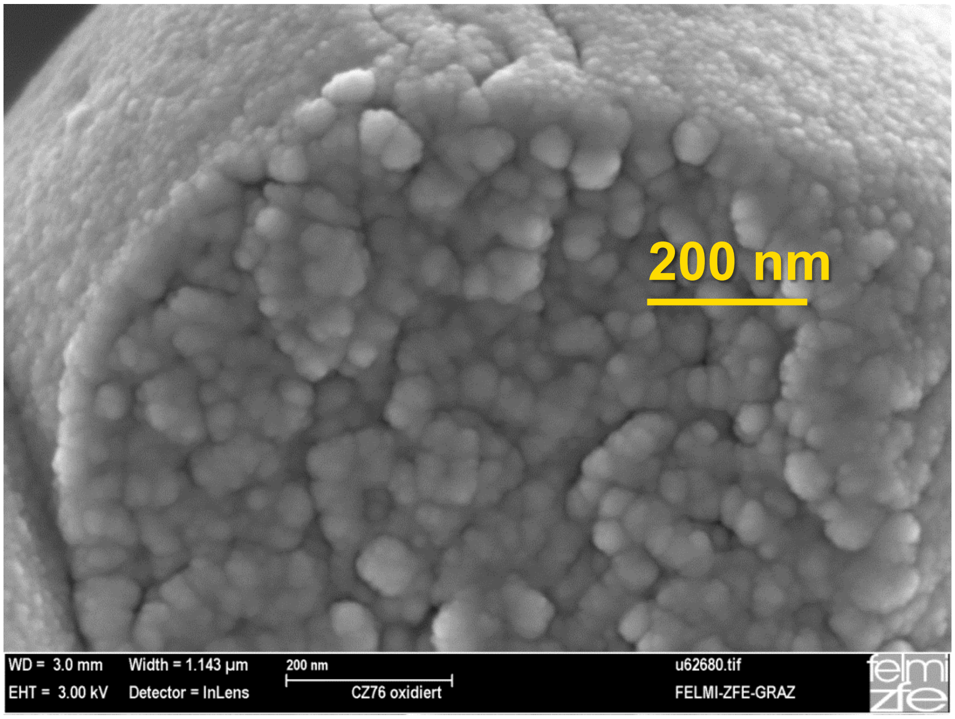
200 nm
WD = 3.0 mm
EHT = 3.00 kV
Width = 1.143 µm
Detector = InLens
200 nm
CZ76 oxidiert
u62680.tif
FELMI-ZFE-GRAZ
felmi zfe

Figure 51: *FESEM showing spherical substructures of* ***o-tolyl@Sn*** *(~ 7-30 nm).*

Consequently, the determined size range elucidated by FESEM images made additional SAXS measurements of the tin polymer ***o*-tolyl@Sn** essential. SAXS analysis revealed a discrete nanostructure in the material with a correlation length of ~1 nm which suggests that the nanosized subunits are formed when subjecting *o*-tolylSnH$_3$ (**36**) to a dehydrogenative coupling reaction. The nano-substructures agglomerate over reaction time under the formation of superstructures in the µm range (Figures 50,51). As displayed in Figure 52, SAXS analysis on the oxidized material (blue) showed that the nanostructure is altered as compared to the unexposed polymer (red). This leads to less pronounced features (Figure 52). The correlation length increases as the substructure particle size increased to ~2 nm. The size distribution and therefore polydispersity increases expressed by the peak width of the blue curve. The latter is found to be broader than for the unoxidized sample (red) (Figure 52).

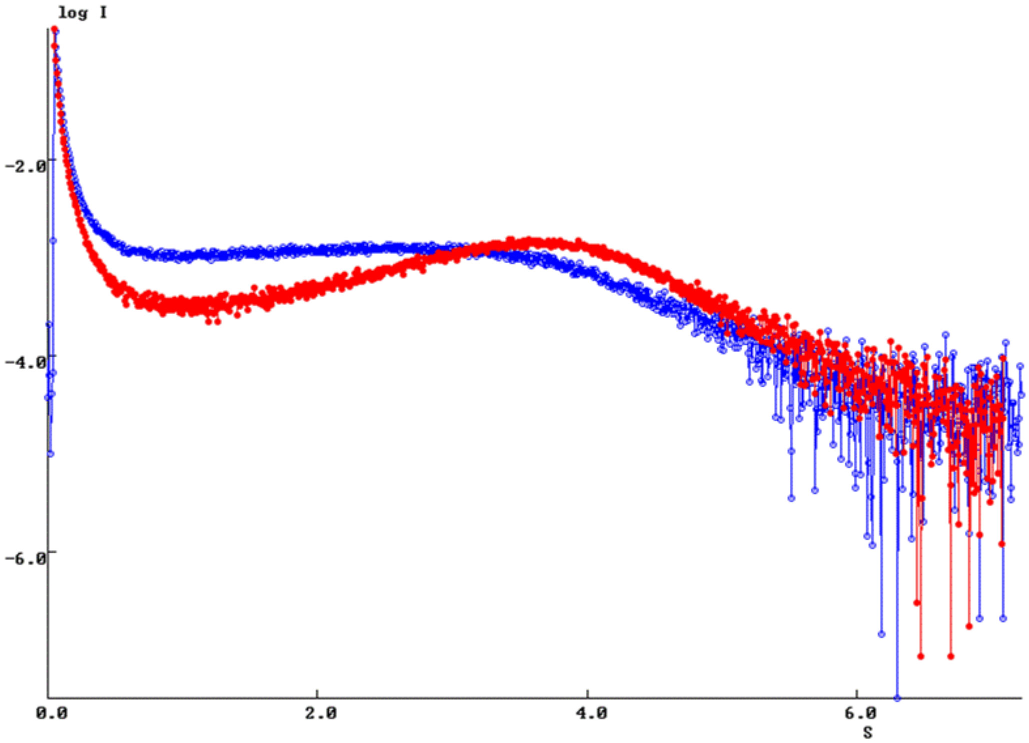

Figure 52: *SAXS pattern for* ***o-tolyl@Sn*** *(red) and* ***o-tolyl@Sn*** *oxidized (blue).*

6.2.3 Particle Formation – *In situ* Synchrotron SAXS Measurements

The found nanostructures in the synthesized polymer, as well as the interesting morphological features displayed in FESEM, provided motivation to investigate and determine the formation of sub- and super structure upon the dehydrogenative coupling reaction of *o*-tolylSnH$_3$ (**36**). Hence, *in situ* synchrotron SAXS measurements were conducted as a 0.08 M solution of diethyl ether and **36** was placed in a quartz glass capillary (OD: 1.5 mm) and sealed with a rubber septum in the dry box. Afterwards, an excess of dried and degassed TMEDA was added *via* the septum and the reaction monitored *in situ* after the capillary was placed in the beamline (Figure 53). The evolution of hydrogen was monitored by the transmission and bubbles were removed by stopping the acquisition, shaking the capillary and remounting the latter on the sample stage.

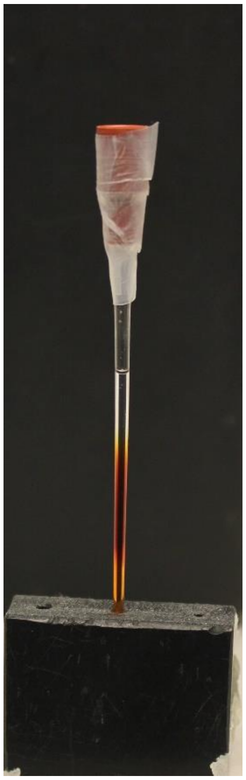

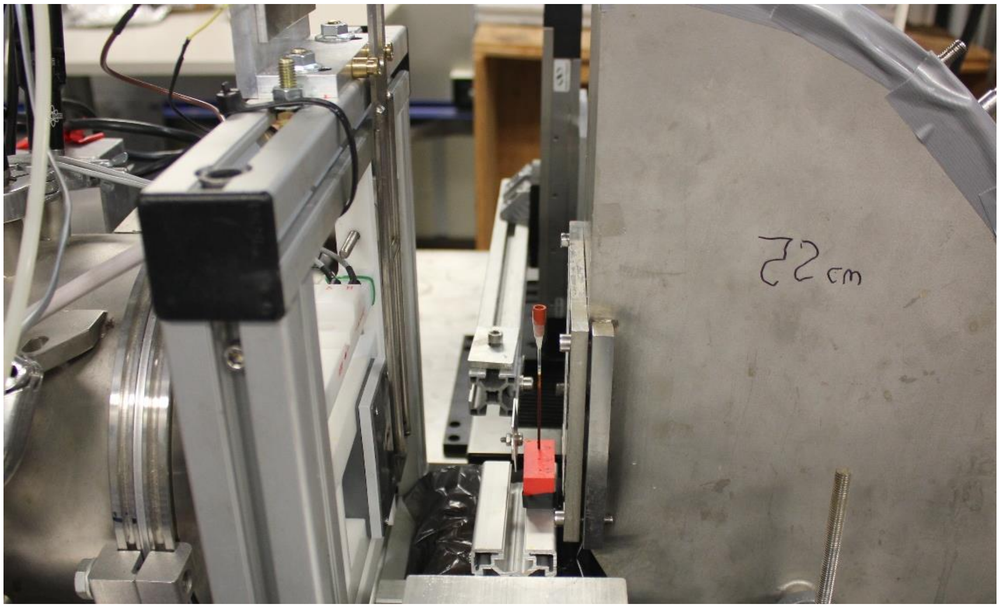

Figure 53: *SAXS in situ measurements in a septum sealed capillary.*

The SAXS data were analyzed according to the structural model reported by Pontoni *et al.*, however modified by including diffuse aggregate scattering from large agglomerates by a generalized power law term $B \cdot q^{-\alpha}$ added to the fitting function.[283,284] The polydispersity of the nanoparticle size was taken into account by considering the Schultz statistical distribution of the nanoparticle core diameters.[285] For simplicity, the hard-sphere potential combined with rectangular well attractive potential was considered to model the nanoparticle-nanoparticle interaction in decoupling approximation (Figure 54).[283] Figure 54 schematically depicts the model showing that the effective interparticle potential can be approximately described by hard-sphere repulsion with an attractive square-well.

The formula for the detected intensity reads:[284]

$$I = A \cdot < F^2(q) >_{rsph} \cdot S(q, \sigma_{hs}, \Delta_A, p_{hs}, \varepsilon_{hs}) + B \cdot q^{-\alpha}$$

Here, q is the magnitude of the scattering vector, *F(q)* is the form factor amplitude of a nanoparticle. Further, the function $f(x)=(3\ \sin x - x \cdot \cos x)/x^3$ in the form factor amplitude *F(q)* stems from the Fourier transform of a sphere, r_{sph} is the mean radius of the nanoparticle where Schultz distribution is the weighting function. $S(q,\sigma_{hs},p_{hs},\varepsilon_{hs})$ is the structure factor based on the sticky hard-sphere nanoparticle interaction potential model. Here, σhs, Δ_A and ε_{hs} are the diameter of the hard-sphere, the thickness and depth of the rectangular potential well (*i.e.* of the attractive potential, see Figure 54), and p_{hs} is the apparent volume fraction of the nanoparticles in the solution. Optimal model parameters were obtained *via* minimization of sum of squares of differences between the experimental and model data using the Marquardt-Leventberg algorithms. The estimation of the confidence intervals of the fitted parameters was obtained from the covariance matrix, which is the inverted curvature matrix involved in the Marquardt-Levenberg fitting algorithm.[286]

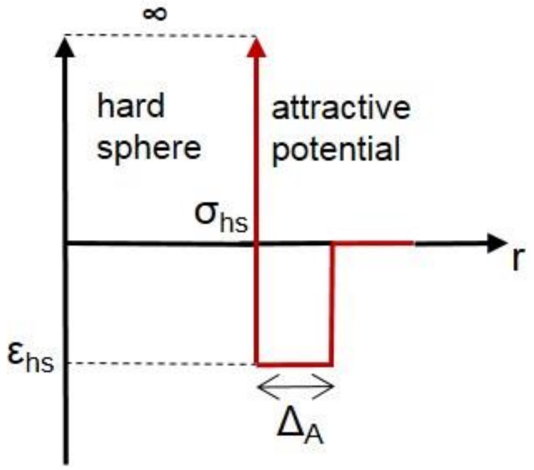

Figure 54: *Sticky hard-sphere potential model for the attractive square-well potential with a short ranged attraction and hard-sphere repulsion. Here* $\boldsymbol{\sigma_{hs}}$ *is the hard-sphere diameter,* $\boldsymbol{\varepsilon_{hs}}$ *is the depth of attractive well and* $\boldsymbol{\lambda}$***-1*** *is the range of the potential in units of* $\boldsymbol{\sigma}$*.*[283]

Figure 55 displays the normalized and background subtracted SAXS scattering pattern of the particle formation upon dehydrogenative coupling reaction of **36** with the amine base TMEDA in diethyl ether over 2 h reaction time with a time resolution of 4 min. To extract information on size evolution, size distribution and interaction of the nanoparticles, the data were fitted according to the structural model described above.

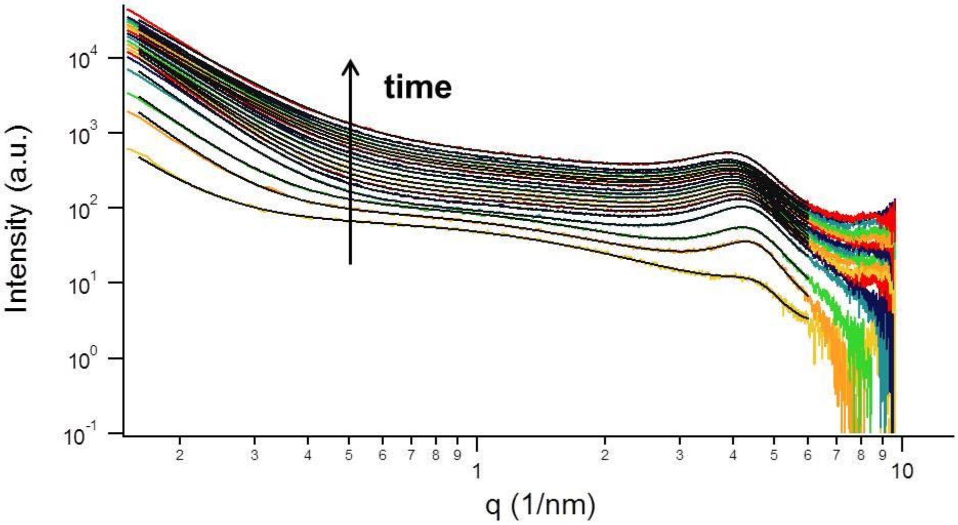

Figure 55: *Scattering pattern of o-tolylSnH*$_3$ *(**36**)/TMEDA reaction in Et*$_2$*O over the first 2 h. Time resolution for each pattern is 4 min.*

The structure development is expressed by the Porod constant strongly increasing in the first 20 min of the reaction. An immediate formation of globular nano-substructures with a diameter of 1.6 nm is observed which is expressed by the Porod parameter which reaches its maximum of 3.65 after 20 min (Figure 56). The sphere formation process is completed after 20 min reaction time which is also stated by the constant height of the peak at 4.3 nm^{-1} in Figure 55. Afterwards, the nano-substructures aggregate to bigger structures. The size of these bigger structures cannot be resolved as they fall out of the *q* area, however the scattering of these aggregates is observed as a decrease of the Porod exponent lower than 3.4 (Figure 56). This is due to a bigger distribution function caused by the aggregation of smaller subunits to bigger structures showing higher porosity which has been evidenced by FESEM (Figures 50,51).

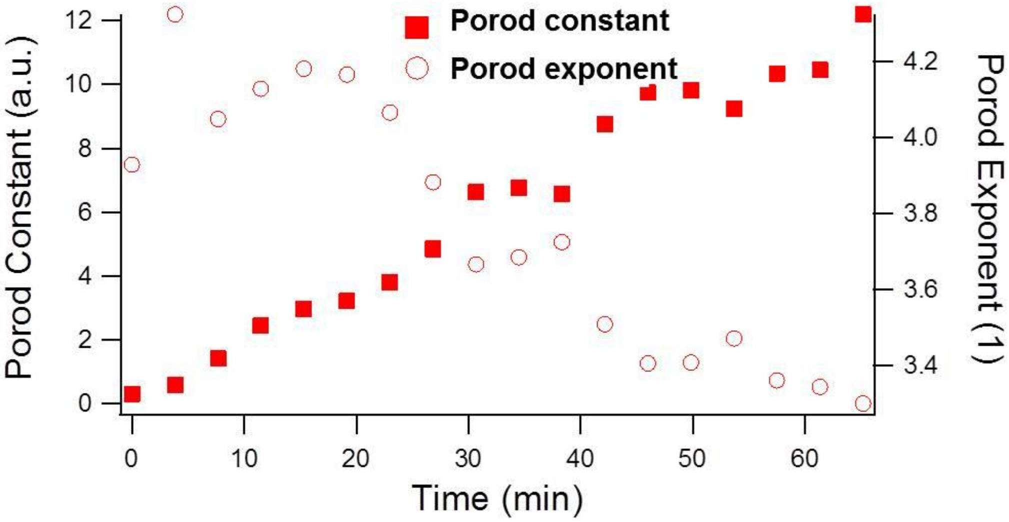

Figure 56: *Porod constant (a.u.) and Porod exponent fitted on the low q part of the scattering pattern of o-tolylSnH*$_3$ *(**36**)/TMEDA reaction in Et*$_2$*O versus time (min).*

A Lorentz fit with linear background for the size distribution of the formed particles also shows a fast structure formation in the first 20 min expressed by an increase of the structure peak which is related to the dimension of the formed particles. This d-spacing increases to ~ 1.6 nm and stagnates afterwards (Figure 57). Since the number of formed particles increases especially in the beginning of the polymerization reaction a rise in intensity is observed as well (Figure 57).

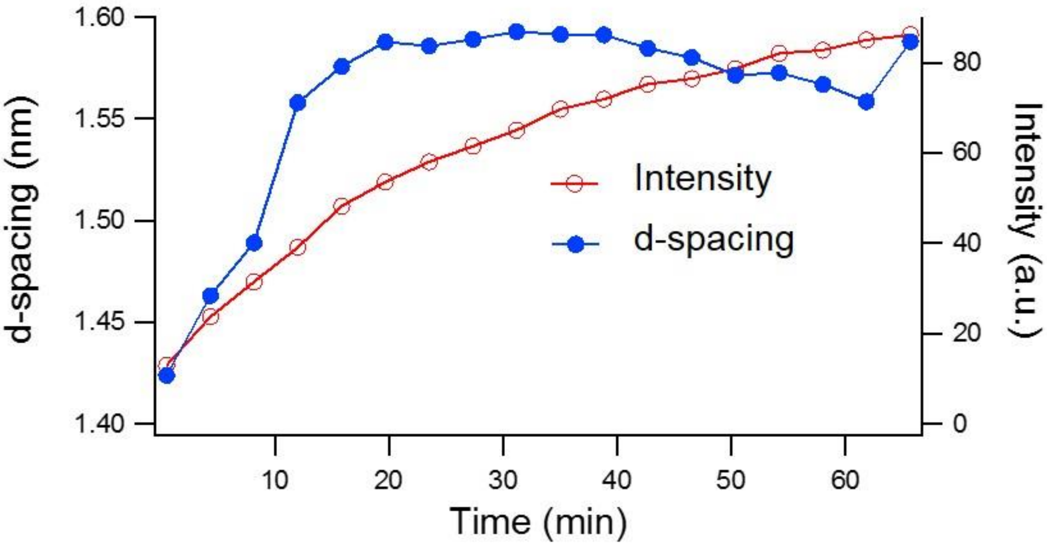

***Figure 57:** Lorentz peak fit with linear background of the scattering pattern of o-tolylSnH_3 (**36**)/TMEDA reaction in Et_2O. d-spacing (nm) and the intensity (a.u.) versus time.*

The hard sphere radius (r_{hs}) evolution is in accordance with the d-spacing increase seen in Figure 57 revealing the growth of nano-substructures. In this manner, two times the r_{hs} equals the calculated d-spacing. Furthermore, a slight volume fraction (p_{hs}) decrease is observed from 0.2 to 0.15. The regime of the stickiness potential (λ_{hs}) reduces from 0.7 to 0.5 over reaction time. The strong increase in ε_{hs} from 0.2 to 2.5 indicating an attractive potential between the particles, correlates to the agglomeration of nano-substructures to bigger aggregates.

Scheme 83 schematically illustrates the fast nano-substructure formation of spherical particles with a diameter of 1.6 nm in the first 20 min. Consequently, the nanospheres agglomerate to bigger superstructures which leads to an intensity increase. After 25 min the attachment of substructures to aggregates and therefore, reduction of spherical character is suggested.

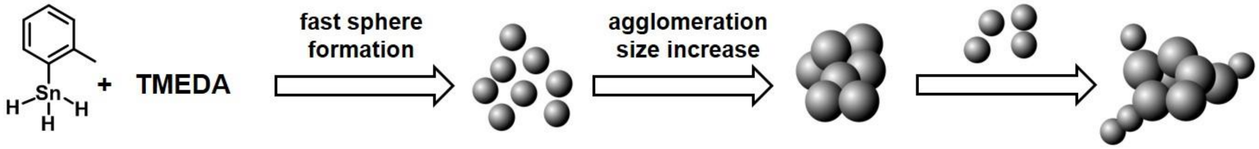

***Scheme 83**: Schematic growth process of nanoparticles **o-tolyl@Sn** in Et_2O.*

6.2.4 TEM Imaging

TEM measurements on ***o*-tolyl@Sn** were carried out in order to complement the data acquired by *in situ* SAXS measurements on the evolution of spherical nanostructures in the dehydrogenative coupling reaction of *o*-tolylSnH$_3$ (**36**) with TMEDA in diethyl ether. Therefore, the isolated powder was deagglomerated by ultrasonication in the dry box and small amounts of the suspension (THF) transferred onto a holey carbon coated copper grid. By using an especially designed sample holder (Gatan), sample transport and measurement was feasible under inert conditions (Figure 107). While acquiring the TEM images, several obstacles were encountered, as the expected substructures with a size of only 1.4 nm could not be resolved, as well as the particles' surface easily interact with the electron beam and beam induced damage could be observed. This interaction can be best described by a morphing of a particle due to evaporation or cleavage of the organic shell, suggesting a Sn core being surrounded by an organometallic layer. This tin core exhibits a higher contrast as visualized in Figure 58 B. In addition, an ordered structure was observed by the presence of interplanar distances of 0.2841 nm suggesting a crystalline arrangement. However, the presence of a lighter contrast (organic nature) in the inside of the particle could suggest a layered structure as schematically represented in Figure 59.

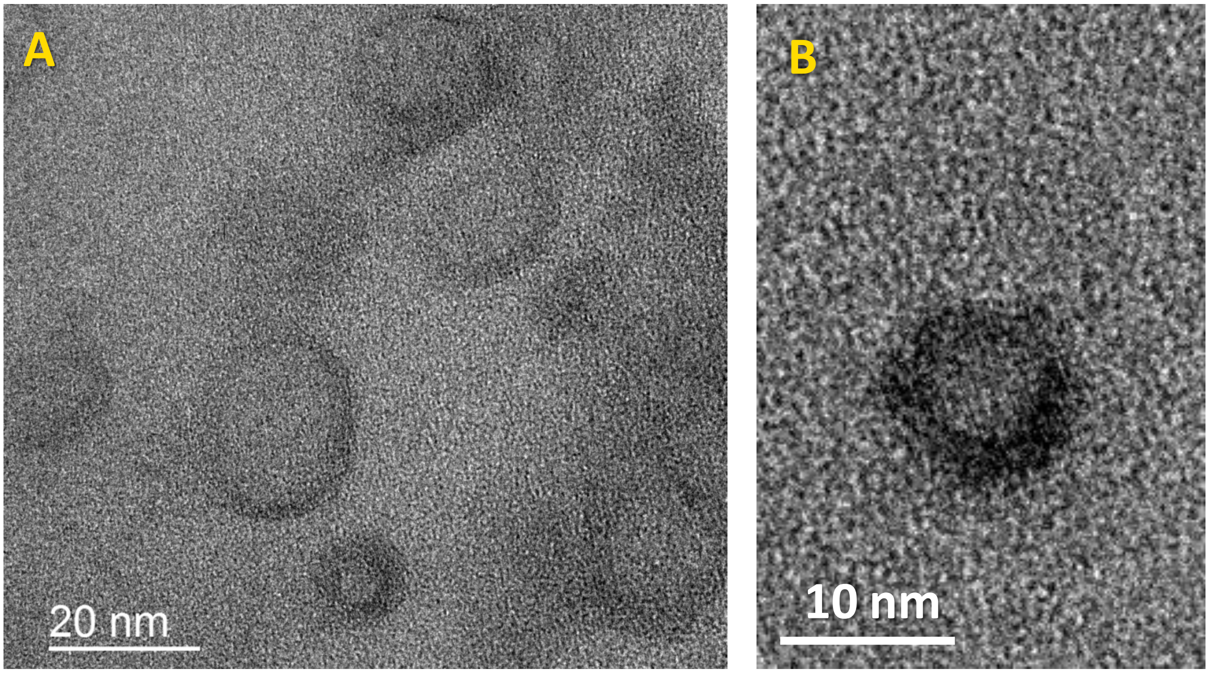

Figure 58: *TEM images of* ***o-tolyl@Sn*** *from diethyl ether.*

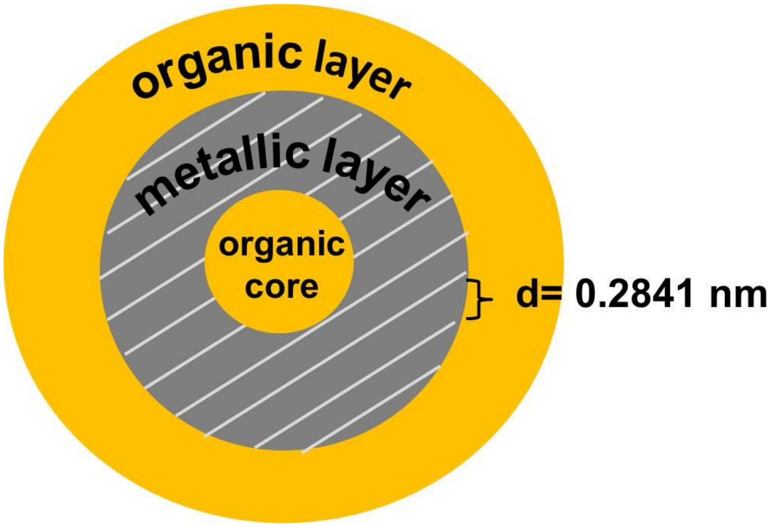
organic layer
metallic layer
organic core
d= 0.2841 nm

Figure 59: *Schematic structure of aryl@Sn as a layered core shell particle.*

Images acquired in the STEM modus, however at lower resolutions, showed bright spots in the case of sample containing elements with high number of electrons (Figure 60). Figure 61 displays agglomerates in a size up to 100 µm and sample fractions smaller than 10 nm. Additional EDX measurements were carried out on the larger agglomerates proving the existence of Sn (Figure 61).

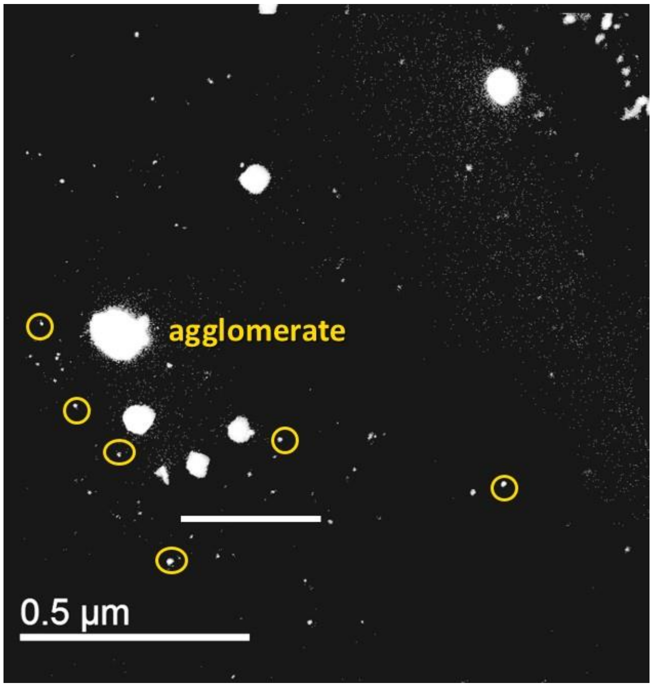
agglomerate
0.5 µm

Figure 60: *STEM images of* ***o-tolyl@Sn*** *from diethyl ether.*

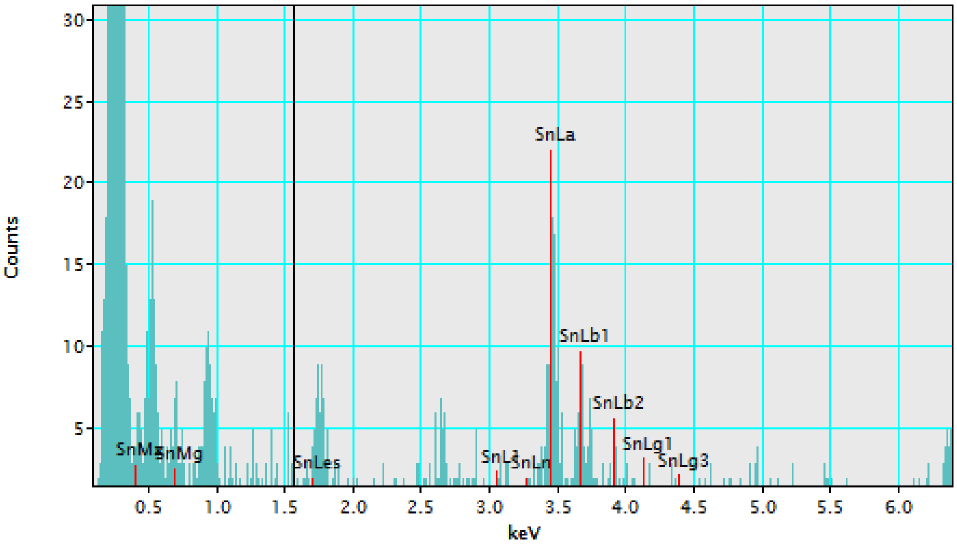

Figure 61: *EDX spectrum of* ***o-tolyl@Sn*** *from diethyl ether.*

6.2.5 *In situ* DLS Measurements

Despite SAXS analysis being a powerful tool to resolve nanostructural information of the sample in the range from 1 to 100 nm in real space, data on the growth process for bigger structures bigger cannot be acquired. However, dynamic light scattering (DLS) allows for the investigation of particle growth from 1 nm up to µm. Thus, the dehydrogenative coupling reaction of *o*-tolylSnH$_3$ (**36**) was subjected to an *in situ* DLS measurement over reaction time. Therefore, a 8.9 mg/L solution of **36** in dried and degassed diethyl ether was prepared in the dry box and carefully filtered through a 20 nm syringe filter in order to remove undesired particles. The solution was transferred into a glass GC vial and closed with an air tight septum crimp cap. The amine base TMEDA was also filtered. Before the addition of TMEDA, the trihydride solution was measured as a blank. Subsequently, two drops of TMEDA were added *via* the septum and the particle formation monitored over reaction time of 40 min using a green laser. As the scattering intensity increases with r^6 of the hydrodynamic radius of the measured particles, little intensity was observed in the very beginning of the reaction which does not allow for reliable data analysis as the signal cannot be distinguished from eventual impurities in the sample itself. However, as known from SAXS analysis nano-substructures are formed within the first minutes of reaction time. After 4 min reaction time, a main population of 100 nm could be observed as indicated with a blue line in Figure 62.

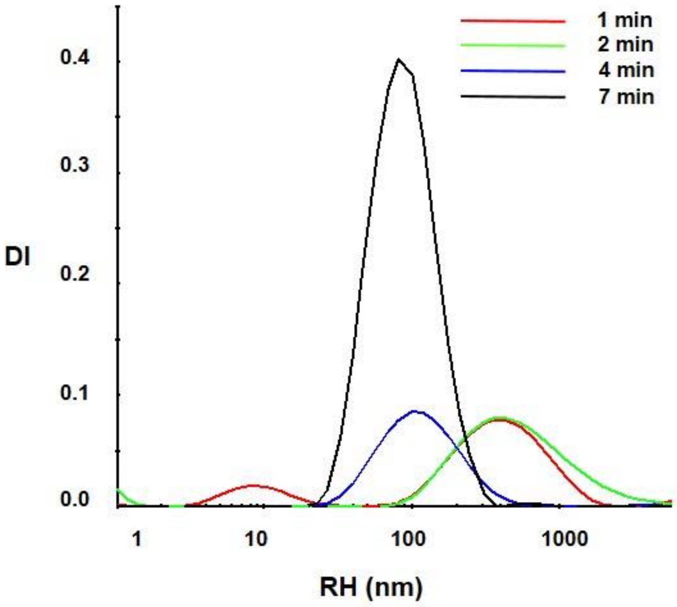

***Figure 62**: Evolution of the hydrodynamic radius RH (nm) after 1, 2, 4 and 7 min reaction time.*

Figure 63 displays a more or less linear growth process of particles from 100 nm (5 min) up to 600 nm radius (40 min), whereas the intensity evolution over reaction time (Figure 64) can be separated into three different stages as it does not proceed in a linear manner. During stage **I** (0-5 min), little to no intensity can be measured, however based on SAXS data analysis this stage belongs to the formation of nano-substructures. After 5 min reaction time a strong increase in intensity is observed (stage **II**) as the particles grow to the main population of 100 nm RH, as well as they are suggested to agglomerate forming bigger structures (Figure 63). This is followed by stage **III**, showing a flattening of the intensity (Figure 64). This evolution is hard to interpret since particles are not monodisperse and their larger sizes do not allow for direct correlation of intensity and size evolution. Additionally, sedimentation of bigger particles is likely to occur. However, this stage is suggested to be mainly dominated by aggregation processes to bigger super-structures. After 40 min reaction time, the particles exhibit a radius of 600 nm (Figure 63).

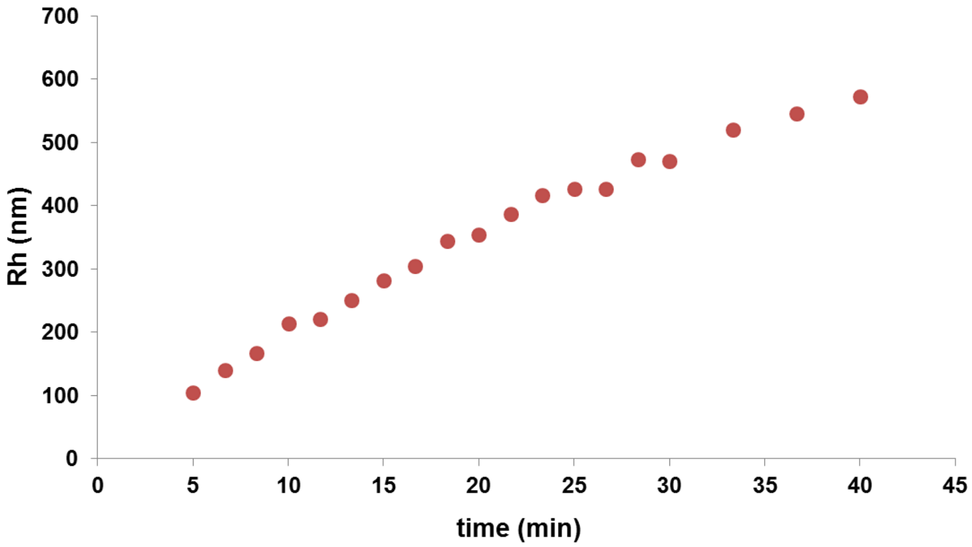

Figure 63: *Size evolution (nm) over reaction time (min).*

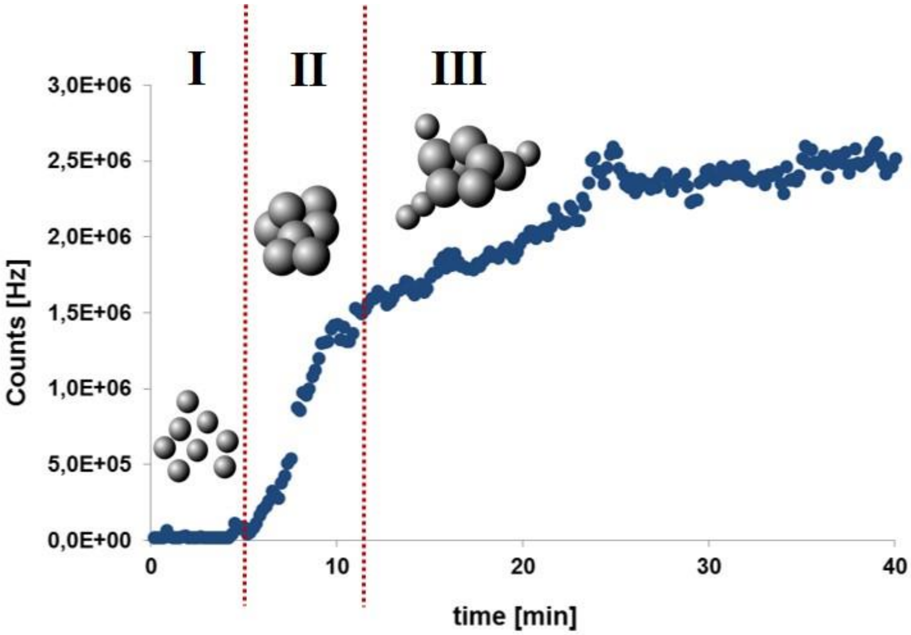

Figure 64: *Intensity increase (Hz) over reaction time (min),* ***I****: substructure formation,* ***II****: growth and aggregation,* ***III****: mainly aggregation.*

6.2.6 Insights into the Reaction Mechanism

There is a fundamental lack of knowledge on how the amine base interacts with the tinhydride in order to form Sn–Sn bonds and molecular hydrogen. The nature of the Sn–H bond can be interpreted in different ways leading to various reaction possibilities. Depending on the reaction conditions and the agent added to organo stannanes, the Sn–H bond can be cleaved homolytically forming Sn and H radicals which is mainly exploited for radical addition, rearrangement and elimination reactions.[5] However, this oxygen labile bond is also known to react as a hydride donor making the tin atom an electropositive center. Controversially, the hydrogen can also undergo a deprotonation using a strong base like LDA (lithium diisopropylamide) or *n*-BuLi in order to form tin anions. Furthermore, no information is available on the conversion of trifunctionalized educts and the formed polymeric materials. Hence, the reaction progress and its mechanism as well as the material's characteristic and the composition on a molecular level are the key investigation questions.

The synthesized polymer was subjected to elemental analysis in order to reveal the elemental composition (C,H,N) (Table 15). As the GC-MS measurements of the supernatant liquid, gained by filtration of the insoluble product, show the presence of toluene, a cleavage of aromatic groups is expected to be reflected in a lack of C and H content of the polymer.

In the calculated composition **(*o*-tolylSn)$_n$** every Sn atom is still bonded to one organic moiety, as it is seen in the educt **36**. This structure represents a reaction product obtained by the exclusive abstraction of hydrogen. However, the filtered material shows a lower carbon content than expected (Table 15). This is in accordance to the loss of toluene evidenced by GC-MS measurements of the filtrate. It can be concluded that the isolated material, ***o*-tolyl@Sn**, must contain tin atoms in the structure that are exclusively surrounded by other tin atoms, thus tin in oxidation state zero.

Table 15: *Elemental composition of* ***o-tolyl@Sn****.*

***o*-tolylSn polymer**	**element (%)**		
	C	H	N
found *o*-tolyl@Sn	27.57	2.42	0.72
calculated (*o*-tolylSn)$_n$	40.07	3.36	0

***o*-tolyl@Sn** was further subjected to a TGA/DSC-MS measurement. Therefore, the product was transferred in a small aluminum pot with a lid in the dry box. The material showed the melting point of elemental tin (232 °C) upon heating which supports the existence of tin in the oxidation state zero encumbered by an organometallic layer. This is again in accordance to the loss of organic residues and therefore changing the bonding environment by partially reducing Sn(IV) to oxidation state 0, suggesting a reductive reaction mechanism. Furthermore, an irreversible phase transition is observed at 466 °C.

6.2.7 Proposed Reaction Mechanism

In order to understand the interaction of aryltin trihydrides with the amine base TMEDA, the conversion of the model substrate phenylSnH_3 with the amine base is investigated by DFT calculations (MPW1PW91/sdd). The free phenylSnH_3 (**I**) exhibits a Sn–H bond length of 1.723 Å (Figure 65). According to calculations, phenylSnH_3 can undergo either a penta (**II**) or hexa (**III**) coordination with the electron donating nitrogen atoms of the TMEDA structure. Figure 65 displays the minimum geometries for all three possibilities. The relative energy gains in comparison to the uncoordinated phenylSnH_3 can be calculated with -8.2 kJ/mol for the penta coordinated adduct (**II**) and -8.7 kJ/mol for the hexa coordinated species (**III**). Therefore, phenylSnH_3 most likely undergoes a hexa coordination (**III**) with the both nitrogen atoms of the amine base TMEDA.

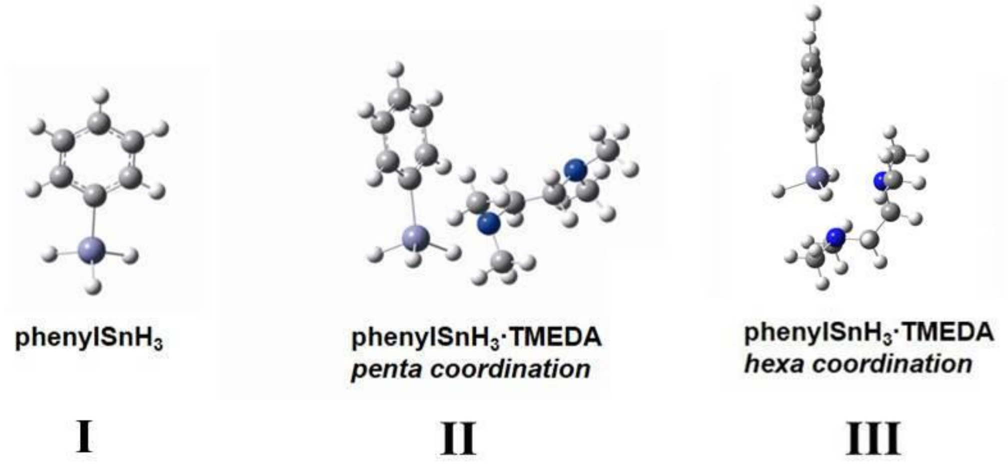

Figure 65: *Calculated minimum geometries for uncoordinated phenylSnH_3 (**I**), penta coordinated phenylSnH_3·TMEDA (**II**) and hexa coordinated phenylSnH_3·TMEDA (**III**).*

Furthermore, it can be stated that double coordination of the nitrogen atoms to the tin in adduct **III** results in a notable increase in the Sn–H bond length (1.758 Å) for the hydrogen atom located orthogonal to the N–Sn–N plane in comparison to uncoordinated phenylSnH_3 (**I**) and therefore weakening it (Table 16). This is consistent with a stronger Sn–N interaction which is nicely reflected in the shorter Sn–N bond for the hexa coordinated species (**III**) (2.781 Å).The Sn–H bond elongation is less pronounced in the case of penta coordination **II** (Table 16).

Table 16: *Selected calculated bond lengths for uncoordinated (I), penta (II) and hexa (III) coordinated phenylSnH_3.*

	I	**II**	**III**
	calculated bond length (Å)		
Sn–H_1	1.721	1.724	**1.758**
Sn–H_2	1.721	1.723	1.749
Sn–H_3	**1.723**	**1.746**	1.749
Sn–C	2.151	2.154	2.187
Sn–N		**2.947**	**2.781**

The coordination of TMEDA to the Sn atom of the educt and thus Sn–H bond elongation and weakening, facilitates the formation of H_2 and therefore initializes the dehydrogenative coupling reaction of arylSnH_3. It has to be noted that DFT calculations, as well as experiments showed that the donor ability of the phosphorous equivalent of TMEDA, DMPE (dimethylphosphinoethane), is not sufficient to induce hydrogen abstraction and Sn–Sn bond formation. This has also been reported by Sindlinger who has not observed any reaction when converting Ar*SnH_3 with DMPE.[259] However, DFT calculations showed a preferred interaction from DMPE to the phenyl group of the model substrate phenylSnH_3 and therefore a computed elongation of the Sn-C bond from 2.150 Å to 2.164 Å.

Applying DFT calculations, the dehydrogenative coupling reaction on the model substrate phenylSnH_3 and the amine base TMEDA a reaction pathway (Scheme 84), as well as the corresponding energy levels can be elucidated (Figure 66).

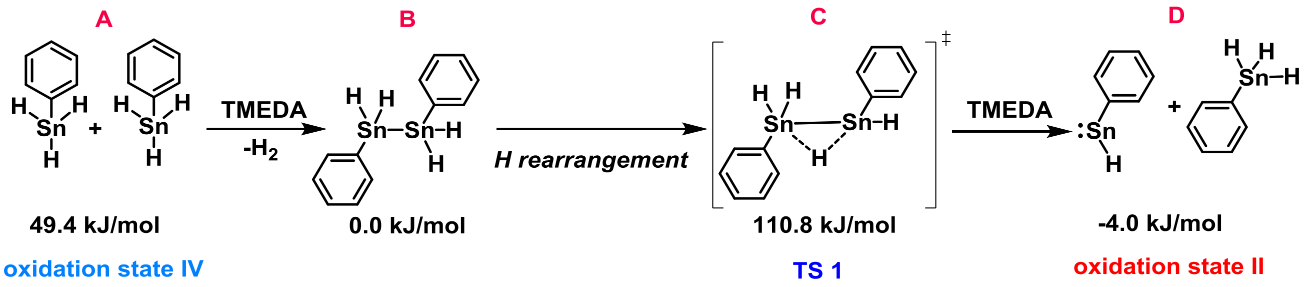
A
B
C
D
TMEDA
-H2
H rearrangement
TMEDA
‡
49.4 kJ/mol
0.0 kJ/mol
110.8 kJ/mol
-4.0 kJ/mol
oxidation state IV
TS 1
oxidation state II

Scheme 84: *Suggested redox mechanism for the formation of a reactive Sn(II) intermediate upon the dehydrogenative coupling reaction of phenyl*SnH_3 *calculated by DFT (MPW1PW91/sdd).*

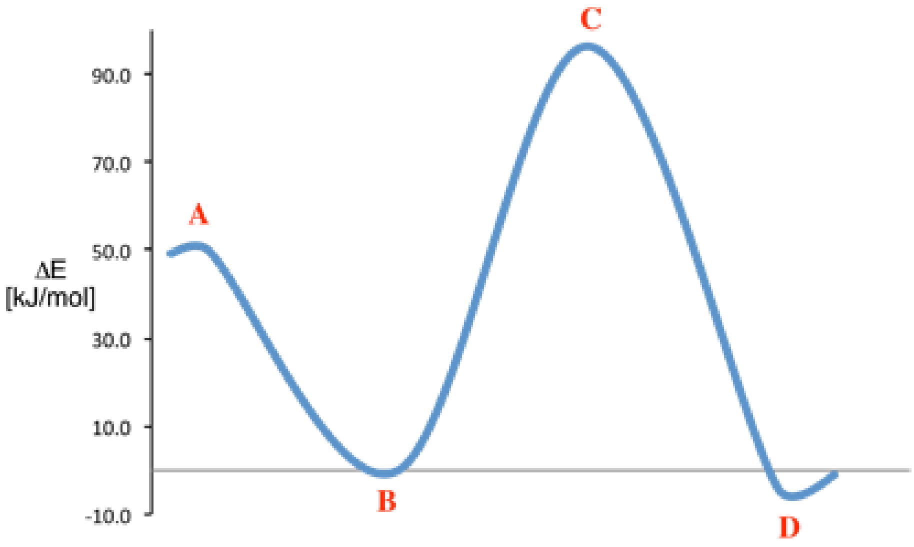

Figure 66: *Reaction pathway for the dehydrogentive coupling reaction of phenyl*SnH_3 *(MPW1PW91/sdd).*

In this reaction sequence, the distannane **B** is found as the first intermediate with an energy of 0 kJ/mol, which corresponds to the loss of one molecule of hydrogen (Scheme 84).

The respective Sn–Sn coupled product (Ar*H_2Sn–SnH_2Ar*) was also observed by Sindlinger and coworkers when converting the sterically highly encumbered Ar*SnH_3 (Ar*=2,6-trip$_2$(C_6H_3), trip= 2,4,6-triisopropylphenyl) with a catalytic amount of amine bases such as pyridine, DMAP or TMEDA.[259] However, when applying an amine catalyzed dehydrogenative coupling on the sterically less encumbered educt *o*-tolylSnH_3 (**36**), the suggested intermediate **B** could not be isolated. The *o*-tolyl residue is too small to allow for steric stabilization of this intermediate **B** and therefore the latter continuous reacting along the reaction pathway.

Subsequently, the transition state **C** (**TS 1**) (110.8 kJ/mol) displaying a hydrogen rearrangement is observed for the model substrate phenylSnH_3 (Figure 67). This transition state **C** (**TS 1**) further allows for Sn–Sn bond cleavage under the formation of a Sn(II) (phenylHSn:) intermediate and the educt phenylSn(IV)H_3 (**D**). Thus, the conversion of phenylSnH_3 with TMEDA is a reductive process in which the educt Sn(IV) (**A**) is converted to a stannylene intermediate (**D**) which corresponds to the loss of two molecules of hydrogen. This proposed reductive process is in accordance to the findings of Sindlinger *et al*., who converted Ar*SnH_3 with an excess of DMAP and successfully determined the existence of a DMAP stabilized Sn(II) hydride species (Ar*SnH·DMAP) by NMR studies also suggesting a reductive process.

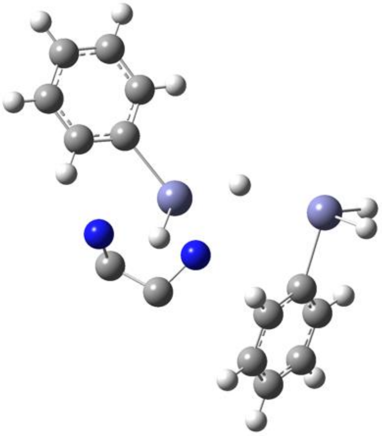

Figure 67: *Calculated minimum geometry for* ***C*** *(****TS 1****) in the dehydrogenative coupling reaction of phenylSnH_3 with TMEDA.*

However, in the case of Ar*SnH_3 the dehydrogenative coupling reaction stops after cleavage of two molecules of hydrogen, as the formed stannylene (Ar*SnH·DMAP) is thermodynamically stable due to the large aromatic substituents. Even upon heating of Ar*SnH_3 in the presence of a variety of amine bases (*e.g*. pyridine, DMAP, TMEDA) Sindlinger did not observe the formation of higher molecular Sn species.[259]

In stark contrast, converting less sterically stabilized aryltin trihydride as postulated for the model substrate phenylSnH_3, the reductive process does not stop at this stage. The unstabilized stannylene (**D**), which is a very reactive and short term intermediate, consequently inserts into the Sn–Sn bond of **B** to realize chain elongation as well as network formation *via* a reductive process (Scheme 85).

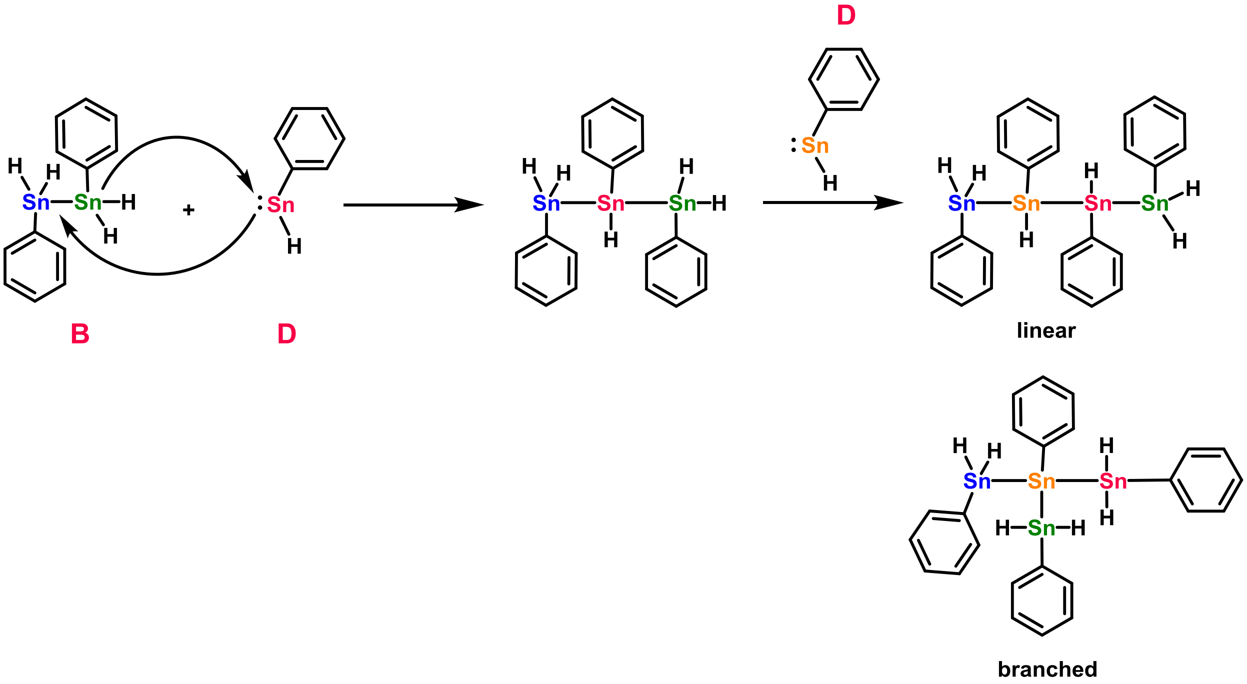

Scheme 85: *Suggested mechanism for chain elongation by Sn(II) insertion forming phenyl@Sn.*

Similarly found as for phenylSnH_3, DFT calculations on the conversion of *o*-tolylSnH_3 (**36**) with TMEDA also show the formation of the distannane **B** (Scheme 86). Most likely, **B** undergoes formation of toluene and the instable intermediate **E** *via* ***TSi*** on route ***i)***. ***TSi*** is displayed in Figure 68. **E** immediately decomposes to *o*-tolylSnH_3 and the stannylene H_2Sn: (**F**). The formation of toluene as a side product was experimentally evidenced by GC-MS analysis as well as NMR measurements. Another possible reaction pathway is route ***ii)*** *via* transition state **TS*ii***, which is in accordance to the reaction process found for phenylSnH_3 (Scheme 84). However, **TS*ii*** which should correspond to **TS1** (Scheme 84) could not be localized by calculations. The least favored reaction pathway is route ***iii)*** which represents a homolytic cleavage of the Sn–Sn of **B** forming two *o*-tolylSnH_2 radicals (Scheme 86). The low probability is also reflected in *in situ* EPR measurements which did not show the presence of radicals.

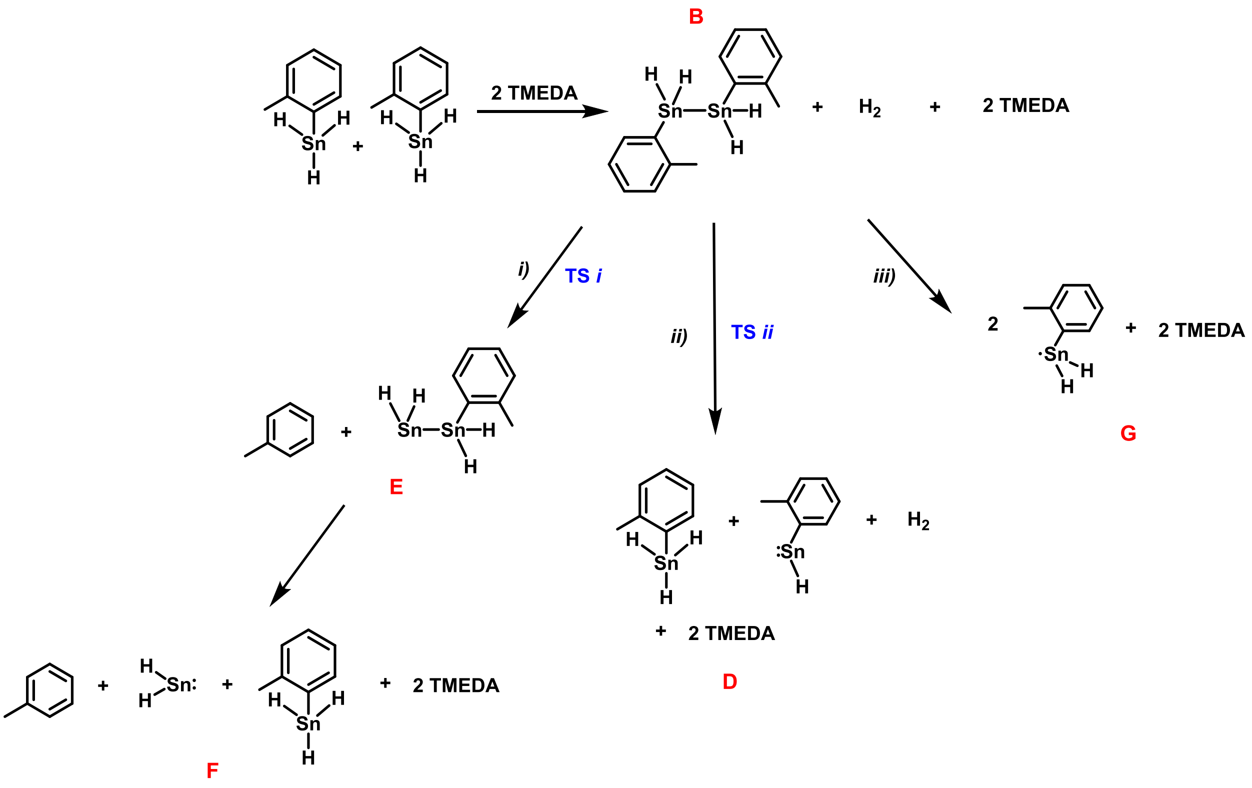
B
2 TMEDA
+ H2 + 2 TMEDA
i)
TS *i*
ii)
TS *ii*
iii)
2
+ 2 TMEDA
G
E
+ H2
+ 2 TMEDA
D
+ 2 TMEDA
F

Scheme 86: *Suggested redox mechanism for the formation of toluene as a side product in the dehydrogenative coupling reaction of o-tolylSnH$_3$ (**36**) calculated by DFT (MPW1PW91/sdd).*

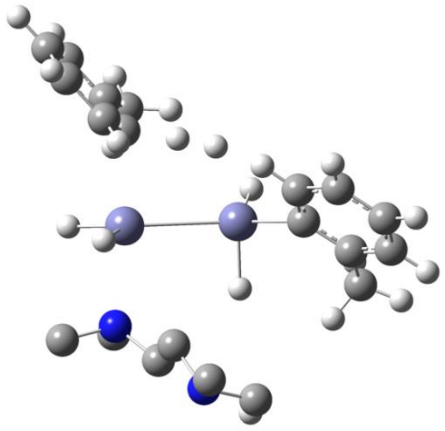

Figure 68: *Calculated minimum geometry for transition state i (**TS i**) in the dehydrogenative coupling reaction of o-tolylSnH$_3$ (**36**) with TMEDA.*

As already described in section 6.2.1, the conversion of arylSnH_3 with TMEDA proceeds with a pronounced color change over reaction time (Figure 48). Linear polystannanes have been reported to significantly exhibit electron delocalization along the Sn backbone. This leads to characteristic yellow or orange-yellow color showing absorption maxima in UV-VIS spectra at around 375-410 nm.[135,150,163,177] Furthermore, the proposed Sn(II) intermediate (**D**) (Scheme 84) is suggested to exhibit an absorption maximum in the visible region. For that matter, additional DFT calculation on the absorption maxima of possible intermediates in the conversion of the model substrate phenylSnH_3 were carried out. These calculations serve as reference points in the *in situ* UV-VIS measurements of the dehydrogenative coupling reaction of *o*-tolylSnH_3 (**36**) with TMEDA. The use of standard quartz glass cuvettes sealed with a screw cap was not possible as an optic pathlength of even 4 mm led to complete saturation of the signal. This effect usually can be circumvented by lowering the concentration of the educt solution. In this case, this resulted in decreased reaction speed which did not allow for reasonable data acquisition. Therefore, the measurements were conducted under inert conditions in a quartz glass capillary (OD: 1.5 mm) sealed with a rubber septum. According to detailed concentration studies, the *o*-tolylSnH_3/diethyl ether concentration of choice is 3.4 mM to monitor changes in the absorption maxima over time Figure 69 displays the UV-VIS measurements (200-700 nm) over 2 h reaction time. The time resolution for each scan accounts for 1 min. After addition of TMEDA, an immediate change from the first measurement (black curve) to the subsequent one (red curve) was detected expressed by an increase of intensity at 280 nm. Comparing these findings to calculated absorption maxima in the conversion of the model substrate phenylSnH_3, this peak compares nicely to the postulated distannane intermediate H_2(phenyl)Sn–Sn(phenyl)H_2 (**B**) calculated at 278 nm exhibiting a strong HOMO-LUMO transition. This also supports that the formation of **B** as a local minimum (Figure 66) proceeds very fast (3 min), as addition of TMEDA to the educts facilitates H_2 abstraction. The peak maximum at 240 nm relates to the theoretical absorption maximum of a hexa coordinated phenylSnH_3·TMEDA complex (235 nm) which is displayed in Figure 65, as the starting point for the subsequent H_2 formation by Sn–H bond elongation. Furthermore, a pronounced bathochromic shift as well as an increase in intensity could be observed as the number of Sn–Sn bonds is growing over reaction time. Three notable wavelengths at lower energies are located in the spectra at 459, 480 and 527 nm (Figure 69). Furthermore, the possible short term intermediates phenyl$_2$Sn: and phenylHSn: (**D**) exhibit theoretical absorption maxima at 526 and 537 nm, respectively. These two maxima fall in the range of the peak observed in Figure 69 at 527 nm.

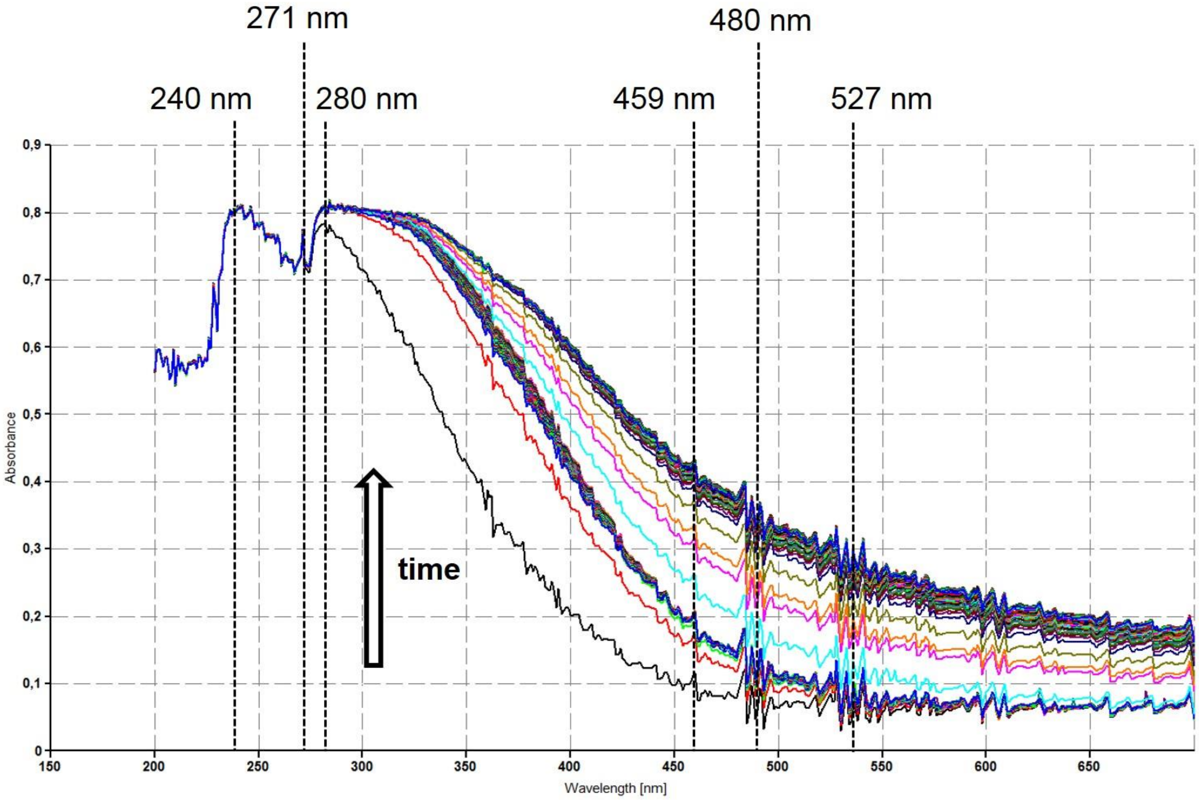

Figure 69: *In situ UV measurements of the dehydrogenative coupling reaction of o-tolylSnH*$_3$ *(**36**) in diethyl ether. Time resolution for each scan is 1 min.*

6.2.8 Thermally Induced Dehydrocoupling

The use of TMEDA in the dehydrogenative coupling reaction of sterically unstabilized aryltin trihydride, *o*-tolylSnH$_3$ provokes fast polymer formation *via* the short term distannane intermediate **B** (Scheme 84). In an effort to circumvent the immediate polymer formation and therefore verify the formation of **B**, a dehydrogenative coupling reaction in the absence of the amine base was studied. The knowledge that Sn–H bonds exhibit a high degree of temperature lability, which is exploited for Sn–Sn bond formation upon hydrogen cleavage, provided motivation to investigate the thermally induced dehydrocoupling of *o*-tolylSnH$_3$ (**36**).[10]

In this case, **36** was warmed up for 20 min to 80 °C under *vacuo* (10^{-4} mbar) to afford a dark red to brown solid which was taken up in benzene to precipitate insoluble polymers. The supernatant solution was subjected to ^{1}H, ^{119}Sn and ^{13}C NMR analysis which successfully proved the formation of a Sn–Sn coupled intermediate H_2[(*o*-tolyl)Sn–Sn(*o*-tolyl)]H_2 (**55**). The structure of **55** is in accordance to the postulated intermediate **B** (Scheme 84) and the findings of Sindlinger and coworkers who described the formation of H_2[(aryl*)Sn–Sn(aryl*)]H_2.[259] Furthermore, formation of **55** also compares nicely to Khan's results who reported on the solvent and catalyst free dehydrocoupling of *n*-butyl$_2$SnH$_2$ forming hydrogen terminated distannanes H[(*n*-butyl)$_2$Sn–Sn(*n*-butyl)$_2$]H in the presence of the polystannane [(*n*-butyl)$_2$Sn]$_n$ and cyclic byproducts [(*n*-butyl)$_2$Sn]$_{n=5,6}$.[10]

Figure 70 displays the ^{1}H NMR (C_6D_6) of H_2[(*o*-tolyl)Sn–Sn(*o*-tolyl)]H_2 (**55**), as well as and Figure 71 shows selected regions of this spectrum. Coupling constants and characteristic coupling patterns are illustrated with dotted lines. In Figure 71 the $^{1}J(^{119}\text{Sn-}^{1}\text{H})$ and $^{1}J(^{117}\text{Sn-}^{1}\text{H})$ values (1734 and 1656 Hz) compare very well with the reported coupling constants for H_2[(aryl*)Sn–Sn(aryl*)]H_2 (1777 and 1700 Hz).[259] The $^{2}J(^{119/117}\text{Sn-}^{1}\text{H})$ along the Sn–Sn bond (135 Hz) also fits to the published value of 145 Hz. However, the Sn–$\underline{\text{H}}$ shift of **55** at 5.07 ppm is located more upfield than in the case of H_2[(aryl*)Sn–Sn(aryl*)]H_2 (3.94 ppm). In the ^{119}Sn spectrum, H_2[(*o*-tolyl)Sn–Sn(*o*-tolyl)]H_2 (**55**) is found at -370.7 ppm and shows expected splitting when measured ^{1}H coupled (Figure 72). H_2[(aryl*)Sn–Sn(aryl*)]H_2 exhibits a shift of -393.4 ppm.[259]

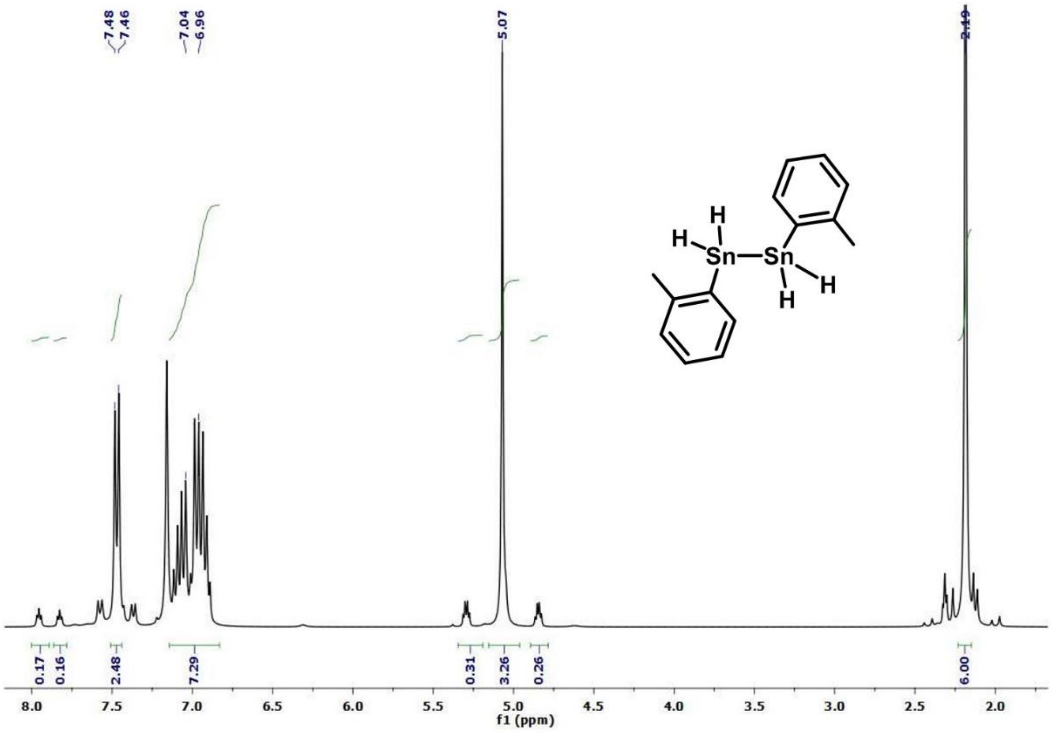

Figure 70: *^{1}H spectrum of H_2[(o-tolyl)Sn–Sn(o-tolyl)]H_2 (**55**) in C_6D_6.*

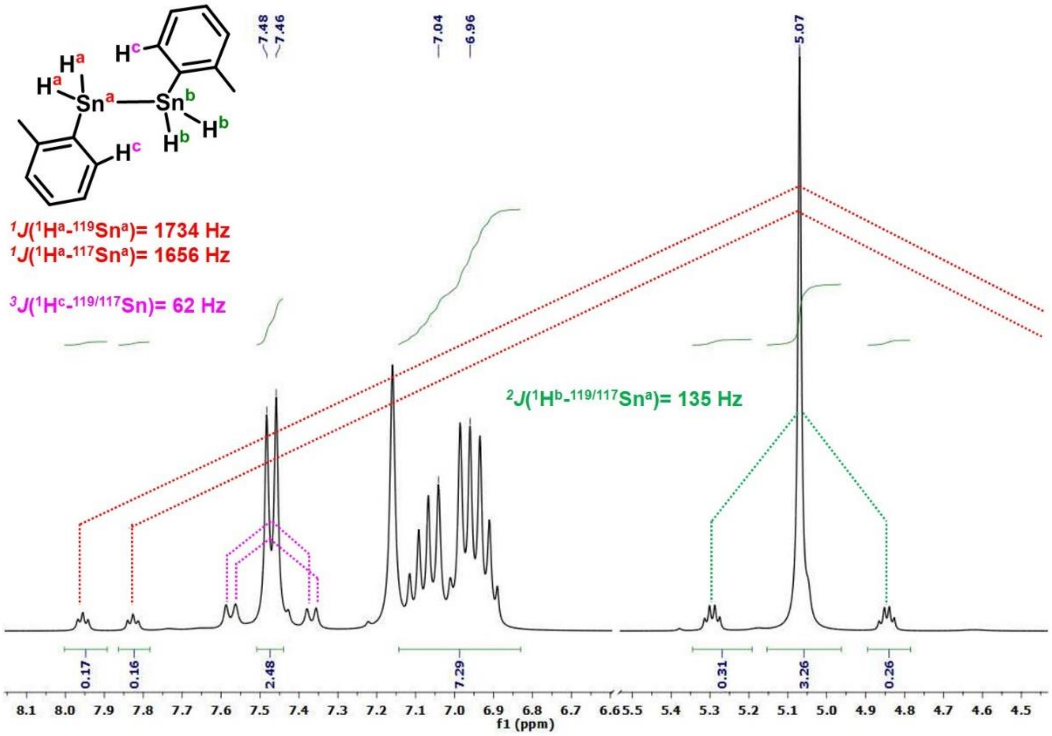

***Figure 71**: Selected regions of the ^{1}H spectrum of H_2[(o-tolyl)Sn–Sn(o-tolyl)]H_2 (**55**). $^1H\text{-}^{119/117}Sn$ coupling patterns are indicated by dotted lines.*

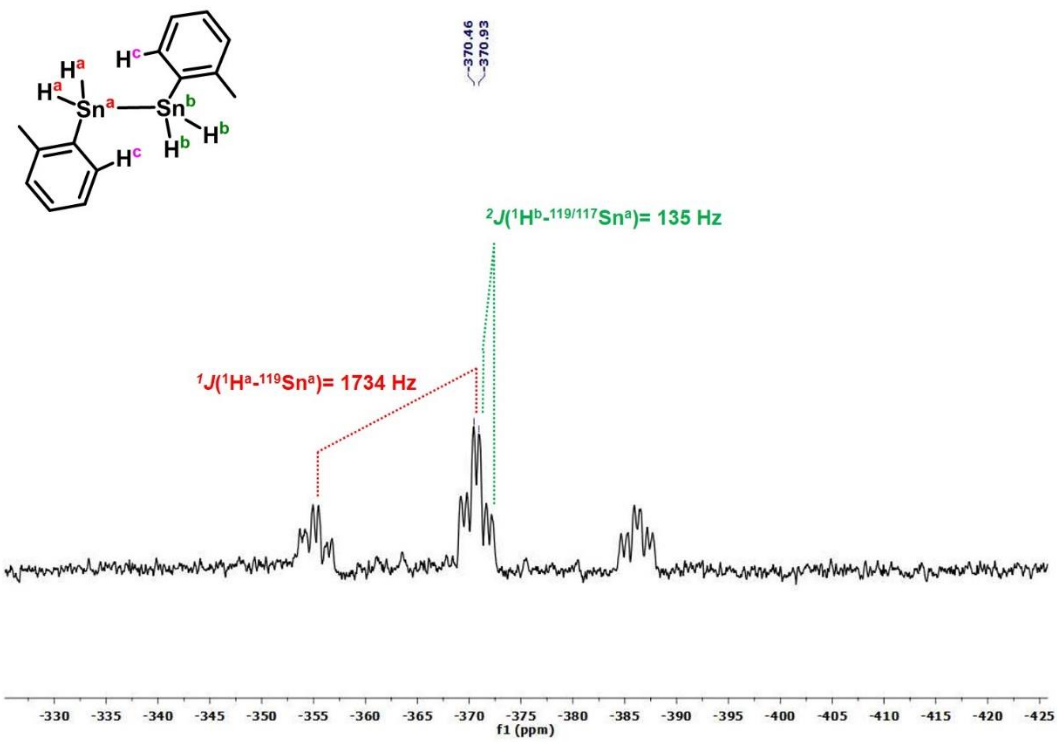

Figure 72: *^{119}Sn spectrum (^{1}H coupled) of $H_2[(o\text{-tolyl})Sn–Sn(o\text{-tolyl})]H_2$ (**55**) in C_6D_6. $^{119/117}$Sn-^{1}H coupling patterns are indicated by dotted lines.*

Not only do ^{1}H and ^{119}Sn NMR (Figures 70-72) support the formation of intermediate **B**, but the characteristic coupling patterns further elucidated in Figure 73 essentially provide a spectroscopic fingerprint and are only possible for **55**. Figure 73 shows two selected areas of the ^{1}H NMR spectrum of **55** illustrating the vicinal $^{3}J(^{1}H-^{1}H)$ coupling. The $^{1}J(^{119}Sn-^{1}H)$ and $^{1}J(^{117}Sn-^{1}H)$ satellites form a triplet, indicated by an intensity ratio of 1:2:1 which is caused by a $^{1}J\ (^{1}H^{a}-^{1}H^{b})$ coupling with a size of 3.9 Hz. The same pattern is expected for the $^{2}J(^{119}Sn-^{1}H)$ and $^{2}J(^{117}Sn-^{1}H)$ satellites to occur, however the expected signals fall in a close ppm range and therefore cannot be resolved. This results in a superposition of two triplets which forms a “pseudo quadruplet” with integrated intensities of 1:3:3:1 and a $^{3}J(^{1}H^{b}-^{1}H^{a})$ of 3.9 Hz (Figure 73). Attempts to recrystallize **55** proved challenging, as the compound easily reacts under polymer formation even at -30 °C.

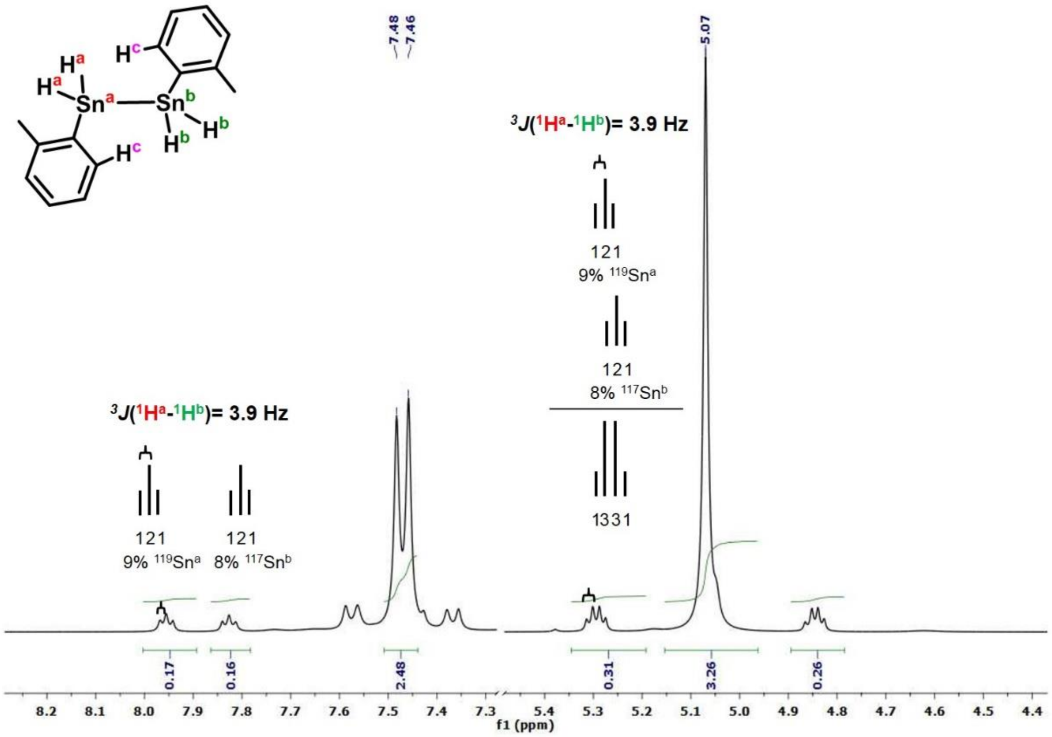

Figure 73: *Selected regions of the* ^1H *spectrum of* $H_2[(o\text{-tolyl})Sn–Sn(o\text{-tolyl})]H_2$ *(**55**) and* $^3J(^1H\text{-}^1H)$ *coupling patterns.*

6.2.9 *In situ* Synchrotron Stopped Flow XANES and EXAFS studies

The X-ray absorption near edge structure (XANES) is sensitive to the electronic environment around a nucleus (absorber) of interest as well as the edge position is indicative for the oxidation state and local geometry. Since the dehydrogenative coupling reaction of the aryltin trihydrides *o*-tolylSnH$_3$ (**36**) is postulated to proceed *via* a reductive process, as described in detail in the last section (6.2.7), the time resolved investigation in the change in oxidation state is indispensable. The amine base TMEDA, acting as a strong Lewis base, is suggested to donate electron density to the Sn(IV) educt forming a hexa coordinated adduct (Figure 65). The increased coordination number of Sn results in hyperconjugated tin centers. Subsequently, the Sn–H and Sn–aryl bonds are supposed to be weakened by elongation facilitating the redox process which forms the reactive Sn(II) intermediate. In this case, *in situ* XANES measurements display a powerful tool to reveal these possible dynamic changes in the oxidation state of Sn upon dehydropolymerization.

The extended X-ray absorption fine structure (EXAFS) reveals information on the local atomic arrangement, structural information, coordination number and interatomic distances of the absorbing element. It is known that Sn–Sn bond formation takes place generating nanostructured Sn particles which are suggested to be capped by an organometallic layer. These Sn core structures are thought to be surrounded by Sn in higher oxidation states still bonded to aryl moieties. As EXAFS measurements reveal the local order around the element of interest, changes in the local structure and composition of the synthesized nanostructured agglomerates can be monitored by *in situ* EXAFS. These findings complement existing results, and are critical to understanding the role of TMEDA in the formation of polyarylstannanes. The X-ray absorption spectra at the Sn K edge were collected at the beamline BM26A (DUBBLE) of the ESRF-The European Synchrotron in Grenoble, France as well as at the BM18 at the Diamond Lightsource Innovation campus.

6.2.9.1 Set-Up

In order to monitor the reaction over time, a novel stopped flow set-up has been designed using standard liquid flow equipment from IDEX Health & Science. This set-up successfully allows inert handling of all substances. Since hydrogen gas evolves upon Sn–Sn bond formation the reaction needs to be carried out in a pressurized system. Thus, the pressure is realized by the use of a Harvard PHD 4400 Hpsi syringe pump, infusing the two reactant feeds against a constant back pressure of 75 psi (5.2 bar) which is maintained by the use of a back pressure regulator assembly (BPR). The constant pressure avoids hydrogen bubble formation which would disturb the measurements.

The set-up consists of three different syringe pumps that feed the stopped flow circuit *via* a custom made adaptor piece (Anton Paar, Graz) that connects the stainless steel syringes and the chemically resistant PFA tubing (Figure 74). With the use of shut-off valves the circuit can be maintained under inert conditions when filling the syringes with trihydride and TMEDA solution in the dry box, respectively. Shut-off valves before and after the measuring cell circumvent back diffusion when the pumps are turned off. To avoid twisting of the tubing when refilling and cleaning the system, the portable part of the set-up is attached to a custom made metal grid (Figure 75). After testing all connection for leak tightness, and measuring a solvent, as well as a trihydride blank, the amine base and the trihydride solution are infused into the circuit with an infusion rate of 2 mL/min. When the cell is filled and bubble free, the three way valve is put to back pressure to pressurize the system. When 75 psi are reached, the sample cell is shut off the circuit by closing the valves and the reaction is monitored *in situ* with a time resolution of 2.5 min.

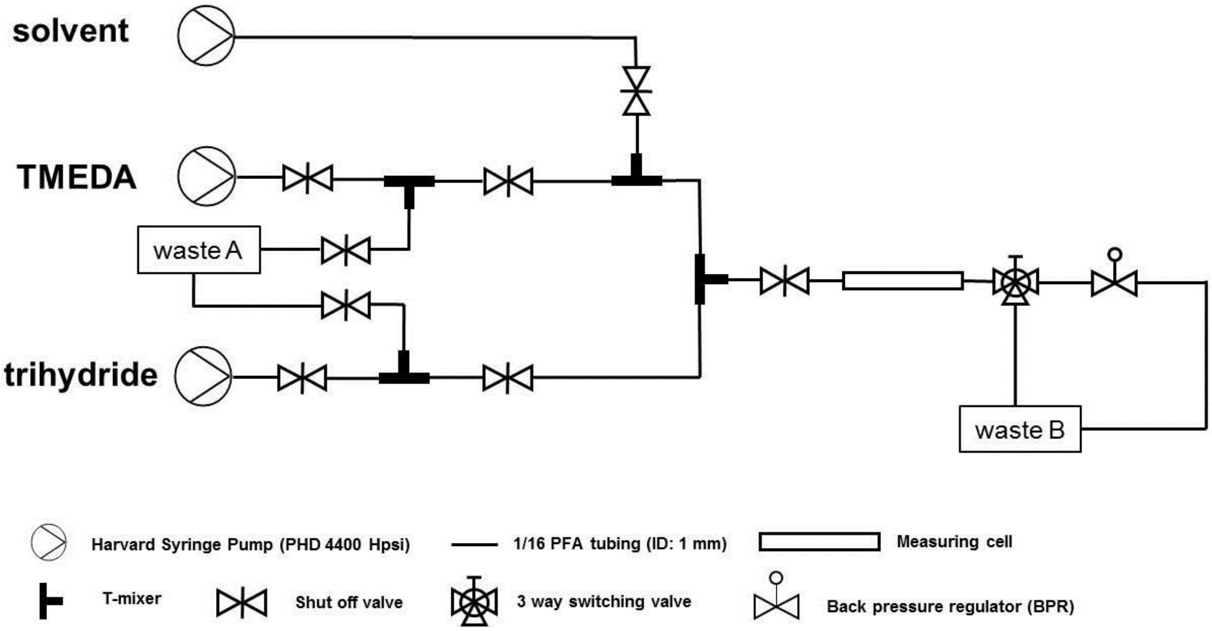
solvent
TMEDA
waste A
trihydride
waste B
Harvard Syringe Pump (PHD 4400 Hpsi)
1/16 PFA tubing (ID: 1 mm)
Measuring cell
T-mixer
Shut off valve
3 way switching valve
Back pressure regulator (BPR)

Figure 74: *Schematic stopped flow set-up for the in situ synchrotron measurements.*

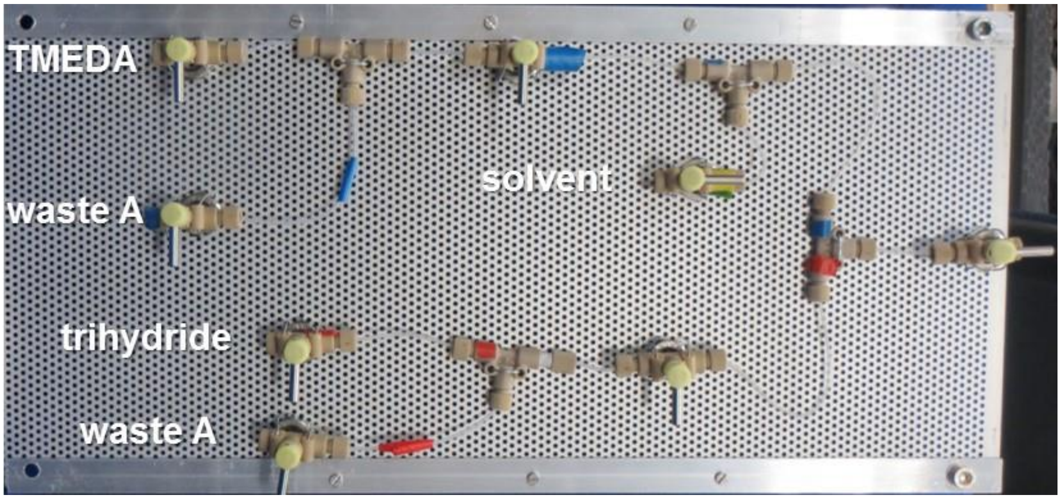
TMEDA
waste A
solvent
trihydride
waste A

Figure 75: *Portable stopped flow set-up for in situ synchrotron measurements.*

6.2.9.2 Data Analysis

Background subtraction, calibration, spectra alignment and normalization of the EXAFS data were performed using the program Athena.[287] EXAFS spectra were then Fourier transformed (FT) over a k range of 0-15 Å^{-1} with an adaptive Hanning window and back FT over a non-phase corrected radial distance R range of 0-6 Å. Spectra were plotted with a k-weight of 2.

Figure 76 displays the normalized near edge structure (XANES) spectra of the *in situ* reaction of *o*-tolylSnH$_3$ (**36**)/TMEDA in diethyl ether over a reaction time of 1.7 h. Time resolution for each pattern is 2.8 min.

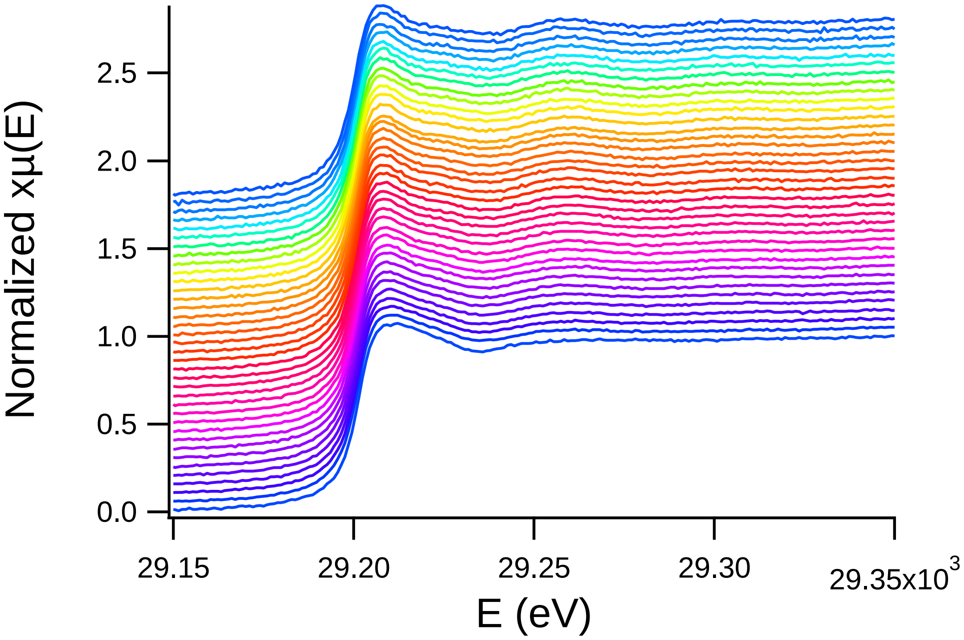

Figure 76: *Normalized XANES data at the Sn K edge of the in situ reaction of o-tolylSnH$_3$ (**36**)/TMEDA reaction in diethyl ether over 1.7 h. Time resolution for each pattern is 2.8 min.*

The edge energies (E0) are monitored over reaction time, as they indicate a change in oxidation state. E0 values are expected to change as Sn is reduced from oxidation IV to II. E0 values were calculated from the peak maximum of the first derivative of each spectrum showing a change from 29202.8 eV for the unreacted educt *o*-tolylSnH$_3$ (**36**) (Sn(IV)) to 29200.4 eV for the final polymeric product (Sn(0)). Energy shifts of the XANES edge of the *in situ* reaction of *o*-tolylSnH$_3$ (**36**)/TMEDA in diethyl ether *versus* time were determined by Lorentz peak fitting of the normalized difference spectra of the XANES signal. The position of the Lorentz peak is shown and the difference related to 29200 eV for the Sn(0) ionization stage (Figure 77). Figure 77 illustrates a fast decrease in E0 in the first 10 min of the reaction which is followed by a slow convergence towards the final energy state for tin in oxidation state zero. However, a decrease in energy of only 2.4 eV is less than expected for a reductive process from Sn(IV) to Sn(0). The edge energy of 29202.8 eV measured for *o*-tolylSnH_3 (**36**) exhibiting Sn in a formal oxidation of IV does not fall in the range with energies reported for other Sn (IV) compounds such as SnO_2 (29206 eV).[288] This large deviation is not entirely surprising as the formal oxidation state assumes that all shared electrons are assigned to the element exhibiting a higher electronegativity.[289] Indeed, this assumption works well for ionic or highly polarized bonds, however is not suitable for the reported Sn–H bond. This effect has already been mentioned for *in situ* Gallium K-edge XAS measurements, where the authors show only a marginal edge energy difference of GaH_x (10368.0 eV) and Ga metal (10367.1 eV).[290]

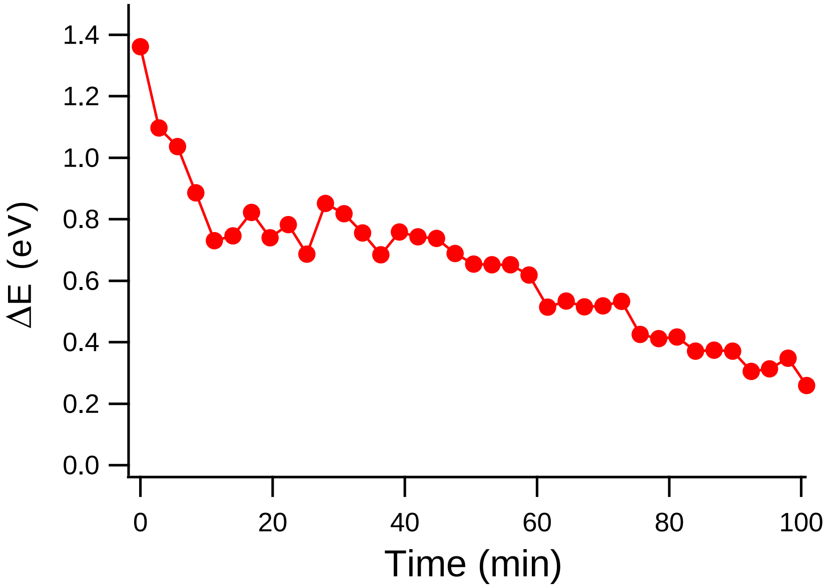

Figure 77: *Energy shift of the XANES edge of the in situ reaction of o-tolylSnH_3 (**36**)/TMEDA in diethyl ether versus time determined by Lorentz peak fitting of the normalized difference spectra of the XANES signal. The position of the Lorentz peak is shown and the difference related to 29200 eV for the Sn(0) ionization stage.*

However, partial charges computed by quantum chemical calculations correlate much better with XANES results than charges estimated by a formal oxidation state.[289] This is in accordance with NBO analysis on the model substrates phenyl$_4$Sn, phenyl$_3$SnH, phenyl$_2$SnH$_2$ and phenylSnH$_3$. The calculations show that an increase of hydrogen substitution at the tin leads to a significant decrease in the partial charge of tin (q(Sn)), although all compounds exhibit the same formal oxidation state of +4 (Table 17).

Table 17: *Partial charges of Sn (q(Sn)) obtained by DFT calculations.*

	Ph_4Sn	Ph_3SnH	Ph_2SnH_2	$PhSnH_3$	*o*-tolylSnH$_3$ (**36**)
q(Sn)	1.96	1.55	1.30	1.04	1.07
formal oxidation state	+4	+4	+4	+4	+4

Even though the XANES data (Figure 76) do not allow for precise identification of the expected Sn intermediates in the oxidation states ranging from IV to 0, a reductive process can be confirmed expressed by decreased edge energy of 2.4 eV, as well it is displayed in Figure 77. From the energy scans, extracted and k^2 weighted EXAFS data allows better monitoring of the structural changes over reaction time as illustrated in Figure 78. Figure 78 shows the evolution of a discrete peak, continuously growing over time at a k position of 3.8 Å^{-1} indicated by a dashed line which corresponds to a change in the local coordination of tin due to polymerization. The increase in intensity is also depicted in Figure 79 which displays the increase in peak intensity of k^2 weighted EXAFS data integrated between 3.64 and 4.2 Å^{-1}.

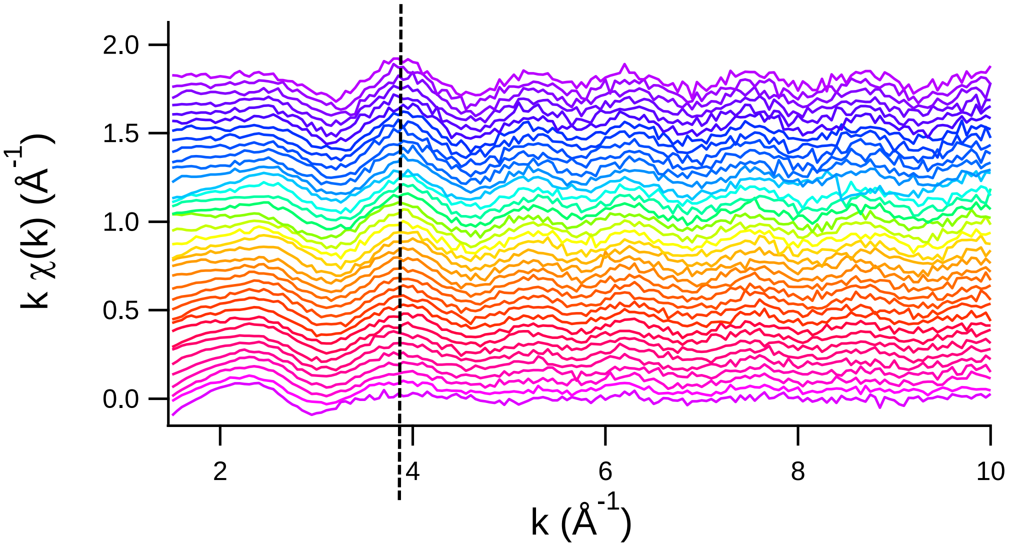

Figure 78: *k^2 weighted EXAFS data of the in situ reaction of o-tolylSnH$_3$ (**36**)/TMEDA reaction in diethyl ether over 1.7 h. Time resolution for each pattern 2.8 min.*

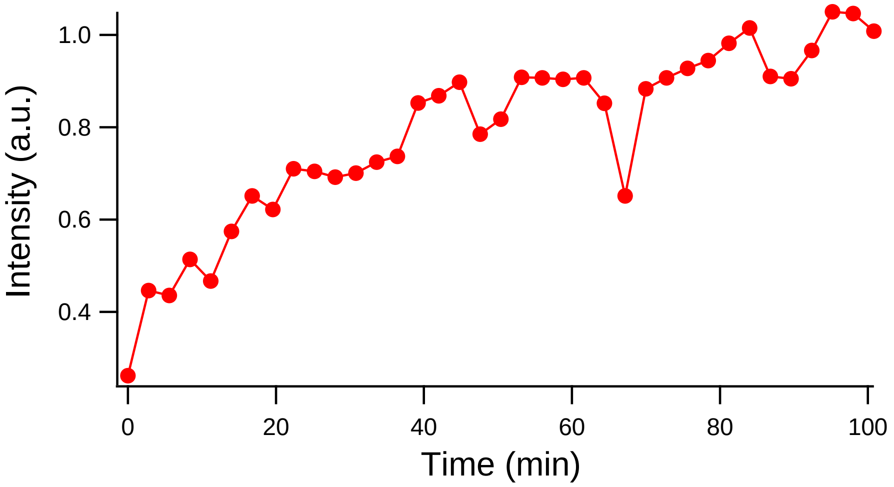

Figure 79: *Peak intensity of k^2 weighted EXAFS data integrated between 3.64 and 4.2 Å^{-1}.*

The Fourier transform magnitudes of the EXAFS oscillations show a growing signal at a real space correlation length of 2.6 Å corresponding to the Sn–Sn distance formed over reaction time (Figure 80).

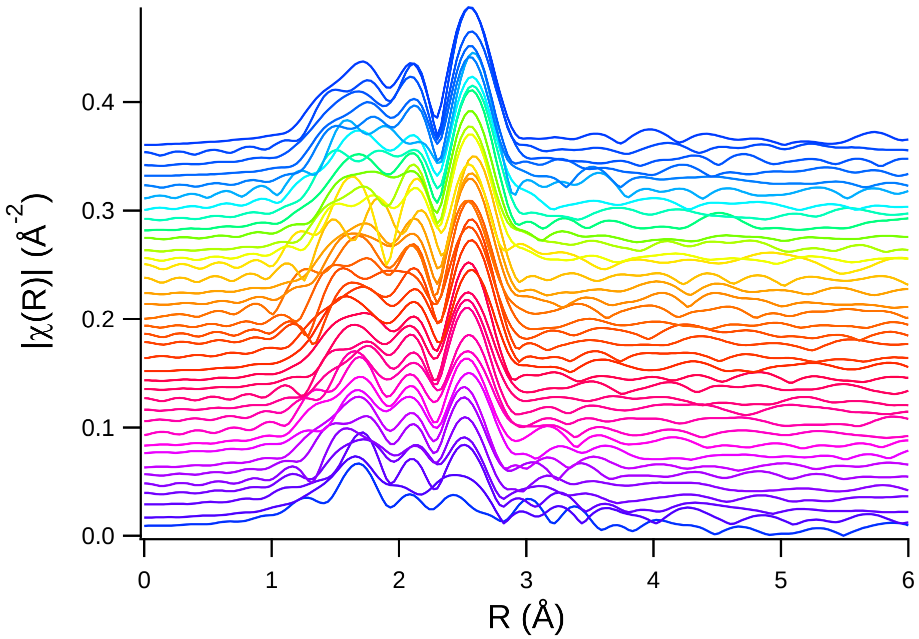

Figure 80: *Fourier transform magnitudes of* k^2*-weighted* $\chi(k)$ *data obtained during the in situ reaction of o-tolylSnH*$_3$ *(**36**)/TMEDA reaction in diethyl ether over the first 1.7 h. Time resolution for each pattern 2.8 min.*

6.3 Conclusions

o-tolylSnH$_3$ (**36**) was subjected to a dehydrogenative coupling reaction with the amine base TMEDA to form the insoluble, oxygen labile *o*-tolyl decorated tin nanoparticles (***o*-tolyl@Sn**). SAXS measurements on the non oxidized, as well as the oxidized powder, showed a discrete correlation length of ~1 nm in the material. It could be shown that the size increases (~2 nm) as well as monodispersity decreases upon oxidation. Furthermore, FESEM imaging revealed that the nanostructured polymer is built up by spherical superstructure in the range of 1 µm. These superstructures are composed by nano-substructures which could also be evidenced by *in situ* synchrotron SAXS measurements at Elettra Trieste in Italy. These measurements show a fast spherical nano-substructure (1.6 nm) formation in the first 10 min, which agglomerate to bigger structures over reaction time. Additional TEM images suggest the formation of a core shell structure of ***o*-tolyl@Sn**, where a metallic tin core is surrounded by an organometallic or organic layer. Additionally, a reductive dehydrogentive coupling mechanism is proposed. It is postulated that the educt *o*-tolylSnH$_3$ (**36**) interacts with TMEDA under the formation of a hexa coordinated Lewis adduct. This adduct formation allows for Sn−H bond elongation and therefore weakening of the latter. Subsequently, the cleavage of H$_2$ and the formation of a distannane (H$_2$[(*o*-tolyl)Sn−Sn(*o*-tolyl)]H$_2$) (**55**) intermediate is facilitated. Consequently, the Sn−Sn bond of **55** is cleaved *via* a proposed H shift rearrangement which forms the educt *o*-tolylSnH$_3$ (**36**) and a reduced, reactive Sn(II) intermediate (*o*-tolylHSn:). This short term stannylene then immediately inserts into existing Sn−Sn bonds of distannanes (**55**) in order to generate branched polymeric products. The immediate polymer formation can be circumvented by performing the dehydrogenative coupling in the absence of the amine base which allows to verify the formation of (H$_2$[(*o*-tolyl)Sn−Sn(*o*-tolyl)]H$_2$) (**55**). The knowledge that Sn−H bonds exhibit a high degree of temperature lability, which is exploited for Sn−Sn bond formation upon hydrogen cleavage, provided motivation to investigate the thermally induced dehydrocoupling of *o*-tolylSnH$_3$ (**36**). This conversion successfully led to the formation of (**55**) proving the distannane as an intermediate in the reductive amine base or thermally induced dehydrogenative coupling reaction of *o*-tolylSnH$_3$ (**36**). **55** could be fully characterized by ^{1}H, ^{13}C and ^{119}Sn.

In addition a novel stopped flow set-up is reported which allows for inert *in situ* EXAFS/XANES measurements. The edge energies (E0) were monitored over reaction time indicating a change in oxidation state. A decrease in edge energy over reaction time of 2.4 eV confirms a reductive mechanism, however is less than expected for a reductive process from Sn(IV) to Sn(0). Nevertheless, this large deviation is not entirely surprising as the formal oxidation state assumes that all shared electrons are assigned to the element exhibiting a higher electronegativity. NBO calculations could show that the partial charge calculated at the Sn correlate much better with XANES results than charges estimated by a formal oxidation state.

The Fourier transform magnitudes of the EXAFS oscillations revealed a real space correlation length of 2.6 Å corresponding to the Sn–Sn distance formed over reaction time.

7 “Basic” Changes in the Dehydrogenative Coupling Reaction of Aryltin Trihydrides

Graphical Abstract

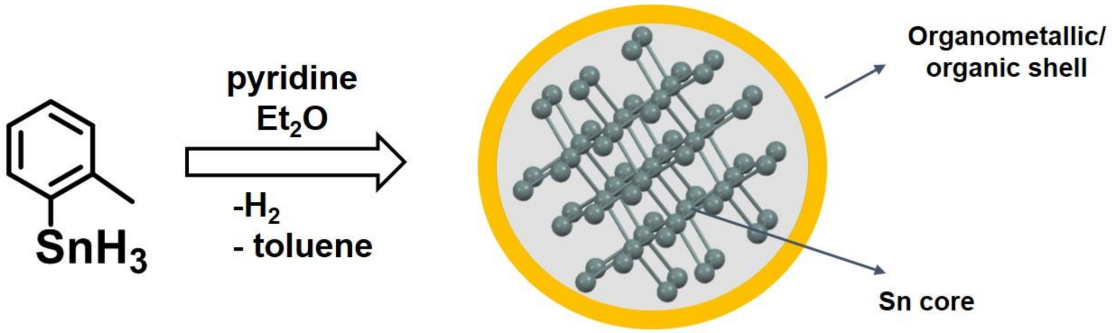

Abstract

*A variety of amine bases, such as TMEDA (N,N,N’,N’-tetramethylethylenediamine), DETA (diethylenetriamine), DMAP (4-dimethylaminopyridine), pyridine, Et_3N (triethylamine) and phenanthroline exhibiting different steric demand, basicity, aromaticity and donor capacity was applied to convert o-tolylSnH_3 (**36**) to the corresponding polymeric material o-tolyl@Sn. Amine bases exhibiting a high degree of donor capacity and basicity, such as DETA or DMAP enhanced the reaction speed. Surprisingly, DMF did not lead to polymer formation. Furthermore, the resulting nanostructure of the formed materials was investigated by SWAXS measurements showing that the type of base used affects the common correlation length found in the polymer. DETA and Et_3N led to the smallest substructures (1.5 nm), followed by TMEDA and DMAP (1.7 nm). The aromatic base pyridine did not only lead to increased sizes of nanostructures (2.1 nm), but the generated material also featured discrete reflections in the WAXS corresponding to white tin in the cubic space group I41/amd. The nature of the amine base catalyst used in the conversion of less sterically demanding aryltin trihydrides exerts a controlling influence on the nanostructure, composition and morphology of the formed aryl decorated tin nanoparticles, which is of high importance for the further application of these materials.*

7.1 Introduction

Since the pioneering work of Neumann and Davies, who reported on the successful formation of Sn–Sn bonds by converting diorganotin dihydrides to cyclostannanes (5- and 6 membered rings) using amine bases such as pyridine, diethylamine, triethylamine, piperidine, aniline and DMF (dimethylformamide), the dehydrogenative coupling reaction applying cheap and easy to be handled amines has remained a quite neglected topic in organotin chemistry.[264,265,291,292] This lasted until the working group of Uhlig described the application of TMEDA in the formation of not only cyclic stannanes, but also linear polystannanes such as poly[bis(*p*-^{n}butylphenyl)stannane] exhibiting a molar mass of 46,000 gmol^{-1} which corresponds to approximately 120 (*p*-^{n}butylphenyl)$_2$Sn units.[11] Furthermore, based on Neumann's results on the condensation of stannylamines with organotin hydrides mainly forming cyclostannanes,[157] Foucher *et al.* have very recently reported on a synthetic protocol for the generation of alternating polystannanes which involves the stoichiometric reaction of organotin dihydrides and organotin diamides in diethyl ether or toluene under mild reaction conditions.[158,159]

Nevertheless, the role of amine bases in the synthesis of polystannanes, as well as the mechanistic background on Sn–Sn bond formation upon hydrogen evolution, has been unclear and dubious as literature has not provided conclusive evidence on the chemical process apart from suggestions and general observations mainly conducted by Neumann.[55,267,292,293]

However, Sindlinger and coworkers proposed a mechanism for the nitrogen-base catalyzed reductive dihydrogen elimination of bulky aryltin trihydrides resulting in organotin(II) hydrides.[259] In this work the authors subjected Ar^*SnH_3 (Ar^*= 2,6-trip$_2$(C_6H_3), trip= 2,4,6-triisopropylphenyl) variety of amine bases such as pyridine, DMAP (4-dimethylaminopyridine), triethylamine and TMEDA. In case of catalytic amounts of base, the dehydrocoupling product diorganodistannane $Ar^*H_2Sn–SnH_2Ar^*$ could be obtained quantitatively, whereas the use of excessive amounts (>4 eq.) led to almost exclusive formation of the monomeric base adduct Ar*SnH. However, the formation of higher molecular Sn species by full hydrogen release has not been observed as the formed organotin(II) hydrides are relatively thermally robust.

By reducing the bulkiness of the converted aryltin trihydrides by converting educts such as *o*-tolylSnH_3 (**36**) with the amine base TMEDA, we were able to realize the formation of aryl decorated tin nanoparticles (***o*-tolyl@Sn**) (Chapter 6). Detailed DFT calculations, as well as *in* *situ* EXAFS studies on the dehydrogenative coupling reactions support a reductive mechanism upon Sn–Sn bond formation, however the reaction does not stop at this stage and formed Sn(II) intermediates serve as reactive species in the polymer formation.

Since the formation of aryl decorated tin nanoparticles (aryl@Sn) is well described for TMEDA being the catalyst (Chapter 6), the lack of information on the conversion of non-bulky aryltin trihydrides with various amine bases provided motivation to convert *o*-tolylSnH_3 (**36**) with pyridine, DMAP, triethylamine, DMF, phenanthroline as well as DETA (diethylenetriamine). The reaction process, as well as morphology, nanostructure and elemental composition as a function of donor ability and basicity of the amine base is a fundamental key in further understanding the dehydrogenative coupling, as well as in tuning the particles' characteristics.

7.2 Results and Discussion

In order to better understand the conversion or aryltin trihydrides lacking steric hindrance, *o*-tolylSnH_3 (**36**) was converted with various amine bases. The bases are chosen according to their basicity, donor ability, aromaticity and steric demand. **36** was synthesized according to literature, subjecting the corresponding trichloride to a hydrogenation reaction using excess of $LiAlH_4$.[80]

Since Sindlinger *et al*. were able to identify a Sn(II) species by converting Ar*SnH_3 with DMAP, the question arose whether increased bulkiness of the base would aid in generating a thermodynamically stable intermediate formed along the suggested reaction pathway even converting small aryltin hydrides as **36**.[259] Therefore, phenanthroline was chosen as a sterically demanding and chelating base. Furthermore, the influence of aromatic bases was investigated by using the smaller pyridine and DMAP. The donor ability was increased by applying amine bases exhibiting different amounts of nitrogen atoms in their structure: DETA, TMEDA, DMAP and Et_3N. DMF was chosen as a non-basic but donating catalyst.

Thus, the influence of the used amine base on the dehydrogenative coupling reaction was qualitatively analyzed in terms of reaction speed by monitoring the visible color change. The nanostructure of the formed polymer was investigated by SAXS analysis. Additionally, SEM images should reveal the monodispersity in the overall morphology of the material, as well as the loss of organic groups upon polymerization was determined by elemental analysis.

For a typical amine base induced dehydrogenative coupling reaction of *o*-tolylSnH$_3$ (**36**), an equimolar amount of amine base was dissolved in diethyl ether if possible and the trihydride was added with a syringe (Scheme 87). The reaction was carried out at room temperature and the formed polymer was filtered off to subject it to further analysis.

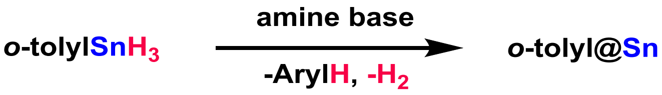

Scheme 87: *Formation of o-tolyltin decorated Sn nanoparticles by dehydrogenative coupling of o-tolylSnH$_3$ (**36**) with amine bases.*

It could be observed that the reaction speed is strongly affected by the donor ability, as well as basicity of the amine base used in the conversion, as DETA showed the fastest polymer formation followed by DMAP, TMEDA pyridine and Et$_3$N. This is not surprising since it is has already been established that phosphorous based donors such as DMPE do not induce Sn−Sn bond formation and hydrogen evolution due to their limited donor capacity (Chapter 6).[259] Surprisingly, DMF did not induce polymerization which is in contrast to Neumann's findings, who reported on the conversion of diphenyltin dihydride (phenyl$_2$SnH$_2$) with DMF which leads to the formation of cyclostannanes as well as insoluble polymeric material.[265] In the case of phenanonthrolin, the reaction progress was very fast, forming a dark brown to black suspension already after 4 min, however no polymer could be filtered off, as the formed particles might be too small. Attempts to crystallize intermediates from the reaction at low temperatures have not been successful.

7.3 SWAXS Measurements and Elemental Composition

The synthesized and isolated powders were subjected to SWAXS analysis in order to reveal the common correlation length on a nano scale (Figure 81). It can be observed that DETA and Et$_3$N formed polymers exhibiting a common correlation length of 1.5 nm which is the shortest one found for all investigated polymers. This is followed by structures with a size of 1.7 nm produced in the case of TMEDA and DETA. However, pyridine led to the generation of particles exhibiting the longest correlation length of 2.1 nm. These results suggest that a higher basicity as well as donor capacity of the bases used results in smaller structural features.

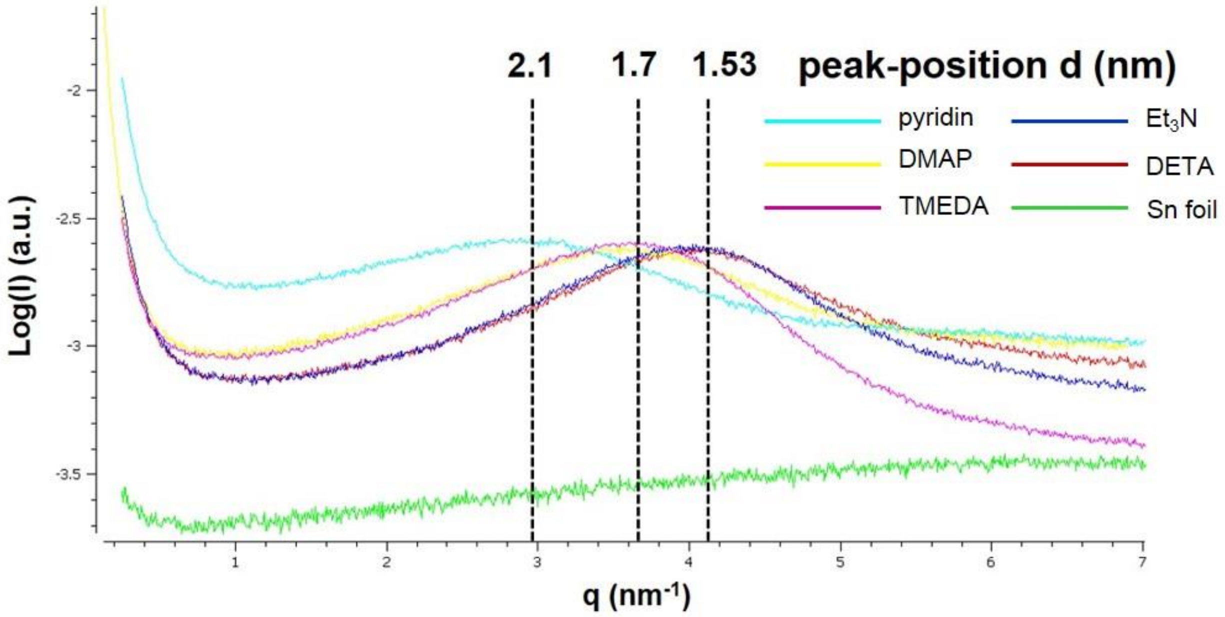

Figure 81: *SAXS spectra of* ***o-tolyl@Sn*** *formed using pyridine (turquois), Et_3N (blue), TMEDA (pink), DMAP (yellow) and DETA (red) as polymerization catalyst.*

In contrast to all other polymers, the material generated from pyridine exhibits discrete reflections in the WAXS range as illustrated in Figure 82. According to the literature, these reflections can be assigned as the 2/0/0 as well as 1/0/1 planes of white tin. Figure 83 displays the powder pattern of Sn as well as the packing diagram.[294] This is the first time to successfully, partially describe the structure of the particles formed which corresponds to white tin in the cubic space group I41/amd.

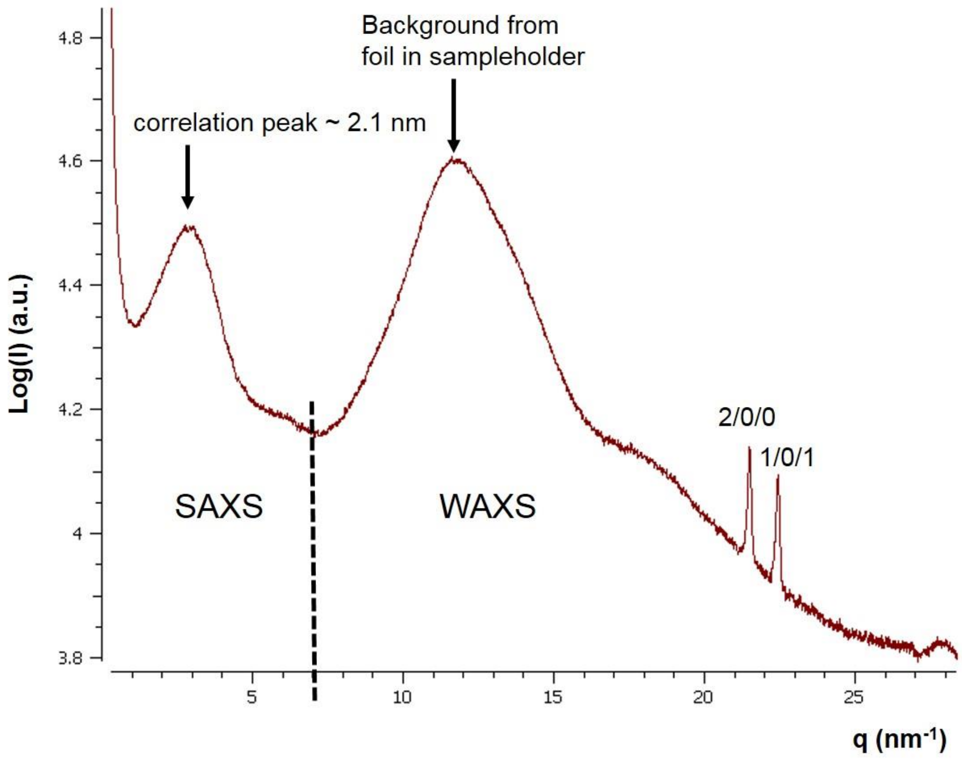

Figure 82: *SWAXS spectrum of* ***o-tolyl@Sn*** *made in diethyl ether and pyridine.*

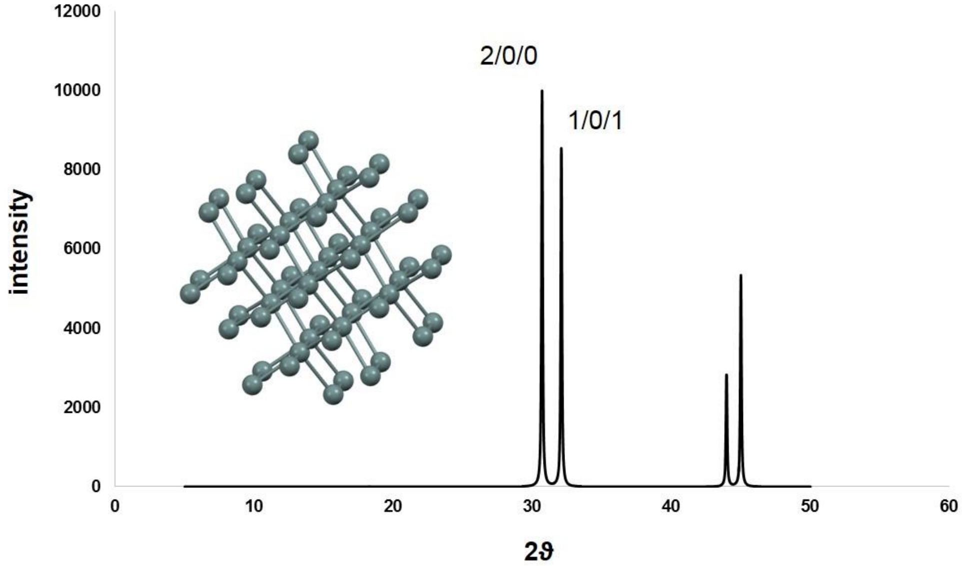

Figure 83: *Powder diffraction pattern of white tin (I41/amd).*[294]

Apparently, pyridine induces a higher degree of aromatic cleavage which leads to the formation of an increased ratio of elemental tin in the material which is not only expressed by the WAXS analysis, but also by the elemental compositions revealing a carbon content of less than 6 %. That implies that 34 % of the initial aryl content is cleaved upon particle formation which is the highest organic loss found for all investigated polymers (Table 18).

Table 18: *Comparison of the elemental composition (%) of* ***o-tolyl@Sn*** *synthesized using a variety of amine bases.*

	C	**H**	**N**
(*o*-tolylSn)$_n$	40.07	3.36	0
o-tolyl@Sn DMAP	32.80	3.01	2.68
o-tolyl@Sn TMEDA	27.57	2.42	0.72
o-tolyl@Sn DETA	26.95	3.08	4.49
o-tolyl@Sn Et$_3$N	22.63	1.89	0.29
o-tolyl@Sn pyridine	5.63	0.69	0.39

7.4 SEM Imaging

As the use of different amine bases induces an appreciable change in the nanostructure of the synthesized material, the polymers were also subjected to a SEM analysis in order to reveal the morphology differences on a µm scale. Figures 84 and 85 illustrate the materials' morphology change as an effect of the base used. Figure 84 (A) shows the polymer made in diethyl ether and pyridine (B). The latter exhibits the most regular assembly of spherical particles followed by ***o*-tolyl@Sn** from Et$_3$N (Figure 84 (B)). This could be explained by the reaction time, being the longest for pyridine and Et$_3$N which allows for organization of particles in a more controlled fashion. Faster reactions using highly donating amine bases such as DMAP and DETA, lead to a less pronounced spherical arrangement as it is displayed in Figure 85 C and D.

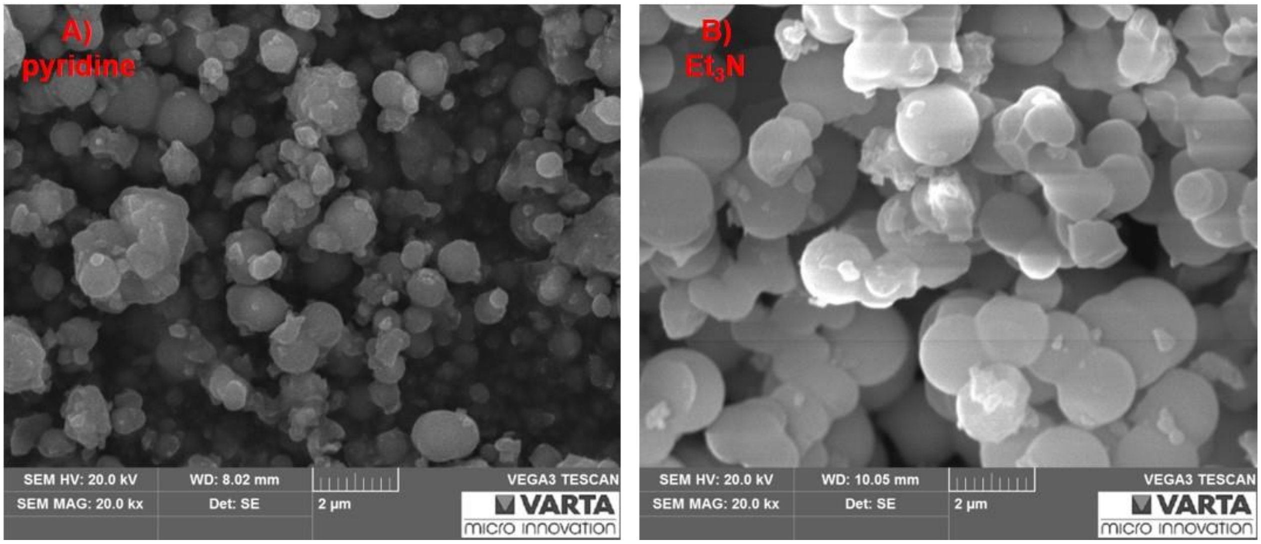
A)
pyridine
SEM HV: 20.0 kV
WD: 8.02 mm
VEGA3 TESCAN
SEM MAG: 20.0 kx
Det: SE
2 µm
VARTA
micro innovation
B)
Et₃N
SEM HV: 20.0 kV
WD: 10.05 mm
VEGA3 TESCAN
SEM MAG: 20.0 kx
Det: SE
2 µm
VARTA
micro innovation

Figure 84: *SEM images from* ***o-tolyl@Sn*** *generated in the presence of pyridine (A) and Et$_3$N (B).*

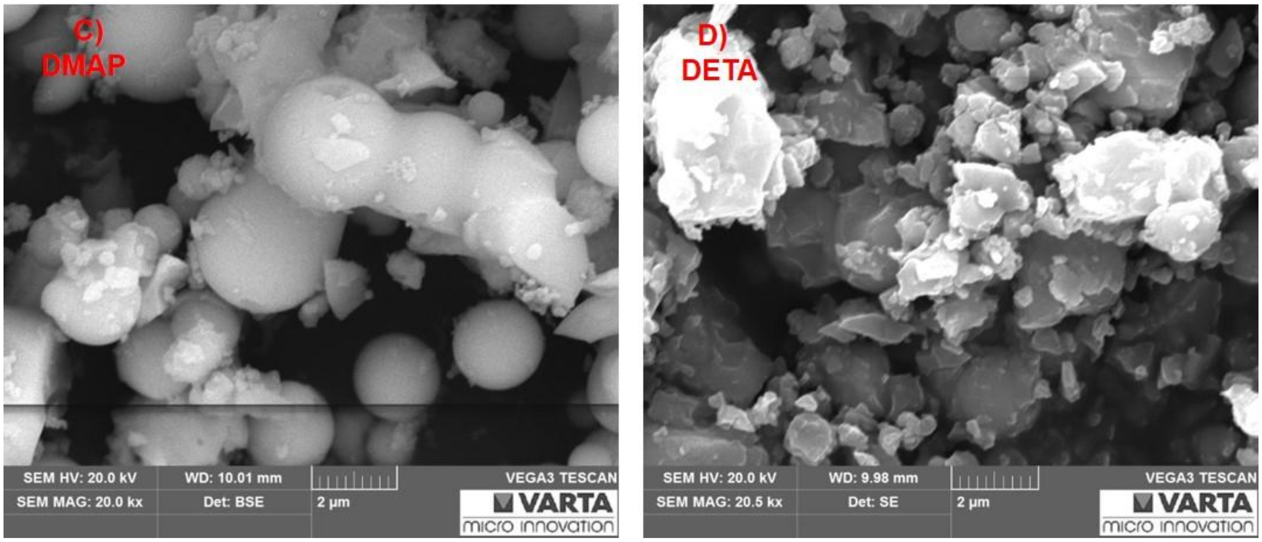
C)
DMAP
SEM HV: 20.0 kV
WD: 10.01 mm
VEGA3 TESCAN
SEM MAG: 20.0 kx
Det: BSE
2 µm
VARTA
micro innovation
D)
DETA
SEM HV: 20.0 kV
WD: 9.98 mm
VEGA3 TESCAN
SEM MAG: 20.5 kx
Det: SE
2 µm
VARTA
micro innovation

Figure 85: *SEM images from* ***o-tolyl@Sn*** *generated in the presence of DMAP (C) and DETA (D).*

7.5 Conclusion

In summary, a variety of amine bases exhibiting different steric demand, basicity, aromaticity and donor capacity was applied to convert *o*-tolylSnH$_3$ (**36**) to the corresponding polymeric material ***o*-tolyl@Sn**. The influence of the used amine base on the dehydrogenative coupling reaction was qualitatively analyzed in terms of reaction speed by monitoring the visible color change. It could be observed that amine bases exhibiting a high degree of donor capacity and basicity enhance the reaction speed. Surprisingly, DMF did not lead to polymer formation, which can be explained by the lack of basicity. Furthermore, the resulting nanostructure of the formed materials was investigated by SWAXS measurements showing that the type of base used indeed affects the common correlation length found in the polymer. DETA and Et$_3$N lead to the smallest substructures found (1.5 nm), followed by TMEDA and DMAP (1.7 nm). The aromatic base pyridine did not only lead to increased sizes of nanostructures (2.1 nm), but also featured discrete reflections in the WAXS area which allowed for comparison to literature reported powder patterns of white tin. This is the first time to successfully, partially describe the structure of the particles formed which contain tin in the cubic space group I41/amd. Carrying out elemental analysis on all synthesized polymers supports the formation of an increased amount of elemental tin in the case of pyridine; as the carbon content was detected to be less than 6 % which is the highest loss of aromatic groups found for all polymers included in this study.

Additionally, SEM images revealed the monodispersity in the overall morphology of the material on a µm scale. The material synthesized with pyridine as a catalyst exhibits the most regular assembly of spherical particles which is comparable to the morphology found for products formed in the TMEDA induced polymerization (Chapter 6). This is followed by ***o*-tolyl@Sn** from Et$_3$N, DMAP and DETA.

The nature of the amine base catalyst used in the conversion of sterically less demanding aryltin trihydrides exerts a controlling influence on the nanostructure, composition and morphology of the formed aryltin decorated tin nanoparticles, which is of high importance for the further use of these materials. These findings allow for further fine tuning of the materials' characteristics and will indeed by one of the key investigation criteria in future work.

8 Control the Morphology of Aryl Decorated Tin Nanoparticles

Graphical Abstract

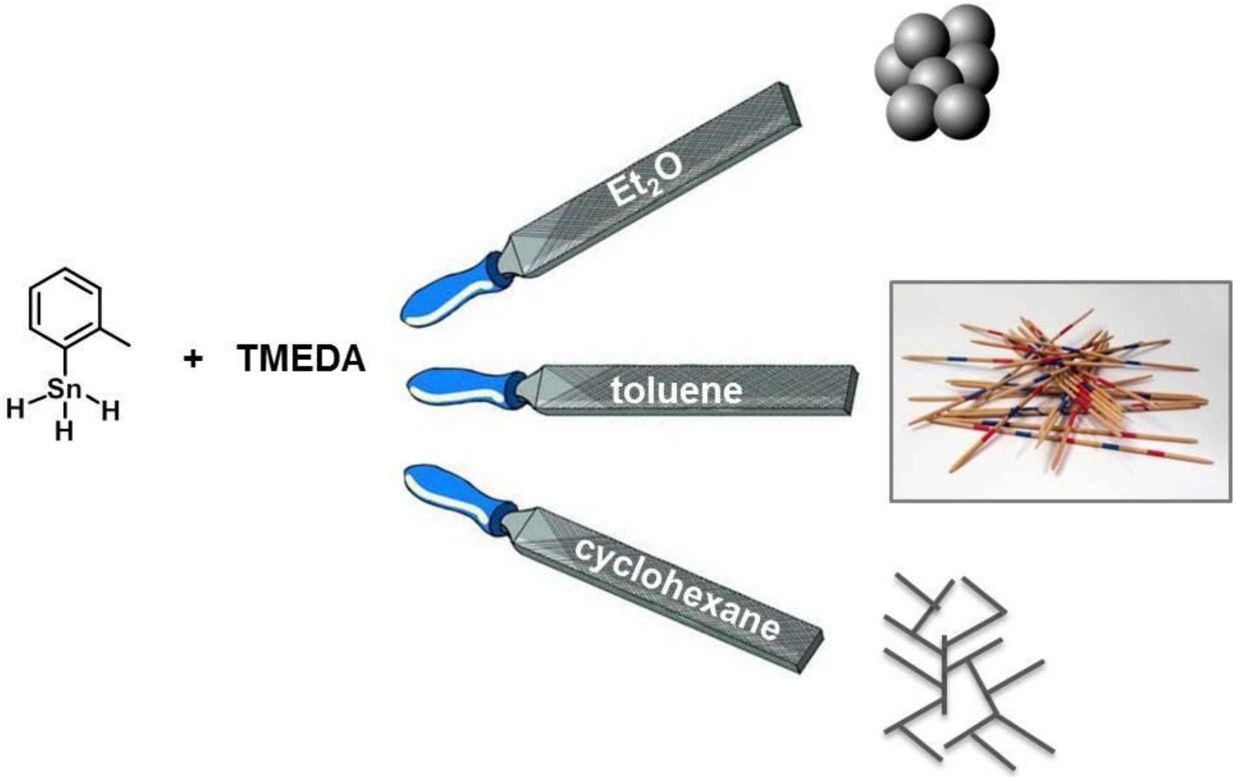

Abstract

Detailed in situ synchrotron SAXS measurements on the dehydrogenative coupling reaction of o-tolylSnH$_3$ with the amine base TMEDA revealed that the nature of the solvent used exerts a strong impact on the nanomorphology and the growth process of the aryl@Sn formed. Donating solvents such as diethyl ether and DME (dimethoxyethane) form spherical particles (~1-2 nm), whereas cyclohexane as apolar solvent, as well as aromatic, apolar solvents such as toluene lead to the generation of nanorods with different lengths and a cross section of 1.5 nm. Furthermore, it could be shown that variation of the aryl residue bonded to the tin alters the common correlation lengths and polydispersity of aryl@Sn as evidenced by SAXS analysis.

8.1 Introduction

The quest for novel electrode materials exhibiting excellent performance is one of the key research topics since lithium ion batteries (LIBs) have been considered one of the most important power sources used in vehicles and portable electronics.[295,296] In the modern age the energy density of existing systems is still not efficient to meet our decreasing demands in energy storage and delivery.[297]

The anode is required to reversibly accommodate as well as release lithium ions upon discharging and charging. Among various interesting candidates in the research field of novel anode materials, tin has recently gained considerable attention due to its high theoretical capacity of 944 mAh/g which is in accordance to the formation of $Li_{22}Sn_{59}$.[298] Therefore, a series of tin based materials, such as tin dioxide (SnO_2),[299] tin disulfide (SnS_2),[300] tin diselenide ($SnSe_2$),[301] as well as intermetallic compounds such as nickel (Ni–Sn)[302] and cooper (Cu–Sn)[303] have been investigated as potential high-energy density anode material since all of them show higher capacity than the commercialized graphite anodes (~372 mAh/g). Despite the high abundance and low price of tin, its application has not been commercialized yet, since one of the main drawbacks of Sn based anode materials is the severe capacity fading upon cycling which is caused by an enormous volume change of the metal (about 300 %).[302,304,305] Thus, the structure of these promising Sn based materials ought to be tuned to effectively accommodate the volume expansion.[297,306]

This issue is proposed to be elegantly circumvented by utilizing electrode materials at the nanoscale which are reported to provide significantly improved performance of LIBs.[295,296,305,307,308] This is due to an increased number of electrochemically active sites as well as to a high ability to buffer the stress which is induced upon lithiation and delithiation. In particular, nanostructured composites of carbon and tin have been proposed as a high capacity substitute for the carbon anode of lithium ion batteries. A variety of Sn-carbon hybrids such as Sn nanoparticles embedded in porous carbon,[302,309-317] Sn or Sn@C nanoparticles encapsulated with carbon nanotubes,[318-322] and carbon-encapsulated Sn nanostructures[323-326] have been designed. Deliberately manufactured composites of tin and carbon on the nanoscale may solve the poor cyclability of the tin electrodes as they provide space to buffer mechanical stress.

Recent work of Uhlig *et al.* has provided a successful route towards aryl decorated tin nanoparticles (aryl@Sn) by converting aryltin trihydrides with cheap and easy to be handled amine bases such as TMEDA and pyridine in diethyl ether (Chapter 6,7). The latter have been carefully investigated by SEM, TEM and SAXS analysis revealing a spherical nano-substructure which is considered to be a core shell assembly where metallic tin is decorated with an organometallic and organic layer. These particles show a diameter of only 1.4 nm according to SAXS experiments.

However, engineering Sn-based materials into desired nanoarchitectures represents an efficient principle towards improving their electrochemical performance, including specific capacity, rate capability, and/or cycling stability. This work deals with the tailoring of the nanomorphology generated upon dehydrogenative coupling reaction of aryltin trihydrides with TMEDA by simply changing the nature of the used solvent. This tool, which can be seen as a “chemical file”, allows for the efficient materials’ fine tuning on a nm scale.

8.2 Results and Discussion

In order to investigate the effect of the solvent used on the polymeric materials formed upon dehydrogenative coupling reaction, several aryltin trihydrides, such as *o*-tolylSnH$_3$ (**36**), *p*-^{n}butylphenylSnH$_3$ (**37**), mesitylSnH$_3$ (**40**) and 1-napththylSnH$_3$ (**41**) were converted with the amine base TMEDA in different solvents. The solvents were chosen according to their donor capacity, polarity and aromaticity. Diethyl ether and DME represent ethereal, donating solvents. Toluene was applied as a non polar, aromatic solvent, while cyclohexane exhibits non polar, non donating characteristics. In these studies, the isolated polymers were subjected to a SAXS analysis to reveal the common correlation length, as well as the morphology on a µm range was investigated by SEM analysis. Furthermore, the evolution of nano-substructure over reaction time and the dependence of the used solvent on the formed nanomorphology were carefully analyzed by *in situ* synchrotron SAXS experiments applying a novel, inert atmosphere stopped flow set-up.

8.2.1 Synthesis

The educts *o*-tolylSnH$_3$ (**36**), *p*-^{n}butylphenylSnH$_3$ (**37**), mesitylSnH$_3$ (**40**) and 1-napththylSnH$_3$ (**41**) were synthesized according to a literature known procedure subjecting the corresponding trichlorides (**21,24-26**) to a hydrogenation reaction using excess of LiAlH$_4$ at -30 °C.[80] The resulting thermally labile compounds were stored at -80 °C. In a typical dehydrogenative coupling reaction, an equimolar amount of TMEDA was added to a 0.4 M solution of dried and degassed diethyl ether, DME (dimethoxyethane), cyclohexane or toluene respectively and **36** at room temperature (Scheme 82). After completion of the reaction the synthesized black solid was filtered off and washed with the respective solvent.

8.2.2 SAXS Measurements

Three different trihydrides (**36**, **37**, **41**) exhibiting a range of substituents were subjected to a dehydrogenative coupling reaction in four different solvents (diethyl ether, DME, cyclohexane and toluene). In this manner, the steric demand of the aryl moieties was altered as well as their solubility. The resulting black products, ***o*-tolyl@Sn**, 1-naphthyl@Sn and *p*-^{n}butylphenyl@Sn were investigated by SAXS measurements. These experiments allowed for insights into how the nature of the solvent, as well as the aromatic substituent, alters the size and the structure of resulting materials on a nanoscale (Figure 86). Figure 86 illustrates the SAXS patterns for all isolated polymers and Table 19 sums up all peak positions in real dimension D(Å) of the correlation peaks in real space and their intensity A. Conclusively, the nature of the solvent as well as the bonded aryl residue alters the common correlation length of the nanostructure as well as its homogeneity. In general, the data suggests that the smallest sizes are realized using DME followed by diethyl ether, toluene and cyclohexane independently of the used aryl residue. The *o*-tolyl based materials generated in diethyl ether showed similar correlation lengths as the 1-naphthyl analogues of 16.5 and 16.8 Å, respectively. However, the *p*-^{n}butylphenyl group induces bigger structures (22.0 Å in diethyl ether), which can be explained by the sterically demanding butyl group in *para* position of the aromatic ring as well as by the better solubility of intermediates in the used solvents. This leads to longer reaction times in solution allowing for bigger particle formation. Thus, nanoporosity of the resulting material can be regulated by the use of differently sized aryl residues as well as by the nature of the solvent which provides a nice tool to alter the materials' characteristics.

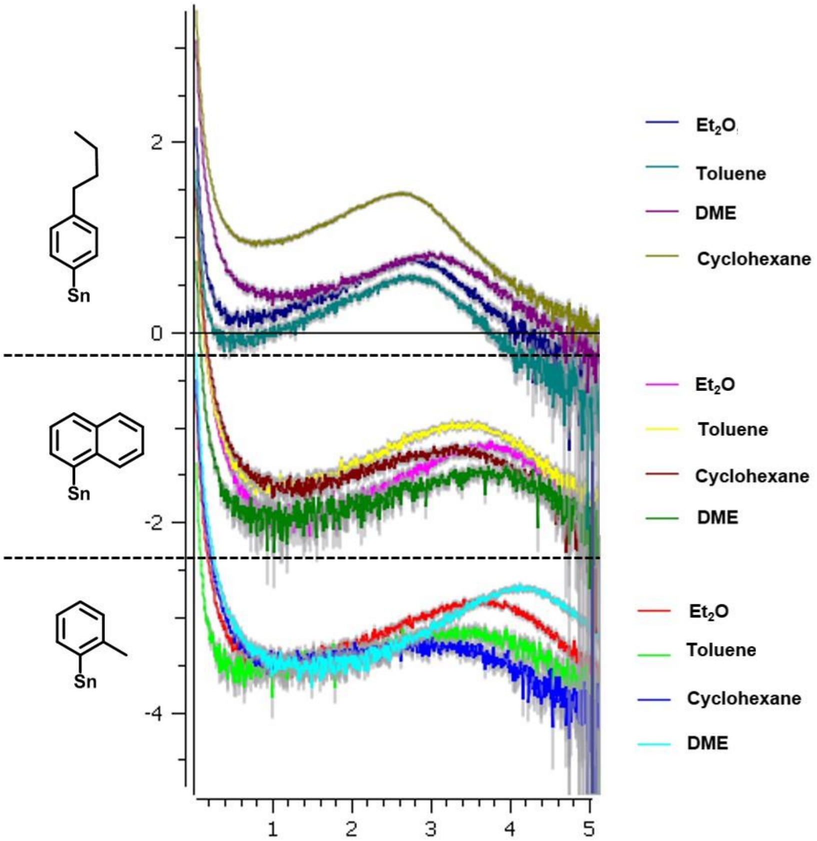

Figure 86: *SAXS pattern from **o-tolyl@Sn**, **1-naphthyl@Sn** and **p-^{n}butylphenyl@Sn** synthesized in Et$_2$O, DME, toluene and cyclohexane.*

Table 19: *Position of correlation peak in real dimension (D(Å)) and peak height (A) for **o-tolyl@Sn**, **1-naphthyl@Sn** and **p-^{n}butylphenyl@Sn** synthesized in Et$_2$O, DME, toluene and cyclohexane.*

	***o*-tolyl@Sn**				**1-naphthyl@Sn**				***p*-^{n}butylphenyl@Sn**			
	DME	Et$_2$O	toluene	cyclohexane	DME	Et$_2$O	toluene	cyclohexane	DME	Et$_2$O	toluene	cyclohexane
D(Å)	15.0	16.5	17.4	18.0	16.6	16.8	18.0	18.0	20.6	22.0	22.1	23.2
A	0.52	0.52	0.12	0.23	0.20	0.40	0.40	0.20	0.29	0.39	0.48	0.60

8.2.3 SEM Imaging

The polymers ***o*-tolyl@Sn**, **1-naphthyl@Sn** and ***p*-^{n}butylphenyl@Sn** were synthesized in diethyl ether, DME, toluene and cyclohexane are subjected to SEM measurements in order to reveal the changes in morphology on a µm range. Investigating the surface structure of the resulting polymers showed that especially, in the case of ***o*-tolyl@Sn** the nature of the used solvent strongly influences the morphology of the material. Carrying out the dehydrogenative coupling reaction of *o*-tolylSnH$_3$ in donating, ethereal solvents like DME and diethyl ether led homogeneous spherical morphologies with an average diameter of 2 µm. However, using aromatic, non polar solvents such as toluene resulted in jagged edged and tighter-packed materials. Apolar and non-donating solvents such as cyclohexane induced no specific arrangement in the solid state as illustrated in the SEM images in Figure 87. When using 1-naphthylSnH$_3$ (**41**) as educt, the effect on the morphology of the material is very similar as described for *o*-tolyl, however less pronounced. In the case of ***p*-^{n}butylphenyl@Sn**, the nature of the solvent used did not exhibit such a pronounced effect on the overall morphology as in the case of ***o*-tolyl@Sn** and **1-naphthyl@Sn**.

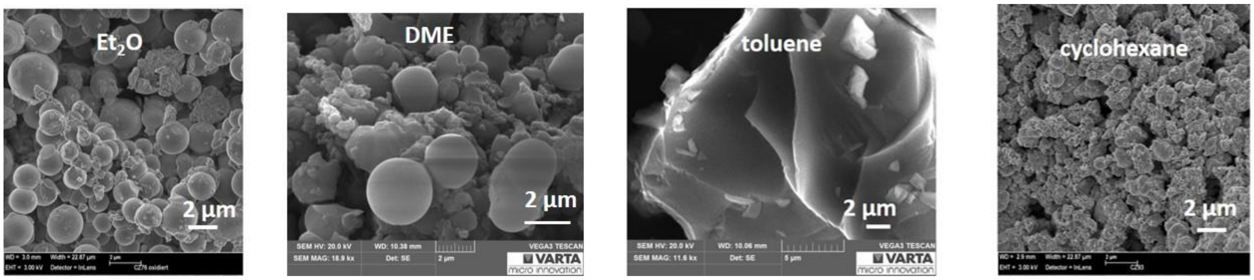

Figure 87: *SEM images of **o-tolyl@Sn** synthesized from Et$_2$O, DME, toluene and cyclohexane.*

Especially, in the case of ***o*-tolyl@Sn**, it can be suggested that the donor capacity of the solvent strongly influences the morphology and the monodispersity of the materials formed. Thus, donor capable solvents such as DME and diethyl ether induced spherical particles, whereas the other investigated solvents did not lead to specific, regular arrangements in the powder.

8.2.4 *In situ* Synchrotron SAXS Measurements

Previous work by Uhlig and coworkers revealed the detailed information on the growth process of the ***o*-tolyl@Sn** using TMEDA as a catalyst in diethyl ether (Chapter 6.2.3). It could successfully be shown that a fast nano-substructure formation of spherical particles (20 min) with a diameter of 1.6 nm takes place which is followed by agglomeration processes to bigger superstructures (Chapter 6 and Scheme 88). As suggested by SEM analysis, appreciable changes in the surface structure (µm scale) were observed for ***o*-tolyl@Sn** synthesized from different solvents. This provided motivation to investigate the *in situ* particle formation in DME, cyclohexane and toluene in order to compare the evolution to the findings for diethyl ether systems.

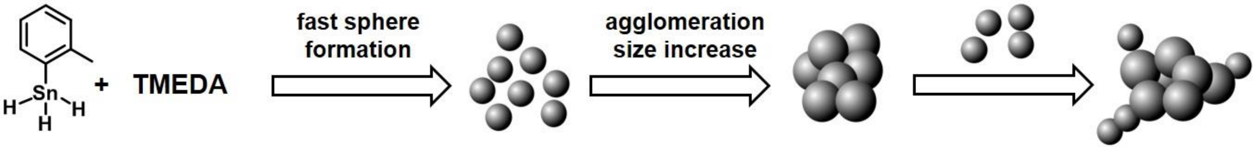

Scheme 88: *Schematic growth process of nanoparticles* ***o-tolyl@Sn*** *in diethyl ether.*

8.2.4.1 Dimethoxyethane (DME)

Figure 88 displays the normalized and background subtracted SAXS scattering pattern of the particle formation upon dehydrogenative coupling reaction of **36** with the amine base TMEDA in DME over 2 h reaction time with a time resolution of 4 min. To extract information on size evolution, size distribution and interaction of the nanoparticles, the data were fitted according to the structural model described in 6.2.3.

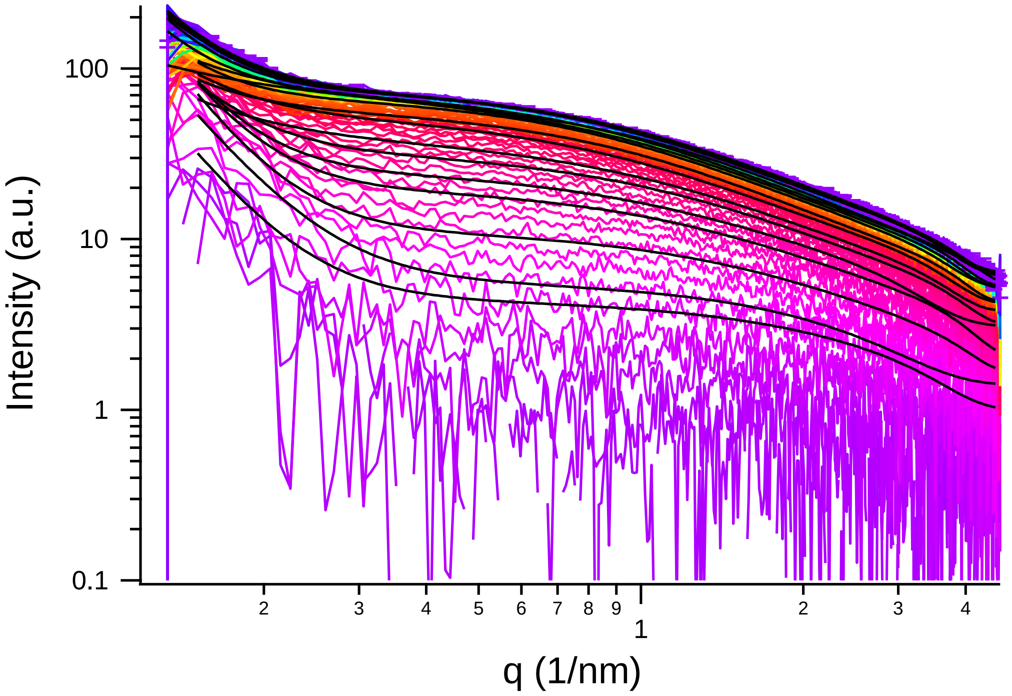

Figure 88: *Scattering pattern of o-tolylSnH$_3$ (**36**)/TMEDA reaction in DME over the first 2 h. Time resolution for each pattern is 4 min.*

Figure 89 displays the fit results for the integrated intensity, as well as the correlation length which is a direct measure for particle size, continuously increasing at the beginning of the reaction. After 10 minutes, the integrated intensity and the correlation length stay constant (Figure 89). At the same time an increase in intensity is observed (Figure 90) accompanied by a mass and volume fraction increase (Figures 90). The increase in intensity at constant correlation length is due to the generation of nano-substructures exhibiting the same shape and size. As already observed for the dehydrogenative coupling reaction in diethyl ether, spherical substructures with a diameter of 1.9 nm are also formed in DME. However, the reaction progress is faster as the maximum correlation length is already reached after 10 min reaction time (Figure 89).

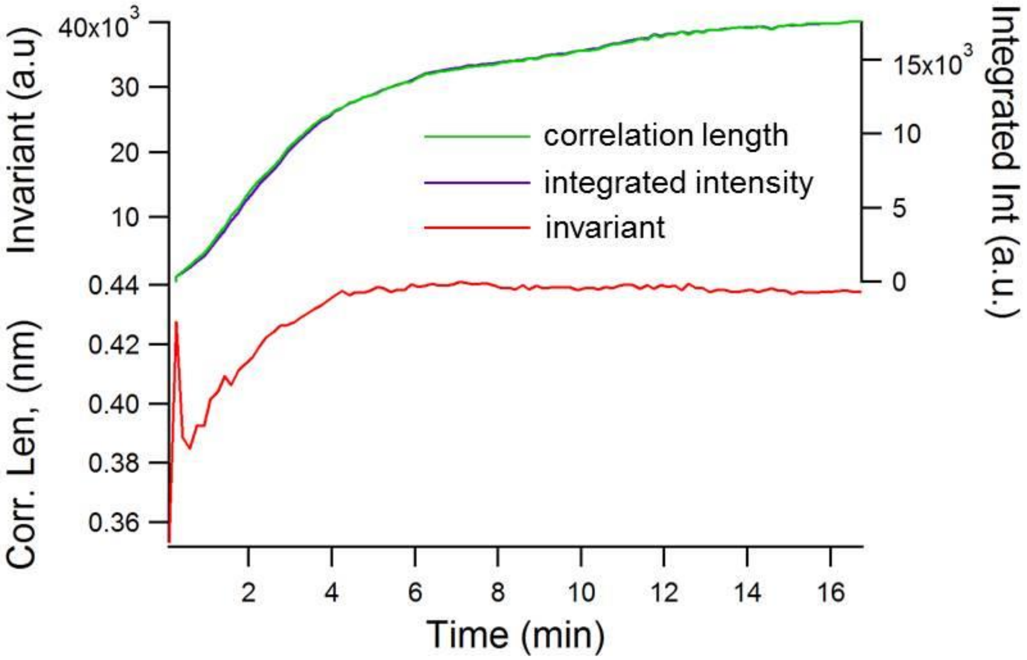

Figure 89: *Fit results for the invariant (a.u.), correlation length (nm) and integrated intensity of the Scattering pattern of o-tolylSnH$_3$ (**36**)/TMEDA reaction in DME.*

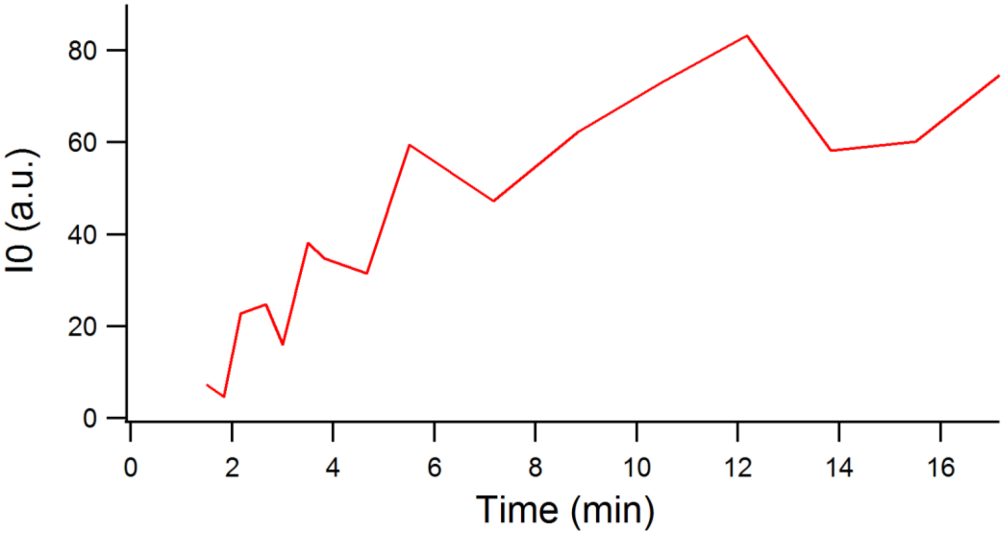

Figure 90: *Intensity increase over time for the dehydrogenative coupling reaction of o-tolylSnH$_3$ (**36**) and TMEDA in DME.*

Figure 91 depicts the development of the hard-sphere radius r_{hs}, the mean particle radius r_{sph} (determined by a Schulz distribution function) and the root mean square deviation of the radius $\sigma_{sph.}$ Interestingly, the mean particle radius r_{sph} (0.95 nm) is 30 % increased in size in comparison to the hard-sphere interaction term (0.77 nm). This is only possible if the formed particles exhibit a soft surface which allows for a 0.2 nm thick overlapping area of interpenetrating particles.

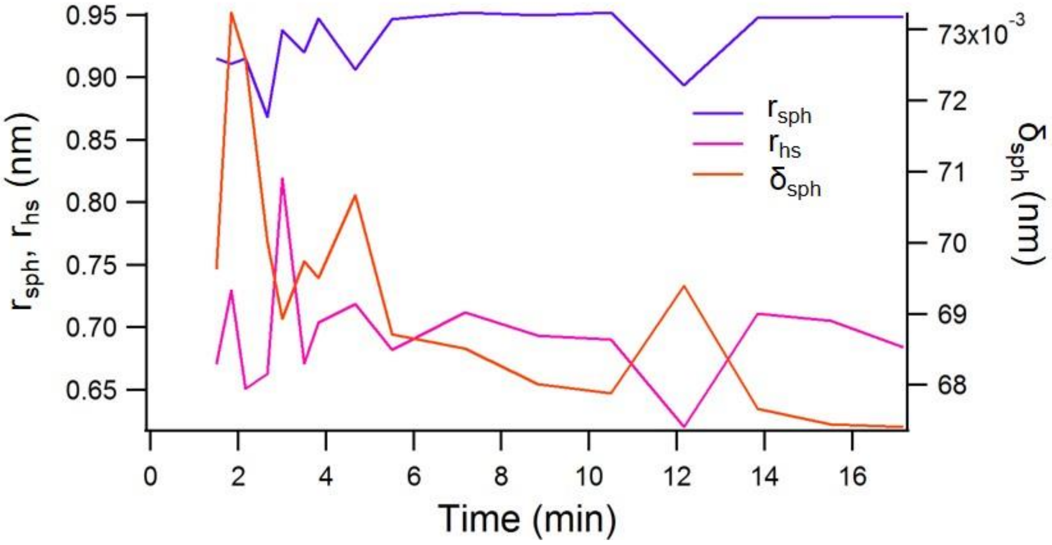

Figure 91: *Hard-sphere radius (r_{hs}), mean radius (r_{sph}) and root mean square deviation of the radius (σ_{sph}) of the particles formed in the dehydrogenative coupling reaction of o-tolylSnH$_3$* ***(36)*** *and TMEDA in DME versus time.*

An overlapping process is also expressed by a striking increase of ε_{hs} in the first 4 min of the dehydrogenative coupling reaction in DME reflecting a high attractive potential and strong propensity to agglomeration (Figure 92). The volume fraction stays constant (Figure 92).

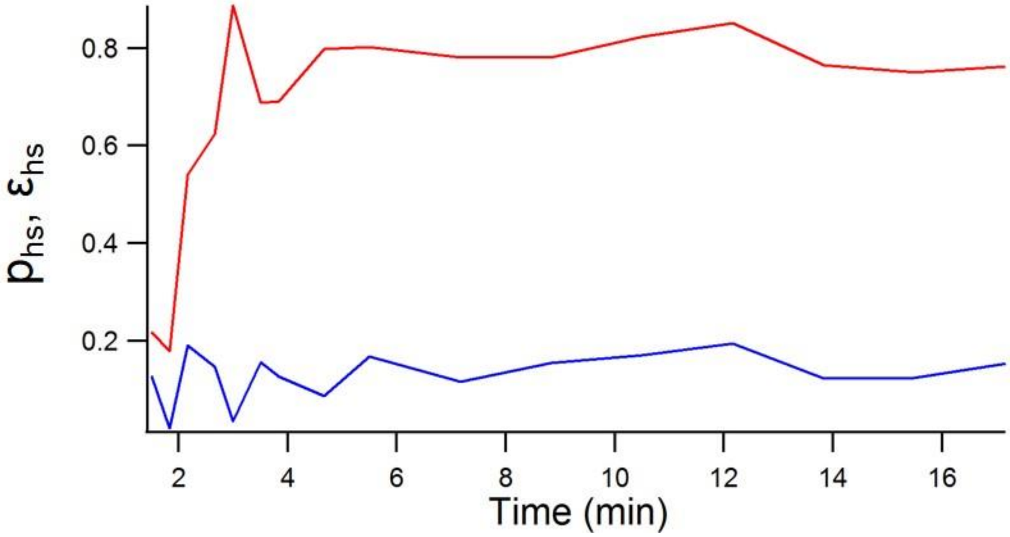

Figure 92: *Calculated hard-sphere parameters, p_{hs} (volume fraction of the sticky hard-sphere potential), and ε_{hs} (well of attractive potential) for the reaction of o-tolylSnH$_3$ (**36**) and TMEDA in DME versus time.*

Since the particles overlap, SAXS measurements of the isolated powder of ***o*-tolyl@Sn** synthesized in DME show smaller distances than for diethyl ether (Table 19). However, the actual diameter (r_{sph}) for the particles formed in DME is bigger (1.9 nm) than for the structures synthesized in diethyl ether (1.4 nm) which fits well to the dimension determined from the structure factor r_{hs}.

8.2.4.2 Cyclohexane

Figure 93 displays the normalized and background subtracted SAXS scattering pattern of the particle formation upon dehydrogenative coupling reaction of **36** with the amine base TMEDA in cyclohexane over 2 h reaction time with a time resolution of 4 min. To extract information on particle shape and morphology, the data were fitted according to a power law fitting in the intermediate range which allows the morphology identification.[327]

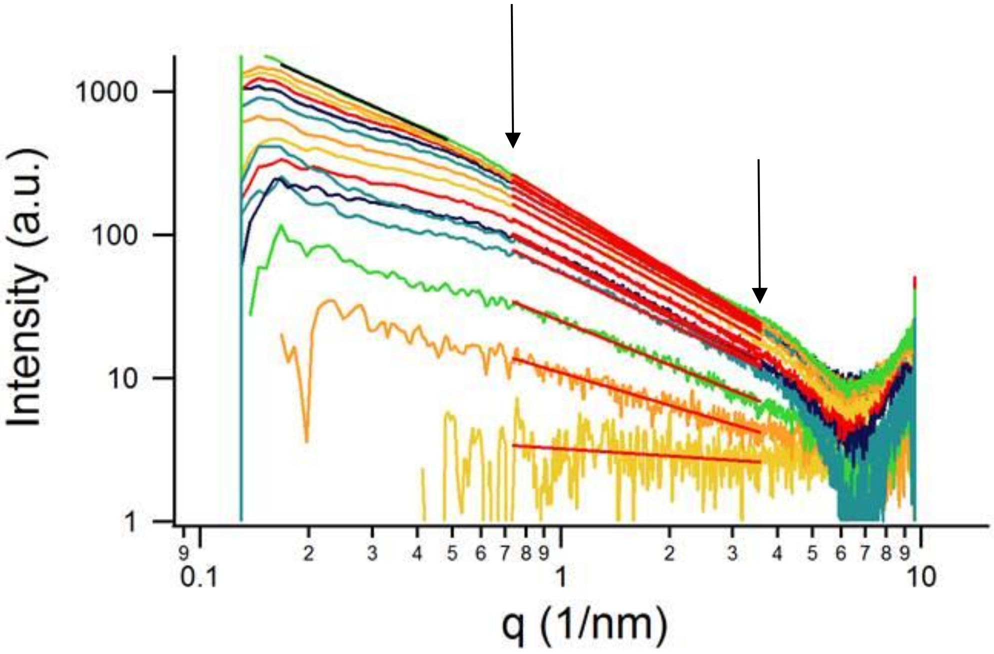

Figure 93: *Scattering pattern of o-tolylSnH$_3$ (**36**)/TMEDA reaction in cyclohexane over the first 2 h. Time resolution for each pattern is 4 min.*

According to the Power law fitting in the intermediate range, the particle formation in the dehydrogenative coupling reaction in cyclohexane shows a q^{-1} behavior. Thus, the formation rod like structures can be observed as the Porod exponent already reaches 1 after 10 minutes reaction time (Figure 94). The principal rod formation is fast, generating rods exhibiting a cross section of 1.4 nm and a length of 8.6 nm as indicated by the position of arrows in Figure 93. The change of the slope below 0.3 nm^{-1} indicates structural changes. These changes are suggested to happen due to the agglomeration processes of rods forming random networks. Figure 95 displays the evolution of the Porod constant over reaction time. The morphology evolution is schematically depicted in Scheme 89.

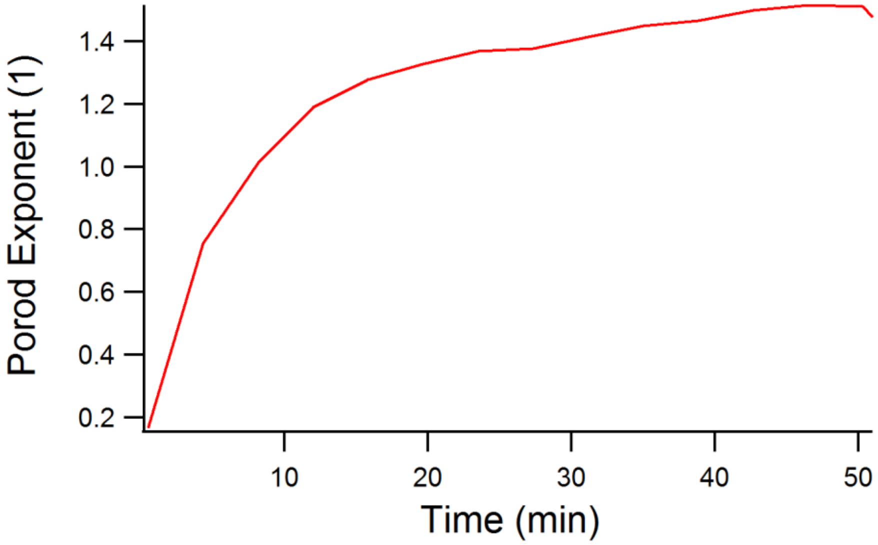

Figure 94: *Porod exponent fitted on the low q part (4-0.7 nm^{-1}) of the scattering pattern of o-tolylSnH$_3$ (**36**)/TMEDA reaction in cyclohexane versus time (min).*

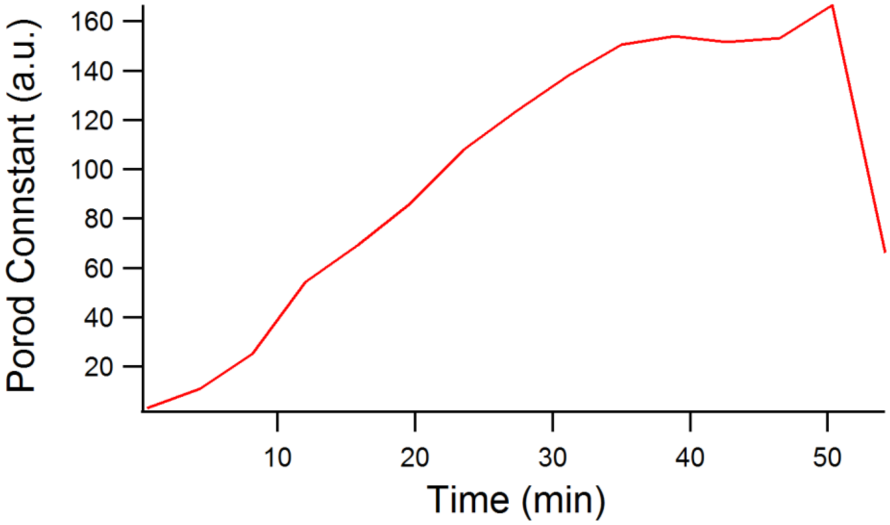

Figure 95: *Porod constant (a.u.) fitted on the low q part (4-0.7 nm^{-1}) of the scattering pattern of o-tolylSnH$_3$ (**36**)/TMEDA reaction in cyclohexane versus time (min).*

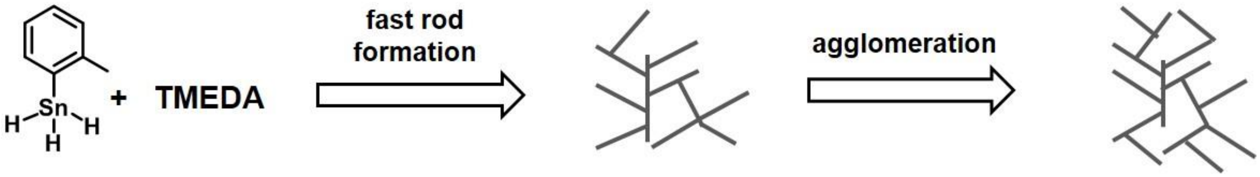
Sn
H
H
H
+
TMEDA
fast rod formation
agglomeration

Scheme 89: *Schematic growth process of nanoparticles* ***o-tolyl@Sn*** *in cyclohexane.*

8.2.4.3 Toluene

Figure 96 displays the normalized and background subtracted SAXS scattering pattern of the particle formation upon dehydrogenative coupling reaction of **36** with the amine base TMEDA in toluene over 2 h reaction time with a time resolution of 4 min. To extract information on size evolution, size distribution and interaction of the nanoparticles, the data were fitted according to a power law fitting in the intermediate range.[327]

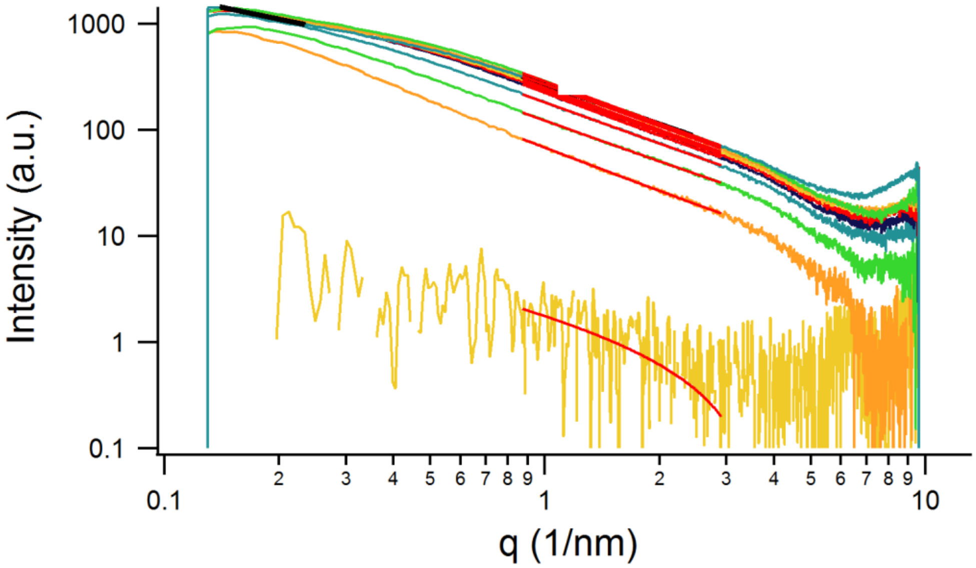

Figure 96: *Scattering pattern of o-tolylSnH$_3$ (**36**)/TMEDA reaction in toluene over the first 2 h. Time resolution for each pattern is 4 min.*

The nanoparticle formation in toluene shows a q^{-1} behavior at the beginning of the reaction as it was also observed for cyclohexane. The reaction is observed to proceed faster in toluene as the Porod exponent increases to 1 in the first 4 min of the reaction (Figure 97). The evolution of a small shoulder of the structure factor is observed which is derived by rod-rod aggregation (Figure 96). The formed nanorods feature infinite length, a cross section of 1.5 nm and an average distance to each other of 15.7 nm. These nano rods do not aggregate in random networks as shown for cyclohexane, however approach each other over reaction time generating an interacting network which can be best described as a “mikkado” like assembly (Scheme 90).

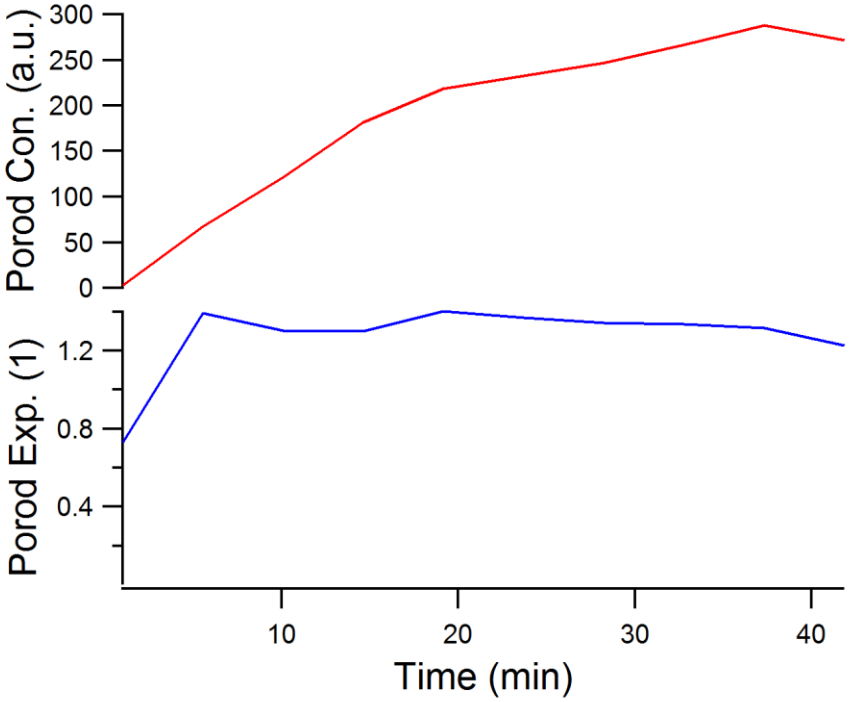

***Figure 97:** Porod exponent and Porod constant (a.u.) fitted on the low q part (3-0.9 nm^{-1}) of the scattering pattern of o-tolylSnH_3 (**36**)/TMEDA reaction in toluene versus time (min).*

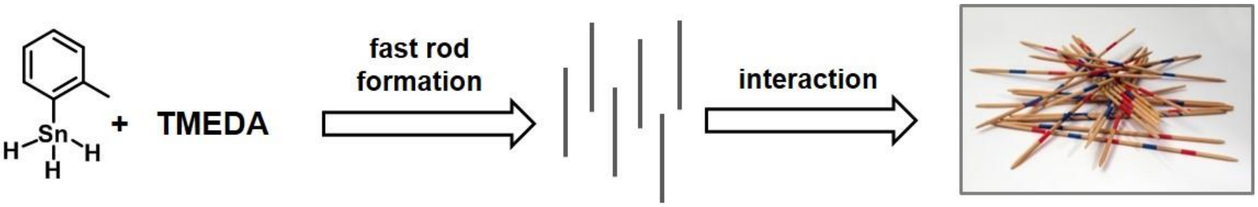

***Scheme 90:** Schematic growth process of nanoparticles **o-tolyl@Sn** in toluene.*

8.2.5 *In situ* Synchrotron Stopped Flow XANES and EXAFS Measurements

The X-ray absorption near edge structure (XANES) is sensitive to the electronic environment around a nucleus (absorber) of interest as well as the edge position is indicative of the oxidation state and local geometry. The dehydrogenative coupling reaction of the aryltin trihydrides, *o*-tolylSnH_3 (**36**) using TMEDA in diethyl ether is postulated to proceed *via* a reductive process (6.2.7) which could be supported by time resolved investigation of the oxidation state (6.2.9). *In situ* synchrotron SAXS measurements revealed differences in the nano-substructure formation kinetics if the nature of the solvent is altered (8.2.4). These solvent effects on the morphology provided motivation to perform *in situ* stopped flow synchrotron EXAFS/XANES analysis on the dehydrogenative coupling of *o*-tolylSnH$_3$ (**36**) using TMEDA in diethyl ether, DME, cyclohexane and toluene. The X-ray absorption spectra at the Sn K edge were collected at the beamline BM26A (DUBBLE) of the ESRF-The European Synchrotron in Grenoble, France as well as at the BM18 at the Diamond Lightsource Innovation campus.

As already reported for the dehydrogenative coupling of *o*-tolylSnH$_3$ (**36**) in diethyl ether, only small changes in the edge energy of 2.4 eV are observed when reducing tin from IV to II (6.2.9). However, the reductive process can also be supported for all the solvents investigated (DME, cyclohexane, toluene) as an overall decrease of E0 is observed (~ 2.2 eV).

The Fourier transform magnitudes of the EXAFS oscillations over reaction time in the solvents diethyl ether, DME and toluene show a growing signal at a correlation length of 2.6 Å (Figure 98). The reaction in cyclohexane proceeds much slower and the pattern does not show this correlation length. This real space distance, which is the same for all solvent systems, corresponds to the Sn–Sn distance formed upon dehydrogenative coupling reaction of *o*-tolylSnH$_3$ (**36**) (Figure 98). Thus, coordination number and local environment in the formed material is not dependent of the nature of the solvent used.

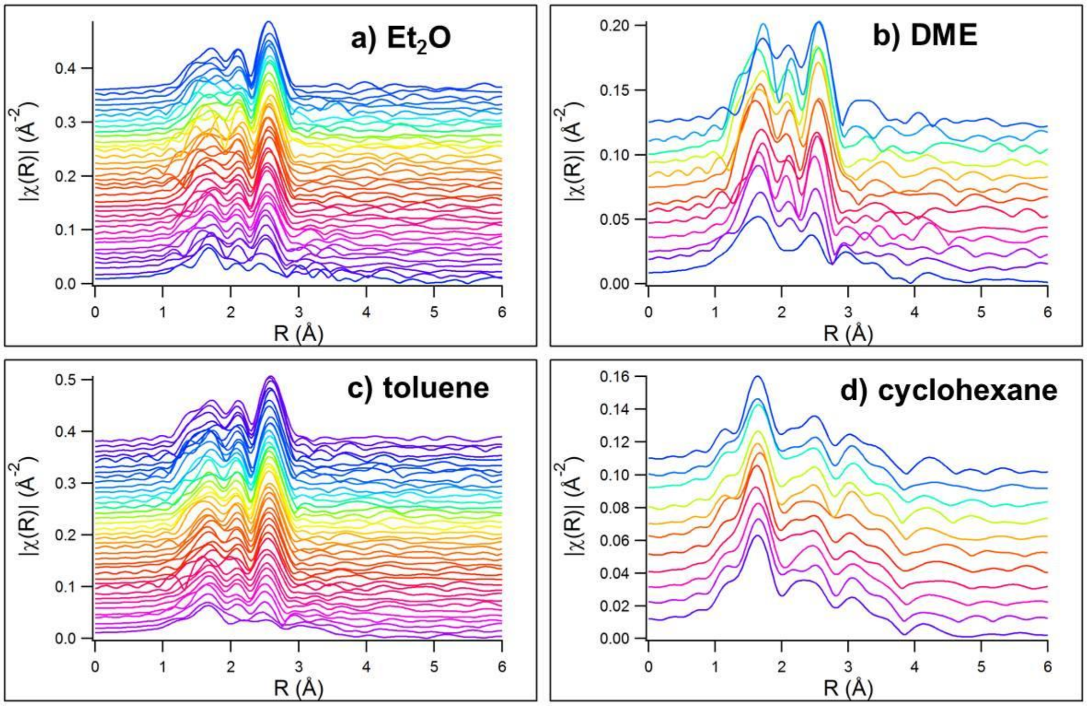

Figure 98: *Fourier transform magnitudes of k^2-weighted $\chi(k)$ data of the EXAFS data of the in situ reaction of o-tolylSnH$_3$ (**36**)/TMEDA reaction in **a)** Et$_2$O (1.7 h), **b)** DME (1.1 h), **c)** toluene (1.4 h), **d)** cyclohexane (0.6 h). Time resolution for each pattern is 2.7 min.*

Final products of (***o*-tolyl@Sn**) were generated in the dry box by adding three drops of TMEDA to 0.5 mL of 0.08 M solution of **36** in the respective solvent. The polymeric products were then subjected to three frames of XANES measurements (Figure 99). Furthermore, three XANES frames were taken from polydiphenylstannane ((phenyl$_2$Sn)$_n$) dry powder as a reference. A comparison of the Fourier transformed magnitudes of the final product ***o*-tolyl@Sn** (from diethyl ether, DME, toluene, cyclohexane) and polydiphenylstannane ((phenyl$_2$Sn)$_n$) powder show the same correlation length of 2.6 Å (Figure 99). This real space distance can be assigned to the Sn–Sn bonds, which are postulated to arrange as a linear Sn backbone in the case of polydiphenylstannane.[179] Although the formation of ***o*-tolyl@Sn** proceeds the slowest in cyclohexane, the final state of the polymer exhibits the same structural features as found for the other solvents (Figure 99).

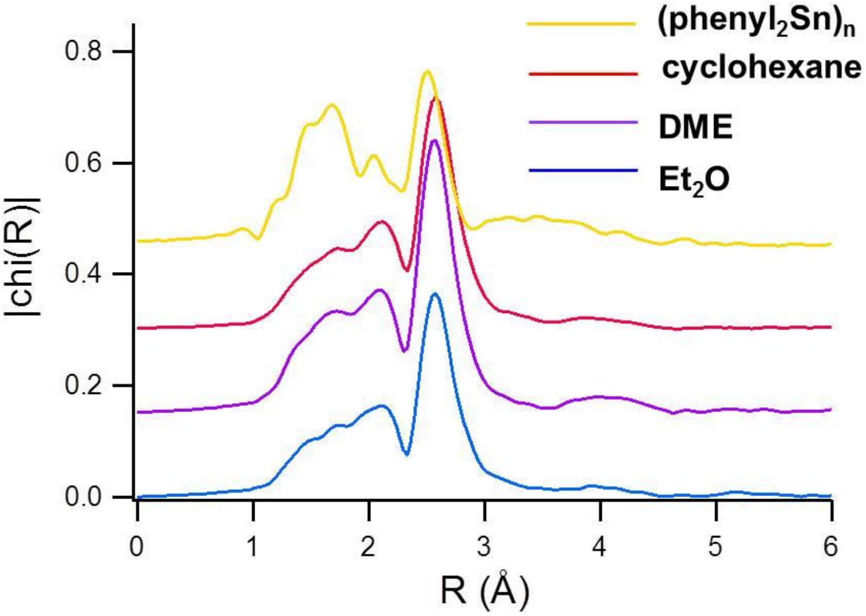

Figure 99: *Fourier transform magnitudes of k^2-weighted $\chi(k)$ data obtained from of* ***o-tolyl@Sn*** *synthesized in Et$_2$O, DME, toluene, cyclohexane and (phenyl$_2$Sn)$_n$ powder (3 frames each).*

8.3 Conclusions

In summary, we were able to provide insights into the control of the nanomorphology of aryl decorated nanoparticles (aryl@Sn). Not only does the alteration of the aryl group lead to significant differences in the common correlation length of the polymers formed, but also the nature of the solvent strongly influences the particle size and shape. Using *o*-tolyl and 1-naphthyl containing aryltin trihydrides led to comparable results in SAXS analysis (16.5 and 16.8 Å), however more sterically hindered aryl residues such as *p*-^{n}butylphenyl formed materials showing a correlation length of 22.0 Å. The solvent effects were investigated by *in situ* synchrotron SAXS measurements revealing detailed information on the growth process for ***o*-tolyl@Sn** in the solvents diethyl ether, DME, toluene and cyclohexane. It could be shown that according to the donor ability of the solvent, different growth processes can be distinguished forming either nanospheres or rods. Performing the reaction in diethyl ether led to nanospheres exhibiting a cross section of only 1.6 nm, whereas the use of cyclohexane induced the formation of nanorods which agglomerate over reaction time forming bigger networks. The nanorods have a cross section of 1.4 nm and a length of 8.6 nm. Interestingly, toluene as an aromatic solvent also led to the formation of rods with a cross section of 1.4 nm, however their length could not be assigned with SAXS resolution. Furthermore, the growth process to bigger assemblies is different in the case of toluene, as the rods do not agglomerate but form “mikkado” like structures over reaction time. These findings provide deeper understanding in the structure and morphology tailoring of carbon coated tin nanoparticles, allowing for precise tuning of electrochemical characteristics which is one of the key future investigation fields in our working group.

Although the nano-substructure formation kinetics strongly differ with respect to the used solvent, *in situ* synchrotron stopped flow XAS measurements showed that the coordination number and local environment in the formed material (***o*-tolyl@Sn**) is not dependent of the nature of the solvent used. The materials formed in diethyl ether, DME, cyclohexane and toluene respectively exhibit a common correlation length of 2.6 Å which can be assigned as the formed Sn–Sn upon dehydrogenative coupling reaction.

9 Hydrogenation of *C,N*- Chelated Organotin Halides- Autocatalytic Reductive Dehydropolymerization

Graphical Abstract

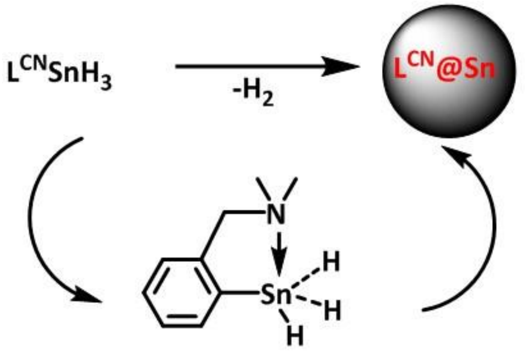
$L^{CN}SnH_3$
$-H_2$
L^{CN}@Sn
N
Sn
H
H
H

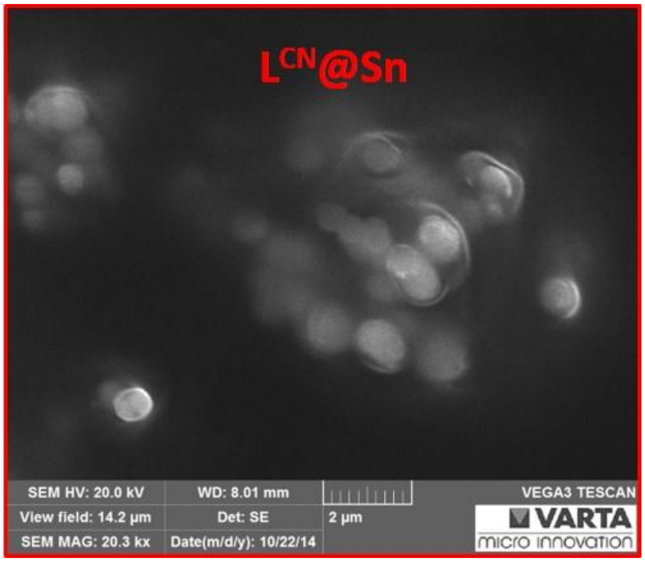
L^{CN}@Sn
SEM HV: 20.0 kV
WD: 8.01 mm
VEGA3 TESCAN
View field: 14.2 µm
Det: SE
2 µm
SEM MAG: 20.3 kx
Date(m/d/y): 10/22/14
VARTA
micro innovation

Abstract

The C,N-chelated organotin halides $L^{CN}_{2}SnBuCl$ *(**49**),* $L^{CN}SnPhCl_2$ *(**50**) and* $L^{CN}SnBr_3$ *(**51**) were subjected to hydrogenation reactions, applying different hydrogenation agents such as* $LiAlH_4$*,* $K(BEt_3){\cdot}H$ *and* $BH_3{\cdot}THF$ *in order to generate the corresponding mono-, di- and trihydrides:* $L^{CN}_{2}SnBuH$ *(**52**),* $L^{CN}SnPhH_2$ *(**53**),* $L^{CN}SnH_3$ *(**54**). The effect of the donor ability of the* L^{CN} *ligand on the thermal stability of the synthesized organotin hydrides is also described reporting on thermally induced, autocatalytic dehydrogenative coupling reaction of* $L^{CN}SnPhH_2$ *(**53**),* $L^{CN}SnH_3$ *(**54**) forming polyarylstannanes. By applying in situ variable temperature NMR studies, the undesired dehydropolymerization could be successfully circumvented to afford the desired organotin hydrides. In addition, DFT studies were carried out in order to reveal the effect of chelating ligands on the* $^{1}J(^{1}H\text{-}^{119}Sn)$ *coupling constants and the Sn–H bond lengths. Furthermore, the solid state structure of* $L^{CN}_{2}SnBuCl$ *(**49**) as the second one known in literature for the compound family of* $L^{CN}_{2}SnRX$ *(R= alkyl, aryl; X= halide) is elucidated.*

9.1 Introduction

The compound family of organotin(IV) compounds exhibiting 2-(dimethylaminomethyl)phenyl groups (L^{CN}) or related chelating moieties has been extensively studied starting in the 1970s (Figure 100). This high interest can be rationalized by remarkable structural properties. According to the number of chelating ligands, these compounds exhibit either trigonal bipyramidal or octahedral coordination geometries.[328,329] The existence of strong N→Sn interactions and therefore the increased coordination number of tin have been evidenced by single crystal diffraction analysis as well as solution and solid state NMR studies.[330-333] A series of organotin(IV) compounds displaying one or more chelating ligands, especially 2-(dimethylaminomethyl)phenyl (L^{CN}) has been successfully synthesized and characterized mostly by the working group of Růžička.[329-332,334-343] These tetravalent organostannanes containing a N→Sn intermolecular interaction have also been reported to show potential biological activity as antimycotical agents,[344] practical use as transesterification or esterification catalyst,[345,346] fluorinating agents,[347,348] and being parts of ion selective electrodes.[349] Furthermore, the particular use of some of these complexes in various types of catalytically driven conversions, such as CO_2 activation to dimethyl carbonate has been developed.[350,351]

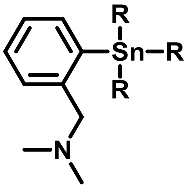

Figure 100: *Organotin(IV) compounds exhibiting 2-(dimethylaminomethyl)phenyl groups (L^{CN})*

Furthermore, Růžička *et al.* reported on the hydrolysis of $L^{CN}SnCl_3$ *via* ligand migration, $[L^{CN}SnCl_4]^-[HL^{CN}{}_2SnCl_2]^+$, [335] as well as the reaction of CN chelated organotin(IV) halides towards carboxylic, mineral and various Lewis acids forming zwitterionic tri- and diorganostannates.[352] The basic hydrolysis of diorganotin(IV) dichlorides of the formula $L^{CN}RSnCl_2$ (R= Bu, Ph) using aqueous sodium hydroxide in benzene generates $(L^{CN}RSnCl)_2(\mu\text{-}O)$. In the case of $(L^{CN}PhSnCl)_2(\mu\text{-}O)$, catalytic activity could be demonstrated.[353] In 2009, Turek described the hydrogenation of $L^{CN}R_2SnCl$ (R= *n*-Bu, Ph, *t*-Bu) using $K(BEt_3)H \cdot THF$ at -40 °C. In this manner, the corresponding hydrides could be formed as well as preliminary reactivity studies such as activation of small molecules and hydrostannation reactions have been reported.[354] According to their assumptions based on ^{119}Sn NMR shifts, $L^{CN}R_2SnH$ (R= *n*-Bu, Ph, *t*-Bu) display strong N→Sn interactions. However, the latter is suggested to be more pronounced for the alkylated species. However, no solid state structure determining the intramolecular Sn–N coordination was successful.

Based on the pioneering work of Neumann *et al*. using amine bases in the dehydrogenation reaction of tin dihydrides, Uhlig *et al*. have successfully reported on the dehydrogenative coupling reaction of organotin dihydrides using TMEDA as an amine base catalyst.[11,55,355]

Very recently, Wesemann and coworkers could show the interaction of amine bases such as DMAP and pyridine with sterically encumbered aryltin trihydrides. According to these findings, the dehydrogenative coupling reaction either proceeds *via* a nucleophilic attack of the amine base at the tin center forming a Lewis adduct, or towards a heterolytic cleavage of a proton by the base.[259] In any case, the authors suggest a reductive process forming a Sn(II) compound, as well as it is described in this work (Chapter 6). Therein, the reductive dehydrogenative coupling or *o*-tolylSnH_3 using the amine base TMEDA is described to successfully form aryl decorated tin nanoparticles (***o*-tolyl@Sn**) (Chapter 6 and 8). Furthermore, a mechanism including a stannylene intermediate is proposed and supported by DFT calculations, elemental analysis, NMR and *in situ* synchrotron EXAFS studies.

These findings provided motivation to investigate the synthesis and properties of L^{CN} containing organotin hydrides, as the present amine functionality strongly interacts with the tin and therefore can be seen as an intramolecular amine base catalyst allowing for Sn–H bond cleavage, H_2 evolution, Sn–Sn bond formation and therefore material generation.

9.2 Results and Discussion

This work focuses on the conversion of organotin halides exhibiting one or two L^{CN} moieties ($L^{CN}{}_2SnBuCl$ **49**, $L^{CN}SnPhCl_2$ **50**, $L^{CN}SnBr_3$ **51**) to their corresponding mono-, di- and trihydrides ($L^{CN}{}_2SnBuH$ **52**, $L^{CN}SnPhH_2$ **53**, $L^{CN}SnH_3$ **54**) as well as on stability studies on the latter. For this reason a variety of different hydrogenation agents and synthetic methods were applied.

For the formation of $L^{CN}{}_2SnBuH$ (**52**), a monoorganotin hydride containing two potentially electron donating L^{CN} moieties, the standard synthetic method using $LiAlH_4$ in diethyl ether turned out to be successful (Scheme 91). The corresponding chloride $L^{CN}{}_2SnBuCl$ (**49**) was converted at room temperature. Surprisingly, the product **52** was stable for several weeks when stored at -20 °C without formation of elemental tin or the corresponding distannane ($L^{CN}{}_2BuSn{-}SnBuL^{CN}{}_2$) *via* dehydrogenative coupling.

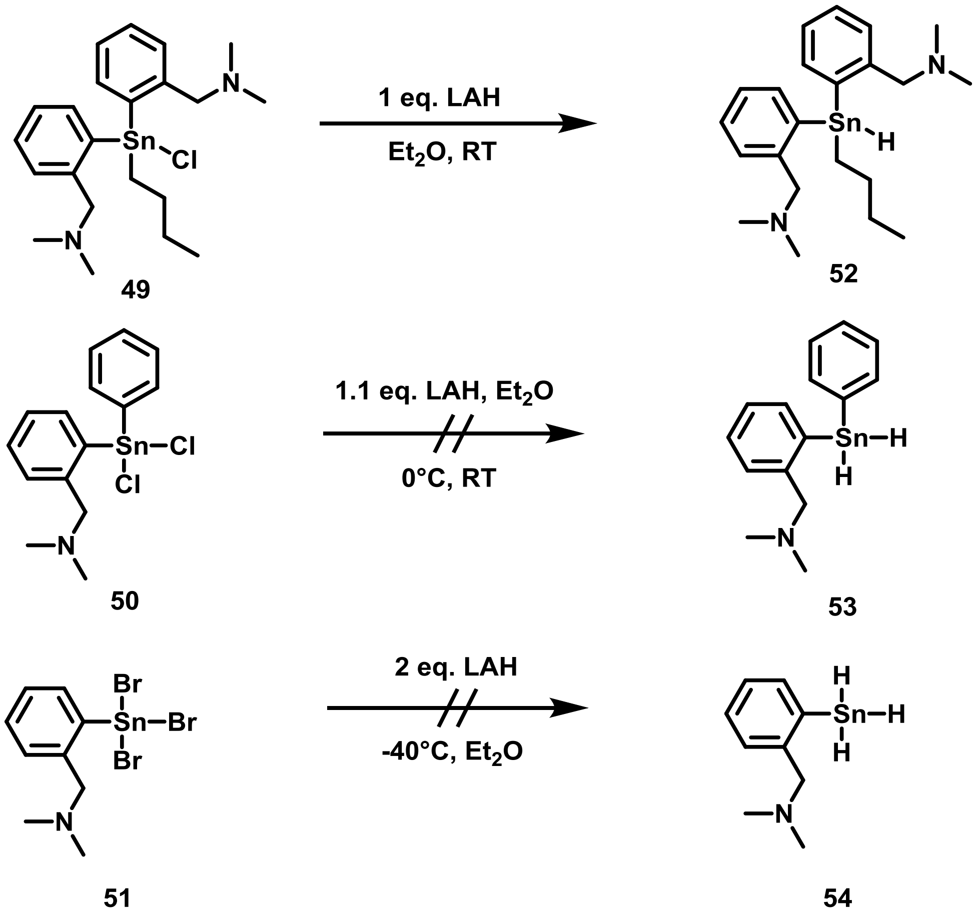

***Scheme 91**: Formation of $L^{CN}{}_2SnBuH$ (**52**), $L^{CN}SnPhH_2$ (**53**), $L^{CN}SnH_3$ (**54**).*

However, applying this standard procedure for the conversion of organotin di- and trihalides exhibiting one L^{CN} moieties (**50**,**51**) was not successful. Although the hydrogenation reaction was carried out at lower temperatures (Scheme 91), undesired dehydrogenative coupling reactions and hydrogen formation were observed. When $L^{CN}SnPhCl_2$ (**50**) was subjected to the hydrogenation reaction, according to Scheme 91, the resulting product was an orange solid which was partly soluble in C_6D_6. The ^{1}H NMR did not show any Sn–H functionalities. In general, Sn–H functionalities reveal a typical hydride shift in the ^{1}H NMR showing ^{1}H-^{119}Sn as well as ^{1}H-^{117}Sn satellites. Phenyl$_2$SnH$_2$ (**31**) shows the Sn–H shift at 6.11 ppm in C_6D_6. In the case of **53** the Sn–H shift was expected to be found in this area. The ^{119}Sn NMR showed a main signal at -172 ppm which most likely corresponds to the unreacted educt **50**. No Sn–H couplings could be detected in the ^{119}Sn NMR which is in accordance to the ^{1}H NMR. It is suggested that the dihydride **53** was formed during the hydrogenation reaction, however it formed polymeric material at higher temperature (RT) upon H_2 evolution and Sn–Sn bond formation (Scheme 92). This is supported by the insolubility of the resulting product, as well as by its orange color, which has been reported for polyarylstannanes (aryl$_2$Sn)$_n$.[11] The observed reactivity could be rationalized by the presence of an internal amine base of the donating ligand (L^{CN}) allowing for Sn–H bond weakening, H_2 evolution and polymer formation (Scheme 92).[259] The orange solid was taken up in toluene, filtered and stored at -80 °C in order to grow crystals. However, an orange, turbid suspension was formed from the solution and unfortunately no crystals were obtained.

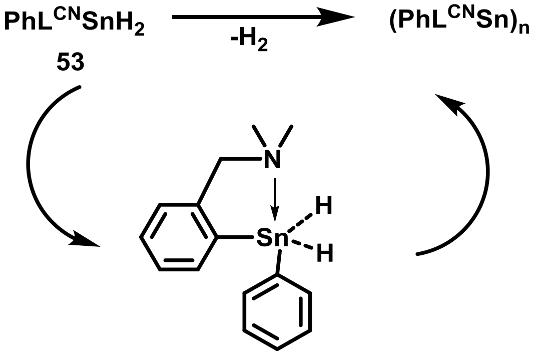

Scheme 92: Internal amine base acting as polymerization catalyst.

Turek reported on the successful formation of triorganotin hydrides exhibiting only one 2-(dimethylaminomethyl)phenyl residue (L^{CN}Bu$_2$SnH and L^{CN}Ph$_2$SnH) using K(BEt$_3$)H·THF instead of lithium aluminum hydride because of higher yields.[354] Therefore, it was tried to convert L^{CN}SnPhCl$_2$ (**50**) applying Turek's procedure. A (BEt$_3$)H·THF solution was added to a solution of **50** in THF at -50 °C. An immediate color change to yellow could be observed. The reaction mixture turned slightly orange upon evaporation of the solvent yielding orange oil. For the NMR investigations, a small amount of sample was taken up in diethyl ether and C_6D_6. The spectra were measured at -60 °C. However, the ^1H NMR was not conclusive and does not show any Sn–H peaks. The ^{119}Sn NMR showed a signal at -220.6 ppm, however no Sn–H coupling were observed, which is in accordance to the ^1H NMR. The attempt to gain crystals from toluene was not successful.

For comparison reasons it has to be mentioned that Lechner and coworkers had reported a ^{119}Sn NMR shift of -197 ppm in $CDCl_3$ when polymerizing *p*-^{n}butylphenyl$_2$SnH$_2$ using TMEDA.[11] Therefore, similar polymers were expected to be found in this spectral region. However, a consistent solvent system is necessary to allow for comparison.

In order to synthesize $L^{CN}SnH_3$ (**54**), the hydrogenation reaction of **51** was carried out at -40 °C (Scheme 91). Further work-up was carried out while cooling using an ice bath. However, the product/diethyl ether solution turned yellowish to orange color, as well as the formation of H_2 could be detected upon handling at 0 °C. After complete removal of diethyl ether, a dark brown solid was gained. The product was taken up in in C_6D_6 in order to measure ^{119}Sn and ^1H NMR. However, it was only partially soluble. The ^{119}Sn NMR did not show a signal. The ^1H NMR showed diethyl ether residues but no signals belonging to the desired product in the Sn–H, nor in the aromatic region.

As for $L^{CN}SnPhSnH_2$ (**53**), it is suggested that the trihydride $L^{CN}SnH_3$ (**54**) was formed during the hydrogenation reaction, however exhibits high thermal lability. Hence, the internal amine base enables Sn–H bond cleavage, hydrogen evolution and Sn–Sn bond formation (Scheme 93). This leads to the formation of a black powder, which is not soluble and therefore could not be characterized by NMR.

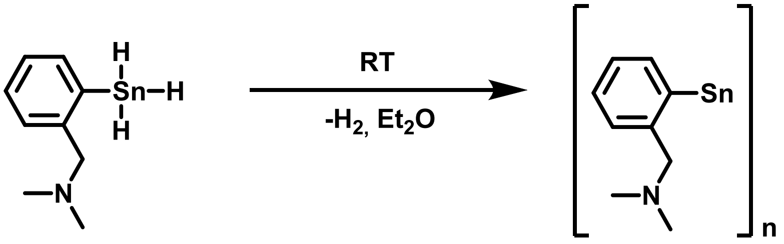

54

Scheme 93: *Thermally induced dehydrogentive coupling reaction of $L^{CN}SnH_3$ (**54**) forming **L^{CN}@Sn**.*

These findings are in accordance to the dehydrogentive coupling reaction with TMEDA of sterically not hindered aryltin trihydrides such as *o*-tolylSnH$_3$ (**36**) and 1-napththylSnH$_3$ (**41**) generating black, insoluble powders exhibiting a discrete nanostructure and morphology depending on the nature of the solvent used (Chapter 6-8). Therefore, the resulting material **L^{CN}@Sn** was subjected to SEM measurements, showing a very similar spherical morphology as found for ***o*-tolyl@Sn** produced from *o*-tolylSnH$_3$ with TMEDA in diethyl ether (Figure 101). It is suggested that an alteration of the morphology of **L^{CN}@Sn** could be achieved by synthesizing it in other solvents than diethyl ether. This morphology control has also been reported for the conversion of **36** in various solvents (Chapter 8).

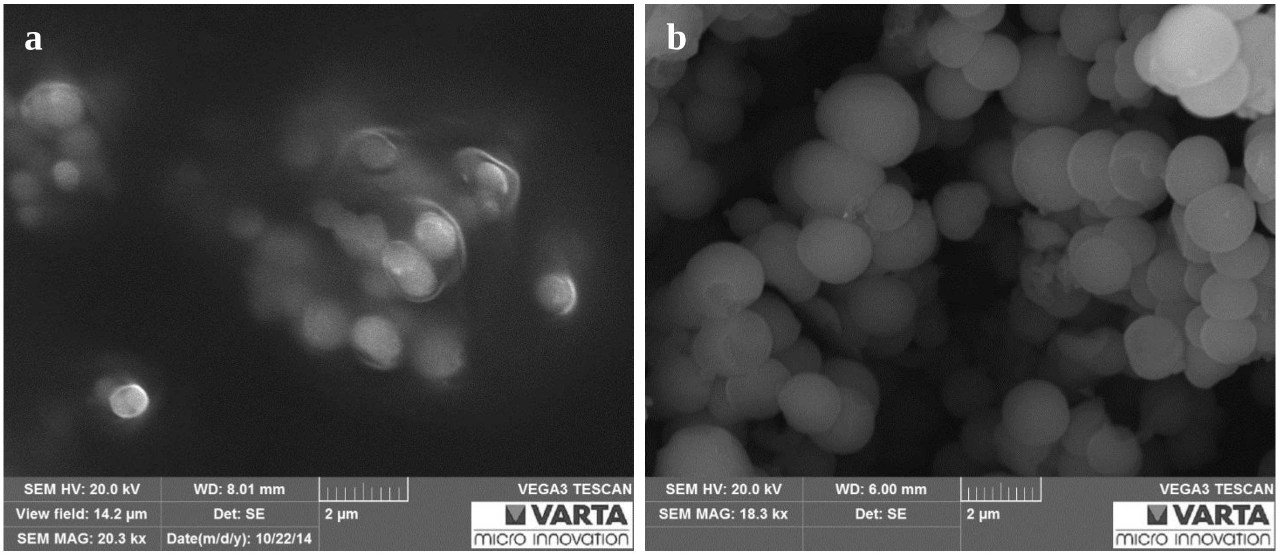
a
b
SEM HV: 20.0 kV
WD: 8.01 mm
View field: 14.2 µm
Det: SE
2 µm
SEM MAG: 20.3 kx
Date(m/d/y): 10/22/14
VEGA3 TESCAN
VARTA
micro innovation
SEM HV: 20.0 kV
WD: 6.00 mm
SEM MAG: 18.3 kx
Det: SE
2 µm
VEGA3 TESCAN
VARTA
micro innovation

Figure 101: *SEM images of* ***a) L^{CN}@Sn*** *and* ***b) o-tolyl@Sn****.*

The observed thermal instability of organotin di- (**53**) and trihydrides (**54**) exhibiting one L^{CN} residue can be explained by the presence of an internal amine function (Scheme 92) allowing for thermally induced reductive dehydropolymerization even at room temperature. This fact provided motivation to evidence the existence of the thermally unstable compounds **53** and **54** as intermediates in the reaction at low temperature.

9.2.1 VT-NMR studies and DFT calculations

In order to evidence the generation of $L^{CN}SnPhH_2$ (**53**) and $L^{CN}SnH_3$ (**54**) as thermally unstable intermediates in the hydrogenation reaction of the corresponding halogenides **50** and **51**, detailed variable temperature NMR studies were carried out measuring ^1H and ^{119}Sn NMR.

In this manner the hydrogenation process was monitored over reaction time at different temperatures using $LiAlH_4$, $K(BEt_3H)\cdot THF$ and $BH_3\cdot THF$ as hydrogenation agents.

9.2.1.1 Blanks

In order to get insight into the shift and coupling constant dependency of the temperature the educts were subjected to blank measurements at different temperatures from -60 °C to room temperature. $L^{CN}SnPhCl_2$ (**51**) was dissolved in THF and 0.1 mL of C_6D_6 were added. Table 19 lists the compound's shift as a function of temperature. It can be seen that a decrease of the temperature leads to a highfield shift in the ^{119}Sn NMR.

Table 20: *Temperature dependency of the ^{119}Sn NMR shifts of $L^{CN}SnPhCl_2$ (**50**).*

temperature (°C)	^{119}Sn shift of **50** (THF, C_6D_6) (ppm)
-60	-223.9
-40	-203.1
-20	-189.6
0	-180.3
RT	-173.8

Koten *et al*. carried out in-depth studies on the ^{119}Sn NMR of organotin compounds displaying intramolecular N→Sn coordination. The authors reported that such ligands exhibit a high impact on the ^{119}Sn shift of divalent organotin compounds leading to signals at relatively high frequencies. In contrast, additional coordination in tri- and diorganotin halides causes a large shift to lower frequency of about 100 ppm compared to compounds lacking N→Sn coordination. Furthermore, Koten and coworkers report that the ^{119}Sn chemical shift values of penta coordinated diorganotin dihalides, such as **50** are independent of the temperature between -70 and 100 °C in apolar solvents such as toluene.[333] These findings are in stark contrast to the temperature dependency found for $L^{CN}SnPhCl_2$ (**50**), which shows a shift range of 50 ppm from room temperature to -60 °C. However, Koten also described that the addition of half an equivalent of pyridine to the solutions of $L^{CN}RSnCl_2$ affects the ^{119}Sn shift at temperatures lower than -10 °C if the ratio is 1:1. In this case, two ^{119}Sn resonances were observed. One belongs to the pentacoordinated species (**a**), whereas the second one at 150 ppm highfield shifted is ascribed to the hexacoordinated pyridine adduct (**b**) (Scheme 94). At lower temperatures, the equilibrium completely driven to the side of (**b**).[333]

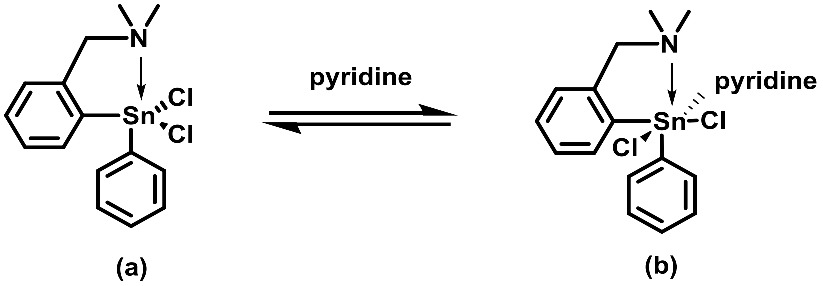

Scheme 94: *Donor induced equilibrium for $L^{CN}RSnCl_2$ between a pentacoordinated species (**a**) and a hexacoordinated pyridine adduct (**b**).*

The pronounced shift deviation in the case of **49** might be explained by the use of THF, having the intrinsic ability to donate electron density to the tin and therefore forming a THF adduct. As THF is a weaker donor compared to pyridine, the presence of both species (**a** and **b** type, Scheme 94) would be expected at a certain temperature. However, just a single one could be observed. In addition, it might also be explained by a stronger N→Sn interaction at lower temperature leading to a higher electron density at the tin atom.

Furthermore, it was detected in ^1H NMR that the $^3J(^1H-^{119/117}Sn)$ coupling constant of the *ortho* proton on the L^{CN} ligand and the tin decreases with higher temperature. This effect could be due to changes in the overall geometry upon cooling. Table 20 summarizes these coupling constants.

Table 21: *Temperature dependency $^3J(H6-^{119/117}Sn)$ of $L^{CN}SnPhCl_2$ (**50**).*

temperature (°C)	$^3J(H_{ortho}-^{119/117}Sn)$ of **50** (Hz)
-60	105
-40	101
-20	97
0	96
RT	n.r.

9.2.1.2 In situ NMR Measurements

The halogenides **50** and **51** were either dissolved in THF/C_6D_6 or THF-*d_8* in a screwable NMR tube with septum. The educt solution was cooled to -80 °C using an ethanol/N_2 (*l.*) bath. Afterwards, the hydrogenation agent solution was added *via* the septum with a syringe and the NMR tube placed in the precooled (-80 °C) NMR spectrometer. ^{1}H and ^{119}Sn NMR measurements were carried out from -80 °C to room temperature.

When a $LiAlH_4$/THF-*d_8* was added to a solution of $L^{CN}SnPhCl_2$ (**50**) in THF-*d_8* at -80 °C an immediate color change to yellow could be observed. It could be detected that the desired product $L^{CN}SnPhH_2$ (**53**) was already formed at the lowest temperature monitored (-80 °C) giving rise to a shift of -246.2 ppm and a triplet in ^{119}Sn NMR (^{1}H coupled) which is comparable to phenyl$_2$SnH_2 (**31**). **31** exhibits a ^{119}Sn chemical shift of -233 ppm in C_6D_6. The ^{1}H NMR showed a chemical shift of 5.99 ppm for the Sn-$\underline{H}_2$, as well as the ^{119}Sn and ^{117}Sn satellites could be detected with a $^{1}J(^{1}H\text{-}^{119}Sn)$ and $^{1}J(^{1}H\text{-}^{117}Sn)$ coupling constant of 2074 and 1983 Hz, respectively. For phenyl$_2$SnH_2 (**31**) the Sn-H_2 is found at 6.11 ppm in C_6D_6 which is comparable with **53**. The $^{1}J(^{1}H\text{-}^{119/117}Sn)$ coupling constants of **31** are 1926 Hz and 1841 Hz.

The main product **53** was found in the presence of a compound with low signal intensity at -166.1 ppm (Figure 102). The formed product showed instability towards temperature and the reaction mixture turned red-brown over time forming an insoluble orange to brown solid, as already reported in the previous chapter.

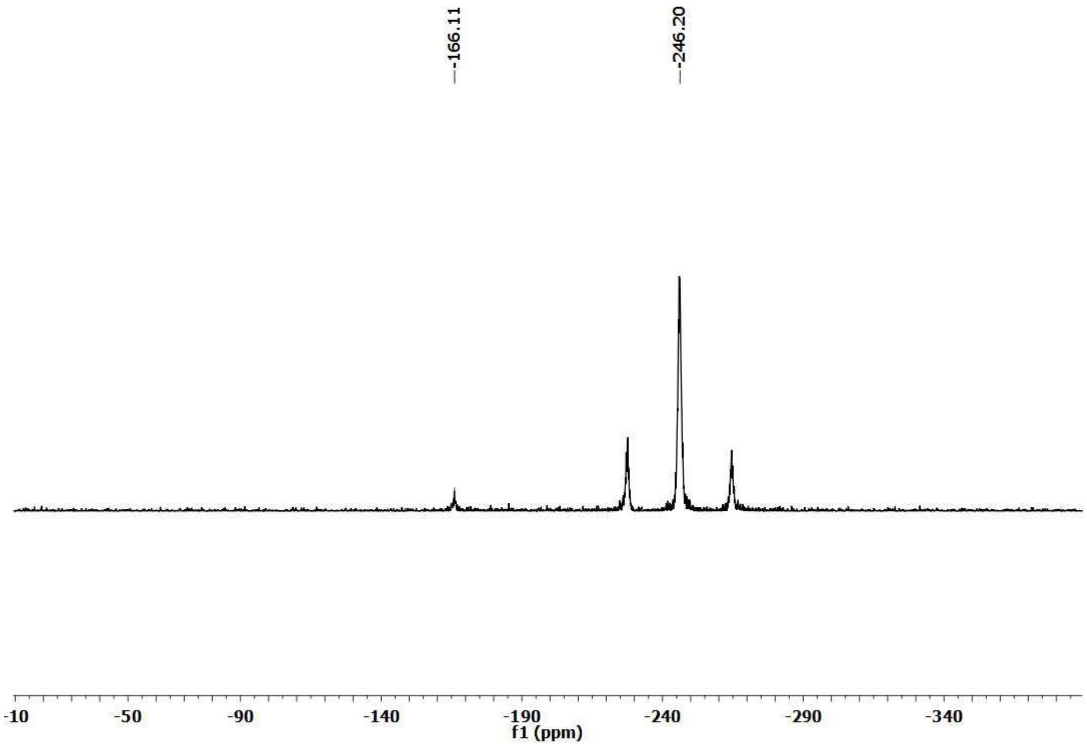

Figure 102: *^{119}Sn NMR (^{1}H coupled) (THF-d_8) of $L^{CN}SnPhH_2$ (**53**) at -80 °C using $LiAlH_4$.*

When trying to convert $L^{CN}SnPhCl_2$ (**50**) and $L^{CN}SnPhH_2$ (**53**) using $K(BEt_3)H\cdot THF$ as a hydrogenation agent in THF/C_6D_6, the reaction mixture immediately turned yellow at -80 °C. It can be shown that the desired product **54** did not form. However, it could be detected that the educt **50** (-196 ppm) reacted at -30 °C forming a product exhibiting a ^{119}Sn shift of -166.5 ppm (Figure 82). This side product was also observed in the formation of $L^{CN}SnPhH_2$ (**53**) using $LiAlH_4$ in deuterated THF. According to the ^{1}H spectrum at -30 °C, the product at -166.5 ppm in the ^{119}Sn NMR did not display a Sn–H functionality (Figure 103).

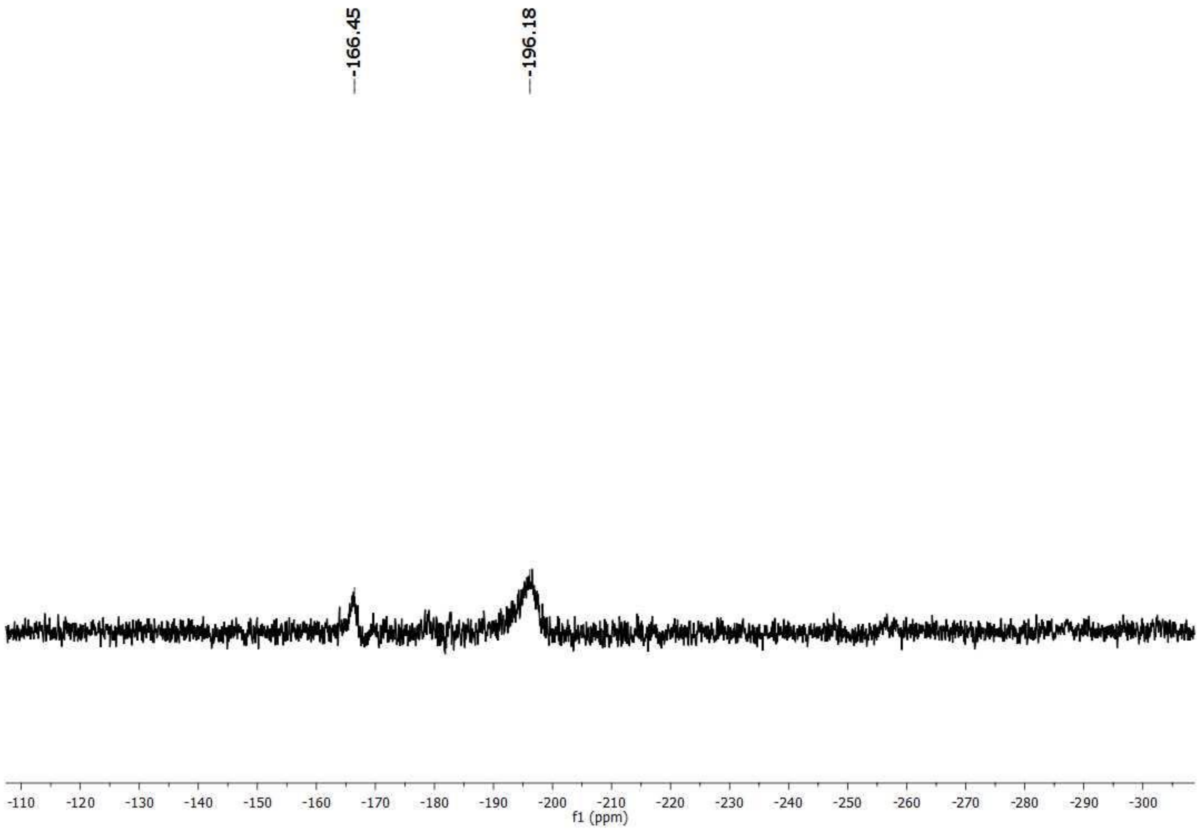

Figure 103: *^{119}Sn NMR (^{1}H coupled) (THF, C_6D_6): Hydrogenation reaction of L^{CN}SnPhCl$_2$ (**50**) using K(BEt$_3$)H·THF in THF at -30 °C.*

Converting L^{CN}SnPhCl$_2$ THF-*d$_8$* (**50**) with an excess of BH_3·THF did not lead to the formation of L^{CN}SnPhH$_2$ (**53**). No color change was observed when adding BH_3·THF *via* the septum at -80 °C. The reaction was monitored by NMR from -80 °C to room temperature. However, no reaction could be observed. Even carrying the reaction mixture at room temperature for up to two days did not lead to any change. L^{CN}SnPhCl$_2$ (**50**) did not react leading to no color change or alteration of the ^{1}H and ^{119}Sn NMR spectra, respectively.

L^{CN}SnBr$_3$ (**51**) was converted with $LiAlH_4$ in THF-*d$_8$* solution as a hydrogenation agent in order to form the desired product L^{CN}SnH$_3$ (**54**) at -80 °C. After addition of the $LiAlH_4$ solution an immediate yellow color change was observed, as already seen for **53**. The formation of **54** was monitored at -80 °C measuring ^{1}H, ^{119}Sn and ^{13}C NMR. No side products were observed. However, upon warming up to room temperature, a black precipitate was formed and the formation of H_2 could be detected, as already reported in the previous chapter, forming **L^{CN}@Sn**. The trihydride **54** was generated successfully at -80 °C and showed a ^{119}Sn NMR shift of -339.5 ppm and a $^{1}J(^{1}H-^{119}Sn)$ and $^{1}J(^{1}H-^{117}Sn)$ of 1877 Hz and 1795 Hz, respectively. The ^{119}Sn (^{1}H coupled) spectrum displayed a quadruplet according to three bonded hydrogens which is comparable to $PhSnH_3$ (**35**) exhibiting a ^{119}Sn chemical shift of -345 ppm in C_6D_6 (Figure 104).

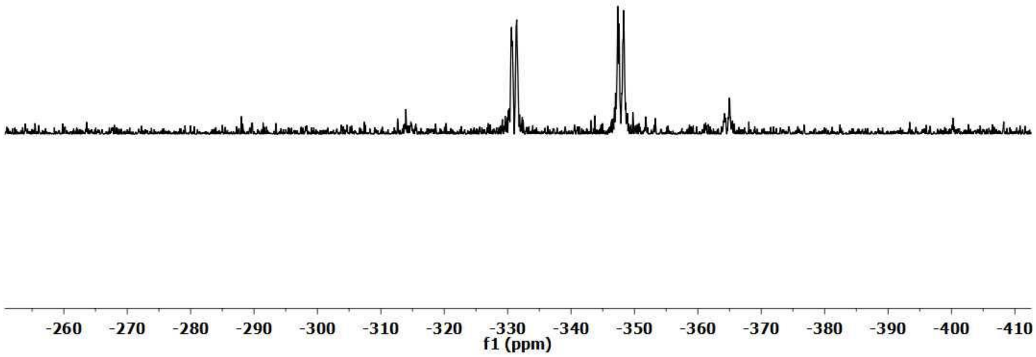

Figure 104: *^{119}Sn NMR (coupled) (THF-d8) of $L^{CN}SnH_3$ (**54**) at -80 °C using $LiAlH_4$.*

The Sn–H functionality gave rise to a shift of 5.10 ppm in ^{1}H NMR which is comparable to the one found for $PhSnH_3$ (**35**) (5.01 ppm). The $^{1}J(^{1}H-^{119/117}Sn)$ coupling constants for $PhSnH_3$ (**35**) (1924, 1688 Hz) are slightly increased in comparison to the L^{CN} containing trihydride **54**. This could be rationalized by a coordination of the L^{CN} moiety to the tin which should weaken and elongate the Sn–H bond, consecutively allowing for hydrogen evolution and Sn–Sn bond formation and thus decrease the size of the $^{1}J(^{1}H-^{119/117}Sn)$ coupling constant. DFT studies show that the coordination of the L^{CN} moiety in $L^{CN}SnH_3$ (**54**) to the tin results in a stabilization of the compound by 19 kJ/mol in comparison to the uncoordinated species. N→Sn coordination leads to elongation of the Sn–H bond across from the N donor (1.752 vs. 1.727 Å). The other two Sn–H bonds are less affected by the electron donation. DFT calculations on the $^{1}J(^{1}H-^{119}Sn)$ coupling constant therefore reveal two different values. The longer Sn–H bond which is more effected by the electron donation shows a $^{1}J(^{1}H-^{119}Sn)$ coupling constant of -1081 Hz, whereas the second one is -1495 Hz. No interaction of the L^{CN} moiety with the Sn leads to a calculated $^{1}J(^{1}H-^{119}Sn)$

coupling constants of -1366 Hz. The values are averaged in Table 22. The sign of the ${}^{1}J({}^{1}H\text{-}{}^{119}Sn)$ coupling constants has not been determined by experiments, however computed values are found to be negative. Therefore experimental and calculated coupling constants are reported as absolute values (Table 22). Calculations support the experimental data for the absolute values of ${}^{1}J({}^{1}H\text{-}{}^{119}Sn)$ coupling constants being increased for $PhSnH_3$ (**35**) (exp:1924 Hz; calcd: 1378 Hz) in comparison to $L^{CN}SnH_3$ (**54**) (exp: 1877 Hz calcd: 1357 Hz) (Table 22).

***Table 22:** Absolute values of ${}^{1}J({}^{1}H\text{-}{}^{119/117}Sn)$ coupling constants for **35** and **54**. Calculated values obtained by DFT calculations are shown in parenthesis.*

	${}^{1}J({}^{1}H\text{-}{}^{119}Sn)$ (Hz)	${}^{1}J({}^{1}H\text{-}{}^{117}Sn)$ (Hz)
$PhSnH_3$ (**35**)	1924 (1378)	1838
$L^{CN}SnH_3$ (**54**)	1877 (1357)	1795
$L^{CN}SnH_3$ (no interaction)	(1366)	-

9.2.2 X-Ray Crystallography

Although Růžička *et al.* reported on the synthesis of $L^{CN}SnBuCl$ (**49**) in 1988 no crystal structure data is available.[331] However, Švec and coworkers described the conversion of **49** with equimolar amounts as well as with excess of hydrochloric acid forming of $L^{CN}SnBuCl\cdot HCl$ and $L^{CN}SnBuCl\cdot 2HCl$, respectively. The authors also reported on the crystal structure of the latter.

$L^{CN}SnBuCl$ (**49**) is successfully recrystallized from pentane at -15 °C forming colorless blocks. Surprisingly, **49** crystallizes in two different space groups concurrently. At one hand it crystallizes in the monoclinic space group $P2_1/n$ and on the other hand in the monoclinic space group C2/c. If **49** crystallizes in the space group $P2_1/n$ significant intermolecular $N(CH)_3\cdots Cl$ interactions of 2.75 Å can be found stabilizing the three dimensional structure (Figure 82), whereas the crystal in C_2/C lacks these interactions. In both cases, coordination between the nitrogen of one of the two L^{CN} units and the Sn can be found, forming a pentacoordinated structure as already reported for a plethora of similar species. This leads to a distorted trigonal bipyramidal conformation where the Sn–C bonds lie in the equatorial plane, whereas the Sn–C and Sn–N bond of the coordinating L^{CN} arm are found in the axial position (Figure 105). Solid state structures of all possible diorganotin dihalides displaying two 2-(dimethylaminomethyl)phenyl residues have been published ($L^{CN}{}_2SnF_2$[342,343], $L^{CN}{}_2SnCl_2$[329,342,356], $L^{CN}{}_2SnBr_2$[357] and $L^{CN}{}_2SnI_2$[329,342]), however in the compound class $L^{CN}{}_2SnRX$ (R= alkyl, aryl; X=

halogen) only L$^{CN}_2$SnPhCl has been reported so far and thus is the only compound comparable to L^{CN}SnBuCl (**49**).[329] Table 23 summarizes selected bond lengths, angles, as well as intra- and intermolecular interactions of **49** and L$^{CN}_2$SnPhCl. In both cases, the structure can be described as a trigonal bipyramid with an average Sn–Cl of 2.52 Å. L$^{CN}_2$SnPhCl does not show a noteworthy deviation to the structure of **49**, however the Sn···N(L^{CN}) interaction found in **49** is 0.25 Å longer than for L$^{CN}_2$SnPhCl.

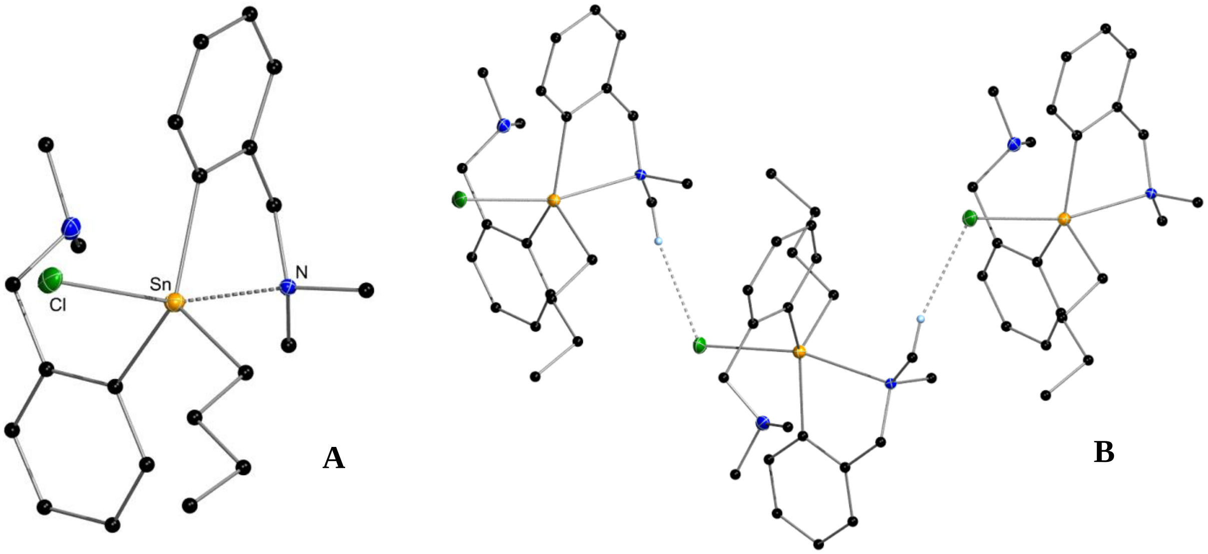

Figure 105: ***A****) Crystal structure of L$^{CN}_2$BuSnCl (**49**).* ***B****) Crystal packing diagram for L$^{CN}_2$BuSnCl (**49**). CH-Cl interactions are highlighted by dashed bonds. All non-carbon atoms shown as 30 % shaded ellipsoids. Hydrogen atoms not involved in intermolecular interactions removed for clarity.*

***Table 23:** Selected bond lengths, angles, intra- and intermolecular interactions of $\mathrm{L^{CN}_2BuSnCl}$ (**49**) and $\mathrm{L^{CN}_2PhSnCl}$.*

	Space Group	**Sn–Cl (Å) (avg.)**	**Sn–C($\mathrm{L^{CN}}$) (Å) (avg.)**	**Sn–C (Å) (avg.)**	**Sn–N (Å) (avg.)**	**Sn···N($\mathrm{L^{CN}}$*) (Å) (avg.)**	**C($\mathrm{L^{CN}}$) –Sn–C($\mathrm{L^{CN}}$*) (°) (avg.)**	**Cl–Sn–N($\mathrm{L^{CN}}$) (°) (avg.)**	**C($\mathrm{L^{CN}}$*)–Sn–C (°) (avg.)**	**C($\mathrm{L^{CN}}$) –Sn–C (°) (avg.)**
$\mathrm{L^{CN}_2BuSnCl}$ (**49**)	$P2_1/n$	2.542(2)	2.141(3)	2.158(2)	2.520(2)	3.52	131.22(4)	166.74(3)	110.80(6)	115.53(6)
$\mathrm{L^{CN}_2PhSnCl}$[329]	$P2_1/c$	2.503(2)	2.145(2)	2.152(2)	2.534(2)	3.27	134.16(8)	168.61(5)	115.27(8)	108.06(8)

	N($\mathrm{CH_3}$)···Cl (Å)	**C($\mathrm{L^{CN}}$) –Sn–Cl (°) (avg.)**	**C($\mathrm{L^{CN}}$*)–Sn–Cl (°) (avg.)**	**C–Sn–Cl (°) (avg.)**	**N($\mathrm{L^{CN}}$) –Sn–C(Bu or Ph) (°) (avg.)**
$\mathrm{L^{CN}_2BuSnCl}$ (**49**)	2.75	93.02	94.34	98.79	91.84
$\mathrm{L^{CN}_2PhSnCl}$[329]	2.965	95.10(8)	95.68(6)	94.58	92.48

$\mathrm{L^{CN}}$*… uncoordinated $\mathrm{L^{CN}}$

9.3 Conclusions

In summary, we were able to successfully report on the conversion of organotin halides exhibiting one or two L^{CN} moieties ($L^{CN}_2SnBuCl$ **49**, $L^{CN}SnPhCl_2$ **50**, $L^{CN}SnBr_3$ **51**) to their corresponding mono-, di- and trihydrides (L^{CN}_2SnBuH **52**, $L^{CN}SnPhH_2$ **53**, $L^{CN}SnH_3$ **54**) as well as on stability studies of the latter. A variety of different hydrogenation agents such as $LiAlH_4$, $K(BEt_3)\cdot THF$ and $BH_3\cdot THF$ and synthetic methods were applied. It could be shown that the hydrogenation agent indeed displays a high influence on the nature of the formed product. In every case, the use of $LiAlH_4$applied in diethyl ether was the hydrogenation agent of choice. It could be shown that with increased number of hydrogens bonded to the tin, the thermal stability decreases dramatically, provoked by the presence of the L^{CN} moieties allowing for strong N→Sn interaction in the molecule. Thus, organotin monohydrides containing two donating L^{CN} residues, as shown for L^{CN}_2SnBuH (**52**) could be generated according to the standard protocol for organotin monohydrides and can be stored at -20 °C without formation of elemental tin, decomposition or dimer formation ($L^{CN}_2BuSn{-}SnBu\ L^{CN}_2$). In contrast, applying the standard synthetic protocol for the hydrogenation of organotin di- and trihalides exhibiting one 2-(dimethylaminomethyl)phenyl moiety (**50**,**51**) the desired di- and trihydride $L^{CN}SnPhH_2$ (**53**) and $L^{CN}SnH_3$ (**54**) were only generated as thermally unstable intermediates forming polystannanes upon Sn–Sn bond formation *via* a dehydrogenative coupling reaction. This reactivity can be rationalized by the internal amine function, donating electron density to the tin and therefore allowing for Sn–H bond weakening, H_2 formation and Sn–Sn bond formation. In the case of $L^{CN}SnPhH_2$ (**52**), an orange colored, insoluble polymer was obtained, comparable to $(phenyl_2Sn)_n$ or (p-^{n}butylphenyl$_2$Sn)$_n$. $L^{CN}SnH_3$ immediately formed an insoluble, black polymer **L^{CN}@Sn** exhibiting a spherical morphology as shown by SEM measurements. This is in accordance to the polymer formed in the dehydrogenative coupling reaction of *o*-tolylSnH_3 and TMEDA, ***o*-tolyl@Sn**.

However, the formation of $L^{CN}PhSnH_2$ (**53**) and $L^{CN}SnH_3$ (**54**) could successfully be carried out and compounds fully characterized *via in situ* ^1H, ^{13}C and ^{119}Sn NMR measurements at variable temperatures. The reaction conditions of choice involve the use of d_8-THF as reaction solvent at -80 °C. The ^{119}Sn chemical shifts found for **53** and **54** are comparable to the ones found for phenyl$_2$SnH$_2$ (**31**) and phenylSnH$_3$ (**35**). $^1J(^1H\text{-}^{119/117}Sn)$ coupling constants are found to be decreased for L^{CN} containing hydrides (**53**, **54**) in comparison to the phenyl derivatives (**31**, **35**), which is reproduced by DFT calculations.

Part C

Summary & Outlook

Experimental Part

References

Appendix

10 Summary & Outlook

In the course of this work a series of novel aryltin halogenides and aryltin hydrides featuring at least one *ortho*-substituent on the phenyl ring, a naphthyl, *p*-^{n}butylphenyl, *p*-biphenyl or 9-anthracenyl group as organic residue were synthesized and fully characterized. Organotin chlorides were generated according to the Kozeshkov equilibrium and subsequently hydrogenated to the corresponding organotin hydride using $LiAlH_4$. In the case of 9-anthracenyl based systems, we could show that the lithiation needs to be carried out fast at low temperature to avoid anthracene or radical anion formation. A big excess of organolithium reagents should be avoided in order to circumvent alkylation of the anthracenyl moiety as well as of the tin generating 9-butylanthracene and tri-9-anthracenyltin butyl, respectively. All solid arylhalogenides and hydrides were characterized *via* X-ray diffraction studies showing interesting stabilizing, non-covalent, intermolecular interactions in the solid state. Three different types of aromatic, non-covalent interactions could be detected including the most prominent edge to face interaction, a parallel displaced stacking, as well as a $C–H\cdots\pi$ interaction of methyl groups to the neighboring ring system. Detailed ^1H, ^{13}C and ^{119}Sn NMR studies, based on experimental data, as well as DFT calculations for these compound classes is provided, which represent a comprehensive work of reference particularly for ^{119}Sn NMR shifts of Sn(IV) halogenides and hydrides.

The synthesized di- and trihydrides were used as educts in the dehydrogenative coupling reaction with the amine base TMEDA. In this work, we show that the formation of polydiphenylstannane $(phenyl_2Sn)_n$ is accompanied by the generation of soluble cyclic side products in the dehydrogenative coupling reaction of $phenyl_2SnH_2$ (**31**) using TMEDA as a catalyst. Depending on the reaction temperature, the generation of a thermodynamically stable six membered, perphenylated tin ring $(phenyl_2Sn)_6$ (**42**), or the seven membered derivative $(phenyl_2Sn)_7$ (**43**) is favored.

However, the use of aryltin trihydrides as potential monomeric building blocks in the generation of novel material, as well as the reaction mechanism of the amine base catalyzed Sn–Sn bond formation has been neglected thus far. Within this work, we propose a reductive dehydropolymerization reaction mechanism based on DFT calculations and *in situ* synchrotron EXAFS/XANES measurements of aryltin trihydrides. The reaction is postulated to proceed *via* a short term Sn(II) intermediate which allows for Sn−Sn bond formation and hydrogen evolution upon insertion. Finally, this conversion forms hitherto unknown aryl decorated nanoparticles (aryl@Sn) containing Sn in oxidation state zero. An autocatalytic reductive dehydropolymerization was observed when *C*,*N*- chelated organotin halides were subjected to a hydrogenation reaction with $LiAlH_4$. The intermediately formed aryltin dihydrides and trihydrides exhibit high thermal lability due to the donating L^{CN} ligand and form (L^{CN}_2Sn) or decorated tin nanoparticles (**L^{CN}@Sn**), respectively.

The shape and size of these nanostructures formed can easily be controlled by the nature of the solvent, which was elucidated by in situ synchrotron SAXS measurements. Ethereal, donating solvents such as diethyl ether lead to spherical nano-substructures in the size range of 1-2 nm, whereas the use of cyclohexane or toluene results in nanorods. Furthermore, size and shape can be altered by the aryl substituent bonded to the tintrihydride. This tool, which can be seen as a “chemical file”, allows for the efficient materials’ fine tuning on a nm scale. Although the nano-substructure formation kinetics strongly differ with respect to the used solvent, *in situ* synchrotron stopped flow EXAFS/XANES measurements showed that the coordination number and local environment in the formed material (***o*-tolyl@Sn**) is not dependent of the nature of the solvent used. The materials formed in diethyl ether, DME, cyclohexane and toluene respectively exhibit a common correlation length of 2.6 Å which can be assigned as the formed Sn−Sn upon dehydrogenative coupling reaction.

Since nanostructured composites of carbon and tin have been proposed as a high capacity substitute for the carbon anode of lithium ion batteries, manufactured composites of tin and carbon on the nanoscale may solve the poor cyclability of the tin electrodes as they provide space to buffer mechanical stress. Therefore, the engineering of Sn-based materials into desired nanoarchitectures represents an efficient principle towards improving their electrochemical performance, including specific capacity, rate capability, and/or cycling stability.

Scheme 95 illustrates the formation of anode material by reacting the aryltin trihydride neat, stirring it with graphite, carbon, NMP and binder (**a**), *in situ* in the presence of the polymerization catalyst TMEDA (**b**), or by utilizing the isolated aryl@Sn which is subsequently mixed with graphite and all other necessary additives (**c**).[358]

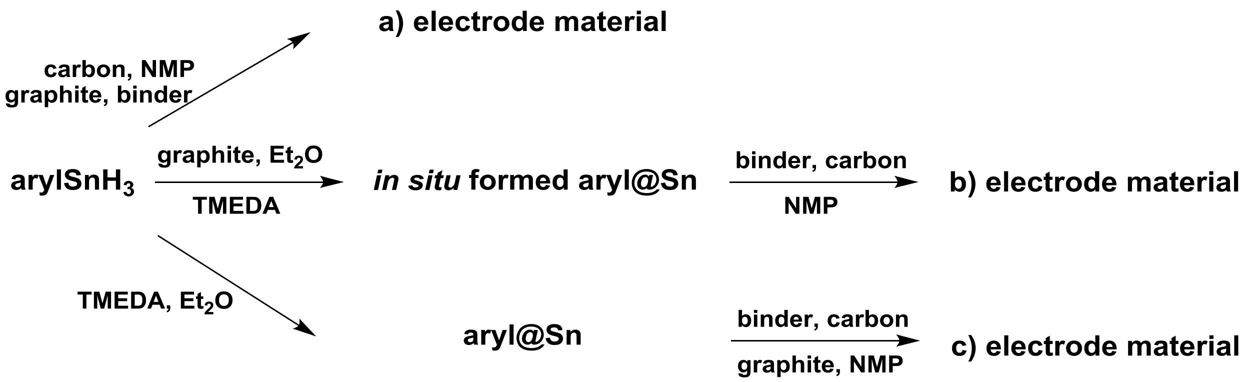
arylSnH$_3$
carbon, NMP
graphite, binder
a) electrode material
graphite, Et$_2$O
TMEDA
in situ formed aryl@Sn
binder, carbon
NMP
b) electrode material
TMEDA, Et$_2$O
aryl@Sn
binder, carbon
graphite, NMP
c) electrode material

***Scheme 95:** Preparation methods of potential anode materials from aryltin trihydrides- **a**) neat trihydride in the presence of graphite **b**) in situ formation of aryl@Sn in the presence of graphite **c**) isolation of aryl@Sn and subsequent addition of graphite.*[358]

Initial electrochemical investigations of the novel materials formed from 1-naphthylSnH$_3$ and mesitylSnH$_3$ have shown electrochemical activity. Cyclovoltammogramms of anode materials prepared from 1-naphthylSnH$_3$ and mesitylSnH$_3$ *via* route a (Scheme 95) illustrate discrete peaks that are not found in the blank measurements (Figure 83). The latter broaden upon cycling however do not vanish. These peaks in the area of 0.2-0.7 V can be assigned as multistep electrochemical reduction reactions of tin with lithium to form discrete Li$_x$Sn alloys upon charging and discharging (Figure 106).[358,359]

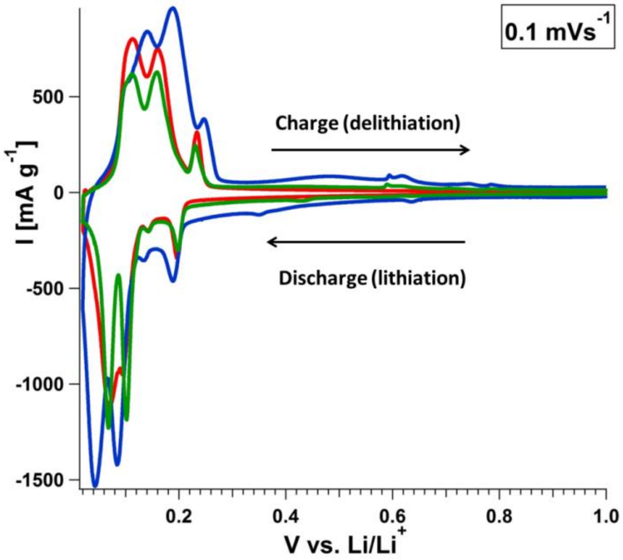

***Figure 106**: Cyclovoltammogramms of anode material synthesized from mesitylSnH$_3$ (blue) and 1-naphthylSnH$_3$ (green) via route **a** in comparison to the blank (red)*

The exact mechanism of the electrochemical reactions or aryl@Sn and arylSnH_3, respectively in graphite electrodes, their long time performance, as well as the influence of morphology on the battery efficiency will be in the focus of future investigations

.

Experimental Part

11 Experimental Part

11.1 Materials and Methods

All reactions, unless otherwise stated, were carried out using standard Schlenk line techniques under nitrogen atmosphere. All dried and deoxygenated solvents were obtained from a solvent drying system (Innovative Technology, Inc.). $SnCl_4$ anhydrous (98 % v/v) was purchased at Alfa Aesar, distilled and stored under nitrogen. C_6D_6 and TMEDA (*N,N,N’,N’*-tetramethylethylenediamine) were distilled over sodium and stored under nitrogen. All other chemicals from commercial sources (arylbromides, Ph_3SnCl and Ph_4Sn) were utilized without further purification. Elemental analysis was performed with an Elementar Vario EL III. Melting point measurements were carried out by threefold determination with a Stuart Scientific SMP 10 (up to 300 °C).

11.2 NMR Spectroscopy

^1H (300.22 MHz), ^{13}C (75.5 MHz) and ^{119}Sn (111.92 MHz) NMR spectra were recorded on a Mercury 300 MHz spectrometer from Varian at 25 °C if not otherwise stated. Chemical shifts are given in parts per million (ppm) relative to TMS (δ= 0 ppm) regarding ^{13}C and ^1H and relative to Me_4Sn in the case of ^{119}Sn. Coupling constants (J) are reported in Hertz (Hz). The letters s, d, t, q and m are used to indicate singlet, doublet, triplet, quadruplet and multiplet. For complete peak assignment, multinuclear NMR experiments were also carried out (H,H-COSY and C,H-HETCOR) as well as shift comparisons to already known and similar compounds in literature were made.[208,360]

11.3 GC-MS Measurements

GC-MS measurements were carried out on an Agilent Technologies 7890A GC system coupled with an Agilent Technologies 5975C VLMSD mass spectrometer using a HP5 column (30 m×0.250mm×0.025 µm) and a carrier helium gas flow of 0.92726 ml/min. A „hot-needle“, manual injection method at an injector temperature of 280 °C was performed. After 2 min at 40

°C the temperature was increased in 12 °C/min steps up to 300 °C and kept at 300 °C for 10 min. The MS conditions included positive EI ionization at an ionization energy of 70 eV and a full scan mode (50-500 m/z).

11.4 Impedance Spectroscopy

The electrical impedance and resistance measurements were performed using a HAMEG HM8118 LCR bridge circuit (frequency range 20 Hz-200 kHz). The sample was prepared in the dry box. It was transferred into a sample holder (polypropylene measurement cell) with polished plane-parallel brass contacts. The data was analyzed using the program Matlab.

11.5 Theoretical Calculations

Density functional calculations were performed using the Gaussian03 software package.[361] For geometry optimizations and analytical frequencies the MPW1PW91[362] functional was applied in basis set combination denoted SDD consisting of a Stuttgart-Dresden relativistic pseudopotential on tin and D95V double-zeta all electron basis sets on the remaining atoms. Magnetic shieldings and nuclear spin-spin coupling constants were obtained with the same functional using Iglo-II basis sets for all atoms.

11.6 Crystal Structure Determination

All crystals suitable for single crystal X-ray diffractometry were removed from a flask and immediately covered with a layer of silicone oil. Due to the low melting point of *o*-tolyl$SnCl_3$ (**21**) the compound was recrystallized neat in the fridge and placed in silicon oil cooled down with dry ice. A single crystal was selected, mounted on a glass rod on a copper pin, and placed in the cold N_2 stream provided by an Oxford Cryosystems cryometer. XRD data collection was performed on a Bruker APEX II diffractometer with use of either a fine-focus sealed tube or an Incoatec microfocus sealed tube with Mo Kα radiation (λ= 0.71073 Å) and a CCD area detector. The determination of compound $Phenyl_2SnH_2$ (**31**) was obtained by crystallization of the sample in a capillary tube while mounted on an Agilent SuperNova diffractometer with use of Mo Kα radiation (λ= 0.71073 Å). Data collection, cell refinement and data reduction were performed with CrysAlisPro.[363] Empirical absorption corrections were applied using SADABS.[364,365] The structures were solved with use of either direct methods or the Patterson option in SHELXS and refined by the full-matrix least-squares procedures in SHELXL.[366,367] The space group assignments and structural solutions were evaluated using PLATON.[368,369] The solvent of crystallization (toluene) for 9-anthracenyl$_3$SnCl (**8**) and 9-anthracenyl$_3$SnMe (**44**) was removed from the refinement by using the "squeeze" option available in the PLATON program suite.[370] Non-hydrogen atoms were refined anisotropically. Hydrogen atoms next to the heavy atom Sn were found on the difference Fourier map, however it should be noted that a common problem exists with locating light atoms (hydrogen) next to heavy atoms because of their poor scattering abilities as seen in 2,6-xylyl$_3$SnH (**30**). All other hydrogen atoms were located in calculated positions corresponding to standard bond lengths and angles. For 1-naphthyl$_4$Sn (**5**), several restraints and constraints (FRAG 17, AFIX 173) were used to afford idealized naphthalene geometry for one of the naphthyl groups. Disorder was handled by modeling the occupancies of the individual orientations using free variables to refine the respective occupancy of the affected fragments. For *p*-^{n}butylphenyl$_4$Sn (**3**), disorder on one of the ^{n}butyl groups was refined using 50/50 split positions. For anthracenyl$_3$SnI (**11**), the solvent of crystallization CHCl$_3$ was refined using 60/40 split positions. Compound 9-anthracenylSnCl$_3$ (**28**) was twinned and is refined using the TWIN option in SHELXL and the matrix (1 0 0 0 1 0 0 0 1) was applied. The main contribution of the twin components refined to a BASF of 0.146. Compound phenyl$_2$SnH$_2$ (**31**) was twinned and is refined using the TWIN option in SHELXL and the matrix (1 0 -1 0 0 0 1 0 0) was applied. The main contribution of the twin components refined to a BASF of 0.157. Intermolecular interactions for presented and published compounds based on a Cambridge Structural Database[371] search were determined by the calculation of centroids and planes feature of the programs Mercury[372] and Diamond[373] and fall within expected ranges.[374]

11.7 Powder Diffraction Studies

The sample was transferred into a quartz glass capillary (OD: 1.5 nm) in the dry box and flame sealed. X-Ray powder diffraction (XRPD) patterns were recorded on a Bruker D8 Advance diffractometer with Bragg Brentano geometry using Cu Kα radiation (9–100° 2ϑ, step size 0.02°

2ϑ, step time 30s/step) and a LYNXEYE detector. Rietveld refinement was carried out with X-PertHighScorePlus (PANalytical) and Topas (Bruker).

11.8 EPR Measurements

EPR spectra were recorded using MiniScope MS300 benchtop X-band EPR spectrometer (Magnettech, Germany) at 77 K up to room temperature. 0.5 mL of 0.08M solution of *o*-tolylSnH_3 (**36**) in degassed Et_2O were transferred in a screwable NMR tube with a septum cap and measured as a blank from -90 °C up to room temperature in 20 °C steps. Subsequently, 2 drops of dried and degassed TMEDA were added *via* the septum and the reaction monitored in situ starting at -90 °C up to room temperature in 10 °C temperature steps.

11.9 SAXS Measurements

Solid powder samples were transferred in the dry box into a sealable (by screw caps) sample holder (Anton Paar, Graz, Austria) where the sample was sandwiched (1 mm) between two vacuum-tight sealing polycarbonate foils (100 µm each). Small-angle (wide-angle) X-ray scattering, S(W)AXS, measurements were carried by a high-flux SAXSess camera (Anton Paar, Graz, Austria) connected to a Debye flex 3003 X-ray generator (GE-Electric, Germany), operating at 40 kV and 50 mA with a sealed-tube Cu anode. The Goebel mirror focused and Kratky slit collimated X-ray beam was line shaped (17 mm horizontal dimension at the sample) and scattered radiation from the sample in the SAXS-range was recorded by a one-dimensional MYTHEN-1k microstrip solid-state detector (Dectris, Switzerland) for 200 s within a *q*-range of 0.1 to 5 nm^{-1} (with *q* being the magnitude of the scattering vector). Additionally, also SWAXS data were recorded separately by a highly X-ray sensitive image plates (Fuji, Japan) within a *q*-range up to 25 nm^{-1}. After each SWAXS measurement with an exposure time of 5 min, the image plates were transferred to a Cyclone Plus image plate reader (Perkin Elmer, USA), laser-scanned and converted digitally into intensity values (*I*). The 2D recorded intensity data were then integrated with a 10 mm width, normal to the direction of the scattering angle, to result in a 1D-scattering curve *I*(*q*) within the angular range mentioned above. Converting the *q*-scale into 2θ

(°), with 2θ being the scattering angle with respect to the incident beam and λ the wavelength of the X-rays, the maximal *q*-value would correspond to an angular rage of 7° (SAXS) and 40° (SWAXS), using CuKα radiation of wavelength 0.154 nm and a sample-to-detector distance of 309 mm (SAXS) and 269 mm (SWAXS), respectively.

11.10 SEM and FESEM Measurements

In the dry box, a small amount of sample was transferred with a spatula onto a SEM sample holder equipped with a carbon tape. SEM pictures were taken with an ESEM TESCAN 500 PA (VEGA 3 control software) with a heated tungsten filament and an OXFORD INSTRUMENTS INCAx-act detector was used for EDX measurements. If the sample needed to be sputtered with Au, a CRESSINGTON 108auto Sputter Coater was used.

FESEM measurements were carried out at the FELMI institute (Graz, Austria). Samples were sputtered with 10 nm chrom and analyzed by a ZEISS Ultra 55 (Gemini) applying excitation energy of 3 keV and a SE-Inlens detector.

11.11 TEM Measurements

A small amount of powder (covering the tip of a spatula) was suspended in 15 mL dried and degassed THF in the dry box. Afterwards the sample was deagglomerated in the dry box using a homogenizer from Sonopuls (70 W) equipped with a micro tip MS 73 (Ø 3 mm) at a working frequency of 20 kHz. One droplet of resulting suspension was transferred onto a holey (Bioloform) carbon coated (5 mm) copper grid. After drying of the solvent the grid was transferred in a double tilt sample holder (Gatan) for Tecnai equipment which allows for sample transfer under inert conditions (Figure 107).

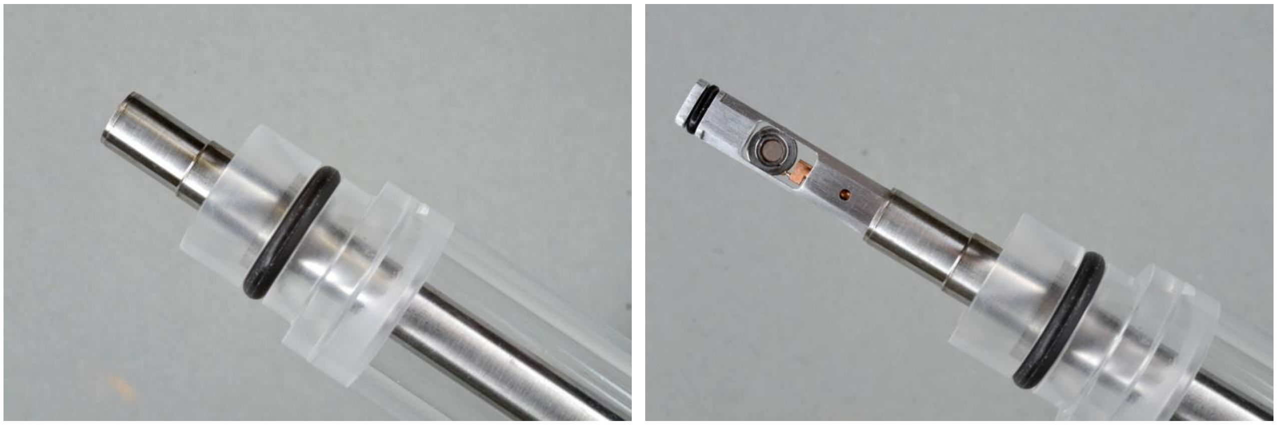

Figure 107: *Double tilt sample holder (Gatan).*

All images were acquired with an FEI Tecnai F20 transmission electron microscope equipped with a field emission gun and operated at 200 kV acceleration voltage. The EDX spectra were recorded with an EDAX Saphire Si(Li) system.

11.12 *In situ* UV-VIS Measurements

A 3.4 mM solution of *o*-tolylSnH$_3$ (**36**) in Et$_2$O was transferred in a quartz glass capillary in the dry box and sealed with a rubber septum. The capillary was placed in the spectrometer and the educt solution measured as a blank. Subsequently, TMEDA was added with a syringe *via* the septum and the resulting opening covered with Teflon grease. Spectra were acquired with an Agilent Cary 60 UV-VIS spectrophotometer, with a scan rate of 600 nm/min and an interval time of 1 min. Base line correction was applied. The resulting data were analyzed using Spekwin 32.

11.13 *In situ* DLS Measurements

Solutions of *o*-tolylSnH$_3$ (**36**) in Et$_2$O (8.9 mg/L) was prepared in the dry box and filtered through a 20 nm pore size syringe filter. Dried and degassed TMEDA was also filtered. Afterwards 0.5 mL of the trihydride solution were transferred into a crimp cap sealed GC vial with septum cap. The trihydride solution was measured as a blank and afterwards two drops of TMEDA were added *via* the septum to *in situ* monitor the reaction progress. The DLS equipment consists of a Helium-Neon-Laser (Spectra Physics λ=632.8nm) with a fixed power of 25mW and a goniometer with single-mode fiber detection optics (OZ from GMP, Zürich, Switzerland). The data were acquired using a Perkin Elmer precisely Photon Counting Module (Perkin Elmer, Voudreuil, Canada) and an ALV 7002/USB Digital Multiple Tau Real Time Correlator (ALV, Langen, Germany). The ALV software package was used to record and store the correlation functions. The light scattering was measured five times 30 s at a scattering angle of 90° and a temperature of 25 °C. The resulting correlation functions were averaged and the hydrodynamic radius calculated by optimized regulation technique software.[375]

11.14 *In situ* Synchrotron Measurements

11.14.1 SAXS

Synchrotron X-ray scattering data was collected at the Austrian SAXS beamline at ELETTRA (Trieste, Italy).[376] The measurements were carried out at a wavelength of 0.154 nm (8 keV). In all set-ups all detectors have been calibrated with silver behenate in order to calibrate the q-scale (θ-scale). The scattering vector q is given by:

$$q = \frac{4\pi(sin\theta)}{\lambda}$$

where 2θ is the scattering angle and λ is the wavelength.

11.14.1.1 Capillary Set-Up

Data were recorded with two detectors depending on the required time resolution for following the reactions. For slow reactions (toluene and cyclohexane) an image-plate detector with online read out was used (Mar300, MarResearch, Norderstedt, Germany) with a sample-detector distance of 790.655 mm. For the fast reactions (diethyl ether, DME) a Pilatus detector (PILATUS 100 K, DECTRIS Ltd., Villigen PSI, Switzerland) with a sample-detector distance of 764.636 mm was used.

A quartz glass capillary (OD: 1.5 mm, wall thickness: 0.01 mm) was filled with a 0.08 M solution of *o*-tolylSnH_3 (**36**) in the respective solvent (diethyl ether, DME, cyclohexane, toluene) and afterwards sealed with a rubber septum in the dry box. Subsequently, the capillary was placed on the sample stage and measured as a blank ("static"). Afterwards, 20 µl of degassed and dried TMEDA were added *via* the septum and the measurement started to follow the *in situ* formation and aggregation of nanoparticles. Data analysis was performed using Fit2D[377] and Igor Pro (Version 6.37, WaveMetrics Inc., USA). Experimental intensities were normalized to sample transmission and corrected for background. Custom made procedures were used to analyze the data in particular for the full pattern refinement.

11.14.1.2 Stopped Flow Set-Up

The liquid flow equipment was purchased from IDEX Health & Science and delivered from the local distributor VWR. All fittings used were flat-bottom fittings with a ¼-28'' thread made out of PEEK. Tubing connection that needed to be twisted upon change of sample or sample cell cleaning were equipped with super flangeless fittings containing ferrules, swadged lock ring and the nut. The others were connected using flangeless fittings set together by ferrule and nut. PFA tubing with $^{1}/_{16}$ OD and 1 mm ID was used. The pressure was realized by the use of Harvard PHD 4400 Hpsi syringe pumps which were connected to the ¼-28'' fittings by a custom made adapter piece (Anton Paar, Graz, Austria). The pressure was controlled and maintained by a back pressure regulator assembly realizing a constant pressure of 75 psi. For the measuring cell a quartz glass capillary (OD 1.5 mm) was glued into a custom made capillary holder (Anton Paar, Graz) using solvent resistant glue (Araldite, 2014-1). The capillary holder was connected to the ¼-28'' fittings by a custom made stainless steel adaptor piece. The solvent waste was collected in NALGENE bottles fixed with waste caps and a vapor trap (Western Analytical Products). The liquid flow system was connected to stainless steel syringe (Harvard) by a custom made adapter piece (Anton Paar, Graz, Austria) made out of PEEK, which connected the ⅜-28'' thread (female) of the syringe to the ¼-28'' thread (male) of the setup. Steel to fitting and plastic adaptor connections were covered with Teflon tape to avoid leaking at high pressures. The system was filled using three syringe pumps (Harvard PHD 4400 Hpsi) for the trihydride, TMEDA and solvent feed, respectively. The portable part of the set-up was affixed onto to a custom made metal grid using wire.

11.14.2 EXAFS/XANES

On part of the X-ray absorption at the Sn K edge (29200.1 eV) was collected at the beamline BM26A (DUBBLE) of the ESRF-The European Synchrotron in Grenoble, France mainly in the XANES regime operating under beam conditions of 6 GeV, 400 mA using a monochromator with both Si(111) and Si(311) crystal pairs.

The other part of the X-ray absorption spectra at the Sn K edge (29200.1 eV) were collected on beamline BM18 at the Diamond Lightsource Innovation campus operating under beam conditions of 3 GeV, 300 mA using a collimating mirror, a water-cooled double crystal monochromator and a focusing mirror. Background subtraction, spectra alignment and normalization as well as forward and backward Fourier Transformation of the EXAFS data were performed with ATHENA.[287]

11.14.2.1 Stopped Flow Set-Up

The liquid flow equipment was purchased from IDEX Health & Science and delivered from the local distributor VWR. All fittings used were flat-bottom fittings with a ¼-28’’ thread made out of PEEK. Tubing connection that needed to be twisted upon change of sample or sample cell cleaning were equipped with super flangeless fittings containing ferrule, swadged lock ring and the nut. The others were connected using flangeless fittings set together by ferrule and nut. PFA tubing with $^{1}/_{16}$ OD and 1 mm ID was used. The pressure was realized by the use of Harvard PHD 4400 Hpsi syringe pumps which were connected to the ¼-28’’ fittings by a custom made adapter piece (Anton Paar, Graz, Austria). The pressure was controlled and maintained by a back pressure regulator assembly realizing a constant pressure of 75 psi. For the measuring cell, a 5 cm long piece of high purity PFA tubing (OD: ¼’’; ID: 4.8 mm) was on both sides furnished with a large bore fitting (½-20’’ thread). These fittings could then by connected to the standard ¼-28’’ thread (used in the whole system) by applying an adaptor assembly (½-20’’ female to ¼-28’’ female). The solvent waste was collected in NALGENE bottles fixed with waste caps and a vapor trap (Western Analytical Products). The liquid flow system was connected to stainless steel syringe (Harvard) by a custom made adapter piece (Anton Paar, Graz, Austria) made out of PEEK, which connected the $^3/_8$-28'' thread (female) of the syringe to the ¼-28'' thread (male) of the setup. Steel to fitting and plastic adaptor connections were covered with Teflon tape to avoid leaking at high pressures. The system was filled using three syringe pumps (Harvard PHD 4400 Hpsi) for the trihydride, TMEDA and solvent feed, respectively. The portable part of the set-up was affixed onto to a custom made metal grid using wire.

11.14.3 General Procedure for Stopped Flow Experiments

0.08 M solutions of *o*-tolylSnH_3 and TMEDA in dried and degassed solvent was prepared in the dry box and transferred in the respective stainless steel syringe by using a glass pipette. Subsequently, the syringes were connected to the stopped flow system by the adaptor piece (Anton Paar, Graz, Austria). All valves were closed to avoid any contamination of the two reactant feeds. After inert filling of the syringes, the stopped flow equipment was affixed onto the metal grid and transferred into the hutch, where it was connected to the solvent feed, waste bottles, as well as the sample cell by screwing the threads into the respective shut off valves. The whole system was filled with solvent until it was filled bubble free (2 mL/min). Subsequently, the three way valve was opened to back pressure in order to perform a leak test. The filled cell was used to measure a solvent blank. Afterwards, the pressure was released and the system filled with trihydride solution until the solvent was pushed through completely. The system was set under back pressure to ensure leak tightness at the syringe/set-up connections. A trihydride blank measurement was carried out. Then, the trihydride solution was removed by flushing the system carefully with solvent. Next, the circuit was filled with TMEDA-solvent solution until back pressure is reached. This was followed by a solvent washing step to remove the base. Afterwards, simultaneous injection of trihydride and TMEDA solution was started with a 2 mL/min. When the cell was filled with reactants the flow rate was reduced to 1 mL/min and the three way valve opened to back pressure. As soon the back pressure had been reached (dropping), the cell was shut off by closing the shut-off valves. This was followed by shutting all other valves and finally stopping the pump. The interlock was set as quickly as possible and the reaction monitored *in* *situ*. When the reaction was finished, the pressure was released and subsequently the system was flushed with solvent. Insoluble polymer was dissolved by using diluted HCl which was injected manually by detaching the sample cell from the feed circuit. The latter was shut off in order to avoid air contamination. After cleaning the sample cell, it was washed with distilled H_2O, isopropanol and afterwards with the respective reaction solvent. The cleanness of the cell was confirmed by running a scan. The washing step was repeated if necessary. If the cell was clean, the feed circuit could be attached and the system washed with reaction solvent to prepare for a next *in situ* measurement. For changing the feed, the metal grid was removed from the sample stage, syringes were disconnected and washed with acetone and isopropanol. The circuit was flushed with isopropanol, diluted HCl and afterwards isopropanol again. Before transferring the pieces in the dry box, the equipment as well as the syringes was dried using compressed air.

11.15 Synthesis

11.15.1 List of Compounds

Table 24: *Summary of all compounds presented.*

	Compound	no.
	$SnCl_4$	**1**
Ar_4Sn	phenyl$_4$Sn	**2**
	p-^{n}butylphenyl$_4$Sn[63]	**3**
	p-biphenyl$_4$Sn[80]	**4**
	1-naphthyl$_4$Sn[63,80]	**5**
	2- naphthyl$_4$Sn[63,80]	**6**
Ar_3SnCl	phenyl$_3$SnCl	**7**
	9-anthracenyl$_3$SnCl*	**8**
Ar_3SnBr	2,6-xylyl$_3$SnBr[63]	**9**
	mesityl$_3$SnBr	**10**
Ar_3SnI	9-anthracenyl$_3$SnI	**11**
Ar_2SnCl_2	phenyl$_2$SnCl$_2$	**12**
	p-^{n}butylphenyl$_2$SnCl$_2$	**13**
	p-biphenyl$_2$SnCl$_2$[80]	**14**
	1-naphthyl$_2$SnCl$_2$[80]	**15**
	2-naphthyl$_2$SnCl$_2$ [80]	**16**
	9-anthracenyl$_2$SnCl$_2$*	**17**
Ar_2SnBr_2	mesityl$_2$SnBr$_2$	**18**
Ar_2SnI_2	9-anthracenyl$_2$SnI$_2$*	**19**
$ArSnCl_3$	phenylSnCl$_3$	**20**
	o-tolylSnCl$_3$ [63,80]	**21**
	2,4-xylylSnCl$_3$[80]	**22**
	2,6-xylylSnCl$_3$ [80]	**23**
	mesitylSnCl$_3$*	**24**
	p-^{n}butylphenylSnCl$_3$[63]	**25**
	1-naphthylSnCl$_3$ [63,80]	**26**
	2-naphthylSnCl$_3$[63]	**27**
	9-anthracenylSnCl$_3$*	**28**
Ar_3SnH	phenyl$_3$SnH [131]	**29**
	2,6-xylyl$_3$SnH[63]	**30**
Ar_2SnH_2	phenyl$_2$SnH$_2$*	**31**
	1-naphthyl$_2$SnH$_2$[80]	**32**
	2-naphthyl$_2$SnH$_2$ [80]	**33**
	p-biphenyl$_2$SnH$_2$[80]	**34**
$ArSnH_3$	phenylSnH$_3$	**35**
	o-tolylSnH$_3$ [80]	**36**
	p-^{n}butylphenylSnH$_3$[63]	**37**
	2,4-xylylSnH$_3$[80]	**38**
	2,6-xylylSnH$_3$[80]	**39**
	mesitylSnH$_3$*	**40**
	1-naphthylSnH$_3$ [80]	**41**
Perphenylated rings	(phenyl$_2$Sn)$_6$	**42**
	(phenyl$_2$Sn)$_7$*	**43**
Anthracene containing educt and side products	9-iodoanthracene	**44**
	9-anthracenyl$_3$SnMe	**45**
	9-anthracenylLi(TMEDA)·LiBr(TMEDA)	**46**
	anthraquinone derivative	**47**
	9-anthracenyl$_3$SnBu	**48**
L^{CN} Sn halogenides	$L^{CN}{}_2SnBuCl$	**49**
	$L^{CN}SnPhCl_2$	**50**
	$L^{CN}SnBr_3$	**51**
L^{CN} Sn hydrides	$L^{CN}{}_2SnBuH$	**52**
	$L^{CN}SnPhH_2$	**53**
	$L^{CN}SnH_3$	**54**
$H_2[(aryl)Sn–Sn(aryl)]H_2$	H$_2$[(*o*-tolyl)Sn–Sn(*o*-tolyl)]H$_2$ *	**55**

* unpublished results

11.15.2 Published Compounds

The following compounds were either purchased or synthesized according to published procedures and only ^{1}H, ^{13}C and ^{119}Sn NMR are provided. [11,12,81,84,102,184]

SnCl$_4$ 1: ^{119}Sn NMR (C$_6$D$_6$, 112 MHz): δ -148.6 ppm.

Phenyl$_4$Sn 2: ^{1}H NMR (C$_6$D$_6$, 300 MHz): δ 7.64-7.58 (m, 20H, ^{3}J(H2-^{119}Sn)= 48.8 Hz, ^{3}J(H2-^{117}Sn)= 46.6 Hz, ^{4}J(H3-$^{119/117}$Sn)= 14.5 Hz, H2, H3, H4) ppm. ^{13}C NMR (C$_6$D$_6$, 75.5 MHz): δ 138.3 (^{1}J(^{13}C-^{119}Sn)= 530 Hz, ^{1}J(^{13}C-^{117}Sn)= 506 Hz, C1), 137.7 (^{2}J(^{13}C-$^{119/117}$Sn)= 37.0 Hz, C2), 129.4 (^{4}J(^{13}C-$^{119/117}$Sn)= 11.1 Hz, C4), 129.0 (^{3}J(^{13}C-^{119}Sn)= 50.7 Hz, ^{3}J(^{13}C-^{117}Sn)= 48.4 Hz, C3) ppm. ^{119}Sn NMR (C$_6$D$_6$, 112 MHz): δ -126.5 ppm.

Phenyl$_3$SnCl 7: ^{1}H NMR (C$_6$D$_6$, 300 MHz): δ 7.59-7.52 (m, 6H, H2), 7.13-7.08 (m, 9H, ^{4}J(H3-$^{119/117}$Sn)= 12.6 Hz, H3,H4) ppm. ^{13}C NMR (C$_6$D$_6$, 75.5 MHz): δ 137.6 (^{1}J(^{13}C-^{119}Sn)= 614 Hz, ^{1}J(^{13}C-^{117}Sn)= 586 Hz, C1), 136.5 (^{2}J(^{13}C-^{119}Sn)= 50.7 Hz, ^{2}J(^{13}C-^{117}Sn)= 48.4 Hz, C2), 130.6 (^{4}J(^{13}C-$^{119/117}$Sn)= 13.0 Hz, C4), 129.4 (^{3}J(^{13}C-^{119}Sn)= 64.5 Hz, ^{3}J(^{13}C-^{117}Sn)= 62.1 Hz, C3) ppm. ^{119}Sn NMR (C$_6$D$_6$, 112 MHz): δ -44.4 ppm.

Mesityl$_3$SnBr 10: ^{1}H NMR (C$_6$D$_6$, 300 MHz): δ 6.71 (s, 2H, ^{4}J(H3,5-$^{119/117}$Sn)= 24.6 Hz, H3), 2.51 (s, 6H, H6), 2.06 (s, 3H, H5) ppm. ^{119}Sn NMR (C$_6$D$_6$, 112 MHz): δ -121.9 ppm.

Phenyl$_2$SnCl$_2$ 12: ^{1}H NMR (C$_6$D$_6$, 300 MHz): δ 7.40 (m, 4H, H2), 7.07-6.91 (m, 6H, H3, H4) ppm. ^{13}C NMR (C$_6$D$_6$, 75.5 MHz): δ 137.1 (^{1}J(^{13}C-^{119}Sn)=785 Hz, ^{1}J(^{13}C-^{117}Sn)=750 Hz, C1), 135.2 (^{2}J(^{13}C-^{119}Sn)= 64.7 Hz, ^{2}J(^{13}C-^{117}Sn)= 61.8 Hz, C2), 131.7 (^{4}J(^{13}C-$^{119/117}$Sn)= 17.5, C4), 129.8 (^{3}J(^{13}C-^{119}Sn)= 86.3 Hz, ^{3}J(^{13}C-^{117}Sn)= 82.5 Hz, C3) ppm. ^{119}Sn NMR (C$_6$D$_6$, 112 MHz): δ -26.4 ppm.

***p*-^{n}Butylphenyl$_2$SnCl$_2$ 13**: ^{1}H NMR (C$_6$D$_6$, 300 MHz): 7.45 (d, 2H, ^{3}J(H2-H3)=7.70 Hz, ^{3}J(H2-$^{119/117}$Sn)=79.83 Hz, H2), 6.99 (d, 2H, ^{3}J(H3-H2)=7.70 Hz, ^{3}J(H3-$^{119/117}$Sn)=27.85 Hz, H3), 2,41-2.29 (2H, t, H5), 1.41-1.32 (2H, dd, H6), 1.27-1.11 (2H, dd, H7), 0.89-0.78 (3H, t, H8).^{13}C NMR (C$_6$D$_6$, 75.5 MHz): δ 147.09 (^{4}J(^{13}C-$^{119/117}$Sn)=16.97 Hz, C4), 135.28 (^{2}J(^{13}C-$^{119/117}$Sn)=65.8, C2), 134.03 (^{1}J(^{13}C-^{119}Sn)=793.45, ^{1}J(^{13}C-^{117}Sn)=758.23 Hz, C1), 130.06 (^{3}J(^{13}C-$^{119/117}$Sn)=86.36 Hz, C3), 35.88 (C5), 33.59 (C6), 22.56 (C7), 14.11 (C8).^{119}Sn NMR (C_6D_6, 112 MHz): δ -19.9 ppm

Mesityl$_2$Br$_2$ 18: ^{1}H NMR (C_6D_6, 300 MHz): δ 6.56 (s, 2H, ^{4}J(H3,5-$^{119/117}$Sn)= 36.7 Hz, H3), 2.51 (s, 6H, H6), 1.98 (s, 3H, H5) ppm. ^{119}Sn NMR (C_6D_6, 112 MHz): δ -148.9 ppm.

PhenylSnCl$_3$ 20: ^{1}H NMR (C_6D_6, 300 MHz): δ 6.99- 6.91 (m, 3H, H2, H4), 6.88-6.81 (m, 2H, H3) ppm. ^{13}C NMR (C_6D_6, 75.5 MHz): δ 135.8 (^{1}J(^{13}C-^{119}Sn)= 1120 Hz, ^{1}J(^{13}C-^{117}Sn)= 1069 Hz, C1), 133.9 (^{2}J(^{13}C-^{119}Sn)= 78.8 Hz, ^{2}J(^{13}C-^{117}Sn)= 75.3 Hz, C2), 132.8 (^{4}J(^{13}C-$^{119/117}$Sn)= 25.9 Hz, C4), 130.2 (^{3}J(^{13}C-^{119}Sn)= 126 Hz, ^{3}J(^{13}C-^{117}Sn)= 121 Hz, C3) ppm. ^{119}Sn NMR (C_6D_6, 112 MHz): δ -61.0 ppm.

MesitylSnCl$_2$Br: ^{1}H NMR (C_6D_6, 300 MHz): 6.70 (s, 2H, H3), 2.28 (s, 6H, H5), 1.88 (s, 3H, H6).^{13}C NMR (C_6D_6, 75.5 MHz): δ 143.41 (^{2}J(^{13}C-^{119}Sn)=78.73 Hz, ^{2}J(^{13}C-^{117}Sn)=75.78 Hz, C2), 143.13 (C4), 135.46 (C1), 130.20 (^{3}J(^{13}C-^{119}Sn)=122.64 Hz, ^{3}J(^{13}C-^{117}Sn)=116.82 Hz, C3), 24.62 (C6), 21.34 (C5). ^{119}Sn NMR (C_6D_6, 112 MHz): δ -149.2 ppm

Phenyl$_3$SnH 29: ^{1}H NMR (C_6D_6, 300 MHz): δ 7.54-7.48 (m, 6H, H2), 7.15-7.11 (m, 9H, H3, H4), 6.91 (s, 1H, ^{1}J(^{1}H-^{119}Sn)= 1934 Hz, ^{1}J(^{1}H-^{117}Sn)= 1848 Hz, Sn-H) ppm. ^{13}C NMR (C_6D_6, 75.5 MHz): δ 137.7 (^{2}J(^{13}C-^{119}Sn)= 41.4 Hz, ^{2}J(^{13}C-^{117}Sn)= 39.2 Hz, C2), 137.3 (^{1}J(^{13}C-^{119}Sn)= 534 Hz, ^{1}J(^{13}C-^{117}Sn)= 511 Hz, C1), 129.3 (^{4}J(^{13}C-$^{119/117}$Sn)= 11.4 Hz, C4), 129.0 (^{3}J(^{13}C-^{119}Sn)= 53.0 Hz, ^{3}J(^{13}C-^{117}Sn)= 50.7 Hz, C3) ppm. ^{119}Sn NMR (C_6D_6, 112 MHz): δ -162.8 (^{1}J(^{119}Sn-^{1}H)=1932 Hz) ppm.

Phenyl$_2$SnH$_2$ 31: ^{1}H NMR (C_6D_6, 300 MHz): δ 7.46-7.38 (m, 4H, H2), 7.17-7.07 (m, 6H, H3, H4), 6.11 (s, 2H, ^{1}J(^{1}H-^{119}Sn)= 1926 Hz, ^{1}J(^{1}H-^{117}Sn)= 1841 Hz, SnH_2) ppm. ^{13}C NMR (C_6D_6, 75.5 MHz): δ 137.8 (^{2}J(^{13}C-^{119}Sn)= 41.3 Hz, ^{2}J(^{13}C-^{117}Sn)= 39.7 Hz, C2), 135.5 (^{1}J(^{13}C-^{119}Sn)= 544 Hz, ^{1}J(^{13}C-^{117}Sn)= 520 Hz, C1), 129.2 (^{4}J(^{13}C-$^{119/117}$Sn)= 11.9 Hz, C4), 128.9 (^{3}J(^{13}C-^{119}Sn)= 54.4 Hz, ^{3}J(^{13}C-^{117}Sn)= 52.0 Hz, C3) ppm. ^{119}Sn NMR (C_6D_6, 112 MHz): δ -233.7 (^{1}J(^{119}Sn-^{1}H)=1939 Hz) ppm.

PhenylSnH$_3$ 35: ^{1}H NMR (C_6D_6, 300 MHz): δ 7.34-7.25 (d, 2H, ^{3}J(^{1}H-$^{117/119}$Sn)= 57.3 Hz, H2), 7.13-7.03 (m, 3H, H3, H4), 5.01 (s, 3H, ^{1}J(^{1}H-^{119}Sn)= 1924 Hz, ^{1}J(^{1}H-^{117}Sn)= 1838 Hz, ^{1}J(^{1}H-

^{115}Sn)= 1688 Hz, Sn$\underline{H_3}$) ppm. ^{13}C NMR (C_6D_6, 75.5 MHz): δ 138.1 ($^{2}J(^{13}C\text{-}^{119}Sn)$= 44.3 Hz, $^{2}J(^{13}C\text{-}^{117}Sn)$= 41.1 Hz, C2), 132.7 ($^{1}J(^{13}C\text{-}^{119}Sn)$= 562 Hz, $^{1}J(^{13}C\text{-}^{117}Sn)$= 532 Hz, C1), 129.1 ($^{4}J(^{13}C\text{-}^{119}Sn)$= 14.1 Hz, $^{4}J(^{13}C\text{-}^{117}Sn)$= 12.2 Hz, C4), 128.8 ($^{3}J(^{13}C\text{-}^{119}Sn)$= 57.8 Hz, $^{3}J(^{13}C\text{-}^{117}Sn)$= 53.7 Hz, C3) ppm. ^{119}Sn NMR: δ -344.9 ($^{1}J(^{119}Sn\text{-}^{1}H)$= 1924 Hz) ppm.

11.15.3 Chapter 2 & 4

11.15.3.1 General Procedure for Ar_4Sn (3-6) and 2,6-xylyl$_3$SnBr (9)

A flask equipped with a dropping funnel and a reflux condenser was charged with Mg in THF. The dropping funnel was charged with arylbromide in THF. 1 ml dibromoethane was added and the solution was heated to start the reaction. The arylbromide was subsequently added slowly. After complete addition, the reaction was refluxed for 2 h. A second flask equipped with a mechanical stirrer and a reflux condenser was charged with 1 eq. $SnCl_4$ in THF cooled with an ice bath. The Grignard solution was then transferred *via* a cannula to the $SnCl_4$ solution whilst hot in order to avoid precipitation of the Grignard reagent. The solution was refluxed for 2 h and stirred overnight at room temperature. Two possible work-up procedures were carried out. In one case (**a**), the solution was filtered through celite and the solvent evaporated under reduced pressure. To the resulting residue, water was added and then extracted with dichloromethane. The organic phase was dried over Na_2SO_4, filtered and the solvent evaporated under reduced pressure. The product was suspended in Et_2O, filtered and washed with Et_2O and subsequently with pentane. The product was then dried in an oven at 110 °C overnight. Alternatively (**b**), H_2O was added and subsequently all of the solvent was removed under reduced pressure. The resulting residue was extracted with a soxhlet apparatus for 4 h with pentane and for another 4 h with chloroform. The pentane solution was discharged. The chloroform in the second fraction was evaporated under reduced pressure. The product was then dried in an oven at 110 °C overnight.

***p*-^{n}Butylphenyl$_4$Sn 3**: 14.3 g (0.59 mol, 5 eq.) Mg in 270 ml THF, 100 g (0.47 mol, 4 eq.) p-^{n}butylphenylbromide in 30 ml THF, 13.7 ml (0.12 mmol, 1 eq.) $SnCl_4$ in 300 ml of THF, work-up procedure (**b**): 10 ml of H_2O to quench, refluxed in 800 ml of pentane, washed with 50 ml pentane. The resulting solid was recrystallized from ^{n}BuOH in the fridge to obtain colorless crystals. Yield: 65 % (53.9 g, 83 mmol). M.p.: 42 °C. Anal. Calcd. For $C_{40}H_{52}Sn$: C, 73.74; H, 8.04. Found: C, 75.25; H, 8.04. ^{1}H NMR (C_6D_6, 300 MHz): δ 7.73 (d, 8H, ^{3}J(H2-H3)= 7.80 Hz, $^{3}J(^{1}\text{H}-^{119}\text{Sn})$= 48.1 Hz, $^{3}J(^{1}\text{H}-^{117}\text{Sn})$= 45.7 Hz, H2), 7.12 (d, 8H, ^{3}J(H3-H2)= 7.7 Hz, $^{4}J(^{1}\text{H}-^{119/117}\text{Sn})$= 13.9 Hz, H3), 2.52-2.40 (t, 8H, H5), 1.55-1.41 (dd, 8H, H6), 1.30-1.14 (dd, 8H, H7), 0.88-0.77 (t, 12H, H8) ppm. ^{13}C NMR (C_6D_6, 75.5 MHz): δ 143.9 ($^{4}J(^{13}\text{C}-^{119/117}\text{Sn})$= 11.5 Hz, C4), 137.8 ($^{2}J(^{13}\text{C}-^{119}\text{Sn})$= 39.2 Hz, $^{2}J(^{13}\text{C}-^{117}\text{Sn})$= 36.9 Hz, C2), 135.4 ($^{1}J(^{13}\text{C}-^{119}\text{Sn})$= 535 Hz, $^{1}J(^{13}\text{C}-^{117}\text{Sn})$= 511 Hz, C1), 129.3 ($^{3}J(^{13}\text{C}-^{119}\text{Sn})$= 53.0 Hz, $^{3}J(^{13}\text{C}-^{117}\text{Sn})$= 50.7 Hz, C3), 36.0 (C5), 33.9 (C6), 22.6 (C7), 14.1 (C8) ppm. ^{119}Sn NMR (C_6D_6, 112 MHz): δ -121.5 ppm.

***p*-Biphenyl$_4$Sn 4**: 6.3 g (260 mmol, 5.5 eq.) Mg in 150 ml THF, 50.9 g (220 mmol, 4.7 eq.) 4-bromobiphenyl in 150 ml THF, 5.5 ml (47 mmol, 1 eq.) $SnCl_4$ in 500 ml THF, work-up procedure (**a**): 6 ml of H_2O. For analysis a small amount was recrystallized from chloroform to obtain a colorless solid. Yield: 99 % (34 g, 46.4 mmol). M.p., 262-264 °C. Anal. Calcd. For $C_{48}H_{36}Sn$: C, 78.81; H, 4.96. Found: C, 79.03; H, 5.01. ^{1}H NMR ($CDCl_3$, 300 MHz): δ 7.80 (d, 8H, ^{3}J(H2-H3)= 7.4 Hz, $^{3}J(\text{H2}-^{119/117}\text{Sn})$= 47.4 Hz, H2), 7.75-7.62 (m, 16H, H3, H6), 7.53-7.45 (dd, 8H, H7), 7.43-7.35 (m, 4H, H8) ppm. ^{13}C NMR ($CDCl_3$, 75.5 MHz): δ 142.1 (C1), 141.0 (C4), 137.6 ($^{2}J(^{13}\text{C}-^{119/117}\text{Sn})$= 38.3 Hz, C2), 136.6 (C5), 128.8 (C7), 127.5 (C8), 127.4 ($^{3}J(^{13}\text{C}-^{119}\text{Sn})$= 53.0, $^{3}J(^{13}\text{C}-^{117}\text{Sn})$= 50.7 Hz, C3), 127.2 (C6) ppm. ^{119}Sn NMR ($CDCl_3$, 112 MHz): δ -124.5 ppm.

1-Naphthyl$_4$Sn 5: 17.0 g (700 mmol, 7 eq.) Mg in 700 ml THF, 83.4 ml (600 mmol, 6 eq.) 1-bromonaphthaline in 150 ml THF, 11.7 ml (100 mmol, 1 eq.) $SnCl_4$ in 1000 ml THF, work-up procedure (**a**): 1000 ml H_2O, 250 ml Et_2O, 250 ml Et_2O, 250 ml pentane. For analysis a small amount was recrystallized from ethyl acetate to obtain colorless crystals. Yield: 72 % (45.2 g, 72.0 mmol). M.p., 230-232 °C. Anal. Calcd. For $C_{20}H_{14}Sn$: C, 76.58; H, 4.50. Found: C, 75.36; H, 4.40. ^{1}H NMR (C_6D_6, 300 MHz): δ 8.33 (d, 4H, ^{3}J(H4-H3)= 8.3 Hz, H4), 8.12 (d, 4H, ^{3}J(H2-H3)= 6.6 Hz, H2), 7.62 (d, 4H, ^{3}J(H8-H7)= 8.2 Hz, H8), 7.54 (d, 4H, ^{3}J(H5-H6)= 8.1 Hz, H5), 7.12-7.00 (m, 8H, H6, H7), 6.83 (dd, 2H, H3) ppm. ^{13}C NMR (C_6D_6, 75.5 MHz): δ 140.7 ($^{1}J(^{13}\text{C}-^{119}\text{Sn})$= 520 Hz, $^{1}J(^{13}\text{C}-^{117}\text{Sn})$= 497 Hz, C1), 139.4 ($^{2}J(^{13}\text{C}-^{119}\text{Sn})$= 34.7 Hz, $^{2}J(^{13}\text{C}-^{117}\text{Sn})$= 33.8 Hz, C8a), 137.6 ($^{2}J(^{13}\text{C}-^{119/117}\text{Sn})$= 38.1 Hz, C2), 134.5 ($^{3}J(^{13}\text{C}-^{119}\text{Sn})$= 37.6 Hz, $^{3}J(^{13}\text{C}-^{117}\text{Sn})$= 36.4 Hz, C4a), 130.6 ($^{4}J(^{13}\text{C}-^{119/117}\text{Sn})$= 32.2 Hz, C4), 130.3 ($^{3}J(^{13}\text{C}-^{119/117}\text{Sn})$= 11.7 Hz, C8), 129.3 ($^{3}J(^{13}\text{C}-^{119/117}\text{Sn})$= 43.8 Hz, C3), 126.4 (C7), 126.1 (C6) ppm. ^{119}Sn NMR (C_6D_6, 112 MHz): δ -118.8 ppm.

2-Naphthyl$_4$Sn 6: 3.2 g (131 mmol, 4.5 eq.) Mg in 250 ml THF, 25.9 g (125 mmol, 4.3 eq.) 2-bromonaphthaline in 50 ml THF, 3.4 ml (29.1 mmol, 1 eq.) $SnCl_4$ in 500 ml of THF, work-up procedure (**a**): 250 ml H_2O, 500 ml of dichloromethane, 100 ml Et_2O, 100 ml of Et_2O, 100 ml pentane. For analysis a small amount was recrystallized from ethyl acetate to obtain colorless crystals. Yield: 56 % (10.2 g, 16.2 mmol). M.p., 199-200 °C. Anal. Calcd. For $C_{20}H_{14}Sn$: C, 76.58; H, 4.50. Found: C, 76.64; H, 4.46. ^{1}H NMR (C_6D_6, 300 MHz): δ 8.14 (s, 4H, ^{3}J(H1-$^{119/117}$Sn)= 55.2 Hz, H1), 7.92 (d, 4H, ^{3}J(H3-H4)= 8.2 Hz, ^{3}J(H3-$^{119/117}$Sn)= 40.7 Hz, H3), 7.75 (d, 4H, ^{3}J(H4-H3)= 8.2 Hz, ^{4}J(H4-$^{119/117}$Sn)= 12.8 Hz, H4), 7.63 (d, 4H, ^{3}J(H8-H7)= 7.8 Hz, H8), 7.45 (d, 4H, ^{3}J(H5-H6)= 7.7 Hz, H5), 7.28-7.16 (m, 8H, H6, H7) ppm. ^{13}C NMR (C_6D_6, 75.5 MHz): δ 138.7 (^{2}J(^{13}C-^{119}Sn= 36.9 Hz, ^{2}J(^{13}C-^{117}Sn= 35.4 Hz, C1), (^{1}J(^{13}C-^{119}Sn= 529 Hz, ^{1}J(^{13}C-^{117}Sn= 505 Hz, C2), 134.5 (^{4}J(^{13}C-$^{119/117}$Sn= 9.9 Hz, C4a), 134.3 (^{3}J(^{13}C-^{119}Sn= 57.8 Hz, ^{3}J(^{13}C-^{117}Sn= 55.3 Hz, C8a), 133.7 (^{2}J(^{13}C-^{119}Sn= 40.3 Hz, ^{2}J(^{13}C-^{117}Sn= 38.7 Hz, C3), 128.6 (^{3}J(^{13}C-^{119}Sn= 50.6 Hz, ^{3}J(^{13}C-^{117}Sn= 48.3 Hz, C4), 128.3 (^{5}J(^{13}C-$^{119/117}$Sn= 4.6 Hz, C5), 128.2 (C8), 126.8 (C6), 126.4 (^{5}J(^{13}C-$^{119/117}$Sn= 4.3 Hz, C7) ppm. ^{119}Sn NMR (C_6D_6, 112 MHz): δ -117.6 ppm.

2,6-Xylyl$_3$SnBr 9: 7.59 g (0.25 mol, 7.8 eq.) Mg in 300 ml THF, 46.3 g (0.25 mol, 6.3 eq.) 2,6-xylylbromide in 60 ml THF, 4.9 ml (0.04 mol, 1 eq.) $SnCl_4$ in 100 ml of THF, work-up procedure I 1 L of pentane. The resulting solid was recrystallized from pentane to obtain colorless crystals. Yield: 90 % (16.9 g, 36 mmol). M.p.: 175 °C. Anal. Calcd. For $C_{24}H_{27}BrSn$: C, 56.07; H, 5.29. Found: C, 54.67; H, 5.48. ^{1}H NMR (C_6D_6, 300 MHz): δ 7.03-6.96 (t, 3H, H4), 6.85 (d, 6H, ^{3}J(H3-H4)= 7.47 Hz, ^{4}J(^{1}H-$^{119/117}$Sn)= 32.8 Hz, H3), 2.45 (s, 18H, ^{3}J(^{1}H-$^{119/117}$Sn)= 6.50 Hz, $\mathrm{C\underline{H}_3}$) ppm. ^{13}C NMR ($C_6D_6$, 75.5 MHz): δ 145.0 ($^{1}J$(^{13}C-^{119}Sn)= 571 Hz, ^{1}J(^{13}C-^{117}Sn)= 546 Hz, C1), 144.5 (^{2}J(^{13}C-^{119}Sn)= 43.9 Hz, ^{2}J(^{13}C-^{117}Sn)= 42.0 Hz, C2), 130.1 (^{3}J(^{13}C-^{119}Sn)= 52.7 Hz, ^{3}J(^{13}C-^{117}Sn)= 50.5 Hz, C3), 26.0 (^{3}J(^{13}C-^{119}Sn)= 41.8 Hz, ^{3}J(^{13}C-^{117}Sn)= 40.1 Hz, $\mathrm{\underline{C}H_3}$) ppm. ^{119}Sn NMR ($C_6D_6$, 112 MHz): δ -131.6 ppm.

11.15.3.2 General Procedure for Ar_2SnCl_2 (14-16)

Two possible routes (**A**,**B**) were applied to synthesize all diaryltin dichlorides followed by the same work-up procedure.

Route (**A**): A Schlenk tube was charged with tetraarylstannane. Subsequently, $SnCl_4$ was added and the flask heated up to 180 °C for 2 h in an oil bath. Afterwards, the reaction mixture was suspended in dichloromethane, filtered through celite and the solvent evaporated under reduced pressure. The crude product was suspended in pentane and filtered again. The filter residue was dried in *vacuo*.

Route (**B**): A Schlenk tube was charged with tetraarylstannane. Subsequently, $SnCl_4$ is added and the flask heated up to 200 °C with an oil bath for 2 h. The excess $SnCl_4$ was removed under *vacuo* at room temperature. Afterwards, the reaction mixture was suspended in dichloromethane, filtered through celite and the solvent evaporated under reduced pressure. The residue was charged in a Schlenk tube and tetraarylstannane is added. The mixture was heated up to 200 °C for 2 h. The reaction mixture was the suspended in dichloromethane, filtered through celite and the solvent evaporated under reduced pressure. The crude product was suspended in pentane and filtered again. The resulting powder was then dried in *vacuo*.

***p*-Biphenyl$_2$SnCl$_2$ 14**: Route (**A**): 8.0 g (11 mmol, 1 eq.) tetra-*p*-biphenyltin (**4**), 1.3 ml (11 mmol, 1 eq.) $SnCl_4$. For analysis a small amount was recrystallized from toluene as colorless blocks. Yield: 70 % (7.6 g, 15 mmol). M.p., 142-143 °C. Anal. Calcd. For $C_{24}H_{18}Cl_2Sn$: C, 58.11; H, 3.66. Found: C, 58.33; H, 3.61. ^{1}H NMR (C_6D_6, 300 MHz): δ 7.50 (d, 4H, ^{3}J(H2-H3)= 8.2 Hz, ^{3}J(H2-^{119}Sn= 81.2 Hz, ^{3}J(H2-^{117}Sn= 77.2 Hz), H2), 7.35 (d, 4H, ^{3}J(H3-H2)= 8.2 Hz, H3), 7.37-7.31 (m, 4H, H6), 7.22-7.13 (m, 4H, H7), 7.13-7.11 (m, 2H, H8) ppm. ^{13}C NMR (C_6D_6, 75.5 MHz): δ 144.9 (^{4}J(^{13}C-$^{119/117}$Sn= 17.9 Hz, C4), 140.3 (^{5}J(^{13}C-$^{119/117}$Sn= 7.67 Hz, C5), 135.7 (^{1}J(^{13}C-^{119}Sn= 795 Hz, ^{1}J(^{13}C-^{117}Sn= 760 Hz, C1), 135.7 (^{2}J(^{13}C-^{119}Sn= 67.1 Hz, ^{2}J(^{13}C-^{117}Sn= 64.9 Hz, C2), 129.2 (C7), 128.5 (^{3}J(^{13}C-^{119}Sn= 88.8 Hz, ^{3}J(^{13}C-^{117}Sn= 84.8 Hz, C3), 128.3 (C8), 127.5 (C6) ppm. ^{119}Sn NMR (C_6D_6, 112 MHz): δ -22.0 ppm.

1-Naphthyl$_2$SnCl$_2$ 15: Route (**B**): 3.9 g (6.2 mmol, 1 eq.) tetra-1-naphthyltin (**5**), 2.5 ml (3.4 eq., 21 mmol) SnCl$_4$, 2.5 g (0.5 eq., 4.0 mmol) tetra-1-naphthyltin (**5**). For analysis a small amount was recrystallized from ethyl acetate as colorless blocks. Yield: 2.8 g (17 % based on 6.2 mmol tetra-1-naphthyltin **5**). M.p., 139-141 °C. Anal. Calcd. For $C_{20}H_{14}Cl_2Sn$: C, 54.11; H, 3.18. Found: C, 53.30; H, 3.18. ^{1}H NMR (C_6D_6, 300 MHz): δ 8.12 (d, 2H, ^3J(H8-H7)= 8.1 Hz, H8), 8.00 (d, 2H, ^3J(H2-H3)= 7.0 Hz, ^3J(H2-^{119}Sn)= 50.4 Hz, H2), 7.54 (2H, d, ^3J(H4-H3)= 8.2 Hz, H4), 7.47 (d, 2H, ^3J(H5-H6)= 8.2 Hz, H5), 7.13-7.02 (m, 4H, H3, H6), 7.01-6.93 (dd, 2H, H7) ppm. ^{13}C NMR (C_6D_6, 75.5 MHz): δ 138.0 (^1J(^{13}C-^{119}Sn)= 772 Hz, ^1J(^{13}C-^{117}Sn)= 736 Hz, C1), 136.7 (^2J(^{13}C-^{119}Sn)= 67.1 Hz, ^2J(^{13}C-^{117}Sn)= 64.1 Hz, C8a), 135.76 (^2J(^{13}C-^{119}Sn)= 54.4 Hz, ^2J(^{13}C-^{117}Sn)= 52.1 Hz, C2), 134.8 (^3J(^{13}C-^{119}Sn= 66.2 Hz, ^3J(^{13}C-^{117}Sn)= 63.4 Hz, C4a), 132.4 (^4J(^{13}C-$^{119/117}$Sn)= 13.2 Hz, C4), 129.4 (^4J(^{13}C-$^{119/117}$Sn)= 13.8 Hz, C5), 128.4 (^3J(^{13}C-^{119}Sn)= 52.4 Hz, ^3J(^{13}C-^{117}Sn)= 50.7 Hz, C8), 128.0 (^4J(^{13}C-$^{119/117}$Sn)= 24.4 Hz, C7), 126.9 (C6), 126.1 (^3J(^{13}C-^{119}Sn)= 95.6 Hz, ^3J(^{13}C-^{117}Sn)= 91.5 Hz, C3) ppm. ^{119}Sn NMR (C_6D_6, 112 MHz): δ -9.0 ppm.

2-Naphthyl$_2$SnCl$_2$ 16: Route (**A**): 3.0 g (4.8 mmol, 1 eq.) tetra-2-naphthyltin (**6**), 0.55 ml (4.8 mmol, 1 eq.) SnCl$_4$. For analysis a small amount was recrystallized from ethyl acetate as colorless blocks. Yield: 50 % (2.1 g, 4.7 mmol). M.p., 112-113 °C. Anal. Calcd. For $C_{20}H_{14}Cl_2Sn$: C, 54.11; H, 3.18. Found: C, 53.66; H, 3.10. ^{1}H NMR (C_6D_6, 300 MHz): δ 8.09 (s, 2H, ^3J(H1-$^{119/117}$Sn= 94.3 Hz, H1), 7.55-7.51 (d, 4H, H3, H4), 7.49 (d, 2H, ^3J(H5-H6)= 7.7 Hz, H5), 7.40 (d, 2H, ^3J(H8-H7)= 7.7 Hz, H8), 7.27-7.13 (m, 2H, H6, H7) ppm. ^{13}C NMR (C_6D_6, 75.5 MHz): δ 137.0 (^2J(^{13}C-^{119}Sn= 64.1 Hz, ^2J(^{13}C-^{117}Sn= 61.4 Hz, C1), 135.0 (^4J(^{13}C-^{119}Sn= 16.2 Hz, ^4J(^{13}C-^{117}Sn= 15.5 Hz, C4a), 134.5 (^1J(^{13}C-^{119}Sn= 788 Hz, ^1J(^{13}C-^{117}Sn= 753 Hz, C2), 133.8 (^3J(^{13}C-^{119}Sn= 96.8 Hz, ^3J(^{13}C-^{117}Sn= 92.6 Hz, C8a), 130.0 (^3J(^{13}C-^{119}Sn= 67.5 Hz, ^3J(^{13}C-^{117}Sn= 64.6 Hz, C3), 129.6 (^3J(^{13}C-^{119}Sn= 84.3 Hz, ^3J(^{13}C-^{117}Sn= 80.7 Hz, C4), 128.7 (^5J(^{13}C-$^{119/117}$Sn= 3.1 Hz, C5), 128.1 (^4J(^{13}C-$^{119/117}$Sn= 6.8 Hz, C8), 128.0 (^6J(^{13}C-$^{119/117}$Sn= 3.7 Hz, C6), 127.0 (^5J(^{13}C-^{119}Sn= 7.4 Hz, ^5J(^{13}C-^{117}Sn= 7.0 Hz, C7) ppm. ^{119}Sn NMR (C_6D_6, 112 MHz): δ -23.9 ppm.

11.15.3.3 General Procedure for $ArSnCl_3$ (21-27)

Different ratios of Ar_4Sn, Ar_3SnX and Ar_2SnX_2 or pure Ar_3SnBr were combined with an excess of $SnCl_4$ in a Schlenk flask furnished with a reflux condenser. The mixture was heated up to 150-190 °C using an oil bath and stirred for 2 h to obtain complete conversion. The excess $SnCl_4$ was removed under reduced pressure to obtain a dark brown liquid. Subsequently, the mixture was subjected to fractional distillation under reduced pressure to afford pure product.

***o*-TolylSnCl$_3$ 21**: 48.14 g of a mixture of tetra-*o*-tolyltin and triaryltinbromide (1:4), 22.8 ml $SnCl_4$ (50.67 g, 1.3 mol, 6.2 eq. calculated for tetra-*o*-tolylstannane), 150 °C, Yield: 7 % (12.19 g, 38 mmol referring to 2-bromotoluene). Anal. Calcd. For $C_7H_7Cl_3Sn$: C, 26.59; H, 2.23. Found: C, 26.12; H, 2.13.^{1}H NMR (C_6D_6, 300 MHz): δ 7.21 (d, 1H, ^{3}J(H6-H5)= 8.5 Hz, ^{4}J (H6-$^{119/117}$Sn)= 64.6 Hz, H6), 7.06-6.97 (dd, 1H, H4), 6.91-6.82 (dd, 1H, H5), 6.81-6.76 (d, 1H, H3), 2.18 (s, 3H, ^{4}J(H7-$^{119/117}$Sn)= 13.7 Hz, H6) ppm. ^{13}C NMR (C_6D_6, 75.5 MHz): δ 142.9 (^{2}J(^{13}C-^{119}Sn)= 75.2 Hz, ^{2}J(^{13}C-^{117}Sn)= 72.0 Hz, C2), 136.7 (^{1}J(^{13}C-^{119}Sn)= 1085 Hz, ^{1}J(^{13}C-^{117}Sn)= 1036 Hz, C1), 134.4 (^{2}J(^{13}C-^{119}Sn)= 77.8 Hz, ^{2}J(^{13}C-^{117}Sn)= 74.4 Hz, C6), 133.3 (^{4}J(^{13}C-$^{119/117}$Sn)= 23.9 Hz, C4), 131.6 (^{3}J(^{13}C-^{119}Sn)= 119 Hz, ^{3}J(^{13}C-^{117}Sn)= 114 Hz, C3), 127.2 (^{3}J(^{13}C-^{119}Sn)= 128 Hz, ^{3}J(^{13}C-^{117}Sn)= 122 Hz, C5), 24.3 (^{3}J(^{13}C-^{119}Sn)= 55.3 Hz, ^{3}J(^{13}C-^{117}Sn)= 53.4 Hz, C7) ppm. ^{119}Sn NMR (C_6D_6, 112 MHz): δ -60.7 ppm.

2,4-XylylSnCl$_3$ 22: 22.55 g of a mixture of tetra-2,4-xylyltin, tri-2,4-xylyltinchloride and di-2,4-xylyltindichloride (1:22:2), 16.85 ml $SnCl_4$ (37.52 g, 0.14 mol, 3.4 eq. calculated for 2,4-xylyl$_3$SnCl), 170 °C, Yield: 18 % (30.24 g, 91 mmol, related to 4-bromo-*m*-xylol). Anal. Calcd. For $C_8H_9Cl_3Sn$: C, 29.10; H, 2.75. Found: C, 28.3; H, 2.64. ^{1}H NMR (C_6D_6, 300 MHz): δ 7.17-7.12 (d, 1H, ^{3}J(H6-H5)= 7.8 Hz, ^{3}J(H6-^{119}Sn)= 131 Hz, ^{3}J(H6-^{117}Sn)= 114 Hz, H6), 6.68 (d, 1H, ^{3}J(H5-H6)= 7.8 Hz, H5), 6.60 (s, 1H, H3), 2.17 (s, 3H, ^{4}J(H7-$^{119/117}$Sn= 13.5 Hz, H7), 1.96 (^{5}J(H8-$^{119/117}$Sn= 7.6 Hz, H8) ppm. ^{13}C NMR (C_6D_6, 75.5 MHz): δ 144.0 (^{4}J(^{13}C-$^{119/117}$Sn)= 24.2 Hz, C4), 142.8 (^{2}J(^{13}C-^{119}Sn)= 79.4 Hz, ^{2}J(^{13}C-^{117}Sn)= 75.9 Hz, C2), 134.2 (^{2}J(^{13}C-^{119}Sn)= 82.2 Hz, ^{2}J(^{13}C-^{117}Sn)= 78.5 Hz, C6), 133.4 (^{1}J(^{13}C-^{119}Sn)= 1098 Hz, ^{1}J(^{13}C-^{117}Sn)= 1049 Hz, C1), 132.5 (^{3}J(^{13}C-^{119}Sn)= 124 Hz, ^{3}J(^{13}C-^{117}Sn)= 118 Hz, C3), 128.0 (^{3}J(^{13}C-^{119}Sn)= 132 Hz, ^{3}J(^{13}C-^{117}Sn)= 126 Hz, C5), 24.2 (^{3}J(^{13}C-^{119}Sn)= 54.8 Hz, ^{3}J(^{13}C-^{117}Sn)= 52.4 Hz, C7), 21.4 (^{5}J(^{13}C-$^{119/117}$Sn)= 14.3 Hz, C8) ppm. ^{119}Sn NMR (C_6D_6, 112 MHz): δ -56.5 ppm.

2,6-XylylSnCl$_3$ 23: 9.28 g tri-2,6-xylyltin bromide (**9**) (18 mmol, 1 eq.), 7.05 ml SnCl$_4$ (15.69 g, 60 mmol, 3.4 eq.), 190 °C. The resulting solid was recrystallized from pentane to afford colorless crystals. Yield: 44 % (10.53 g, 0.03 mol). M.p., 56-59 °C. Anal. Calcd. For $C_8H_9Cl_3Sn$: C, 29.10; H, 2.75. Found: C, 29.45; H, 2.66. ^{1}H NMR (C_6D_6, 300 MHz): δ 6.85-6.76 (t, 1H, H4), 6.57-6.51 (d, 2H, ^4J(H3-H4)= 7.4 Hz, ^4J(H3-$^{119/117}$Sn)= 32.4 Hz, H3), 2.21 (s, 6H, ^4J(H5-$^{119/117}$Sn)= 14 Hz, H5) ppm. ^{13}C NMR (C_6D_6, 75.5 MHz): δ 138.5 (^1J(^{13}C-^{119}Sn)= 1064 Hz, ^1J(^{13}C-^{117}Sn)= 1016 Hz, C1), 143.6 (^2J(^{13}C-^{119}Sn)= 75.5 Hz, ^2J(^{13}C-^{117}Sn)= 72.6 Hz, C2), 132.9 (^4J(^{13}C-$^{119/117}$Sn)= 23.4 Hz, C4), 129.3 (^3J(^{13}C-^{119}Sn)= 121Hz, ^3J(^{13}C-^{117}Sn)= 116 Hz, C3), 24.9 (^3J(^{13}C-^{119}Sn)= 57.5 Hz, ^3J(^{13}C-^{117}Sn)= 54.9 Hz, C5) ppm. ^{119}Sn NMR (C_6D_6, 112 MHz): δ -90.5 ppm.

MesitylSnCl$_3$ 24: 20 g of a mixture of mesityl$_2$SnBr$_2$, mesityl$_3$SnBr and mesityl$_2$SnClBr (73:11:16), 9.12 mL SnCl$_4$ (20.29 g, 77.9 mmol), 160 °C. The resulting solid was recrystallized from pentane to afford colorless crystals Yield: 64 % (49.6 mmol). ^{1}H NMR (C_6D_6, 300 MHz): 6.37 (s, 2H, ^4J(^{1}H-$^{119/117}$Sn)=61.5 Hz, H3), 2.23 (s, 6H, ^4J(^{1}H-$^{119/117}$Sn)=50.5 Hz, H5), 1.88 (s, 3H, H6).^{13}C NMR (C_6D_6, 75.5 MHz): δ 143.49 (^2J(^{13}C-^{119}Sn)=79.83 Hz, ^2J(^{13}C-^{117}Sn)=76.70 Hz, C2), 143.27 (C4), 135.17 (^1J(^{13}C-^{119}Sn)=1075.6 Hz, ^1J(^{13}C-^{117}Sn)=1029.5 Hz), C1), 130.11 (^3J(^{13}C-^{119}Sn)=126.58 Hz, ^3J(^{13}C-^{117}Sn)=121.0 Hz, C3), 24.65 (^3J(^{13}C-^{119}Sn)=56.25 Hz, ^3J(^{13}C-^{117}Sn)=54.13 Hz, C6), 20.90 (^5J(^{13}C-$^{119/117}$Sn)=15.08 Hz, C5). ^{119}Sn NMR (C_6D_6, 112 MHz): δ -84.9ppm

***p*-^{n}ButylphenylSnCl$_3$ 25:** 2.0 g tetra-*p*-^{n}butyltin (**3**) (3.1 mmol, 1 eq.), 1.07 ml SnCl$_4$ (2.4 g, 9.2 mmol, 3 eq.), 150 °C, work-up procedure (**a**) Yield: 87 % ^{1}H NMR (C_6D_6, 300 MHz): δ 6.99 (d, 2H, ^3J(H3-H2)= 7.9 Hz, H3), 6.75 (d, 2H, ^3J(H2-H3)= 7.8 Hz, ^3J(H2-$^{119/117}$Sn)=48.5 Hz, H2), 2.21 (t, 2H, H5), 1.37-1.21 (dd, 2H, H6), 1.20-1.04 (dd, 2H, H7), 0.81 (t, 3H, H8) ppm. ^{13}C NMR (C_6D_6, 75.5 MHz): δ 148.6 (^4J(^{13}C-^{119}Sn)=28.8 Hz, ^4J(^{13}C-^{117}Sn)=25.4 Hz, C4), 133.9 (^2J(^{13}C-^{119}Sn)=82.2 Hz, ^2J(^{13}C-^{117}Sn)=80.0 Hz, C2), 132.8 (^1J(^{13}C-^{119}Sn)=1137 Hz, ^1J(^{13}C-^{117}Sn)=1083 Hz, C1), 130.5 (^3J(^{13}C-^{119}Sn)=130.2 Hz, ^3J(^{13}C-^{117}Sn)=124.8 Hz, C3), 35.7 (^5J(^{13}C-$^{119/117}$Sn)=12.4 Hz, C5), 33.4 (^6J(^{13}C-$^{119/117}$Sn= 5.8 Hz, C6), 22.5 (C7), 14.0 (C8) ppm. ^{119}Sn NMR (C_6D_6, 112 MHz): δ –58.2 ppm.

1-NaphthylSnCl$_3$ 26: 3.00 g of tetra-1-naphthyltin (**5**) (4.78 mmol, 1 eq.) were combined with 1.67 ml SnCl$_4$ (3.73 g, 14.3 mmol, 3 eq.). Black solid was taken up in 50 ml CH$_2$Cl$_2$. The suspension was filtered through celite and the solvent is evaporated under reduced pressure. The obtained colorless solid was recrystallized from toluene to afford **26** as colorless crystals. Yield: 51 % (3.43 g, 9.73 mmol). M.p., 71-73 °C. Anal. Calcd. For $C_{10}H_7Cl_3Sn$: C, 34.10; H, 2.00. Found: C, 33.99; H, 1.87. ^{1}H NMR (C_6D_6, 300 MHz): δ 7.97-7.89 (dd, 1H, H6), 7.50-7.30 (m, 3H, H2, H4, H5), 7.12-7.03 (m, 2H, H7, H8), 6.91-6.83 (m, 1H, H3) ppm. ^{13}C NMR (C_6D_6, 75.5 MHz): δ 136.1 (^{1}J(^{13}C-^{119}Sn= 1098 Hz, ^{1}J(^{13}C-^{117}Sn= 1050 Hz, C1), 135.1 (^{2}J(^{13}C-^{119}Sn= 85.5 Hz, ^{2}J(^{13}C-^{117}Sn= 81.7 Hz, C8a), 134.8 (^{3}J(^{13}C-^{119}Sn= 103 Hz, ^{3}J(^{13}C-^{117}Sn= 98.3 Hz, C4a), 134.7 (^{2}J(^{13}C-$^{119/117}$Sn= 63.4 Hz, C2), 133.3 (^{4}J(^{13}C-$^{119/117}$Sn= 27.5 Hz, C4), 129.4 (^{4}J(^{13}C-$^{119/117}$Sn= 20.7 Hz, C5), 128.7 (^{4}J(^{13}C-$^{119/117}$Sn= 6.9 Hz, C7), 125.5 (^{3}J(^{13}C-$^{119/117}$Sn= 58.3 Hz, C8), 127.3 (C6), 125.8 (^{3}J(^{13}C-^{119}Sn= 141 Hz, ^{3}J(^{13}C-^{117}Sn= 135 Hz, C3) ppm. ^{119}Sn NMR (C_6D_6, 112 MHz): δ -62.3 ppm.

2-NaphthylSnCl$_3$ 27: 3.71 g tetra-2-naphthyltin (**6**) (5.7 mmol, 1 eq.), 1.99 ml SnCl$_4$ (4.5 g, 17 mmol, 3 eq.), 160 °C, work-up procedure (**b**) The resulting solid was recrystallized from chloroform to obtain colorless crystals. Yield: 90 % (7.2 g, 20 mmol). M. p.: 82 °C. Anal. Calcd. For $C_{10}H_7Cl_3Sn$: C, 34.10; H, 2.00. Found: C, 35.82; H, 2.13. ^{1}H NMR (C_6D_6, 300 MHz): δ 7.64 (s, 1H, ^{3}J(H1-^{119}Sn)=135.4 Hz, ^{3}J(H1-^{117}Sn)=134.9 Hz, H1), 7.40-7.31 (m, 2H, H4, H6), 7.28-7.23 (m, 2H, H5, H7), 7.20-7.10 (m, 1H, H3), 7.04 (d, ^{3}J(H8-H7)=8.38 Hz, H8).^{13}C NMR (C_6D_6, 75.5 MHz): δ 136.0 (^{2}J(^{13}C-^{119}Sn)=74.6 Hz, ^{2}J(^{13}C-^{117}Sn)=71.5 Hz, C1), 135.1 (^{4}J(^{13}C-$^{119/117}$Sn)=23.1 Hz, C4a), 133.4 (^{3}J(^{13}C-^{119}Sn)=141.4 Hz, ^{3}J(^{13}C-^{117}Sn)=135.3 Hz, C8a), 135.2 (^{1}J(^{13}C-^{119}Sn)=1130 Hz, ^{1}J(^{13}C-^{117}Sn)=1081 Hz, C2), 130.1 (^{3}J(^{13}C-^{119}Sn)=124.7 Hz, ^{3}J(^{13}C-^{117}Sn)=119.3 Hz, C4), 128.8 (^{5}J(^{13}C-$^{119/117}$Sn=5.5, C5/C7), 128.7 (^{5}J(^{13}C-$^{119/117}$Sn=5.8 Hz, C5/C7), 128.2 (C6), 128.1 (^{2}J(^{13}C-^{119}Sn)=85.4 Hz, ^{2}J(^{13}C-^{117}Sn)=81.8 Hz, C3), 127.4 (^{4}J(^{13}C-$^{119/117}$Sn=11.3 Hz, C8).^{119}Sn NMR (C_6D_6, 112 MHz): δ -63.5 ppm.

11.15.3.4 General Procedure for Ar_3SnH (29) and Ar_2SnH_2 (32-34)

A Schlenk tube was charged with $LiAlH_4$ and Et_2O. A solution of diaryltin dichloride in Et_2O was added *via* a syringe at 0 °C. The reaction was stirred for 5 minutes and quenched with degassed H_2O. The organic layer was dried over Na_2SO_4, filtered and the solvent removed under reduced pressure to result in colorless to yellowish powders.

2,6-Xylyl$_3$SnH 29: 5.38 g tri-2,6-xylyltinbromide (**9**) (10.5 mmol, 1 eq.) in 40 ml Et_2O, 0.60 g LAH pellets (15.7 mmol, 1.5 eq.) in 40 ml Et_2O, 50 ml degassed H_2O, 2 x 40 ml Et_2O. The resulting solid was recrystallized from toluene to obtain colorless crystals. Yield: 57 % (2.59 g, 59.5 mmol). M.p.: 139 °C. Anal. Calcd. For $C_{10}H_7Cl_3Sn$: C, 66.24; H, 6.49. Found: C, 67.94; H, 6.78. ^{1}H NMR (C_6D_6, 300 MHz): δ 7.09-7.02 (t, 3H, H4), 6.91 (d, 6H, ^{3}J(H3-H4)= 7.6, H3), 6.86 (s, 1H, $^{1}J(^{1}H-^{119}Sn)$=1776 Hz, $^{1}J(^{1}H-^{117}Sn)$=1697 Hz, Sn-H), 2.32 (s, 6H, C$\underline{H}_3$) ppm. ^{13}C NMR (C_6D_6, 75.5 MHz): δ 145.0 ($^{2}J(^{13}C-^{119/117}Sn)$= 32.5 Hz, C2), 142.9 ($^{1}J(^{13}C-^{119}Sn)$= 534 Hz, $^{1}J(^{13}C-^{117}Sn)$= 511 Hz, C1), 129.3 ($^{4}J(^{13}C-^{119/117}Sn)$= 9.4 Hz, C4), 127.7 ($^{3}J(^{13}C-^{119}Sn)$= 43.8 Hz, $^{3}J(^{13}C-^{117}Sn)$= 41.5 Hz, C3), 25.8 ($^{3}J(^{13}C-^{119}Sn)$= 42.6 Hz, $^{3}J(^{13}C-^{117}Sn)$= 40.3 Hz, $\underline{C}H_3$) ppm.^{119}Sn NMR (C_6D_6, 112 MHz): δ -286.6 ($^{1}J(^{119/117}Sn-^{1}H)$=1780 Hz) ppm.

1-Naphthyl$_2$SnH$_2$ 32: 0.20 g $LiAlH_4$ (5.3 mmol, 2.3 eq.), 100 ml Et_2O, di-1-naphthyltin dichloride (**15**) (1.0 g, 2.3 mmol, 1eq.) in 50 ml Et_2O, 50 ml of degassed H_2O. Yield: 0.60 g (71 %, 1.6 mmol). M.p., 62-64 °C. Anal. Calcd. For $C_{20}H_{16}Sn$: C, 64.05 H, 4.30. Found: C, 63.05; H, 4.45. ^{1}H NMR (C_6D_6, 300 MHz): δ 7.99-7.91 (m, 2H, H8), 7.68-7.56 (m, 6H, H2, H4, H5), 7.25-7.06 (m, 6H, H3, H6, H7), 6.41 (s, 2H, $^{1}J(^{1}H-^{119}Sn)$= 1937 Hz, $^{1}J(^{1}H-^{117}Sn)$= 1851 Hz, Sn$\underline{H_2}$) ppm. ^{13}C NMR (C_6D_6, 75.5 MHz): δ 139.2 ($^{2}J(^{13}C-^{119}Sn)$= 36.3 Hz, $^{2}J(^{13}C-^{117}Sn)$= 34.8 Hz, C8a), 138.0 ($^{3}J(^{13}C-^{119}Sn)$= 39.2 Hz, $^{3}J(^{13}C-^{117}Sn)$= 38.0 Hz, C4a), 136.7 ($^{1}J(^{13}C-^{119}Sn)$= 544 Hz, $^{1}J(^{13}C-^{117}Sn)$= 519 Hz, C1), 134.3 ($^{2}J(^{13}C-^{119}Sn)$= 36.3 Hz, $^{2}J(^{13}C-^{117}Sn)$= 38.0 Hz, C2), 130.6 ($^{3}J(^{13}C-^{119}Sn)$= 41.2 Hz, $^{3}J(^{13}C-^{117}Sn)$= 39.4 Hz, C8), 130.1 ($^{4}J(^{13}C-^{119/117}Sn)$= 12.4 Hz, C4), 129.2 (C6), 126.1 ($^{3}J(^{13}C-^{119}Sn)$= 62.7 Hz, $^{3}J(^{13}C-^{117}Sn)$= 60.2 Hz, C3), 126.1 ($^{4}J(^{13}C-^{119/117}Sn)$= 5.8 Hz, C4) ppm. ^{119}Sn NMR (C_6D_6, 112 MHz): δ -249.7 ($^{1}J(^{119}Sn-^{1}H)$= 1948 Hz) ppm.

2-Naphthyl$_2$SnH$_2$ 33: 0.20 g (5.3 mmol, 2.3 eq.) $LiAlH_4$, 100 ml Et_2O, 1.0 g (2.3 mmol, 1 eq.) di-2-naphthyltin dichloride (**16**) in 50 ml Et_2O, 50 ml of degassed H_2O. Yield: 95% (0.80 g, 2.1 mmol). M.p., 107-111 °C (decomposition). Anal. Calcd. For $C_{20}H_{16}Sn$: C, 64.05; H, 4.30. Found: C, 59.37; H, 4.64. ^{1}H NMR (C_6D_6, 300 MHz): δ 7.98 (2H, s, ^3J(H1-$^{119/117}$Sn= 60.9 Hz, H1), 7.66-7.43 (m, 8H, H3, H4, H5, H8), 7.29-7.17 (m, 4H, H6, H7), 6.27 (s, 2H, ^1J(^{1}H-^{119}Sn= 1941 Hz, ^1J(^{1}H-^{117}Sn= 1855 Hz) Sn$\underline{H_2}$) ppm. ^{13}C NMR (C_6D_6, 75.5 MHz): δ 138.7 (^2J(^{13}C-^{119}Sn= 40 Hz, ^2J(^{13}C-^{117}Sn= 38.6 Hz, C1), 134.2 (^4J(^{13}C-$^{119/117}$Sn= 9.8 Hz, C4a), 134.1 (^3J(^{13}C-$^{119/117}$Sn= 63.9 Hz, C8a), 133.8 (^2J(^{13}C-^{119}Sn= 44.3 Hz, ^2J(^{13}C-^{117}Sn= 42.5 Hz, C3), 133.0 (^1J(^{13}C-^{119}Sn= 542 Hz, ^1J(^{13}C-^{117}Sn= 519 Hz, C2), 128.2 (^3J(^{13}C-^{119}Sn= 52.5 Hz, ^3J(^{13}C-^{117}Sn= 50.4 Hz, C4), 128.1 (^5J(^{13}C-$^{119/117}$Sn= 5.2 Hz, C5), 128.1 (C8), 126.6 (C6), 126.3 (^5J(^{13}C-$^{119/117}$Sn= 4.4 Hz, C7) ppm. ^{119}Sn NMR (C_6D_6, 112 MHz): δ -230.0 (^1J(^{119}Sn-^{1}H)= 2022 Hz) ppm.

***p*-Biphenyl$_2$SnH$_2$ 34**: 0.15 g (4.0 mmol, 2 eq.) $LiAlH_4$, 250 ml Et_2O, 1.0 g (2.0 mmol, 1 eq.) di-*p*-biphenyltin dichloride (**14**) in 150 ml THF, 15 ml of degassed H_2O. The residue was then suspended in 250 ml toluene, filtered and the solvent evaporated. Yield: 99 % (0.85 g, 2.0 mmol). M.p., 143-145 °C. Anal. Calcd. For $C_{24}H_{20}Sn$: C,67.49; H, 4.72. Found: C, 67.76; H, 4.99. ^{1}H NMR (C_6D_6, 300 MHz): δ 7.49 (d, 4H, ^3J(H2-H3)= 8.0 Hz, ^3J(H2-$^{119/117}$Sn= 49.5 Hz, H2), 7.46-7.37 (m, 8H, H3, H6), 7.21-7.14 (m, 4H, H7), 7.13-7.06 (m, 2H, H8), 6.14 (s, 2H, ^1J(^{1}H-^{119}Sn= 1936 Hz, ^1J(^{1}H-^{117}Sn= 1850 Hz) Sn$\underline{H_2}$) ppm. ^{13}C NMR (C_6D_6, 75.5 MHz): δ 142.4 (^4J(^{13}C-$^{119/117}$Sn= 11.8 Hz, C4), 141.4 (^5J(^{13}C-$^{119/117}$Sn= 5.5 Hz, C5), 138.3 (^2J(^{13}C-^{119}Sn= 42.8 Hz, ^2J(^{13}C-^{117}Sn)= 41.3 Hz, C2), 134.2 (^1J(^{13}C-^{119}Sn)= 546 Hz, ^1J(^{13}C-^{117}Sn)= 522 Hz, C2) ppm. ^{119}Sn NMR (C_6D_6, 112 MHz): δ -233.2 (^1J(^{119}Sn-^{1}H)= 1937 Hz) ppm.

11.15.3.5 General procedure for ArSnH$_3$ (36-41)

A flask furnished with a reflux condenser and a dropping funnel was charged with a $LiAlH_4$-solution (2 eq., 2 M in Et_2O) or $LiAlH_4$ pellets and 50 ml Et_2O. A solution of aryltin trichloride in 50 ml Et_2O was added slowly *via* the dropping funnel while cooling to -30 °C. The reaction mixture was stirred for 1.5 h and allowed to warm up to room temperature. Subsequently, 50 ml degassed water were added. The phases were separated *via* a cannula and the aqueous layer washed twice with 40 ml Et_2O. The combined organic phases were extracted with saturated sodium tartrate in degassed water and the resulting organic phase dried over $CaCl_2$. If not otherwise stated the solvent was evaporated gently at 200 mbar and the product was distilled at room temperature or the lowest temperature possible using the turbomolecular pump while the receiving flask was placed in a dewar filled with liquid nitrogen to obtain a colorless liquid.

***o*-TolylSnH$_3$ 36**: 15.8 ml LiAlH$_4$-solution (2 eq., 2 M in Et$_2$O, 31.6 mmol), *o*-tolyltin trichloride (**21**) (4 g, 1 eq., 12.1 mmol). Yield: 50 % (1.86 g, 7.89 mmol). Anal. Calcd. For $C_7H_{10}Sn$: C, 39.50; H, 4.74. Found: C, 39.13; H, 4.63. ^{1}H NMR (C$_6$D$_6$, 300 MHz): δ 7.47 (d, 1H, ^{3}J(H6-H5)= 8.4 Hz, ^{4}J (H6-$^{119/117}$Sn)= 70.5 Hz, H6), 7.26-7.16 (dd, 1H, H5), 7.14-7.03 (m, 2H, H4, H3), 4.96 (s, 3H, ^{1}J(^{1}H-^{119}Sn)= 1908 Hz, ^{1}J(^{1}H-^{117}Sn)= 1823 Hz, Sn$\underline{H_3}$), 2.15 (s, 3H, ^{4}J(^{1}H-$^{119/117}$Sn)= 5.3, H7) ppm. ^{13}C NMR (C$_6$D$_6$, 75.5 MHz): δ 144.8 (^{2}J(^{13}C-^{119}Sn)= 33.4 Hz, ^{2}J(^{13}C-^{117}Sn)= 31.7 Hz, C2), 139.0 (^{2}J(^{13}C-^{119}Sn)= 45.0 Hz, ^{2}J(^{13}C-^{117}Sn)= 43.5 Hz, C6), 134.4 (^{1}J(^{13}C-^{119}Sn)= 568 Hz, ^{1}J(^{13}C-^{117}Sn)=542 Hz, C1), 129.8 (^{4}J(^{13}C-$^{119/117}$Sn)= 11.6 Hz, C4), 129.4 (^{3}J(^{13}C-^{119}Sn)= 43.5 Hz, ^{3}J(^{13}C-^{117}Sn)= 42.2 Hz, C3), 126.0 (^{3}J(^{13}C-^{119}Sn)= 58.6 Hz, ^{3}J(^{13}C-^{117}Sn)= 56.2 Hz, C5), 25.8 (^{3}J(^{13}C-^{119}Sn)= 40.9 Hz, ^{3}J(^{13}C-^{117}Sn)=39.7 Hz, C7) ppm. ^{119}Sn NMR (C$_6$D$_6$, 112 MHz): δ -358.4 (^{1}J(^{119}Sn-^{1}H)= 1920 Hz) ppm.

***p*-^{n}ButylphenylSnH$_3$ 37:** 5.0 g *p*-^{n}butylphenylSnCl$_3$ (**25**) (14.0 mmol, 1 eq.) in 40 ml Et$_2$O 1.1 g LiAlH$_4$ pellets (27.9 mmol, 2 eq.) in 40 ml Et$_2$O, 50 ml degassed H$_2$O, 2 x 40 ml Et$_2$O. Yield: 83 % (2.95 g, 11.5 mmol). Anal. Calcd. For $C_{10}H_{16}Sn$: C, 47.11; H, 6.40. Found: C, 47.88.; H, 6.38.^{1}H NMR (C$_6$D$_6$, 300 MHz): 7.30 (d, 2H, ^{3}J(H2-H3)=6.96, ^{3}J(H2-$^{119/117}$Sn)=55.9 Hz, H2), 6.99 (d, 2H, ^{3}J(H3-H2)=7.0 Hz, ^{3}J(H3-$^{119/117}$Sn)=24.8 Hz, H3), 5.05 (s, 3H, ^{1}J(^{1}H-^{119}Sn=1913 Hz, ^{1}J(^{1}H-^{117}Sn=1828 Hz, Sn-H), 2.47-2.37 (t, 2H, H5), 1.52-1.39 (dd, 2H, H6), 1.30-1.15 (dd, 2H, H7), 0.09-0.80 (t, 3H, H8). ^{13}C NMR (C$_6$D$_6$, 75.5 MHz): 143.8 (^{4}J(^{13}C-$^{119/117}$Sn=11.9 Hz, C4), 138.1 (^{2}J(^{13}C-^{119}Sn)=45.2 Hz, ^{2}J(^{13}C-^{117}Sn)=42.7 Hz, C2), 129.1 (^{3}J(^{13}C-^{119}Sn)=62.6 Hz, ^{3}J(^{13}C-^{117}Sn)=56.3 Hz, C3), 129.0 (^{1}J(^{13}C-^{119}Sn)=571.2 Hz, ^{1}J(^{13}C-^{117}Sn)=545.5 Hz, C1), 35.9 (C5), 33.9 (C6), 22.6 (C7), 14.1 (C8) ppm.^{119}Sn NMR (C$_6$D$_6$, 112 MHz): δ -344.6 ppm (^{1}J($^{119/117}$Sn-^{1}H)=1910 Hz) ppm.

2,4-XylylSnH$_3$ 38: 15.1 ml LiAlH$_4$-solution (2 eq., 2M in Et$_2$O, 30.3 mmol), 2,4-xylyltin trichloride (**22**) (5 g, 1 eq., 15.1 mmol) Yield: 68 % (2.33 g, 10 mmol). Anal. Calcd. For $C_8H_{11}Sn$: C, 42.35; H, 5.33. Found: C, 42.10; H, 5.22. ^{1}H NMR (C_6D_6, 300 MHz): δ 7.26 (d, 1H, ^{3}J(H6-H5)= 7.4 Hz, ^{4}J(H6-$^{119/117}$Sn)= 69.4 Hz, H6), 6.90-9.72 (m, 2H, H5, H3), 4.96 (s, 3H, ^{1}J(^{1}H-^{119}Sn)= 1898 Hz, ^{1}J(^{1}H-^{117}Sn)= 1814 Hz, Sn$\underline{H_3}$), 2.18 (3H, s, H7), 2.12 (3H, s, H8). ^{13}C NMR (C_6D_6, 75.5 MHz): δ 144.6 (^{2}J(^{13}C-^{119}Sn= 35.7 Hz, ^{2}J(^{13}C-^{117}Sn)= 33.4 Hz, C2), 139.2 (^{4}J(^{13}C-$^{119/117}$Sn)= 11.6 Hz, C4), 139.0 (C6), 130.4 (^{3}J(^{13}C-$^{119/117}$Sn)= 43.8 Hz, C3), 130.4 (^{1}J(^{13}C-^{119}Sn)= 579 Hz, ^{1}J(^{13}C-^{117}Sn)= 551 Hz, C1), 126.8 (^{3}J(^{13}C-$^{119/117}$Sn)= 59.5 Hz, C5), 25.7 (^{3}J(^{13}C-$^{119/117}$Sn)= 40 Hz, C7), 21.5 (C8) ppm. ^{119}Sn NMR (C_6D_6, 112 MHz): δ -352.5 (^{1}J(^{119}Sn-^{1}H)= 1913 Hz) ppm.

2,6-XylylSnH$_3$ 39: 0.86 g LiAlH$_4$ pellets (22.8 mmol, 2 eq.), 2,6-xylyltin trichloride (**23**) (3.76 g, 11.4 mmol, 1 eq.). Yield: 86 % (2.70 g, 11.9 mmol). Anal. Calcd. For $C_8H_{11}Sn$: C, 42.35; H, 5.33. Found: C, 43.08; H, 5.29. ^{1}H NMR (C_6D_6, 300 MHz): δ 7.04-6.95 (m, 1H, H4), 6.85 (d, 2H, ^{3}J(H3-H4)= 4.5 Hz, H3), 4.81 (s, 3H, ^{1}J(^{1}H-^{119}Sn)= 1896 Hz, ^{1}J(^{1}H-^{117}Sn)= 1812 Hz, Sn$\underline{H_3}$), 2.23 (s, 6H, ^{3}J(H5-$^{119/117}$Sn)= 126 Hz, H5 ppm. ^{13}C NMR (C_6D_6, 75.5 MHz): δ 144.9 (^{2}J(^{13}C-$^{119/117}$Sn)= 30.4 Hz, C2), 135.3 (^{1}J(^{13}C-^{119}Sn)= 582 Hz, ^{1}J(^{13}C-^{117}Sn)= 558 Hz, C1), 129.4 (^{4}J(^{13}C-$^{119/117}$Sn)= 8.8 Hz, C4), 126.9 (^{3}J(^{13}C-$^{119/117}$Sn)= 43.5 Hz, C3), 26.7 (^{3}J(^{13}C-$^{119/117}$Sn)= 47.3 Hz, C5) ppm. ^{119}Sn NMR (C_6D_6, 112 MHz): δ -417.5 (^{1}J(^{119}Sn-^{1}H)= 1915 Hz) ppm.

MesitylSnH$_3$ 40 : 2.21 g LiAlH$_4$ pellets (58.2 mmol, 2 eq.), mesitylSnCl$_3$ (**24**) (10 g, 29.1 ,1 eq.). Et$_2$O is removed under reduced pressure to afford a yellowish solid which is recrystallized from diethyl ether to obtain colorless crystals. Yield: 87 % (6.12 g, 25.4 mmol). Anal. Calcd. For $C_9H_{14}Sn$: C, 44.87; H, 5.86. Found: C, 44.93; H, 5.97. ^{1}H NMR (C_6D_6, 300 MHz): 6.73 (s, 2H, ^{4}J(^{1}H-$^{119/117}$Sn)=18.5 Hz, H3), 4.83 (s, ^{1}J(^{1}H-^{119}Sn=1886.8 Hz, ^{1}J(^{1}H-^{117}Sn=1845.1 Hz, Sn-$\underline{H}$), 2.24 (s, 6H, H5), 2.10 (s, 3H, H6). ^{13}C NMR (C_6D_6, 75.5 MHz): 144.91 (^{2}J(^{13}C-^{119}Sn)=32.24 Hz, ^{2}J(^{13}C-^{117}Sn)=31.09 Hz, C2), 138.78 (^{4}J(^{13}C-$^{119/117}$Sn)=9.68 Hz, C4), 131.28 (^{1}J(^{13}C-^{119}Sn)=591.93 Hz, ^{1}J(^{13}C-^{117}Sn)=565.44 Hz, C1), 127.97 (^{3}J (^{13}C-$^{119/117}$Sn)=under benzene, C3), 26.44 (^{3}J (^{13}C-$^{119/117}$Sn)=48.34 Hz, C5), 21.12 (^{5}J (^{13}C-$^{119/117}$Sn)=5.18, C6) ppm. ^{119}Sn NMR (C_6D_6, 112 MHz): δ –420.7 ^{1}J(^{119}Sn-^{1}H=1898.0 Hz) ppm.

1-NaphthylSnH_3 41: 0.67 g $LiAlH_4$ pellets (17.6 mmol, 2 eq.) 1-naphthyltin trichloride (**26**) (3.10 g, 10.5 mmol, 1 eq.), distillation under slight heating (~ 50 °C). Yield: 75 % (1.64 g, 6.59 mmol). Anal. Calcd. For $C_{10}H_{10}Sn$: C, 48.26; H, 4.05. Found: C, 49.06; H, 3.98. ^{1}H NMR (C_6D_6, 300 MHz): δ 7.70-7.63 (m, 1H, H8), 7.62-7.53 (m, 2H, H4, H5), 7.48 (d, 1H, ^{3}J(H2-H3)= 6.5 Hz, ^{3}J(H2-$^{119/117}$Sn= 14.8 Hz, H2), 7.28-7.18 (m, 2H, H6, H7), 7.16-7.09 (dd, 1H, H3), 5.14 (s, 3H, ^{1}J(^{1}H-^{119}Sn)= 1934 Hz, ^{1}J(^{1}H-^{117}Sn)= 1848 Hz, $Sn\underline{H_3}$) ppm. ^{13}C NMR (C_6D_6, 75.5 MHz): δ 139.1 (^{2}J(^{13}C-$^{119/117}$Sn= 35.8 Hz, C8a), 138.2 (^{2}J(^{13}C-$^{119/117}$Sn=39.2 Hz, C2), 134.4 (^{1}J(^{13}C-^{119}Sn= 534 Hz, ^{1}J(^{13}C-^{117}Sn= 510 Hz, C1), 134.1 (^{3}J(^{13}C-$^{119/117}$Sn= 37.6 Hz, C4a), 130.7 (^{3}J(^{13}C-$^{119/117}$Sn= 42.4 Hz, C8), 130.0 (^{4}J(^{13}C-$^{119/117}$Sn=12.6 Hz, C4), 129.2 (^{4}J(^{13}C-$^{119/117}$Sn= 7.16 Hz, C5), 126.6 (C6), 126.0 (^{4}J(^{13}C-$^{119/117}$Sn= 10.9 Hz, C7), 125.9 (^{3}J(^{13}C-^{119}Sn= 64.5 Hz, ^{3}J(^{13}C-^{117}Sn=61.6 Hz, C3) ppm. ^{119}Sn NMR (C_6D_6, 112 MHz): δ -353.9 (^{1}J(^{119}Sn-^{1}H)= 1953 Hz) ppm.

11.15.4 Chapter 3

11.15.4.1 Synthesis of $ASnCl_3$ via the Lithiation Route (a)

a1) 4 g 9-bromoanthracene **ABr** (15.6 mmol, 1 eq.) were dissolved in 150 mL THF and cooled to -78 °C using an ethanol/N_2(*l*) bath. Subsequently, 6.2 mL of an *n*-BuLi solution (15.6 mmol, 1 eq., 2.5 M in hexane) were added. A color change from yellow to bright orange was observed immediately. The lithiation reaction was stirred for 1.5 h at -78 °C. $SnCl_4$ (1.8 mL, 15.6 mmol, 1 eq.) was added to 30 mL ice cooled THF. The lithiated species **LiA** was transferred to the $SnCl_4$ solution leading to an amberlike color. After complete addition of **LiA** the reaction mixture was allowed to warm up to room temperature and stirred overnight. THF was completely removed in *vacuo* and part of the solid taken up in $CDCl_3$ in order to subject to ^{1}H and ^{119}Sn NMR spectroscopy revealing a mixture of A_3SnCl (**8**) and $ASnCl_3$ (**28**). ^{119}Sn NMR ($CDCl_3$, 112 MHz): δ -49.6, -84.8 ppm.

a2) 3 g 9-bromoanthracene **ABr** (11.7 mmol, 1 eq.) were dissolved in 20 mL THF and cooled to -78 °C. Subsequently, 1 eq. of *n*-BuLi (4.7 mL, 11.7 mmol, 2.5 M in hexane) was added resulting in a dark orange reaction mixture which is stirred for 1h. Afterwards, the latter was transferred onto a solution of 0.46 mL $SnCl_4$ (0.3 eq., 3.9 mmol) and 10 mL THF cooled to -50 °C. The reaction mixture was stirred for 1 h and then allowed to warm up to room temperature and stirred overnight to give a dark red, clear solution. THF was removed under *vacuo* and the resulting solid is taken up in 15 mL toluene. The supernatant dark yellow solution was filtered off and the toluene removed under *vacuo*. ^{1}H and ^{119}Sn NMR spectra were taken in $CDCl_3$ revealing a mixture of A_3SnCl (**8**) and $ASnCl_3$ (**28**). ^{119}Sn NMR ($CDCl_3$, 112 MHz): δ -45.1, -84.7, -92.7 ppm.

a3) 1.88 g 9-bromoanthracene **ABr** (7.3 mmol, 1 eq.) were dissolved in 15 mL THF and cooled to -78 °C. Subsequently, 1 eq. of *n*-BuLi (2.9 mL, 2.5 M in hexane) was added resulting in a dark orange reaction mixture which was stirred for 1h. Afterwards the latter was transferred onto a solution of 0.86 mL $SnCl_4$ (1 eq., 7.3) and 10 mL THF cooled to -50 °C. The reaction mixture turned red and after 15 min brown and turbid. It was stirred for 3 h at -50 °C and then allowed to warm up to room temperature and stirred overnight to result in a dark red reaction mixture. Subsequently, approximately 10 mL of the reaction were transferred in a separate flask and the solvent removed under reduced pressure. The resulting dark red solid was taken up in $CDCl_3$ and precipitates filtered off. The ^{119}Sn spectrum showed the formation of $ASnCl_3$ (**28**). ^{119}Sn NMR ($CDCl_3$, 112 MHz): δ -84.3,-258.9 ppm.

a4) 2 g 9-bromoanthracene **ABr** (7.8 mmol, 1 eq.) were dissolved in 15 mL THF and cooled to -78 °C. Subsequently, 1 eq. of *n*-BuLi (3.1 mL, 2.5 M in hexane) was added resulting in a dark orange reaction mixture which was stirred for 1 h. Afterwards the mixture was transferred onto a solution of 0.9 mL $SnCl_4$ (1 eq., 7.8 mmol) and 15 mL THF. The reaction mixture turned dark red (clear) and was stirred at room temperature overnight forming a slightly brown precipitate. The solvent was removed under reduced pressure to afford a brownish red solid which was taken up in 15 mL toluene. The precipitate was filtered off and toluene removed in *vacuo* to afford a yellow solid. The latter was subjected to NMR analysis in $CDCl_3$ revealing a mixture of A_3SnCl (**8**) and $ASnCl_3$ (**28**). ^{119}Sn NMR ($CDCl_3$, 112 MHz): δ -45.1,-84.5 ppm.

a5) 2 g 9-bromoanthracene **ABr** (7.8 mmol, 1 eq.) were dissolved in 15 mL THF and cooled to -78 °C. Subsequently, 1 eq. of *n*-BuLi (3.1 mL, 2.5 M in hexane) was added resulting in a dark orange reaction mixture which was stirred for 1h. Afterwards the mixture was transferred onto a solution of 0.9 mL $SnCl_4$ (1 eq., 7.8 mmol) and 15 mL THF at -78 °C. The reaction mixture was stirred at -78 °C for 3 h and then allowed to warm up to room temperature resulting in a clear solution without formation of salt precipitation. For a micro work-up, a small amount of solution was transferred to a separate flask and the solvent evaporated under reduced pressure. The resulting yellow oil was taken up in $CDCl_3$ and ^{1}H and ^{119}Sn NMR measurements are performed. Di-9-anthracenyl$_2$SnCl$_2$ (**17**) could be recrystallized from toluene. ^{119}Sn NMR ($CDCl_3$, 112 MHz): δ -50.6,-84.0 ppm.

***a6*)** 2 9-bromoanthracene **ABr** (7.8 mmol, 1 eq.) were dissolved in 13 mL THF and cooled to -78 °C. Subsequently, 2 eq. of *n*-BuLi (6.2 mL, 2.5 M in hexane) were added resulting in a dark orange reaction mixture which was stirred for 3h and allowed to warm up to -10 °C. Afterwards, the reaction solution was transferred onto a solution of 0.9 mL $SnCl_4$ (1 eq., 7.8 mmol) and 18 mL THF at 0 °C. The reaction mixture turned olive green (clear) and is stirred for 3h forming a brown and turbid reaction suspension. For a micro work-up, a small amount of solution was transferred to a separate flask and the solvent evaporated under reduced pressure. The resulting solid was taken up in $CDCl_3$ and ^{1}H and ^{119}Sn NMR measurements are performed, however no signal was detected.

***a7*)** 0.6 g 9-bromoanthracene **ABr** (2.3 mmol, 1 eq.) were dissolved in 15 mL THF and cooled to -78 °C. Subsequently, 1.2 eq. of *n*-BuLi (1.8 mL, 1.6 M in hexane) were added resulting in a dark orange reaction mixture which was stirred overnight and allowed to warm up to room temperature. The reaction mixture turned dark green. Afterwards, the latter was transferred onto a solution of 0.27 mL $SnCl_4$ (1 eq., 2.3 mmol) and 18 mL THF at 0 °C. The reaction mixture turned turbid yellow and gets clear orange after 10 min stirring. Approximately 5 mL of reaction solution were transferred in a separate flask and the solvent was removed under reduced pressure. The resulting orange to brown solid is then taken up in $CDCl_3$.

***a8*)** 0.6 g 9-bromoanthracene **ABr** (2.3 mmol, 1 eq.) were dissolved in 10 mL THF and cooled to -78 °C. Subsequently, 2.2 eq. of *n*-BuLi (3.2 mL, 5.1 mmol, 1.6 M in hexane) were added resulting in a dark orange reaction mixture which was stirred for 1h. Afterwards, the latter was transferred onto a solution of 0.27 mL $SnCl_4$ (1 eq., 2.3 mmol) and 10 mL THF at 0 °C. The reaction mixture turned turbid and yellow and gets clear after 10 min reaction time. For reaction monitoring a small amount of the reaction solution was transferred into a separate flask and the solvent removed under *vacuo*. a) The resulting solid was taken up in $CDCl_3$ and ^{1}H, ^{119}Sn NMR were recorded. ^{119}Sn NMR ($CDCl_3$, 112 MHz): δ -62.3,-100.1 ppm. b) The resulting solid was taken up in toluene and the precipitate filtered off. Toluene was evaporated and the solid taken up in $CDCl_3$. Di-9-anthracenyltin dichloride (**17**) could be recrystallized from toluene. ^{119}Sn NMR ($CDCl_3$, 112 MHz): δ 1.5, -32.2, -45.0, -92.0, -92.4, -145.2, -153.7, -165.4 ppm

a9) 0.5 g 9-bromoanthracene **ABr** (1.9 mmol, 1 eq.) were dissolved in 15 mL THF and 1.38 eq. of *n*-BuLi (1.68 mL, 2.6 mmol, 1.6 M in hexane) are added at 0 °C. After complete addition the reaction mixture was stirred for 15 min and subsequently cannulated onto a solution of $SnCl_4$ (0.23 mL, 1.9 mmol, 1 eq.) in 10 mL Et_2O at 0 °C leading to a bright yellow color change. After 10 min stirring time the ice bath was removed and the formed yellow precipitate filtered off. The resulting yellow powder was taken up in 15 mL chloroform and the precipitating salts removed by filtration. The gained filtrate was concentrated in *vacuo* to give 0.22 g of a mixture containing A_3SnCl (**8**), $ASnCl_3$ (**28**) and anthracene. **8** could be recrystallized from the mixture using ethyl acetate. ^{119}Sn NMR ($CDCl_3$, 112 MHz):-44.5, -84.7 ppm.

a10) 0.5 g 9-bromoanthracene **ABr** (1.9 mmol, 1 eq.) were dissolved in 15 mL THF and cooled to -95 °C. Subsequently, 2.5 eq. of *t*-BuLi (3.04 mL, 4.8 mmol, 1.6 M in pentane) were added resulting in a dark orange reaction mixture. Afterwards, the reaction mixture was allowed to warm up to -50 °C and stirred for 55 min. Subsequently, 1.5 eq. of $SnCl_4$ (2.9 mmol, 0.76 g, 0.34 mL) were added with a syringe under the formation of an orange turbid solution which got clear after stirring for 5 min. After 30 min reaction time, the cooling bath was removed and the mixture slowly warms up to room temperature. THF was completely removed under reduced pressure and the resulting solid taken up in toluene to form a yellow precipitate. The supernatant liquid showed two phases. The lower phase was dark orange, clear and the upper phase slightly orange and clear. For NMR analysis, the two phases as well as the precipitate were separated. Toluene was completely removed under reduced pressure and the resulting solids taken up in $CDCl_3$. The lower phase did not show a tin signal. The upper phase and the precipitate showed the following. Di-9-anthracenyltin dichloride (**17**) and tri-9-anthracenyltrin chloride (**8**) could be recrystallized from toluene. ^{119}Sn NMR ($CDCl_3$, 112 MHz): δ -45.3,-92.3 ppm.

a11) 0.5 g 9-bromoanthracene **ABr** (1.9 mmol, 1 eq.) were dissolved in 15 mL Et_2O and cooled to 0 °C. Subsequently, 1.1 eq. of *n*-BuLi (1.33 mL, 2.1 mmol, 1.6 M in pentane) were added resulting in a dark orange reaction mixture and subsequent precipitation of a yellow solid. The reaction mixture was allowed to warm up to room temperature and stirred overnight. The clear yellow supernatant solution was filtered off using a cannula. The resulting precipitate was dissolved in 15 mL toluene and converted with 0.27 mL $SnCl_4$ (2.3 mmol, 0.61 g, 1.1 eq.) in 5 mL toluene at 0 °C. After complete addition of **ALi** to $SnCl_4$, the reaction mixture was allowed to warm up to room temperature and subsequently refluxed for 1h. No ^{119}Sn NMR signal found.

***a12*)** 2 g 9-bromoanthracene **ABr** (7.8 mmol, 1 eq.) were dissolved in 30 mL THF and cooled to 0 °C. Subsequently, 1.1 eq. of *n*-BuLi (5.35 mL, 8.6 mmol, 1.6 M in pentane) were added resulting in a dark orange reaction mixture which was stirred for 25 min. Subsequently, 0.91 mL of $SnCl_4$ (7.8 mmol, 1 eq.) were added. After complete addition of $SnCl_4$ the reaction mixture was allowed to warm up to room temperature and stirred overnight. Afterwards, the solvent was removed under *vacuo* and the resulting brown oil. The lithium coordinated anthraquinone derivative **48** could be recrystallized from toluene. ^{119}Sn NMR (C_6D_6, 112 MHz): δ -201 ppm.

***a13*)** 1.5 g 9-bromoanthracene **ABr** (5.8 mmol, 1 eq.) were suspended in 20 mL pentane and 0.88 mL of TMEDA (5.8 mmol, 1 eq.) were added. The mixture was cooled to 0 °C. Subsequently, 1.1 eq. of *n*-BuLi (4.01 mL, 6.4 mmol, 1.6 M in pentane) were added resulting in a dark red, clear reaction mixture which turned brightly yellow and turbid after 1 min reaction time. The latter was stirred for 15 min and then the ice bath was removed. The gained orange precipitate (1.29 g) was filtered off and redisolved in 30 mL THF to give a red solution to which 1 eq. of $SnCl_4$ (5.8 mmol, 0.68 mL) was added at room temperature. The mixture was stirred for 5 h. Subsequently, the solvent was removed under reduced pressure to resulting in a brownish solid which was taken up in 20 mL toluene to precipitate salts. 9-Anthrancenyl$_3$SnCl (**8**) could be recrystallized from toluene. ^{119}Sn NMR ($CDCl_3$, 112 MHz): δ -44.5 ppm.

***a14*)** 9-Anthracenyltin trichloride (**28**): 1.5 g 9-bromoanthracene **ABr** (5.8 mmol, 1 eq.) were suspended in 20 mL pentane and 0.88 mL of TMEDA (5.8 mmol, 1 eq.) were added. The mixture was cooled to 0 °C. Subsequently, 1.1 eq. of *n*-BuLi (4.01 mL, 6.4 mmol, 1.6 M in pentane) were added resulting in a dark red, clear reaction mixture which turned brightly yellow and turbid after 1 min reaction time. The latter was stirred for 15 min and then the ice bath was removed. The gained orange precipitate (1.29 g) was filtered off and redisolved in 30 mL toluene to give a red solution to which 1.4 eq. of $SnCl_4$ (8.2 mmol, 0.96 mL) were added at 0 °C. The ice bath was removed after 20 min and the mixture stirred overnight. Subsequently, the precipitates were filtered off and the solvent of the filtrate removed under reduced pressure resulting in 0.34 g of a yellow powder containing anthracene (44 %), 9-bromoanthracene (15 %) and 9-AnthrancenylSnCl_3 (**23**) (41 %). 9-AnthrancenylSnCl_3 (**23**) could be purified by sublimation for 1.5 h at 80 °C and recrystallized from toluene. ^{1}H NMR ($CDCl_3$, 300 MHz): δ 8.75 (d, 1H, $^4J(^1H-^{119/117}Sn)$= 20.1 Hz, H10), 8.57 (d, 2H, $^3J(H_{1,8}- H_{2,7})$= 9.2 Hz) H1, H8), 8.13 ($^3J(H_{4,5}- H_{3,6})$= 8.8 Hz, H4, H4), 7.77-7.67 (dd, 2H, H2, H7), 7.60 (t, 2H, $^3J(H_{3,6}- H_{2,4}/H_{7,5})$= 7.6, H3, H6) ppm. ^{119}Sn NMR ($CDCl_3$, 112 MHz): δ -84.5 ppm.

***a15*)** 1.5 g 9-bromoanthracene **ABr** (5.8 mmol, 1 eq.) were suspended in 20 mL pentane and 1.76 mL of TMEDA (11.7 mmol, 2 eq.) were added. The mixture is cooled to 0 °C. Subsequently, 2.2 eq. of *n*-BuLi (8.02 mL, 12.8 mmol, 1.6 M in pentane) were added resulting in a dark red, clear reaction mixture which turned orange and turbid after 20 min reaction time. The latter was stirred for 20 min and then the ice bath is removed and the reaction mixture stirred for 30 min at room temperature. The gained yellow precipitate was filtered off and suspended in 20 mL toluene which was cannulated onto a 1.2 eq. solution of $SnCl_4$ (7.0 mmol, 0.82 mL) in toluene at 0 °C to result in a red reaction mixture. After complete addition, the ice bath was removed and the reaction stirred at room temperature overnight. The formed precipitates are filtered off and toluene from the filtrate removed under *vacuo* to give the following Sn shifts: ^{119}Sn NMR (C_6D_6, 112 MHz): δ -84, -154 ppm. Unreacted 9-bromoanthracene could be removed by sublimation. Tri-9-anthracenyltin butyl (**49**) could be recrystallized from the red brown powder.

***a16*)** 1.8 mL TMEDA (11.7 mmol, 2 eq.) were mixed with 25 mL pentane and cooled to 0 °C. 2.2 eq. of MeLi (12.8 mmol, 8.02 mL, 1.6 M in Et_2O) were added. Subsequently, 1.5 g 9-bromoanthracene **ABr** (5.8 mmol, 1 eq.) were added to give a yellow suspension which was stirred for 30 min. Afterwards the ice was is removed and the mixture stirred for 20 min at room temperature. The yellow precipitate was filtered off, washed with 10 mL of pentane, dried under *vacuo* and suspended in 40 mL toluene to give an orange solution. The latter was added to a mixture of $SnCl_4$ (1.2 eq., 7.0 mmol, 0.82 mL) and 20 mL toluene at 0 °C to yield a yellow, turbid reaction mixture. After complete addition, the ice bath was removed and the reaction solution allowed to warm up to room temperature and stirred overnight. The formed precipitate was filtered through celite and solvent of the filtrate removed under *vacuo* resulting in an orange solid which is subjected to sublimation to remove left over 9-bromoanthracene and anthracene. ^{119}Sn NMR (C_6D_6, 112 MHz): δ -48.8, -84.0, -102.2, -165.3, -172.9 ppm. Tri-9-anthracenyltin methyl could be recrystallized from the mixture using benzene.

***a17*)** 1.8 mL TMEDA (11.7 mmol, 2 eq.) were mixed with 20 mL pentane and cooled to 0 °C. 1.1 eq. of MeLi (6.4mmol, 4.01 mL, 1.6 M in Et_2O) are added. Subsequently, 1.5 g 9-bromoanthracene **ABr** (5.8 mmol, 1 eq.) were added to give an orange suspension which was stirred for 25 min. Afterwards the ice bath is removed and the mixture stirred for 15 min at room temperature. The yellow to orange precipitate was filtered off, washed with twice with 10 mL of pentane, dried under *vacuo* and suspended in 20 mL toluene to give a red solution. The latter was added to a mixture of $SnCl_4$ (1.2 eq., 7.0 mmol, 0.82 mL) an 20 mL toluene at 0 °C to yield in a yellow to brown, turbid reaction mixture. After complete addition, the ice was removed and the reaction solution allowed to warm up to room temperature and stirred overnight. Toluene was removed under reduced pressure to afford 3.18 g of crude product which is subsequently taken up in benzene. The formed precipitate was filtered through celite and solvent of the filtrate removed under *vacuo* resulting in 0.83 g of an orange solid. ^{119}Sn NMR (C_6D_6, 112 MHz): δ -43.7, -50.4, -87.0 ppm.

9-iodoanthracene AI (44):[217] 15.06 g 9-bromoanthracene **ABr** (59 mmol) were dissolved in 300 mL Et_2O and 50.5 mL of *n*-BuLi (1.38 eq., 81 mmol, 1.6 M in pentane) were added at room temperature to form an orange precipitate. After stirring the reaction mixture for 30 min, 25.3 g I_2 (1.7 eq., 0.10 mol) were added and the reaction stirred overnight. The solution was washed with aqueous sodium thiosulfate solution (25 %) and the combined organic phases were dried over Na_2SO_4. The solvent was removed under reduced pressure to afford yellow oil. **44** could be recrystallized from ethyl acetate to afford yellow crystals. Yield: 11.31 g (37 mmol, 63 %). ^{1}H NMR (C_6D_6, 300 MHz): 8.47 (d, 2H, $^3J(H_{1/8}\text{-}H_{2/7})$=8.8 Hz, H1,H8), 7.95 (s, 1H, H 10), 7.51 (d, 2H, $^3J(H_{4/5}\text{-}H_{3/6})$=8.4 Hz, H4, H5), 7.23-7.14 (t, 2H, H2, H7), 7.13-7.01 (m, 2H, H3, H6) ppm. ^{13}C NMR ($CDCl_3$, 75.5 MHz): 134.0 (Cq), 133.3, 132.2 (Cq), 128.9, 128.7, 128.3 (Cq), 125.7 ppm.

***a18*)** 0.5 g 9-ioidoanthracene **AI** (**44**) (1.6 mmol, 1 eq.) were dissolved in 20 mL Et_2O and 2.06 mL *t*-BuLi (3.2 mmol, 2 eq.) were added and the reaction mixture stirred at room temperature for 20 min. Subsequently, the latter was added to a mixture of 1.03 g SnI_4 (1.6 mmol, 1 eq.) in 30 mL Et_2O and stirred overnight. The formed precipitate was filtered off and taken up in chloroform to separate the product from the salt. ^{119}Sn NMR ($CDCl_3$, 112 MHz): δ -221.5, -438.3 ppm. Di-9-anthracenyltin diiodide (**19**) could be recrystallized from $CHCl_3$.

a19) 0.5 g 9-ioidoanthracene **AI** (**44**) (1.6 mmol, 1 eq.) were dissolved in 10 mL Et_2O and 1.42 mL *n*-BuLi (2.2 mmol, 1.38 eq.) were added and the reaction mixture stirred at room temperature for 15 min. Subsequently, the latter was added to a mixture of 1.03 g SnI_4 (1.6 mmol, 1 eq.) in 20 mL Et_2O and stirred overnight. The formed precipitate was filtered off and afterwards taken up in chloroform to separate the product from the salt. ^{119}Sn NMR ($CDCl_3$, 112 MHz): δ -221.5, -223.6, -438.4 ppm. Di-9-anthracenyltin diiodide (**19**) and tri-9-anthracenyltin (**11**) iodide could be recrystallized from $CHCl_3$.

11.15.4.2 Synthesis of $ASnCl_3$ via the Grignard Route (b)

***b1*)** A flask equipped with a dropping funnel and a reflux condenser was charged with 1.18 g Mg (48.6 mmol, 1.25 eq.) in 60 mL THF. The dropping funnel was charged with 9-bromoanthracene **ABr** (38.9 mmol, 1 eq.) in 60 mL THF. 1 ml dibromoethane was added and the solution heated to start the reaction. The 9-bromoanthracene/THF solution was subsequently added slowly. After complete addition, the reaction is refluxed for 1.5 h. The formation of anthracenylMgBr is estimated with 80 %. The brownish reaction mixture showing a precipitate was cannulated onto a mixture of $SnCl_4$ (0.83 mL, 1.86 g, 7.16 mmol, 0.23 eq.) in 150 mL THF cooled with an ice bath. After dropwise addition of the Grignard reagent the reaction solutions showed a brownish color with precipitation. The reaction suspension is stirred for 72 h at room temperature. For a reaction monitoring approximately 20 mL of the supernatant liquid were transferred in a separate flask and the THF is removed under *vacuo*. The resulting brown solid was taken up in $CDCl_3$. ^{119}Sn NMR ($CDCl_3$, 112 MHz): δ -124.0, -145.9 ppm.

***b1**)** 1g of the product mixture of **B1** was converted with an excess of 1.5 eq. $LiAlH_4$ at -30 °C in 30 mL Et_2O. The excess of $LiAlH_4$ was quenched with degassed water and phases are separated using a cannula. The aqueous phase was washed with 30 mL of Et_2O. The organic phase was dried over $CaCl_2$ and the Et_2O removed under *vacuo*. The resulting solid was subjected to ^1H as well as to a ^{119}Sn hydrogen coupled NMR measurement in C_6D_6. NMR ($CDCl_3$, 112 MHz): δ -272.6, -345.9 ppm.

11.15.4.3 Synthesis of ASnCl$_3$ via a Sn(II) Species (c)

0.5 g 9-bromoanthracene **ABr** (1.9 mmol, 1 eq.) were dissolved in 20 mL THF and cooled to -78 °C using an ethanol/N_2(*l*) bath. Then 1.1 *n*-BuLi (0.86 mL, 2.5 M in hexane) were added which led to an immediate dark orange color. The reaction mixture as stirred for 1h. Afterwards 0.41 g $SnCl_2$ (2.1 mmol, 1.1 eq.) in 14 mL THF were added and the reaction mixture changes color from orange to dark red. The suspension was stirred for another 1h at -30 °C and afterwards 2.7 mL CCl_4 (14 eq.) were added leading to a color change from dark red to yellowish green. The reaction mixture is stirred overnight and allowed to warm up to room temperature. The solvent was removed under *vacuo* and the resulting solid taken up in toluene forming a precipitate which was filtered off. The solvent was removed under reduced pressure to result in a brown solid and a ^{1}H, ^{13}C and ^{119}Sn NMR were taken in $CDCl_3$. NMR ($CDCl_3$, 112 MHz): δ -45.4 ppm.

11.15.4.4 Synthesis of ASnCl$_3$ via Oxidative Addition (d)

0.5 g 9-bromoanthracene **ABr** (1.9 mmol, 1 eq.) were dissolved in 10 mL THF and a solution of 0.37 $SnCl_2$ (1.9 mmol, 1 eq.) in 10 mL THF was added at room temperature using a syringe. The reaction mixture was stirred at room temperature for 2 d and afterwards refluxed for 5 d. The reaction was monitored *via* NMR spectroscopy. No reaction took place.

11.15.5 Chapter 5

11.15.5.1 Synthesis of (phenyl$_2$Sn)$_6$ 42 & (phenyl$_2$Sn)$_7$ 43

1 ml of phenyl$_2$SnH$_2$ (**31**) (1.53 g, 5.6 mmol, 1 eq.) was diluted in 10 mL dried and deoxygenated diethyl ether. The mixture was cooled to -30 °C using a liquid nitrogen ethanol bath. Afterwards, 1.2 ml TMEDA (0.92 g, 8.0 mmol, 1.4 eq.) was added with a syringe *via* a septum. After 15 min reaction time the reaction mixture was brightly yellow. The mixture was stirred at -30 °C for 1 h and afterwards allowed to warm up to room temperature. Subsequently, the yellow polystannane was filtered off, washed twice with 5 mL ether and dried in *vacuo* to result in 1.25 g yellow solid.

Measuring the ether filtrate using a D_2O capillary revealed two peaks in the ^{119}Sn NMR (-210 ppm and 221 ppm). The filtrate was concentrated and toluene was added until all precipitate dissolved while heating. Two separate crystals could be subjected to single crystal analysis and where identified as (phenyl$_2$Sn)$_6$ (**42**) and (phenyl$_2$Sn)$_7$ (**43**).

11.15.6 Chapter 6

11.15.6.1 Thermally Induced Dehydrocoupling

H$_2$[(*o*-tolyl)Sn–Sn(*o*-tolyl)]H$_2$ 55: *o*-tolylSnH$_3$ (**36**) is warmed up to 80 °C under *vacuo* (10^{-4} mbar) to afford mainly dark red to brown polymeric product. The latter is taken up in benzene to precipitate the polymer which is filtered off. The resulting filtrate is subjected to NMR analysis. ^{1}H NMR (C_6D_6, 300 MHz): δ 7.47 (d, 2H, $^3J(^1\text{H-}^{119/117}\text{Sn})$= 62.6 Hz, H6), 7.13-6.85 (m, 6H, H3-H5), 5.07 (s, 4H, $^1J(^1\text{H-}^{119}\text{Sn})$= 1734 Hz, $^1J(^1\text{H-}^{117}\text{Sn})$= 1656 Hz, $^2J(^1\text{H-}^{119/117}\text{Sn})$= 135 Hz, $^3J(^1\text{H-}^1\text{H})$= 3.9 Hz, Sn-H), 2.19 (s, 6H, CH_3) ppm. ^{13}C NMR (C_6D_6, 75.5 MHz): δ 144.8 (C2), 139.2 ($^4J(^{13}\text{C-}^{119/117}\text{Sn})$= 12.3 Hz, C4), 135.5 (C1), 129.8 (C6), 129.5 (C5), 126.1 ($^3J(^{13}\text{C-}^{119/117}\text{Sn})$= 56.0 Hz, C3), 26.1 (C7) ppm. ^{119}Sn (^{1}H coupled) NMR (C_6D_6, 112 MHz): -370.7 (tt, $^1J(^{119}\text{Sn-}^1\text{H})$= 1734 Hz, $^2J(^1\text{H-}^{119}\text{Sn})$= 135 Hz) ppm.

11.15.7 Chapter 7 & 8

11.15.7.1 General Procedure for the Amine Base Induced Dehydrocoupling

A Schlenk equipped with a stirring bar is charged with dried and degassed solvent and amine base. Subsequently, an equimolar amount of *o*-tolylSnH$_3$ (**36**) is added using a syringe. The reaction is stirred overnight. Afterwards, the precipitated polymer is filtered off and the resulting filtrate subjected to a GC-MS as well as ^{1}H and ^{119}Sn NMR analysis.

***o*-tolyl@Sn** from **TMEDA**: 4.43 g **36** (20.8 mmol, 2.8 mL), 11 mL Et_2O, 3.1 mL TMEDA (20.8 mmol, 2.42 g, 1 eq.). Anal. Found: C, 27.57; H, 2.42; N, 0.72.

***o*-tolyl@Sn** from **pyridine**: 0.17 g **36** (0.8 mmol, 1 mL 0.8 M Et_2O solution), 5 mL Et_2O, 0.8 mmol pyridine (0.06 g, 0.06 mL, 1 eq.). Anal. Found: C, 5.63; H, 0.69; N, 0.39.

***o*-tolyl@Sn** from **DMF**: 0.17 g **36** (0.8 mmol, 1 mL 0.8 M Et_2O solution), 5 mL Et_2O, 0.8 mmol DMF (0.06 g, 0.06 mL, 1 eq.).

***o*-tolyl@Sn** from **Et_3N**: 0.17 g **36** (0.8 mmol, 1 mL 0.8 M Et_2O solution), 5 mL Et_2O, 0.8 mmol Et_3N (0.08 g, 0.11 mL, 1 eq.). Anal. Found: C, 22.63; H, 1.89; N, 0.39.

***o*-tolyl@Sn** from **DMAP**: 0.80 g **36** (3.76 mmol, 0.5 mL), 14 mL benzene, 3.76 mmol DMAP (0.46 g, 1 eq.). Anal. Found: C, 32.80; H, 3.01; N, 2.68.

***o*-tolyl@Sn** from **DETA**: 0.80 g **36** (3.76 mmol, 0.5 mL), 12 mL Et_2O, 3.76 mmol DETA (0.39 g, 0.4 mL, 1 eq.). Anal. Found: C, 26.95; H, 3.08; N, 4.49.

***o*-tolyl@Sn** from **phenanthroline**: 0.39 g **36** (1.83 mmol), 10 mL benzene, 1.83 mmol phenanthroline (0.33 g, 1 eq.).

11.15.8 Chapter 9

11.15.8.1 VT-NMR Studies of the Dehydrogenative Coupling Reaction of phenyl$_2$SnH$_2$ (31)

A NMR tube with a screw cap and septum is filled with 0.4 ml Et_2O, 0.05 ml phenyl$_2$SnH$_2$ (**31**) (0.08 g, 0.28 mmol, 1 eq.) and 0.1 ml C_6D_6. The solution is cooled to -80 °C using an ethanol/N_2 (*l.*) bath and afterwards 0.2 ml TMEDA (1.32 mmol, 4.8 eq.) are added with a syringe *via* the septum. The NMR tube is immediately transferred in the precooled NMR machine (-50 °C). ^{119}Sn NMR spectra are recorded applying a continuous wave decoupling modus with a decoupler power of 63 dB.

Hydrogenation with LAH: 0.07 g of L^{CN} containing organotin halogenide (**49**, **50**) were dissolved in 0.5 ml THF-d_8 in a screwable NMR tube with septum. The educt solution was cooled to -80 °C using an ethanol/N_2 (*l.*) bath. Then 0.06 mL of a 2 M THF-d_8/$LiAlH_4$ solution were added *via* the septum with a syringe and the NMR tube was placed in the precooled (-80 °C) NMR machine.

Hydrogenation with $K(BEt_3)H^{\cdot}THF$: 0.03 g of $L^{CN}SnPhCl_2$ (**49**) (0.075 mmol) were dissolved in 0.5 ml THF and 0.1 mL of C_6D_6 in a screwable NMR tube with septum. The educt solution was cooled to -80 °C using an ethanol/N_2 (*l.*) bath. Then 0.15 mL of the $K(BEt_3)H^{\cdot}THF$ (1 M, 0.15 mmol, 2 eq.) solution were added *via* the septum with a syringe and the NMR tube was placed in the precooled (-80 °C) NMR machine.

Hydrogenation with $BH_3^{\cdot}THF$: 0.05 g of $L^{CN}SnPhCl_2$ (**49**) (0.12 mmol) were dissolved in 0.5 ml THF-d_8 in a screwable NMR tube with septum. The educt solution was cooled to -80 °C using an ethanol/N_2 (*l.*) bath. Then 0.13 mL of $BH_3{\cdot}THF$ solution (1 M, 0.13 mmol, 1 eq.) were added *via* the septum with a syringe and the NMR tube was placed in the precooled (-80 °C) NMR machine.

11.15.8.2 Synthesis of L^{CN} containing organotin hydrides

Schlenk reactions

A flask furnished with a dropping funnel was charged with $LiAlH_4$ in Et_2O. A solution of the *C,N* chelated organotin halide (**49**,**50**,**51**) in Et_2O was added slowly *via* the dropping funnel. After complete addition degassed water was added slowly. The phases were separated *via* a cannula and the aqueous layer washed twice with Et_2O. The combined organic phases were dried over $CaCl_2$ and subsequently the solvent was evaporated.[80]

$L^{CN}{}_2SnBuH$ 52: 0.08 g LAH pellets (20.8 mmol, 1 eq.), $L^{CN}{}_2SnBuCl$ **49** (1 g, 20.8 mmol ,1 eq.). The yellowish oil was recrystallized from pentane at -20 °C to afford colorless crystals. Yield: 54 % (0.5 g, 11.2 mmol). ^1H NMR (C_6D_6, 300 MHz): δ 7.74-7.65 (m, 2H, $^3J(^1H-^{119/117}Sn)$= 54.1 Hz, H6), 7.17-6.91 (m, 6H, H3-h5), 6.38 (s, 1H, $^1J(^1H-^{119}Sn)$= 1980 Hz, $^1J(^1H-^{117}Sn)$= 1894 Hz), Sn-H), 3.30-3.13 (m, 4H, N-CH_2), 1.82 (s, 12H, $N(CH_3)_2$), 1.77-1-69 (m, 2H, H9), 1.52-1.36 (q, 2H, H8), 1.37-1.21 (t, 2H, H7), 0.91-0.84 (t, 3H, H10) ppm. ^{13}C NMR (C_6D_6, 75.5 MHz): δ 145.7 ($^2J(^{13}C-^{119/117}Sn)$= 24.1, C2), 143.8 ($^1J(^{13}C-^{119}Sn)$= 539.5 Hz, $^1J(^{13}C-^{117}Sn)$= 517.2 Hz, C1), 138.0 ($^3J(^{13}C-^{119/117}Sn)$= 40.0 Hz,C6), 128.6 ($^4J(^{13}C-^{119/117}Sn)$= 10.3 Hz, C4), 128.2 (couplings under $C_6D_{6,}$ C3 or C5), 126.9 ($^3J(^{13}C-^{119/117}Sn)$= 52.3 Hz, C3 or C5), 66.3 ($^3J(^{13}C-^{119/117}Sn)$= 21.0 Hz, N-$\underline{C}H_2$), 44.5 (N-$(\underline{C}H_3)_2$), 30.7 ($^3J(^{13}C-^{119/117}Sn)$= 17.4 Hz, C9), 27.9 ($^2J(^{13}C-^{119/117}Sn)$= 66.9, C8), 14.1 (C10), 12.6 $^{1}J(^{13}C-^{119}Sn)$= 396.4 Hz, $^{1}J(^{13}C-^{117}Sn)$= 379.2, C7) ppm. ^{119}Sn NMR (C_6D_6, 112 MHz): -161.9 ($^{1}J(^{119}Sn-^{1}H)$= 1980 Hz) ppm.

L^{CN}SnPhH$_2$ 53: ^{1}H NMR (d_8-THF, 300 MHz, -80 °C): δ 7.67-7.09 (m, 9H), 5.99 (s, 2H, $^{1}J(^{1}H-^{119}Sn)$= 2074 Hz, $^{1}J(^{1}H-^{117}Sn)$= 1983 Hz), Sn-H$_2$), 3.59 (s, 2H, N-C$\underline{H}_2$), 2.17 (s, 6H, N(C$\underline{H}_3$)$_2$) ppm. ^{13}C NMR (d_8-THF, 75.5 MHz, -80 °C): δ 146.7 ($^{x}J(^{13}C-^{119/117}Sn)$ = 28.5 Hz, 144.1, 138.6, 138.0, 137.7, 130.0, 129.3, 129.1, 128.8, 128.6, 128.0, 64.3 (N-$\underline{C}$H$_2$), 43.8 ($\underline{N}$-(CH$_3$)$_2$) ppm. ^{119}Sn NMR (d_8-THF, 112 MHz, -80 °C): -246.2 ($^{1}J(^{1}H-^{119}Sn)$= 2075) ppm.

L^{CN}SnH$_3$ 54: ^{1}H NMR (d_8-THF, 300 MHz, -80 °C): δ 7.54 (d, 1H, $^{3}J(^{1}H-^{119/117}Sn)$= 66.7 Hz, H6), 7.46-6.80 (m, 5H, aromatic Hs), 5.10 (s, 3H, $^{1}J(^{1}H-^{119}Sn)$= 1877 Hz, $^{1}J(^{1}H-^{117}Sn)$= 1795 Hz), Sn-H$_3$), 3.47 (s, 2H, N-C$\underline{H}_2$), 2.13 (s, 6H, N(C$\underline{H}_3$)$_2$) ppm. ^{13}C NMR (d_8-THF, 75.5 MHz, -80 °C): δ 145.5 ($^{2}J(^{13}C-^{119/117}Sn)$= 29.6 Hz, C2), 139.5 ($^{3}J(^{13}C-^{119/117}Sn)$= 52.4 Hz, C3/C5) 136.1 (C1), 130.1 ($^{4}J(^{13}C-^{119/117}Sn)$= 11.6 Hz, C4), 128.6 ($^{3}J(^{13}C-^{119/117}Sn)$= 48.2 Hz, C3/C5) 128.1 (C6), 64.0 ($^{3}J(^{13}C-^{119/117}Sn)$= 28.2 Hz, N-$\underline{C}H_2$), 43.6 ($^{3}J(^{13}C-^{119/117}Sn)$= 9.7 Hz $\underline{N}$-(CH$_3$)$_2$) ppm. ^{119}Sn NMR (d_8-THF, 112 MHz, -80 °C): -339.3 ($^{1}J(^{1}H-^{119}Sn)$= 1880) ppm.

12 References

[1] von Frankland, E. *Justus Liebigs Ann. Chem.* **1849**, *71*, 171.
[2] von Frankland, E. *Justus Liebigs Ann. Chem.* **1849**, *71*, 213.
[3] Seyferth, D. *Organometallics* **2001**, *20*, 1488.
[4] C., Z. W. *Ann. Phys.* **1827**, *2*.
[5] Zard, S. Z. *Radical Reactions in Organic Synthesis*; Oxford University Press, 2003.
[6] Choffat, F.; Smith, P.; Caseri, W. *J. Mater. Chem.* **2005**, *15*, 1789.
[7] Bukalov, S. S.; Leites, L. A.; Lu, V.; Tilley, T. D. *Macromolecules* **2002**, *35*, 1757.
[8] Schittelkopf, K.; Fischer, R. C.; Meyer, S.; Wilfling, P.; Uhlig, F. *Appl. Organomet. Chem.* **2010**, *24*, 897.
[9] Sharma, H. K.; Arias-Ugarte, R.; Metta-Magana, A. J.; Pannell, K. H. *Angew. Chem. Int. Ed.* **2009**, *48*, 6309.
[10] Khan, A.; Gossage, R. A.; Foucher, D. A. *Can. J. Chem.* **2010**, *88*, 1046.
[11] Lechner, M.-L.; Trummer, M.; Braeunlich, I.; Smith, P.; Caseri, W.; Uhlig, F. *Appl. Organomet. Chem.* **2011**, *25*, 769.
[12] Finholt, A. E.; Bond, A. C., Jr.; Wilzbach, K. E.; Schlesinger, H. I. *J. Am. Chem. Soc.* **1947**, *69*, 2692.
[13] van der Kerk, G. J. M.; Luijten, J. G. A. *J. Appl. Chem.* **1957**, *7*, 369.
[14] Sonika; Narula, A. K. *Int. J. Chem. Sci.* **2003**, *1*, 141.
[15] Wrackmeyer, B. In *Annual Reports on NMR Spectroscopy*; Webb, G. A., Ed.; Academic Press: 1985; Vol. Volume 16, p 73.
[16] Davies, A. G. In *Tin Chemistry*; John Wiley & Sons, Ltd: 2008, p 1.
[17] Harrison, P. G. *Chemistry of tin*; Blackie, 1989.
[18] *Mineral commodity summaries 2015*, 2015.
[19] Hoch, M. *Appl. Geochem.* **2001**, *16*, 719.
[20] Guard, H. E.; Cobet, A. B.; Coleman, W. M. *Science* **1981**, *213*, 770.
[21] van der Kerk, G. J. M.; Luijten, J. G. A. *J. Appl. Chem.* **1954**, *4*, 314.
[22] van der Kerk, G. J. M.; Luijten, J. G. A. *J. Appl. Chem.* **1956**, *6*, 56.
[23] Nath, M.; Eng, G.; Song, X.; Beraldo, H.; de Lima, G. M.; Pettinari, C.; Marchetti, F.; Whalen, M. M.; Beltrán, H. I.; Santillan, R.; Farfán, N. In *Tin Chemistry*; John Wiley & Sons, Ltd: 2008, p 413.
[24] Smith, P. J.; Luijten, J. G. A.; Klimmer, O. R.; Institute, I. T. R. *Toxicological Data on Organotin Compounds*; International Tin Research Institute, 1978.
[25] Chagot, D.; Alzieu, C.; Sanjuan, J.; Grizel, H. *Aquat. Living Resour.* **1990**, *3*, 121.
[26] Iwata, H.; Tanabe, S.; Mizuno, T.; Tatsukawa, R. *Environ. Sci. Technol.* **1995**, *29*, 2959.
[27] Randall, L.; Weber, J. H. *Sci. Total Environ.* **1986**, *57*, 191.
[28] Buckton, G. B. *Philos. T. R. Soc. Lond.* **1859**, *149*, 417.
[29] Pope, W. J.; Peachey, S. J. *Proceedings Chem. Soc.* **1903**, *19*, 290.
[30] Pfeiffer, P.; Schnurmann, K. *Ber. Dtsch. Chem. Ges.* **1904**, *37*, 319.
[31] Pfeiffer, P. *Ber. Dtsch. Chem. Ges.* **1911**, *44*, 1269.
[32] Thoonen, S. H. L.; Deelman, B.-J.; Van Koten, G. *J. Organomet. Chem.* **2004**, *689*, 2145.
[33] Ingham, R. K.; Rosenberg, S. D.; Gilman, H. *Chem. Rev.* **1960**, *60*, 459.
[34] Edgell, W. F.; Ward, C. H. *J. Am. Chem. Soc.* **1954**, *76*, 1169.
[35] Clark, H. C.; Willis, C. J. *J. Am. Chem. Soc.* **1960**, *82*, 1888.
[36] Foldesi, I. *Acta Chim. Acad. Sci. Hung.* **1965**, *45*, 237.
[37] Zimmer, H.; Gold, H. *Chem. Ber.* **1956**, *89*, 712.
[38] van der Kerk, G. J. M.; Luijten, J. G. A. *Org. Synth.* **1956**, *36*, 86.

[39] Saitow, A.; Rochow, E. G.; Seyferth, D. *J. Org. Chem.* **1958**, *23*, 116.

[40] Bogdanovic, B.; Bons, P.; Konstantinovic, S.; Schwickardi, M.; Westeppe, U. *Chem. Ber.* **1993**, *126*, 1371.

[41] Natoli, J. G.; M and T Chemicals Inc. . 1968, p 3 pp.

[42] Rosenberg, S. D.; Gibbons, A. J., Jr.; Ramsden, H. E. *J. Am. Chem. Soc.* **1957**, *79*, 2137.

[43] Fishwick, M.; Wallbridge, M. G. H. *J. Organomet. Chem.* **1970**, *25*, 69.

[44] Naruta, Y.; Nishigaichi, Y.; Maruyama, K. *Tetrahedron* **1989**, *45*, 1067.

[45] Denmark, S. E.; Wilson, T.; Willson, T. M. *J. Am. Chem. Soc.* **1988**, *110*, 984.

[46] Ballczo, H.; Schiffner, H. *Fresenius' Z. Anal. Chem.* **1956**, *152*, 3.

[47] Sharma, R. K.; Sharma, C. P.; Sharma, A. *J. Indian Chem. Soc.* **1987**, *64*, 205.

[48] Srivastava, T. N.; Bhattacharya, S. N. *Z. Anorg. Allg. Chem.* **1966**, *344*, 102.

[49] Smith, T. A.; Kipping, F. S. *J. Chem. Soc., Trans.* **1912**, *101*, 2553.

[50] Morris, H.; Byerly, W.; Selwood, P. W. *J. Am. Chem. Soc.* **1942**, *64*, 1727.

[51] Ramsden, H. E.; Gloskey, C. R.; Metal & Thermit Corp. . 1954.

[52] van der Kerk, G. J. M.; Luijten, J. G. A. *J. Appl. Chem.* **1954**, *4*, 301.

[53] Chambers, R. F.; Scherer, P. C. *J. Am. Chem. Soc.* **1926**, *48*, 1054.

[54] Takeda, Y.; Okuyama, T.; Fueno, T.; Furukawa, J. *Makromol. Chem.* **1964**, *76*, 209.

[55] Neumann, W. P.; Koenig, K. *Justus Liebigs Ann. Chem.* **1964**, *677*, 1.

[56] Sundermeyer, W.; Verbeek, W. *Angew. Chem., Int. Ed. Engl.* **1966**, *5*, 1.

[57] Sisido, K.; Kozima, S. *J. Organomet. Chem.* **1968**, *11*, 503.

[58] Koermer, G. S.; Hall, M. L.; Traylor, T. G. *J. Amer. Chem. Soc.* **1972**, *94*, 7205.

[59] San Filippo, J., Jr.; Silbermann, J. *J. Am. Chem. Soc.* **1982**, *104*, 2831.

[60] Kitching, W.; Olszowy, H.; Waugh, J.; Doddrell, D. *J. Org. Chem.* **1978**, *43*, 898.

[61] Shaikh, N. S.; Parkin, S.; Lehmler, H.-J. *Organometallics* **2006**, *25*, 4207.

[62] Abraham, M. H.; Hill, J. A. *J. Organomet. Chem.* **1967**, *7*, 11.

[63] Zeppek, C.; Fischer, R. C.; Torvisco, A.; Uhlig, F. *Can. J. Chem.* **2014**, *92*, 556.

[64] Gilman, H.; Melvin, H. W., Jr. *J. Am. Chem. Soc.* **1949**, *71*, 4050.

[65] d'Ans, J.; Zimmer, H. *Chem. Ber.* **1952**, *85*, 585.

[66] Cuthbertson, M. J.; Wells, P. R. *J. Organomet. Chem.* **1981**, *216*, 331.

[67] Smith, G. F.; Kuivila, H. G.; Simon, R.; Sultan, L. *J. Am. Chem. Soc.* **1981**, *103*, 833.

[68] Shishido, K.; Takeda, Y.; Kinugawa, J. *J. Am. Chem. Soc.* **1961**, *83*, 538.

[69] Anderson, H. H. *Inorg. Chem.* **1962**, *1*, 647.

[70] Rosenberg, S. D.; Debreczeni, E.; Weinberg, E. L. *J. Am. Chem. Soc.* **1959**, *81*, 972.

[71] Srivastava, T. N.; Tandon, S. K. *Indian J. Appl. Chem.* **1963**, *26*, 171.

[72] Krause, E. *Ber. Dtsch. Chem. Ges.* **1918**, *51*, 912.

[73] Sisido, K.; Kozima, S.; Hanada, T. *J. Organomet. Chem.* **1967**, *9*, 99.

[74] Ziegler, K. 1963, p 5 pp.

[75] Neumann, W. P. *Justus Liebigs Ann. Chem.* **1962**, *653*, 157.

[76] Van Koten, G.; Schaap, C. A.; Noltes, J. G. *J. Organomet. Chem.* **1975**, *99*, 157.

[77] Coffer, P. K.; Dillon, K. B.; Howard, J. A. K.; Yufit, D. S.; Zorina, N. V. *Dalton Trans.* **2012**, *41*, 4460.

[78] Aminabhavi, T. M.; Biradar, N. S.; Patil, S. B.; Hoffman, D. E. *Inorg. Chim. Acta* **1985**, *108*, L31.

[79] Aminabhavi, T. M.; Biradar, N. S.; Patil, S. B.; Hoffman, D. E.; Biradar, V. N. *Inorg. Chim. Acta* **1987**, *135*, 139.

[80] Zeppek, C.; Pichler, J.; Torvisco, A.; Flock, M.; Uhlig, F. *J. Organomet. Chem.* **2013**, *740*, 41.

[81] Kozeshkov, K. A. *Ber. Dtsch. Chem. Ges. B* **1929**, *62B*, 996.

[82] Gilman, H.; Gist, L. A., Jr. *J. Org. Chem.* **1957**, *22*, 368.

[83] Seyferth, D.; Stone, F. G. A. *J. Am. Chem. Soc.* **1957**, *79*, 515.

[84] Kocheshkov, K. A. *Ber. Dtsch. Chem. Ges. B* **1933**, *66B*, 1661.

[85] Buschhoff, M.; Neumann, W. P.; Schering A.-G., Fed. Rep. Ger. . 1985, p 18 pp.
[86] Dillon, K. B.; Hewitson, G. F. *Polyhedron* **1984**, *3*, 957.
[87] Zakharkin, L. I.; Okhlobystin, O. Y.; Strunin, B. N. *Izv. Akad. Nauk SSSR, Ser. Khim.* **1962**, 2002.
[88] Grosse, A. V.; Mavity, J. M. *J. Org. Chem.* **1940**, *5*, 106.
[89] Brown, P.; Mahon, M. F.; Molloy, K. C. *J. Organomet. Chem.* **1992**, *435*, 265.
[90] Jaekle, F.; Manners, I. *Organometallics* **1999**, *18*, 2628.
[91] Armitage, D. A.; Tarassoli, A. *Inorg. Chem.* **1975**, *14*, 1210.
[92] Bade, V.; Huber, F. *J. Organomet. Chem.* **1970**, *24*, 387.
[93] Narula, S. P.; Sharma, R. K.; Lata, S.; Walia, R. *Indian J. Chem., Sect. A* **1983**, *22A*, 246.
[94] Oakes, V.; Hutton, R. E. *J. Organomet. Chem.* **1965**, *3*, 472.
[95] Oakes, V.; Hutton, R. E. *J. Organomet. Chem.* **1966**, *6*, 133.
[96] Matsuda, H.; Hayashi, J.; Matsuda, S. *Kogyo Kagaku Zasshi* **1961**, *64*, 1951.
[97] Boga, C.; Savoia, D.; Tagliavini, E.; Trombini, C.; Umani-Ronchi, A. *J. Organomet. Chem.* **1988**, *353*, 177.
[98] Verbeek, F.; Bulten, E. J.; Van den Hurk, J. W. G.; Commer S.r.l., Italy . 1976, p 11 pp.
[99] Smith, A. C., Jr.; Rochow, E. G. *J. Am. Chem. Soc.* **1953**, *75*, 4103.
[100] Ugo, R.; Chiesa, A.; Fusi, A. *J. Organomet. Chem.* **1987**, *330*, 25.
[101] Kocheshkov, K. A.; Nesmeyanov, A. N. *Ber. Dtsch. Chem. Ges. B* **1931**, *64B*, 628.
[102] Kocheshkov, K. A.; Nadi, M. M. *Ber. Dtsch. Chem. Ges. B* **1934**, *67B*, 717.
[103] Neumann, W. P.; Burkhardt, G. *Justus Liebigs Ann. Chem.* **1963**, *663*, 11.
[104] Zimmer, H.; Sparmann, H. W. *Chem. Ber.* **1954**, *87*, 645.
[105] Burley, J. W.; AKZO G.m.b.H., Fed. Rep. Ger. . 1977, p 9 pp.
[106] Buschhoff, M.; Mueller, K. H.; Schering A.-G., Fed. Rep. Ger. . 1976, p 10 pp.
[107] Janiak, C.; Schwichtenberg, M.; Hahn, F. E. *J. Organomet. Chem.* **1989**, *365*, 37.
[108] Bulten, E. J. *J. Organomet. Chem.* **1975**, *97*, 167.
[109] Elhamzaoui, H.; Jousseaume, B.; Toupance, T.; Allouchi, H. *Organometallics* **2007**, *26*, 3908.
[110] Matsuda, S.; Kudara, H.; Chugoku Marine Paints, Ltd., Japan . 1976, p 3 pp.
[111] Lazarev, I. M.; Dolgushin, G. V.; Feshin, V. P.; Voronkov, M. G. *Mendeleev Commun.* **1996**, 150.
[112] Saito, M.; Hashimoto, H.; Tajima, T.; Ikeda, M. *J. Organomet. Chem.* **2007**, *692*, 2729.
[113] Voronkov, M. G.; Egorochkin, A. N. In *The Chemistry of Organic Germanium, Tin and Lead Compounds*; John Wiley & Sons, Ltd: 2003, p 131.
[114] Dillard, C. R.; McNeill, E. H.; Simmons, D. E.; Yeldell, J. B. *J. Am. Chem. Soc.* **1958**, *80*, 3607.
[115] Paneth, F. *Ber. Dtsch. Chem. Ges. B* **1920**, *53B*, 1710.
[116] Kraus, C. A.; Greer, W. N. *J. Am. Chem. Soc.* **1922**, *44*, 2629.
[117] Wittig, G.; Meyer, F. J.; Lange, G. *Justus Liebigs Ann. Chem.* **1951**, *571*, 167.
[118] Bullard, R. H.; Vinger, R. A. *J. Am. Chem. Soc.* **1929**, *51*, 892.
[119] Gilman, H.; Eisch, J. *J. Org. Chem.* **1955**, *20*, 763.
[120] Lorenz, D. H.; Shapiro, P.; Stern, A.; Becker, E. I. *J. Org. Chem.* **1963**, *28*, 2332.
[121] Stern, A.; Becker, E. I. *J. Org. Chem.* **1964**, *29*, 3221.
[122] Considine, W. J.; Ventura, J. J. *Chem. Ind.* **1962**, 1683.
[123] Ziegler, K.; Gellert, H. G.; Zosel, K.; Lehmkuhl, W.; Pfohl, W. *Angew. Chem.* **1955**, *67*, 424.
[124] Kula, M. R.; Amberger, E.; Rupprecht, H. *Chem. Ber.* **1965**, *98*, 629.
[125] van der Kerk, G. J. M.; Noltes, J. G.; Luijten, J. G. A. *Chem. Ind.* **1958**, 1290.
[126] Tamborski, C.; Soloski, E. J. *J. Am. Chem. Soc.* **1961**, *83*, 3734.
[127] Tamborski, C.; Ford, F. E.; Soloski, E. J. *J. Org. Chem.* **1963**, *28*, 181.
[128] Tamborski, C.; Ford, F. E.; Soloski, E. J. *J. Org. Chem.* **1963**, *28*, 237.
[129] Kula, M. R.; Lorberth, J.; Amberger, E. *Chem. Ber.* **1964**, *97*, 2087.
[130] Emeleus, H. J.; Kettle, S. F. A. *J. Chem. Soc.* **1958**, 2444.

[131] Pichler, J.; Torvisco, A.; Bottke, P.; Wilkening, M.; Uhlig, F. *Can. J. Chem.* **2014**, *92*, 565.

[132] Gilman, H.; Rosenberg, S. D. *J. Org. Chem.* **1953**, *18*, 1554.

[133] Anderson, H. H. *J. Am. Chem. Soc.* **1957**, *79*, 4913.

[134] Choffat, F.; Smith, P.; Caseri, W. *Adv. Mater.* **2008**, *20*, 2225.

[135] de Lima, G. M.; Toupance, T.; Arkis, E.; Chaniotakis, N.; Cusack, P. A.; Lacroix, P. G.; Farfán, N.; Jousseaume, B.; Sharma, H. K.; Pannell, K. H.; Haiduc, I.; Tiekink, E. R. T.; Zukerman-Schpector, J. In *Tin Chemistry*; John Wiley & Sons, Ltd: 2008, p 285.

[136] Adams, S.; Draeger, M. *Angew. Chem.* **1987**, *99*, 1280.

[137] Adams, S.; Draeger, M. *Main Group Met. Chem.* **1988**, *11*, 151.

[138] Lu, V. Y.; Tilley, T. D. *Macromolecules* **2000**, *33*, 2403.

[139] Skotheim, T. A. *Handbook of Conducting Polymers, Second Edition*; Taylor & Francis, 1997.

[140] Brédas, J. L.; Silbey, R. *Conjugated Polymers: The Novel Science and Technology of Highly Conducting and Nonlinear Optically Active Materials*; Springer Netherlands, 2012.

[141] Carraher, C. E.; Currell, B.; Pittman, C.; Sheats, J.; Zeldin, M. *Inorganic and Metal-Containing Polymeric Materials*; Springer US, 2012.

[142] Miles, D.; Burrow, T.; Lough, A.; Foucher, D. *J. Inorg. Organomet. Polym. Mater.* **2010**, *20*, 544.

[143] Löwig, C. *J. Prakt. Chem.* **1852**, *57*, 385.

[144] Cahours, A. *Compt. rend.* **1879**, *88*, 725.

[145] Cahours, A.; Demarcay, E. *Compt. rend.* **1879**, *88*, 1112.

[146] Devylder, N.; Hill, M.; Molloy, K. C.; Price, G. J. *Chem. Commun.* **1996**, 711.

[147] Mustafa, A.; Achilleos, M.; Ruiz-Iban, J.; Davies, J.; Benfield, R. E.; Jones, R. G.; Grandjean, D.; Holder, S. J. *React. Funct. Polym.* **2006**, *66*, 123.

[148] Priestley, R.; Walser, A. D.; Dorsinville, R.; Zou, W. K.; Xu, D. Y.; Yang, N. L. *Opt. Commun.* **1996**, *131*, 347.

[149] Imori, T.; Lu, V.; Cai, H.; Tilley, T. D. *J. Am. Chem. Soc.* **1995**, *117*, 9931.

[150] Harada, T. *Sci. Pap. Inst. Phys. Chem. Res. (Jpn.)* **1939**, *35*, 290.

[151] Holder, S. J.; Jones, R. G.; Benfield, R. E.; Went, M. J. *Polymer* **1996**, *37*, 3477.

[152] Bratton, D.; Holder, S. J.; Jones, R. G.; Wong, W. K. C. *J. Organomet. Chem.* **2003**, *685*, 60.

[153] Jones, R. G.; Holder, S. J. *Polym. Int.* **2006**, *55*, 711.

[154] Trummer, M.; Solenthaler, D.; Smith, P.; Caseri, W. *RSC Adv.* **2011**, *1*, 823.

[155] Jousseaume, B.; Noiret, N.; Pereyre, M.; Saux, A.; Frances, J. M. *Organometallics* **1994**, *13*, 1034.

[156] Beckmann, J.; Duthie, A.; Grassmann, M.; Semisch, A. *Organometallics* **2008**, *27*, 1495.

[157] Sommer, R.; Neumann, W. P.; Schneider, B. *Tetrahedron Lett.* **1964**, *5*, 3875.

[158] Harrypersad, S.; Foucher, D. *Chem. Commun.* **2015**, *51*, 7120.

[159] Harrypersad, S.; Liao, L.; Khan, A.; Wylie, R. S.; Foucher, D. *J. Inorg. Organomet. Polym.* **2015**, *25*, 515.

[160] Okano, M.; Matsumoto, N.; Arakawa, M.; Tsuruta, T.; Hamano, H. *Chem. Commun.* **1998**, 1799.

[161] Okano, M.; Watanabe, K. *Electrochem. Commun.* **2000**, *2*, 471.

[162] Okano, M.; Watanabe, K.; Totsuka, S. *Electrochemistry* **2003**, *71*, 257.

[163] Thompson, S. M.; Schubert, U. *Inorg. Chim. Acta* **2003**, *350*, 329.

[164] Imori, T.; Tilley, T. D. *J. Chem. Soc., Chem. Commun.* **1993**, 1607.

[165] Neale, N. R.; Tilley, T. D. *J. Am. Chem. Soc.* **2002**, *124*, 3802.

[166] Woo, H.-G.; Park, J.-M.; Song, S.-J.; Yang, S.-Y.; Kim, I.-S.; Kim, W.-G. *Bull. Korean Chem. Soc.* **1997**, *18*, 1291.

[167] Woo, H.-G.; Song, S.-J.; Kim, B.-H. *Bull. Korean Chem. Soc.* **1998**, *19*, 1161.

[168] Choffat, F.; Kaeser, S.; Wolfer, P.; Schmid, D.; Mezzenga, R.; Smith, P.; Caseri, W. *Macromolecules* **2007**, *40*, 7878.

[169] Khan, A.; Komejan, S.; Patel, A.; Lombardi, C.; Lough, A. J.; Foucher, D. A. *J. Organomet. Chem.* **2015**, *776*, 180.

[170] Khan, A.; Lough, A. J.; Gossage, R. A.; Foucher, D. A. *Dalton Trans.* **2013**, *42*, 2469.

[171] Ward, J.; Al-Alul, S.; Harrypersad, S.; Foucher, D. A. *Can. J. Chem.* **2014**, *92*, 525.

[172] Davies, A. G.; Osei-Kissi, D. K. *J. Organomet. Chem.* **1994**, *474*, C8.

[173] Mathiasch, B. *Inorg. Nucl. Chem. Lett.* **1977**, *13*, 13.

[174] Neumann, W. P. *The Organic Chemistry of Tin*; Interscience, 1970.

[175] Poller, R. C. *The chemistry of organotin compounds*; Logos P., 1970.

[176] Choffat, F.; Wolfer, P.; Smith, P.; Caseri, W. *Macromol. Mater. Eng.* **2010**, *295*, 210.

[177] Choffat, F.; Buchmueller, Y.; Mensing, C.; Smith, P.; Caseri, W. *J. Inorg. Organomet. Polym. Mater.* **2009**, *19*, 166.

[178] Trummer, M.; Nauser, T.; Lechner, M.-L.; Uhlig, F.; Caseri, W. *Polym. Degrad. Stab.* **2011**, *96*, 1841.

[179] Trummer, M.; Choffat, F.; Smith, P.; Caseri, W. *Macromol. Rapid Commun.* **2012**, *33*, 448.

[180] Voronkov, M. G.; Abzaeva, K. A. In *The Chemistry of Organic Germanium, Tin and Lead Compounds*; John Wiley & Sons, Ltd: 2003, p 1.

[181] Neumann, W. P.; Niernmann, H. *Justus Liebigs Ann. Chem.* **1962**, *653*, 164.

[182] Hayes, P. G.; Gribble, C. W.; Waterman, R.; Tilley, T. D. *J. Am. Chem. Soc.* **2009**, *131*, 4606.

[183] Peng, Y.; Brynda, M.; Ellis, B. D.; Fettinger, J. C.; Rivard, E.; Power, P. P. *Chem. Commun.* **2008**, 6042.

[184] Schneider-Koglin, C.; Behrends, K.; Draeger, M. *J. Organomet. Chem.* **1993**, *448*, 29.

[185] Schneider-Koglin, C.; Mathiasch, B.; Draeger, M. *J. Organomet. Chem.* **1994**, *469*, 25.

[186] Buckton, G. B. *Justus Liebigs Ann. Chem.* **1859**, *112*, 220.

[187] Keay, B. A. *Sci. Synth.* **2002**, *4*, 685.

[188] Wharf, I.; Simard, M. G. *J. Organomet. Chem.* **1997**, *532*, 1.

[189] Barbieri, G.; Taddei, F. *J. Chem. Soc., Perkin Trans. 2* **1972**, 1327.

[190] Allen, C. W.; Burroughs, A. E.; Anstey, R. G. *Inorg. Nucl. Chem. Lett.* **1973**, *9*, 1211.

[191] Colton, R.; Dakternieks, D. *Inorg. Chim. Acta* **1988**, *143*, 151.

[192] Al-Allaf, T. A. K. *J. Organomet. Chem.* **1986**, *306*, 337.

[193] Mathiasch, B. *Org. Magn. Resonance* **1981**, *17*, 296.

[194] Trummer, M.; Caseri, W. *Organometallics* **2010**, *29*, 3862.

[195] Bagno, A.; Casella, G.; Ferrante, F.; Saielli, G. *J. Organomet. Chem.* **2013**, *724*, 139.

[196] Casella, G.; Ferrante, F.; Saielli, G. *Org. Biomol. Chem.* **2010**, *8*, 2711.

[197] Wharf, I. *Inorg. Chim. Acta* **1989**, *159*, 41.

[198] Doddrell, D.; Burfitt, I.; Kitching, W.; Bullpitt, M.; Lee, C.-H.; Mynott, R. J.; Considine, J. L.; Kuivila, H. G.; Sarma, R. H. *J. Am. Chem. Soc.* **1974**, *96*, 1640.

[199] Kalinowski, H. O.; Berger, S.; Braun, S. *13C-NMR-Spektroskopie*; Thieme, 1984.

[200] Bent, H. A. *Chem. Rev.* **1961**, *61*, 275.

[201] Kelly, T. R.; Tellitu, I.; Sestelo, J. P. *Angew. Chem., Int. Ed. Engl.* **1997**, *36*, 1866.

[202] Lu, V.; Tilley, T. D. *Macromolecules* **1996**, *29*, 5763.

[203] Brieva, A. C.; Jäger, C.; Huisken, F.; Šiller, L.; Butenko, Y. V. *Carbon* **2009**, *47*, 2812.

[204] Niemann, U.; Marsmann, H. C. *Z. Naturforsch., B: Anorg. Chem., Org. Chem.* **1975**, *30B*, 202.

[205] McDowell, M.; Hill, I. G.; McDermott, J. E.; Bernasek, S. L.; Schwartz, J. *Appl. Phys. Lett.* **2006**, *88*, 073505.

[206] Kelly, T. R.; Sestelo, J. P.; Tellitu, I. *J. Org. Chem.* **1998**, *63*, 3655.

[207] Mueller, U.; Baumgarten, M. *J. Am. Chem. Soc.* **1995**, *117*, 5840.

[208] Bullpitt, M.; Kitching, W.; Adcock, W.; Doddrell, D. *J. Organomet. Chem.* **1976**, *116*, 161.

[209] Kitching, W.; Olszowy, H. A.; Schott, I.; Adcock, W.; Cox, D. P. *J. Organomet. Chem.* **1986**, *310*, 269.

[210] Weisemann, C.; Schmidtberg, G.; Brune, H.-A. *J. Organomet. Chem.* **1989**, *365*, 403.

[211] Sergeeva, N. N.; Scala, A.; Bakar, M. A.; O'Riordan, G.; O'Brien, J.; Grassi, G.; Senge, M. O. *J. Org. Chem.* **2009**, *74*, 7140.

[212] Wolf, C.; Xu, H. *J. Org. Chem.* **2008**, *73*, 162.

[213] Yamada, I.; Yamazaki, N.; Yamaguchi, M.; Yamagishi, T. *J. Mol. Catal. A: Chem.* **1997**, *120*, L13.

[214] Zimmerman, S. C.; Zeng, Z. *J. Org. Chem.* **1990**, *55*, 4789.

[215] Viñas, C.; Barberà, G.; Oliva, J. M.; Teixidor, F.; Welch, A. J.; Rosair, G. M. *Inorg. Chem.* **2001**, *40*, 6555.

[216] Gerbino, D. C.; Fidelibus, P. M.; Mandolesi, S. D.; Ocampo, R. A.; Scoccia, J.; Podestá, J. C. *J. Organomet. Chem.* **2013**, *741–742*, 24.

[217] Ke, I.-S.; Myahkostupov, M.; Castellano, F. N.; Gabbaï, F. P. *J. Am. Chem. Soc.* **2012**, *134*, 15309.

[218] Yamaguchi, S.; Shirasaka, T.; Tamao, K. *Organometallics* **2002**, *21*, 2555.

[219] van den Ancker, T. R.; Raston, C. L. *J. Organomet. Chem.* **1998**, *550*, 283.

[220] Baumgarten, M.; Gherghel, L.; Friedrich, J.; Jurczok, M.; Rettig, W. *J. Phys. Chem. A* **2000**, *104*, 1130.

[221] Kendall, J. K.; Engler, T. A.; Shechter, H. *J. Org. Chem.* **1999**, *64*, 4255.

[222] Vrancken, E.; Alexakis, A.; Mangeney, P. *Eur. J. Org. Chem.* **2005**, *2005*, 1354.

[223] Stern, D.; Finkelmeier, N.; Stalke, D. *Chem. Commun.* **2011**, *47*, 2113.

[224] Neugebauer, W.; Clark, T.; von Ragué Schleyer, P. *Chem. Ber.* **1983**, *116*, 3283.

[225] Chieh, P. C.; Trotter, J. *J. Chem. Soc. A* **1970**, 911.

[226] Bel'skii, V. K.; Simonenko, A. A.; Reikhsfel'd, V. O.; Saratov, I. E. *J. Organomet. Chem.* **1983**, *244*, 125.

[227] Karipides, A.; Oertel, M. *Acta Crystallogr. Sect. B: Struct. Sci.* **1977**, *B33*, 683.

[228] Karipides, A.; Wolfe, K. *Acta Crystallogr. Sect. B: Struct. Sci.* **1975**, *B31*, 605.

[229] Wharf, I.; Belanger-Gariepy, F. *Acta Crystallogr., Sect. E: Struct. Rep. Online* **2003**, *59*, m661.

[230] Wharf, I.; Lebuis, A.-M. *Main Group Met. Chem.* **2000**, *23*, 497.

[231] Bokii, N. T.; Zakharova, G. N.; Struchkov, Y. T. *Zh. Strukt. Khim.* **1970**, *11*, 895.

[232] Geller, J. M.; Butler, I. S.; Gilson, D. F. R.; Morin, F. G.; Wharf, I.; Belanger-Gariepy, F. *Can. J. Chem.* **2003**, *81*, 1187.

[233] Wharf, I.; Simard, M. G.; McGinn, K. *Acta Crystallogr., Sect. C: Cryst. Struct. Commun.* **1995**, *C51*, 236.

[234] Wharf, I.; Lebuis, A. M.; Roper, G. A. *Inorg. Chim. Acta* **1999**, *294*, 224.

[235] Wharf, I.; Lebuis, A.-M. *Acta Crystallogr., Sect. C: Cryst. Struct. Commun.* **1996**, *C52*, 3025.

[236] Bojan, R. V.; Lopez-de-Luzuriaga, J. M.; Monge, M.; Olmos, M. E. *J. Organomet. Chem.* **2010**, *695*, 2385.

[237] Sharma, H. K.; Cervantes-Lee, F.; Mahmoud, J. S.; Pannell, K. H. *Organometallics* **1999**, *18*, 399.

[238] Baxter, J. L.; Holt, E. M.; Zuckerman, J. J. *Organometallics* **1985**, *4*, 255.

[239] Greene, P. T.; Bryan, R. F. *J. Chem. Soc. A* **1971**, 2549.

[240] Leonhardt, T.; Latscha, H. P. *Z. Naturforsch., B: Chem. Sci.* **1997**, *52*, 25.

[241] Kraeuter, T.; Neumueller, B. *Z. Naturforsch., B: Chem. Sci.* **1998**, *53*, 503.

[242] Batsanov, A. S.; Cornet, S. M.; Dillon, K. B.; Goeta, A. E.; Thompson, A. L.; Xue, B. Y. *Dalton Trans.* **2003**, 2496.

[243] Weidenbruch, M.; Schaefers, K.; Pohl, S.; Saak, W.; Peters, K.; Von Schnering, H. G. *J. Organomet. Chem.* **1988**, *346*, 171.

[244] Meyer, E. A.; Castellano, R. K.; Diederich, F. *Angew. Chem., Int. Ed.* **2003**, *42*, 1210.

[245] Jennings, W. B.; Farrell, B. M.; Malone, J. F. *Acc. Chem. Res.* **2001**, *34*, 885.

[246] Janiak, C. *Dalton* **2000**, 3885.

[247] Hunter, C. A.; Sanders, J. K. M. *J. Am. Chem. Soc.* **1990**, *112*, 5525.

[248] Nayak, S. K.; Sathishkumar, R.; Row, T. N. G. *CrystEngComm* **2010**, *12*, 3112.

[249] Brock, C. P.; Dunitz, J. D. *Acta Crystallogr. Sect. B: Struct. Sci.* **1982**, *B38*, 2218.

[250] Geller, J.; Wharf, I.; Belanger-Gariepy, F.; Lebuis, A.-M.; Butler, I. S.; Gilson, D. F. R. *Acta Crystallogr. Sect. C: Cryst. Struct. Commun.* **2002**, *58*, m466.

[251] Tse, J. S.; Lee, F. L.; Gabe, E. J. *Acta Crystallogr. Sect. C: Cryst. Struct. Commun.* **1986**, *42*, 1876.

[252] Balas, V. I.; Banti, C. N.; Kourkoumelis, N.; Hadjikakou, S. K.; Geromichalos, G. D.; Sahpazidou, D.; Male, L.; Hursthouse, M. B.; Bednarz, B.; Kubicki, M.; Charalabopoulos, K.; Hadjiliadis, N. *Aust. J. Chem.* **2012**, *65*, 1625.

[253] Ng, S. *Acta Crystallogr. Sect. C: Cryst. Struct. Commun.* **1995**, *51*, 2292.

[254] Geller, J. M.; Butler, I. S.; Gilson, D. F. R.; Morin, F. G.; Wharf, I.; Bélanger-Gariépy, F. *Can. J. Chem.* **2003**, *81*, 1187.

[255] Preut, H.; Huber, F. *Acta Crystallogr. Sect. B: Struct. Sci.* **1979**, *B35*, 744.

[256] Dakternieks, D.; Lim, A. E. K.; Tiekink, E. R. T. *Main Group Met. Chem.* **2000**, *23*, 325.

[257] Simard, M. G.; Wharf, I. *Acta Crystallogr. Sect. C: Cryst. Struct. Commun.* **1994**, *50*, 397.

[258] Bajue, S. A.; Bramwell, F. B.; Charles, M.; Cervantes-Lee, F.; Pannell, K. *Inorg. Chim. Acta* **1992**, *197*, 83.

[259] Sindlinger, C. P.; Stasch, A.; Bettinger, H. F.; Wesemann, L. *Chem. Sci.* **2015**, Ahead of Print.

[260] Bernal, J. D. *Proc. R. Soc. London, Ser. A* **1924**, *106*, 749.

[261] Ahmad, S. U.; Beckmann, J.; Duthie, A. *Chem. - Asian J.* **2010**, *5*, 160.

[262] Johnson, B. P.; Almstaetter, S.; Dielmann, F.; Bodensteiner, M.; Scheer, M. *Z. Anorg. Allg. Chem.* **2010**, *636*, 1275.

[263] Ritter, H. P.; Neumann, W. P. *J. Organomet. Chem.* **1973**, *56*, 199.

[264] Neumann, W. P.; Koenig, K. *Angew. Chem.* **1962**, *74*, 215.

[265] Neumann, W. P. *Angew. Chem.* **1962**, *74*, 122.

[266] Draeger, M.; Mathiasch, B.; Ross, L.; Ross, M. *Z. Anorg. Allg. Chem.* **1983**, *506*, 99.

[267] Neumann, W. P.; Pedain, J.; Sommer, R. *Justus Liebigs Ann. Chem.* **1966**, *694*, 9.

[268] Watta, B.; Neumann, W. P.; Sauer, J. *Organometallics* **1985**, *4*, 1954.

[269] Babcock, J. R.; Sita, L. R. *J. Am. Chem. Soc.* **1996**, *118*, 12481.

[270] Davies, A. G. In *Organotin Chemistry*; Wiley-VCH Verlag GmbH & Co. KGaA: 2004, p 244.

[271] Zhou, Z.; Kuemmerle, R.; Qiu, X.; Redwine, D.; Cong, R.; Taha, A.; Baugh, D.; Winniford, B. *J. Magn. Reson.* **2007**, *187*, 225.

[272] Puff, H.; Bach, C.; Reuter, H.; Schuh, W. *J. Organomet. Chem.* **1984**, *277*, 17.

[273] Olson, D. H.; Rundle, R. E. *Inorg. Chem.* **1963**, *2*, 1310.

[274] Bocian, D. F.; Strauss, H. L. *J. Am. Chem. Soc.* **1977**, *99*, 2876.

[275] Ivanov, P. M.; Osawa, E. *J. Comput. Chem.* **1984**, *5*, 307.

[276] Favini, G. *J. Mol. Struct.: THEOCHEM* **1983**, *10*, 139.

[277] Wiberg, K. B. *J. Org. Chem.* **2003**, *68*, 9322.

[278] Brough, L. F.; West, R. *J. Organomet. Chem.* **1980**, *194*, 139.

[279] Watanabe, H.; Muraoka, T.; Kageyama, M.; Yoshizumi, K.; Nagai, Y. *Organometallics* **1984**, *3*, 141.

[280] Shafiee, F.; Damewood, J. R., Jr.; Haller, K. J.; West, R. *J. Am. Chem. Soc.* **1985**, *107*, 6950.

[281] Fogarty, H. A.; Casher, D. L.; Imhof, R.; Schepers, T.; Rooklin, D. W.; Michi, J. *Pure Appl. Chem.* **2003**, *75*, 999.

[282] Hoelbling, M.; Flock, M.; Baumgartner, J.; Hassler, K. *Eur. J. Inorg. Chem.* **2007**, 4952.

[283] Pontoni, D.; Finet, S.; Narayanan, T.; Rennie, A. R. *J. Chem. Phys.* **2003**, *119*, 6157.

[284] Rath, T.; Novák, J.; Amenitsch, H.; Pein, A.; Maier, E.; Haas, W.; Hofer, F.; Trimmel, G. *Mater. Chem. Phys.* **2014**, *144*, 310.

[285] Kotlarchyk, M.; Chen, S. H. *J. Chem. Phys.* **1983**, *79*, 2461.

[286] Bjorck, M.; Andersson, G. *J. Appl. Crystallogr.* **2007**, *40*, 1174.

[287] Ravel, B.; Newville, M. *J. Synchrotron Rad.* **2005**, *12*, 537.

[288] Dulnee, S.; Banerjee, D.; Merkel, B. J.; Scheinost, A. C. *Environ. Sci. Technol.* **2013**, *47*, 12852.

[289] Li, L.; Morrill, M. R.; Shou, H.; Barton, D. G.; Ferrari, D.; Davis, R. J.; Agrawal, P. K.; Jones, C. W.; Sholl, D. S. *J. Phys. Chem. C* **2013**, *117*, 2769.

[290] Meitzner, G. D.; Iglesia, E.; Baumgartner, J. E.; Huang, E. S. *J. Catal.* **1993**, *140*, 209.

[291] Neumann, W. P.; König, K. *Angew. Chem., Int. Ed. Engl.* **1964**, *3*, 751.

[292] Neumann, W. P.; Pedain, J. *Justus Liebigs Ann. Chem.* **1964**, *672*, 34.

[293] Neumann, W. P.; König, K. *Justus Liebigs Ann. Chem.* **1964**, *677*, 12.

[294] Wyckoff, R. W. G. *Crystal Structures*; Wiley, 1963.

[295] Armand, M.; Tarascon, J. M. *Nature* **2008**, *451*, 652.

[296] Tarascon, J. M.; Armand, M. *Nature* **2001**, *414*, 359.

[297] Kamali, A. R.; Fray, D. J. *Rev. Adv. Mater. Sci* **2011**, *27*, 14.

[298] Courtney, I. A.; Dahn, J. R. *J. Electrochem. Soc.* **1997**, *144*, 2045.

[299] Idota, Y.; Kubota, T.; Matsufuji, A.; Maekawa, Y.; Miyasaka, T. *Science* **1997**, *276*, 1395.

[300] Zhi Xiang, H.; Ye, W.; Jen It, W.; Hui Ying, Y. *2D Materials* **2015**, *2*, 024010.

[301] Ibarz, A.; Ruiz, E.; Alvarez, S. *Chem. Mater.* **1998**, *10*, 3422.

[302] Wang, B.; Luo, B.; Li, X.; Zhi, L. *Mater. Today* **2012**, *15*, 544.

[303] Shin, H. C.; Liu, M. *Adv. Funct. Mater.* **2005**, *15*, 582.

[304] Hu, R.; Zhu, M.; Wang, H.; Liu, J.; Liuzhang, O.; Zou, J. *Acta Mater.* **2012**, *60*, 4695.

[305] Kravchyk, K.; Protesescu, L.; Bodnarchuk, M. I.; Krumeich, F.; Yarema, M.; Walter, M.; Guntlin, C.; Kovalenko, M. V. *J. Am. Chem. Soc.* **2013**, *135*, 4199.

[306] Chen, J. S.; Lou, X. W. *Mater. Today* **2012**, *15*, 246.

[307] Goodenough, J. B.; Kim, Y. *Chem. Mater.* **2010**, *22*, 587.

[308] Xu, L.; Kim, C.; Shukla, A. K.; Dong, A.; Mattox, T. M.; Milliron, D. J.; Cabana, J. *Nano Lett.* **2013**, *13*, 1800.

[309] Xu, Y.; Liu, Q.; Zhu, Y.; Liu, Y.; Langrock, A.; Zachariah, M. R.; Wang, C. *Nano Lett.* **2013**, *13*, 470.

[310] Xu, Y.; Guo, J.; Wang, C. *J. Mater. Chem.* **2012**, *22*, 9562.

[311] Deng, D.; Lee, J. Y. *Angew. Chem. Int. Ed.* **2009**, *48*, 1660.

[312] Derrien, G.; Hassoun, J.; Panero, S.; Scrosati, B. *Adv. Mater.* **2007**, *19*, 2336.

[313] Hassoun, J.; Derrien, G.; Panero, S.; Scrosati, B. *Adv. Mater.* **2008**, *20*, 3169.

[314] Hassoun, J.; Lee, K.-S.; Sun, Y.-K.; Scrosati, B. *J. Am. Chem. Soc.* **2011**, *133*, 3139.

[315] Hwang, J.; Woo, S. H.; Shim, J.; Jo, C.; Lee, K. T.; Lee, J. *ACS Nano* **2013**, *7*, 1036.

[316] Qiu, Y.; Yan, K.; Yang, S. *Chem. Commun.* **2010**, *46*, 8359.

[317] Yu, Y.; Gu, L.; Zhu, C.; van Aken, P. A.; Maier, J. *J. Am. Chem. Soc.* **2009**, *131*, 15984.

[318] Hou, X.; Jiang, H.; Hu, Y.; Li, Y.; Huo, J.; Li, C. *ACS Appl. Mater. Interfaces* **2013**, *5*, 6672.

[319] Seo, S.-D.; Lee, G.-H.; Lim, A.-H.; Min, K.-M.; Kim, J.-C.; Shim, H.-W.; Park, K.-S.; Kim, D.-W. *RSC Adv.* **2012**, *2*, 3315.

[320] Wang, Y.; Wu, M.; Jiao, Z.; Lee, J. Y. *Chem. Mater.* **2009**, *21*, 3210.

[321] Yu, Y.; Gu, L.; Wang, C.; Dhanabalan, A.; van Aken, P. A.; Maier, J. *Angew. Chem. Int. Ed.* **2009**, *48*, 6485.

[322] Zhang, H.; Song, H.; Chen, X.; Zhou, J. *J. Phys. Chem. C* **2012**, *116*, 22774.

[323] Hsu, K.-C.; Liu, C.-E.; Chen, P.-C.; Lee, C.-Y.; Chiu, H.-T. *J. Mater. Chem.* **2012**, *22*, 21533.

[324] Lee, K. T.; Jung, Y. S.; Oh, S. M. *J. Am. Chem. Soc.* **2003**, *125*, 5652.

[325] Li, X.; Dhanabalan, A.; Gu, L.; Wang, C. *Adv. Energy Mater.* **2012**, *2*, 238.

[326] Zhang, W.-M.; Hu, J.-S.; Guo, Y.-G.; Zheng, S.-F.; Zhong, L.-S.; Song, W.-G.; Wan, L.-J. *Adv. Mater.* **2008**, *20*, 1160.

[327] Glatter, O.; Kratky, O. *Small Angle X-ray Scattering*; Academic Press, 1982.

[328] Jastrzebski, J. T. B. H.; Van Koten, G. In *Adv. Organomet. Chem.*; Stone, F. G. A., Robert, W., Eds.; Academic Press: 1993; Vol. Volume 35, p 241.

[329] Novak, P.; Padelkova, Z.; Kolarova, L.; Cisarova, I.; Ruzicka, A.; Holecek, J. *Appl. Organomet. Chem.* **2005**, *19*, 1101.

[330] Ruzicka, A.; Jambor, R.; Brus, J.; Cisarova, I.; Holecek, J. *Inorg. Chim. Acta* **2001**, *323*, 163.

[331] Ruzicka, A.; Pejchal, V.; Holecek, J.; Lycka, A.; Jacob, K. *Collect. Czech. Chem. Commun.* **1998**, *63*, 977.

[332] Biesemans, M.; Martins, J. C.; Willem, R.; Lycka, A.; Ruzicka, A.; Holecek, J. *Magn. Reson. Chem.* **2002**, *40*, 65.

[333] Jastrzebski, J. T. B. H.; Grove, D. M.; Boersma, J.; Van Koten, G.; Ernsting, J. M. *Magn. Reson. Chem.* **1991**, *29*, S25.

[334] Coza, C.; Stegarescu, A.; Suteu, R.; Silvestru, A. *J. Organomet. Chem.* **2015**, *777*, 71.

[335] Novak, P.; Padelkova, Z.; Cisarova, I.; Kolarova, L.; Ruzicka, A.; Holecek, J. *Appl. Organomet. Chem.* **2006**, *20*, 226.

[336] Varga, R. A.; Silvestru, C.; Deleanu, C. *Appl. Organomet. Chem.* **2005**, *19*, 153.

[337] Svec, P.; Padelkova, Z.; Cernosek, Z.; De Proft, F.; Ruzicka, A. *J. Organomet. Chem.* **2008**, *693*, 2937.

[338] Padelkova, Z.; Havlik, A.; Svec, P.; Nechaev, M. S.; Ruzicka, A. *J. Organomet. Chem.* **2010**, *695*, 2651.

[339] Svec, P.; Padelkova, Z.; Stepnicka, P.; Ruzicka, A.; Holecek, J. *J. Organomet. Chem.* **2011**, *696*, 1809.

[340] Varga, R. A.; Schuermann, M.; Silvestru, C. *J. Organomet. Chem.* **2001**, *623*, 161.

[341] Varga, R. A.; Jurkschat, K.; Silvestru, C. *Eur. J. Inorg. Chem.* **2008**, 708.

[342] Varga, R. A.; Rotar, A.; Schurmann, M.; Jurkschat, K.; Silvestru, C. *Eur. J. Inorg. Chem.* **2006**, 1475.

[343] Novak, P.; Brus, J.; Cisarova, I.; Ruzicka, A.; Holecek, J. *J. Fluorine Chem.* **2005**, *126*, 1531.

[344] Růžička, A.; Dostál, L.; Jambor, R.; Buchta, V.; Brus, J. í.; Císařová, I.; Holčapek, M.; Holeček, J. *Appl. Organomet. Chem.* **2002**, *16*, 315.

[345] Padelkova, Z.; Weidlich, T.; Kolarova, L.; Eisner, A.; Cisarova, I.; Zevaco, T. A.; Ruzicka, A. *J. Organomet. Chem.* **2007**, *692*, 5633.

[346] Weidlich, T.; Dusek, L.; Vystrcilova, B.; Eisner, A.; Svec, P.; Ruzicka, A. *Appl. Organomet. Chem.* **2012**, *26*, 293.

[347] Svec, P.; Novak, P.; Nadvornik, M.; Padelkova, Z.; Cisarova, I.; Kolarova, L.; Ruzicka, A.; Holecek, J. *J. Fluorine Chem.* **2007**, *128*, 1390.

[348] Svec, P.; Eisner, A.; Kolarova, L.; Weidlich, T.; Pejchal, V.; Ruzicka, A. *Tetrahedron Lett.* **2008**, *49*, 6320.

[349] Chandra, S.; Ruzicka, A.; Svec, P.; Lang, H. *Anal. Chim. Acta* **2006**, *577*, 91.

[350] Svec, P.; Padelkova, Z.; Ruzicka, A.; Weidlich, T.; Dusek, L.; Plasseraud, L. *J. Organomet. Chem.* **2011**, *696*, 676.

[351] Svec, P.; Olejnik, R.; Padelkova, Z.; Ruzicka, A.; Plasseraud, L. *J. Organomet. Chem.* **2012**, *708-709*, 82.

[352] Svec, P.; Cernoskova, E.; Padelkova, Z.; Ruzicka, A.; Holecek, J. *J. Organomet. Chem.* **2010**, *695*, 2475.

[353] Padelkova, Z.; Weidlich, T.; Cisarova, I.; Ruzicka, A. *Appl. Organomet. Chem.* **2009**, *23*, 253.

[354] Turek, J.; Padelkova, Z.; Cernosek, Z.; Erben, M.; Lycka, A.; Nechaev, M. S.; Cisarova, I.; Ruzicka, A. *J. Organomet. Chem.* **2009**, *694*, 3000.

[355] Neumann, W. P.; Schneider, B. *Angew. Chem.* **1964**, *76*, 891.

[356] Rotar, A.; Varga, R. A.; Silvestru, C. *Acta Crystallogr., Sect. E: Struct. Rep. Online* **2008**, *64*, m45.

[357] Padelkova, Z.; Cisarova, I.; Ruzicka, A. *Acta Crystallogr., Sect. E: Struct. Rep. Online* **2005**, *61*, m2691.

[358] Biedermann, J. M. Master Thesis, Graz University of Technology, 2014.

[359] Jung, Y. S.; Lee, K. T.; Ryu, J. H.; Im, D.; Oh, S. M. *J. Electrochem. Soc.* **2005**, *152*, A1452.

[360] Schaeffer, C. D.; Lefferts, J. L.; Zuckerman, J. J. *Org. Magn. Resonance* **1984**, *22*, 125.

[361] Frisch, M. J.; Trucks, G. W.; Schlegel, H. B.; Scuseria, G. E.; Robb, M. A.; Cheeseman, J. R.; Scalmani, G.; Barone, V.; Mennucci, B.; Petersson, G. A.; Nakatsuji, H.; Caricato, M.; Li, X.; Hratchian, H. P.; Izmaylov, A. F.; Bloino, J.; Zheng, G.; Sonnenberg, J. L.; Hada, M.; Ehara, M.; Toyota, K.; Fukuda, R.; Hasegawa, J.; Ishida, M.; Nakajima, T.; Honda, Y.; Kitao, O.; Nakai, H.; Vreven, T.; Montgomery Jr., J. A.; Peralta, J. E.; Ogliaro, F.; Bearpark, M. J.; Heyd, J.; Brothers, E. N.; Kudin, K. N.; Staroverov, V. N.; Kobayashi, R.; Normand, J.; Raghavachari, K.; Rendell, A. P.; Burant, J. C.; Iyengar, S. S.; Tomasi, J.; Cossi, M.; Rega, N.; Millam, N. J.; Klene, M.; Knox, J. E.; Cross, J. B.; Bakken, V.; Adamo, C.; Jaramillo, J.; Gomperts, R.; Stratmann, R. E.; Yazyev, O.; Austin, A. J.; Cammi, R.; Pomelli, C.; Ochterski, J. W.; Martin, R. L.; Morokuma, K.; Zakrzewski, V. G.; Voth, G. A.; Salvador, P.; Dannenberg, J. J.; Dapprich, S.; Daniels, A. D.; Farkas, Ö.; Foresman, J. B.; Ortiz, J. V.; Cioslowski, J.; Fox, D. J. In *Gaussian 09, Revision D.01*; Gaussian, Inc.: Wallingford, CT, USA, 2013.

[362] Adamo, C.; Barone, V. *J. Chem. Phys.* **1998**, *108*, 664.

[363] In *CrysAlisPro Software system*; version 1.171.36.28c ed.; Agilent Technologies UK Ltd: Oxford, UK, 2014.

[364] Bruker; Bruker AXS Inc.: Madison, Wisconsin, USA, 2012.

[365] Blessing, R. *Acta Crystallogr. Sect. A: Found. Crystallogr.* **1995**, *51*, 33.

[366] Sheldrick, G. *Acta Crystallogr. Sect. A: Found. Crystallogr.* **1990**, *46*, 467.

[367] Sheldrick, G. *Acta Crystallogr. Sect. A: Found. Crystallogr.* **2008**, *64*, 112.

[368] Spek, A. L. *J. Appl. Crystallogr.* **2003**, *36*, 7.

[369] Spek, A. L. *Acta Crystallogr. Sect. D. Biol. Crystallogr.* **2009**, *65*, 148.

[370] van der Sluis, P.; Spek, A. L. *Acta Crystallogr. Sect. A: Found. Crystallogr.* **1990**, *46*, 194.

[371] Allen, F. H. *Acta Crystallogr., Sect. B* **2002**, *B58*, 380.

[372] Macrae, C. F.; Bruno, I. J.; Chisholm, J. A.; Edgington, P. R.; McCabe, P.; Pidcock, E.; Rodriguez-Monge, L.; Taylor, R.; van de Streek, J.; Wood, P. A. *J. Appl. Crystallogr.* **2008**, *41*, 466.

[373] Putz, H.; Brandenburg, K.; 3.2i ed.; Crystal Impact: Bonn, Germany.

[374] Janiak, C. *J. Chem. Soc., Dalton Trans.* **2000**, 3885.

[375] Schnablegger, H.; Glatter, O. *Appl. Opt.* **1991**, *30*, 4889.

[376] Amenitsch, H.; Rappolt, M.; Kriechbaum, M.; Mio, H.; Laggner, P.; Bernstorff, S. *J. Synchrotron Rad.* **1998**, *5*, 506.

[377] Hammersley, A. *ESRF97HA02T, FIT2D: An Introduction and Overview*, European Synchrotron Radiation Facility, **1997**.

13 Appendix

13.1 Crystal Structure Analysis Data

Table 25: *Crystallographic Table for* $Aryl_4Sn$ (***3***,***5***,***6***), $Aryl_3SnX$ (***8***,***9***,***11***) *and* $Aryl_2SnCl_2$ (***14-16***).

Compound	***p-^{n}*butylphenyl$_4$Sn (3)**	**1-naphthyl$_4$Sn (5)**	**2-naphthyl$_4$Sn (6)**	**9-anthracenyl$_3$SnCl (8)**	**2,6-xylyl$_3$SnBr (9)**	**9-anthracenyl$_3$SnI (11)**	***p*-biphenyl$_2$SnCl$_2$ (14)**	**1-naphthyl$_2$SnCl$_2$ (15)**	**2-naphthyl$_2$SnCl$_2$ (16)**
Formula	$C_{40}H_{52}Sn$	$C_{40}H_{28}Sn$	$C_{40}H_{28}NSn$	$C_{42}H_{27}ClSn$	$C_{24}H_{27}BrSn$	$C_{42}H_{27}Isn$	$C_{24}H_{18}Cl_2Sn$, C_6H_6	$C_{20}H_{14}Cl_2Sn$	$C_{20}H_{14}Cl_2Sn$
Fw (g mol^{-1})	651.50	627.31	627.31	685.77	514.05	896.59	574.08	443.90	443.90
a (Å)	10.2809(3)	11.0020(3)	19.0493(17)	19.0194(6)	7.9774(3)	17.1219(7)	15.2013(4)	7.5925(3)	7.6608(5)
b (Å)	13.5926(4)	12.3126(4)	19.0493(17)	19.0194(6)	18.6305(6)	14.8830(6)	18.3258(5)	7.1840(3)	13.8169(10)
c (Å)	26.0182(8)	21.3522(6)	7.8388(8)	19.0194(6)	14.5078(4)	27.2528(11)	11.2285(3)	14.9860(6)	15.9891(12)
α (°)	92.532(2)	90	90	90	90	90	90	90	90
β (°)	96.022(2)	90.789(1)	90	90	94.680(1)	90	125.7040(10)	92.618(2)	94.275(4)
γ(°)	97.922(2)	90	90	90	90	90	90	90	90
V (Å^3)	3574.97(19)	2892.16(15)	2844.5(6)	6880.0(7)	2149.00(12)	6944.7(5)	2540.06(12)	816.55(6)	1687.7(2)
Z	4	4	4	8	4	8	4	2	4
Crystal system	Triclinic	Monoclinic	Tetragonal	Cubic	Monoclinic	Orthorhombic	Monoclinic	Monoclinic	Monoclinic
Space group	P-1	P2$_1$/n	I-4	Pa-3	P2$_1$/c	Pbca	C2/c	P2/n	P2(1)/n
d_{calc} (Mg/m^3)	1.210	1.439	1.465	1.324	1.589	1.715	1.501	1.805	1.747
μ (mm^{-1})	0.74	0.91	0.93	0.85	3.05	1.89	1.232	1.887	1.826
T (K)	100(2)	100(2)	100(2)	100(2)	100(2)	100(2)	100(2)	100(2)	100(2)
2θ range (°)	2.3–26.5	2.5–25.9	2.8–27.6	2.4–26.6	2.6–26.8	2.7–30.4	1.99—27.18	2.72—27.13	1.95 —25.00
F(000)	1368	1272	1272	2545	1024	10648	1152	436	872
R_{int}	0.082	0.097	0.050	133	0.030	461	0.079	0.028	0.077
independent reflns	15766	5911	2833	2768	4448	3520	2820	1804	2951
No. of params	767	358	185	0.097	241	0.147	150	105	208
R$_1$, wR2 (all data)^a	$R_1 = 0.0955$ $wR2 = 0.1195$	$R_1 = 0.1000$ $wR2 = 0.1406$	$R_1 = 0.0429$ $wR2 = 0.0940$	$R_1 = 0.0764$ $wR2 = 0.1128$	$R_1 = 0.0250$ $wR2 = 0.0474$	$R_1 = 0.0707$ $wR2 = 0.0892$	$R1 = 0.0470$ $wR2 = 0.1025$	$R1 = 0.0205$ $wR2 = 0.0493$	$R1 = 0.0704$ $wR2 = 0.1986$
R$_1$, wR2 (>2σ)^b	$R_1 = 0.0535$ $wR2 = 0.1076$	$R_1 = 0.0597$ $wR2 = 0.1246$	$R_1 = 0.0354$ $wR2 = 0.0893$	$R_1 = 0.0412$ $wR2 = 0.1012$	$R_1 = 0.0193$ $wR2 = 0.0452$	$R_1 = 0.0358$ $wR2 = 0.0768$	$R1 = 0.0387$ $wR2 = 0.0975$	$R1 = 0.0194$ $wR2 = 0.0489$	$R1 = 0.0625$ $wR2 = 0.1826$

Table 26: *Crystallographic Table for Aryl$_2$SnX$_2$ (**17,19**) and ArylSnCl$_3$ (**21,23,24,26-28**).*

Compound	**9-anthracenyl$_2$SnCl$_2$ (17)**	**9-anthracenyl$_2$SnI$_2$ (19)**	***o*-tolylSnCl$_3$ (21)**	**2,6-xylylSnCl$_3$ (23)**	**mesitylSnCl$_3$ (24)**	**1-naphthylSnCl$_3$ (26)**	**2-naphthylSnCl$_3$ (27)**	**9-anthracenylSnCl$_3$ (28)**
Formula	$C_{28}H_{18}Cl_2Sn$	$C_{28}H_{18}I_2Sn$	$C_7H_7Cl_3Sn$	$C_8H_9Cl_3Sn$	$C_9H_{11}Cl_3Sn$	$C_{10}H_7Cl_3Sn$	$C_{10}H_7Cl_3Sn$	$C_{14}H_9Cl_3Sn$
Fw (g mol^{-1})	544.01	726.91	316.17	330.19	344.22	352.20	352.20	402.25
a (Å)	13.6544(4)	8.2283(4)	7.1993(8)	8.2836(4)	7.1701(3)	7.2454(3)	9.1965(3)	9.9200(5)
b (Å)	9.3596(3)	8.9854(5)	8.6524(10)	15.1421(7)	8.3365(4)	17.8681(7)	7.0776(2)	9.9586(5)
c (Å)	18.0320(5)	15.9246(7)	17.4519(19)	17.9066(8)	10.7824(5)	9.1734(3)	18.0394(5)	14.9681(7)
a (°)	90	89.055(1)	76.418(3)	90	73.743(1)	90	90	104.478(3)
b (°)	106.913(1)	85.832(1)	78.788(3)	90	74.259(1)	95.325(2)	90	100.524(3)
g (°)	90	76.712(2)	81.902(4)	90	83.947(2)	90	90	98.343(3)
V (°)	2204.81(11)	1142.83(10)	1031.4(2)	4111.1(4)	595.22(5)	1182.48(8)	1174.17(6)	1379.09(12)
Z	4	2	4	8	2	4	4	4
Crystal system	Monoclinic	Triclinic	Triclinic	Orthorhombic	Triclinic	Monoclinic	Orthorhombic	Triclinic
Space group	P2$_1$/c	P-1	P-1	Pbcn	P-1	P2(1)/c	Pnma	P-1
d_{calc} (mg/m^3)	1.639	2.112	2.036	1.953	1.921	1.978	1.992	1.937
μ/ (mm^{-1})	1.42	3.83	3.19	2.936	2.77	2.795	2.82	2.41
T (K)	100(2)	100(2)	100(2)	100(2)	100(2)	100(2)	100(2)	100(2)
2θ range (°)	2.7–31.5	2.6–33.3	2.4–27.2	2.27—30.03	2.6–25.2	2.28—24.99	2.5–27.1	2.8–27.2
F(000)	5040	8816	600	1264	332	672	672	6104
R_{int}	280	280	0.055	0.035	0.073	0.086	0.041	326
independent reflns	1080	684	4157	3273	2089	2078	1397	776
No. of params	0.034	0.092	201	111	121	127	82	0.081
R1, wR2 (all data)^a	R_1 = 0.0334 wR2 = 0.0690	R_1 = 0.0371 wR2 = 0.0561	R_1 = 0.0349 wR2 = 0.0865	R1 = 0.0313, wR2 = 0.0748	R1 = 0.0595 wR2 = 0.1683	R1 = 0.0672 wR2 = 0.1795	R_1 = 0.0232 wR2 = 0.0540	R_1 = 0.0833 wR2 = 0.1150
R1, wR2 (>2σ)^b	R_1 = 0.0298 wR2 = 0.0678	R_1 = 0.0274 wR2 = 0.0593	R_1 = 0.0347 wR2 = 0.0864	R1 = 0.0265 wR2 = 0.0725	R1 = 0.0582 wR2 = 0.1669	R1 = 0.0667 wR2 = 0.1793	R_1 = 0.0202 wR2 = 0.0522	R_1 = 0.0525 wR2 = 0.1047

Table 27: *Crystallographic Table for aryltin hydrides (**29-31**, **40**) and compounds **43-45**.*

Compound	**Phenyl$_3$SnH (29)**	**2,6-xylyl$_3$SnH (30)**	**phenyl$_2$SnH$_2$ (31)**	**mesitylSnH$_3$ (40)**	**(phenyl$_2$Sn)$_7$ (43)**	**9-iodoanthracene (44)**	**9-anthracenyl$_3$SnMe (45)**
Formula	$C_{18}H_{16}Sn$	$C_{24}H_{28}Sn$	$C_{12}H_{12}Sn$	$C_9H_{14}Sn$	$C_{84}H_{70}Sn_7$	$C_{14}H_9I$	$2(C_{43}H_{30}Sn)\cdot C_7H_8$
Fw (g mol^{-1})	351.00	435.15	274.91	240.89	3630.22	304.11	1422.85
a (Å)	10.2387(9)	6.9415(4)	7.61953(12)	8.1935(15)	13.8612(3)	4.3549(2)	19.1155(6)
b (Å)	17.0950(16)	11.9714(7)	5.75092(9)	8.2193(15)	22.7603(6)	14.0522(6) Å	19.8822(6)
c (Å)	8.6077(9)	12.8316(8)	12.13438(18)	14.911(3)	24.8024(6)	17.0995(7)	22.0128(7)
α (°)	90	108.672(2)	90	80.575(6)	95.655(1)	90	89.025(2)
β (°)	99.248(5)	91.291(2)	97.1877(14)	81.037(8)	94.739(1)	91.508(1)	64.881(2)
γ(°)	90	95.958(2)	90	78.712 (8)	92.808(1)	90	79.141(2)
V (Å^3)	1487.0(2)	1002.96(10)	527.54 (1)	963.5 (3)	7747.2(3)	1046.06(8)	7420.6(4)
Z	4	2	2	4	2	4	4
Crystal system	Monoclinic	Triclinic	Monoclinic	Triclinic	Triclinic	Monoclinic	Triclinic
Space group	$P2_1/c$	P-1	$P2_1$	P-1	P-1	$P2_1/c$	P-1
d_{calc} (Mg/m^3)	1.568	1.440	1.731	1.661	1.556	1.931	1.274
μ (mm^{-1})	1.70	1.28	2.37	2.58	2.26	3.02	0.72
T (K)	100(2)	100(2)	100(2)	100(2)	100(2)	100(2)	100(2)
2θ range (°)	2.0–25.0	2.8–26.4	1.0–32.6	2.6–27.1	2.31–27.1°	2.8–27.1°	2.5–27.2
F(000)	2619	444	5840	4174	3350	584	2904
R_{int}	176	0.043	167	211	0.132	0.072	0.052
independent reflns	696	4069	268	472	100631	2310	32958
No. of params	0.089	236	0.012	0.021	821	136	1717
R_1, wR2 (all data)^a	R_1 = 0.0536 wR2 = 0.1327	R_1 = 0.0501 wR2 = 0.1275	R_1 = 0.0179 wR2 = 0.0555	R_1 = 0.0425 wR2 = 0.0883	R_1 = 0.2045 wR2 = 0.1085	R_1 = 0.0395 wR2 = 0.1085	R_1 = 0.0869 wR2 = 0.1929
R_1, wR2 ($>2\sigma$)^b	R_1 = 0.0475 wR2 = 0.1236	R_1 = 0.0480 wR2 = 0.1260	R_1 = 0.0175 wR2 = 0.0553	R_1 = 0.0393 wR2 = 0.0875	R_1 =0.2252 wR2 = 0.3284	R_1 =0.0386 wR2 = 0.1076	R_1 = 0.0698 wR2 = 0.1826

***Table 28:** Crystallographic Table for compounds **46-50**.*

Compound	**9-anthracenylLi(TMEDA)·LiBr(TMEDA) (46)**	**anthraquinone (47)**	**9-anthracenyl$_3$SnBu (48)**	**L$^{CN}{}_2$BuSnCl (50)**	**L$^{CN}{}_2$BuSnCl (50)**
Formula	$C_{26}H_{41}BrLi_2N_4$	$C_{28}H_{20}Li_2O_8 \cdot Cl_6Sn$	$C_{46}H_{36}Sn$	$C_{22}H_{33}ClN_2Sn$	$C_{22}H_{33}ClN_2Sn$
Fw (g mol^{-1})	503.42	829.71	708	479.64	479.64
a (Å)	10.9963(7)	7.5409(2)	27.8957(10)	17.3955(7)	30.816(3)
b (Å)	15.1099(9)	10.3058(3)	27.8957(10)	12.5554(5)	7.6933(6)
c (Å)	17.2799(11)	10.7614(3)	32.1997(18)	20.9929(8)	19.3028(15)
α (°)	74.603(4)	86.1350(18)	90	90	90
β (°)	89.330(4)	78.9170(18)	90	102.010(1)	97.782(6)
γ(°)	82.192(4)	79.2240(18)	90	90	90
V (Å^3)	2741.5(3)	805.82(4)	21700(2)	4484.6(3)	4534.2(6)
Z	4	1	4	8	8
Crystal system	Triclinic	Triclinic	Trigonal	Monoclinic	Monoclinic
Space group	P-1	P-1	$R\bar{3}$	P2$_1$/n	C2/c
d_{calc} (Mg/m^3)	1.220	1.710	0.116	1.421	1.405
μ (mm^{-1})	1.52	1.34	0.12	1.27	1.25
T (K)	100(2)	100(2)	100(2)	100(2)	100(2)
2θ range (°)	2.8–27.3	2.7–27.2	1.8–23.5	2.4–27.2	2.7–27.2
F(000)	1064	410	760	1968	1968
R_{int}	0.080	0.037	0.067	0.025	0.037
independent reflns	12181	2707	7165	9935	5012
No. of params	611	206	565	479	240
R$_1$, wR2 (all data)^a	R$_1$ = 0.0848 wR2 = 0.1764	R$_1$ = 0.0489 wR2 = 0.1075	R$_1$ = 0.2099 wR2 = 0.5614	R$_1$ = 0.0219 wR2 = 0.0583	R$_1$ = 0.0335 wR2 = 0.0905
R$_1$, wR2 (>2σ)^b	R$_1$ = 0.0640 wR2 = 0.1666	R$_1$ = 0.0397 wR2 = 0.1022	R$_1$ = 0.1936 wR2 = 0.5451	R$_1$ = 0.0189 wR2 = 0.0551	R$_1$ = 0.0318 wR2 = 0.0891

13.2 DFT Calculations

13.2.1 Chapter 2

Phenyl$_3$SnCl, E = -1158.028073 a.u.

Sn	-0.001665	-0.004656	0.442356	C	1.666955	-1.198406	-0.151499
C	1.885584	-2.482443	0.390804	C	2.984009	-3.252446	-0.019820
C	3.876695	-2.750477	-0.979347	C	2.574009	-0.702413	-1.112314
C	3.671231	-1.475015	-1.524751	H	1.213349	-2.883135	1.143902
H	3.143035	-4.235984	0.410112	H	4.726702	-3.346632	-1.295325
H	2.435971	0.286835	-1.540776	H	4.361605	-1.080468	-2.263302
C	-1.874401	-0.845164	-0.148063	C	-1.908933	-1.897979	-1.087535
C	-3.133323	-2.448703	-1.498379	C	-4.336754	-1.956175	-0.973139
C	-3.092019	-0.360469	0.374657	C	-4.314591	-0.912974	-0.034757
H	-0.986654	-2.298730	-1.499867	H	-3.144943	-3.258711	-2.220538
H	-5.283038	-2.383650	-1.288688	H	-3.095715	0.438108	1.110796
H	-5.242894	-0.533024	0.379215	C	0.204761	2.038948	-0.145543
C	-0.670951	2.583755	-1.108938	C	-0.539181	3.919807	-1.519534
C	0.466756	4.727721	-0.969887	C	1.211342	2.862710	0.401351
C	1.340484	4.198330	-0.007713	H	-1.462055	1.976013	-1.540149
H	-1.220104	4.325830	-2.260625	H	0.566795	5.761388	-1.284946
H	1.889027	2.475145	1.156419	H	2.116094	4.821571	0.425292
Cl	-0.000233	-0.007259	2.890419				

Phenyl$_2$SnCl$_2$, E = -1386.789561 a.u.

C	4.234380	1.921765	-0.225691	C	3.141054	2.303002	-1.017764
C	1.938216	1.584450	-0.948716	C	1.825492	0.476808	-0.082566
C	2.926257	0.097778	0.710373	C	4.126053	0.821657	0.637804
Sn	0.000072	-0.606800	0.000038	C	-1.825637	0.476330	0.082680
C	-2.925296	0.098794	-0.712507	C	-4.125288	0.822367	-0.640044
C	-4.234931	1.920670	0.225577	C	-3.142726	2.300392	1.019925
C	-1.939704	1.582139	0.951007	Cl	0.217110	-2.079294	1.912768
Cl	-0.216439	-2.079110	-1.912908	H	-2.852165	-0.748642	-1.386941
H	-1.106325	1.892046	1.575222	H	-4.968275	0.526648	-1.255275
H	-3.225220	3.149026	1.690616	H	-5.164960	2.476569	0.281812
H	1.103923	1.895546	-1.571120	H	2.854082	-0.750992	1.383229
H	3.222521	3.153068	-1.686766	H	4.969909	0.524795	1.251291
H	5.164263	2.477900	-0.282025				

PhenylSnCl$_3$, E = -1615.539294 a.u.

Sn	0.710139	0.003559	-0.002247	Cl	1.632754	-1.414910	-1.703378
Cl	1.479307	2.243013	-0.382578	C	-1.404891	-0.027419	0.010724
Cl	1.709096	-0.746651	2.047558	C	-2.093617	-1.255364	0.021510
C	-3.495882	-1.258743	0.031052	C	-4.203987	-0.047475	0.028533
C	-3.513778	1.173178	0.014835	C	-2.110725	1.190101	0.005312

H	-1.561941	-2.201386	0.019115	H	-4.029215	-2.202848	0.038808
H	-5.288564	-0.055557	0.035333	H	-4.060348	2.109730	0.010074
H	-1.589304	2.141753	-0.010007				

1-NaphthylSnCl$_3$, E = -1769.079617 a.u.

Sn	1.259558	-0.041101	0.000000	C	-0.687644	0.798646	-0.000001
C	-1.860030	-0.026188	-0.000002	C	-0.778957	2.184575	-0.000001
C	-1.821691	-1.450071	-0.000003	C	-3.141916	0.624220	-0.000001
C	-2.053879	2.8131570	-0.000001	H	0.108820	2.808997	-0.000002
C	-2.987158	-2.194642	-0.000003	H	-0.868389	-1.973468	-0.000002
C	-4.325145	-0.169207	-0.000002	C	-3.203821	2.047568	0.000000
H	-2.110348	3.895589	-0.000001	C	-4.253376	-1.549570	-0.000003
H	-2.936735	-3.277616	-0.000003	H	-5.288678	0.330840	-0.000002
H	-4.177792	2.527103	0.000000	H	-5.158888	-2.145810	-0.000003
Cl	1.751809	-1.420229	-1.904533	Cl	2.857325	1.747417	-0.000006
Cl	1.751796	-1.420217	1.904545				

***p*-TolylSnCl$_3$**, E = -1654.816827 a.u.

C	-3.909286	-0.002098	0.044561	C	-3.189061	1.207675	0.033405
C	-1.788844	1.218041	0.014020	C	-1.084369	-0.000443	0.008869
C	-1.787094	-1.219310	0.015502	C	-3.188080	-1.210545	0.035096
H	-1.267302	2.169717	-0.002948	Sn	1.026340	0.000322	-0.004824
Cl	1.865827	-1.942753	-1.134574	C	-5.417986	-0.000424	0.037257
Cl	1.863265	1.967140	-1.094233	Cl	2.052935	-0.022861	2.167049
H	-1.264832	-2.170638	-0.000461	H	-3.723496	-2.154719	0.041820
H	-3.725883	2.151226	0.038707	H	-5.819911	0.841595	0.607751
H	-5.799064	0.086514	-0.987283	H	-5.822653	-0.923118	0.461231

***o*-TolylSnCl$_3$**, E = -1654. 817256 a.u.

C	2.126700	-0.976536	0.003488	C	1.337985	0.197846	0.000520
C	1.920750	1.478130	-0.002211	C	3.317262	1.604156	-0.000280
C	4.115082	0.452748	0.004198	C	3.524510	-0.819250	0.006208
Sn	-0.779065	0.075009	0.000268	Cl	-1.706061	-0.994331	1.944237
Cl	-1.689036	2.293592	-0.071254	Cl	-1.699723	-1.116044	-1.874119
H	1.307048	2.373347	-0.005190	H	3.770046	2.589156	-0.001285
H	5.196070	0.542712	0.006770	H	4.153180	-1.703862	0.009507
C	1.507645	-2.354422	-0.007425	H	2.268616	-3.129845	0.101321
H	0.793802	-2.485802	0.815129	H	0.976792	-2.546859	-0.947306

2,4-XylylSnCl$_3$, E = -1694.094626 a.u.

C	3.186849	-0.990890	0.012217	C	1.785739	-1.087718	0.006192
C	1.044548	0.116958	0.003430	C	1.690819	1.365460	0.006118
C	3.089897	1.425457	0.011401	C	3.856319	0.247442	0.011367
C	1.108443	-2.438183	-0.000428	Sn	-1.071377	0.093409	-0.000406
Cl	-2.050684	-1.028635	-1.888763	C	5.363847	0.304692	-0.012827
Cl	-2.060895	-0.954120	1.925497	Cl	-1.872963	2.355013	-0.045958
H	1.122222	2.290060	0.007344	H	3.582475	2.392359	0.017025

H	3.771313	-1.906689	0.018099	H	1.838188	-3.247666	0.066065
H	0.422298	-2.550504	0.848027	H	0.532904	-2.592783	-0.920998
H	5.806444	-0.535498	0.529549	H	5.734816	0.261062	-1.043930
H	5.736623	1.231484	0.431131				

2,6-XylylSnCl$_3$, E = -1694.089435 a.u.

C	-3.444683	1.225171	-0.009436	C	-2.038967	1.288805	-0.001147
C	-1.323473	0.067172	0.000571	C	-1.979756	-1.189394	0.001216
C	-3.385979	-1.199046	-0.005677	C	-4.112077	-0.004019	-0.013532
C	-1.366531	2.640842	0.009997	Sn	-0.817881	0.020136	0.001693
Cl	2.052430	2.077331	-0.135343	C	-1.231084	-2.502400	0.000739
Cl	1.687583	-1.027814	1.991388	Cl	1.684117	-1.248687	-1.855720
H	-3.905816	-2.151237	-0.004380	H	-5.196416	-0.030114	-0.019397
H	-4.011895	2.149965	-0.010547	H	-2.111025	3.439538	0.024137
H	-0.728664	2.776378	0.889936	H	-0.737691	2.797080	-0.872489
H	-1.918842	-3.339174	0.137968	H	-0.702289	-2.666723	-0.944842
H	-0.496324	-2.559445	0.813059				

Phenyl$_3$SnH, E = -698.370149 a.u.

C	2.505918	-0.255832	0.974803	C	1.854618	-0.834331	-0.136717
C	2.449842	-1.961499	-0.744713	C	3.652237	-2.496442	-0.256301
C	4.283850	-1.910531	0.851090	C	3.709069	-0.788538	1.465567
Sn	0.002866	-0.018714	-0.862927	H	-0.001955	-0.057936	-2.588742
C	-1.652235	-1.178695	-0.127465	C	-1.493981	-2.038473	0.981526
C	-2.573856	-2.789180	1.473981	C	-3.833474	-2.693541	0.864473
C	4.008446	-1.846627	-0.240152	C	-2.926703	-1.098298	-0.730772
C	-0.193628	2.002731	-0.152414	H	1.981419	-2.432398	-1.605192
H	2.081539	0.618586	1.460916	H	4.092791	-3.363290	-0.738707
H	4.193671	-0.328185	2.320861	H	5.214092	-2.322624	1.229084
H	-0.524798	-2.132836	1.463835	H	-3.087369	-0.453385	-1.591112
H	-2.430299	-3.444873	2.327050	H	-4.979533	-1.770060	-0.719109
H	-4.668473	-3.273756	1.244172	C	0.733365	3.003329	-0.519301
C	0.599637	4.319721	-0.051090	C	-0.467845	4.660631	0.793486
C	-1.397418	3.679929	1.168409	C	-1.260630	2.363288	0.699005
H	1.569445	2.764686	-1.171830	H	1.323163	5.073516	-0.345333
H	-0.572928	5.678600	1.155073	H	-2.225104	3.935896	1.822427
H	-1.990885	1.617896	1.002451				

Phenyl$_2$SnH$_2$, E = -467.483946 a.u.

C	4.067743	1.604394	-0.167465	C	2.922213	1.962711	-0.893579
C	1.775088	1.154957	-0.843831	C	1.751389	-0.025820	-0.069413
C	2.911331	-0.368342	0.658814	C	4.060294	0.437398	0.610323
Sn	0.000062	-1.269982	0.000078	C	-1.751370	-0.025967	0.069435
C	-2.910782	-0.367964	-0.659881	C	-4.059839	0.437653	-0.611515
C	-4.067916	1.603992	0.167248	C	-2.922915	1.961784	0.894458
C	-1.775696	1.154159	0.844828	H	0.136258	-2.277972	1.393005
H	-0.136069	-2.278085	-1.392774	H	-2.926547	-1.264088	-1.274716

H	-0.898725	1.455140	1.411611	H	-4.940746	0.156200	-1.179812
H	-2.920978	2.864714	1.496907	H	-4.955125	2.227953	0.205686
H	0.897698	1.456340	-1.409749	H	2.927589	-1.264972	1.272897
H	2.919789	2.866147	-1.495267	H	4.941618	0.155536	1.177771
H	4.954879	2.228454	-0.205993				

PhenylSnH$_3$, E = -236.599312 a.u.

Sn	-1.567708	0.000093	0.000070	H	-2.178579	-0.750481	1.425347
H	-2.107009	1.632890	-0.064842	C	0.582923	-0.006317	-0.000585
H	-2.175566	-0.865041	-1.359277	C	1.313845	-1.214460	-0.000598
C	2.717408	-1.210361	0.000253	C	3.417945	0.004961	0.000766
C	2.708574	1.214265	0.000241	C	1.303940	1.207519	-0.000619
H	0.796652	-2.170233	-0.001616	H	3.259189	-2.150886	0.000233
H	4.503175	0.008839	0.001333	H	3.242882	2.159045	0.000182
H	0.776867	2.157582	-0.001621				

13.2.2 Chapter 5

(Phenyl$_2$Sn)$_7$ (43) C, E = -3265.71546 a.u.

Sn	0.68779700	2.85014400	-0.64239300
Sn	-1.92935200	2.44313500	0.40749000
Sn	-3.25971600	0.02756500	-0.29350300
Sn	-1.97373600	-2.41894900	0.38220100
Sn	0.62226800	-2.90243700	-0.68129000
Sn	2.87196000	-1.48882000	0.36226100
Sn	2.90126100	1.38126800	0.39684800
C	0.64837800	2.72194500	-2.80638600
C	-0.56904000	2.67847000	-3.52019700
H	-1.51949200	2.64612900	-2.99431400
C	-0.58565100	2.68175200	-4.92469300
H	-1.53567000	2.64557300	-5.44782500
C	0.61844500	2.72962700	-5.64233900
H	0.60658300	2.74097800	-6.72781000
C	1.83885400	2.76426600	-4.94959300
H	2.77643700	2.79956900	-5.49563700
C	1.85357200	2.75814300	-3.54521500
H	2.81212600	2.79063400	-3.03454500
C	1.22114500	4.92243700	-0.24634800
C	1.41223500	5.82712200	-1.31384800
H	1.29343800	5.49193700	-2.34041200
C	1.76088000	7.16577200	-1.06993100
H	1.90426800	7.84535200	-1.90454500
C	1.92571300	7.62307800	0.24611600
H	2.19569200	8.65737700	0.43486000
C	1.74098300	6.73540500	1.31695100

H	1.87014200	7.07881400	2.33860100
C	1.39121000	5.39778100	1.07274100
H	1.26100900	4.73035800	1.91999100
C	-3.17933400	4.09620700	-0.23816800
C	-2.65870700	5.18755300	-0.96533400
H	-1.60269600	5.23046100	-1.21527500
C	-3.48679900	6.24840800	-1.36754300
H	-3.06277400	7.07956300	-1.92213200
C	-4.85271300	6.23487800	-1.05151400
H	-5.49331800	7.05406600	-1.36258400
C	-5.38690500	5.15691400	-0.32913500
H	-6.44302600	5.13829600	-0.07838600
C	-4.55828800	4.09733000	0.07198200
H	-4.99869100	3.27530400	0.62996100
C	-1.86201700	2.58083000	2.57197400
C	-1.69189200	1.44229800	3.38937100
H	-1.59252100	0.45286200	2.95061100
C	-1.66181600	1.55323000	4.78959700
H	-1.53777100	0.65967600	5.39256800
C	-1.80158800	2.80980900	5.39747100
H	-1.78577700	2.89755400	6.47944300
C	-1.97146800	3.95221000	4.59972800
H	-2.08509400	4.92767000	5.06263700
C	-2.00132200	3.83892800	3.20049500
H	-2.14433200	4.73492200	2.60300500
C	-3.76530300	0.08709300	-2.39918500
C	-2.96849700	-0.53671200	-3.38253000
H	-2.06630000	-1.07610900	-3.10775900
C	-3.31112800	-0.46705700	-4.74263500
H	-2.67862800	-0.95500200	-5.47722700
C	-4.45924100	0.23120800	-5.14418000
H	-4.72723300	0.28384800	-6.19484400
C	-5.25961200	0.86287200	-4.17989100
H	-6.14726200	1.41019000	-4.48171100
C	-4.91547600	0.79185600	-2.82071100
H	-5.54959900	1.29042000	-2.09309600
C	-5.16147500	-0.01495000	0.75604300
C	-6.26023600	-0.69980300	0.19012300
H	-6.16408700	-1.18395400	-0.77756200
C	-7.48987200	-0.77183300	0.86392600
H	-8.32059300	-1.30443800	0.41146300
C	-7.64381300	-0.16201600	2.11815600
H	-8.59453000	-0.21778900	2.63894900
C	-6.56103200	0.51727700	2.69626100
H	-6.66877600	0.99022000	3.66746400
C	-5.33113800	0.58838700	2.02176300
H	-4.50686200	1.11346200	2.49666200

C	-3.31260100	-4.01068100	-0.23893700
C	-3.82976000	-4.06537600	-1.55136800
H	-3.57205900	-3.30038300	-2.27856300
C	-4.69043500	-5.10273300	-1.94376800
H	-5.07694900	-5.12586700	-2.95794500
C	-5.05087500	-6.10385400	-1.02953000
H	-5.71611400	-6.90611900	-1.33279600
C	-4.54798900	-6.06110500	0.27911500
H	-4.82465000	-6.82984000	0.99417500
C	-3.68663700	-5.02359400	0.67061900
H	-3.31389100	-5.00608500	1.69124200
C	-1.89526700	-2.53878500	2.54430600
C	-3.09158700	-2.47961900	3.29611400
H	-4.04918400	-2.36484300	2.79591400
C	-3.06720600	-2.56438900	4.69709600
H	-3.99800600	-2.51788200	5.25375700
C	-1.84581000	-2.70592700	5.37445400
H	-1.82784500	-2.77550400	6.45768800
C	-0.64923300	-2.76062200	4.64479000
H	0.30266700	-2.87065800	5.15396000
C	-0.67634000	-2.67737300	3.24259000
H	0.26794100	-2.72983700	2.70772900
C	1.10076100	-4.99823800	-0.37755100
C	0.31941400	-5.83071300	0.45148600
H	-0.56617900	-5.44098300	0.94492600
C	0.66027500	-7.17834800	0.65085000
H	0.04099900	-7.80084200	1.28897400
C	1.79375300	-7.71800800	0.02562600
H	2.05791000	-8.75960900	0.17881100
C	2.58402200	-6.90373400	-0.80003700
H	3.46449000	-7.31131700	-1.28693300
C	2.24149500	-5.55675200	-0.99856700
H	2.87401700	-4.94711800	-1.63782900
C	0.59753500	-2.63500100	-2.83211300
C	0.42012500	-3.75294500	-3.67782000
H	0.29051500	-4.74364100	-3.25190700
C	0.41429800	-3.60562500	-5.07429400
H	0.27853300	-4.47799900	-5.70616400
C	0.58598300	-2.33780700	-5.65114600
H	0.58612300	-2.22516000	-6.73089200
C	0.75909800	-1.21642700	-4.82592800
H	0.88780600	-0.22921000	-5.25633300
C	0.76345000	-1.36679700	-3.42941500
H	0.89711100	-0.47790000	-2.81794300
C	4.53105700	-2.24596300	-0.82461700
C	4.45361700	-2.35600500	-2.23084300
H	3.55108500	-2.06074400	-2.75864400

C	5.53476400	-2.85423000	-2.97610300
H	5.45205900	-2.93245100	-4.05570300
C	6.71415500	-3.25159600	-2.32777500
H	7.55022500	-3.63689800	-2.90290100
C	6.80531700	-3.15100800	-0.93129400
H	7.71293000	-3.45880000	-0.42126700
C	5.72321200	-2.65371000	-0.18677500
H	5.81152800	-2.59074000	0.89396500
C	3.25080000	-2.27076100	2.35162500
C	3.33928200	-3.67134900	2.52731100
H	3.20816700	-4.34252900	1.68326600
C	3.59840900	-4.22486600	3.79102900
H	3.66049100	-5.30291700	3.90144200
C	3.77510200	-3.38892500	4.90448000
H	3.97961800	-3.81690600	5.88098700
C	3.68958600	-1.99804700	4.74659700
H	3.82846600	-1.34085700	5.59928700
C	3.42772600	-1.44439800	3.48185800
H	3.37071800	-0.36482100	3.39010600
C	3.19710900	2.11267100	2.41961100
C	4.49141000	2.47769400	2.85151300
H	5.33589600	2.39688000	2.17310500
C	4.70800500	2.95353400	4.15494300
H	5.71061400	3.22977100	4.46662000
C	3.63407800	3.07383500	5.04998700
H	3.80183800	3.44342800	6.05677400
C	2.34199900	2.71695700	4.63551200
H	1.50070400	2.80846000	5.31479500
C	2.12780000	2.24025900	3.33196900
H	1.11516200	1.97275300	3.04276300
C	4.61428500	2.14812300	-0.69459000
C	5.47666500	1.32935800	-1.45413800
H	5.31691100	0.25743300	-1.50449500
C	6.56563400	1.88071100	-2.15035400
H	7.21834400	1.23031300	-2.72413200
C	6.80930600	3.26083700	-2.10140000
H	7.65050900	3.68641000	-2.63958600
C	5.96010300	4.08896600	-1.35119500
H	6.13879500	5.15874300	-1.30722700
C	4.87271700	3.53819700	-0.65512800
H	4.23003200	4.20171000	-0.08300600

(Phenyl$_2$Sn)$_7$ (**43**) **TT**, E = -3265.71529 a.u.

Sn	1.83915700	2.27112700	-0.85155900
Sn	3.32342300	0.03472600	0.10850500
Sn	1.88835700	-2.36321700	0.71149400
Sn	-0.60698900	-2.85264500	-0.58648300
Sn	-2.94617800	-1.31830500	-0.01209700
Sn	-2.92045200	1.53723700	-0.06731300
Sn	-0.51814900	2.90028100	0.60873200
C	1.37589300	1.96579000	-2.94578300
C	0.91682300	0.72877800	-3.44560300
H	0.78408400	-0.12399600	-2.78458600
C	0.62698200	0.55911600	-4.80948900
C	0.79157900	1.63091600	-5.69953600
C	1.24622500	2.86867000	-5.21966400
H	1.37959000	3.70217900	-5.90249600
C	1.53579400	3.03447900	-3.85567800
H	1.89471500	3.99860100	-3.50682800
C	3.18596800	3.97227000	-0.83792700
C	4.40526100	3.89736100	-1.55013000
H	4.66243700	2.99997200	-2.10691700
C	5.30424400	4.97549100	-1.55532800
H	6.23463300	4.89716800	-2.10904300
C	5.00095500	6.14901700	-0.84749800
H	5.69567400	6.98301300	-0.85160200
C	3.79372600	6.24011700	-0.13956600
H	3.54632500	7.14689500	0.40332600
C	2.89496500	5.16042900	-0.13437500
H	1.96082600	5.26429200	0.40968100
C	4.43678800	0.64200300	1.86998400
C	5.01387300	1.93081800	1.93799600
H	4.88296600	2.63789400	1.12373600
C	5.77062100	2.32501400	3.05350700
H	6.20526100	3.31932500	3.08226200
C	5.96474700	1.43781200	4.12317100
H	6.55113300	1.74152300	4.98474500
C	5.39744200	0.15611900	4.07182500
H	5.53875400	-0.53731900	4.89477500
C	4.63961500	-0.23635900	2.95650900
H	4.20390200	-1.23101500	2.95110000
C	4.84334200	-0.36704500	-1.39109300
C	4.50972200	-0.67433100	-2.72800000
H	3.47097800	-0.71549000	-3.04283700
C	5.50974400	-0.92008100	-3.68207400
H	5.23085900	-1.15092200	-4.70546500
C	6.86298500	-0.86340300	-3.31605400
H	7.63633800	-1.05369100	-4.05359000
C	7.21095200	-0.55605100	-1.99224500

H	8.25578900	-0.50607800	-1.70124600
C	6.20990200	-0.30900200	-1.03830800
H	6.49982400	-0.06697000	-0.01962300
C	1.52888900	-2.44996000	2.85003900
C	1.77589900	-3.64476500	3.56209700
H	2.15899000	-4.52013500	3.04570600
C	1.54404500	-3.71954300	4.94521200
C	1.06446400	-2.60008900	5.64196800
H	0.89135800	-2.65680600	6.71220100
C	0.81919800	-1.40475900	4.94995200
H	0.46155100	-0.52622800	5.47679900
C	1.04856500	-1.33286500	3.56638000
H	0.86485000	-0.38724300	3.06293100
C	3.13700600	-4.07888900	0.24809200
C	4.51230800	-3.93382600	-0.03723200
H	4.96880400	-2.94902800	-0.06639000
C	5.31675700	-5.05374500	-0.30312800
H	6.37073400	-4.91651100	-0.52334400
C	4.76017500	-6.34111700	-0.28961100
H	5.38177100	-7.20677500	-0.49576900
C	3.39410000	-6.50267000	-0.01496200
H	2.95092400	-7.49356100	-0.00914500
C	2.58967500	-5.38227400	0.24818700
H	1.53253200	-5.53738500	0.44347100
C	-1.17916900	-4.87002300	-0.00144800
C	-1.47701500	-5.19474400	1.34065400
H	-1.42840600	-4.43542000	2.11550900
C	-1.84683600	-6.50057000	1.70108600
H	-2.07556300	-6.72659900	2.73783600
C	-1.92466800	-7.50629000	0.72574200
H	-2.21139100	-8.51561100	1.00407900
C	-1.63155600	-7.19966100	-0.61182600
H	-1.68961500	-7.97178100	-1.37301700
C	-1.26236000	-5.89316500	-0.97227300
H	-1.03847500	-5.67655200	-2.01292500
C	-0.27487300	-3.01442600	-2.72460300
C	0.98831600	-3.40722800	-3.22261900
H	1.81996200	-3.57819800	-2.54378700
C	1.19299100	-3.60988700	-4.59736700
H	2.17047000	-3.91771800	-4.95522600
C	0.13616500	-3.42402400	-5.50153000
H	0.29142200	-3.58821900	-6.56324300
C	-1.12342000	-3.03048700	-5.02462300
H	-1.94919400	-2.88881100	-5.71479100
C	-1.32563200	-2.82473400	-3.64960400
H	-2.31353500	-2.53053000	-3.30776800
C	-4.44632900	-2.07225400	-1.38854700

C	-4.73026900	-3.45755300	-1.40757300
H	-4.20512300	-4.13640700	-0.74082200
C	-5.68834000	-3.98451900	-2.28786700
H	-5.89068100	-5.05102900	-2.28534800
C	-6.37764500	-3.13744000	-3.16923300
H	-7.11783800	-3.54515500	-3.85050700
C	-6.10304800	-1.76211600	-3.16627600
H	-6.62919800	-1.09849800	-3.84526300
C	-5.14495600	-1.23466400	-2.28434900
H	-4.95043700	-0.16672800	-2.30642400
C	-3.60682300	-1.97792800	1.94681300
C	-4.89870900	-2.52253700	2.11697900
H	-5.56842000	-2.61624100	1.26697500
C	-5.33810000	-2.95279000	3.37982100
H	-6.33436000	-3.37045900	3.48865500
C	-4.49304600	-2.84814300	4.49481600
H	-4.83184900	-3.18360000	5.47000400
C	-3.20651800	-2.30970300	4.34138200
H	-2.53995800	-2.22803500	5.19400400
C	-2.77041200	-1.87812100	3.07880900
H	-1.76828400	-1.46808100	2.99185900
C	-4.39557200	2.31489400	1.32414900
C	-5.12264300	1.48867000	2.20771400
H	-4.96648600	0.41460800	2.21237700
C	-6.05886800	2.03563400	3.10106200
H	-6.60705400	1.37978500	3.77010300
C	-6.28268400	3.41979700	3.12901900
H	-7.00573900	3.84255100	3.81948900
C	-5.56434200	4.25594800	2.26059900
H	-5.72652500	5.32916000	2.27725900
C	-4.62861900	3.70920400	1.36826200
H	-4.08137700	4.38033800	0.71179300
C	-3.55721200	2.26111500	-2.01128600
C	-4.84325800	2.82471200	-2.16637700
H	-5.51272300	2.90042600	-1.31434600
C	-5.27663300	3.29693300	-3.41607000
H	-6.26836600	3.72800100	-3.51333200
C	-4.43171100	3.21477700	-4.53312700
H	-4.76618600	3.58130400	-5.49859100
C	-3.15182600	2.65696000	-4.39479800
H	-2.48690900	2.58814700	-5.24966200
C	-2.72000000	2.18432600	-3.14499100
H	-1.72359000	1.75818100	-3.07130200
C	-0.97771200	5.00400200	0.31434900
C	-0.89210800	5.90912800	1.39529200
H	-0.59758100	5.55662500	2.38000100
C	-1.19004100	7.27064300	1.21958300

H	-1.11899300	7.95044000	2.06324500
C	-1.58076000	7.75033000	-0.03956300
H	-1.81143100	8.80226500	-0.17545300
C	-1.67395300	6.86224700	-1.12190100
H	-1.97935800	7.22345500	-2.09892300
C	-1.37522700	5.50166500	-0.94625500
H	-1.46284300	4.83554500	-1.80035700
C	-0.11482400	2.71025200	2.72889200
C	-1.17365400	2.69339700	3.66562400
H	-2.20651300	2.73024800	3.33062900
C	-0.91468100	2.63785400	5.04483300
H	-1.74350100	2.63209100	5.74588900
C	0.40745700	2.59270500	5.51401000
H	0.60719000	2.55393300	6.58038000
C	1.46986400	2.59966400	4.59821000
H	2.49678400	2.55589700	4.94608200
C	1.20844200	2.65837200	3.21942900
H	2.05455900	2.66742600	2.53757100
H	1.74188800	-4.64698700	5.47387200
H	0.57354200	1.50113800	-6.75504900
H	0.27919400	-0.40475700	-5.16523200

(Phenyl$_2$Sn)$_7$ (**43**) **TB1**, E = -3265.71152 a.u.

Sn	3.17239600	0.47068300	0.33668500
Sn	1.39650400	2.65525400	0.83355800
Sn	-1.06539000	2.86230200	-0.60171200
Sn	-2.98752400	0.72754000	-0.59777800
Sn	-2.44766900	-1.70524700	0.80413800
Sn	-0.06318200	-3.19342700	0.21178300
Sn	2.10673100	-1.80175400	-1.00111700
C	4.87316200	1.11956700	-0.85221100
C	6.10541600	1.39947200	-0.22103800
H	6.20584300	1.28444800	0.85439800
C	7.21754700	1.82323300	-0.96659400
H	8.15579900	2.03115600	-0.46150500
C	7.11802400	1.97500900	-2.35771600
H	7.97781800	2.30156300	-2.93417500
C	5.90149300	1.69848900	-2.99945400
H	5.81500400	1.80916400	-4.07592900
C	4.79036100	1.27430300	-2.25326000
H	3.86379900	1.06182600	-2.77844800
C	4.05442300	-0.23055400	2.19049100
C	5.07773000	-1.20459000	2.12632600
H	5.40349400	-1.59857400	1.16757600
C	5.69179200	-1.68320300	3.29406900
H	6.47504200	-2.43109000	3.22035200
C	5.29309300	-1.19908700	4.54963300

H	5.77111500	-1.56575000	5.45275300
C	4.27586300	-0.23698400	4.63017100
H	3.95997100	0.14570800	5.59561100
C	3.66097100	0.24196300	3.46088500
H	2.87844800	0.98806100	3.55478700
C	2.40671000	4.54539600	0.48342300
C	3.69911200	4.62121900	-0.07932100
H	4.23687600	3.71820200	-0.35071700
C	4.31867200	5.86331600	-0.29715500
H	5.31442900	5.89649900	-0.72801100
C	3.65527900	7.05177200	0.04049700
H	4.13378900	8.01133200	-0.12864900
C	2.36819700	6.99358400	0.59674100
H	1.84385200	7.90761400	0.85724300
C	1.74896700	5.75281300	0.81451100
H	0.74914200	5.73739100	1.23947900
C	0.85907400	2.69459400	2.93501200
C	-0.06279400	1.77687400	3.48310200
H	-0.53547500	1.02309900	2.85853300
C	-0.39438000	1.80928700	4.84718600
H	-1.10593400	1.09148800	5.24057100
C	0.19432300	2.76501700	5.68916500
H	-0.06039500	2.79227700	6.74398900
C	1.11288000	3.68504300	5.16118600
H	1.57200700	4.42815100	5.80601700
C	1.44262400	3.65001600	3.79644400
H	2.15587500	4.37095400	3.40782200
C	-0.65964000	3.46770700	-2.64662800
C	-1.56606500	3.19940100	-3.69565200
H	-2.46371700	2.61662300	-3.51425700
C	-1.32470100	3.67014100	-4.99722100
H	-2.03812000	3.45304600	-5.78588100
C	-0.16728200	4.41239200	-5.27554300
H	0.01922000	4.77757000	-6.28064100
C	0.74736700	4.68223400	-4.24601900
H	1.64520200	5.25726600	-4.44955800
C	0.50275000	4.21514500	-2.94432300
H	1.22130300	4.45278600	-2.16485500
C	-1.94919100	4.64146400	0.28958600
C	-2.31837800	5.72887400	-0.53273300
H	-2.17426200	5.67199200	-1.60779600
C	-2.86656100	6.89767500	0.02122200
H	-3.14396800	7.72190200	-0.62870900
C	-3.05175700	7.00165200	1.40810900
H	-3.47356500	7.90558100	1.83626500
C	-2.68578900	5.93122800	2.23874400
H	-2.82120500	6.00274700	3.31338300

C	-2.14025500	4.76227100	1.68391100
H	-1.86330600	3.95070000	2.35059200
C	-3.43313800	0.12063500	-2.63574500
C	-2.51777500	-0.62424000	-3.40991500
H	-1.54048200	-0.88656500	-3.01511200
C	-2.84038400	-1.03591100	-4.71303000
H	-2.11747300	-1.60613700	-5.28692500
C	-4.08694600	-0.70717100	-5.26649300
H	-4.33801400	-1.02598000	-6.27332200
C	-5.00707900	0.03629900	-4.51168200
H	-5.97421400	0.29502800	-4.93190600
C	-4.68344100	0.44555400	-3.20757700
H	-5.41289100	1.01268600	-2.63642700
C	-4.90360200	1.42458700	0.15906300
C	-5.14709500	2.77449700	0.49136200
H	-4.36167800	3.51657100	0.39569900
C	-6.40868400	3.18832100	0.95145200
H	-6.57080700	4.23246900	1.19989300
C	-7.44976100	2.25930000	1.08936100
H	-8.42389600	2.57905100	1.44598700
C	-7.22455900	0.91309300	0.76315200
H	-8.02264000	0.18452500	0.86590100
C	-5.96420000	0.49996600	0.30329200
H	-5.81931600	-0.54834900	0.05869100
C	-4.18615700	-2.94312000	0.36275000
C	-4.85327800	-3.60801800	1.41556100
H	-4.50022000	-3.50197100	2.43735500
C	-5.98307900	-4.40406100	1.16457200
H	-6.48054300	-4.90679700	1.98829700
C	-6.46932900	-4.54623000	-0.14381800
H	-7.34379800	-5.15949000	-0.33748500
C	-5.82008400	-3.88868400	-1.19993400
H	-6.19076400	-3.98760800	-2.21538100
C	-4.68822200	-3.09598900	-0.94890900
H	-4.20644300	-2.59827600	-1.78538800
C	-2.63909900	-1.37040500	2.94237300
C	-3.60120100	-0.44924100	3.41710500
H	-4.18825100	0.14373200	2.72139800
C	-3.83387200	-0.29242700	4.79295800
H	-4.58322500	0.41569300	5.13250800
C	-3.10567000	-1.05108600	5.72266100
H	-3.29037400	-0.93547300	6.78614800
C	-2.14014900	-1.96137300	5.26854200
H	-1.56881500	-2.55219900	5.97752900
C	-1.90920700	-2.11902300	3.89131800
H	-1.15999300	-2.83560400	3.57101000
C	0.71573200	-4.08817400	2.03381700

C	1.56532500	-3.38271300	2.91354500
H	1.85582900	-2.35699600	2.70315100
C	2.06616300	-3.98915700	4.07706500
H	2.72522300	-3.42683900	4.73032100
C	1.72087200	-5.31410100	4.38347600
H	2.10690300	-5.78451500	5.28237200
C	0.87914400	-6.03049900	3.51862600
H	0.61168400	-7.05789300	3.74580200
C	0.38319900	-5.42382200	2.35315900
H	-0.25527500	-6.00032000	1.68950700
C	-0.50747800	-4.89528600	-1.06212700
C	-1.81297800	-5.41047500	-1.20879000
H	-2.65229700	-4.93905400	-0.70865200
C	-2.05639600	-6.54334700	-2.00356400
H	-3.06970500	-6.92014400	-2.10125400
C	-0.99834600	-7.18201800	-2.66562400
H	-1.18648600	-8.05736500	-3.27938800
C	0.30602400	-6.68337900	-2.52862700
H	1.13345700	-7.17303700	-3.03286500
C	0.54794000	-5.55030600	-1.73640700
H	1.56953900	-5.19180100	-1.64261700
C	1.63295300	-1.25923700	-3.04569900
C	1.28360200	0.05970300	-3.40607900
H	1.21940600	0.84069000	-2.65217300
C	1.00776400	0.40287400	-4.73943100
H	0.73437800	1.42347400	-4.98414200
C	1.07688700	-0.57558600	-5.74157900
H	0.86645800	-0.31346700	-6.77360000
C	1.41430000	-1.89504900	-5.40260200
H	1.46640900	-2.65930200	-6.17206000
C	1.68788900	-2.23382200	-4.06783800
H	1.94767200	-3.26156900	-3.83075700
C	3.76263400	-3.19996700	-1.16653700
C	4.69137500	-3.06646200	-2.22308900
H	4.56591500	-2.28414400	-2.96623500
C	5.79071600	-3.93315800	-2.33086100
H	6.49342300	-3.81124200	-3.14931800
C	5.98323000	-4.94947700	-1.38284500
H	6.83304300	-5.61963500	-1.46620300
C	5.07235500	-5.09273500	-0.32555700
H	5.21238700	-5.87501600	0.41389900
C	3.97351000	-4.22473100	-0.21759300
H	3.28779400	-4.35488500	0.61486200

(Phenyl$_2$Sn)$_7$ (**43**) **TC**, E = -3265.70995 a.u.

Sn	0.92532000	-2.91946800	-0.52965500
Sn	3.08384400	-1.17593100	0.11320800
Sn	2.70737200	1.61108800	-0.28204800
Sn	0.37076900	2.92702500	0.67217600
Sn	-2.12279600	2.32157700	-0.54389000
Sn	-3.25252400	-0.27211000	-0.10446900
Sn	-1.63044700	-2.50935000	0.65528900
C	1.55806600	-4.92918300	-0.00974500
C	2.74129000	-5.16221400	0.72388400
H	3.36684000	-4.33156200	1.03922900
C	3.13423000	-6.46583800	1.06739400
H	4.04818400	-6.62068500	1.63215100
C	2.34784600	-7.56171600	0.68364300
H	2.64932400	-8.56979000	0.95026000
C	1.16640800	-7.34747500	-0.04210200
H	0.54667600	-8.18867000	-0.33636700
C	0.77373800	-6.04386800	-0.38384600
H	-0.15268800	-5.90599000	-0.93366400
C	0.58882500	-2.93179900	-2.67319500
C	1.10171900	-3.97588600	-3.47427800
H	1.66538300	-4.78609100	-3.01947200
C	0.88304800	-3.99460700	-4.86130200
H	1.28391500	-4.80821500	-5.45807800
C	0.14547500	-2.97032400	-5.47387100
H	-0.02665200	-2.98721300	-6.54534400
C	-0.37436800	-1.92753600	-4.69286700
H	-0.95478900	-1.13425100	-5.15299000
C	-0.15309000	-1.91164600	-3.30675000
H	-0.57630200	-1.09454600	-2.72751600
C	4.81415400	-1.71674500	-1.07825900
C	4.78698500	-2.77862900	-2.00703000
H	3.88200800	-3.36253300	-2.14785900
C	5.92312600	-3.10448000	-2.76557900
H	5.88035700	-3.92665900	-3.47304200
C	7.10807600	-2.37112300	-2.60875600
H	7.98643800	-2.62142300	-3.19521000
C	7.15168500	-1.31011100	-1.69144100
H	8.06351900	-0.73465700	-1.56610900
C	6.01490600	-0.98489800	-0.93507500
H	6.07305200	-0.15548200	-0.23495400
C	3.71400500	-1.44722200	2.17110900
C	2.93342800	-0.98574500	3.25164600
H	1.98438700	-0.48751100	3.07552700
C	3.36144600	-1.15319900	4.57802300
H	2.74351800	-0.78388100	5.39058700
C	4.58241500	-1.78884300	4.84794500

H	4.91671400	-1.91697300	5.87266300
C	5.37088500	-2.25433500	3.78508300
H	6.31925600	-2.74386500	3.98435900
C	4.94122100	-2.08430500	2.45895300
H	5.57259200	-2.44403200	1.65121600
C	2.92138700	2.09418900	-2.38258800
C	2.88040900	3.44484800	-2.79807900
H	2.72133600	4.23935400	-2.07411300
C	3.03886900	3.78860800	-4.14952700
C	3.23797800	2.78808800	-5.11288600
H	3.36411400	3.05445100	-6.15769500
C	3.27541200	1.44263700	-4.71842800
H	3.43220500	0.66044800	-5.45451000
C	3.11845600	1.09985800	-3.36508800
H	3.16560400	0.05031800	-3.08894800
C	4.36225900	2.59477300	0.72261200
C	5.37820800	3.23154000	-0.02282200
H	5.33554700	3.23684500	-1.10821400
C	6.45433200	3.86374300	0.62174800
H	7.22574400	4.34852200	0.03116300
C	6.53278500	3.86965200	2.02248000
H	7.36522300	4.35703300	2.52031800
C	5.53159100	3.23856600	2.77654100
H	5.58738300	3.23212500	3.86059700
C	4.45646000	2.60659700	2.13172500
H	3.69768400	2.11957100	2.73825000
C	0.80959600	5.02864300	0.34164000
C	1.92234600	5.63027900	0.97353000
H	2.56000800	5.05108300	1.63540100
C	2.24133200	6.97818500	0.74394300
H	3.10122300	7.41792100	1.23942300
C	1.45916100	7.74945900	-0.12884700
H	1.70705100	8.79085500	-0.30808300
C	0.36020500	7.16442100	-0.77489100
H	-0.24639900	7.74981000	-1.45864500
C	0.04059200	5.81699700	-0.54224800
H	-0.80903900	5.38818500	-1.06609900
C	0.13364700	2.64006200	2.80834300
C	0.27988700	3.71749600	3.70907500
H	0.52898400	4.70793100	3.33969700
C	0.09475800	3.53344100	5.08914500
H	0.21111600	4.37590400	5.76405200
C	-0.24466300	2.26961200	5.59469700
H	-0.39125000	2.12961700	6.66101200
C	-0.39981500	1.18841100	4.71404200
H	-0.67141400	0.20671200	5.08899700
C	-0.21001500	1.37590000	3.33537500

H	-0.34300300	0.51855700	2.67900200
C	-3.63847500	3.67911700	0.21043700
C	-3.31070200	4.81270000	0.98476300
H	-2.27686100	5.02718000	1.23999700
C	-4.30893800	5.68662400	1.44498600
H	-4.03291200	6.55180700	2.03965300
C	-5.65560500	5.44107700	1.14072200
H	-6.42789800	6.11443600	1.49889300
C	-6.00002100	4.31485800	0.37875800
H	-7.04057200	4.10851900	0.14902000
C	-5.00083000	3.44191400	-0.07825000
H	-5.29988900	2.56669800	-0.64956700
C	-1.97231400	2.75638200	-2.66586700
C	-2.92883000	3.59232900	-3.28441700
H	-3.73454800	4.02627200	-2.69881200
C	-2.85083900	3.88407100	-4.65605100
H	-3.59506800	4.53023300	-5.11159300
C	-1.81312900	3.34788200	-5.43338000
C	-0.85014100	2.52413400	-4.83182100
H	-0.03011200	2.11980600	-5.41616900
C	-0.93113200	2.23243000	-3.46093800
H	-0.15800300	1.60785500	-3.02195200
C	-4.42268000	-0.85688200	-1.83713000
C	-5.16260000	-2.06103800	-1.82771500
H	-5.11476100	-2.73183600	-0.97496100
C	-5.95890100	-2.42821800	-2.92418500
H	-6.51630400	-3.35927200	-2.89331100
C	-6.02803400	-1.60074700	-4.05474500
H	-6.64304200	-1.88521700	-4.90276100
C	-5.29302800	-0.40693600	-4.08421600
H	-5.33365400	0.23884700	-4.95584600
C	-4.49789400	-0.03981100	-2.98637500
H	-3.93618900	0.88755600	-3.04255200
C	-4.69144700	0.03681200	1.49649800
C	-6.02013800	-0.42412200	1.37123100
H	-6.33893000	-0.93718900	0.46888500
C	-6.95533800	-0.21538400	2.39830800
H	-7.97234300	-0.57725900	2.28144500
C	-6.57934200	0.46235600	3.56744800
H	-7.30324800	0.62807000	4.35916900
C	-5.26447100	0.93230500	3.70358700
H	-4.96531400	1.46841500	4.59871500
C	-4.33061300	0.72039800	2.67769400
H	-3.32166400	1.10096300	2.81158300
C	-1.45547700	-2.62169600	2.81377800
C	-0.25077400	-3.03132300	3.42616900
H	0.62548200	-3.26080800	2.82632500

C	-0.15636000	-3.16868000	4.82066600
H	0.78128200	-3.48762500	5.26442200
C	-1.26940100	-2.90012100	5.63105200
H	-1.19981300	-3.01271800	6.70849700
C	-2.47426100	-2.48971200	5.04026400
H	-3.34190900	-2.27796500	5.65727300
C	-2.56556500	-2.34987400	3.64571000
H	-3.50892600	-2.02428600	3.21804400
C	-2.70448100	-4.31287500	0.08675600
C	-3.21411500	-5.18135300	1.07618600
H	-3.09057700	-4.94115300	2.12819000
C	-3.87396500	-6.36929600	0.72042200
H	-4.25749000	-7.02469000	1.49635500
C	-4.03240100	-6.71081800	-0.63109500
H	-4.54079400	-7.62983000	-0.90562500
C	-3.52862400	-5.85864600	-1.62591400
H	-3.64555500	-6.11381700	-2.67462200
C	-2.87123900	-4.67015500	-1.26952100
H	-2.49379600	-4.02614300	-2.05910100
H	3.00183700	4.83211900	-4.44589200
H	-1.75067600	3.57632000	-6.49269300

(Phenyl$_2$Sn)$_7$ (**43**) **TB2**, E = -3265.70555 a.u.

Sn	-1.71549100	2.18126400	1.10394800
Sn	-3.27540600	0.05630100	0.00587700
Sn	-1.79000400	-2.11060300	-1.11299900
Sn	0.41900100	-2.94967100	0.48040900
Sn	2.76829600	-1.31009600	0.70055400
Sn	2.81682300	1.20108700	-0.70052300
Sn	0.53180300	2.92950600	-0.48253300
C	-2.96820800	3.95069100	1.19425500
C	-2.96232500	4.78236100	2.33571100
C	-3.78050600	4.32194900	0.10046600
C	-3.74851900	5.94435600	2.38485200
H	-2.34474500	4.53214200	3.19382900
C	-4.56594500	5.48446200	0.14920900
H	-3.81305600	3.71105600	-0.79647900
C	-4.55293600	6.29801200	1.29153200
H	-3.72903700	6.57032900	3.27180700
H	-5.18483300	5.74825500	-0.70263500
H	-5.16033400	7.19691000	1.32917400
C	-1.10317300	1.79422000	3.14933000
C	0.23349500	1.48390300	3.48036600
C	-2.05031100	1.84792800	4.19801500
C	0.61642600	1.23126700	4.80804700
H	0.99763000	1.43678900	2.70815100
C	-1.67084700	1.60324300	5.52737200

H	-3.09032500	2.08026200	3.98592500
C	-0.33707100	1.29233400	5.83481400
H	1.64958100	0.98604700	5.03016500
H	-2.41463600	1.65519900	6.31667200
H	-0.04323300	1.10264400	6.86237200
C	-4.56497400	0.95587300	-1.48700300
C	-5.86238900	1.39696800	-1.14288800
C	-4.11397400	1.17483400	-2.80639700
C	-6.68649900	2.02221900	-2.09201300
H	-6.23448400	1.26917700	-0.13093700
C	-4.93504800	1.80542700	-3.75476800
H	-3.11678600	0.86687600	-3.10588200
C	-6.22562000	2.22618100	-3.40134200
H	-7.68019600	2.35322000	-1.80615100
H	-4.56156900	1.97212100	-4.76009200
H	-6.86162900	2.71250200	-4.13429800
C	-4.58255400	-0.80738800	1.50428700
C	-5.87283800	-1.26201600	1.15052000
C	-4.15501800	-0.98504100	2.83758300
C	-6.71339900	-1.85852900	2.10355400
H	-6.22678800	-1.16701800	0.12833100
C	-4.99278400	-1.58661000	3.79017100
H	-3.16354500	-0.66720700	3.14537700
C	-6.27637100	-2.01983700	3.42697700
H	-7.70135200	-2.19991000	1.81013900
H	-4.63781900	-1.72099300	4.80702000
H	-6.92537700	-2.48323500	4.16337800
C	-1.16046900	-1.72783600	-3.15343300
C	0.19190900	-1.49238600	-3.48244400
C	-2.10987500	-1.71087400	-4.20136500
C	0.58786000	-1.24425800	-4.80716400
H	0.95843800	-1.50162800	-2.71117900
C	-1.71760600	-1.47190900	-5.52797400
H	-3.16168800	-1.88468100	-3.99154500
C	-0.36807400	-1.23605400	-5.83337900
H	1.63314500	-1.05595900	-5.02762300
H	-2.46390200	-1.46955800	-6.31660200
H	-0.06429500	-1.04997100	-6.85868500
C	-3.10777800	-3.83101100	-1.22126800
C	-3.16614200	-4.62546300	-2.38727900
C	-3.90291900	-4.20548900	-0.11605800
C	-3.99837300	-5.75444800	-2.44919800
H	-2.56240700	-4.37197500	-3.25409500
C	-4.73401100	-5.33520200	-0.17735400
H	-3.88625200	-3.62208400	0.79946500
C	-4.78508100	-6.11172900	-1.34423500
H	-4.02832100	-6.35221100	-3.35513300

H	-5.33871800	-5.60227400	0.68363400
H	-5.42796600	-6.98512300	-1.39166400
C	1.03789300	-4.86956600	-0.32098600
C	1.72450800	-5.79575100	0.49466500
C	0.78802800	-5.22279400	-1.66432200
C	2.14661500	-7.03320400	-0.01552900
H	1.93639200	-5.56007500	1.53402000
C	1.21086700	-6.45937900	-2.17804000
H	0.25609100	-4.54097500	-2.32253700
C	1.89208100	-7.36739700	-1.35431500
H	2.67412200	-7.72963900	0.62874000
H	1.00325700	-6.71160000	-3.21328300
H	2.21820100	-8.32443600	-1.74916100
C	-0.39419000	-3.39683300	2.44146000
C	-0.95309000	-4.67312800	2.67856800
C	-0.43110600	-2.44760200	3.48483900
C	-1.52383500	-4.98962600	3.92153600
H	-0.94858000	-5.42632800	1.89596300
C	-1.00138700	-2.76357200	4.72865700
H	-0.00879800	-1.45636800	3.34995500
C	-1.54831600	-4.03583000	4.95016500
H	-1.94761800	-5.97614900	4.08220300
H	-1.01196500	-2.01569900	5.51529900
H	-1.98808100	-4.28200400	5.91171000
C	4.45932200	-2.47017800	-0.03258500
C	4.34100600	-3.45750500	-1.03407100
C	5.74017700	-2.21822500	0.50835900
C	5.46596900	-4.16782800	-1.48430900
H	3.37249600	-3.69879900	-1.46117900
C	6.86579200	-2.92536500	0.05669600
H	5.86779600	-1.47753800	1.29274300
C	6.73176600	-3.90112700	-0.94255100
H	5.34762300	-4.93149500	-2.24667800
H	7.84028100	-2.71615000	0.48708300
H	7.60145800	-4.45041700	-1.28932200
C	3.31616500	-0.96172400	2.77612000
C	4.04307800	0.18802300	3.15632300
C	3.05528400	-1.93869000	3.76217800
C	4.49774700	0.35341900	4.47581400
H	4.27910000	0.95849500	2.42905900
C	3.50580100	-1.77401300	5.08158700
H	2.49833300	-2.83693800	3.51326200
C	4.23012300	-0.62740000	5.44208000
H	5.06345900	1.24165400	4.73949300
H	3.29259600	-2.53996900	5.82057200
H	4.58524200	-0.50308100	6.46028600
C	3.35515400	0.83226000	-2.77529100

C	3.13035500	1.81749400	-3.76202200
C	4.04209200	-0.34233400	-3.15412200
C	3.57818500	1.63719300	-5.08030200
H	2.60392300	2.73447100	-3.51493300
C	4.49436000	-0.52335900	-4.47236500
H	4.24906800	-1.12075100	-2.42643300
C	4.26376800	0.46640800	-5.43901300
H	3.39329700	2.41000200	-5.81975400
H	5.02952600	-1.43074500	-4.73473600
H	4.61719600	0.32986900	-6.45624100
C	4.55047200	2.29695300	0.03228300
C	5.81901600	2.00298000	-0.51640300
C	4.47219500	3.28120300	1.04079400
C	6.97141200	2.66600900	-0.06544000
H	5.91594600	1.26367400	-1.30645200
C	5.62406000	3.94764000	1.49016300
H	3.51510900	3.55428100	1.47443600
C	6.87705700	3.63919600	0.94076800
H	7.93577300	2.42475500	-0.50185300
H	5.53659100	4.70999400	2.25799000
H	7.76752300	4.15446300	1.28702900
C	-0.25182800	3.42219700	-2.44438500
C	-0.74250500	4.72582000	-2.68287500
C	-0.33544400	2.47608200	-3.48782800
C	-1.29247200	5.07169700	-3.92742300
H	-0.70110800	5.47754600	-1.90018900
C	-0.88521300	2.82112200	-4.73318700
H	0.03429400	1.46437600	-3.35122400
C	-1.36410900	4.12032500	-4.95615900
H	-1.66387400	6.07894000	-4.08907200
H	-0.93257400	2.07463900	-5.51974400
H	-1.78748200	4.38918300	-5.91899800
C	1.23046700	4.81499400	0.33692800
C	1.95444800	5.72010700	-0.46991600
C	1.00088100	5.16254100	1.68539900
C	2.43178000	6.93178000	0.05344100
H	2.15427400	5.48698500	-1.51220600
C	1.47937500	6.37299100	2.21242100
H	0.44275700	4.49618100	2.33776000
C	2.19667500	7.26050600	1.39702100
H	2.98752500	7.61213200	-0.58427300
H	1.28716100	6.62104800	3.25164900
H	2.56589800	8.19745200	1.80198400

13.2.3 Chapter 6

A, E +ZPVE = -1010.913967

Sn	2.40711300	-0.40409400	0.02527500
H	2.49310700	-0.86474800	-1.66041600
H	0.75272800	0.22737000	0.10644400
H	2.63698700	-0.93062000	1.67789900
C	3.70631300	1.35653000	0.00889800
C	4.02113200	2.02695700	-1.19472300
C	4.25606600	1.87276200	1.20389900
C	4.84130100	3.16778500	-1.20688900
H	3.62320200	1.65704400	-2.13755600
C	5.07907600	3.01217800	1.20147600
H	4.03982000	1.38297800	2.15134600
C	5.37262200	3.66360700	-0.00615400
H	5.06472700	3.66566900	-2.14610000
H	5.48714600	3.38910100	2.13496600
H	6.00718800	4.54456500	-0.01185900
N	1.34283400	-2.83145100	0.07947300
C	0.67015800	-3.09009800	-1.20696400
H	-0.14764500	-2.37675800	-1.33351200
H	1.36401200	-2.94147700	-2.03685500
H	0.25934800	-4.11174600	-1.25784800
C	0.38199000	-2.85627600	1.20167700
H	0.88083900	-2.51181100	2.11205500
H	-0.44506900	-2.17450200	0.99084900
H	-0.02711000	-3.86450000	1.37535600
C	2.47977500	-3.74824500	0.33106500
H	2.73345400	-3.67549600	1.39276600
H	2.17397000	-4.79341900	0.14740000
C	3.72024200	-3.45370800	-0.51880600
H	4.40959200	-4.31324800	-0.43472900
H	3.43487000	-3.37917600	-1.57261600
N	4.41563100	-2.19829000	-0.15716800
C	5.12872000	-2.28032400	1.12886000
H	5.89781000	-3.07114200	1.12509100
H	5.61123000	-1.32116900	1.33193900
H	4.42663700	-2.46931000	1.94371300
C	5.31149600	-1.75391100	-1.24237800
H	5.79224200	-0.81582800	-0.95606100
H	6.09120300	-2.49948600	-1.47054200
H	4.72225900	-1.56762600	-2.14496000
H	-2.32337900	-0.31213700	1.03806900
Sn	-3.49533200	0.70482400	0.27673900
H	-4.09711900	1.91966600	1.34613600
H	-3.15929400	1.16902100	-1.34957100

C	-5.20961700	-0.62586600	-0.01024600
C	-5.65630700	-0.95579200	-1.30946800
C	-5.90668000	-1.19356900	1.08058000
C	-6.74856700	-1.81669500	-1.51400500
H	-5.15177400	-0.53715100	-2.17755500
C	-6.99912000	-2.05409900	0.88523600
H	-5.60267600	-0.96482800	2.09977700
C	-7.42278900	-2.36874100	-0.41519700
H	-7.07133800	-2.05182500	-2.52409300
H	-7.51751000	-2.47461400	1.74206100
H	-8.26800400	-3.03259200	-0.56904600
C	-1.03428000	3.35500500	-0.53926000
C	-1.80731400	4.65052300	-0.22746700
H	-1.37126600	2.95232900	-1.50229800
H	-1.48908100	5.02620000	0.75464500
H	-1.49996900	5.41049200	-0.95473400
N	-1.25449200	2.31461800	0.49202600
H	-0.57385000	1.55474300	0.40832500
H	-1.21096800	2.70119200	1.43454300
N	-3.26490300	4.56928500	-0.23739500
H	-3.66986400	3.97361400	0.47429000
H	-3.67917400	4.41469600	-1.14828300
H	0.03487200	3.60274800	-0.63908500

B, E + ZPVE = -1010.932959

Sn	0.06480600	2.37559400	-1.13088700
H	-0.81100200	3.87190200	-1.23022900
H	4.54686600	0.14437600	3.03154000
H	0.62195600	2.07962800	-2.75543800
C	1.91416900	2.85152100	-0.06450400
C	1.91009100	3.02101700	1.34068800
C	3.15646000	2.97026700	-0.72968600
C	3.09043100	3.30628200	2.04872100
H	0.97614400	2.94442800	1.89259100
C	4.34059100	3.25191500	-0.02687900
H	3.20294200	2.85590900	-1.80967700
C	4.31101200	3.42096500	1.36591700
H	3.05460100	3.44470100	3.12547400
H	5.27887700	3.34664800	-0.56573500
H	5.22350300	3.64575300	1.90942000
N	0.80452600	-4.65394200	-0.16509600
C	-0.52825800	-4.46511600	-0.75319900
H	-1.29096900	-4.61258400	0.01838100
H	-0.64037200	-3.44851600	-1.13696800
H	-0.73648200	-5.18143000	-1.57158700
C	0.88923800	-5.90403500	0.60205000
H	1.86489000	-5.97445300	1.09247200

H	0.11907500	-5.91477000	1.37938500
H	0.75369700	-6.80778900	-0.02338300
C	1.88348000	-4.56771300	-1.16166300
H	2.81560800	-4.87615200	-0.67685700
H	1.70954100	-5.29521600	-1.98294300
C	2.08017400	-3.20526500	-1.82974400
H	2.79048900	-3.37174300	-2.66606400
H	1.14199700	-2.86843900	-2.28254100
N	2.57479400	-2.10906200	-0.97150200
C	3.81597500	-2.43986300	-0.25609200
H	4.62984100	-2.75434800	-0.93585500
H	4.15862900	-1.55961200	0.29541100
H	3.63734700	-3.23796900	0.46783200
C	2.73029300	-0.88376700	-1.77804400
H	3.04240400	-0.05036600	-1.14266200
H	3.47962800	-1.00198600	-2.58220100
H	1.77370300	-0.61978400	-2.23686200
H	4.69533200	-0.49427100	3.38172700
Sn	-1.19819600	0.22099700	0.31082900
H	-0.93401200	-1.12150100	-0.79413900
H	-1.09084900	0.97325900	1.90618900
C	-3.37298800	0.40077800	0.04977800
C	-4.14736300	1.22445100	0.89677000
C	-4.05213500	-0.32247100	-0.95559200
C	-5.54041800	1.32836800	0.74485300
H	-3.65892800	1.79674200	1.68314100
C	-5.44515200	-0.22552900	-1.11496400
H	-3.48808400	-0.96702900	-1.62755500
C	-6.19320100	0.60167000	-0.26299600
H	-6.11223100	1.97296900	1.40649200
H	-5.94304200	-0.78909300	-1.89913600
H	-7.26936400	0.68073100	-0.38409200
C	0.80099200	-1.25927100	2.46367200
C	-0.25328500	-2.35979300	2.31430800
H	0.45214800	-0.49755000	3.17117800
H	0.07604100	-3.04851500	1.52870500
H	-0.31262300	-2.92844600	3.25433100
N	1.04276900	-0.60542000	1.16339800
H	1.62362200	0.22826300	1.25471300
H	1.44115100	-1.25168300	0.45660800
N	-1.56237500	-1.79037300	1.92723400
H	-2.16684500	-2.44341500	1.43665500
H	-2.05998000	-1.34714100	2.69551600
H	1.71563000	-1.70595300	2.88043400

C, E + ZPVE= -1009.725189

Sn	2.98578300	1.58277400	-1.47340000
H	4.38865900	2.67296900	-1.44532600
H	3.63575300	0.38363600	-2.63479000
C	3.54926400	0.37217600	0.33956700
C	3.33785100	0.87585800	1.65086400
C	4.06428400	-0.94872800	0.25710300
C	3.63970700	0.12627300	2.80284600
H	2.95413000	1.88652100	1.77772800
C	4.35833400	-1.71307000	1.40197200
H	4.27519900	-1.37041000	-0.72294600
C	4.14812900	-1.17751200	2.68309300
H	3.49109900	0.56329600	3.78711400
H	4.77165600	-2.71281600	1.29390100
H	4.39194400	-1.75679700	3.56879200
N	-2.82678600	-3.15861900	-0.30159000
C	-3.60993900	-2.04637000	-0.85737900
H	-4.16782100	-1.55099200	-0.05692700
H	-2.95774000	-1.29877900	-1.31234900
H	-4.34040400	-2.37928200	-1.61925100
C	-3.67059700	-4.06181400	0.49591500
H	-3.05268700	-4.83701200	0.95911000
H	-4.16675400	-3.50083000	1.29404400
H	-4.45401700	-4.56112400	-0.10487100
C	-2.08621900	-3.91000900	-1.32997600
H	-1.62706500	-4.77756600	-0.84424600
H	-2.78755200	-4.31809300	-2.08798000
C	-1.02248100	-3.12997300	-2.10512000
H	-0.70392800	-3.78435900	-2.94107500
H	-1.46842900	-2.24321200	-2.56687100
N	0.16788600	-2.68525200	-1.34749500
C	0.91336100	-3.80946200	-0.75037300
H	1.23213000	-4.54819000	-1.50713200
H	1.80789200	-3.42384300	-0.25325500
H	0.30363200	-4.32053600	-0.00170200
C	1.04753400	-1.89318000	-2.23829000
H	1.92958200	-1.55208100	-1.69352900
H	1.38875700	-2.47626400	-3.11058600
H	0.51818300	-1.00770500	-2.59917800
Sn	-0.65482800	1.30424100	0.54978200
H	0.62013800	1.53966200	-0.75476500
H	-0.15846000	2.13128200	2.00285800
C	-2.69743800	2.02156200	0.10296900
C	-3.56868300	2.52533400	1.09684900
C	-3.15283400	2.03538800	-1.23415400
C	-4.84608400	3.01114900	0.77164600
H	-3.24573900	2.57203100	2.13499800

C	-4.43106400	2.51535600	-1.56621000
H	-2.50108300	1.68469300	-2.03120800
C	-5.28201300	3.00087000	-0.56248100
H	-5.49155000	3.40509900	1.55108100
H	-4.75546300	2.51938800	-2.60236600
H	-6.26738900	3.37782600	-0.81715500
C	0.06079800	-1.42658500	2.20865900
C	-1.46079200	-1.46413400	2.36092400
H	0.52687600	-0.83425800	3.00240700
H	-1.87898200	-2.08254200	1.55782200
H	-1.73104700	-1.91137400	3.32600900
N	0.38572000	-0.80831300	0.90780700
H	1.37787300	-0.55099400	0.84313000
H	0.14716900	-1.44581800	0.10994800
N	-1.99598900	-0.09256300	2.21322800
H	-2.94709400	-0.05655200	1.85491800
H	-1.92749500	0.45436400	3.06917700
H	0.45977000	-2.44561600	2.28121300

D, E + ZPVE = -1009.763387

Sn	-3.54346700	-0.93099200	-1.37685200
H	-3.34113000	-2.61750000	-1.13534700
H	-4.95047700	-0.64849500	-2.33728100
C	-3.87636400	0.08419300	0.49548300
C	-3.17103200	-0.26898500	1.66762400
C	-4.84025400	1.11300000	0.58408100
C	-3.42111300	0.38634100	2.88491300
H	-2.42202700	-1.05527500	1.63277000
C	-5.08688200	1.77350400	1.79913800
H	-5.41237100	1.40337000	-0.29311700
C	-4.37804500	1.40998800	2.95336400
H	-2.87584300	0.09256500	3.77688100
H	-5.83337500	2.56042700	1.84367500
H	-4.57276800	1.91374500	3.89488300
N	3.77471700	3.01764500	0.06228700
C	4.28912900	1.82429300	-0.62286700
H	4.71202600	1.13337700	0.11367200
H	3.48510700	1.29782200	-1.14238100
H	5.08602600	2.06622200	-1.35327900
C	4.77083200	3.58953500	0.97812400
H	4.33165700	4.42534200	1.53123100
H	5.08524700	2.83252500	1.70332700
H	5.67718600	3.95913100	0.45956300
C	3.27048300	4.03466700	-0.87514100
H	3.07277000	4.94904800	-0.30611400
H	4.05671800	4.29742000	-1.61478300
C	2.02765900	3.65213200	-1.68347800

H	1.93068500	4.41167400	-2.48740600
H	2.18709200	2.69078900	-2.18188000
N	0.75880500	3.55287300	-0.93669300
C	0.38814400	4.78899100	-0.23587900
H	0.30499300	5.65845800	-0.91542700
H	-0.57932900	4.64806400	0.25487900
H	1.12003500	5.02399600	0.54002500
C	-0.31729500	3.09334100	-1.83304700
H	-1.25126900	2.99541300	-1.27166600
H	-0.49358300	3.78895700	-2.67408500
H	-0.06151600	2.11008400	-2.23786100
Sn	1.03277300	-1.00537100	-0.49008500
H	-2.19169700	-0.28216600	-2.22087800
H	-0.50934400	-1.54927900	0.29642300
C	1.95749700	-3.04755100	-0.06071000
C	1.29757100	-4.08198900	0.64932200
C	3.26619700	-3.33742600	-0.52344300
C	1.90571600	-5.32780000	0.88917200
H	0.28360200	-3.91505500	1.00732900
C	3.88761300	-4.57688500	-0.28710900
H	3.80827900	-2.58776500	-1.10032100
C	3.20671900	-5.57712600	0.42405500
H	1.36684700	-6.10096500	1.43091000
H	4.89040600	-4.76496500	-0.66211600
H	3.67872000	-6.53832900	0.60534200
C	0.62977600	1.19925000	2.29441300
C	2.07623500	0.69924400	2.26684100
H	0.00601700	0.50308600	2.86918800
H	2.66180300	1.38261700	1.64344900
H	2.49443000	0.70493700	3.28394300
N	0.11512600	1.27852600	0.93117000
H	-0.89230800	1.18454900	0.85991000
H	0.48885600	2.05442300	0.36528000
N	2.13801400	-0.65335500	1.66437800
H	3.08739300	-0.96052200	1.45789300
H	1.69150300	-1.36568200	2.24161900
H	0.61222300	2.16193400	2.83147000

TSi, E +ZPVE = -1246.459388

Sn	1.94067900	1.01422100	0.75982500
H	2.41684400	0.34076600	2.29022700
H	2.67558300	-0.85316400	-1.51016700
Sn	0.57541400	-0.55097000	-1.33910200
H	0.60077600	0.13538900	-2.93389400
H	3.30565800	-0.29624100	-0.97204500
H	-1.05332100	-0.06314300	-0.84132500

C	4.07535200	0.59753300	-0.28234000
C	4.55652700	1.61420600	-1.16457300
C	4.97991100	0.06963700	0.67771900
C	5.87907700	2.07231600	-1.05030100
C	6.29791100	0.53321700	0.78393400
H	4.64268300	-0.71704100	1.34840200
C	6.74589200	1.54304000	-0.08103800
H	6.23680200	2.84399200	-1.72668900
H	6.96678300	0.11418800	1.52912100
H	7.76495100	1.91032600	-0.00836000
C	0.40862200	-2.72283200	-1.29214900
C	-0.78000100	-3.41647700	-1.64418600
C	1.52761900	-3.46943200	-0.86963900
C	-0.80602300	-4.82216300	-1.55288300
C	1.48881100	-4.87003900	-0.77950100
H	2.45205300	-2.95255000	-0.62495800
C	0.31257900	-5.54876800	-1.12076700
H	-1.71364900	-5.35188200	-1.82985300
H	2.36698600	-5.41906500	-0.45445100
H	0.26607000	-6.63171300	-1.06044400
H	2.15213000	2.74262200	0.85304000
C	3.64557800	2.15662500	-2.23697000
H	2.83642300	2.76082300	-1.80543300
H	4.18606300	2.78645900	-2.94901000
H	3.17353400	1.33698900	-2.79182900
C	-2.01770100	-2.69168000	-2.12520600
H	-1.78697900	-2.01215300	-2.95341700
H	-2.77644000	-3.39846700	-2.47372300
H	-2.46017500	-2.08501900	-1.32667100
N	-5.41350300	0.04657300	0.37880700
C	-6.38053300	0.55637700	1.34693900
H	-6.84832100	-0.28227200	1.87411400
H	-5.86717000	1.17427800	2.09057000
H	-7.19272300	1.16234400	0.90083800
C	-5.98604600	-0.87816800	-0.59711800
H	-6.76414500	-0.42862900	-1.24250000
H	-5.19407100	-1.26738900	-1.24468400
H	-6.44025800	-1.72782700	-0.07534300
C	-4.46936600	1.03282300	-0.15497600
H	-3.69470000	0.48559800	-0.70417300
H	-3.97303200	1.53001000	0.68624900
C	-5.06925800	2.13723000	-1.05264900
H	-5.59493300	1.68476700	-1.91761100
H	-5.82053500	2.68848700	-0.47563000
N	-4.04574400	3.10113400	-1.49039100
C	-4.61596600	4.39392700	-1.88335300
H	-3.80961700	5.09865800	-2.11005900

H	-5.27176800	4.32983700	-2.77395600
H	-5.20280600	4.80816600	-1.05804500
C	-3.14575600	2.56883800	-2.52030900
H	-3.67476200	2.32067100	-3.46178400
H	-2.37509400	3.31062800	-2.75111100
H	-2.63990600	1.66743200	-2.16700800
N	-0.20010700	1.63875900	1.99731300
C	-0.86667000	2.67115500	1.15723200
H	-1.16134500	2.23770600	0.19979900
H	-1.76639900	3.06614100	1.65015200
H	-0.17351900	3.49618500	0.97537300
C	0.25712100	2.25711600	3.26792700
H	-0.59301500	2.67249100	3.82950400
H	0.76444100	1.51903100	3.89025400
H	0.96449800	3.06010400	3.04686300
C	-1.15893300	0.51736000	2.25546600
H	-1.91884600	0.84712100	2.98159900
H	-1.66160900	0.30593400	1.30961000
C	-0.50409100	-0.75965600	2.79147600
H	0.05956600	-1.25472100	1.97486000
H	0.22225100	-0.50950600	3.57128800
N	-1.49917300	-1.66022400	3.38753500
C	-2.49162700	-2.16572700	2.42842900
H	-2.03133000	-2.74528400	1.60499400
H	-3.19427600	-2.81999200	2.95275700
H	-3.07334100	-1.34913600	1.99432800
C	-0.86724700	-2.74652500	4.14432100
H	-1.63704300	-3.33340400	4.65426700
H	-0.27773100	-3.43413600	3.50781100
H	-0.20089300	-2.33027700	4.90625200

13.2.4 Chapter 9

$\mathrm{L^{(CN)}SnH_3}$ (54), conformer 1, E + ZPVE = -409.711125 a.u.

Sn	-1.05755900	-1.19332400	-0.05266600
C	0.07674500	1.84342500	-0.67978000
H	-0.17322900	1.70851200	-1.74042600
H	0.37735300	2.89773700	-0.55159400
N	-1.13725700	1.52828900	0.09723800
C	0.96775900	-0.44286400	-0.04759000
C	1.22582900	0.91946500	-0.31963900
C	2.05743600	-1.29302000	0.22265900
C	2.54296000	1.40641100	-0.30543500
C	3.37556100	-0.80644300	0.23413800
H	1.88301500	-2.34696600	0.42299500

C	3.61769100	0.54833100	-0.02988500
H	2.72985300	2.45789000	-0.50898200
H	4.20108900	-1.47784500	0.44817900
H	4.63197500	0.93441400	-0.01893500
H	-1.95155400	-0.83181100	-1.48596900
H	-1.98731500	-0.96332900	1.38491800
H	-0.79382600	-2.92432800	-0.10876600
C	-2.36256700	2.06714600	-0.51085100
H	-3.23102800	1.74083700	0.06840000
H	-2.36503800	3.16978700	-0.54674600
H	-2.47036300	1.68228000	-1.52862100
C	-1.01291300	1.91047300	1.51394100
H	-0.95644500	3.00482700	1.64208800
H	-1.87526600	1.53508900	2.07114500
H	-0.11148000	1.46354600	1.93962800

L$^{(CN)}$SnH$_3$ (54), conformer 2, E + ZPVE = -409.702147 a.u.

Sn	-1.92034900	-0.82452400	0.01763400
C	1.46766700	-0.69017200	-0.53606700
H	1.49777500	-0.85772900	-1.62087700
H	0.80687900	-1.48144400	-0.12006000
N	2.83627400	-0.82160300	-0.03113700
C	-0.53907500	0.82902200	-0.05646400
C	0.85045900	0.67462400	-0.27393500
C	-1.05905700	2.13128300	0.11593700
C	1.67983100	1.81059900	-0.30772300
C	-0.22526500	3.25873400	0.08206400
H	-2.12321700	2.27467500	0.28304700
C	1.15070200	3.09422800	-0.12943000
H	2.74244200	1.65810600	-0.46594000
H	-0.64623300	4.24923300	0.22193600
H	1.80594800	3.95916700	-0.15661800
H	-1.58502500	-1.89245500	1.32821900
H	-1.90394900	-1.74972000	-1.43622100
H	-3.48840600	-0.14592500	0.23536700
C	3.57579200	-1.92316000	-0.64964500
H	4.61337600	-1.90786200	-0.30258700
H	3.15437600	-2.92009300	-0.41482400
H	3.58173700	-1.80322700	-1.73732100
C	2.91379500	-0.83634700	1.43195900
H	2.43846700	-1.73255900	1.87618600
H	3.96150600	-0.81403700	1.74604100
H	2.41877200	0.04842100	1.83971700

CURRICULUM VITAE

PERSONAL DATA

Name: **Cathrin Zeppek**, BSc, MSc
Address: Schönaugasse 13/3
8010 Graz
Austria
Telephone: +43650 2727348
Email: cathrin_zeppek@hotmail.com
Nationality: Austria
Date of Birth: January 25, 1988
Place of Birth: Klagenfurt, Austria

EDUCATION

09/2012 – 12/2015	**PhD study** in Chemistry, Graz University of Technology, Institute for Inorganic Chemistry, Prof. Frank Uhlig, Title: „*Amine Base Induced Polymerization of Aryltin Hydrides: Mechanistic Insights & Nanomaterial Characterization”*
09/2012	**Bachelor Study Psychology**, University of Graz, entrance exam
10/2009 – 06/2012	**Master Study in Chemistry**, University of Graz and Graz University of Technology **Master Thesis**, Graz University of Technology, Institute for Inorganic Chemistry, Prof. Frank Uhlig, Title: “*Synthesis and characterization of novel aryltin trichlorides and trihydrides: precursors for polyarylstannanes*” **Master degree with distinction**
10/2006 – 08/2009	**Bachelor Study in Chemistry**, University of Graz and Graz University of Technology **Bachelor Thesis**, Graz University of Technology, Institute for Organic Chemistry, Prof. Arnold Stütz,
09/1998 – 06/2006	**Europagymnasium**, Klagenfurt **Degree with distinction**

OUTGOINGS

07/2015	**Research work** at Diamond Lightsource, Oxford, Great Britain *Measurements at the EXAFS Beamline*
05/2015	**Research work** at the ESRF, Grenoble, France *Measurements at the EXAFS Beamline*
09/2013, 02/2014, 08/2015	**Research work** at the Synchrotron Elettra in Trieste, Italy *Measurements at the Austrian SAXS Beamline*
05/2013	**Research work** at the University of Bielefeld, Germany, Institute for Inorganic Chemistry, Prof. Norbert Mitzel
02/2011 – 07/2011	**Erasmus stay**, Universidad de Sevilla, Seville, Spain

WORK EXPERIENCE

Since 09/2012	**Scientific assistant**, Graz University of Technology, Institute for Inorganic Chemistry, Prof. Frank Uhlig *Research, supervision of students in the laboratory, teaching*
02/2010 – 09/2012	Part of the **Promotion- and event organization team** at Marketing Kleine Zeitung GmbH und Co KG, Graz *Coordination and assistance of social events, direct costumer support*
08/2010 – 09/2010	**Project worker**, University of Graz, Institute for Organic and Bioorganic Chemistry, Prof. Wolfgang Kroutil *Research in the field of biocatalysis*
Summer 2008 – 2010	**Scientific researcher**, Cytec Austria GmbH, Graz, Dr. Roland Feola *Research and development in the field of cationic epoxy resins*
10/2009 – 01/2012	**Student supervisor**, University of Graz, Institute for Chemistry
08/2008 – 09/2008	**Project worker,** University of Graz, Institute for Organic and Bioorganic Chemistry, Prof. Renate Dworzak *Research in the field of natural dies*

ADDITIONAL EDUCATION

Leadership & communication	**Leading Diverse Teams**, Interne Education, Graz University of Technology, April **2015** **Basics of NLP**, VHS Graz, October **2014** **Conflict Management**, Interne Education, Graz University of Technology, November 2014 **Leadership and Management**, Interne Education, Graz University of Technology, April 11, **2014** **Basics in Communication**, GÖCH, September 27, **2013**
Presentation techniques	**Presentation Skills for Scientists**, University of Graz, winter **2012**
Other	**Projektmanagement,** Bildungsforum Institut Dr. Rampitsch, September 8, **2014**

SCHOLARSHIPS & AWARDS

2015	**e-fellows** scholarship
2014	**Best Presentation Award** Doc Days and Summer School 2014, University of Graz
2013	**“8. März Mobilitätsstipendium”**, Graz University of Technology **“Erasmus Personalmobilität”**, TU Graz
2011	**Erasmus scholarship** for Spain, Graz University of Technology **Scholarship for outstanding study success** Graz University of Technology
2009	**Scholarship for outstanding study success** Graz University of Technology

MEMBERSHIP

Since 01/2014	**Circle of Excellence Graz** (High Potential Program)

PERSONAL COMPETENCES

Languages	German (mother tongue), English (C2), Spanish (B2), French (B1), Latin
IT- Knowledge	MS-Office, SciFinder, ChemOffice, ISIS Draw, SciDex CLAKS, VNMRJ, MestReNova/ MestReC
Interests and Hobbies	Travel, Sport (Functional Training, Jogging), Psychology, Reading, Languages, Cooking

SCIENTIFIC RECORD

POSTER PRESENTATION AT CONFERENCES

1. Amenitsch, H., Hanzu, I., Flock, M., Uhlig, F., Wilkening, M., Biedermann, J. M., Binder, J.; Torvisco, A., Wolf, M.; Zeppek, C.: “From Molecules Towards Energy Related Materials”, **10 Years NAWI Graz**, July 10, **2014**, Graz, Austria
2. Torvisco, A., Binder, J., Pichler, J., Wolf, M., Zeppek, C., Stammler, H. G., Mitzel, N., Uhlig, F.: “Crystallographic studies of novel aryl heavy Group 14/15 halides and hydrides”, **23rd International Union of Crystallography (IUCr) Congress and General Assembly**, August 4, **2014**, Montreal, Canada
3. Zeppek, C., Pichler, J., Flock M., Torvisco, A., Uhlig, F.: **“**Aryltin Chlorides and Hydrides: Precursors for Polyarylstannanes”, **14th International Conference on the Coordination and Organometallic Chemistry of Germanium, Tin and Lead**, July 14, **2013**, Baddeck, Canada
4. Suljanovic, A.; Zeppek, C.; Albering, J.; Flock, M.; Fischer, R.: “Low-valent Group 14 Derivatives with Aminopyridine Ligands”**,** 13th International Conference on the Coordination and Organometallic Chemistry of Germanium Tin and Lead, July 11, **2010**, Graz, Austria

ORAL PRESENTATIONS

1. Zeppek, C., Torvisco, A., Amenitsch, H., Uhlig, F.: “Aryl Decorated Tin Nanoparticles from Aryltin Trihydrides”, **14th International Seminar of PhD Students on Organometallic and Coordination Chemistry**, October 19, **2015**, Lichtenfels, Germany
2. Zeppek, C., Torvisco, A., Uhlig, F.: “Aryl Decorated Tin Nanoparticles from Aryltin Trihydrides”, **1st European Conference on Smart Inorganic Polymers**, September 21, **2014**, Maribor, Slovenia
3. Chemelli, A., Zeppek, C., Amenitsch, H, Uhlig, F.: “Statische und dynamische Lichtstreuung anorganischer Proben”, **Deutsch-Österreichischer Mitarbeiter Workshop Hauptgruppenelement Chemie**, September, 19-21, **2014**, Freiberg, Germany
4. Zeppek, C.: “Aryl Decorated Tin Nanoparticles”, **Doc Days and Summer School**, July 1, **2014**, Graz, Austria
5. Zeppek, C.: “Aryltin Chlorides and Hydrides: Precursors for Polyarylstannanes**”, 6. Deutsch-Österreichischer Mitarbeiterworkshop Hauptgruppenelement Chemie,** 5. April 2013, Bonn, Germany
6. Zeppek, C.: „Synthesis and Characterization of Novel Aryltin trichlorides- and hydrides: Precursors for Polyarylstannanes”**, 14th International Seminar of PhD Students on Organometallic and Coordination Chemistry**, September 9, **2012**, Admont, Austria

PUBLICATIONS IN PEER REVIEWED JOURNALS

1. Zeppek, C., Fischer R., Torvisco A., Uhlig., F. “Stabilizing, non-covalent interactions in the solid state structure of novel aryltin hydrides and halogenides” *Canad. J. Chem.*, **2014**, *92(6)*, 556-564.
2. Zeppek, C., Pichler, J., Flock, M., Torvisco, A., Uhlig, F. “Aryltin chlorides and hydrides: Preparation, detailed NMR studies and DFT calculations” *J. Organomet. Chem.*, **2013**, *740*, 41-49.